Advances in Mathematical Physics

Nonlinear Evolution Equations and their Analytical and Numerical Solutions

Lead Guest Editor: Mohammad Mirzazadeh
Guest Editors: Kamyar Hosseini, Sachin Kumar, and F. Rabiei

Nonlinear Evolution Equations and their Analytical and Numerical Solutions

Advances in Mathematical Physics

Nonlinear Evolution Equations and their Analytical and Numerical Solutions

Lead Guest Editor: Mohammad Mirzazadeh
Guest Editors: Kamyar Hosseini, Sachin Kumar, and F. Rabiei

Contents

Contents

Hindawi
Advances in Mathematical Physics
Volume 2021, Article ID 5570788, 6 pages
https://doi.org/10.1155/2021/5570788

Research Article

The Soliton Solutions and Long-Time Asymptotic Analysis for an Integrable Variable Coefficient Nonlocal Nonlinear Schrödinger Equation

Guiying Chen, Xiangpeng Xin, and Feng Zhang

School of Mathematical Sciences, Liaocheng University, Liaocheng, Shandong 252059, China

Correspondence should be addressed to Guiying Chen; chenguiying@lcu.edu.cn

Received 24 February 2021; Revised 6 June 2021; Accepted 8 November 2021; Published 10 December 2021

Academic Editor: Mohammad Mirzazadeh

An integrable variable coefficient nonlocal nonlinear Schrödinger equation (NNLS) is studied; by employing the Hirota's bilinear method, the bilinear form is obtained, and the N-soliton solutions are constructed. In addition, some singular solutions and period solutions of the addressed equation with specific coefficients are shown. Finally, under certain conditions, the asymptotic behavior of the two-soliton solution is analyzed to prove that the collision of the two-soliton is elastic.

1. Introduction

In 1998, Bender and coworker first proposed the $\mathcal{PT}$- (parity-time-) symmetry for non-Hermitian quantum mechanics [1]. Now, $\mathcal{PT}$-symmetry has been extensively studied in diverse areas such as lasers [2], acoustics [3], nonlinear optics [4], Bose-Einstein condensation [5], and quantum mechanics [6, 7]. The nonlinear Schrödinger equation has been regarded as the basic model to describe the propagation of solitons in optical fiber, and its spatial solitons have become the research frontier of nonlinear science [8, 9]. In 2013, Ablowitz and Musslimani incorporated the $\mathcal{PT}$-symmetry with nonlinear integrable systems and proposed the nonlocal or $\mathcal{PT}$-symmetry nonlinear Schrödinger equation (NLS) [10],

$$iq_t(x,t) + q_{xx}(x,t) + 2q^2(x,t)q^*(-x,t) = 0, \tag{1}$$

where $*$ represents complex conjugation. Obviously, Equation (1) is invariant under the parity-time (PT) transformation, and its solution is evaluated at (x, t) and $(-x, t)$. Since Equation (1) was proposed, many researchers have carried out a lot of work on it. The integrability [10, 11], the Cauchy problem [12], the inverse scattering transform [13], and exact solutions, such as breathers, periodic, and rational solutions [14], general rogue waves [15], multiple bright soliton [16], higher order rational solutions [17], and N-soliton solutions [18] of (1) have been derived. Moreover, other nonlocal integrable systems have also been investigated like nonlocal modified Korteweg-de Vries equation [19, 20], nonlocal KP equation [21], nonlocal vector nonlinear nonlinear Schrödinger equation [22, 23], nonlocal discrete nonlinear Schrödinger equation [24–26], nonlocal Davey-Stewartson I equation [27], etc.

Although much advance has been made in nonlocal systems, there are very few studies on nonlocal equations with variable coefficients. From the realistic point of view, it is more accurate to describe the physical phenomena by using the variable coefficient equations in many physics situations [28]. So it is a meaningful work to study the exact solutions for nonlocal equations with variable coefficients. In [29], authors constructed the soliton solutions for the variable coefficient nonlocal NLS equation by using Darboux transformation. In [30], analytical matter wave solutions of a $(2+1)$-dimensional nonlocal Gross-Pitaevskii equation are investigated. In this paper, we consider the variable coefficient nonlocal NLS equation,

$$iq_t(x,t) - \delta(t)q_{xx}(x,t) - 2\delta(t)q(x,t)^2q^*(-x,t) + \alpha(t)q(x,t) = 0, \tag{2}$$

where the dispersion coefficient $\delta(t)$ and the gain/loss coefficient $\alpha(t)$ are arbitrary real continuous even functions of

variable t. Obviously, Equation (2) keeps the parity-time transformation $x \longrightarrow -x$, $t \longrightarrow -t$, $q(x,t) \longrightarrow q^*(-x,-t)$ invariant, so it is $\mathscr{PT}$-symmetric. When $\delta(t) = -1$ and $\alpha(t) = 0$, Equation (2) reduces to the constant coefficient self-focusing nonlocal NLS equation (1). When $\alpha(t) = 0$, Equation (2) becomes variable coefficient nonlocal NLS equation which has been solved by Darboux transformations in [29]. The novelty of this paper is that the variable coefficient NLS equation is firstly solved by Hirota's bilinear method, the more general two-soliton solution and N-soliton solution are reported, and the collision of the two solitons is firstly discussed.

The paper is organized as follows: In Section 2, the bilinear form and the one-soliton, two-soliton, and N-soliton solutions of Equation (2) are obtained based on the Hirota's direct method. In Section 3, the asymptotic behavior is studied to prove that the two-soliton collision is elastic. Finally, conclusions are given in Section 4.

2. The Bilinear Form and Soliton Solutions

We implement the following dependent variable transformation to Equation (2)

$$q = e^{i\beta(t)}\frac{g}{f}, \tag{3}$$

where g and f are complex functions and $\beta(t)$ is a real function; then, the following bilinear equations of Equation (2) are obtained as follows:

$$\begin{aligned} &\left(iD_t - \delta(t)D_x^2\right) g \cdot f = 0, \\ &f^*(-x,t)D_x^2 f \cdot f = 2fgg^*(-x,t), \end{aligned} \tag{4}$$

where $\beta(t) = \int \alpha(t)dt$ and D is the bilinear operator [24]:

$$D_t^l D_x^m f(x,t)\cdot g(x,t) = \left(\frac{\partial}{\partial t} - \frac{\partial}{\partial t'}\right)^l \left(\frac{\partial}{\partial x} - \frac{\partial}{\partial x'}\right)^m f(x,t)g\left(x',t'\right)\Big|_{x}^{t'=x,t'=t}. \tag{5}$$

2.1. One-Soliton Solution. In order to construct the soliton solutions for Equation (2), we expend f and g as follows:

$$\begin{aligned} f &= 1 + \varepsilon^2 f_2 + \varepsilon^4 f_4 + \varepsilon^6 f_6 + \cdots, \\ g &= \varepsilon g_1 + \varepsilon^3 g_3 + \varepsilon^5 g_5 + \cdots, \end{aligned} \tag{6}$$

where ε is an arbitrary small parameter. Then, substituting Equation (6) into the bilinear equations (4) and collecting the same power coefficients in ε, we get the following equations:

$$\varepsilon^1 : \left(iD_t - \delta(t)D_x^2\right) g_1 \cdot 1 = 0, \tag{7}$$

$$\varepsilon^2 : D_x^2(f_2 \cdot 1 + 1 \cdot f_2) = 2g_1 g_1^*(-x,t), \tag{8}$$

$$\varepsilon^3 : \left(iD_t - \delta(t)D_x^2\right)(g_3 \cdot 1 + g_1 \cdot f_2) = 0, \tag{9}$$

$$\begin{aligned} \varepsilon^4 : {} & D_x^2(1\cdot f_4 + f_4 \cdot 1 + f_2 \cdot f_2) + f_2^*(-x,t)D_x^2(1\cdot f_2 + f_2 \cdot 1) \\ &= 2(g_1 g_3^*(-x,t) + g_1^*(-x,t)g_3) + 2f_2 g_1 g_1^*(-x,t), \end{aligned} \tag{10}$$

$$\varepsilon^5 : \left(iD_t - \delta(t)D_x^2\right)(g_5 \cdot 1 + g_3 \cdot f_2 + g_1 \cdot f_4) = 0, \tag{11}$$

$$\begin{aligned} \varepsilon^6 : {} & D_x^2(1\cdot f_6 + f_6 \cdot 1 + f_2 \cdot f_4 + f_4 \cdot f_2) + f_2^*(-x,t)D_x^2(1\cdot f_4 \\ &+ f_4 \cdot 1 + f_2 f_2) + f_4^*(-x,t) \times D_x^2(1\cdot f_2 + f_2 \cdot 1) \\ &= 2(g_5 g_1^*(-x,t) + g_3 g_3^*(-x,t) + g_1 g_5^*(-x,t)) \\ &+ 2f_2(g_1 g_3^*(-x,t) + g_3 g_1^*(-x,t)) + 2f_4 g_1 g_1^*(-x,t). \end{aligned} \tag{12}$$

Now, we construct the one-soliton solution for Equation (2). Assuming $g_1 = e^{\eta}$ with $\eta = kx + w(t)$, $\eta^*(-x,t) = -k^*x + w^*(t)$, Equation (7) yields the dispersive relation with $w(t) = -ik^2\int\delta(t)dt$. Then, substituting the obtained g_1 into Equation (8), we get $f_2 = Ae^{\eta+\eta^*(-x,t)}$ with $A = 1/(k-k^*)^2$. Hence, g_1 and f_2 can be expressed as

$$\begin{aligned} g_1 &= e^{kx - ik^2\int\delta(t)dt}, \\ f_2 &= \frac{1}{(k-k^*)^2} e^{(k-k^*)x - i\left(k^2-k^{*2}\right)\int\delta(t)dt}. \end{aligned} \tag{13}$$

Other left equations are satisfied if we set $g_3 = g_5 = \cdots = 0$ and $f_4 = f_6 = \cdots = 0$. Hence, we get the one-soliton solution for Equation (2) as

$$q = e^{i\int\alpha(t)dt}\left(\varepsilon e^{kx-ik^2\int\delta(t)dt}/1+\varepsilon^2\left(1/(k-k^*)^2\right)e^{(k-k^*)x-i\left(k^2-k^{*2}\right)\int\delta(t)dt}\right). \tag{14}$$

Now, setting $\varepsilon = 1$ and $\alpha(t) = 0$, we get several special solutions for Equation (2):

(i) If $k = -2\lambda_2 i$ and $-4\lambda_2 i = \gamma_2$, where λ_2 is a real number, Equation (14) turns into the following period solution which has been reported in [29],

$$q = -\frac{4i\lambda_2\gamma_2 e^{4i\lambda_2^2\int\delta(t)\mathrm{d}t}}{\gamma_2^2 e^{2i\lambda_2 x} + e^{-2i\lambda_2 x}}. \tag{15}$$

(ii) If $k = a + ib$ $(a, b \in \mathbf{R}$, and $ab \neq 0)$, Equation (14) becomes

$$q = \frac{e^{ax+2ab\int\delta(t)\mathrm{d}t}e^{i\left(bx+\int\left(\alpha(t)-\left(a^2-b^2\right)\delta(t)\right)\mathrm{d}t\right)}}{1-\left(1/4b^2\right)e^{4ab\int\delta(t)\mathrm{d}t}e^{2ibx}}. \tag{16}$$

Obviously, Equation (16) is the one-soliton solution with the singular point $(x_0, t_0) = (l\pi/b, t_0)$, where t_0 satisfies $\int\delta(t)\mathrm{d}t = -\ln 4b^2/4ab$, and $l \in \mathbf{Z}$.

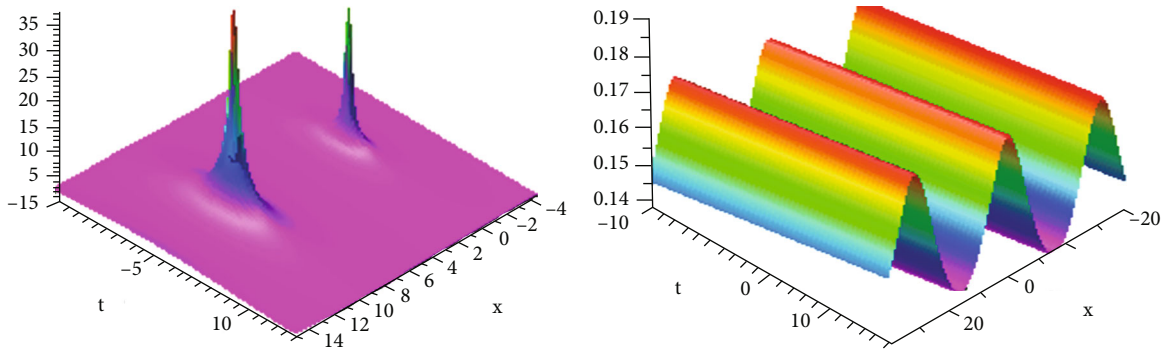

(a) Singular solution ($\delta(t) = -1$) (b) Period solution ($\delta(t) = -1$)

FIGURE 1: (a) Soliton solution with singularity with parameters $a = 0.12$ and $b = -0.35$. (b) Spatial period soliton solution with parameters $a = 0$ and $b = 0.2$, period $M = 5\pi$.

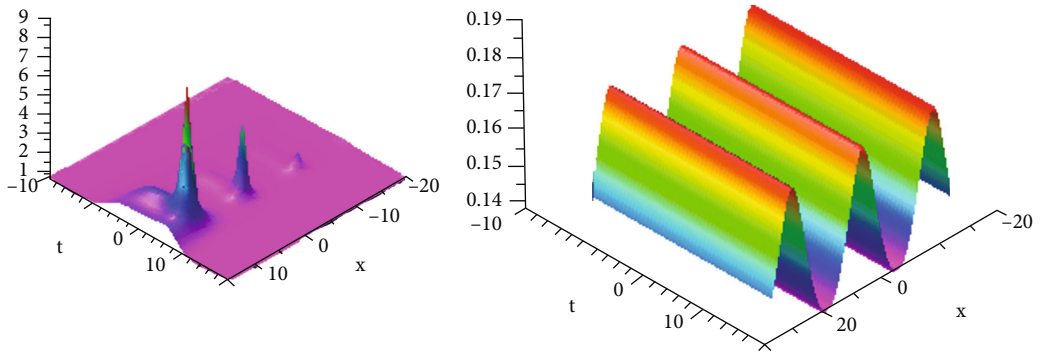

(a) Singular solution ($\delta(t) = t^2$) (b) Period solution ($\delta(t) = t^2$)

FIGURE 2: (a) Soliton solution with singularity when $a = 0.1$ and $b = -0.3$. (b) Spatial period soliton solution with parameter $a = 0$ and $b = 0.2$, period $M = 5\pi$.

(iii) If $k = ib$, $b \in \mathbf{R}$, and $b \neq 0$, we get the spatial period solution

$$|q| = \frac{4b^2}{\sqrt{16b^4 - 8b^2 \cos 2bx + 1}}, \tag{17}$$

where the period $M = \pi/b$.

To show the characteristics of the one-soliton solution, we illustrate the singular solution (16) and the period solution (17) in Figure 1 (when $\delta(t) = -1$) and Figure 2 (when $\delta(t) = t^2$).

2.2. Two-Soliton Solution. To get the two-soliton solution, we let $g_1 = e^{\eta_1} + e^{\eta_2}$ with $\eta_j = k_j x + w_j(t)$, $\eta_j^*(-x,t) = -k_j^* x + w_j^*(t)$, $j = 1, 2$. From Equation (7), we have $w_j(t) = -ik^2 \int \delta(t)dt$, $j = 1, 2$. Plugging the obtained g_1 into Equation (8) leads to

$$\begin{aligned} f_2 = {} & a(1,1^*)e^{\eta_1+\eta_1^*(-x,t)} + a(1,2^*)e^{\eta_1+\eta_2^*(-x,t)} \\ & + a(2,1^*)e^{\eta_2+\eta_1^*(-x,t)} + a(2,2^*)e^{\eta_2+\eta_2^*(-x,t)}, \end{aligned} \tag{18}$$

where $a(l, m^*) = 1/(k_l - k_m^*)^2$, $l, m = 1, 2$.

Then, plugging the known g_1 and f_2 into Equation (9) and Equation (10), we derive g_3 and f_4 as

$$\begin{aligned} g_3 &= a(1,2,1^*)e^{\eta_1+\eta_2+\eta_1^*(-x,t)} + a(1,2,2^*)e^{\eta_1+\eta_2+\eta_2^*(-x,t)}, \\ f_4 &= a(1,2,1^*,2^*)e^{\eta_1+\eta_2+\eta_1^*(-x,t)+\eta_2^*(-x,t)}. \end{aligned} \tag{19}$$

where

$$\begin{aligned} a(l,m) &= \frac{1}{(k_l - k_m)^2}, a(l,m*) = \frac{1}{(k_l - k_m^*)^2}, l, m = 1, 2, \\ a(1,2,1^*) &= a(1,2)a(1,1^*)a(2,1^*), \\ a(1,2,2^*) &= a(1,2)a(1,2^*)a(2,2^*), \\ a(1,2,1^*,2^*) &= a(1,2)a(1,1^*)a(1,2^*)a(2,1^*)a(2,2^*)a(1^*,2^*). \end{aligned} \tag{20}$$

Other equations are satisfied if we let $f_6 = f_8 = \cdots = 0$ and $g_5 = g_7 = \cdots = 0$. Therefore, for $\varepsilon = 1$, we get the two-soliton solution as

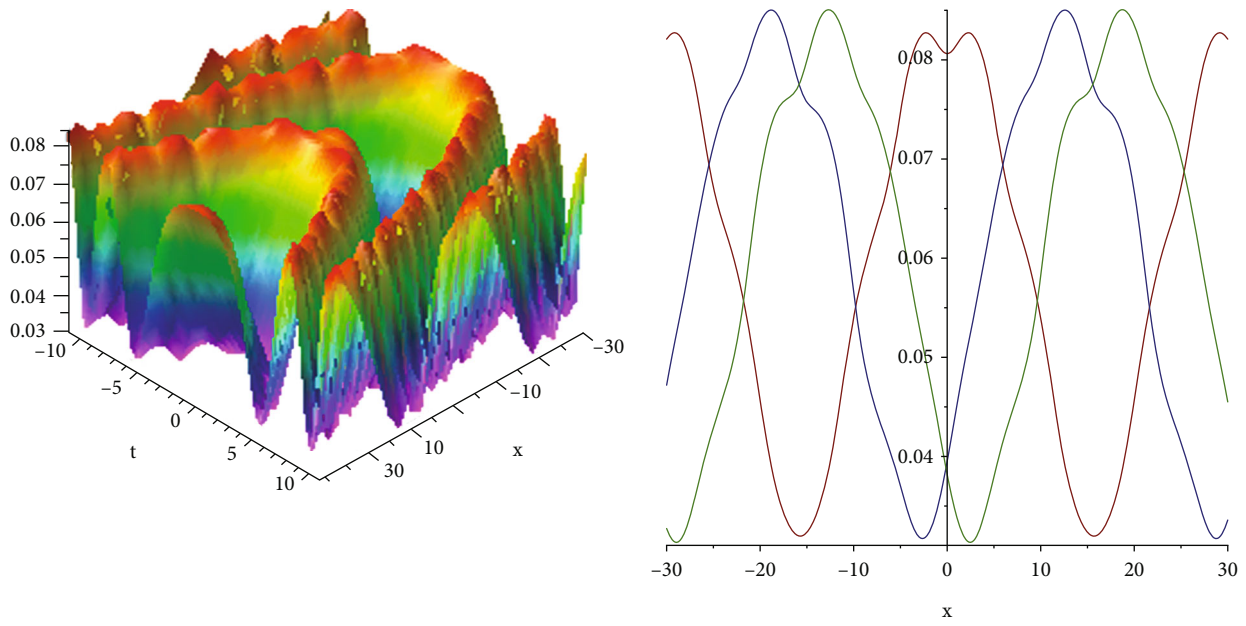

(a) Two-soliton solution ($\delta(t) = t^2$)

(b) Cross-sectional display diagrams ($\delta(t) = t^2$)

FIGURE 3: (a) Double spatial-period soliton solution with parameters: $k_1 = 0.4i$, $k_2 = 0.6i$. (b) Cross-sectional shots of solution (a) at $t = 0$ (red), $t = 5$ (blue), and $t = 10$ (green).

$$q = e^{i\int \alpha(t)dt} \frac{e^{\eta_1} + e^{\eta_2} + \gamma_1 e^{\eta_1+\eta_2+\eta_1^*(-x,t)} + \gamma_2 e^{\eta_1+\eta_2+\eta_2^*(-x,t)}}{1 + \rho_1 e^{\eta_1+\eta_1^*} + \rho_2 e^{\eta_1+\eta_2^*} + \rho_3 e^{\eta_2+\eta_1^*} + \rho_4 e^{\eta_2+\eta_2^*} + \theta e^{\eta_1+\eta_2+\eta_1^*+\eta_2^*}}. \tag{21}$$

where $\gamma_1 = a(1, 2, 1^*)$, $\gamma_2 = a(1, 2, 2^*)$, $\rho_1 = a(1, 1^*)$, $\rho_2 = a(1, 2^*)$, $\rho_3 = a(2, 1^*)$, $\rho_4 = a(2, 2^*)$, $\rho_5 = a(1, 2)$, and $\theta = a(1, 2, 1^*, 2^*)$. Specially, if $k_1 = b_1 i$ and $k_2 = b_2 i$, the solution Equation (21) becomes a double spatial-period solution which is illustrated in Figure 3 (when $\delta(t) = t^2$).

2.3. N-Soliton Solution. The N-soliton solution for Equation (2) can be shown as follows:

$$q = e^{i\int \alpha(t)dt} \frac{g}{f}, \tag{22}$$

where

$$\begin{aligned} f &= \sum_{\mu=0,1}^{(e)} \exp\left(\sum_{l=1}^{2N} \mu_l \eta_l + \sum_{l<m}^{2N} \mu_l \mu_m A_{lm}\right), \\ g &= \sum_{\mu=0,1}^{(o)} \exp\left(\sum_{l=1}^{2N} \mu_l \eta_l + \sum_{l<m}^{2N} \mu_l \mu_m A_{lm}\right), \\ g^*(-x,t) &= \sum_{\mu=0,1}^{(c)} \exp\left(\sum_{l=1}^{2N} \mu_l \eta_l + \sum_{l<m}^{2N} \mu_l \mu_m A_{lm}\right), \end{aligned} \tag{23}$$

where

$$\begin{aligned} &\eta_l = k_l x + \omega_l(t), \omega_l(t) = -ik^2 \int \delta(t)dt, \\ &\eta_{l+N} = \eta_l^*(-x,t), k_{l+N} = k_l^* (l = 1, 2, \cdots, N), \\ &A_{lm} = \ln \frac{1}{(k_l - k_m)^2} (l = 1, 2, \cdots, N, m = N+1, \cdots, 2N), \\ &A_{lm} = \ln (k_l - k_m)^2 (l, m = 1, 2, \cdots, N, orl, m = N+1, \cdots, 2N), \end{aligned} \tag{24}$$

and for $\mu_l = 0$ or 1 $(l = 1, 2, \cdots N)$, $\sum_{\mu=0,1}^{(e)}$, $\sum_{\mu=0,1}^{(o)}$, and $\sum_{\mu=0,1}^{(c)}$ satisfy the following conditions, respectively,

$$\sum_{l=1}^{N} \mu_l = \sum_{l=1}^{N} \mu_{l+N}, \sum_{l=1}^{N} \mu_l = 1 + \sum_{l=1}^{N} \mu_{l+N}, 1 + \sum_{l=1}^{N} \mu_l = \sum_{l=1}^{N} \mu_{l+N}. \tag{25}$$

3. Asymptotic Analysis on Two-Soliton Solution

The asymptotic behavior of the two-soliton solution is dependent on $\delta(t)$. In this section, under certain assumption that $\lim_{t\longrightarrow+\infty} \int \delta(t)dt = +\infty$, we investigate the asymptotic behavior of the two-soliton solution. Since $\delta(t)$ is an even real function, we have $\lim_{t\longrightarrow-\infty} \int \delta(t)dt = -\infty$. For simplicity, we denote $-ik_j^2$ by ω_j, $j = 1, 2$, then $\eta_j = k_j x + \omega_j \int \delta(t)dt$, $j = 1, 2$.

For fixed η_1, we get

$$\eta_2 = \frac{k_2}{k_1}\eta_1 + \left(w_2 - \frac{k_2}{k_1}w_1\right)\int \delta(t)dt,$$
$$\eta_2^*(-x,t) = \frac{k_2^*}{k_1^*}\eta_1^*(-x,t) + \left(w_2^* - \frac{k_2^*}{k_1^*}w_1^*\right)\int \delta(t)dt,$$
$$\eta_2 + \eta_2^*(-x,t) = 2\,\mathrm{Re}\left(\frac{k_2}{k_1}\xi_1\right) + 2\,\mathrm{Re}\left(w_2 - \frac{k_2}{k_1}w_1\right)\int \delta(t)dt. \tag{26}$$

where $w_2 - (k_2/k_1)w_1 = i(-k_2^2 + k_2k_1)$.

Suppose that $\mathrm{Re}\,(w_2 - (k_2/k_1)w_1) > 0$, that is, $\mathrm{Im}\,(k_2^2 - k_2k_1) < 0$. The two-soliton solution asymptotically tends to be one-soliton solution as follows:

$$q \sim \frac{1}{2}e^{(\eta_1 - \eta_1^*(-x,t) - \ln\,\rho_1/2) + i\int \delta(t)dt}\,\mathrm{sec}\,h\frac{\eta_1 + \eta_1^*(-x,t) + \ln\,\rho_1}{2}, t \longrightarrow -\infty, \tag{27}$$

$$q \sim \frac{\rho_2\rho_5}{2}e^{(\eta_1 - \eta_1^*(-x,t) - \ln\,(\theta/\rho_4)/2) + i\int \delta(t)dt}\,\mathrm{sec}\,h\frac{\xi_1 + \xi_1^*(-x,t) + \ln\,(\theta/\rho_4)}{2}, t \longrightarrow +\infty. \tag{28}$$

For fixed η_2, suppose that $\mathrm{Re}\,(w_2 - (k_2/k_1)w_1) > 0$, in a similar way, we get the asymptotic expressions of Equation (21):

$$q \sim \frac{1}{2}e^{(\eta_2 + \eta_2^*(-x,t) - \ln\,\rho_4/2) + i\int \delta(t)dt}\,\mathrm{sec}\,h\frac{\eta_2 + \eta_2^*(-x,t) + \ln\,\rho_4}{2}, t \longrightarrow -\infty, \tag{29}$$

$$q \sim \frac{\rho_3\rho_5}{2}e^{(\eta_2 + \eta_2^*(-x,t) - \ln\,(\theta/\rho_1)/2) + i\int \delta(t)dt}\,\mathrm{sec}\,h\frac{\eta_2 + \eta_2^*(-x,t) + \ln\,(\theta/\rho_1)}{2}, t \longrightarrow +\infty. \tag{30}$$

We can see that the asymptotic solutions Equation (27) and Equation (28), Equation (29) and Equation (30) have the same form, which implies that the two-soliton collision is elastic. But the two-soliton solution is not a travelling wave. If we suppose that $\lim_{t\longrightarrow+\infty}\int \delta(t)dt = -\infty$, the same conclusion can be drawn.

4. Conclusion and Remarks

In the current paper, we studied an integrable variable coefficient nonlocal nonlinear Schrödinger equation via the Hirota's bilinear method. We first constructed the bilinear form and then the N-soliton solution. Furthermore, under certain conditions, we analyzed the asymptotic behavior of the two-soliton solution and proved that the collision of the two soliton is elastic. Also, we demonstrated that by choosing different special parameters, the obtained soliton solutions can reduce to spatial period solution or singular solution. We know that sometimes the higher-dimensional nonlinear systems are more suitable to model the physical phenomena such as ultrafast nonlinear optics, so we hope to investigate the $(2+1)$-dimensional variable coefficient nonlocal partial equations in the future.

Data Availability

All data used to support the findings of this study is included in the submitted paper.

Conflicts of Interest

The authors declare that they have no conflicts of interest.

Acknowledgments

This work was supported by the National Natural Science Foundation of China under grant No. 11505090 and PHD Research Foundation of Liaocheng University under grant No. 318051431.

References

[1] C. M. Bender and S. Boettcher, "Real spectra in non-Hermitian Hamiltonians having $\mathscr{PT}$-symmetry," *Physical Review Letters*, vol. 80, p. 5243, 1998.

[2] S. Longhi, "Bloch oscillations in complex crystals with $\mathscr{PT}$-symmetry," *Physical Review Letters*, vol. 103, article 123601, 2009.

[3] R. Fleury, D. Sounas, and A. Alu, "An invisible acoustic sensor based on parity-time symmetry," *Nature Communications*, vol. 6, no. 1, p. 5905, 2015.

[4] Z. Zhang, Y. Zhang, J. Sheng et al., "Observation of parity-time symmetry in optically induced atomic lattices," *Physical Review Letters*, vol. 117, no. 12, article 123601, 2016.

[5] H. Cartarius and G. Wunner, "Model of a $\mathscr{PT}$-symmetric Bose-Einstein condensate in a δ-function double-well potential," *Physical Review A*, vol. 86, article 013612, 2012.

[6] F. E. Bouzenna, Z. Korichi, and M. T. Meftah, "Solutions of nonlocal Schrodinger equation via the Caputo-Fabrizio definition for some quantum systems," *Reports on Mathematical Physics*, vol. 85, no. 1, pp. 57–67, 2020.

[7] K. G. Atman and H. Sirin, "Nonlocal phenomena in quantum mechanics with fractional calculus," *Reports on Mathematical Physics*, vol. 86, no. 2, pp. 263–270, 2020.

[8] D. Bilman, R. Buckingham, and D. S. Wang, "Far-field asymptotics for multiple-pole solitons in the large-order limit," *Journal of Differential Equations*, vol. 297, pp. 320–369, 2021.

[9] C. Q. Dai, R. P. Chen, Y. Y. Wang, and Y. Fan, "Dynamics of light bullets in inhomogeneous cubic-quintic-septimal nonlinear media with $\mathscr{PT}$-symmetric potentials," *Nonlinear Dynamics*, vol. 87, pp. 1675–1683, 2017.

[10] M. J. Ablowitz and Z. H. Musslimani, "Integrable nonlocal nonlinear Schrödinger equation," *Physical Review Letters*, vol. 110, no. 6, article 064105, 2013.

[11] V. S. Gerdjikov and A. Saxena, "Complete integrability of nonlocal nonlinear Schrödinger equation," *Journal of Mathematical Physics*, vol. 58, no. 1, article 013502, 2017.

[12] Y. Rybalko and D. Shepelsky, "Long-time asymptotics for the nonlocal nonlinear Schrodinger equation with step-like initial data," *Journal of Differential Equations*, vol. 270, pp. 694–724, 2021.

[13] W. X. Ma, "Inverse scattering for nonlocal reverse-time nonlinear Schrodinger equations," *Applied Mathematics Letters*, vol. 102, article 106161, 2020.

[14] X. Huang and L. M. Ling, "Soliton solutions for the nonlocal nonlinear Schrödinger equation," *The European Physical Journal Plus*, vol. 131, no. 5, p. 148, 2016.

[15] B. Yang and J. K. Yang, "On general rogue waves in the parity-time-symmetric nonlinear Schrodinger equation," *Journal of Mathematical Analysis and Applications*, vol. 487, no. 2, article 124023, 2020.

[16] J. C. Chen, Q. X. Yan, and H. Zhang, "Multiple bright soliton solutions of a reverse-space nonlocal nonlinear Schrodinger equation," *Applied Mathematics Letters*, vol. 106, article 106375, 2020.

[17] X. Y. Wen, Z. Yan, and Y. Yang, "Dynamics of higher-order rational solitons for the nonlocal nonlinear Schrödinger equation with the self-induced parity-time-symmetric potential," *Chaos*, vol. 26, no. 6, article 063123, 2016.

[18] J. K. Yang, "General *N*-solitons and their dynamics in several nonlocal nonlinear Schrodinger equations," *Physics Letters A*, vol. 383, no. 4, pp. 328–337, 2019.

[19] J. L. Ji and Z. N. Zhu, "On a nonlocal modified Korteweg-de Vries equation: integrability, Darboux transformation and soliton solutions," *Communications in Nonlinear Science and Numerical Simulation*, vol. 42, pp. 699–708, 2017.

[20] W. X. Ma, "Inverse scattering and soliton solutions of nonlocal complex reverse-spacetime mKdV equations," *Journal of Geometry and Physics*, vol. 157, article 103845, 2020.

[21] X. E. Zhang, Y. Chen, and Y. Zhang, "Breather, lump and X soliton solutions to nonlocal KP equation," *Computers & Mathematics with Applications*, vol. 74, no. 10, pp. 2341–2347, 2017.

[22] D. Sinha and P. K. Ghosh, "Integrable nonlocal vector nonlinear Schrodinger equation with self-induced parity-time-symmetric potential," *Physics Letters A*, vol. 381, no. 3, pp. 124–128, 2017.

[23] Z. Y. Yan, "Nonlocal general vector nonlinear Schrodinger equations: integrability, PT symmetribility, and solutions," *Applied Mathematics Letters*, vol. 62, pp. 101–109, 2016.

[24] L. Y. Ma and Z. N. Zhu, "N-soliton solution for an integrable nonlocal discrete focusing nonlinear Schrodinger equation," *Applied Mathematics Letters*, vol. 59, pp. 115–121, 2016.

[25] J. C. Chen, B. F. Feng, and Y. Y. Jin, "Gram determinant solutions to nonlocal integrable discrete nonlinear Schrodinger equations via the pair reduction," *Wave Motion*, vol. 93, article 102487, 2020.

[26] Y. Hanif and U. Saleem, "Degenerate and non-degenerate solutions of $\mathcal{PT}$-symmetric nonlocal integrable discrete nonlinear Schrodinger equation," *Physics Letters A*, vol. 384, no. 32, article 126834, 2020.

[27] J. G. Rao, J. S. He, D. Mihalache, and Y. Cheng, "PT-symmetric nonlocal Davey-Stewartson I equation: general lump-soliton solutions on a background of periodic line waves," *Applied Mathematics Letters*, vol. 104, article 106246, 2020.

[28] Y. Y. Yan, W. Liu, Q. Zhou, and A. Biswas, "Dromion-like structures and periodic wave solutions for variable-coefficients complex cubic-quintic Ginzburg-Landau equation influenced by higher-order effects and nonlinear gain," *Nonlinear Dynamics*, vol. 99, no. 2, pp. 1313–1319, 2020.

[29] X. P. Xin, Y. Xia, H. Liu, and L. Zhang, "Darboux transformation of the variable coefficient nonlocal equation," *Journal of Mathematical Analysis and Applications*, vol. 490, no. 1, article 124227, 2020.

[30] Q. Liu, "Analytical matter wave solutions of a (2+1)-dimensional partially nonlocal distributed-coefficient Gross-Pitaevskii equation with a linear potential," *Optik*, vol. 200, article 163434, 2020.

Hindawi
Advances in Mathematical Physics
Volume 2021, Article ID 4213939, 6 pages
https://doi.org/10.1155/2021/4213939

Research Article

New Traveling Wave Solutions and Interesting Bifurcation Phenomena of Generalized KdV-mKdV-Like Equation

Yiren Chen[1] **and Shaoyong Li**[2]

[1]*College of Mathematics and Statistics, Shenzhen University, Shenzhen 518060, China*
[2]*School of Mathematics and Statistics, Shaoguan University, Shaoguan 512005, China*

Correspondence should be addressed to Shaoyong Li; lishaoyongok@qq.com

Received 18 June 2021; Revised 5 August 2021; Accepted 7 November 2021; Published 20 November 2021

Academic Editor: Mohammad Mirzazadeh

Using the bifurcation method of dynamical systems, we investigate the nonlinear waves and their limit properties for the generalized KdV-mKdV-like equation. We obtain the following results: (i) three types of new explicit expressions of nonlinear waves are obtained. (ii) Under different parameter conditions, we point out these expressions represent different waves, such as the solitary waves, the 1-blow-up waves, and the 2-blow-up waves. (iii) We revealed a kind of new interesting bifurcation phenomenon. The phenomenon is that the 1-blow-up waves can be bifurcated from 2-blow-up waves. Also, we gain other interesting bifurcation phenomena. We also show that our expressions include existing results.

1. Introduction

Most relationships in nature and human society are intrinsically nonlinear rather than linear in nature, so many phenomena in nature and human society can be described by nonlinear equations, such as automatic control, meteorology, engineering calculation, engineering budget, economy, and finance [1, 2]. Nowadays, many scientists are very interested in nonlinear equations and their solutions and have done a lot of related work [3–5].

In the paper, we consider the generalized KdV-mKdV-like equation [6, 7].

$$u_t + \left(\alpha + \beta u^p + \gamma u^{2p}\right) u_x + u_{xxx} = 0, \tag{1}$$

where $p > 0, \alpha, \beta, \gamma \neq 0$ are real constants. By using appropriate parameters, the generalized KdV-mKdV-like equation becomes the classical KdV equation [8–11], the mKdV equation [12–16], the KdV-like equation [17–20], and the generalized mKdV equation [21].

Up to now, many authors have been interested in the study of the many forms of KdV-like equations [22–25], and there are several explicit solutions results of the generalized KdV-mKdV-like equation based on the significant physical background. For example, Li and Wang [6] gave the following traveling wave solution:

$$u_w(\xi) = \left[\frac{-2(p+1)(p+2)(2p+1)\beta}{(2p+1)\beta^2(p\xi)^2 + (p+1)(p+2)^2\gamma}\right]^{1/p}, \tag{2}$$

where $\beta < 0, \gamma > 0, \xi = x - \alpha t$.

In recent years, the bifurcation method of dynamical systems has been widely used in investigating the nonlinear partial differential equations, for instance [26–29].

In this paper, we study the nonlinear wave solutions and the bifurcation phenomena for Eq. (1). First, we obtain three types of explicit waves which represent the solitary waves, the 1-blow-up waves, and the 2-blow-up waves. Second, we reveal the new bifurcation phenomena which are introduced in the abstract above. Furthermore, we obtain other interesting bifurcation phenomena. The first phenomenon is that the 1-blow-up waves can be bifurcated from the solitary waves. The second phenomenon is that the trivial waves can be bifurcated from the solitary waves.

This paper is organized as follows. In Section 2, we give some notations and state our main results. Our main

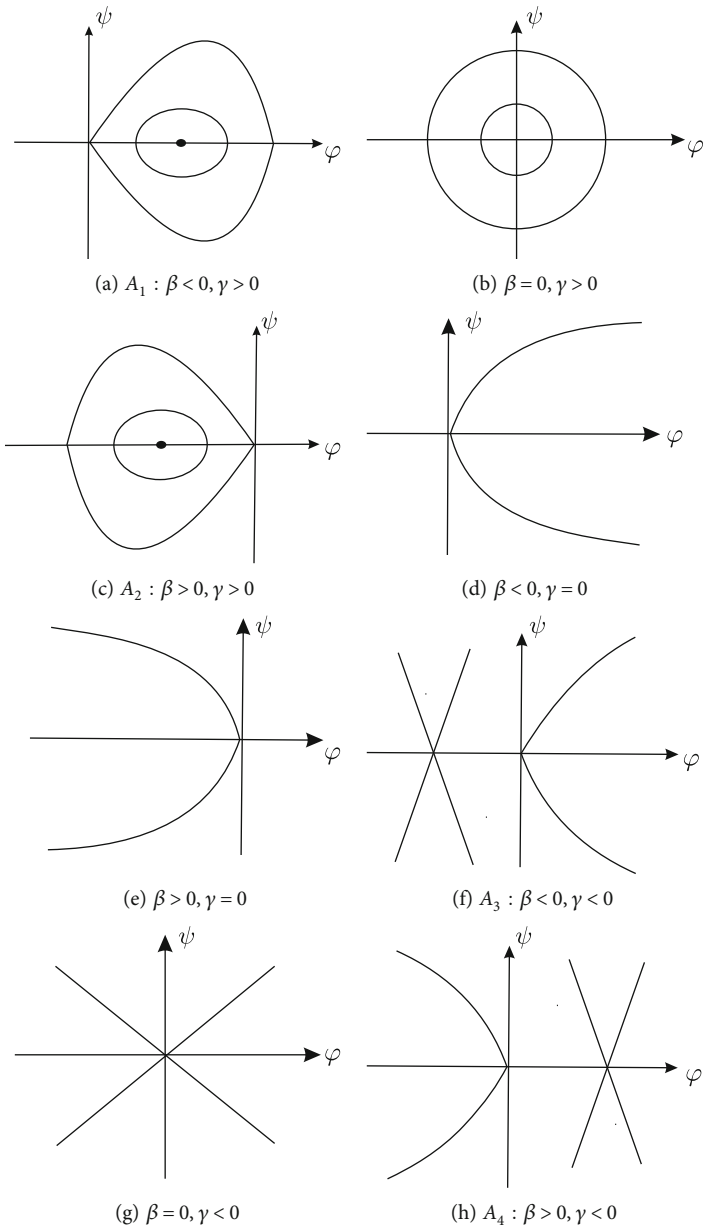

Figure 1: The phase portraits of the system (12).

derivations are listed in Section 3. A brief conclusion is given in Section 4.

2. Our Main Results

In this paper, p is odd and the situation of even is similar to study. In this section, we state our main results. In order to state these results conveniently, we give some notations which will be used in the latter statement and the derivations.

The zones A_j $(j = 1, 2, 3, 4)$ are given in Figure 1, and κ is an arbitrary real constant. In this article, we only consider the case $\alpha - c = 0$. For other cases, due to the complexity, we will investigate them in our future works.

Proposition 1. *If $\alpha - c = 0$, then, the explicit solutions are*

$$u_1(\xi) = \left(\frac{-2(p+1)(p+2)(2p+1)\,\beta}{(2p+1)\beta^2 (p\,\xi + \kappa)^2 + (p+1)(p+2)^2\,\gamma} \right)^{1/p}, \quad (3)$$

and

$$u_2(\xi) = \left(\frac{1}{p\sqrt{-\gamma/(p+1)(p+2)}\,\xi + \kappa} \right)^{1/p}, \quad (4)$$

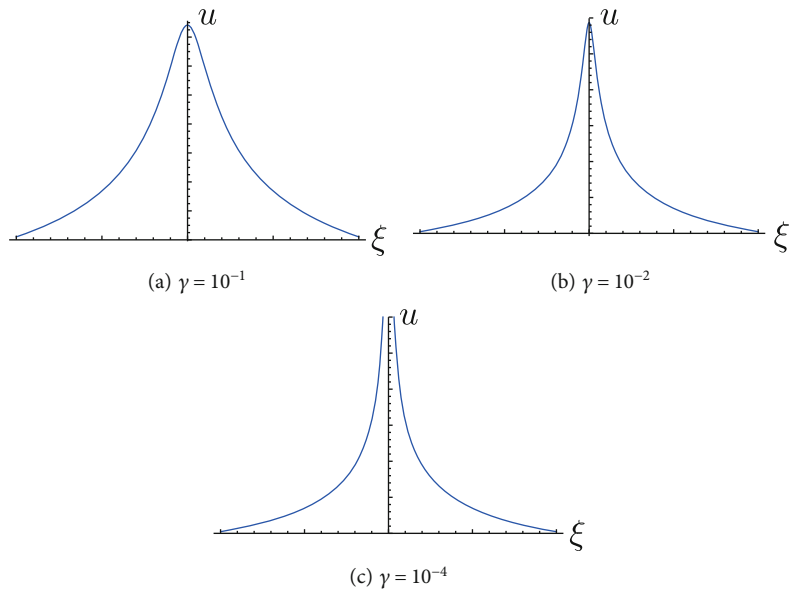

(a) $\gamma = 10^{-1}$ (b) $\gamma = 10^{-2}$

(c) $\gamma = 10^{-4}$

FIGURE 2: The varying figures of the example of $u = u_1(\xi)$ when $\kappa = 0, p = 5, \alpha - c = 0, \beta = -3$, and $\gamma \longrightarrow 0 + 0$.

when $\kappa = 0$, u_1 becomes

$$u_1^0(\xi) = \left(\frac{-2(p+1)(p+2)(2p+1)\beta}{(2p+1)(\beta p \xi)^2 + (p+1)(p+2)^2 \gamma} \right)^{1/p}, \quad (5)$$

After selecting the appropriate parameters, u_1^0 is equivalent to u_w.

when $\gamma = 0$, u_1 becomes

$$u_1^1(\xi) = \left(\frac{-2(p+1)(p+2)}{\beta (p\xi + \kappa)^2} \right)^{1/p}, \quad (6)$$

(i) *If $(\beta, \gamma) \in A_1$ or A_2, then, u_1 is symmetric solitary wave (the example is given in Figure 2(a) or Figure 3(a)). Specially, when $\gamma \longrightarrow 0 + 0$, then, the symmetric solitary wave u_1 becomes single-side 1-blow-up wave u_1^1 (the example is given in Figure 2(c)), and for the varying process of the example, see Figure 2. When $\beta \longrightarrow 0 \pm 0$, then, the symmetric solitary wave u_1 becomes the trivial wave (the example is given in Figure 3(c)), and for the varying process of the example, see Figure 3*

(ii) *If $(\beta, \gamma) \in A_3$ or A_4, then, u_1 is 2-blow-up solitary wave (the example is given in Figure 4(a)). Specially, when $\gamma \longrightarrow 0 - 0$, then, the 2-blow-up wave u_1 becomes the single-side 1-blow-up wave u_1^1 (the example is given in Figure 4(c)), and for the varying process of the example, see Figure 4*

(iii) *If $\beta = 0, \gamma < 0$, then, u_2 is 1-blow-up solitary wave*

3. The Derivation of Main Results

To derive our results, we give some preliminaries in this section. For simplicity of the derived expression, we use the following notation

$$A = \frac{\gamma}{2(p+1)(2p+1)}, \quad (7)$$

$$B = \frac{\beta}{(p+1)(p+2)}, \quad (8)$$

$$C = \frac{\alpha - c}{2}. \quad (9)$$

then we derive our main results.

3.1. The Derivations to Proposition 1. For given constant c and $c - \alpha = 0$, substituting $u = \varphi(\xi)$ with $\xi = x - ct$ into Eq.(1), it follows that

$$\beta \varphi^p \varphi' + \gamma \varphi^{2p} \varphi' + \varphi''' = 0. \quad (10)$$

Integrating (10) once and letting the integral constant be zero, we get

$$\frac{\beta}{p+1} \varphi^{p+1} + \frac{\gamma}{2p+1} \varphi^{2p+1} + \varphi'' = 0. \quad (11)$$

Letting $\psi = \varphi'$, we obtain a planar system

$$\begin{cases} \dfrac{d\varphi}{d\xi} = \psi, \\ \dfrac{d\psi}{d\xi} = -\dfrac{\gamma}{2p+1} \varphi^{2p+1} - \dfrac{\beta}{p+1} \varphi^{p+1}, \end{cases} \quad (12)$$

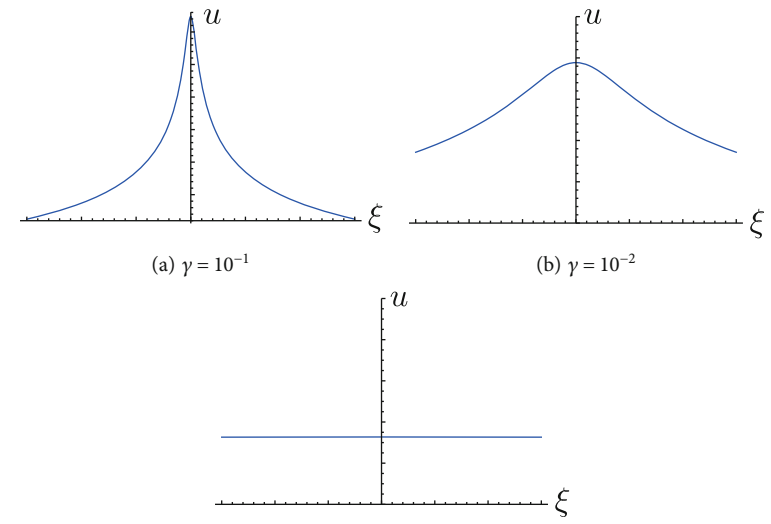

(a) $\gamma = 10^{-1}$ (b) $\gamma = 10^{-2}$

(c) $\gamma = 10^{-4}$

FIGURE 3: The varying figures of the example of $u = u_1(\xi)$ when $\kappa = 0, p = 9, \alpha - c = 0, \gamma = 1$, and $\beta \longrightarrow 0 - 0$.

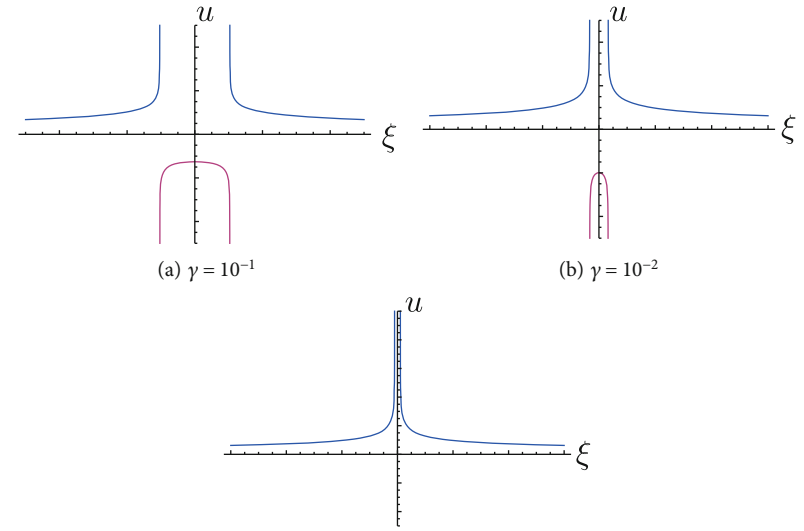

(a) $\gamma = 10^{-1}$ (b) $\gamma = 10^{-2}$

(c) $\gamma = 10^{-4}$

FIGURE 4: The varying figures of the example of $u = u_1(\xi)$ when $\kappa = 0, p = 9, \alpha - c = 0, \gamma = 1$, and $\beta \longrightarrow 0 - 0$.

with the first integral

$$H(\varphi, \psi) = \frac{1}{2}\psi^2 + \frac{\gamma}{2(p+1)(2p+1)}\varphi^{2p+2} + \frac{\beta}{(p+1)(p+2)}\varphi^{p+2} = h, \tag{13}$$

where h is the integral constant. According to the qualitative theory, we obtain the bifurcation phase portraits of system (12) as Figure 1. By means of the bifurcation phase portraits, we can derive Proposition 1.

In the first integral (13), letting $h = H(0, 0)$, we obtain

$$\psi^2 = -2\varphi^2\left(A\varphi^{2p} + B\varphi^p\right), \tag{14}$$

Substituting (14) into the first equation of (12) and integrating it, we get

$$\int_l^{\varphi} \frac{ds}{s\sqrt{As^{2p} + Bs^p}} = |\xi|, \tag{15}$$

where l is an arbitrary constant or $\pm\infty$.

When $\beta \neq 0$ and completing the integral above and solving the equation for φ, it will follow that

$$\varphi = \left(\frac{-2(p+1)(p+2)(2p+1)\beta}{(2p+1)\beta^2(p\xi + \kappa)^2 + (p+1)(p+2)^2\gamma}\right)^{1/p}, \tag{16}$$

and letting $\kappa = 0$, we can obtain (5) from (3). Similarly, when $\beta = 0$ and completing the integral above and solving the equation for φ, we gain (4). Therefore, we have completed the derivations for Proposition 1.

4. Conclusion

In this paper, we have investigated the explicit expressions of the nonlinear waves and their bifurcations in Eq. (1).

First, we obtained three types of new expressions. And they represent different waves, such as the solitary waves, the 1-blow-up waves, and the 2-blow-up waves.

Second, we revealed three kinds of bifurcation phenomena which include a new bifurcation phenomena. The first phenomenon which is new bifurcation phenomenon is that 1-blow-up waves can be bifurcated from 2-blow-up waves. The second phenomenon is that the trivial waves can be bifurcated from the solitary waves. The third phenomenon is that the 1-blow-up waves can be bifurcated from the solitary waves.

Third, we showed that a previous result is our special case, that is, u_w is included in u_1^0.

Furthermore, the bifurcation method of dynamical systems can be used to find the new traveling solutions and bifurcations of many nonlinear equations such as the extended quantum Zakharov-Kuznetsov equation [37], the Fujimoto-Watanabe equation [38], and b-family-like equation [39]. We will continue to use the bifurcation method of dynamical systems to study other important nonlinear equations.

Data Availability

No data were used to support this study.

Conflicts of Interest

The authors declare that there is no conflict of interests regarding the publication of this article.

Acknowledgments

This work was supported by the National Natural Science Foundation of China Grant (12001377 and 11971176), the Outstanding Innovative Young Talents of Guangdong Province (2019KQNCX122), Natural Science Foundation of Guangdong Province (2018A0303100015), and Characteristic Innovative Project from Guangdong Provincial Department of Education (2018KTSCX204).

References

[1] X. P. Zhai and Y. R. Chen, "Global solutions and large time behavior for the chemotaxis-shallow water system," *Journal of Differential Equations*, vol. 275, pp. 332–358, 2021.

[2] Y. R. Chen, B. F. Feng, and L. M. Ling, "The robust inverse scattering method for focusing Ablowitz-Ladik equation on the non-vanishing background," *Physica D: Nonlinear Phenomena*, vol. 424, article 132954, 2021.

[3] L. Kaur and A. M. Wazwaz, "Bright - dark optical solitons for Schrodinger-Hirota equation with variable coefficients," *Optik*, vol. 179, pp. 479–484, 2019.

[4] I. Ahmed, A. R. Seadawy, and D. Lu, "M-shaped rational solitons and their interaction with kink waves in the Fokas-Lenells equation," *Physica Scripta*, vol. 94, no. 5, article 055205, 2019.

[5] S. Singh, L. Kaur, R. Sakthivel, and K. Murugesan, "Computing solitary wave solutions of coupled nonlinear Hirota and Helmholtz equations," *Physica A: Statistical Mechanics and its Applications*, vol. 560, article 125114, 2020.

[6] X. Z. Li and M. L. Wang, "A sub-ODE method for finding exact solutions of a generalized KdV-mKdV equation with high-order nonlinear terms," *Physics Letters A*, vol. 361, no. 1-2, pp. 115–118, 2007.

[7] Z. L. Li, "Constructing of new exact solutions to the GKdV-mKdV equation with any-order nonlinear terms by $G'G$-expansion method," *Applied Mathematics and Computation*, vol. 217, no. 4, pp. 1398–1403, 2010.

[8] M. Song, X. J. Hou, and J. Cao, "Solitary wave solutions and kink wave solutions for a generalized KDV-mKDV equation," *Applied Mathematics and Computation*, vol. 217, no. 12, pp. 5942–5948, 2011.

[9] R. M. Miura, "The Korteweg–deVries equation: a survey of results," *SIAM Review*, vol. 18, no. 3, pp. 412–459, 1976.

[10] A. H. Khater, O. H. El-Kalaawy, and M. A. Helal, "Two new classes of exact solutions for the KdV equation via Backlund transformations," *Chaos, Solitons & Fractals*, vol. 8, no. 12, pp. 1901–1909, 1997.

[11] M. Kovalyov and M. H. A. Abadi, "An explicit formula for a class of solutions of the KdV equation," *Physics Letter A*, vol. 254, no. 1-2, pp. 47–52, 1999.

[12] M. Lakshmanan and K. M. Tamizhmani, "Lie–Bäcklund symmetries of certain nonlinear evolution equations under perturbation around their solutions," *Journal of Mathematical Physics*, vol. 26, no. 6, pp. 1189–1200, 1985.

[13] L. R. T. Gardner, G. A. Gardner, and T. Geyikli, "Solitary wave solutions of the MKdV^{-} equation," *Computer Methods in Applied Mechanics and Engineering*, vol. 124, no. 4, pp. 321–333, 1995.

[14] B. Li, Y. Chen, and H. Q. Zhang, "Explicit exact solutions for compound KdV-type and compound KdV-Burgers-type equations with nonlinear terms of any order," *Solitons & Fractals*, vol. 15, no. 4, pp. 647–654, 2003.

[15] J. Gorsky and A. Himonas, "Construction of non-analytic solutions for the generalized KdV equation," *Journal of Mathematical Analysis and Application*, vol. 303, no. 2, pp. 522–529, 2005.

[16] N. A. Kudryashov and D. I. Sinelshchikov, "A note on the lie symmetry analysis and exact solutions for the extended mKdV equation," *Acta Applicandae Mathematicae*, vol. 113, no. 1, pp. 41–44, 2011.

[17] B. Dey, "Domain wall solutions of KdV like equations with higher order nonlinearity," *Journal of Physics A: Mathematical and General*, vol. 19, no. 1, pp. L9–L12, 1986.

[18] B. Dey, "K-dV like equations with domain wall solutions and their Hamiltonians," *Solitons, Springer Series in Nonlinear Dynamics*, pp. 188–194, 1988.

[19] R. Grimshaw, D. Pelinovsky, E. Pelinovsky, and A. Slunyaev, "Generation of large-amplitude solitons in the extended Korteweg-de Vries equation," *Chaos*, vol. 12, no. 4, pp. 1070–1076, 2002.

[20] L. Zhengrong, J. Tianpei, Q. Peng, and X. Qinfeng, "Trigonometric function periodic wave solutions and their limit forms for the KdV-like and the PC-like equations," *Mathematical Problems in Engineering*, vol. 2011, Article ID 810217, 23 pages, 2011.

[21] Z. R. Liu and J. B. Li, "Bifurcations of solitary waves and domain wall waves for KdV-like equation with higher order

nonlinearity," *International Journal of Bifurcation and Chaos*, vol. 12, no. 2, pp. 397–407, 2002.

[22] K. Roy, A. Saha, P. Chatterjee, and C. S. Wong, "Head on collision of dust acoustic multi-solitons in a nonextensive plasma," *Jurnal Fizik Malaysia*, vol. 36, no. 1, pp. 01009–01028, 2015.

[23] D. Lu, C. Yue, and M. Arshad, "Traveling wave solutions of space-time fractional generalized fifth-order KdV equation," *Advances in Mathematical Physics*, vol. 2017, Article ID 6743276, 6 pages, 2017.

[24] S. B. G. Karakoc, A. Saha, and D. Sucu, "A novel implementation of Petrov-Galerkin method to shallow water solitary wave pattern and superperiodic traveling wave and its multistability: generalized Korteweg-de Vries equation," *Chinese Journal of Physics*, vol. 68, pp. 605–617, 2020.

[25] B. Pradhan, A. Abdikian, and A. Saha, "Characteristics of supernonlinear and coexistence features for electron-acoustic waves in an adiabatic quantum plasma," *The European Physical Journal D*, vol. 75, no. 2, 2021.

[26] B. G. Zhang, W. B. Li, and X. P. Li, "Peakons and new exact solitary wave solutions of extended quantum Zakharov-Kuznetsov equation," *Physics of Plasmas*, vol. 24, no. 6, article 062113, 2017.

[27] Z. S. Wen, "Bifurcations and exact traveling wave solutions of the celebrated Green-Naghdi equations," *International Journal of Bifurcation and Chaos*, vol. 27, no. 7, article 1750114, 2017.

[28] S. K. El-Labany, W. F. El-Taibany, and A. Atteya, "Bifurcation analysis for ion acoustic waves in a strongly coupled plasma including trapped electrons," *Physics Letters A*, vol. 382, no. 6, pp. 412–419, 2018.

[29] J. P. Yang, R. Liu, and Y. R. Chen, "Bifurcations of solitary waves of a simple equation," *International Journal of Bifurcation and Chaos*, vol. 30, no. 9, article 2050138, 2020.

Hindawi
Advances in Mathematical Physics
Volume 2021, Article ID 3346387, 17 pages
https://doi.org/10.1155/2021/3346387

Research Article

Numerical Approximation of Generalized Burger's-Fisher and Generalized Burger's-Huxley Equation by Compact Finite Difference Method

Ravneet Kaur,[1] **Shallu**,[1] **Sachin Kumar**,[2] **and V. K. Kukreja**[1]

[1]*Department of Mathematics, SLIET, Longowal, 148106 Punjab, India*
[2]*Department of Mathematics and Statistics, Central University of Punjab, Bathinda, 151001 Punjab, India*

Correspondence should be addressed to V. K. Kukreja; vkkukreja@gmail.com

Received 16 May 2021; Accepted 7 October 2021; Published 9 November 2021

Academic Editor: Giuseppe Pellicane

In this work, computational analysis of generalized Burger's-Fisher and generalized Burger's-Huxley equation is carried out using the sixth-order compact finite difference method. This technique deals with the nonstandard discretization of the spatial derivatives and optimized time integration using the strong stability-preserving Runge-Kutta method. This scheme inculcates four stages and third-order accuracy in the time domain. The stability analysis is discussed using eigenvalues of the coefficient matrix. Several examples are discussed for their approximate solution, and comparisons are made to show the efficiency and accuracy of CFDM6 with the results available in the literature. It is found that the present method is easy to implement with less computational effort and is highly accurate also.

1. Introduction

The excerpt approximation of the Navier-Stokes equation is represented by a prominent nonlinear mathematical model known as Burger's equation. It is the perfect combination of advection and diffusion terms. This equation was introduced by Bateman [1]. Later, Burger [2] extensively worked on this problem, considering the turbulence effect and the statistical aspects. Burger's equation describes the process of simulating shock wave phenomena, dispersion in a porous medium, heat conduction, diffusion flow, modeling of gas dynamics, traffic flow, propagation and reflection of the nonlinear fluid, boundary layer flow, electrohydrodynamics, sound waves, oil reservoir simulation, etc. The spreading of any species due to the favorable environment of the invasive species or predicting the pattern of spreading was an important issue in the early twenties. The great researcher Fisher [3] proposed a model for the temporal and spatial propagation, depicting the wave of increase in gene frequency in an infinite medium and termed it as Fisher's equation. It represents the biological processes, ecological systems, pattern formation, etc. Petrovskii and Shigesada [4] combined both the models by assuming that the distribution of species is symmetrical and the environment is homogeneous. The following 1D equation was proposed:

$$\frac{\partial z}{\partial t} = \frac{\partial^2 z}{\partial x^2} + \mathfrak{f}(x, t, z, z_x), \quad \text{in } \Phi = \Phi_x \times \Phi_t, \tag{1}$$

with the initial and boundary conditions:

$$\begin{aligned} z &= z^0, \quad \text{in } \bar{\Phi}_x \times t_0, \\ \mathfrak{B}z &= \Omega, \quad \text{on } \partial\Phi_x \times \bar{\Phi}_t, \end{aligned} \tag{2}$$

where $\Phi_x = (a, b)$, $\Phi_t = (0, t)$, and $\mathfrak{B}$ is the boundary operator. A mathematical model for $\mathfrak{f}(x, t, z, z_x) = -\beta z^\delta z_x + \gamma z(1 - z^\delta)$ in (1) with the above conditions is known as the generalized Burger's-Fisher (gBF) equation and is expressed as follows:

$$\frac{\partial z}{\partial t} - \frac{\partial^2 z}{\partial x^2} + \beta z^\delta \frac{\partial z}{\partial x} - \gamma z\left(1 - z^\delta\right) = 0, \quad 0 \le x \le 1, t \ge 0, \tag{3}$$

subject to the initial condition:

$$z(x,0)=\left[\frac{1}{2}+\frac{1}{2}\tanh\left(\frac{-\beta\delta x}{2(1+\delta)}\right)\right]^{1/\delta}, \tag{4}$$

and the boundary conditions:

$$z(0,t)=\left(\frac{1}{2}+\frac{1}{2}\tanh\left(\frac{\beta\delta}{2(1+\delta)}\left[\left(\frac{\beta^2+\gamma(1+\delta)^2}{\beta(1+\delta)}t\right)\right]\right)\right)^{1/\delta},\quad t\geq 0, \tag{5}$$

$$z(1,t)=\left(\frac{1}{2}+\frac{1}{2}\tanh\left(\frac{-\beta\delta}{2(1+\delta)}\left[1-\left(\frac{\beta^2+\gamma(1+\delta)^2}{\beta(1+\delta)}t\right)\right]\right)\right)^{1/\delta}, \tag{6}$$

where β, γ, and δ are the constants. The choice of the value of these constants reduces the model to different forms of PDEs. For $\gamma=0$, it reduces to the generalized Burger's equation. Taking $\beta=0$, it becomes the generalized Fisher's equation. The exact solution of Equation (3) was given by Chen and Zhang [5] as follows:

$$z(x,t)=\left(\frac{1}{2}+\frac{1}{2}\tanh\left(\frac{-\beta\delta}{2(1+\delta)}\left[x-\left(\frac{\beta^2+\gamma(1+\delta)^2}{\beta(1+\delta)}t\right)\right]\right)\right)^{1/\delta}. \tag{7}$$

Over the past many years, work has been done for the explicit solution of Equation (3). Numerical methods provide a tool for the physical behaviour of the system, although theoretical results are available in the literature. Sari et al. [6] applied the compact finite difference method along with the third-order total variation-diminishing Runge-Kutta scheme in the time domain. Zhao et al. [7] implemented the pseudospectral method using the time discretization by Crank-Nicolson as well as the leapfrog scheme and space discretization by Legendre-Galerkin and Chebyshev-Gauss-Lobatto for nodes. Mohammadi [8] proposed the exponential spline and finite difference approximations. Tatari et al. [9] analyzed the radial basis function collocation technique with the predictor-corrector method. Malik et al. [10] discussed the hybridization of the Exp-function method with the nature-inspired algorithm. Yadav and Jiwari [11] analyzed the finite element analysis with the existence and uniqueness of the weak solution using Galerkin's finite element method. Macias-Diaz and Gonzalez [12] implemented the finite difference method. Soori [13] obtained the exact solution of the Burger's-Fisher equation using the variational iteration method and homotopy perturbation method. An exponential time differencing scheme using the method of lines was developed by Bratsos and Khaliq [14]. Gurbuz and Sezer [15] discussed the modified Laguerre matrix-collocation method.

The significance and various applications motivated the researchers to compute the analytical and numerical solutions of the Burger's-Fisher equation. Recently, the dynamical behaviour and exact parametric representations of the traveling wave solutions under different parametric conditions have been discussed by Li [16]. In the findings, the exact monotonic and nonmonotonic kink wave solutions, two-peak solitary wave solutions, and periodic wave solutions, as well as unbounded traveling wave solutions have been obtained. Onyejekwe et al. [17] applied a boundary integral element-based numerical technique, in which the boundary and domain values calculate the fundamental integral inside the domain. The domain integrals due to nonlinearity are considered for computing the solution. Investigation of the global existence and uniqueness of a periodic wave solution has been conducted by Zhang et al. [18].

Another important nonlinear equation, describing the interaction between reaction mechanism, convection effect, and diffusion transport is the 1D generalized Burger's-Huxley (gBH) equation, for which $\mathfrak{f}(x,t,z,z_x)=-\beta z^{\delta}z_x+\gamma z(1-z^{\delta})(z^{\delta}-\eta)$. The equation is expressed as follows:

$$\frac{\partial z}{\partial t}-\frac{\partial^2 z}{\partial x^2}+\beta z^{\delta}\frac{\partial z}{\partial x}=\gamma z\left(1-z^{\delta}\right)\left(z^{\delta}-\eta\right),\quad a\leq x\leq b,\ t\geq 0. \tag{8}$$

The parameters β, γ, and δ are the constants and parameter $\eta\in(0,1)$. The initial and boundary conditions are as follows:

$$z(x,0)=\left(\frac{\eta}{2}+\frac{\eta}{2}\tanh\left(A_1x\right)\right)^{1/\delta}, \tag{9}$$

$$\begin{aligned} z(a,t)&=\left[\frac{\eta}{2}+\frac{\eta}{2}\tanh\left(A_1(a-A_2t)\right)\right]^{1/\delta}, z(b,t)\\ &=\left[\frac{\eta}{2}+\frac{\eta}{2}\tanh\left(A_1(b-A_2t)\right)\right]^{1/\delta}. \end{aligned} \tag{10}$$

The exact solution derived by Wang [19], using nonlinear transformations, is reproduced hereunder:

$$z(x,t)=\left[\frac{\eta}{2}+\frac{\eta}{2}\tanh\left(A_1(x-A_2t)\right)\right]^{1/\delta}, \tag{11}$$

where

$$\begin{aligned} A_1&=\eta\delta\left(\frac{-\beta+\sqrt{\beta^2+4\gamma(1+\delta)}}{4(\delta+1)}\right), A_2\\ &=\frac{\beta\eta}{\delta+1}-\frac{(1-\eta+\delta)\left(-\beta+\sqrt{\beta^2+4\gamma(\delta+1)}\right)}{2(\delta+1)}. \end{aligned} \tag{12}$$

For $\gamma=0$, the above model conforms to the generalized Burger's equation, and considering $\beta=0$ and $\delta=1$, the Huxley equation [20] is obtained. For $\beta=0$, $\gamma=1$, and $\delta=1$, it corresponds to the Fitzhugh-Nagoma equation [21]. Yefimova and Kudryashov [22] applied the Hopf-Cole transformation for solving the gBH equation. The Adomian decomposition method was implemented by Ismail et al. [23]. Gao and Zhao [24] proposed the Exp-function method for a series of exact solutions of the gBH equation. A high-order difference scheme using Taylor's series expansion was presented by Sari et al. [25]. Celik [26] introduced a numerical method based on the Haar wavelet approach.

Zhang et al. [27] reduced the Burger's-Huxley and Burger's-Fisher equations into first-order systems and then applied the discontinuous Galerkin method. A numerical scheme based on the finite differences for time integration and cubic B-spline for space integration was proposed by Mohammadi [28]. A fourth-order finite difference method was implemented by Bratsos [29] in a two-time level recurrence relation for the solution of the gBH equation. El-Kady et al. [30] discussed the methods based on cardinal Chebyshev and Legendre basis functions with the Galerkin method, Gauss quadrature formula, and El-Gendi method to convert the problem into ordinary differential equations. Technique based on modified cubic B-spline as the basis function with differential quadrature method was discussed by Singh et al. [31]. The nonstandard finite difference method was analyzed by Zibaei et al. [32]. Bukhari [33] applied local radial basis function differential collocation method. Macias-Diaz [34] used the explicit exponential method. Gilani and Saeed [35] applied the CAS wavelet in conjunction with the Picard technique. Cardinal B-spline wavelet numerical method was used by Shiralashetti and Kumbinarasaiah [36]. A technique based on the hyperbolic-trigonometric tension B-spline method was applied by Alinia and Zarebnia [37]. Loyinmi and Akinfe [38] proposed an algorithm using the coupling of the Elzaki transform with the homotopy perturbation method.

Recently, the exact solution has been computed by Kushner and Matviichuk [39] using the theory of finite-dimensional dynamics. Shukla and Kumar [40] applied the numerical scheme based on the Crank-Nicolson finite difference method in collaboration with the Haar wavelet analysis, to obtain the numerical solution. A feed-forward artificial neural network technique is applied by Panghal and Kumar [41] in which the constructed error function is minimized using the quasi-Newton algorithm.

Based on the traditional finite difference approximations, Lele [42] proposed well-regulated compact schemes to provide a better representation of shorter proportionate lengths. Many researchers have extended the compact finite difference scheme for linear/nonlinear differential equations, partial differential equations having Dirichlet or Neumann boundary conditions. Ansari et al. [43] implemented the CFD6 scheme for free vibration phenomena of nanobeams in an elastic medium. A similar scheme for incompressible Navier-Stokes and scalar transport equation was analyzed by Boersma [44], a reaction-diffusion equation with delay was approximated by Li et al. [45] and the modified Burger's equation by Kaur et al. [46].

In this work, a numerical scheme based on the sixth-order compact finite difference method (CFDM6) followed by the strong stability-preserving Runge-Kutta method (SSP-RK43) for time integration is used to solve gBF and gBH equations. The advantage of CFDM6 with the SSP-RK43 method is that it computes the results at more mesh points, giving a better approximate solution. The proposed method gives the sixth order of convergence in the spatial domain and the third order in the temporal domain. The proposed method is easy to implement and has less computational cost. The future scope of the method is to solve various arduous linear and nonlinear PDEs.

The paper is organized as follows: in Section 2, first- and second-order spatial derivatives of the CFDM6 are derived. In Section 3, the proposed method is implemented followed by SSP-RK43. In Section 4, convergence is discussed. In Section 5, stability analysis for the proposed scheme is presented. In Section 6, several test problems are discussed to demonstrate and justify the applicability of the proposed scheme. In Section 7, the conclusion explaining the efficiency of CFDM6 is given.

2. Compact Finite Difference Method

The spatial domain $\phi_x = (a, b)$ is divided into uniform mesh with step iteration $x_i = a + ih$, $i = 0, 1, 2, \cdots, N$, $h = (b - a)/N$ and for time domain $\phi_t = (t_0, t)$, with $t_0 = 0$, a uniform step of size $\Delta t = t^{j+1} - t^j$ such that $t^j = t_0 + j\Delta t$, $j = 0, 1, 2, \cdots$, is followed. The method for calculating first-order and second-order derivatives using the compact finite difference scheme is given hereunder.

2.1. Spatial Derivatives of First Order. The first-order spatial derivatives for CFDM6 at the inner nodes are calculated as follows [42]:

$$\varphi z'_{i-1} + z'_i + \varphi z'_{i+1} = \chi\left(\frac{z_{i+2} - z_{i-2}}{4h}\right) + \psi\left(\frac{z_{i+1} - z_{i-1}}{2h}\right). \quad (13)$$

For the optimality of the scheme with higher-order accuracy, consider $\varphi = 1/3$ representing the implicit form of the first-order derivative. The unknown parameters on the other side are calculated by the relation $\chi = (1/3)(4\varphi - 1)$ and $\psi = (2/3)(2 + \varphi)$. By simple calculation, Equation (13) reduces to a sixth-order tridiagonal matrix as a linear system of equations given below with truncation error $(4/7!)h^6 z_i^{(7)}$:

$$z'_{i-1} + 3z'_i + z'_{i+1} = \frac{-z_{i-2} - 28z_{i-1} + 28z_{i+1} + z_{i+2}}{12h}, \quad i = 2, 3, \cdots, N-2. \quad (14)$$

For the value of the derivative at x_0, x_1, x_{N-1}, and x_N, one-sided forward and backward schemes have been implemented, which produce following results:

$$\begin{aligned}
z'_0 + 5z'_1 &= \frac{1}{60h}(-197z_0 - 25z_1 + 300z_2 - 100z_3 + 25z_4 - 3z_5),\\
2z'_0 + 11z'_1 + 2z'_2 &= \frac{1}{12h}(-80z_0 - 35z_1 + 136z_2 - 28z_3 + 8z_4 - z_5),\\
2z'_{N-2} + 11z'_{N-1} + 2z'_N &= \frac{1}{12h}(z_{N-5} - 8z_{N-4} + 28z_{N-3}\\
&\quad - 136z_{N-2} + 35z_{N-1} + 80z_N),\\
5z'_{N-1} + z'_N &= \frac{1}{60h}(3z_{N-5} - 25z_{N-4} + 100z_{N-3}\\
&\quad - 300z_{N-2} + 25z_{N-1} + 197z_N).
\end{aligned} \quad (15)$$

The relations (14) and (15) can be represented in the form of a matrix system as

$$\mathbb{A}z' = \mathbb{B}z, \quad (16)$$

where

$$\mathbb{A}z' = \begin{bmatrix} 1 & 5 & & & & & & & \\ 2 & 11 & 2 & & & & & & \\ & 1 & 3 & 1 & & & & & \\ & & . & . & . & & & & \\ & & & . & . & . & & & \\ & & & & & 1 & 3 & 1 & \\ & & & & & & 2 & 11 & 2 \\ & & & & & & & 5 & 1 \end{bmatrix} \begin{bmatrix} z'_0 \\ z'_1 \\ z'_2 \\ . \\ . \\ z'_{N-2} \\ z'_{N-1} \\ z'_N \end{bmatrix},$$

$$\mathbb{B}z = \frac{1}{h} \begin{bmatrix} -\frac{197}{60} & -\frac{25}{60} & \frac{300}{60} & -\frac{100}{60} & \frac{25}{60} & -\frac{3}{60} & & & \\ -\frac{80}{12} & -\frac{35}{12} & \frac{136}{12} & -\frac{28}{12} & \frac{8}{12} & -\frac{1}{12} & & & \\ -\frac{1}{12} & -\frac{28}{12} & 0 & \frac{28}{12} & \frac{1}{12} & & & & \\ & -\frac{1}{12} & -\frac{28}{12} & 0 & \frac{28}{12} & \frac{1}{12} & & & \\ & & . & . & . & & & & \\ & & & . & . & . & & & \\ & & & -\frac{1}{12} & -\frac{28}{12} & 0 & \frac{28}{12} & \frac{1}{12} & \\ & & & & -\frac{1}{12} & -\frac{28}{12} & 0 & \frac{28}{12} & \frac{1}{12} \\ & & & \frac{1}{12} & -\frac{8}{12} & \frac{28}{12} & -\frac{136}{12} & \frac{35}{12} & \frac{80}{12} \\ & & & \frac{3}{60} & -\frac{25}{60} & \frac{100}{60} & -\frac{300}{60} & \frac{25}{60} & \frac{197}{60} \end{bmatrix} \begin{bmatrix} z_0 \\ z_1 \\ z_2 \\ z_3 \\ . \\ . \\ z_{N-3} \\ z_{N-2} \\ z_{N-1} \\ z_N \end{bmatrix}. \tag{17}$$

2.2. Spatial Derivatives of Second Order. Similarly, the second-order derivative is calculated as

$$\tau z''_{i-1} + z''_i + \tau z''_{i+1} = \sigma\left(\frac{z_{i+2} - 2z_i + z_{i-2}}{4h^2}\right) + \varsigma\left(\frac{z_{i+1} - 2z_i + z_{i-1}}{h^2}\right). \tag{18}$$

For $\tau = 0$, this equation represents the explicit method to calculate the derivative, and for $\tau = 1/10$, it will represent the implicit scheme of the second-order derivative. The unknown constants on the R.H.S. are calculated as $\varsigma = (4/3)(1 - \tau)$ and $\sigma = (1/3)(-1 + 10\tau)$. This reduces Equation (18) to a tridiagonal system as follows:

$$z''_{i-1} + 10z''_i + z''_{i+1} = \frac{12}{h^2}(z_{i+1} - 2z_i + z_{i-1}). \tag{19}$$

For the boundary points, one-sided forward and backward schemes have been implemented, which gives the following results:

$$10z''_0 + z''_1 = \frac{12}{h^2}\left(\frac{115}{36}z_0 - \frac{1555}{144}z_1 + \frac{89}{6}z_2 - \frac{773}{72}z_3 + \frac{151}{36}z_4 - \frac{11}{16}z_5\right),$$

$$z''_{N-1} + 10z''_N = \frac{12}{h^2}\left(\frac{115}{36}z_N - \frac{1555}{144}z_{N-1} + \frac{89}{6}z_{N-2} - \frac{773}{72}z_{N-3} + \frac{151}{36}z_{N-4} - \frac{11}{16}z_{N-5}\right). \tag{20}$$

The second-order derivative can be written in the matrix form as

$$\mathbb{C}z'' = \mathbb{D}z,$$

$$\mathbb{C}z'' = \begin{bmatrix} 10 & 1 & & & & & & & \\ 1 & 10 & 1 & & & & & & \\ & 1 & 10 & 1 & & & & & \\ & & . & . & . & & & & \\ & & & . & . & . & & & \\ & & & & . & . & . & & \\ & & & & & 1 & 10 & 1 & \\ & & & & & & 1 & 10 & 1 \\ & & & & & & & 1 & 10 \end{bmatrix} \begin{bmatrix} z''_0 \\ z''_1 \\ z''_2 \\ . \\ . \\ . \\ z''_{N-2} \\ z''_{N-1} \\ z''_N \end{bmatrix},$$

$$\mathbb{D}z = \frac{12}{h^2} \begin{bmatrix} \frac{115}{36} & \frac{-1555}{144} & \frac{89}{6} & \frac{-773}{72} & \frac{151}{36} & \frac{-11}{16} & & & \\ 1 & -2 & 1 & & & & & & \\ & 1 & -2 & 1 & & & & & \\ & & . & . & . & & & & \\ & & & . & . & . & & & \\ & & & & . & . & . & & \\ & & & & 1 & -2 & 1 & & \\ & & & & & 1 & -2 & 1 & \\ & & \frac{-11}{16} & \frac{151}{36} & \frac{-773}{72} & \frac{89}{6} & \frac{-1555}{144} & \frac{115}{36} \end{bmatrix} \begin{bmatrix} z_0 \\ z_1 \\ z_2 \\ z_3 \\ . \\ z_{N-3} \\ z_{N-2} \\ z_{N-1} \\ z_N \end{bmatrix}. \tag{21}$$

3. Implementation of CFDM6

By substituting the values of first-order and second-order derivatives in Equations (3) and (8), a linear system of equations are obtained for $i = 0, 1, \cdots, N$:

(i) *Model-I*: generalized Burger's-Fisher equation:

$$\frac{\partial z_i}{\partial t} = \mathbb{C}^{-1}\mathbb{D}z_i - \beta z_i^\delta \mathbb{A}^{-1}\mathbb{B}z_i + \gamma z_i\left(1 - z_i^\delta\right) \equiv \mathscr{L}(z_i). \tag{22}$$

(ii) *Model-II*: generalized Burger's-Huxley equation:

$$\frac{\partial z_i}{\partial t} = \mathbb{C}^{-1}\mathbb{D}z_i - \beta z_i^\delta \mathbb{A}^{-1}\mathbb{B}z_i + \gamma z_i\left(1 - z_i^\delta\right)\left(z_i^\delta - \eta\right) \equiv \mathscr{L}(z_i). \tag{23}$$

3.1. SSP-RK43 Scheme. Let

$$\frac{dz_i}{dt} = \mathscr{L}(z_i), \quad i = 0, 1, 2 \cdots, N, \tag{24}$$

where $\mathscr{L}$ represents the nonlinear differential operator as defined above. In order to solve this system of ODE's from the t^j to t^{j+1} time level, SSP-RK43 is applied using the following operations:

$$\begin{aligned} z^{(1)} &= z^j + \frac{\Delta t}{2}\mathscr{L}\left(z^j\right), \\ z^{(2)} &= z^{(1)} + \frac{\Delta t}{2}\mathscr{L}\left(z^{(1)}\right), \\ z^{(3)} &= \frac{2}{3}z^j + \frac{1}{3}z^{(2)} + \frac{\Delta t}{6}\mathscr{L}\left(z^{(2)}\right), \\ z^{j+1} &= z^{(3)} + \frac{\Delta t}{2}\mathscr{L}\left(z^{(3)}\right). \end{aligned} \tag{25}$$

By using the initial condition, $z(x, t)$ at every required time level can be calculated.

4. Convergence Analysis

Convergence of the model is investigated below for the desired Equations (22) and (23).

Theorem 1. *It is an assumption that the given initial value problem $dz/dt = \mathscr{L}(z)$ has a unique solution if $\mathscr{L}(z)$ satisfies the following conditions:*

(1) $\mathscr{L}(z)$ is a real function

(2) $\mathscr{L}(z)$ is well defined and continuous in the domain of $t \in \Phi_t$ and $z \in (-\infty, \infty)$

(3) There exists a constant called the Lipschitz constant κ such that $|\mathscr{L}(z, t, \Delta t) - \mathscr{L}(\dot{z}, t, \Delta t)| \le \kappa|z - \dot{z}|$, where $t \in \Phi_t$ and z and $\dot{z}$ be any two different points

It is clearly seen that $\mathscr{L}(z)$ for the generalized Burger's-Fisher equation and generalized Burger's-Huxley equation is real, well defined, and continuous. Hence, above theorem is satisfied.

Lemma 2. *A single-step method (25) is said to be regular, if the incremental function $\phi(z, t, \Delta t)$ satisfies the following conditions:*

(1) The function is well defined and is continuous in the given time and space domain

(2) For every $t \in \Phi_t$ and $z, \dot{z} \in (-\infty,\infty)$, there exit a constant κ such that

$$|\phi(z, t, \Delta t) - \phi(\dot{z}, t, \Delta t)| \le \kappa|z - \dot{z}|. \tag{26}$$

Lemma 3. *Any single-step method is consistent if $\phi(z, t, 0) = \mathscr{L}(z, t)$.*

Theorem 4. *The consistency is the necessary and sufficient condition for the convergence of a regular single-step method with the order (say) $p \ge 1$.*

Proof. This theorem ensures that the approximate solution converges to the exact solution. For the proof, consider the specific incremental function $\phi(z, t, \Delta t)$. Assume that the given differential equation $z_t \equiv \mathscr{L}z$ has a unique solution $z(t)$ on Φ_t and also $z(t) \in C^{(p+1)}\Phi_t$ for $p \ge 1$. Using Taylor's series expansion about any point t^j,

$$\begin{aligned} z(t) = z\left(t^j\right) &+ \left(t - t^j\right)z'\left(t^j\right) + \frac{1}{2!}\left(t - t^j\right)^2 z''\left(t^j\right) \\ &+ \cdots + \frac{1}{p!}\left(t - t^j\right)^p z^p\left(t^j\right) + \frac{1}{(p+1)!}\left(t - t^j\right)^{p+1} z^{p+1}\left(\xi^j\right), \end{aligned} \tag{27}$$

where $\xi \in (t^j, t)$. Taking $t = t^{j+1}$, one gets

$$z\left(t^{j+1}\right) - z\left(t^j\right) = \Delta t z'\left(t^j\right). \tag{28}$$

Thus, the incremental function is defined as

$$\phi\left(z\left(t^j\right), t^j, \Delta t\right) = (\Delta t)z'\left(t^j\right) + \frac{1}{2!}(\Delta t)^2 z''\left(t^j\right) + \cdots + \frac{1}{p!}(\Delta t)^p z^p\left(t^j\right). \tag{29}$$

It is computed using the approximate value of z^j where the exact value $z(t^j)$ is required. Hence, $z^{j+1} = z^j + \Delta t\phi(z(t^j), t^j, \Delta t)$, $j = 0, 1, 2, \cdots, m-1$. To compute the error using Taylor's series,

$$\begin{aligned} z^{j+1} = z^j &+ \Delta t z'^j + \frac{(\Delta t)^2}{2!}z''^j + \frac{(\Delta t)^3}{3!}z'''^j \\ &+ \cdots + \frac{(\Delta t)^p}{p!}z^{pj} + \frac{(\Delta t)^{p+1}}{(p+1)!}z^{p+1}(\xi)^j. \end{aligned} \tag{30}$$

The approximate value using the SSP-RK43 scheme is

$$\begin{aligned} z^{j+1} = z^j &+ \Delta t\mathscr{L}\left(z^j\right) + \frac{(\Delta t)^2}{2!}\mathscr{L}^2\left(z^j\right) + \frac{(\Delta t)^3}{3!}\mathscr{L}^3\left(z^j\right) \\ &+ \cdots + \frac{(\Delta t)^p}{p!}\mathscr{L}^p\left(z^j\right). \end{aligned} \tag{31}$$

The following relation is obtained:

$$\begin{aligned} \Delta t\phi\left(z\left(t^j\right), t^j, \Delta t\right) = \Delta t z'\left(t^j\right) &+ \frac{(\Delta t)^2}{2!}\mathscr{L}^2\left(z^j\right) + \frac{(\Delta t)^3}{3!}\mathscr{L}^3\left(z^j\right) \\ &+ \cdots + \frac{(\Delta t)^p}{p!}\mathscr{L}^p\left(z^j\right). \end{aligned} \tag{32}$$

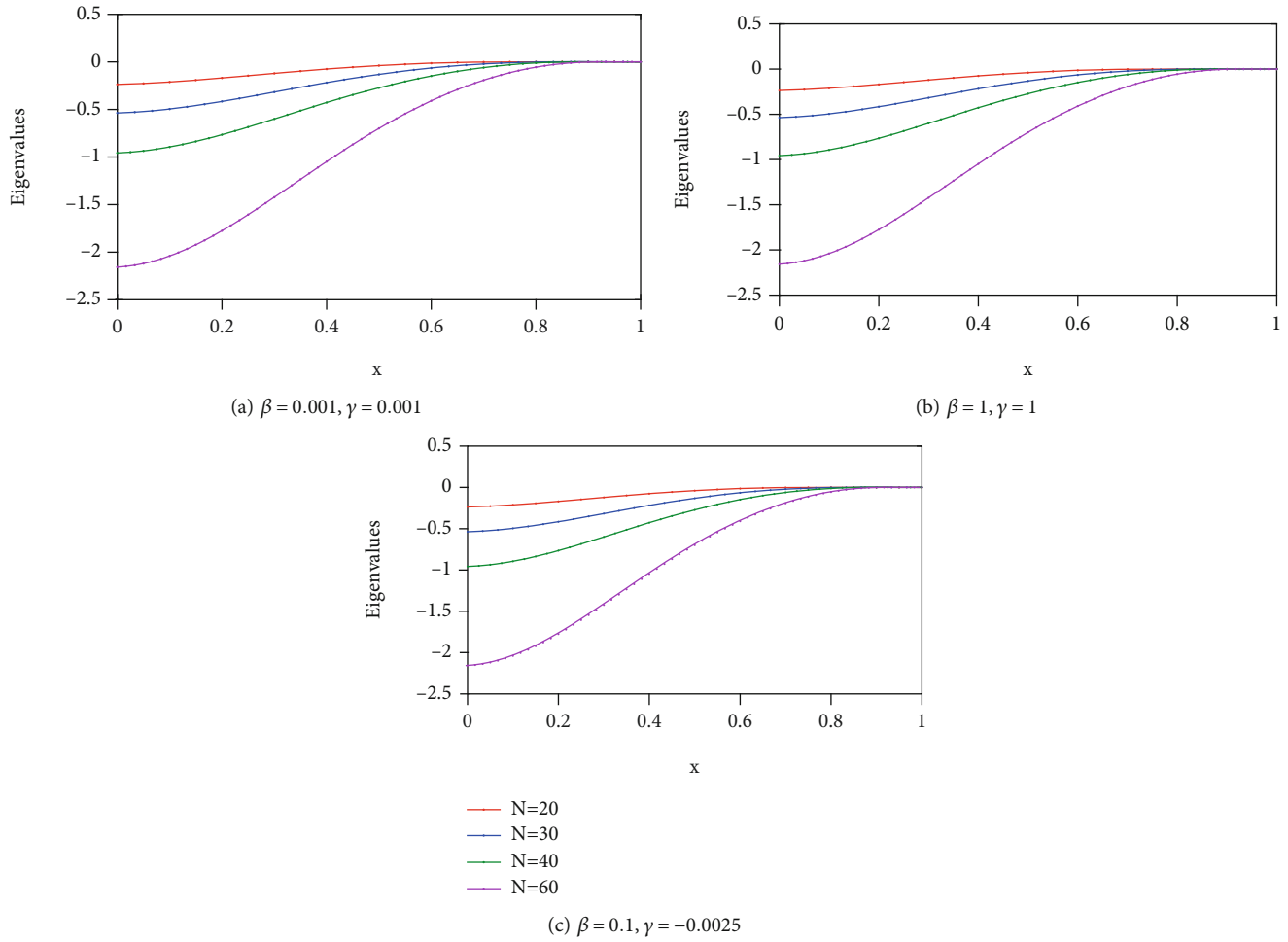

FIGURE 1: Plot of eigenvalues corresponding to gBF equation with $\Delta t = 0.0001$ and $\delta = 8$.

The value of $\Delta t\phi(z^j, t^j, \Delta t)$ is obtained from $\Delta t\phi(z(t^j), t^j, \Delta t)$ by using the exact approximate value of z^j in place of the exact value of $z(t^j)$. According to the SSP-RK43, the approximate value of $z(t^{j+1})$ is obtained as follows:

$$z^{j+1} = z^j + \Delta t\phi\left(z^j, t^j, \Delta t\right) + \frac{(\Delta t)^2}{2!}\phi'\left(z^j, t^j, \Delta t\right) + \frac{(\Delta t)^3}{3!}\phi''\left(z^j, t^j, \Delta t\right) + \cdots. \tag{33}$$

For the above relation, compute the values of $z(t^j), z'(t^j), z''(t^j) \cdots z^p(t^j)$ as follows:

$$\begin{aligned} z'\left(t^j\right) &= \mathscr{L}\left(z\left(t^j\right), t^j\right), \\ z''\left(t^j\right) &= \mathscr{L}_t + \mathscr{L}\mathscr{L}_z, \\ z'''\left(t^j\right) &= \mathscr{L}_{tt} + 2'\mathscr{L}_{tz} + \mathscr{L}^2 L_{zz} + L_z(\mathscr{L}_t + \mathscr{L}\mathscr{L}_z). \\ &\vdots \end{aligned} \tag{34}$$

Thus, from these computed values taking $t = t^j$, the error term is obtained as follows:

$$\frac{\Delta t^{p+1}}{(p+1)!} z^{p+1}\left(\xi^j\right) < \varepsilon. \tag{35}$$

Hence, on simplification,

$$\Delta t^{p+1} z^{p+1}\left(\xi^j\right) < \varepsilon(p+1)!. \tag{36}$$

In other words,

$$\Delta t^{p+1} \mathscr{L}^p\left(\xi^j\right) < \varepsilon(p+1)!. \tag{37}$$

Thus, the given value of p will give the upper bound, and for the computational purpose, the value of $\mathscr{L}^p(\xi^j)$ in Equation (37) is replaced with the max $|\mathscr{L}^p(\xi^j)|$ in the temporal domain Φ_t. The SSP-RK43 as discussed above is rewritten as

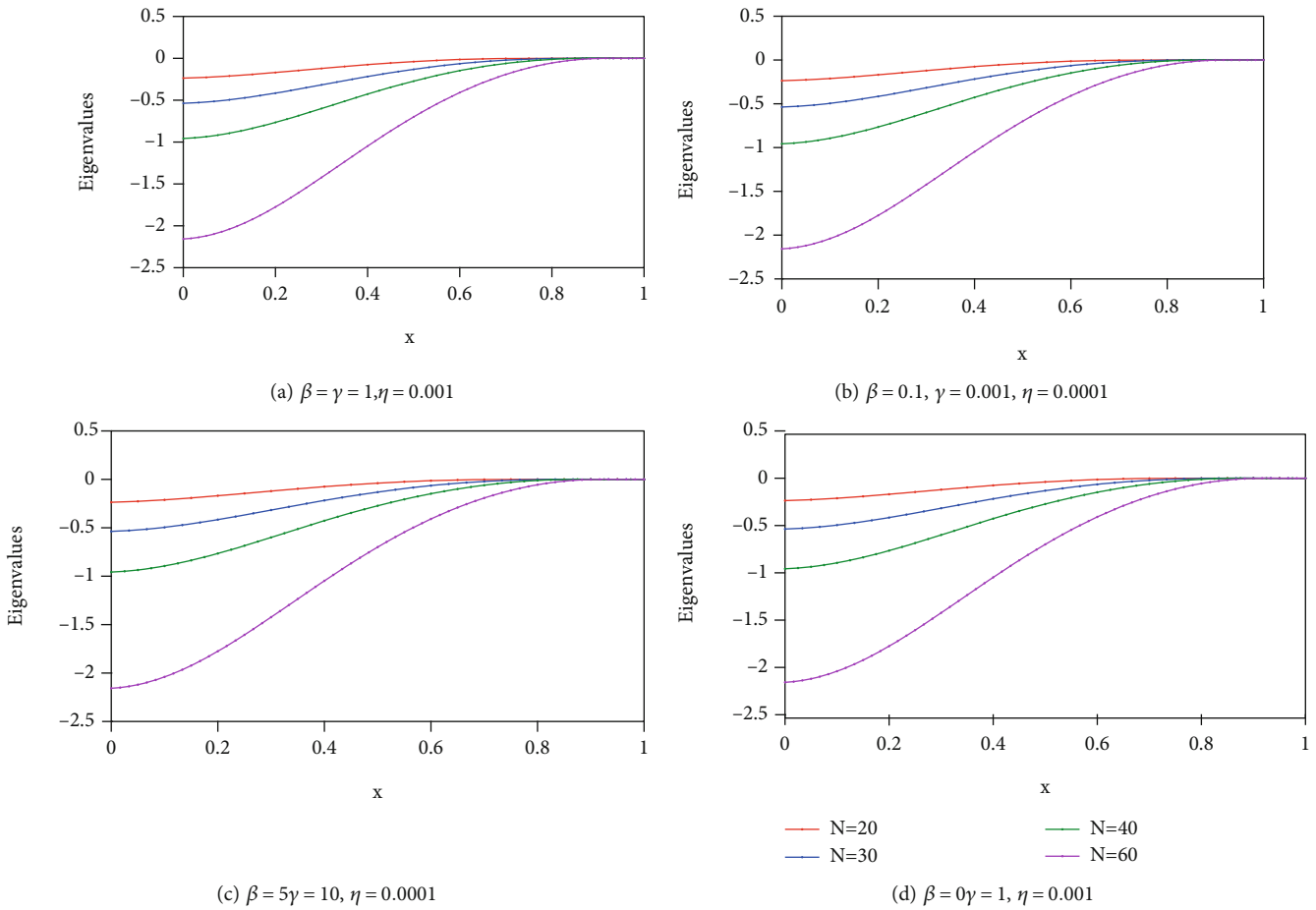

(a) $\beta = \gamma = 1, \eta = 0.001$

(b) $\beta = 0.1$, $\gamma = 0.001$, $\eta = 0.0001$

(c) $\beta = 5\gamma = 10$, $\eta = 0.0001$

(d) $\beta = 0\gamma = 1$, $\eta = 0.001$

Figure 2: Plot of eigenvalues corresponding to gBH equation with $\Delta t = 0.0001$ and $\delta = 8$.

$$
\begin{aligned}
Q_1 &= z^j + \frac{\Delta t}{2}\mathscr{L}\left(z^j, t^j\right),\\
Q_2 &= Q_1 + \frac{\Delta t}{2}\mathscr{L}(Q_1),\\
Q_3 &= \frac{2}{3}z^j + \frac{1}{3}Q_2 + \frac{\Delta t}{6}\mathscr{L}(Q_2),\\
z^{j+1} &= Q_3 + \frac{\Delta t}{2}\mathscr{L}(Q_3).
\end{aligned}
\tag{38}
$$

The iterated value of z^{j+1} can be written as

$$
z^{j+1} = z^j + c_1 Q_1 + c_2 Q_2 + c_3 Q_3. \tag{39}
$$

Using Taylor's series expansion, the incremental function becomes

$$
\phi\left(z^j, t^j, \Delta t\right) = (\Delta t)^{-1}(c_1 Q_1 + c_2 Q_2 + c_3 Q_3). \tag{40}
$$

From the Theorem 1, the proof for convergence is elaborated as follows:

$$
Q_1 - Q_1{}^* = z^j + \frac{\Delta t}{2}\mathscr{L}\left(z^j\right) - z^{j^*} + \frac{\Delta t}{2}\mathscr{L}\left(z^{j^*}\right),
$$

$$
|Q_1 - Q_1{}^*| \le \left|z^j - z^{j^*}\right| + \frac{\Delta t}{2}\left|\mathscr{L}\left(z^j\right) - \mathscr{L}\left(z^{j^*}\right)\right| \le \left(1 + \frac{\Delta t}{2}\kappa\right)\left|z^j - z^{j^*}\right|,
$$

$$
Q_2 - Q_2{}^* = Q_1 + \frac{\Delta t}{2}\mathscr{L}(Q_1) - Q_1{}^* - \frac{\Delta t}{2}\mathscr{L}(Q_1{}^*),
$$

$$
\begin{aligned}
|Q_2 - Q_2{}^*| &\le |Q_1 - Q_1{}^*| + \frac{\Delta t}{2}|\mathscr{L}(Q_1) - \mathscr{L}(Q_1{}^*)|\\
&= |Q_1 - Q_1{}^*| + \frac{\Delta t}{2}\left|\mathscr{L}\left(z^j + \frac{\Delta t}{2}\mathscr{L}\left(z^j\right)\right) - \mathscr{L}\left(z^{j^*} + \frac{\Delta t}{2}\mathscr{L}\left(z^{j^*}\right)\right)\right|\\
&\le \left(1 + \frac{\Delta t}{2}\kappa\right)\left|z^j - z^{j^*}\right|\\
&\quad + \frac{\Delta t}{2}\left[\mathscr{L}\left(z^j\right) + \frac{\Delta t}{2}\mathscr{L}\left(z^j\right)\mathscr{L}_z\left(z^j\right) + \left(\frac{\Delta t}{2}\mathscr{L}\left(z^j\right)\right)^2\mathscr{L}_{zz}\left(z^j\right)\right.\\
&\quad \left. + \cdots - \mathscr{L}\left(z^{j^*}\right) - \frac{\Delta t}{2}\mathscr{L}\left(z^{j^*}\right)\mathscr{L}_z\left(z^{j^*}\right) - \left(\frac{\Delta t}{2}\mathscr{L}\left(z^{j^*}\right)\right)^2\mathscr{L}_{zz}\left(z^{j^*}\right)\right]\\
&\le \left(1 + \frac{\Delta t}{2}\kappa\right)\left|z^j - z^{j^*}\right| + \frac{\Delta t}{2}\left[\mathscr{L}\left(z^j\right) - \mathscr{L}\left(z^{j^*}\right)\right]\\
&\quad + \left(\frac{\Delta t}{2}\right)^2\left|\mathscr{L}\left(z^j\right)\mathscr{L}_z\left(z^j\right) - \mathscr{L}\left(z^{j^*}\right)\mathscr{L}_z\left(z^{j^*}\right)\right|\\
&\quad + \left(\frac{\Delta t}{2}\right)^3\left|\left(\mathscr{L}\left(z^j\right)\right)^2\mathscr{L}_{zz}\left(z^j\right) - \left(\mathscr{L}\left(z^{j^*}\right)\right)^2\mathscr{L}_{zz}\left(z^{j^*}\right)\right| + \cdots\\
&\le (1 + \Delta t\kappa)\left|z^j - z^{j^*}\right| + \left(\frac{\Delta t}{2}\right)^2\kappa^2\left|z^j - z^{j^*}\right|\\
&= \left[1 + \Delta t\kappa + \left(\frac{\Delta t}{2}\kappa\right)^2\right]\left|z^j - z^{j^*}\right|,
\end{aligned}
$$

Table 1: Comparison of absolute error of Example 1 with $\beta = 0.001$, $\gamma = 0.001$, $h = 0.1$, and $\Delta t = 0.0001$.

t	x	$\delta = 1$				$\delta = 4$		
		CFDM6	ADM [23]	CFDM [6]	ETDM [14]	CFDM6	CFDM [6]	ETDM [14]
0.001	0.1	2.2204E-16	1.94E-06	1.01E-07	1.15E-08	1.1102E-16	1.75E-08	7.71E-09
	0.5	1.1102E-16	1.94E-06	1.04E-07	3.07E-13	1.1102E-16	1.75E-08	2.07E-13
	0.9	4.4409E-17	1.94E-06	1.01E-07	1.15E-08	3.3307E-16	1.75E-08	7.71E-09
0.010	0.1	5.8818E-16	1.94E-05	7.53E-07	6.02E-08	4.4409E-15	1.27E-06	4.05E-08
	0.5	1.6653E-16	1.94E-05	1.04E-06	8.96E-13	4.2188E-15	1.75E-06	5.56E-13
	0.9	1.1102E-15	1.94E-05	7.53E-07	6.02E-08	4.8850E-15	1.27E-06	4.05E-08
100	0.1	2.2204E-16	—	7.53E-07	1.01E-07	5.5511E-16	—	5.73E-08
	0.5	1.1102E-15	—	1.04E-06	1.50E-11	2.7756E-15	—	3.51E-12
	0.9	1.1102E-16	—	7.53E-07	1.01E-07	1.3323E-15	—	5.73E-08

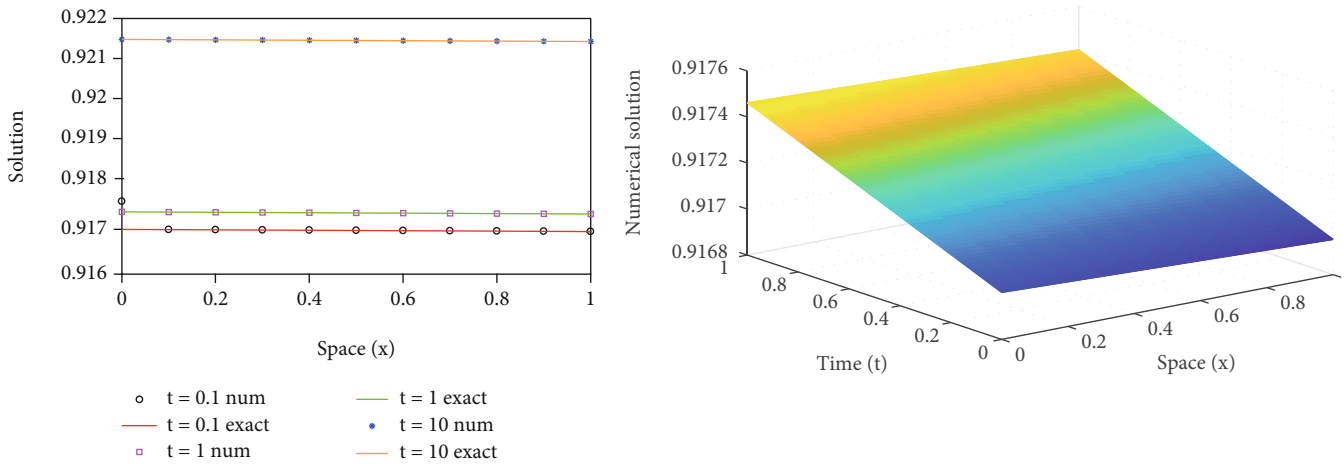

(a) Comparison of numerical and exact solution

(b) Surface plot of numerical solution

Figure 3: Graphical representation of solutions corresponding to Example 1 with $N = 10$ and $\Delta t = 0.001$.

$$Q_3 - Q_3^* = \frac{2}{3}z^j + \frac{Q_2}{3} + \frac{\Delta t}{2}\mathscr{L}(Q_2) - \frac{2}{3}z^{j*} - \frac{Q_2^*}{3} - \frac{\Delta t}{2}\mathscr{L}(Q_2^*)),$$

$$\begin{aligned}
|Q_3 - Q_3^*| &= \frac{2}{3}\left|z^j - z^{j*}\right| + \frac{1}{3}|Q_2 - Q_2^*| + \frac{\Delta t}{2}|\mathscr{L}(Q_2) - \mathscr{L}(Q_2^*)| \\
&\le \frac{2}{3}\left|z^j - z^{j*}\right| + \frac{1}{3}|Q_2 - Q_2^*| \\
&\quad + \left|\frac{\Delta t}{2}\left[\mathscr{L}\left(Q_1 + \frac{\Delta t}{2}\mathscr{L}(Q_1)\right) - \mathscr{L}\left(Q_1^* + \frac{\Delta t}{2}\mathscr{L}(Q_1^*)\right)\right]\right| \\
&\le \frac{2}{3}\left|z^j - z^{j*}\right| + \frac{1}{3}|Q_2 - Q_2^*| \\
&\quad + \frac{\Delta t}{2}\left[\left|\left(\mathscr{L}(z^j) - \mathscr{L}\left(z^{j*}\right)\right)\right| + \frac{\Delta t}{2}\left|\mathscr{L}(z^j)\mathscr{L}_z(z^j) - \mathscr{L}_z\left(z^{j*}\right)\right|\right] \\
&\le \left|z^j - z^{j*}\right| + \frac{\Delta t}{2}\kappa\left(2 + \frac{\Delta t}{2}\kappa\right)\left|z^j - z^{j*}\right| \\
&\quad + \frac{\Delta t}{2}\kappa\left|z^j - z^{j*}\right| + \left(\frac{\Delta t}{2}\kappa\right)^2\left|z^j - z^{j*}\right| \\
&\le \left|z^j - z^{j*}\right| + \left[\frac{3\Delta t}{2}\kappa + 2\left(\frac{\Delta t}{2}\kappa\right)^2\right]\left|z^j - z^{j*}\right|,
\end{aligned} \tag{41}$$

As discussed by [47], the free parameters are largely taken according to the range of absolute stability. The other possibility is minimizing the sum of the absolute value of the coefficients of the truncation error. Thus $\mathscr{L}_z < \kappa$ and $\mathscr{L}_{zz} < \kappa^2/M$ where M is the upper bound of convergence. For the incremental function,

$$\begin{aligned}
&\left|\phi(z^j, t^j, \Delta t) - \phi\left(z^{j*}, t^j, \Delta t\right)\right| \\
&= (\Delta t)^{-1}|c_1Q_1 + c_2Q_2 + c_3Q_3 - c_1Q_1^* - c_2Q_2^* - c_3Q_3^*| \\
&= (\Delta t)^{-1}(c_1|Q_1 - Q_1^*| + c_2|Q_2 - Q_2^*| + c_3|Q_3 - Q_3^*|) \\
&\le (\Delta t)^{-1}\left[c_1\left(1 + \frac{\Delta t}{2}\kappa\right)\left|z^j - z^{j*}\right| + c_2\left(\left[1 + \Delta t\kappa + \left(\frac{\Delta t}{2}\kappa\right)^2\right]\left|z^j - z^{j*}\right|\right)\right. \\
&\quad \left. + c_3\left(\left|z^j - z^{j*}\right| + \left[\frac{3\Delta t}{2}\kappa + 2\left(\frac{\Delta t}{2}\kappa\right)^2\right]\left|z^j - z^{j*}\right|\right)\right] \\
&\le \left[(\Delta t)^{-1}(c_1 + c_2 + c_3) + [c_1 + 2c_2 + c_3]\frac{\kappa}{2} + [c_2 + 2c_3]\Delta t\left(\frac{\kappa}{2}\right)^2\right]\left|z^j - z^{j*}\right|.
\end{aligned} \tag{42}$$

The backward substitution of (38) and its comparison with general Taylor's series [47] gives $c_1 = 1/4$, $c_2 = 1/2$, $c_3 = 1/4$. Hence, these values generate the inequality as

$$\left|\phi(z^j, t^j, \Delta t) - \phi\left(z^{j*}, t^j, \Delta t\right)\right| \le \kappa\left(1 + \frac{1}{2}\Delta t\kappa + \frac{1}{6}(\Delta t\kappa)^2\right)\left|z^j - z^{j*}\right|. \tag{43}$$

Table 2: Comparison of absolute error of Example 2 with $\beta = 1$, $\gamma = 1$, $h = 0.1$, and $\Delta t = 0.0001$.

t	x	$\delta = 2$				$\delta = 8$		
		CFDM6	ADM [23]	CFDM [6]	ETDM [14]	CFDM6	CFDM [6]	ETDM [14]
0.0005	0.1	2.2547*E*-11	1.40*E*-03	7.62*E*-05	5.67*E*-06	4.8073*E*-11	1.02*E*-04	2.44*E*-06
	0.5	8.4710*E*-14	1.35*E*-03	9.14*E*-05	5.75*E*-09	1.6162*E*-12	1.37*E*-04	1.82*E*-10
	0.9	1.8019*E*-11	1.28*E*-03	1.02*E*-04	5.95*E*-06	6.3383*E*-13	1.69*E*-04	3.15*E*-06
0.0010	0.1	4.3846*E*-11	2.80*E*-03	1.50*E*-04	1.08*E*-05	9.3434*E*-11	2.00*E*-04	4.65*E*-06
	0.5	1.8086*E*-13	2.69*E*-03	1.83*E*-04	1.15*E*-08	3.2596*E*-12	2.74*E*-04	4.02*E*-10
	0.9	3.5862*E*-12	2.55*E*-03	2.00*E*-04	1.14*E*-05	1.6023*E*-12	3.31*E*-04	6.00*E*-06

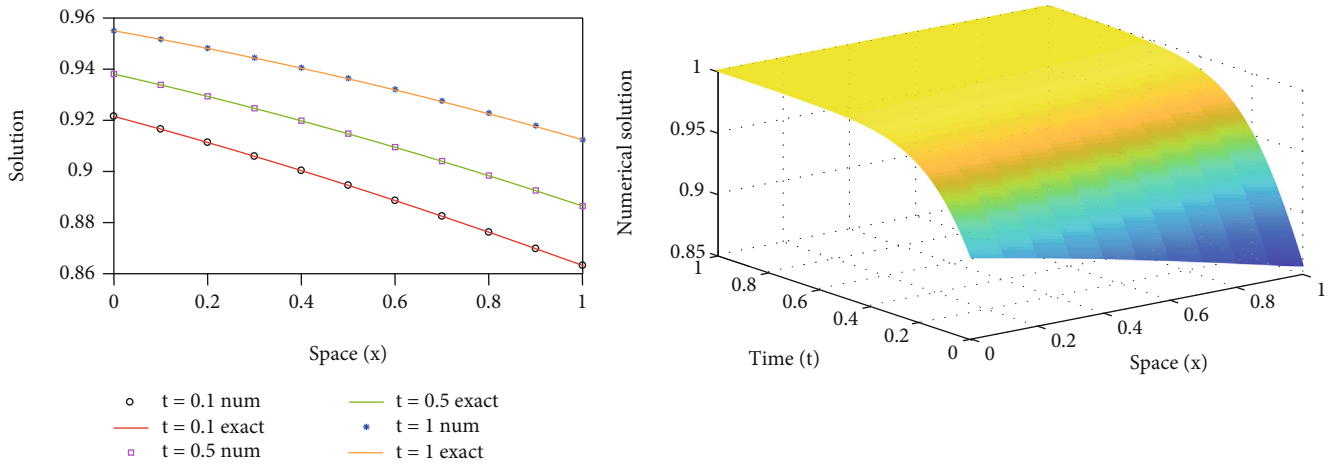

(a) Comparison of numerical and exact solution

(b) Surface plot of numerical solution

Figure 4: Graphical representation of solutions corresponding to Example 2 with $N = 10$ and $\Delta t = 0.001$.

It is observed that $|\phi(z^j, t^j, \Delta t)|$ satisfies the Lipschitz condition in z^j and is a continuous function in Δt. Thus, it is concluded that SSP-RK43 is convergent. □

5. Stability Analysis

The stability analysis of both the models is discussed below by taking nonlinearity coefficient $z = m$ (say), where $m = \max z$, in the entire process to handle the nonlinear term in Equations (22) and (23). The eigenvalue-based technique [45] is followed to establish the stability of the system.

(1) *Model-I*: generalized Burger's-Fisher equation:

$$\frac{\partial z}{\partial t} = \mathbb{C}^{-1}\mathbb{D}z_i - \beta m^{\delta}\mathbb{A}^{-1}\mathbb{B}z_i + \gamma\left(1 - m^{\delta}\right)z_i,$$
$$z_t = \left(\mathbb{C}^{-1}\mathbb{D} - \left(\beta m^{\delta}\mathbb{A}^{-1}\mathbb{B} + \gamma\left(1 - m^{\delta}\right)\right)I\right)z_i \equiv \mathfrak{T}z_i. \tag{44}$$

(2) *Model-II*: generalized Burger's-Huxley equation:

$$\frac{\partial z_i}{\partial t} = \mathbb{C}^{-1}\mathbb{D}z_i - \beta m^{\delta}\mathbb{A}^{-1}\mathbb{B}z_i + \gamma\left(1 - m^{\delta}\right)\left(m^{\delta} - \eta\right)z_i, \tag{45}$$

$$z_t = \left(\mathbb{C}^{-1}\mathbb{D} - \left(\beta m^{\delta}\mathbb{A}^{-1}\mathbb{B}z_i + \gamma\left(1 - m^{\delta}\right)\left(m^{\delta} - \eta\right)\right)I\right)z_i \equiv \mathfrak{T}z_i, \frac{dz}{dt} = \mathfrak{T}z. \tag{46}$$

The matrix $\mathfrak{T}$ is constant for both the Model-I and Model-II with the assumption that it has distinct or possibly complex eigenvalues with a negative real part. Using the given initial condition for the analytic solution, the relation becomes

$$z(t) = \exp(\mathfrak{T}t)z^0, \tag{47}$$

whereas on expanding the exponent as a matrix function where I is the identity matrix,

$$\exp(\mathfrak{T}t) = I + \mathfrak{T}t + \frac{(\mathfrak{T}t)^2}{2!} + \frac{(\mathfrak{T}t)^3}{3!} + \cdots. \tag{48}$$

For Model-I and Model-II, consider the transformation matrix P such that $P^{-1}\mathfrak{T}P = \mathscr{D}$ where $\mathscr{D}$ is the diagonal matrix; thus, the relation becomes

$$P^{-1}\exp(\mathfrak{T}t)P = \exp(\mathscr{D}t), \tag{49}$$

Table 3: Comparison of absolute error of Example 3 with $\beta = 0.1$, $\gamma = -0.0025$, $h = 0.1$, and $\Delta t = 0.0001$.

t	x	$\delta = 2$			$\delta = 4$			$\delta = 8$		
		CFDM6	CFDM [6]	ETDM [14]	CFDM6	CFDM [6]	ETDM [14]	CFDM6	CFDM [6]	ETDM [14]
0.1	0.1	6.661E-16	1.21E-05	9.47E-06	2.220E-16	1.34E-05	6.76E-06	1.110E-15	1.47E-05	4.09E-06
	0.5	6.661E-16	2.90E-05	2.74E-08	5.551E-16	3.49E-05	1.03E-08	6.661E-16	3.83E-05	1.84E-08
	0.9	2.220E-16	1.54E-05	9.57E-06	7.772E-16	1.39E-05	6.92E-08	3.331E-16	1.53E-05	4.24E-06
0.5	0.1	1.341E-16	1.67E-05	9.58E-06	6.661E-16	2.00E-05	6.83E-06	4.441E-16	2.20E-05	4.14E-06
	0.5	1.887E-15	4.69E-05	5.18E-08	2.331E-15	5.64E-05	1.93E-08	6.661E-16	6.22E-05	3.47E-08
	0.9	4.441E-16	1.71E-05	9.66E-06	1.665E-15	2.07E-05	7.01E-06	1.332E-15	2.28E-05	4.30E-06
2.0	0.1	5.551E-16	—	9.59E-06	1.221E-15	—	6.86E-06	1.221E-15	—	4.20E-06
	0.5	3.331E-15	—	5.26E-08	1.776E-15	—	1.89E-08	3.997E-15	—	3.45E-08
	0.9	6.661E-16	—	9.67E-06	7.772E-16	—	7.04E-06	3.331E-16	—	4.35E-06

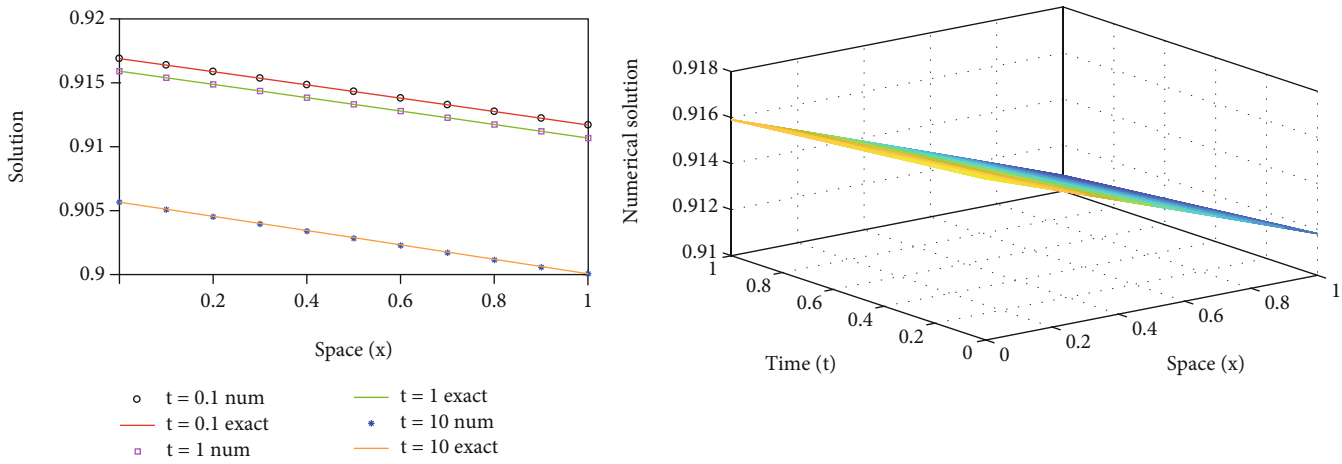

(a) Comparison of numerical and exact solution

(b) Surface plot of numerical solution

Figure 5: Graphical representation of solutions corresponding to Example 3 with $N = 10$ and $\Delta t = 0.001$.

Table 4: Comparison of absolute error of Example 4 with $\beta = 1$, $\gamma = 1$, $\eta = 0.001$, $\delta = 2$, $h = 0.1$, and $\Delta t = 0.0001$.

Method	$t = 0.1$			$t = 1$		
	$x = 0.1$	$x = 0.5$	$x = 0.9$	$x = 0.1$	$x = 0.5$	$x = 0.9$
CFDM6 ($\Delta t = 0.1$)	6.4123E-08	6.4126E-08	6.4129E-08	6.4099E-07	6.4102E-07	6.4105E-07
EFD [49]	2.0510E-06	5.2339E-06	2.0511E-06	3.0562E-06	8.4901E-06	3.0564E-06
HSCM [50]	5.1820E-07	1.3220E-06	5.1820E-07	7.7340E-07	2.1480E-06	7.7340E-07
UAHT [37]	2.8510E-07	7.8223E-07	2.8507E-07	3.0616E-07	8.5042E-07	3.0614E-07
UAH [37]	5.2629E-07	1.3423E-06	5.2620E-07	7.8705E-07	2.1860E-06	7.8690E-07
UAT [37]	5.3131E-07	1.3585E-06	5.3121E-07	7.8706E-07	2.1861E-06	7.8691E-07

Table 5: Comparison of L_∞ error norm of Example 4 with $\beta = 1$, $\gamma = 1$, $\eta = 0.001$, $h = 0.1$, and $\Delta t = 0.001$.

Method	$t = 0.2$			$t = 1$		
	$\delta = 1$	$\delta = 4$	$\delta = 8$	$\delta = 1$	$\delta = 4$	$\delta = 8$
CFDM6 ($\Delta t = 0.1$)	7.4965E-08	1.3207E-07	1.3587E-07	3.7494E-07	6.6011E-07	6.7896E-07
MCSCM [51]	3.7487E-08	1.2271E-05	3.3191E-05	4.2940E-08	1.4046E-05	3.7949E-05
MGT [52]	4.0305E-08	1.3193E-05	3.5687E-05	4.6849E-08	1.5325E-05	4.1407E-05
UAHT [37]	1.8104E-08	5.9274E-06	1.6034E-05	1.8219E-08	5.9602E-06	1.6102E-05
UAH [37]	4.0069E-08	1.3118E-05	3.5485E-05	4.6833E-08	1.5321E-05	4.1400E-05
UAT [37]	4.0326E-08	1.3202E-05	3.5712E-05	4.6834E-08	1.5322E-05	4.1400E-05

Table 6: Comparison of error norms of Example 4 with $\beta = 1$, $\gamma = 1$, $\eta = 0.001$, $\delta = 2$, $h = 0.1$, and $\Delta t = 0.01$.

Method	Error (time)	$t = 0.05$	$t = 0.1$	$t = 1$	$t = 5$
CFDM6	L_∞	3.2065E-08	6.4129E-08	6.4105E-07	3.1999E-06
	L_2	3.0418E-08	6.0835E-08	6.0812E-07	3.0355E-06
UAHT [37]	L_∞	6.0735E-07	7.8321E-07	8.5042E-07	8.4946E-07
	L_2	4.4929E-07	5.7352E-07	6.2103E-07	6.2033E-07
UAH [37]	L_∞	8.0770E-07	1.3430E-06	2.1860E-06	2.1837E-06
	L_2	6.2288E-07	1.0009E-06	1.5964E-06	1.5947E-06
UAT [37]	L_∞	8.2028E-07	1.3587E-06	2.1861E-06	2.1837E-06
	L_2	6.3230E-07	1.0124E-06	1.5964E-06	1.5947E-06

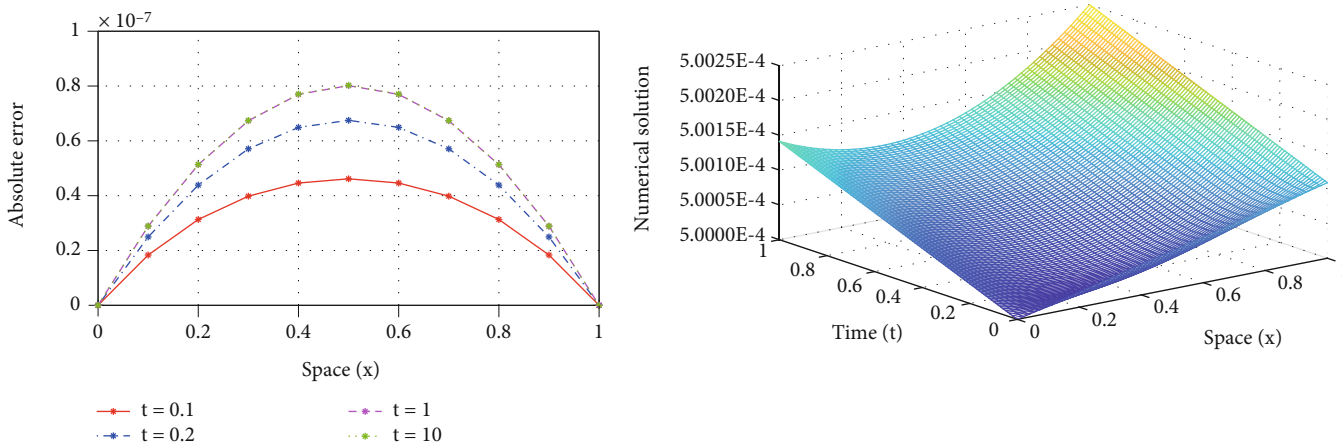

(a) Absolute error at different time levels

(b) Surface plot of numerical solution

Figure 6: Error and solution profile of Example 4 with $N = 50$ and $\Delta t = 0.01$.

where

$$\mathscr{D} = \begin{bmatrix} \eta_1 & & & & & \\ & \eta_2 & & & & \\ & & \eta & & & \\ & & & \ddots & & \\ & & & & \eta_{n-1} & \\ & & & & & \eta_n \end{bmatrix}. \quad (50)$$

Taking $P^{-1}z = v$ in Equation (46), the differential equation becomes

$$\frac{dv}{dt} = \mathscr{D}v. \quad (51)$$

Similarly, as discussed above, the solution of Equation (52) is $v = \exp(\mathscr{D}t)v^0$, and the recursive relation is

$$v^{j+1} = E(\mathscr{D}\Delta t)v^j. \quad (52)$$

In this diagonal matrix, $E(\mathscr{D}\Delta t)$ is an approximate matrix of $\exp(\mathscr{D}\Delta t)$. The diagonal elements of the approximated matrix are $E^j(\eta^j\Delta t)$. Implementing Equation (25) on the scalar Equation (44),

$$z' = \eta^j z. \quad (53)$$

Thus, the method discussed in Equation (25) is absolutely stable if

$$\left|E^j\left(\eta^j\Delta t\right)\right| < 1, \quad (54)$$

where $\mathrm{Re}(\eta) < 0$. The stability of the system exclusively depends on the eigenvalues of the coefficient matrix $\mathfrak{T}$ of the form $\sum_{m=0}^{4}(\mathfrak{T}\Delta t)^m/m!$ which should satisfy Equation (54). The necessary conditions that eigenvalues of $\mathfrak{T}$ should satisfy are given below [47]:

Table 7: Comparison of absolute error of Example 5 with $\beta = 0.1$, $\gamma = 0.001$, $\eta = 0.0001$, $\delta = 2$, $h = 0.1$, and $\Delta t = 0.0001$.

Method	$t = 0.5$			$t = 0.8$		
	$x = 0.1$	$x = 0.5$	$x = 0.9$	$x = 0.1$	$x = 0.5$	$x = 0.9$
CFDM6 ($\Delta t = 0.1$)	2.7448*E*-12	2.7405*E*-12	2.7442*E*-12	4.3917*E*-12	4.3848*E*-12	4.3908*E*-12
EFD [49]	4.3493*E*-11	1.2069*E*-10	4.3494*E*-11	4.3758*E*-11	1.2154*E*-10	4.3759*E*-11
HSCM [50]	2.1847*E*-11	6.0620*E*-11	2.1840*E*-11	2.1980*E*-11	6.1050*E*-11	2.1980*E*-11
UAHT [37]	7.3920*E*-12	2.0534*E*-11	7.3920*E*-12	7.3920*E*-12	2.0534*E*-11	7.3920*E*-12
UAH [37]	1.8881*E*-11	5.2390*E*-11	1.8881*E*-11	1.8998*E*-11	5.2769*E*-11	1.8998*E*-11
UAT [37]	1.8892*E*-11	5.2427*E*-11	1.8892*E*-11	1.8999*E*-11	5.2772*E*-11	1.8999*E*-11

Table 8: Comparison of L_∞ error norm of Example 5 with $\beta = 0.1$, $\gamma = 0.001$, $\eta = 0.0001$, $h = 0.1$, and $\Delta t = 0.001$ for different values of δ.

Method	$t = 0.2$			$t = 1$		
	$\delta = 1$	$\delta = 4$	$\delta = 8$	$\delta = 1$	$\delta = 4$	$\delta = 8$
CFDM6 ($\Delta t = 0.1$)	5.7337*E*-13	1.1345*E*-12	1.1825*E*-12	2.8669*E*-12	5.6727*E*-12	5.9123*E*-12
MCSCM [51]	3.0271*E*-13	5.6344*E*-10	2.0904*E*-09	3.4889*E*-13	6.4937*E*-10	2.4085*E*-09
MGT [52]	3.0804*E*-13	5.7325*E*-10	2.1267*E*-09	3.5806*E*-13	6.6634*E*-10	2.4720*E*-09
UAHT [37]	1.3929*E*-13	2.5756*E*-10	9.5551*E*-10	1.4017*E*-13	2.5918*E*-10	9.6154*E*-10
UAH [37]	3.0631*E*-13	5.7006*E*-10	2.1148*E*-09	3.5847*E*-13	6.6629*E*-10	2.4718*E*-09
UAT [37]	3.0790*E*-13	5.7372*E*-10	2.1284*E*-09	3.5746*E*-13	6.6630*E*-10	2.4719*E*-09

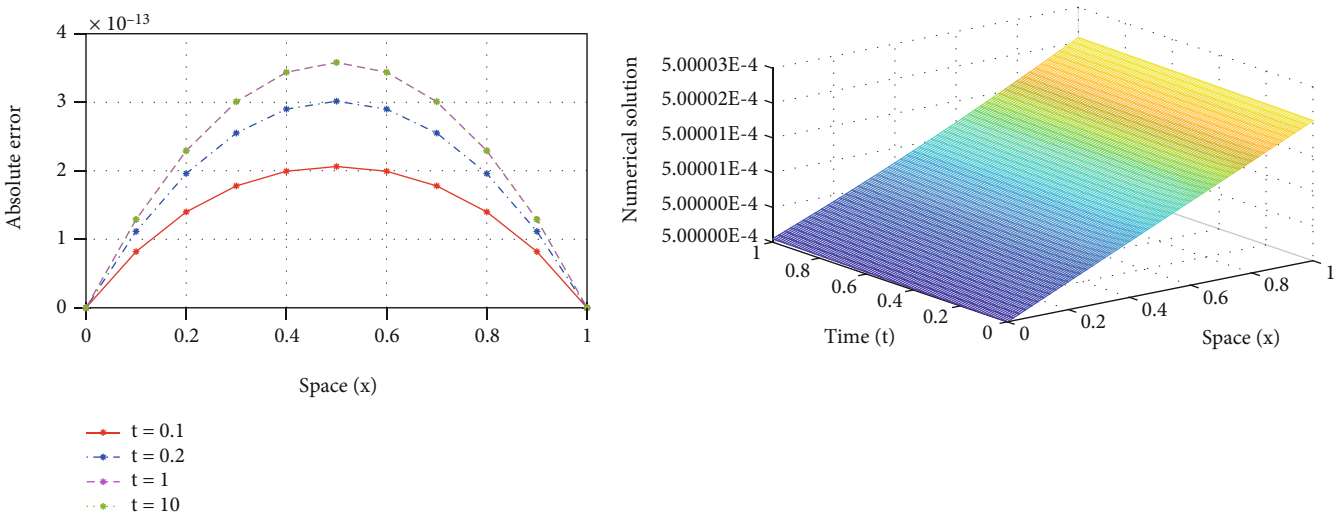

(a) Absolute error at different time levels

(b) Surface plot of numerical solution

Figure 7: Error and solution profile of Example 5 with $N = 50$ and $\Delta t = 0.01$.

(i) For real η^j::$-2.78 < \Delta t\eta^j < 0$

(ii) For pure imaginary η^j : $-2\sqrt{2} < \Delta t\eta^j < 2\sqrt{2}$

(iii) For complex η^j : $\Delta t\eta^j$ should lie in the region as given by [48]

For different values of parameters, eigenvalues corresponding to gBF and gBH equations are given in Figures 1 and 2, respectively. It can be clearly observed that the eigenvalues of all the considered problems satisfy the above defined conditions; therefore, the proposed technique is unconditionally stable.

6. Numerical Experiments

The accuracy of compact finite difference scheme is measured using the L_2 and L_∞ error norms, which are defined as follows:

$$L_\infty = \max_{0 \le i \le N} |z_i - Z_i|, L_2 = \sqrt{h \sum_{i=0}^{N} (z_i - Z_i)^2}, \quad (55)$$

Table 9: Comparison of absolute error of Example 6 with $\beta = 5$, $\gamma = 10$, $\eta = 0.0001$, $\delta = 2$, $h = 0.1$, and $\Delta t = 0.0001$.

t	x	CFDM6 ($\Delta t = 0.1$)	EFD [49]	HSCM [50]	UAHT [37]
0.2	0.1	1.2065*E*-08	6.58058*E*-07	1.971*E*-07	8.69755*E*-08
	0.5	1.2065*E*-08	1.78564*E*-06	5.350*E*-07	2.41380*E*-07
	0.9	1.2065*E*-08	6.58087*E*-07	1.971*E*-07	8.69729*E*-08
0.5	0.1	3.0158*E*-08	7.45354*E*-07	2.233*E*-07	8.74403*E*-08
	0.5	3.0158*E*-08	2.06834*E*-06	6.198*E*-07	2.42887*E*-07
	0.9	3.0159*E*-08	7.45392*E*-07	2.233*E*-07	8.74376*E*-08
0.8	0.1	4.8246*E*-08	7.49483*E*-07	2.247*E*-07	8.74351*E*-08
	0.5	4.8247*E*-08	2.08190*E*-06	6.242*E*-07	2.42873*E*-07
	0.9	4.8247*E*-08	7.49521*E*-07	2.247*E*-07	8.74324*E*-08

Table 10: Comparison of absolute error of Example 6 with $\beta = 5$, $\gamma = 10$, $\eta = 0.00001$, $\delta = 2$, $h = 0.1$, and $\Delta t = 0.0001$.

t	x	CFDM6 ($\Delta t = 0.1$)	EFD [49]	HSCM [50]	UAHT [37]
0.2	0.1	1.2066*E*-10	2.08154*E*-08	6.235*E*-09	2.75063*E*-09
	0.5	1.2066*E*-10	5.64806*E*-08	1.692*E*-08	7.63381*E*-09
	0.9	1.2066*E*-10	2.08155*E*-08	6.235*E*-09	2.75062*E*-09
0.5	0.1	3.0164*E*-10	2.35874*E*-08	7.065*E*-09	2.76548*E*-09
	0.5	3.0164*E*-10	6.54514*E*-08	1.960*E*-08	7.68188*E*-09
	0.9	3.0164*E*-10	2.35875*E*-08	7.065*E*-09	2.76547*E*-09
0.8	0.1	4.8262*E*-10	2.37299*E*-08	7.108*E*-09	2.76547*E*-09
	0.5	4.8262*E*-10	6.59132*E*-08	1.974*E*-08	7.68186*E*-09
	0.9	4.8262*E*-10	2.37300*E*-08	7.108*E*-09	2.76546*E*-09

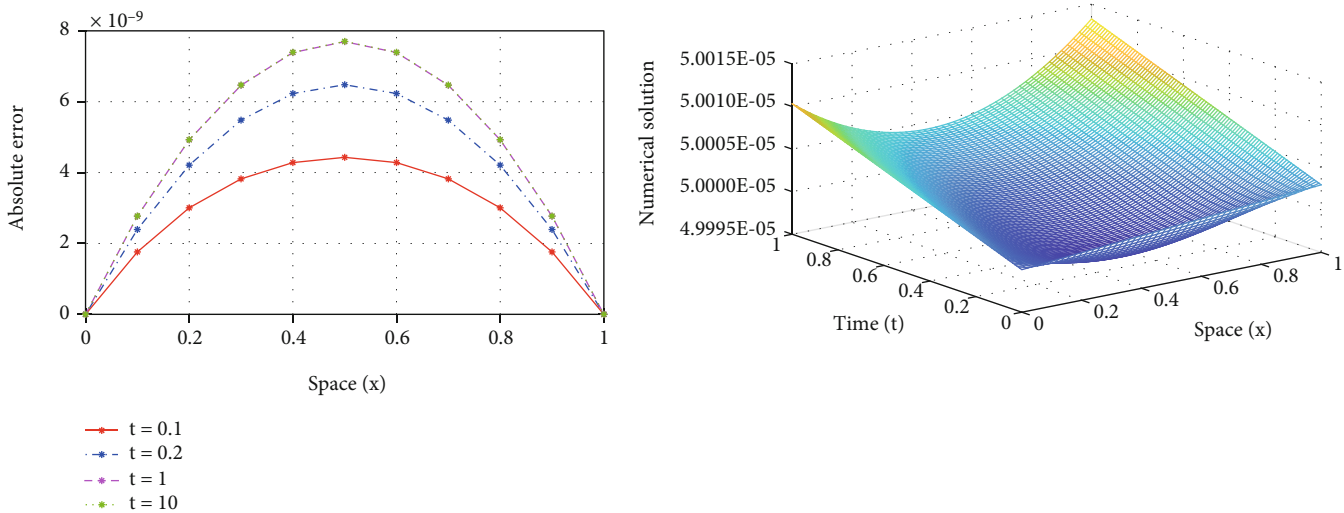

(a) Absolute error at different time levels

(b) Surface plot of numerical solution

Figure 8: Error and solution profile of Example 6 with $N = 50$ and $\Delta t = 0.01$.

where z_i and Z_i represent the exact and numerical solutions, respectively, at the node point x_i for some fixed time.

Example 1. Consider gBF Equation (3) with the parameters $\beta = 0.001$ and $\gamma = 0.001$ for the initial condition as Equation (4) and the boundary conditions as (5) and (6). The exact solution is given by Equation (7). Table 1 gives a comparison of the absolute error for fixed spatial step size $h = 0.1$ and temporal step size $\Delta t = 0.0001$. Absolute error is calculated at time levels $t = 0.001, 0.010, 100$ with $\delta = 1$ and $\delta = 4$. The results are found to be more accurate in comparison to the Adomian decomposition method [23], compact FDM [25],

Table 11: Comparison of absolute error of Example 7 with $\beta = 0$, $\gamma = 1$, $\eta = 0.001$, $\delta = 2$, $h = 0.1$, and $\Delta t = 0.0001$.

t	x	CFDM6	ADM [23]	FDS4 [29]	GCG [30]	MCQDQM [31]
	0.1	3.7491*E*-08	5.5890*E*-07	1.1176*E*-06	4.8110*E*-07	4.4924*E*-07
0.05	0.5	3.7493*E*-08	5.5884*E*-07	1.1175*E*-06	3.9966*E*-07	1.0307*E*-06
	0.9	3.7494*E*-08	5.5877*E*-07	1.1174*E*-06	3.9240*E*-07	4.4917*E*-07
	0.1	7.4981*E*-08	1.1178*E*-06	2.2353*E*-06	1.0397*E*-06	6.6147*E*-07
0.10	0.5	7.4984*E*-08	1.1177*E*-06	2.2350*E*-06	9.5823*E*-07	1.7107*E*-06
	0.9	7.4987*E*-08	1.1175*E*-06	2.2347*E*-06	9.5091*E*-07	6.6139*E*-07
	0.1	7.4953*E*-07	1.1175*E*-05	2.2353*E*-05	1.1021*E*-05	9.9267*E*-07
1.00	0.5	7.4956*E*-07	1.0074*E*-05	2.2350*E*-05	1.1057*E*-05	2.7793*E*-06
	0.9	7.4959*E*-07	1.1173*E*-05	2.2347*E*-05	1.0841*E*-05	9.9260*E*-07

Table 12: Comparison of absolute error of Example 7 with $\beta = 0$, $\gamma = 1$, $\eta = 0.001$, $\delta = 3$, $h = 0.1$, and $\Delta t = 0.0001$.

t	x	CFDM6	ADM [23]	FDS4 [29]	MCSDQM [31]
	0.1	3.7499*E*-08	1.9841*E*-06	3.9673*E*-06	1.5946*E*-06
0.05	0.5	3.7499*E*-08	1.9837*E*-06	3.9665*E*-06	3.6584*E*-06
	0.9	3.7499*E*-08	1.9833*E*-06	3.9657*E*-06	1.5942*E*-06
	0.1	7.4996*E*-08	3.9681*E*-06	7.9346*E*-06	2.3479*E*-06
0.10	0.5	7.4996*E*-08	3.9673*E*-06	7.9330*E*-06	6.0721*E*-06
	0.9	7.4996*E*-08	3.9665*E*-06	7.9314*E*-06	2.3475*E*-06
	0.1	7.4962*E*-07	3.9663*E*-05	7.9346*E*-05	3.5221*E*-06
1.00	0.5	7.4962*E*-07	3.9655*E*-05	7.9330*E*-05	9.8610*E*-06
	0.9	7.4962*E*-07	3.9647*E*-05	7.9314*E*-05	3.5217*E*-06

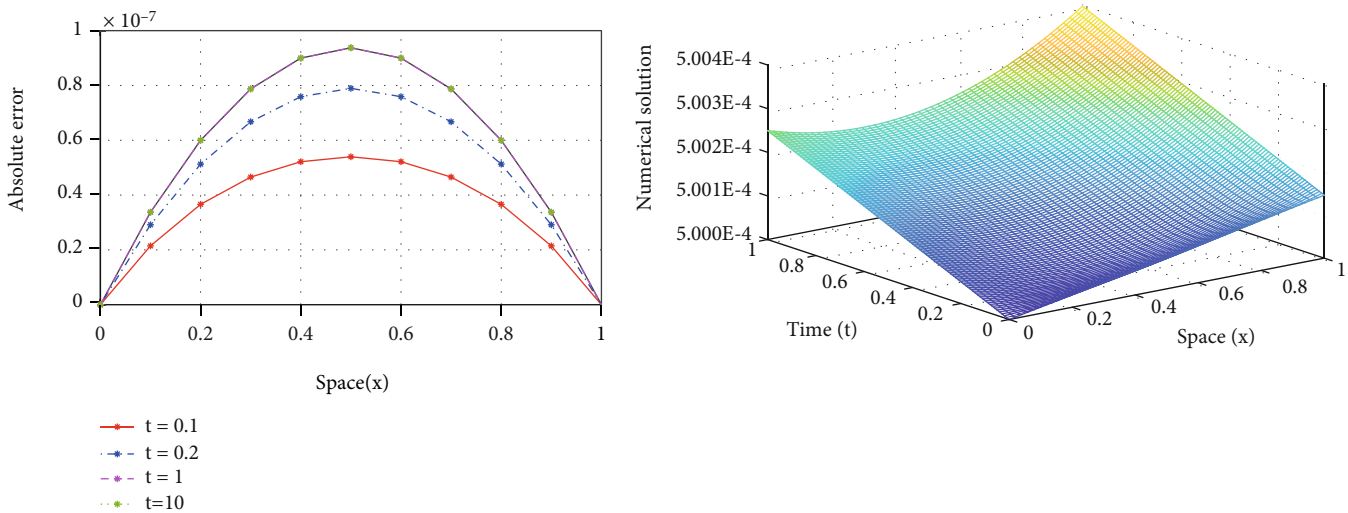

(a) Absolute error at different time levels

(b) Surface plot of numerical solution

Figure 9: Error and solution profile of Example 7 with $N = 50$ and $\Delta t = 0.01$.

and exponential time differencing method of lines [29]. Figure 3(a) compares numerical and exact solution at different time levels, and Figure 3(b) presents the 3D behaviour of the numerical solution with $N = 10$, $\Delta t = 0.01$, and $\delta = 8$.

Example 2. Consider Equation (3) for $\beta = \gamma = 1$ with the initial condition (4) and boundary conditions (5) and (6). The absolute error is compared in Table 2 with those of previous investigators Ismail et al. [23], Sari et al. [25], and Bratsos

[29] for $h = 0.1$, $\Delta t = 0.0001$, and $\delta = 2, 8$ at $t = 0.0005$ and $t = 0.0010$. Figure 4(a) compares the numerical and exact solution at different time levels, and Figure 4(b) represents the 3D behaviour of numerical solution with $N = 10$, $\Delta t = 0.01$, and $\delta = 8$.

Example 3. Consider Equation (3) for the initial and boundary conditions (4) and (6) with $\beta = 0.1$ and $\gamma = -0.0025$. Table 3 depicts the accuracy of the results obtained by CFDM6, by comparing the absolute error with literature data for $h = 0.1$, $\Delta t = 0.0001$, and $\delta = 2, 4, 8$. Figure 5(a) compares the numerical and exact solution at different time levels, and Figure 5(b) represents the 3D behaviour of the numerical solution with $N = 10$, $\Delta t = 0.01$, and $\delta = 8$.

Example 4. Consider gBH Equation (8) with the initial and boundary conditions (9) and (10) for parametric values $\beta = \gamma = 1$ and $\eta = 0.001$. The exact solution is given by (11). The absolute error at node points $x = 0.1, 0.5, 0.9$ is given in Table 4 at $t = 0.1$ and $t = 1$ for $h = 0.1$, $\Delta t = 0.0001$, and $\delta = 2$. Comparison shows that results are better than exponential finite difference scheme [49], hybrid B-spline [50], and tension B-spline collocation method [37]. Table 5 gives a comparison of L_∞ error norm for $\delta = 1, 4$, and 8. Table 6 gives a comparison of L_2 and L_∞ error norms with $\delta = 2$, $h = 0.1$, $\eta = 0.001$, $\Delta t = 0.01$ at $t = 0.05, 0.1, 1, 5$. Figure 6(a) represents the absolute error at different time levels with $N = 10$, and Figure 6(b) gives the 3D profile of numerical solution with $N = 50$, $\Delta t = 0.01$, and $\delta = 8$.

Example 5. The gBH Equation (8) is considered for the initial and boundary conditions (9) and (10). The CFDM6 results are evaluated for $\beta = 0.1$ and $\gamma = 0.001$, and $\eta = 0.0001$, $h = 0.1$, $\Delta t = 0.0001$, and $\delta = 2$ at time $t = 0.5$ and $t = 0.8$ are given in Table 7. The absolute error is compared with [37, 49, 50]. The L_∞ error norm is compared for CFDM6 with the collocation of cubic B-splines [51], multiscale Runge-Kutta Galerkin method (MGT) [52], and a new kind of tension B-spline function [37] and is presented in Table 8 at different values of $\delta = 1, 4, 8$. Figure 7(a) represents the absolute error at different time levels with $N = 10$, and Figure 7(b) gives the 3D profile of numerical solution with $N = 50$, $\Delta t = 0.01$, and $\delta = 8$.

Example 6. Consider gBH Equation (8) with initial and boundary conditions (9) and (10). The absolute error is compared with the schemes discussed by [37, 49, 50] for $\beta = 5$, $\gamma = 10$, $\eta = 0.0001$, $\Delta t = 0.0001$, and $\delta = 2$ at different node points for time $t = 0.2, 0.5$, and 0.8. Tables 9 and 10 give a comparison of absolute error for $\eta = 0.0001$ and $\eta = 0.00001$, respectively. Remarkable closeness of numerical and exact solutions can be seen in the tables. Figure 8(a) represents the absolute error at different time levels with $N = 10$, and Figure 8(b) gives the 3D profile of numerical solution with $N = 50$, $\Delta t = 0.01$, and $\delta = 8$.

Example 7. The gBH Equation (8) is subjected to initial and boundary conditions (9) and (10) for $\beta = 0$, $\gamma = 1$, and $\eta = 0.001$. Table 11 compares absolute error of CFDM6 with the Adomian decomposition method (ADM) [23], fourth-order numerical scheme (FDS4) [29], Gauss Chebyshev Galerkin (GCG) [30], and modified cubic B-spline differential quadrature method (MCSDQM) [31] at $\delta = 2$, $h = 0.1$, and $\Delta t = 0.0001$. Table 12 gives the comparison of absolute error for $\delta = 3$. The efficiency of the numerical solution to approach the exact solution can be easily seen, and the results are better than those of other methods. Figure 9(a) represents the absolute error at different time levels with $N = 10$, and Figure 9(b) gives the 3D profile of the numerical solution with $N = 50$, $\Delta t = 0.01$, and $\delta = 8$.

7. Conclusion

Compact FDM along with the SSP-RK43 scheme has been implemented to solve gBF and gBH equations. Several examples of both the equations are successfully solved with the proposed technique. Absolute error and L_2 and L_∞ error norms are calculated and compared with the previous results. The results with CFDM6 are found to be better than those with many techniques like the Adomian decomposition method, exponential time differencing method of lines, cubic B-spline collocation method, exponential finite difference scheme, hybrid B-spline collocation, tension B-spline collocation, multiscale Runge-Kutta Galerkin method, and modified cubic B-spline differential quadrature method. Comparison shows that the technique is providing highly accurate results with ease in implementation and less computational effort.

Data Availability

The complete data is in the manuscript.

Conflicts of Interest

The authors declare that they have no conflicts of interest.

Acknowledgments

Ms. Shallu is thankful to CSIR New Delhi for providing financial assistance in the form of JRF with File No. 09/797(0016)/2018-EMR-I.

References

[1] H. Bateman, "Some recent researches on the motion of fluids," *Monthly Weather Review*, vol. 43, no. 4, pp. 163–170, 1915.

[2] J. M. Burgers, "Mathematical examples illustrating relations occurring in the theory of turbulent fluid motion," *Transactions of the Royal Netherlands Academy of Arts and Sciences*, vol. 17, pp. 1–53, 1939.

[3] R. A. Fisher, "The wave of advance of advantageous genes," *Annals of Eugenics*, vol. 7, no. 4, pp. 355–369, 1937.

[4] S. Petrovskii and N. Shigesada, "Some exact solutions of a generalized Fisher equation related to the problem of biological

invasion," *Mathematical Biosciences*, vol. 172, no. 2, pp. 73–94, 2001.

[5] H. Chen and H. Zhang, "New multiple soliton solutions to the general Burgers-Fisher equation and the Kuramoto-Sivashinsky equation," *Chaos, Solitons & Fractals*, vol. 19, no. 1, pp. 71–76, 2004.

[6] M. Sari, G. Gurarslan, and I. Dag, "A compact finite difference method for the solution of the generalized Burgers–Fisher equation," *Numerical Methods for Partial Differential Equations*, vol. 26, no. 1, pp. 125–134, 2010.

[7] T. Zhao, C. Li, Z. Zang, and Y. Wu, "Chebyshev-Legendre pseudo-spectral method for the generalised Burgers-Fisher equation," *Applied Mathematical Modelling*, vol. 36, no. 3, pp. 1046–1056, 2012.

[8] R. Mohammadi, "Spline solution of the generalized Burgers-Fisher equation," *Applicable Analysis*, vol. 91, no. 12, pp. 2189–2215, 2012.

[9] M. Tatari, B. Sepehrian, and M. Alibakhshi, "New implementation of radial basis functions for solving Burgers-Fisher equation," *Numerical Methods for Partial Differential Equations*, vol. 28, no. 1, pp. 248–262, 2012.

[10] S. A. Malik, I. M. Qureshi, M. Amir, A. N. Malik, and I. Haq, "Numerical solution to generalized Burgers-Fisher equation using exp-function method hybridized with heuristic computation," *PLoS One*, vol. 10, no. 3, article e0121728, 2015.

[11] O. P. Yadav and R. Jiwari, "Finite element analysis and approximation of Burgers-Fisher equation," *Numerical Methods for Partial Differential Equations*, vol. 33, no. 5, pp. 1652–1677, 2017.

[12] J. E. Macias-Diaz and A. E. Gonzalez, "A convergent and dynamically consistent finite-difference method to approximate the positive and bounded solutions of the classical Burgers-Fisher equation," *Journal of Computational and Applied Mathematics*, vol. 318, pp. 604–615, 2017.

[13] M. Soori, "The variational iteration method and the Homotopy perturbation method to the exact solution of the generalized Burgers-Fisher equation," *Calculus of Variations and Partial Differential Equations*, vol. 5, no. 8, pp. 19–26, 2018.

[14] A. G. Bratsos and A. Q. M. Khaliq, "An exponential time differencing method of lines for Burgers-Fisher and coupled Burgers equations," *Journal of Computational and Applied Mathematics*, vol. 356, pp. 182–197, 2019.

[15] B. Gurbuz and M. Sezer, "A modified Laguerre matrix approach for Burgers-Fisher type nonlinear equations," in *Numerical Solutions of Realistic Nonlinear Phenomena*, vol. 31 of Nonlinear Systems and Complexity, pp. 107–123, Springer International Publishing, Cham, Switzerland, 2020.

[16] J. Li, "Geometric properties and exact travelling wave solutions for the generalized Burger-Fisher equation and the Sharma-Tasso-Olver equation," *Journal of Nonlinear Modeling and Analysis*, vol. 1, no. 1, pp. 1–10, 2019.

[17] O. O. Onyejekwe, B. Minale, F. Habtamu et al., "Numerical discrete-domain integral formulations for generalized Burger-Fisher equation," *Applied Mathematics*, vol. 11, no. 3, pp. 137–145, 2020.

[18] H. Zhang, Y. Xia, and P. R. N'gbo, "Global existence and uniqueness of a periodic wave solution of the generalized Burgers-Fisher equation," *Applied Mathematics Letters*, vol. 121, pp. 1–7, 2021.

[19] X. Y. Wang, Z. S. Zhu, and Y. K. Lu, "Solitary wave solutions of the generalised Burgers-Huxley equation," *Journal of Physics A: Mathematical and General*, vol. 23, no. 3, pp. 271–274, 1990.

[20] A. L. Hodgkin and A. F. Huxley, "A quantitative description of membrane current and its application to conduction and excitation in nerve," *The Journal of Physiology*, vol. 117, no. 4, pp. 500–544, 1952.

[21] R. FitzHugh, *Mathematical Models of Excitation and Propagation in Nerve*, Biological Engineering, McGraw Hill, New York, NY, USA, 1969.

[22] O. Y. Yefimova and N. A. Kudryashov, "Exact solutions of the Burgers-Huxley equation," *Journal of Applied Mathematics and Mechanics*, vol. 68, no. 3, pp. 413–420, 2004.

[23] H. N. Ismail, K. Raslan, and A. Abd Rabboh, "Adomian decomposition method for Burger's-Huxley and Burger's-Fisher equations," *Applied Mathematics and Computation*, vol. 159, no. 1, pp. 291–301, 2004.

[24] H. Gao and R. X. Zhao, "New exact solutions to the generalized Burgers-Huxley equation," *Applied Mathematics and Computation*, vol. 217, no. 4, pp. 1598–1603, 2010.

[25] M. Sari, G. Gurarslan, and A. Zeytinoglu, "High-order finite difference schemes for numerical solutions of the generalized Burgers-Huxley equation," *Numerical Methods for Partial Differential Equations*, vol. 27, no. 5, pp. 1313–1326, 2011.

[26] I. Celik, "Haar wavelet method for solving generalized Burgers-Huxley equation," *Arab Journal of Mathematical Sciences*, vol. 18, no. 1, pp. 25–37, 2012.

[27] R. Zhang, X. Yu, and G. Zhao, "The local discontinuous Galerkin method for Burger's-Huxley and Burger's-Fisher equations," *Applied Mathematics and Computation*, vol. 218, no. 17, pp. 8773–8778, 2012.

[28] R. Mohammadi, "B-spline collocation algorithm for numerical solution of the generalized Burgers-Huxley equation," *Numerical Methods for Partial Differential Equations*, vol. 29, no. 4, pp. 1173–1191, 2013.

[29] A. G. Bratsos, "A fourth order improved numerical scheme for the generalized Burgers-Huxley equation," *American Journal of Computational Mathematics*, vol. 1, no. 3, pp. 152–158, 2011.

[30] M. El-Kady, S. M. El-Sayed, and H. E. Fathy, "Development of Galerkin method for solving the generalized Burger's-Huxley equation," *Mathematical Problems in Engineering*, vol. 2013, no. 4, 2013.

[31] B. K. Singh, G. Arora, and M. K. Singh, "A numerical scheme for the generalized Burgers-Huxley equation," *Journal of the Egyptian Mathematical Society*, vol. 24, no. 4, pp. 629–637, 2016.

[32] S. Zibaei, M. Zeinadini, and M. Namjoo, "Numerical solutions of Burgers-Huxley equation by exact finite difference and NSFD schemes," *Journal of Difference Equations and Applications*, vol. 22, no. 8, pp. 1098–1113, 2016.

[33] M. Bukhari, M. Arshad, S. Batool, and S. M. Saqlain, "Numerical solution of generalized Burgers-Huxley equation using local radial basis functions," *International Journal of Advanced and Applied Sciences*, vol. 4, no. 5, pp. 1–11, 2017.

[34] J. E. Macias-Diaz, "A modified exponential method that preserves structural properties of the solutions of the Burgers-Huxley equation," *International Journal of Computer Mathematics*, vol. 95, no. 1, pp. 3–19, 2018.

[35] K. Gilani and U. Saeed, "CAS wavelet Picard technique for Burgers-Huxley and Burgers equation," *International Journal of Applied and Computational Mathematics*, vol. 4, no. 5, pp. 133–147, 2018.

[36] S. C. Shiralashetti and S. Kumbinarasaiah, "Cardinal B-spline wavelet based numerical method for the solution of generalized Burgers-Huxley equation," *International Journal of Applied and Computational Mathematics*, vol. 4, no. 2, pp. 73–86, 2018.

[37] N. Alinia and M. Zarebnia, "A numerical algorithm based on a new kind of tension B-spline function for solving Burgers-Huxley equation," *Numerical Algorithms*, vol. 82, no. 4, pp. 1121–1142, 2019.

[38] A. C. Loyinmi and T. K. Akinfe, "An algorithm for solving the Burgers-Huxley equation using the Elzaki transform," *SN Applied Sciences*, vol. 2, no. 1, pp. 7–24, 2020.

[39] A. G. Kushner and R. I. Matviichuk, "Exact solutions of the Burgers-Huxley equation via dynamics," *Journal of Geometry and Physics*, vol. 151, article 103615, 2020.

[40] S. Shukla and M. Kumar, "Error analysis and numerical solution of Burgers-Huxley equation using 3-scale Haar wavelets," *Engineering with Computers*, vol. 1-9, 2020.

[41] S. Panghal and M. Kumar, "Approximate analytic solution of Burger Huxley equation using feed-forward artificial neural network," *Neural Processing Letters*, vol. 53, no. 3, pp. 2147–2163, 2021.

[42] S. K. Lele, "Compact finite difference schemes with spectral-like resolution," *Journal of Computational Physics*, vol. 103, no. 1, pp. 16–42, 1992.

[43] R. Ansari, R. Gholami, K. Hosseini, and S. Sahmani, "A sixth-order compact finite difference method for vibrational analysis of nanobeams embedded in an elastic medium based on nonlocal beam theory," *Mathematical and Computer Modelling*, vol. 54, no. 11-12, pp. 2577–2586, 2011.

[44] B. J. Boersma, "A 6th order staggered compact finite difference method for the incompressible Navier-Stokes and scalar transport equations," *Journal of Computational Physics*, vol. 230, no. 12, pp. 4940–4954, 2011.

[45] D. Li, C. Zhang, and J. Wen, "A note on compact finite difference method for reaction-diffusion equations with delay," *Applied Mathematical Modelling*, vol. 39, no. 5-6, pp. 1749–1754, 2015.

[46] R. Kaur, Shallu, V. K. Kukreja, N. Parumasur, and P. Singh, "Two different temporal domain integration schemes combined with compact finite difference method to solve modified Burgers' equation," *Ain Shams Engineering Journal*, 2021.

[47] M. K. Jain, *Numerical Solutions of Differential Equations*, Wiley Eastern Ltd., 1984.

[48] E. J. Kubatko, B. A. Yeager, and D. I. Ketcheson, "Optimal strong-stability-preserving Runge-Kutta time discretizations for discontinuous Galerkin methods," *Journal of Scientific Computing*, vol. 60, no. 2, pp. 313–344, 2014.

[49] B. Inan and A. R. Bahadir, "Numerical solutions of the generalized Burgers-Huxley equation by implicit exponential finite difference method," *Journal of Applied Mathematics, Statistics and Informatics*, vol. 11, no. 2, pp. 57–67, 2015.

[50] I. Wasim, M. Abbas, and M. Amin, "Hybrid B-spline collocation method for solving the generalized Burgers-Fisher and Burgers-Huxley equations," *Mathematical Problems in Engineering*, vol. 2018, Article ID 6143934, 18 pages, 2018.

[51] R. C. Mittal and A. Tripathi, "Numerical solutions of generalized Burgers-Fisher and generalized Burgers-Huxley equations using collocation of cubic B-splines," *International Journal of Computer Mathematics*, vol. 92, no. 5, pp. 1053–1077, 2015.

[52] J. Chen, "An efficient multiscale Runge-Kutta Galerkin method for generalized Burgers-Huxley equation," *Applied Mathematical Sciences*, vol. 11, no. 30, pp. 1467–1479, 2017.

Hindawi
Advances in Mathematical Physics
Volume 2021, Article ID 8484041, 7 pages
https://doi.org/10.1155/2021/8484041

Research Article

New Optical Soliton Solutions to the Fractional Hyperbolic Nonlinear Schrödinger Equation

Ahmad Sharif

Department of Mathematics, Faculty of Sciences, Gonbad Kavous University, Gonbad, Iran

Correspondence should be addressed to Ahmad Sharif; sharif@gonbad.ac.ir

Received 19 June 2021; Revised 14 August 2021; Accepted 21 September 2021; Published 13 October 2021

Academic Editor: Mohammad Mirzazadeh

This paper is aimed at investigating the soliton solutions of the hyperbolic nonlinear Schrödinger equation. Exact analytical solutions of the model are acquired through applying an integration method, namely, the Sine-Gordon method. It is observed that the method is able to efficiently determine the exact solutions for this equation. Graphical simulations corresponding to some of the results obtained in the paper are also drawn. These results can help us better understand the behavior and performance of this model. The procedure implemented in this paper can be recommended in solving other equations in the field. All calculations and graphing are performed using powerful symbolic computational packages in Mathematica software.

1. Introduction

Finding exact solutions for differential equations, including ordinary or partial derivatives, is always an important challenge in mathematics, physics, and engineering. This process is very difficult or even impossible for some of these equations. Therefore, any method that helps us determine these solutions is of great importance and use. Exact solutions can be used to illustrate many nonlinear phenomena observed in mathematical physics. One of the most appropriate tools for describing many events in nature is to employ differential equations. This importance has made the traces to such equations tangible in many branches of science, including mathematics, physics [1–3], electrical engineering, astronomy, mechanics, economics, and many other existing disciplines [4–6]. Based on these remarkable effects, several analytical methods have been successfully applied to obtain exact solutions of such equations. Some of these methods are the homotopy analysis method [7], the variational iteration method [8], the exp-function method [9], the logistic function method [10], the generalized G'/G-expansion [11], the elliptic finder method [12–14], the exponential rational function idea [15], the modified Kudryashov technique [16], and the subequation method [17]. To see more methods, please refer to [18–20], including, biology, nonlinear optics, economy, and applied science [1, 20–34]. In this article, the authors study the HNSE, which is given in the form [35]:

$$iD_y^{\alpha}u + \frac{1}{2}\left(D_x^{2\alpha} - D_t^{2\alpha}\right)u + |u|^2 u = 0, \quad 0 < \alpha \leq 1. \tag{1}$$

It is notable that this equation encompasses a wide range of well-known equations through some specific selection of parameters. So far, a variety of techniques have been used successfully to find the exact solutions to the HNS equation (1). This article contains the following sections. A brief mathematical description of the conformable derivative used in this paper is provided in the second section of this paper. Then, the method used is introduced in the third section. The fourth section involved the exact solutions obtained by employing the analytical method equation and graphical behavior are discovered. Finally, conclusions are presented in the last section of the article.

2. The Conformable Derivative

Biswas proposed an interesting definition of derivative called conformable derivative [1]. This derivative can be considered to be a natural extension of the classical derivative. Furthermore, conformable derivative satisfies all the properties of the standard calculus, for instance, the chain rule.

Definition 1. Let $f : [0,\infty) \longrightarrow \mathbb{R}$, the conformable derivative of a function $f(t)$ of order α, is defined as

$$D_t^{\alpha} f(t) = \lim_{\epsilon \longrightarrow 0} \frac{f\left(t+\epsilon t^{1-\alpha}\right) - f(t)}{\epsilon}, \quad \alpha \in (0,1], t > 0. \tag{2}$$

This new definition satisfies the following properties.

Definition 2. Suppose that $c \geq 0$ and $t \geq c$, let h be a function defined on c, t as well as $\alpha \in R$. Then, the α-fractional integral of h is given by

$${}_tI_c^{\alpha} h(t) = \int_c^{\alpha} \frac{h(x)}{x^{1-\alpha}} dx, \tag{3}$$

if the Riemann improper integral exists.

Theorem 3. *Let $\alpha \in (0,1]$, f, g be α-differentiable at a point t, then*

$$\begin{aligned} D_t^{\alpha}(af + bg) &= aD_t^{\alpha}(f) + bD_t^{\alpha}(g), \text{for } a, b \in \mathbb{R}, \\ D_t^{\alpha}(t^{\mu}) &= \mu t^{\mu-\alpha}, \text{for } \mu \in \mathbb{R}, \\ D_t^{\alpha}(fg) &= fD_t^{\alpha}(g) + gD_t^{\alpha}(f), \\ D_t^{\alpha}\left(\frac{g}{g}\right) &= \frac{gD_t^{\alpha}(f) - fD_t^{\alpha}(g)}{g^2}. \end{aligned} \tag{4}$$

Theorem 4. *Let h be a differentiable function and _ is the order of the conformable derivative. Let g be a differentiable function defined in the range of h, then*

$$D_t^{\alpha}(fog)(t) = t^{1-\alpha} g(t)^{\alpha-1} g'(t) D_t^{\alpha}(f(t))_{t=g(t)}, \tag{5}$$

where "prime" is the classical derivative with respect to t.

3. Structure of the Sine-Gordon Method

In order, we consider the Sine-Gordon equation as follows:

$$\psi_{xyt} = \alpha \sin(\psi); \tag{6}$$

here, α is a nonzero constant. We exert the change

$$\psi(x,y,t) = U(\xi), \quad \xi = \eta(x + y + \upsilon t); \tag{7}$$

here, υ is the traveling wave velocity. Replace Equation (8) in Equation (7)

$$U'' = \frac{\alpha}{\upsilon\mu^2} \sin(u(\xi)). \tag{8}$$

By simplifying Equation (8), we have

$$\left[\left(\frac{U}{2}\right)'\right]^2 = \frac{\alpha}{\upsilon\mu^2} \sin^2\left(\frac{U(\xi)}{2}\right) + C. \tag{9}$$

In Equation (9), C is the integration constant. We suppose $C = 0$, $w(\xi) = U(\xi)/2$, and $f^2 = \alpha/\upsilon\mu^2$, so Equation (9) detracts to

$$w'(\xi)^2 = f^2 \sin^2(w(\xi)). \tag{10}$$

In simple terms, we have

$$w'(\xi) = f \sin(w(\xi)). \tag{11}$$

Inserting $f = 1$, we have

$$w'(\xi) = \sin(w(\xi)). \tag{12}$$

We have solutions of Equation (12) as follows:

$$\begin{aligned} &\sin(w(\xi)) = \operatorname{sech}(\xi) \text{ or } \quad \cos(w(\xi)) = \tanh(\xi), \\ &\sin(w(\xi)) = \operatorname{icsc}h(\xi) \text{ or } \quad \cos(w(\xi)) = \coth(\xi). \end{aligned} \tag{13}$$

For constructing the solutions of NLPDE as follows:

$$N\left(\psi, \psi_t, \psi_x, \psi_y, \psi_{tt}, .. \cdots\right) = 0. \tag{14}$$

Using the following variation:

$$U(w) = \sum_{j=1}^{n} \cos^{j-1}(w) \times \left[B_j \sin(w) + A_j \cos(w)\right] + A_0, \tag{15}$$

by using Equation (13), we have the solution of Equation (15) as follows:

$$\begin{aligned} U_1(\xi) &= \sum_{j=1}^{n} \tanh^{j-1}(\xi) \times \left[B_j \operatorname{sech}(\xi) + A_j \tanh(\xi)\right] + A_0, \\ U_2(\xi) &= \sum_{j=1}^{n} \coth^{j-1}(\xi) \times \left[B_j \operatorname{csch}(\xi) + A_j \coth(\xi)\right] + A_0. \end{aligned} \tag{16}$$

We obtain n by balancing in [10]. Then, by substituting Equation (15) into ODE concluded from Equation (14), we have a system of algebraic equations of $\sin^i(\xi)$ and $\cos^i(\xi)$. Then, by equating of coefficients, we obtain the necessary coefficients. By substituting these coefficients in (15), we extract the solutions of Equation (14).

4. Solution Procedure

To determine the solitary solution of Equation (1), we first define the following new variables:

$$u(x,y,t) = \hbar(\xi)e^{i\theta},$$
$$\xi = \left(\frac{1}{\alpha}\right)x^{\alpha} + \left(\frac{\mu}{\alpha}\right)y^{\alpha} - \left(\frac{\sigma}{\alpha}\right)t^{\alpha}, \tag{17}$$
$$\theta = \left(\frac{a}{\alpha}\right)x^{\alpha} + \left(\frac{b}{\alpha}\right)y^{\alpha} + \left(\frac{d}{\alpha}\right)t^{\alpha} + \theta_0.$$

Substituting Equation (2) in Equation (1) and comparing real and imaginary parts, respectively, one can obtain

$$\left(a^2 + 2b - d^2\right)\hbar - 2\hbar^3 + \left(\sigma^2 - 1\right)\hbar'' = 0,$$
$$\mu = -(a + d\sigma). \tag{18}$$

Taking balance principles between $\hbar''$ and $\hbar^3$ into account in Equation (10) yields $m = 1$. Immediately, the general structure for the solution to the problem, which is presented in (7), is determined as follows:

$$\hbar(\xi) = B_1 \sin(\xi) + A_1 \cos(\xi) + A_0. \tag{19}$$

Following the steps mentioned for the method by substituting Equation (15) along with Equation (8) into Equation (10), we get a polynomial in $\sin(\xi), \cos(\xi)$. Equating the coefficient of same power of $\sin^i(\xi), \cos^i(\xi)(i = 0, 1, 2, \cdots)$, we obtain the system of algebraic equations, and by solving this system, we obtained equations for $A_0, A_1, B_1, a, b, d, \mu$, and σ. Now, by solving obtained systems, we get the following values:

Set 1:

$$A_0 = \frac{\sqrt{2a^2 - 2d^2 - 3\sigma^2 + 4b + 3}}{2},$$
$$A_1 = \frac{\sqrt{2a^2 - 2d^2 + \sigma^2 + 4b - 1}}{4}, \tag{20}$$
$$B_1 = \frac{\sqrt{2a^2 - 2d^2 + \sigma^2 + 4b - 1}}{4}.$$

So, we obtain the following dark optical soliton:

$$\hbar_1(\xi) = \frac{\sqrt{2a^2 - 2d^2 + \sigma^2 + 4b - 1}}{4}\operatorname{sech}(\xi) + \frac{\sqrt{2a^2 - 2d^2 + \sigma^2 + 4b - 1}}{4}\tanh(\xi) + \frac{\sqrt{2a^2 - 2d^2 - 3\sigma^2 + 4b + 3}}{2}. \tag{21}$$

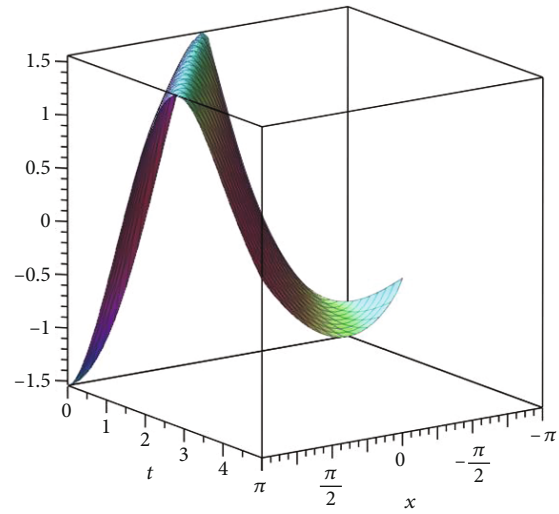

Figure 1: Dynamic behaviors of solution $u_1(x, y, t)$ given by (22) for $t = 0..5, x = -\pi..\pi$, for $\alpha = 0.8$.

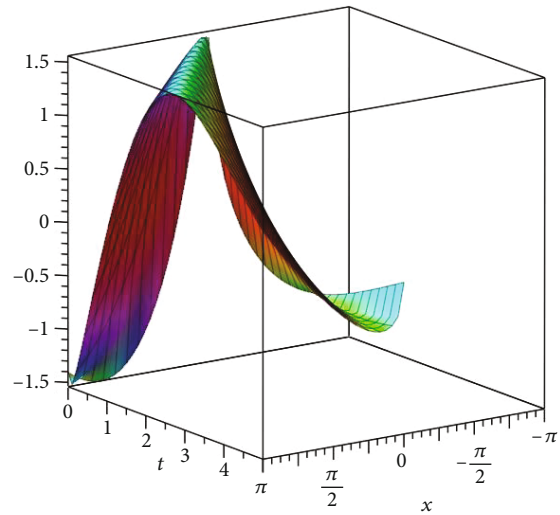

Figure 2: Dynamic behaviors of solution $u_1(x, y, t)$ given by (22) for $t = 0..5, x = -\pi..\pi$, for $\alpha = 0.5$.

So we have optical dark soliton solution of (1) as follows:

$$u_1(x,y,t) = \left[\frac{\sqrt{2a^2 - 2d^2 + \sigma^2 + 4b - 1}}{4}\operatorname{sech} \cdot \left(\left(\frac{1}{\alpha}\right)x^{\alpha} + \left(\frac{\mu}{\alpha}\right)y^{\alpha} - \left(\frac{\sigma}{\alpha}\right)t^{\alpha}\right) + \frac{\sqrt{2a^2 - 2d^2 + \sigma^2 + 4b - 1}}{4}\tanh \cdot \left(\left(\frac{1}{\alpha}\right)x^{\alpha} + \left(\frac{\mu}{\alpha}\right)y^{\alpha} - \left(\frac{\sigma}{\alpha}\right)t^{\alpha}\right) + \frac{\sqrt{2a^2 - 2d^2 - 3\sigma^2 + 4b + 3}}{2}\right]\exp \cdot \left(i\left(\left(\frac{a}{\alpha}\right)x^{\alpha} + \left(\frac{b}{\alpha}\right)y^{\alpha} + \left(\frac{d}{\alpha}\right)t^{\alpha} + \theta_0\right)\right). \tag{22}$$

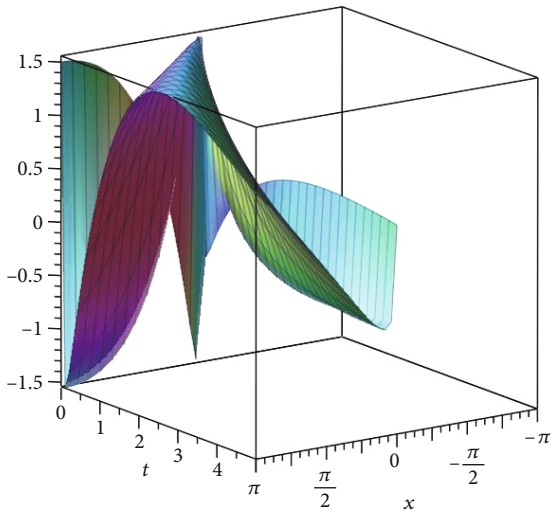

Figure 3: Graphical representation of solution $u_1(x, y, t)$ given by (22) for $t = 0..5, x = -\pi..\pi$, for $\alpha = 0.2$.

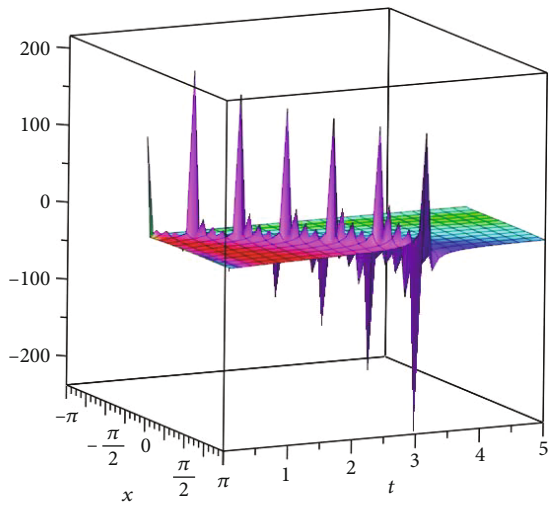

Figure 4: Graphical representation of solution $u_2(x, y, t)$ given by (23) for $t = 0..5, x = -\pi..\pi$, for $\alpha = 0.8$.

And the dark singular soliton is

$$\begin{aligned} u_2(x,y,t) = &\left[\frac{\sqrt{2a^2-2d^2+\sigma^2+4b-1}}{4}\ \text{csch}\right.\\ &\cdot\left(\left(\frac{1}{\alpha}\right)x^\alpha+\left(\frac{\mu}{\alpha}\right)y^\alpha-\left(\frac{\sigma}{\alpha}\right)t^\alpha\right)\\ &+\frac{\sqrt{2a^2-2d^2+\sigma^2+4b-1}}{4}\ \coth\\ &\cdot\left(\left(\frac{1}{\alpha}\right)x^\alpha+\left(\frac{\mu}{\alpha}\right)y^\alpha-\left(\frac{\sigma}{\alpha}\right)t^\alpha\right)\\ &\left.+\frac{\sqrt{2a^2-2d^2-3\sigma^2+4b+3}}{2}\right]\ \exp\\ &\cdot\left(i\left(\left(\frac{a}{\alpha}\right)x^\alpha+\left(\frac{b}{\alpha}\right)y^\alpha+\left(\frac{d}{\alpha}\right)t^\alpha+\theta_0\right)\right). \end{aligned} \tag{23}$$

Set 2:

$$\begin{aligned} A_0 &= 0,\\ A_1 &= \frac{\sqrt{3}}{6}\sqrt{6a^2-6d^2-6\sigma^2+12b+6},\\ B_1 &= \frac{1}{6}\sqrt{6a^2-6d^2-6\sigma^2+12b+6}. \end{aligned} \tag{24}$$

The optical dark soliton solution is

$$\begin{aligned} u_3(x,y,t) = &\left[\frac{1}{6}\sqrt{6a^2-6d^2-6\sigma^2+12b+6}\ \text{sech}\right.\\ &\cdot\left(\left(\frac{1}{\alpha}\right)x^\alpha+\left(\frac{\mu}{\alpha}\right)y^\alpha-\left(\frac{\sigma}{\alpha}\right)t^\alpha\right)\\ &+\frac{\sqrt{3}}{6}\sqrt{6a^2-6d^2-6\sigma^2+12b+6}\ \tanh\\ &\left.\cdot\left(\left(\frac{1}{\alpha}\right)x^\alpha+\left(\frac{\mu}{\alpha}\right)y^\alpha-\left(\frac{\sigma}{\alpha}\right)t^\alpha\right)\right]\\ &\times\exp\left(i\left(\left(\frac{a}{\alpha}\right)x^\alpha+\left(\frac{b}{\alpha}\right)y^\alpha+\left(\frac{d}{\alpha}\right)t^\alpha+\theta_0\right)\right). \end{aligned} \tag{25}$$

And dark singular soliton is

$$\begin{aligned} u_4(x,y,t) = &\left[\frac{1}{6}\sqrt{6a^2-6d^2-6\sigma^2+12b+6}\ \text{csch}\right.\\ &\cdot\left(\left(\frac{1}{\alpha}\right)x^\alpha+\left(\frac{\mu}{\alpha}\right)y^\alpha-\left(\frac{\sigma}{\alpha}\right)t^\alpha\right)\\ &+\frac{\sqrt{3}}{6}\sqrt{6a^2-6d^2-6\sigma^2+12b+6}\ \coth\\ &\left.\cdot\left(\left(\frac{1}{\alpha}\right)x^\alpha+\left(\frac{\mu}{\alpha}\right)y^\alpha-\left(\frac{\sigma}{\alpha}\right)t^\alpha\right)\right]\\ &\times\exp\left(i\left(\left(\frac{a}{\alpha}\right)x^\alpha+\left(\frac{b}{\alpha}\right)y^\alpha+\left(\frac{d}{\alpha}\right)t^\alpha+\theta_0\right)\right). \end{aligned} \tag{26}$$

Set 3:

$$\begin{aligned} A_0 &= \frac{\sqrt{2a^2-2d^2+4b}}{2},\\ A_1 &= \frac{\sqrt{2a^2-2d^2+\sigma^2+4b-1}}{4},\\ B_1 &= 0. \end{aligned} \tag{27}$$

The optical dark soliton solution is

$$\begin{aligned} u_5(x,y,t) = &\left[\frac{\sqrt{2a^2-2d^2+\sigma^2+4b-1}}{4}\ \tanh\left(\left(\frac{1}{\alpha}\right)x^\alpha\right.\right.\\ &\left.\left.+\left(\frac{\mu}{\alpha}\right)y^\alpha-\left(\frac{\sigma}{\alpha}\right)t^\alpha\right)+\frac{\sqrt{2a^2-2d^2+4b}}{2}\right]\ \exp\\ &\cdot\left(i\left(\left(\frac{a}{\alpha}\right)x^\alpha+\left(\frac{b}{\alpha}\right)y^\alpha+\left(\frac{d}{\alpha}\right)t^\alpha+\theta_0\right)\right). \end{aligned} \tag{28}$$

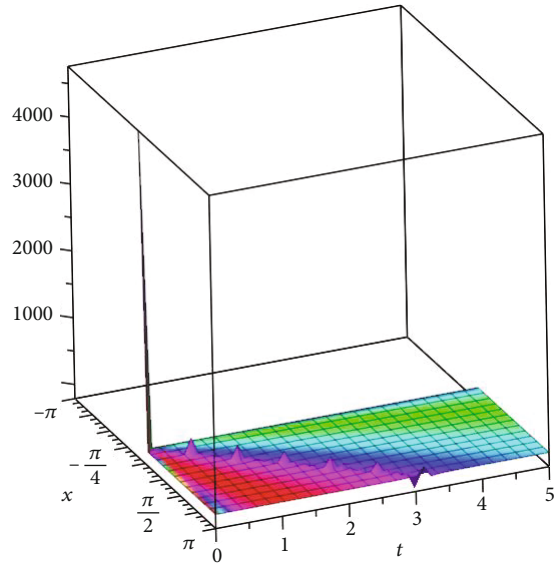

Figure 5: Graphical representation of solution $u_2(x, y, t)$ given by (23) for $t = 0..5, x = -\pi..\pi$, for $\alpha = 0.5$.

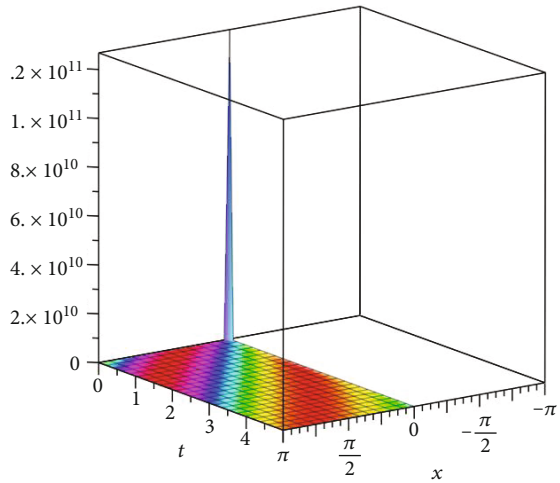

Figure 6: Graphical representation of solution $u_2(x, y, t)$ given by (23) for $t = 0..5, x = -\pi..\pi$, for $\alpha = 0.2$.

And dark singular soliton is

$$u_6(x, y, t) = \left[\frac{\sqrt{2a^2 - 2d^2 + \sigma^2 + 4b - 1}}{4} \coth\left(\left(\frac{1}{\alpha}\right)x^\alpha + \left(\frac{\mu}{\alpha}\right)y^\alpha - \left(\frac{\sigma}{\alpha}\right)t^\alpha\right) + \frac{\sqrt{2a^2 - 2d^2 + 4b}}{2}\right] \exp \cdot \left(i\left(\left(\frac{a}{\alpha}\right)x^\alpha + \left(\frac{b}{\alpha}\right)y^\alpha + \left(\frac{d}{\alpha}\right)t^\alpha + \theta_0\right)\right). \quad (29)$$

In Figures 1–9, we see that the graphs of the answers are very similar and the only difference is in the degree of oscillation of the graph.

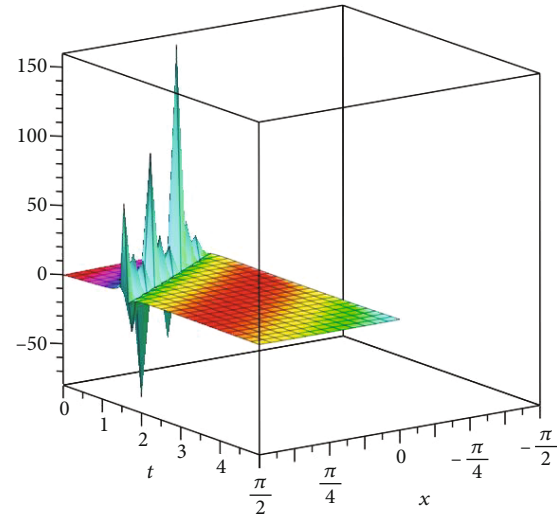

Figure 7: Graphical representation of solution $u_6(x, y, t)$ given by (29) for $t = 0..5, x = -\pi..\pi$, for $\alpha = 0.8$.

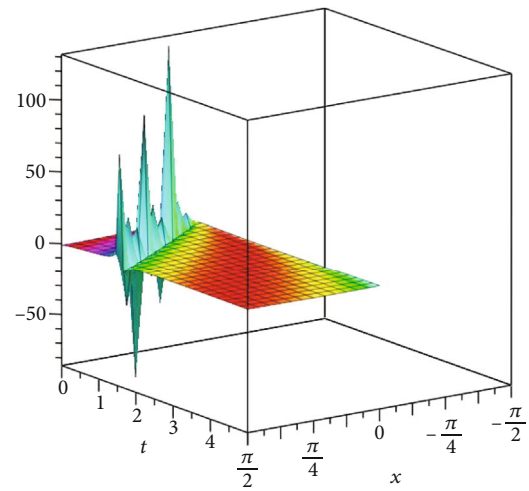

Figure 8: Graphical representation of solution $u_6(x, y, t)$ given by (29) for $t = 0..5, x = -\pi..\pi$, for $\alpha = 0.5$.

5. Concluding Remarks

In this study, some new solitary exact solutions of the hyperbolic Schrödinger equation are obtained with the aid of an efficient analytic method. The structure considered for the equation consists of a series of arbitrary parameters that lead to many well-known models by considering certain options for them. One of the main advantages of this method is the determination of different categories of solutions for the equation in a single framework; this means that the method can determine different types of solutions for the equation in a single process. Furthermore, one can easily deduce that the methods used in this study are very simple but very efficient methodologies for solving NPDEs. We have performed all necessary calculations for obtaining and plotting Figures 1–9 through the implementation of the symbolic computations in Mathematica software.

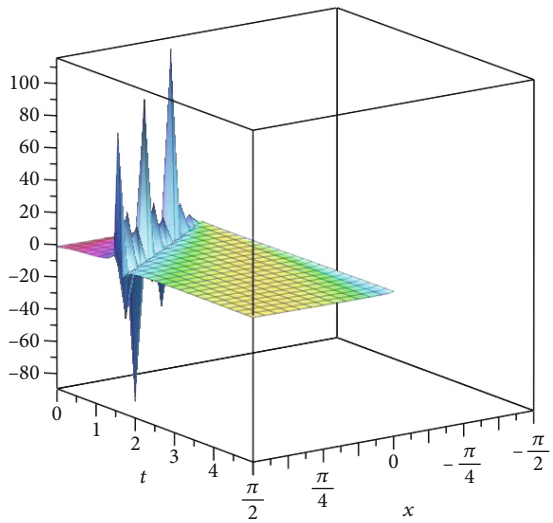

FIGURE 9: Graphical representation of solution $u_6(x, y, t)$ given by (29) for $t = 0..5, x = -\pi..\pi$, for $\alpha = 0.2$.

Data Availability

No data were used to support this study.

Conflicts of Interest

The author declares no conflicts of interest.

References

[1] A. Biswas, "Chirp-free bright optical soliton perturbation with Fokas-Lenells equation by traveling wave hypothesis and semi-inverse variational principle," *Optik*, vol. 170, pp. 431–435, 2018.

[2] A. Biswas, M. Ekici, A. Sonmezoglu, and R. T. Alqahtani, "Optical soliton perturbation with full nonlinearity for Fokas-Lenells equation," *Optik*, vol. 165, pp. 29–34, 2018.

[3] A. Biswas and S. Arshed, "Optical solitons in presence of higher order dispersions and absence of self- phase modulation," *Optik*, vol. 174, pp. 452–459, 2018.

[4] S. W. McCue, M. El-Hachem, and M. J. Simpson, "Exact sharp-fronted travelling wave solutions of the Fisher-KPP equation," *Applied Mathematics Letters*, vol. 114, p. 106918, 2021.

[5] A. Neirameh, "Nonlinear evolution equations and their analytical and numerical solutions," *Advances in Mathematical Physics*, vol. 2021, Article ID 5538516, 2021.

[6] A. Kurt, H. Rezazadeh, M. Senol, A. Neirameh, O. Tasbozan, and M. Eslami, "Two effective approaches for solving fractional generalized Hirota-Satsuma coupled KdV system arising in interaction of long waves," *Journal of Ocean Engineering and Science*, vol. 4, no. 1, pp. 24–32, 2019.

[7] S. J. Liano, *The proposed homotophy analysis technique for the solution of nonlinear problems*, (Ph.D. thesis), Shanghai Jiao Tong University, 1992.

[8] A. M. Wazwaz, "The variational iteration method for solving linear and nonlinear systems of PDEs," *Computers & Mathematics with Applications*, vol. 54, no. 7-8, pp. 895–902, 2007.

[9] J. H. He and X. H. Wu, "Exp-function method for nonlinear wave equations," *Chaos, Solitons and Fractals*, vol. 30, no. 3, pp. 700–708, 2006.

[10] N. A. Kudryashov and P. N. Ryabov, "Analytical and numerical solutions of the generalized dispersive Swift- Hohenberg equation," *Mathematics of Computation*, vol. 286, pp. 171–177, 2016.

[11] J. Manafian, M. Fazli Aghdaei, M. Khalilian, and R. S. Jeddi, "Application of the generalized G'/G-expansion method for nonlinear PDEs to obtaining soliton wave solution," *Optik*, vol. 135, pp. 395–406, 2017.

[12] A. Biswas, M. Ekici, A. Sonmezoglu, A. S. Alshomrani, and M. R. Belic, "Optical solitons with Kudryashov's equation by extended trial function," *Optik*, vol. 202, p. 163290, 2020.

[13] N. Sajid and G. Akram, "Novel solutions of Biswas-Arshed equation by newlyϕ^6-model expansion method," *Optik*, vol. 211, article 164564, 2020.

[14] B. Ghanbari, S. Kumar, M. Niwas, and D. Baleanu, "The Lie symmetry analysis and exact Jacobi elliptic solutions for the Kawahara-KdV type equations," *Results in Physics*, vol. 23, p. 104006, 2021.

[15] K. Hosseini, Z. Ayati, and R. Ansari, "New exact traveling wave solutions of the Tzitzeica type equations using a novel exponential rational function method," *Optik*, vol. 148, pp. 85–89, 2017.

[16] S. M. Ege and E. Misirli, "The modified Kudryashov method for solving some fractional-order nonlinear equations," *Advances in Difference Equations*, vol. 2014, no. 1, 3 pages, 2014.

[17] H. Rezazadeh, A. Neirameh, M. Eslami, A. Bekir, and A. Korkmaz, "A sub-equation method for solving the cubic–quartic NLSE with the Kerr law nonlinearity," *Modern Physics Letters B*, vol. 33, no. 18, article 1950197, 2019.

[18] H. Rezazadeh, M. Mirzazadeh, S. M. Mirhosseini-Alizamini, and A. Neirameh, "Optical solitons of Lakshmanan-Porsezian-Daniel model with a couple of nonlinearities," *Optik*, vol. 164, pp. 414–423, 2018.

[19] H. Rezazadeh, D. Kumar, A. Neirameh, M. Eslami, and M. Mirzazadeh, "Applications of three methods for obtaining optical soliton solutions for the Lakshmanan-Porsezia-Daniel model with Kerr law nonlinearity," *Pramana*, vol. 94, no. 1, pp. 1–11, 2020.

[20] A. Biswas, M. Asma, P. Guggilla et al., "Optical soliton perturbation with Kudryashov's equation by semi-inverse variational principle," *Physics Letters A*, vol. 384, no. 33, p. 126830, 2020.

[21] Y. Shi, M. Pana, and D. Peng, "Replicator dynamics and evolutionary game of social tolerance: the role of neutral agents," *Economics Letters*, vol. 159, pp. 10–14, 2017.

[22] A. Biswas, M. Ekici, A. Sonmezoglu et al., "Chirped optical solitons of Chen-Lee-Liu equation by extended trial equation scheme," *Optik*, vol. 156, pp. 999–1006, 2018.

[23] A. Biswas, Y. Yildrim, E. Yasar, Q. Zhou, S. P. Moshokoa, and M. Belic, "Sub pico-second pulses in mono-mode optical fibers with Kaup-Newell equation by a couple of integration schemes," *Optik*, vol. 167, pp. 121–128, 2018.

[24] A. Biswas, M. Ekici, A. Sonmezoglu, and R. T. Alqahtani, "Sub-pico-second chirped optical solitons in mono-mode fibers with Kaup-Newell equation by extended trial function method," *Optik*, vol. 168, pp. 208–216, 2018.

[25] A. Biswas, "Stochastic perturbation of optical solitons in Schrodinger-Hirota equation," *Optics Communication*, vol. 239, no. 4–6, pp. 461–466, 2004.

[26] S. U. Rehman, A. R. Seadawy, M. Younis, S. T. R. Rizvi, T. A. Sulaiman, and A. Yusuf, "Computing wave solutions and conservation laws of conformable time-fractional Gardner and Benjamin–Ono equations," *Pramana*, vol. 95, p. 43, 2021.

[27] M. Alquran, I. Jaradat, A. Yusuf, and T. A. Sulaiman, "Heart-cusp and bell-shaped-cusp optical solitons for an extended two-mode version of the complex Hirota model: application in optics," *Optical and Quantum Electronics*, vol. 53, p. 26, 2021.

[28] A. Yusuf, "Symmetry analysis, invariant subspace and conservation laws of the equation for fluid flow in porous media," *International Journal of Geometric Methods in Modern Physics*, vol. 17, no. 12, p. 2050173, 2020, (14 pages).

[29] S. Kumar, A. Kumar, and H. Kharbanda, "Abundant exact closed-form solutions and solitonic structures for the double-chain deoxyribonucleic acid (DNA) model," *Brazilian Journal of Physics volume*, vol. 51, no. 4, pp. 1043–1068, 2021.

[30] S. Kumar, D. Kumar, and A. Kumar, "Lie symmetry analysis for obtaining the abundant exact solutions, optimal system and dynamics of solitons for a higher-dimensional Fokas equation," *Chaos Soliton & Fractals*, vol. 142, no. 110507, p. 110507, 2021.

[31] S. Kumar and D. Kumar, "Lie symmetry analysis and dynamical structures of soliton solutions for the (2 + 1)-dimensional modified CBS equation," *International Journal of Modern Physics B*, vol. 34, no. 25, article 2050221, 2020.

[32] B. Kilic and M. Inc, "Soliton solutions for the Kundu-Eckhaus equation with the aid of unified algebraic and auxiliary equation expansion methods," *Journal of Electromagnetic Waves and Applications*, vol. 30, no. 7, pp. 871–879, 2016.

[33] M. Inc, E. Ates, and F. Tchier, "Optical solitons of the coupled nonlinear Schrödinger's equation with spatiotemporal dispersion," *Nonlinear Dynamics*, vol. 85, no. 2, pp. 1319–1329, 2016.

[34] F. Tchier, E. C. Aslan, and M. Inc, "Optical solitons in parabolic law medium: Jacobi elliptic function solution," *Nonlinear Dynamics*, vol. 85, no. 4, pp. 2577–2582, 2016.

[35] K. L. Khalid, A. M. Wazwaz, M. S. Mehanna, and M. S. Osman, "On short-range pulse propagation described by (2+1)-dimensional Schrödinger's hyperbolic equation in nonlinear optical fibers," *Physica Scripta*, vol. 95, no. 7, article 075203, 2020.

Hindawi
Advances in Mathematical Physics
Volume 2021, Article ID 9113423, 7 pages
https://doi.org/10.1155/2021/9113423

Research Article

Lie Symmetry Analysis of $C_1(m, a, b)$ Partial Differential Equations

Hengtai Wang,[1] Aminu Ma'aruf Nass,[2] and Zhiwei Zou[1]

[1]*School of Mathematics and Physics, University of South China, Hengyang, 421001 Hunan, China*
[2]*Department of Actuarial Science, Federal University, Dutse, P.M.B 7156 Jigawa State, Nigeria*

Correspondence should be addressed to Aminu Ma'aruf Nass; aminu.nass@fud.edu.ng

Received 16 April 2021; Revised 11 June 2021; Accepted 9 August 2021; Published 25 August 2021

Academic Editor: Sachin Kumar

In this article, we discussed the Lie symmetry analysis of $C_1(m, a, b)$ fractional and integer order differential equations. The symmetry algebra of both differential equations is obtained and utilized to find the similarity reductions, invariant solutions, and conservation laws. In both cases, the symmetry algebra is of low dimensions.

1. Introduction

In the last century, fractional partial differential equations (FPDEs) have played important rules in the fields of science and engineering, for instance, physics, chemistry, biology, andcontrol theory. Recently, those class of differential equations has also attracted much more interest of mathematicians and physicists [1–6].

Finding the best methods of obtaining the exact solutions of differential equations remains one of the unanswered questions in the field. Many approaches have been developed by mathematicians to study the solutions of PFDEs, such as Adomian decomposition method, the fractional subequation method, numerical method, the first integral method, and Lie symmetry method [7–14]. In this article, we consider one of the powerful techniques of solving and analyzing differential equations, i.e., the Lie symmetry method. The Lie symmetry method is widely used to transformed partial differential equations (PDEs) into ordinary differential equations (ODEs), and the ODE is later solve numerically or analytically using similarity invariant [7, 9, 10, 12, 14–22]. Lie symmetry is also utilized in obtaining the conservation laws (Cls) [23]. The method developed by Noether theorem [24] and Ibraginov's [25] is one of the best and simplest methods of evaluating Cls of differential equations.

Consider general forms of fractional differential equations:

$$\frac{\partial^\alpha u}{\partial t^\alpha} = F[u], \tag{1}$$

where $u = u(x, t)$ denotes the unknown function, and $F[u] = F(x, u, u_x, u_{xx}, \cdots)$ is a known function. The fractional order α is a real number and $\partial^\alpha u/\partial t^\alpha$ denotes Riemann-Liouville(R-L) derivative defined in [1, 3, 26] as

$$D_t^\alpha u = \begin{cases} \dfrac{\partial^n u}{\partial t^n}, \alpha = n \in \mathbb{N}, \\ \dfrac{1}{\Gamma(n-\alpha)} \dfrac{\partial^n}{\partial t^n} \displaystyle\int_0^t \frac{u(\tau, x)}{(t-\tau)^{\alpha+1-n}} d\tau, n-1 < a < n, n \in \mathbb{N}, \end{cases} \tag{2}$$

where $\Gamma(x)$ denotes the standard gamma function defined by

$$\Gamma(x) = \int_0^\infty e^{-t} t^{x-1} dt. \tag{3}$$

The $C_N(m,a,b)$ partial differential equations

$$u_t + (u^m)_x + \frac{1}{b}\left[u^a \nabla^2 u^b\right]_x = 0, m > 1, 1 < n = a + b, \quad (4)$$

where N denotes the spatial dimension , have been introduced in [27]. In particular, if $N = 1$, it becomes

$$u_t + (u^m)x + \frac{1}{b}\left[u^a\left(u^b\right)xx\right]x = 0, \quad (5)$$

which is equivalent to

$$\begin{aligned} u_t &+ mu^{m-1}u_x + (b-1)(a+b-2)u^{a+b-3}u_x^3 \\ &+ (a+3b-3)u^{a+b-2}u_x u_{xx} + u^{a+b-1}u_{xxx} = 0. \end{aligned} \quad (6)$$

Therefore, the fractional form of $C_1(m,a,b)$ differential equation is define as

$$\begin{aligned} \frac{\partial^\alpha u}{\partial t^a} &= -mu^{m-1}u_x - (b-1)(a+b-2)u^{a+b-3}u_x^3 \\ &- (a+3b-3)u^{a+b-2}u_x u_{xx} - u^{a+b-1}u_{xxx}, \end{aligned} \quad (7)$$

where $\partial^a u/\partial t^a$ is given by (2).

2. Lie Symmetries of Eq. (6)

In this section, we first consider the Lie symmetry analysis of Eq.(6). To obtained the Lie symmetry analysis, we first consider a one-parameter Lie group of transformations

$$\begin{aligned} \bar{x} &= x + \varepsilon\xi(x,t,u) + O\left(\varepsilon^2\right), \\ \bar{t} &= t + \varepsilon\tau(x,t,u) + O\left(\varepsilon^2\right), \\ \bar{u} &= u + \varepsilon\varphi(x,t,u) + O\left(\varepsilon^2\right), \end{aligned} \quad (8)$$

with a small parameter $\varepsilon \ll 1$. The vector field associated with the one-parameter group of transformation is

$$V = \xi(x,t,u)\frac{\partial}{\partial x} + \tau(x,t,u)\frac{\partial}{\partial t} + \phi(x,t,u)\frac{\partial}{\partial u}. \quad (9)$$

Thus, expanding the infinitesimals generator to include the transformation of the derivatives, we obtained the following third prolongation $pr^{(3)}V$

$$\boldsymbol{pr}^{(3)}V = V + \phi^x\frac{\partial}{\partial u_x} + \phi^t\frac{\partial}{\partial u_t} + \phi_{xx}\frac{\partial}{\partial u_{xx}} + \phi^{xxx}\frac{\partial}{\partial u_{xxx}}. \quad (10)$$

In (10), ϕ^x, ϕ^t, ϕ^{xx}, and ϕ^{xxx} are all undetermined functions, which are given by the following formulae

$$\phi^x = D_x(\phi - \xi u_x - \tau u_t) + \xi u_{xx} + \tau u_{xt}, \quad (11)$$

$$\phi^t = D_t(\phi - \xi u_x - \tau u_t) + \xi u_{xt} + \tau u_{tt}, \quad (12)$$

$$\phi^{xx} = D_x{}^2(\phi - \xi u_x - \tau u_t) + \xi u_{xxx} + \tau u_{xxt}, \quad (13)$$

$$\phi^{xxx} = D_x^2(\phi - \xi u_x - \tau u_t) + \xi u_{xxx} + \tau u_{xxxt}, \quad (14)$$

where D_x and D_t represent the total derivatives with respect to x and t, respectively. e refers the reader(s) to [28] for details of how to evaluate the prolongation formulae.

If the vector field (9) forms a symmetry of Eq.(6), the infinitesimal generator V must satisfy the following invariance criterion for Eq.(6), given as

$$pr^{(3)}V(\Delta)\Big|_{\Delta=0} = 0, \quad (15)$$

where

$$\begin{aligned} \Delta = u_t &+ mu^{m-1}u_x + (b-1)(a+b-2)u^{a+b-3}u_x^3 \\ &+ (a+3b-3)u^{a+b-2}u_x u_{xx} + u^{a+b-1}u_{xxx}. \end{aligned} \quad (16)$$

Substituting Eqs. (11)–(14) into Eq. (15) and equating the coefficients of various powers of partial derivatives of u to zero, an overdetermined system of equations known as determining equations is obtained. Solving the determining equations the following infinitesimals for $C_1(m,a,b)$ has been derived

$$\begin{aligned} \xi(x,t,u) &= pc_1x + c_2, \\ \tau(x,t,u) &= qc_1t + c_3, \\ \phi(x,t,u) &= c_1u, \end{aligned} \quad (17)$$

where c_1, c_2, and c_3 are arbitrary constants, and throughout this paper, we denote

$$p = \frac{a+b-m}{2}, q\frac{a+b-3m+2}{2}. \quad (18)$$

Therefore, we have the following conclusion.

Theorem 1. *For the arbitrary parameters m, a, b, if $m > 1$, $a + b > 1$, the vector field admitted by the differential equation (6) is*

$$V_1 = \partial_x,\ V_2 = \partial_t,\ V_3 = px\partial_x + qt\partial_t + u\partial_u. \quad (19)$$

The sketch of the proof has been stated above. In details, we should divide it into the following four cases. Obviously, the vector fields of each case are the special cases of (19)

(i) If $a + b = 2$, $a + 3b \neq 3$, the vector field is

$$V_1 = \partial_x, V_2 = \partial_t, V_3 = \left(1 - \frac{m}{2}\right)x\partial_x + \left(2 - \frac{3m}{2}\right)t\partial_t + u\partial_u \quad (20)$$

(ii) If $a + b = 2$, $a + 3b = 3$, the vector field is the same as (i)

(iii) If $a+b\neq 2$, $a+3b=3$, the vector field is

$$V_1=\partial_x,\ V_2=\partial_t,\ V_3=px\partial_x+qt\partial_t+u\partial_u \tag{21}$$

(iv) If $a+b\neq 2$, $a+3b\neq 3$, $b\neq 1$, the vector field is the same as (iii).

The vector fields V_1, V_2, and V_3 form a Lie algebra under the following Lie bracket

$$\left[f\partial_i, g\partial_j\right]=f\partial_i(g)\partial_j-g\partial_j(f)\partial_i, \tag{22}$$

where i and j stand for x, t, u.

That is to say

$$[V_1,V_2]=0,\quad [V_1,V_3]=pV_3,\quad [V_2,V_3]=qV_3. \tag{23}$$

By solving the following ordinary differential equations with the initial conditions:

$$\begin{aligned}\frac{dx^*}{d\varepsilon}&=\xi(x^*,t^*,u^*),\ x^*|_{\varepsilon=0}=x,\\ \frac{dt^*}{d\varepsilon}&=\tau(x^*,t^*,u^*),\ t^*|_{\varepsilon=0}=t,\\ \frac{du^*}{d\varepsilon}&=\phi(x^*,t^*,u^*),\ u^*|_{\varepsilon=0}=u.\end{aligned} \tag{24}$$

We therefore obtain the group transformation which is generated by infinitesimal generators V_1, V_2, V_3, respectively

$$G_1:(x,t,u)\mapsto(x+\varepsilon,t,u), \tag{25}$$

$$G_2:(x,t,u)\mapsto(x,t+\varepsilon,u), \tag{26}$$

$$G_3:(x,t,u)\mapsto(e^{p\varepsilon}x,e^{q\varepsilon}t,e^{\varepsilon}u). \tag{27}$$

Remark 2. In (25)–(27), an arbitrary element in $G_i(i=1,2,3)$ can transfer one solution of Eq. (6) to another one, so do the products of the elements from G_1, G_2, and G_3.

Remark 3. The Lie group $G_1\times G_2$ is a normal Lie subgroup of $G_1G_2G_3$. The Lie algebra generated by V_1 and V_2 is an ideal of L.

Theorem 4. *If $u=f(x,t)$ is a solution of Eq. (1.3), then $u^{(1)}$, $u^{(2)}$, and $u^{(3)}$ as follows are solutions of Eq. (6) as well.*

$$\begin{aligned}u^{(1)}&=f(x-\varepsilon,t),\\ u^{(2)}&=f(x,t-\varepsilon),\\ u^{(3)}&=e^{\varepsilon}f(e^{-p\varepsilon}x,e^{-q\varepsilon}t).\end{aligned} \tag{28}$$

3. Similarity Reductions to Eq. (6)

In the preceding section, we obtained the group symmetry analysis of Eq. (6). In this section, the characteristic equations of vector fields are obtained by making use of (19) and utilized to perform the symmetry reduction.

For $V=V_1$, the characteristic equation can be presented as follows:

$$\frac{dx}{1}=\frac{dt}{0}=\frac{du}{0}. \tag{29}$$

Solving the characteristic equation (29), we have $u=f(\xi)$, where $\xi=t$ which yields a trivial solution.

For $V=V_2$, the characteristic equation can be expressed as follows:

$$\frac{dx}{0}=\frac{dt}{1}=\frac{du}{0}, \tag{30}$$

from which we have $u=f(\xi)$, where $\xi=x$ which transformed (6) to an ODE

$$\begin{aligned}&m^{fm-1}f'+(b-1)(a+b-2)f^{a+b-3}f'^3\\ &\quad+(a+3b-3)f^{a+b-2}f'f''+f^{a+b-1}f'''=0.\end{aligned} \tag{31}$$

For $V=V_3$, the characteristic equation can be written as follows:

$$\frac{dx}{px}=\frac{dt}{qt}=\frac{du}{u}. \tag{32}$$

Solving the characteristic equation, we have the following invariants $\xi=xt^{-p/q}$, $u=t^{1/q}f(\xi)$, which transformed (6) to an ODE

$$\begin{aligned}&\frac{1}{q}t^{\frac{1}{q}-1}f-\frac{p}{q}\left(xt^{-\frac{p}{q}}\right)t^{\frac{1}{q}-1}-f'+mt^{\frac{p}{q}-1}f^{m-1}f'\\ &\quad+(b-1)(a+b-2)t^{\frac{a+b-2m}{q}}f^{a+b-3}f'^3\\ &\quad+(a+3b-3)t^{\frac{a+b-3p}{q}}f'f''+t^{\frac{a+b-3p}{q}}f'f''\\ &\quad+t^{\frac{a+b-3p}{q}}f^{a+b-1}f'''=0.\end{aligned} \tag{33}$$

4. Nonlinear Self-Adjointness of Eq. (6)

In this section, we shall show that Eq. (6) is nonlinearly self-adjoint. Let it start by presenting the definitions of nonlinear self-adjointness of differential equations according to Ibragimov's [13, 25].

Definition 5. Given a differential function F and the new dependent variable $v=v(x)$ known as the adjoint variable or local variable [13, 25], the formal Lagrangian for the differential equation $F=0$ is the differential function given by

$$F^*:=vF. \tag{34}$$

Definition 6. [25]. The differential equation (6) is said to be nonlinearly selfadjoint if there exists a substitution

$$\mathrm{v} = \phi(\mathrm{x}, \mathrm{t}, \mathrm{u}) \neq 0, \tag{35}$$

such that

$$F^*\Big|_{v=\varphi(x,t,u)} = \lambda F, \tag{36}$$

for some undermine function λ.

Theorem 7. *The differential equation (6) is self-adjoint.*

Proof. The formal Lagrangian is

$$\begin{aligned}\mathscr{L} = v\Big(&u_t + mu^{m-1}u_x + (b-1)(a+b-2)u^{a+b-3}u_x^3 \\ &+ (a+3b-3)u^{a+b-2}u_x u_{xx} + u^{a+b-1}u_{xxx}\Big).\end{aligned} \tag{37}$$

Substituting into $(36) = 0$, we have the adjoint equation to Eq. (6)

$$\begin{aligned}&-mu^{m-1}v_{x-a}(a+b-2)u^{a+b-3}v_x u_x^2 - 2au^{a+b-2}v_x u_{xx} \\ &\quad - v_t - 2au^{a+b-2}v_{xx}u_x - u^{a+b-1}v_{xxx} = 0.\end{aligned} \tag{38}$$

Let $v = \phi(x, t, u)$ and the left hand of (38) be $\lambda \cdot \Delta$, we shall get $\lambda = -\varphi_u$, and

$$\begin{cases}\varphi = c_1 u + c_2, b = a+1, \\ \varphi = c_3 u^{b-a-1}, b \neq a+1.\end{cases} \tag{39}$$

Then, we prove that Eq. (6) is self-adjoint. □

Generally speaking, we are now to calculate the conserved vectors. However, by using the method of Ibragimov [25], so we here omit the process.

5. Lie Symmetry and Reductions of Eq. (7)

In this section, we deal with all of the point symmetries of Eq. (7). We now assume that $n-1 < \alpha < n$ in this section. Thus, Eq. (1.4) is an FPDE with the infinitesimal generator given by (2.2). If the vector field (9) generates a symmetry of Eq. (7), then V must satisfy the following Lie symmetry condition:

$$pr^{(3)}V(\Delta_1)\Big|_{\Delta_1=0} = 0, \tag{40}$$

where

$$\begin{aligned}\Delta_1 = &\frac{\partial^\alpha u}{\partial t^\alpha} + mu^{m-1}u_x + (b-1)(a+b-2)u^{a+b-3}u_x^3 \\ &+ (a+3b-3)u^{a+b-2}u_x u_{xx} + u^{a+b-1}u_{xxx}.\end{aligned} \tag{41}$$

Also, the invariant condition yields [29]

$$\tau(x, t, u)\big|_{t=0} = 0, \tag{42}$$

and the αth extended infinitesimal related to Riemann-Liouville fractional time derivative with (42) is given by [30, 31].

$$\begin{aligned}\phi_\alpha^0 = &\frac{\partial^\alpha \phi}{\partial t^\varphi} + (\phi u - \alpha D_t(\tau))\frac{\partial^\alpha u}{\partial t^\alpha} - u\frac{\partial^\alpha \phi_u}{\partial t^\alpha} + \mu \\ &- \sum_{n-1}^{\infty}\binom{\alpha}{n}D_t^n(\xi)D_t^{\alpha-n}(u_x) \\ &+ \sum_{n-1}^{\infty}\left[\binom{\alpha}{n}\frac{\partial^\alpha \phi_u}{\partial t^\alpha} - \binom{\alpha}{n+1}D_t^{n+1}(\tau)\right]D_t^{\alpha-n}(u),\end{aligned} \tag{43}$$

where

$$\begin{aligned}\mu = &\sum_{n=2}^{\infty}\sum_{m=2}^{n}\sum_{k=2}^{m}\sum_{r=0}^{k-1}\binom{\alpha}{n}\binom{n}{m}\binom{k}{r}\frac{1}{k!}\frac{t^{n-\alpha}}{\Gamma(n+1-\alpha)} \\ &\cdot [-u]^{n-\alpha}\frac{\partial}{\partial t^m} \times \left[u^{k-r}\right]\frac{\partial^{n-m+k}\phi}{\partial t^{n-m}\partial u^k}.\end{aligned} \tag{44}$$

The expression of μ is complicated; however, it should converges to zero when the infinitesimal φ is linear in u, because of the existence of the derivatives $\partial^{n-m+k}/\partial t^{n-m}\partial u^k$, $k \geq 2$ in the above expression (44).

Thus, the Lie group classification method for the FPDE leads to the following result.

Theorem 8. *The infinitesimal symmetry group of the equation (7) is spanned by the two vector fields*

$$V_1 = \partial_x \quad V_2 = px\partial_x + \frac{1}{\alpha}qt\partial_t + u\partial_u. \tag{45}$$

Proof. Considering the invariance criterion (40), we have

$$\begin{aligned}&\phi_\alpha^0 + m(m-1)u^{m-2}\phi u_x + mu^{m-1}\phi^x + (b-1)(a+b-2) \\ &\quad \cdot (a+b-3)u^{a+b-4}\phi u_x^3 + 3(b-1)(a+b-2)u^{a+b-3}\phi^x u_x^2 \\ &\quad + (a+3b-3)(a+b-2)u^{a+b-3}\phi u_x u_{xx} + (a+3b-3)\phi^x_{u_{xx}} \\ &\quad + (a+3b-3)\phi^{xx}u_x + (a+b-1)\phi u^{a+b-2}u_{xxx} + u^{a+b-1}\phi^{xxx} = 0\end{aligned} \tag{46}$$

solving the determining equation (46), and we obtained the following infinitesimals

$$\begin{aligned}\xi(x, t, u) &= pc_1 x + c_2, \\ \tau(x, t, u) &= \frac{1}{\alpha}qc_1 t, \\ \phi(x, t, u) &= c_1 u,\end{aligned} \tag{47}$$

which follows that the fractional differential equation (7) admitted two dimensional symmetries and is spanned by (45). □

Next, we utilized the admitted Lie symmetry and perform similarity reductions, present the reduced nonlinear fractional ordinary differential equations (FODEs), and classify the corresponding group-invariant solutions of the fractional $C_1(m, a, b)$.

Case 9. For $V_1 = \partial/\partial x$, the characteristic equation is

$$\frac{dx}{1} = \frac{dt}{0} = \frac{du}{0}, \tag{48}$$

and the following similarity variables are obtained by solving the characteristic equation $u = f(\zeta)$, $\zeta = t$, which yields the following reduced ODE

$$\partial_t^{\alpha} f(t) = 0. \tag{49}$$

The fractional ODE has a polynomial general group-invariant solution

$$u = a_1 t^{\alpha-1}, \tag{50}$$

where a_1 is an arbitrary constant of integration [6, 15, 16].

Case 10. For $V_2 = px\partial_x + 1/2qt\partial_t + u\partial_u$, the characteristic equation is

$$\frac{dx}{px} = \frac{\alpha dt}{qt} = \frac{du}{u}, \tag{51}$$

and by solving the above equation, we get the group-invariant solution

$$u = t^{\frac{\alpha}{q}} g(\zeta), \zeta = xt^{-\frac{p\alpha}{q}}, \tag{52}$$

where g is an arbitrary function of ζ. Using these invariants, Eq. (7) transforms to a special nonlinear ODE of fractional order. Thus, we have the following theorem corresponding to this case.

Theorem 11. *The transformation (52) reduces (7) to the following nonlinear ordinary differential equation of fractional order with the Erd'elyi-Kober fractional differential operator $P_{\beta}^{\tau,\alpha}$ of order [5]*

$$\left(P_{\beta}^{\tau+\alpha,n-\alpha} g\right) := \prod_{j=0}^{n-1}\left(\tau + j - \frac{1}{\beta}\zeta\frac{d}{d\zeta}\right)\left(K_{\beta}^{\tau,\alpha} g\right)(\zeta), n = \begin{cases} |\alpha| + 1, \alpha \neq \mathbb{N} \\ \alpha, \alpha \in \mathbb{N} \end{cases}, \tag{53}$$

where

$$\left(K_{\beta}^{\tau,\alpha} g\right)(\zeta) := \begin{cases} \dfrac{1}{\Gamma(\alpha)}\displaystyle\int_1^{\infty} (u-1)^{\alpha-1} u^{-u(\tau+\alpha)} g\left(\zeta u^{\frac{1}{\beta}}\right) du, \ \alpha > 0, \\ g(\zeta), \ \alpha = 0. \end{cases} \tag{54}$$

is the Erd'elyi-Kober fractional integral operator.

Proof. Let $n-1 < \alpha < n$, $n = 1, 2, 3, \cdots$, according to the Riemann-Liouville fractional derivative, and one can obtain

$$\frac{\partial^{\alpha} u}{\partial t^{\alpha}} = \frac{\partial^n}{\partial t^n}\left[\frac{1}{\Gamma(n-\alpha)}\int_0^t (t-s)^{n-\alpha-1} s^{\frac{\alpha}{q}} g\left(xs^{-\frac{p\alpha}{q}}\right) ds\right]. \tag{55}$$

Let $v = t/s$, and then $ds = -(t/v^2)dv$;so, (55) can be written as

$$\frac{\partial^{\alpha} u}{\partial t^{\alpha}} = \frac{\partial^n}{\partial t^n}\left[t^{n-\alpha+\frac{\alpha}{q}} \frac{1}{\Gamma(n-\alpha)}\int_1^{\infty} (v-1)^{n-\alpha-1} v^{-\left(n-\alpha+\frac{\alpha}{q}+1\right)} g\left(\zeta v^{\frac{p\alpha}{q}}\right) dv\right]. \tag{56}$$

In view of the Erd'elyi-Kober fractional integral operator (54), one can get

$$\frac{\partial^{\alpha} u}{\partial t^{\alpha}} = \frac{\partial^n}{\partial t^n}\left[t^{n-\alpha+\frac{\alpha}{q}}\left(K_{\frac{q}{p\alpha}}^{1+\frac{\alpha}{q},n-\alpha} g\right)(\zeta)\right]. \tag{57}$$

Therefore, the right hand side of (57) becomes

$$\begin{aligned} \frac{\partial^n}{\partial t^n}\left[t^{n-\alpha+\frac{\alpha}{q}}\left(K_{\frac{q}{p\alpha}}^{1+\frac{\alpha}{q},n-\alpha} g\right)(\zeta)\right] &= \frac{\partial^{n-1}}{\partial t^{n-1}}\left[\frac{\partial}{\partial t}\left(t^{n-\alpha+\frac{\alpha}{q}}\left(K_{\frac{q}{p\alpha}}^{1+\frac{\alpha}{q},n-\alpha} g\right)(\zeta)\right)\right] \\ &= \frac{\partial^{n-1}}{\partial t^{n-1}}\left[t^{n-\alpha+\frac{\alpha}{q}-1}\left(n-\alpha+\frac{\alpha}{q}-1-\frac{p\alpha}{q}\zeta\frac{d}{f\zeta}\right)\left(K_{\frac{q}{p\alpha}}^{1+\frac{\alpha}{q},n-\alpha} g\right)(\zeta)\right]. \end{aligned} \tag{58}$$

Repeating the same procedure $n-1$ times, one can obtain

$$\begin{aligned} \frac{\partial^n}{\partial t^n}\left[t^{n-\alpha+\frac{\alpha}{q}}\left(K_{\frac{q}{p\alpha}}^{1+\frac{\alpha}{q},n-\alpha} g\right)(\zeta)\right] &= t^{-\alpha+\frac{\alpha}{q}} \prod_{j=0}^{n-1} \\ &\cdot \left(1-\alpha+\frac{\alpha}{q}+j-\frac{p\alpha}{q}\zeta\frac{d}{d\zeta}\right)\left(K_{\frac{q}{p\alpha}}^{1+\frac{\alpha}{q},n-\alpha} g\right)(\zeta). \end{aligned} \tag{59}$$

Using the definition of the Erd'elyi-Kober fractional differential operator (53), we get

$$\frac{\partial^n}{\partial t^n}\left[t^{n-\alpha+\frac{\alpha}{q}}\left(K_{\frac{q}{p\alpha}}^{1+\frac{\alpha}{q},n-\alpha} g\right)(\zeta)\right] = t^{-\alpha+\frac{\alpha}{q}}\left(P_{\frac{q}{p\alpha}}^{1-\alpha+\frac{\alpha}{q},\alpha} g\right)(\zeta). \tag{60}$$

Substituting (60) into (57), we obtain an expression for the time fractional derivative

$$\frac{\partial^{\alpha} u}{\partial t^{\alpha}} = t^{-\alpha+\frac{\alpha}{q}}\left(P_{\frac{q}{p\alpha}}^{1-\alpha+\frac{\alpha}{q},\alpha} g\right)(\zeta). \tag{61}$$

Thus, the fractional $C_1(m,a,b)$ equation (7) can be reduced into a fractional order.

ODE:

$$\left(P^{1-\alpha+\frac{q}{q'},\alpha}_{\frac{q}{p\alpha}}g\right)(\zeta) = -mg^{m-1}g_\zeta - (b-1)(a+b-2)g^{a+b-3}g_\zeta^3 - (a+3b-3)g^{a+b-2}g_\zeta^3 - (a+3b-3)g^{a+b-2}g_\zeta u_{\zeta\zeta} - g^{a+b-1}g_{\zeta\zeta\zeta}. \tag{62}$$

□

6. Conservation Law of Eq. (7)

In this section, we will construct the conservation laws of the fractional $C_1(m,a,b)$ differential equation (7).

Let $\mathscr{L}$ be the formal Lagrangian of Eq. (7) written as $\mathscr{L} = v\Delta_1$, where $v = v(x,t)$ is the new introduced dependent variable; so, the adjoint equation of (1.4) is written as $\delta\mathscr{L}/\delta u = 0$, where $\delta/\delta u$ is the Euler-Lagrange operator with respect to u and defined by

$$\frac{\delta}{\delta u} = \frac{\partial}{\partial u} + (D_t^\alpha)^* \frac{\partial}{\partial D_t^\alpha u} + \sum_{k=1}^{\infty}(-1)^k D_{i_1}D_{i_2}\cdots D_{i_k}\frac{\partial}{\partial_{u_1 i_2\cdots i_k}}, \tag{63}$$

and $(D_t^\alpha)^*$ is the adjoint operator of D_t^α. For Riemann-Liouville fractional differential operators, we have

$$(D_t^\alpha)^* = (-1)^n I_r^{n-\alpha}(D_t^n) = \sum\nolimits_t^C D_r^\alpha, \tag{64}$$

where

$$I_r^{n-\alpha}(D_t^n) = \frac{1}{\Gamma(n-\alpha)}\int_t^r (\tau - t)^{n-\alpha-1} f(x,\tau)d\tau,\ n = [\alpha] + 1 \tag{65}$$

is the right-sided fractional integral operators of order α.

In this case, the formal Lagrangian of Eq. (7) is written as

$$\mathscr{L} = v(x,t)\left[\frac{\partial^\alpha u}{\partial t^\alpha} + mu^{m-1}u_x + (b-1)(a+b-2)u^{a+b-3}u_x^3 + (a+3b-3)u^{a+b-2}u_x u_{xx} + u^{a+b-1}u_{xxx}\right]. \tag{66}$$

Every Lie point symmetry (45) admitted by the Eq. (7) leads to a conservation law $D_i(C^i) = 0$ where the components C^i constructed by the following formula [5, 32]:

$$C^t = \sum_{k=0}^{n-1}(-1)^k D_t^{\alpha-1-k}(W)D^k\frac{\partial\mathscr{L}}{\partial D_t^\alpha u} - J\left(W, D_t^n\frac{\partial\mathscr{L}}{\partial D_t^\alpha u}\right),$$

$$C^x = W\left[\frac{\partial\mathscr{L}}{\partial u_x} - D_x\left(\frac{\partial\mathscr{L}}{\partial u_{xx}}\right) + D_x^2\left(\frac{\partial\mathscr{L}}{\partial u_{xxx}}\right)\right] + D_x(W)\left[\frac{\partial\mathscr{L}}{\partial u_{xx}} - D_x\frac{\partial\mathscr{L}}{\partial u_{xxx}}\right] + D_x^2(W)\frac{\partial\mathscr{L}}{\partial u_{xxx}}, \tag{67}$$

where $W = \phi - \xi u_x - \tau u_t$ and $\mathscr{L}$ are the formal Lagrangian which are written in the symmetric form, and the mixed derivatives J are given by the integral:

$$J(f,g) = \frac{1}{\Gamma(n-\alpha)}\int_0^t\int_t^r f(x,\xi)g(x,\mu)(\mu-\xi)^{n-\alpha-1}d\mu d\xi, \tag{68}$$

for $0 < \alpha < 1$. For other cases, the calculations of conserved vector components are similar. In this case,

$$C^t = D_t^{\alpha-1}(W)\frac{\partial\mathscr{L}}{\partial D_t^\alpha u} - J\left(W, D_t\frac{\partial\mathscr{L}}{\partial D_t^\alpha u}\right). \tag{69}$$

The conserved vector components C^t, C^x are as follows:

$$\begin{aligned} C^t &= D_t^{\alpha-1}(W_i)v - J(W_{i,vt}),\\ C^x &= W_i\Big[mvu^{m-1} + 3(b-1)(a+b-2)u^{a+b-3}vu_x^2 \\ &\quad + (a+3b-3)u^{a+b-2}vu_{xx} - (a+3b-3)(a+b-2).u^{a+b-3}vu_x^2 \\ &\quad - (a+3b-3)u^{a+b-2}v_x u_x - (a+3b-3)u^{a+b-2}vu_{xx} \\ &\quad + (a+b-1)u^{a+b-2}vu_x + u^{a+b-1}v_x + (a+b-1) \\ &\quad \cdot (a+b-2)u^{a+b-3}vu_x^2 + 2(a+b-1)u^{a+b-2}v_x u_x \\ &\quad + (a+b-1)ua^{+b-2}vu_{xx} + u^{a+b-1}v_{xx}] + D_x(W_i) \\ &\quad \cdot \left[(a+3b-3)u^{a+b-2}vu_x - (a+b-1)u^{a+b-2}vu_x - u^{a+b-1}v_x\right] \\ &\quad + D_x^2(W_i)\left(u^{a+b-1}v\right). \end{aligned} \tag{70}$$

where $W_1 = -u_x$, $W_2 = u - pxu_x - (1/\alpha)qtu_t$.

Data Availability

All the data used to support the findings of this study are included within the article.

Conflicts of Interest

The authors declare that this article has no conflicts of interest.

Acknowledgments

The first and third authors are supported by the National Science Foundation of China [Grant No. 11801264], Hunan Provincial Natural Science Foundation of China [Grant Nos. 2019JJ50505, 2019JJ50490, 2019JJ40240], and Scientific Research Foundation of Hunan Province Education Department (Grant No. 18C0455).

References

[1] K. S. Miller and B. Ross, *An Introduction to the Fractional calculus and Fractional Differentialequations*, Wiley, New York, NY, USA, 1993.

[2] K. B. Oldham and J. Spanier, *The Fractional calculus*, Academic Press, London, UK, 1974.

[3] I. Podlubny, *Fractional Differential Equations*, Academic Press, San Diego, CA, USA, 1974.

[4] S. Samko, A. A. Kilbas, and O. Marichev, *Fractional Integrals and Derivatives: Theory Andapplications*, Gordon and Breach Science Publishers, Yverdon, Switzerland, 1993.

[5] V. Kiryakova, *Generalized Fractional Calculus and Applications, Pitman Research Notes in Mathematics Series*, Longman Scientific and Technical, Longma Group, Harlow, UK, 1994.

[6] A. A. Kilbas, "Srivastava H M and Trujillo J. J., theory and applications of fractional differential equations," in *North-Holland Mathematics Studies*, J. V. Mill, Ed., p. 204, Elsevier, Amsterdam, The Netherlands, 2006.

[7] S. Kumar, W. X. Ma, and A. Kumar, "Lie symmetries, optimal system and group-invariant solutions of the (3+1)-dimensional generalized KP equation," *Chinese Journal of Physics*, vol. 69, pp. 1–23, 2021.

[8] M. Wen-Xiu and M. Chen, "Direct search for exact solutions to the nonlinear Schrodinger equation," *Applied Mathematics and Computation*, vol. 215, no. 8, pp. 2835–2842, 2009.

[9] A. M. Nass, K. Mpungu, and R. I. Nuruddeen, "Group classification of space-time fractional nonlinear Poisson equation," *Mathematical Communications*, vol. 24, no. 2, pp. 221–233, 2019.

[10] A. M. Nass and K. Mpungu, "Symmetry analysis of time fractional convection-reaction-diffusionequation with delay," *Results in Nonlinear Analysis*, vol. 2, no. 3, pp. 113–124, 2019.

[11] R. I. Nuruddeen and A. M. Nass, "Exact solitary wave solution for the fractional and classical GEW-Burgers equations: an application of Kudryashov method," *Journal of Taibah University for Science*, vol. 12, no. 3, pp. 23–30, 2018.

[12] Q. Hussain, F. D. Zaman, A. H. Bokhari, and H. A. Kara, "On a study of symmetries and conservation laws of a class of time fractional Schrodinger equations with nonlocal nonlinearities," *Optik*, vol. 224, article 165619, 2020.

[13] G. Loaiza, Y. Acevedo, O. M. L. Duque, and A. G. H. Danilo, "Lie algebra classification, conservation laws, and invariant solutions for a generalization of the Levinson-Smith equation," *International Journal of Differential Equations*, vol. 2021, Article ID 6628243, 2021.

[14] Q. Hussain, F. D. Zaman, and H. A. Kara, "Invariant analysis and conservation laws of time fractional Schrodinger equations," *Optik*, vol. 206, article 164356, 2020.

[15] A. M. Nass, "Lie symmetry analysis and exact solutions of fractional ordinary differential equations with neutral delay," *Applied Mathematics and Computation*, vol. 347, pp. 370–380, 2019.

[16] A. M. Nass, "Symmetry analysis of space-time fractional Poisson equation with a delay," *Quaestiones Mathematicae*, vol. 42, no. 9, pp. 1221–1235, 2019.

[17] M. Wen-Xiu, "Conservation laws by symmetries and adjoint symmetries," *Discrete & Continuous Dynamical Systems*, vol. 11, no. 4, pp. 707–721, 2018.

[18] L. Kaur and A. M. Wazwaz, "Painlevé analysis and invariant solutions of generalized fifth-order nonlinear integrable equation," *Nonlinear Dyn*, vol. 94, no. 4, pp. 2469–2477, 2018.

[19] L. Kaur and A. Wazwaz, "Einstein's vacuum field equation: Painlevé analysis and lie symmetries," *Waves in Random and Complex Media*, vol. 31, no. 2, pp. 199–206, 2021.

[20] L. Kuar and R. K. Gupta, "Some invariant solutions of field equations with axial symmetry forempty space containing an electrostatic field," *Applied Mathematics and Computation*, vol. 15, article 560565, 2014.

[21] A. Wazwaz and L. Kuar, "Complex simplified Hirota's forms and lie symmetry analysis for multiple real and complex soliton solutions of the modified KdV-Sine-Gordon equation," *Nonlinear Dynamics*, vol. 95, no. 3, pp. 2209–2215, 2019.

[22] V. Kumar, L. Kaur, A. Kumar, and M. E. Koksal, "Lie symmetry based-analytical and numerical approach for modified Burgers-KdV equation," *Results in Physics*, vol. 8, pp. 1136–1142, 2018.

[23] P. J. Olver, *Application of Lie Groups to Differential Equations*, Springer-Verlag, New York, NY, USA, 1993.

[24] E. Noether, "Invariante variations probleme," *Transport Theory and Statistical Physics*, vol. 1, no. 3, article 186C207, 1971.

[25] N. H. Ibragimov, "A new conservation theorem," *Journal of Mathematical Analysis and Applications*, vol. 333, no. 1, pp. 311–328, 2007.

[26] K. Diethelm, *The analysis of fractional differential equations: An application-oriented exposition using differential operators of Caputo type*, Springer Science & Business Media, 2010.

[27] A. Zilburg and P. Rosenau, "On Hamiltonian formulations of the $C_1(m,a,b)$ equations," *Physics Letters A*, vol. 381, no. 18, pp. 1557–1562, 2017.

[28] E. H. Peter, *Symmetry Methods for Differential Equations*, Cambridge University Press, 2000.

[29] G. W. Wang and T. Z. Xu, "Invariant analysis and exact solutions of nonlinear time fractional Sharma-Tasso-Olver equation by Lie group analysis," *Nonlinear Dynamics*, vol. 76, no. 1, pp. 571–580, 2014.

[30] R. K. Gazizov, A. A. Kasatkin, and S. Y. Lukashcuk, "Continuous transformation groups offractional differential equations," *Vestnik Usatu*, vol. 9, pp. 125–135, 2007.

[31] R. K. Gazizov, A. A. Kasatkin, and S. Y. Lukashchuk, "Symmetry properties of fractional diffusionequations," *Physica Scripta*, vol. T136, pp. 014–016, 2009.

[32] R. K. Gazizov, N. H. Ibragimov, and S. Y. Lukashchuk, "Nonlinear selfadjointness, conservationlaws and exact solutions of time-fractional Kompaneets equations," *Communications in Nonlinear Science and Numerical Simulation*, vol. 23, no. 1-3, pp. 153–163, 2014.

Hindawi
Advances in Mathematical Physics
Volume 2021, Article ID 9971505, 5 pages
https://doi.org/10.1155/2021/9971505

Review Article

Fuzzy Meir-Keeler's Contraction and Characterization

Kianoush Fathi Vajargah [1] **and Hamid Mottaghi Golshan** [2]

[1]*Department of Statistics, Islamic Azad University, Tehran North Branch, Iran*
[2]*Department of Statistics, Islamic Azad University, Shahriar Branch, Iran*

Correspondence should be addressed to Kianoush Fathi Vajargah; fathi_kia10@yahoo.com

Received 19 March 2021; Revised 25 April 2021; Accepted 5 July 2021; Published 28 July 2021

Academic Editor: Mohammad Mirzazadeh

In this study, a fuzzy Meir-Keeler's contraction theorem for complete FMS based on George and Veeramani idea is established. Then, we characterize fuzzy Meir-Keeler's contractions as contractive types induced by functions called fuzzy L-function. Moreover, we show that the converse of it is true. Finally, we bring some examples and corollaries certify our results and new improvement.

1. Introduction

Fixed point theory and related topics are an active research field with a wide range of applications in mathematics, engineering, chemistry, physics, economics, and computer sciences. Many authors have been studied this theory in hyperstructure spaces alongside the classical metric spaces and normed spaces. Among them, it could be cited probabilistic (and fuzzy) metric spaces. The phrase of fuzzy metric space (FMS), introduced by Kramosil and Michalek [1], then George and Veeramani [2], modified this idea which has applications in quantum particle physics [3] and in the two-slit experiment [4, 5]. Also, the theory of FMS is, in this framework, very disparate from the usual theory of metric best approximation and completion, e.g., see [6] and [7–9], respectively. Grabiec [10] developed and extended fixed point theory to probabilistic metric space. Later on, several authors have participated to the growth of this theory (see [10–17]).

In 2006, Lim [18] introduced L-functions (LF) and characterized Meir-Keeler's contractive as a self-map T on M that satisfies $d(T(p), T(q)) < \varphi(d(p, q)), p \neq q \in X$ for some LF φ (see also [19]). This characterization prepares it easy to compare such maps with those satisfying Boyd-Wong's condition (see [20]). Then, Meir-Keeler [21] developed Boyd-Wong's result as follows

$$\forall \varepsilon > 0; \exists \delta > 0, \varepsilon \leq d(p, q) < \varepsilon + \delta \Rightarrow d(T(p), T(q)) < \varepsilon. \quad (1)$$

In 2005, Razani ([22], Theorem 2.2) introduced a contraction theorem in FMS. Our main result in this paper is to extend this Theorem to fuzzy Meir-Keeler's contraction. We assert that if $(X, M, *)$ is a FMS and T on X be a fuzzy Meir-Keeler's contractive self-mapping, then, T has a unique fixed point in X. Our works are an extension of some recent results that we notice them. Then, we characterize fuzzy Meir-Keeler's contractive map as a map so that

$$\frac{1}{M(T(p), T(q), t)} - 1 < \varphi\left(\frac{1}{M(p, q, t)} - 1\right), \forall p, q \in X, p \neq q, t > 0, \quad (2)$$

where φ is a fuzzy LF and $*$ is the minimum t-norm, i.e., $r * s = \min\{r, s\}, r, s \in I := [0, 1]$.

2. Preliminaries

In what follows, we mention some reported results, definitions, and examples related to the theory of FMS which are needed. More details and explanations can be followed in [2, 6–9, 23, 24].

Definition 1 (see [24]). A t-norm is a function $* : I \times I \longrightarrow I$ such that $*$ is continuous, commutative, associative, $s * 1 = s$, $s \in I$, and $p * q \leq t * s$, where $p \leq t$ and $q \leq s$, and $p, q, t, s \in I$.

In the study of probabilistic and FM spaces, the presentation of t-norms was raised by the requirement to assign the triangle inequality (condition (iv) below) in the setting of metric spaces to that of fuzzy metric spaces. Numerous examples of this concept have been cited by various researchers, for instance, one may be found in [14, 15].

Definition 2 (George and Veeramani [2]). $(X, M, *)$ is said FMS where $X \neq \varnothing$ is a set, $*$ is a continuous t-norm, and M on $X^2 \times]0,+\infty[\longrightarrow I$ is a function with

(1) $M(p, q, t) > 0$, for all $t > 0$

(2) $M(p, q, t) = 1$, for all $t > 0$ iff $p = q$

(3) $M(p, q, t) = M(q, p, t)$

(4) $M(p, q, t) * M(q, r, s) \leq M(p, r, t + s)$,

(5) $M(p, q, \cdot)$: $]0,+\infty[\longrightarrow I$ be a continuous fuzzy set-where $p, q, r \in X$ and $t, s > 0$.

Now, we bring two theorems and definitions that play as key roles in this paper, and we continue the next sections based on these concepts to reach our aims.

Theorem 3 (see [2]). *In a FMS $(X, M, *)$, $p_n \longrightarrow p$ (i.e., p_n converges to p) iff, $\forall t > 0, M(p_n, p, t) \longrightarrow 1$ as $n \longrightarrow \infty$.*

Definition 4 (see [2]). $(p_n)_{n\geq 1}$ is said a Cauchy sequence in $(X, M, *)$ if for all $t > 0$ and $\varepsilon \in (0, 1)$, $\exists n_0 = n_0(\varepsilon, t) \in \mathbb{N}$ so that $M(p_n, p_m, t) > 1 - \varepsilon$ whenever $n, m \geq n_0$. Also, we call it complete if every Cauchy sequence is convergent.

Theorem 5 (see [9, 17, 23]). *In a FMS $(X, M, *)$, $M : X \times X \times (0,+\infty) \longrightarrow I$ is a continuous function.*

Definition 6 (see [22]). In a FMS $(X, M, *)$, T on X is said a fuzzy contractive self-mapping (FCM), if

$$\frac{1}{M(T(p), T(q), t)} - 1 < \frac{1}{M(p, q, t)} - 1, \forall p, q \in X, p \neq q, t > 0. \tag{3}$$

3. Main Results

In this section, we discuss concerning fuzzy Meir-Keeler's contractive self-mapping. We give a proof of Meir-Keeler's fixed point theorem in FMS. Here, we consider fuzzy Meir-Keeler's contraction (FMK) to state our main results.

Definition 7. In a FMS $(X, M, *)$, T on X is a (FMK), if for all $\varepsilon \in (0, 1)$, $\exists \delta > 0$ such that for all $p \neq q \in X, t > 0$,

$$Mp, q, t) > \frac{1}{\varepsilon + \delta + 1} \quad \text{implies} \quad M(T(p), T(q), t) > \frac{1}{\varepsilon + 1}. \tag{4}$$

Remark 8. Each FMK is a FCM but the inverse is not necessarily true. To prove this claim, we bring the flowing example.

Example 1. It is precise that FMK implies fuzzy contraction but note the inverse is not true because assume that

$$T(p) = \begin{cases} 3 & |p| > 1, \\ 4 & p = 0. \end{cases} \tag{5}$$

and M_d defined as Example 2.9 of [2] with $* = \min$. If $|p| > 1$ and $q = 0$ then $T(p) = 3$ and $T(q) = 4$. Thus, $|T(p) - T(q)| = 1 < |p| = |p - q|$. Therefore, we get $|T(p) - T(q)| < |p - q|$, for all $p, q, p \neq q$, i.e., T is a FCM. But if $|p| > 1$, $q = 0$, and $\varepsilon = 1/2$, then, there exists $\delta > 0$ so that

$$\begin{aligned} M(p, q, t) &= \frac{t}{t+|p|} \\ &> \frac{1}{1 + 1/2 + \delta}, \end{aligned} \tag{6}$$

holds. Hence, if T be a FMK, we easily have that

$$\begin{aligned} M(T(p), T(q), t) &= \frac{t}{t+|T(p) - T(q)|} \\ &= \frac{t}{t+1} \\ &> \frac{1}{1 + 1/2}, \end{aligned} \tag{7}$$

for all $p \neq q \in X$. It means that $t > 2$, which is a contradiction. Thus, T does not satisfy FMK, and this proves our claim.

Theorem 9. *If $(X, M, *)$ is a complete FMS, where t-norm is defined as $* = \min$. Suppose self-mapping T on X is a FMK. Then, T has a unique fixed point.*

Proof. For all $p \neq q \in X$ and $t > 0$, we get $M(T(p), T(q), t) > M(p, q, t)$. Since if there are $p_0, q_0 \in X$ and $t_0 > 0$ so that $M(T(p_0), T(q_0), t_0) \leq M(p_0, q_0, t_0)$. For simplicity, we put $M_2 = M(T(p_0), T(q_0), t_0)$ and $M_1 = M(p_0, q_0, t_0)$. Hence, for each $\delta > 0$

$$\begin{aligned} M_1 \geq M_2 &\geq \frac{M_2}{1 + \delta M_2} \\ &= \frac{1}{(1/M_2 - 1) + \delta + 1}. \end{aligned} \tag{8}$$

Then, by (4), $M_1 > M_2$, which is a contradiction. Let $p_0 \in X$. Set $p_{n+1} = T(p_n)$, $n \in \mathbb{N}$ and suppose that $p_{n+1} \neq p_n$, $\forall n \in \mathbb{N}$, since otherwise T has a fixed point. Assume that $t > 0$ be arbitrary and fixed after choosing. Now, let $c_n = 1/M(p_{n+1}, p_n, t) - 1$. (c_n) is a nonincreasing sequence. So, (c_n)converges to η. Thus, $\exists N \in \mathbb{N}$ such that, $|c_n - \eta| < r$, for all $n \geq N$. We claim that $\eta = 0$. If $0 < \eta$, there is $d > 0$ such that, for all $p, q \in X$ and $t > 0$, where $M(p, q, t) > 1/1 + \eta + d$, we have $M(T(p), T(q), t) > 1/1 + \eta$. Select $r > 0$ such that $(d/2 - r, d/2 + r) \subset [0,+\infty)$. We have

$$|d/2 - (c_n - \eta) - d/2| < r, \tag{9}$$

thus

$$\frac{d}{2} - (c_n - \eta) \in \left(\frac{d}{2} - r, \frac{d}{2} + r\right), \tag{10}$$

so $1/M(p_{n+1}, p_n, t) - 1 - \eta < d$. It means that $M(p_{n+1}, p_n, t) > 1/1 + \eta + d$. Hence by 2, $M(p_{n+2}, p_{n+1}, t) > 1/1 + \eta$, which is a contradiction, since $c_j = 1/M(p_{j+1}, p_j, t) - 1 \geq \eta$, for all $j \in \mathbb{N}$.

Now, we prove that (p_n) is a Cauchy sequence. If (p_n) is not, then there is $0 < \varepsilon_0 < 1$, so that, for any $m \in \mathbb{N}$, there are $i_m, j_m > m$ such that $M(p_{i_m}, p_{j_m}, t) \leq 1 - \varepsilon_0$. For each $0 < e < \varepsilon_0$, there is $d > 0$ such that for any $p, q \in X$ and $t > 0$, if $M(p, q, t) > 1/1 + e + d$ then $M(T(p), T(q), t) > 1/1 + e$. There exists $M > 0$ such that for all $i \geq M$ and $t > 0$, $M(p_i, p_{i+1}, t) \geq 1 - e + d/1 + e + d$. Take $j_M > i_M \geq M$ such that

$$M\left(p_{j_M}, p_{i_M}, t\right) \leq 1 - \varepsilon_0. \tag{11}$$

Then, we get

$$\begin{aligned} M\left(p_{i_{M-1}}, p_{i_{M+1}}, t\right) &> M\left(p_{i_{M-1}}, p_{i_M}, \frac{t}{2}\right) * M\left(p_{i_M}, p_{i_{M+1}}, \frac{t}{2}\right) \\ &\geq \left(1 - \frac{e+d}{1+e+d}\right) * \left(1 - \frac{e+d}{1+e+d}\right) \\ &= \frac{1}{1+e+d}. \end{aligned} \tag{12}$$

It presents that $1/M(p_{i_{M-1}}, p_{i_{M+1}}, t) - 1 < e + d$. Thus, by (4), $1/M(p_{i_M}, p_{i_{M+2}}, t) - 1 < e$. Also,

$$\begin{aligned} M\left(p_{i_{M-1}}, p_{i_{M+2}}, t\right) &> M\left(p_{i_{M-1}}, p_{i_M}, \frac{t}{2}\right) * M\left(p_{i_M}, p_{i_{M+2}}, \frac{t}{2}\right) \\ &\geq \left(1 - \frac{e+d}{1+e+d}\right) * \left(\frac{1}{1+e}\right) \\ &= \frac{1}{1+e+d}. \end{aligned} \tag{13}$$

In other words, $M(p_{i_{M-1}}, p_{i_{M+2}}, t) > 1/1 + e + d$. Thus, by (4), $M(p_{i_M}, p_{i_{M+3}}, t) > 1/1 + e$. By induction, $M(p_{i_M}, p_{j_M}, t) > 1/1 + \varepsilon_0$. By (11), $1 - \varepsilon_0 > 1/1 + \varepsilon_0$, i.e., $1 - \varepsilon_0^2 > 1$, which is a contradiction. Thus, (p_n) is convergent to $p^* \in X$. We get

$$M(p_{n+1}, Tp^*, t) = M(Tp_n, Tp^*, t) > M(p_n, p^*, t) \longrightarrow 1. \tag{14}$$

Then, $M(p_{n+1}, Tp^*, t) \longrightarrow 1$. So, $Tp^* = p^*$.

For proving the uniqueness of p^*, suppose there is a $q^* \neq p^*$ with $T(q^*) = q^*$, it follows that

$$M(p^*, q^*, t) = M(T(p^*), T(q^*), t) > M(p^*, q^*, t). \tag{15}$$

This is a contradiction, then, the uniqueness is proved.

Note that Theorem 9 is a generalization of ([22], Theorem 2.2); when we consider t-norm $* = \min$, this shows one of the most reason of improvement of [22]. □

4. Characterization of Fuzzy Meir-Keeler's Contractions

In this part of the paper, we characterize FMK maps. In Theorem 11, we provided a sufficient and necessary condition for FMK maps by tools of fuzzy L-function. Also, this generalizes Theorem 1 of [21]. More precisely, we show that if a self-mapping T on X be a FMK then there is a fuzzy L-function ϕ from $(0, +\infty)$ into itself such that, for all $t > 0, p \neq q \in X$, $1/M(T(p), T(q), t) - 1 < \phi(1/M(p, q, t) - 1)$. Also, we show that the converse of it is true. In some sense, our work is very close to Suzuki [19], and Lim [18].

Definition 10 (see [18]). Function φ from $[0, +\infty)$ into itself is said to be a fuzzy LF if $\varphi^{-1}(0) = 0$ and $\forall s \in (0,+\infty)$, $\exists \delta > 0$ so that $\varphi(t) \leq s, \forall t \in [s, s + \delta]$.

In the following, we bring a theorem to show the condition of reaching a self-map T on X in a FMS to FMK.

Theorem 11. *Suppose $(X, M,*)$ is a FMS, and the t-norm is defined as $* = \min$. Then, a self-map T on X is FMK iff there exists a (nondecreasing) fuzzy LF φ as (2) is satisfied.*

Proof. Assume that T is a FMK. By Definition 7, let a function η from $(0, 1)$ into $(0, +\infty)$ is defined such that

$$\frac{1}{M(p, q, t)} - 1 < \varepsilon + 2\eta(\varepsilon) \text{implies} \frac{1}{M(T(p), T(q), t)} - 1 < \varepsilon, \tag{16}$$

for $\varepsilon \in (0, 1)$. With such η, let present a nondecreasing function κ from $(0, 1)$ into $[0, +\infty)$ by

$$\kappa(t) = \inf\{\varepsilon > 0 : t \leq \eta(\varepsilon) + \varepsilon\}, \tag{17}$$

for any $t \in (0, 1), p, q \in X, p \neq q$. Since $t \leq t + \eta(t)$, we get $\kappa(t) \leq t$ for $t \in (0,+\infty)$. Suppose that the function $\bar{\varphi} : [0,+\infty) \longrightarrow [0,+\infty)$ is defined by

$$\bar{\varphi}(t) = \begin{cases} \kappa(t) & \text{if } \min\{\varepsilon > 0 : t \leq \eta(\varepsilon) + \varepsilon\} \text{exists, where} t > 0, \\ 0 & \text{if } t = 0, \\ \dfrac{t + \kappa(t)}{2} & \text{otherwise.} \end{cases} \tag{18}$$

It is obvious that $\bar{\varphi}(0) = 0$. $0 < \bar{\varphi}(s) \leq s$ for $s \in (0,+\infty)$. Let $s \in (0,+\infty)$ be fixed. If $\bar{\varphi}(t) \leq s$, where $t \in (s, s + \eta(s)]$, one can

put $\delta = \kappa(s)$. Otherwise, $\exists\sigma \in (s, s+\eta(s)]$ with $s < \bar{\varphi}(\sigma)$. But $\sigma \le s + \eta(s)$, then, we get $\kappa(\sigma) \le s$, and if $\kappa(\sigma) = s$ then

$$\bar{\varphi}(\sigma) = \kappa(\sigma) = s. \tag{19}$$

Thus, we get $s = \bar{\varphi}(\sigma)$. This is a contradiction. Thus, it is concluded that

$$\kappa(\sigma) < s < \bar{\varphi}(\sigma) = \frac{\sigma + \kappa(\sigma)}{2}. \tag{20}$$

Now, we shall select $u \in (\kappa(\sigma), s)$ with $\sigma \le u + \eta(u)$, and let $\delta = s - u > 0$. Consider $t \in [s, s+\delta]$. Since

$$u + \eta(u) \ge \sigma = 2\frac{\sigma + \kappa(\sigma)}{2} - \kappa(\sigma) > 2s - u = \delta + s \ge t, \tag{21}$$

we obtain $\kappa(t) \le u$. Therefore

$$s = \frac{u + s + \delta}{2} \ge \frac{\kappa(t) + t}{2} \ge \bar{\varphi}(t). \tag{22}$$

Hence, $\bar{\varphi}$ is a fuzzy LF. If we consider $p, q \in X$ with $p \ne q$ and fixed. The definition of $\bar{\varphi}$ implies that $\forall t > 0$ there is $\varepsilon \in (0, \bar{\varphi}(t)]$ in which $t \le \eta(\varepsilon) + \varepsilon$. Thus, $\exists\varepsilon \in (0, \varphi(1/M(p, q, l) - 1))$ where $1/M(p, q, l) - 1 \le \varepsilon + \eta(\varepsilon)$. Therefore,

$$\frac{1}{M(T(p), T(q), l)} - 1 \le \varepsilon \le \bar{\varphi}\left(\frac{1}{M(p, q, l)} - 1\right), \tag{23}$$

holds. Therefore, $\bar{\varphi}$ satisfies (2). We define function $\bar{\bar{\varphi}}$ as

$$\bar{\bar{\varphi}}(t) = \sup\{\bar{\varphi}(s) : s \le t\}, \tag{24}$$

for any $t \in (0, 1)$, we get

$$0 < \bar{\varphi}(t) \le \bar{\bar{\varphi}}(t) \le t, \forall t \in (0, 1). \tag{25}$$

Hence, $\bar{\bar{\varphi}}$ also satisfies (2). Easily can be verified that $\bar{\bar{\varphi}}$ is a nondecreasing fuzzy LF. This completes the proof. □

Considering the following example, we briefly explain the Theorems 9 and 11.

Example 2. Let $X = I \cup \{3n, 3n+1\}_{n\in\mathbb{N}}$ with usual distance on $\mathbb{R}$ and T on X be defined as follows:

$$T(p) = \begin{cases} \dfrac{p}{2} & 0 \le p \le 1, \\ 1 - \dfrac{1}{n+2} & p = 3n+1, \\ 0 & p = 3n. \end{cases} \tag{26}$$

Let we set M as Example 2.9 of [2] and $* = \min$ then,

$$\delta(\varepsilon) = \begin{cases} 2\varepsilon & 0 < \varepsilon \le \dfrac{1}{2}, \\ 1 & \dfrac{1}{2} < \varepsilon < 1. \end{cases} \tag{27}$$

Therefore, T satisfies the conditions of Theorem 9. Hence, T has a (unique) fixed point in X. Also, if we consider

$$\varphi(t) = \begin{cases} \dfrac{2}{3}t & 0 \le t \le \dfrac{3}{4}, \\ 2t - 1 & \dfrac{3}{4} < t \le 1, \\ 1 & 1 \le t < \infty. \end{cases} \tag{28}$$

Thus, φ is a fuzzy LF and

$$\begin{aligned} \frac{1}{M(T(p), T(q), t)} - 1 &= \frac{|T(p) - T(q)|}{t}, \\ &\le \varphi\left(\frac{|p - q|}{t}\right), \\ &= \varphi\left(\frac{1}{M(p, q, t)} - 1\right). \end{aligned} \tag{29}$$

In this step, we can easily reach to the following corollaries.

Corollary 12. *Suppose $(X, M, *)$ is a FMS, where $* = \min$ and T are a self-mapping on X. If there exists a fuzzy L-function $\varphi : (0, +\infty) \longrightarrow (0, +\infty)$ where (2) is satisfied, then, T has a unique fixed point.*

Proof. Let $\varepsilon > 0$ has given. By Definition 10 there is $\delta > 0$ such that for all $t \in [\varepsilon, \varepsilon + \delta]$, $\varphi(t) \le \varepsilon$. It means that if

$$\varepsilon \le \frac{1}{M(p, q, t)} - 1 < \varepsilon + \delta, \tag{30}$$

then by (2)

$$\frac{1}{M(T(p), T(q), t)} - 1 < \varphi\left(\frac{1}{M(p, q, t)} - 1\right) < \varepsilon. \tag{31}$$

It means that (4) holds. Thus, T has a (unique) fixed point. □

Based on theorems in Section 3 and 4, we have the following result:

Corollary 13. *Suppose that $(X, M, *)$ be a FMS where $* = \min$ and T is a self-mapping on X. The followings statements are equivalent:*

(1) T is a FMK

(2) There is a fuzzy LF φ such that (2) satisfies

Proof. By Theorem 11 and Corollary 12, we easily obtain the desired results. □

5. Conclusion

In this paper motivated by the results of Razani [22], a new class of FMK contractions in a complete FMS was introduced by reducing the contractive condition of the so-called Meir-Keeler's contractive maps. In Theorems 9, we established a fixed point theorem; and in Theorem 11, we provided a sufficient and necessary condition for fuzzy FMK maps. Our work generalizes Theorem 1.1 of [22] and Theorem 1 of [21].

Data Availability

No data were used to support this study.

Conflicts of Interest

The authors declare that they have no competing interests.

Authors' Contributions

All authors contributed equally. All authors read and approved the final manuscript.

References

[1] I. Kramosil and J. Michálek, "Fuzzy metrics and statistical metric spaces," *Kybernetika*, vol. 11, no. 5, pp. 336–344, 1975.

[2] A. George and P. Veeramani, "On some results in fuzzy metric spaces," *Fuzzy Sets and Systems*, vol. 64, no. 3, pp. 395–399, 1994.

[3] M. El Naschie, "A review of _E_ infinity theory and the mass spectrum of high energy particle physics," *Chaos, Solitons & Fractals*, vol. 19, no. 1, pp. 209–236, 2004.

[4] M. El Naschie, "The two-slit experiment as the foundation of E-infinity of high energy physics," *Chaos Solitons and Fractals*, vol. 25, no. 3, pp. 509–514, 2005.

[5] V. Gregori, S. Romaguera, and P. Veeramani, "A note on intuitionistic fuzzy metric spaces," *Chaos, Solitons & Fractals*, vol. 28, no. 4, pp. 902–905, 2006.

[6] A. Abbasi and H. Mottaghi Golshan, "On best approximation in fuzzy metric spaces," *Kybernetika*, vol. 51, no. 2, pp. 374–386, 2015.

[7] V. Gregori and S. Romaguera, "Characterizing completable fuzzy metric spaces," *Fuzzy Sets and Systems*, vol. 144, no. 3, pp. 411–420, 2004.

[8] V. Gregori and S. Romaguera, "On completion of fuzzy metric spaces," *Fuzzy Sets and Systems*, vol. 130, no. 3, pp. 399–404, 2002.

[9] K. Fathi Vajargah and H. Mottaghi Golshan, "Probabilistic modular metric spaces," *Journal of Hyperstructures*, vol. 9, no. 1, pp. 18–34, 2020.

[10] M. Grabiec, "Fixed points in fuzzy metric spaces," *Fuzzy Sets and Systems*, vol. 27, no. 3, pp. 385–389, 1988.

[11] N. Abbasi and H. Mottaghi Golshan, "Caristi's fixed point theorem and its equivalences in fuzzy metric spaces," *Kybernetika*, vol. 52, no. 6, pp. 929–942, 2016.

[12] V. Gregori, S. Morillas, and A. Sapena, "On a class of completable fuzzy metric spaces," *Fuzzy Sets and Systems*, vol. 161, no. 16, pp. 2193–2205, 2010.

[13] L. Ćirić, "Some new results for Banach contractions and Edelstein contractive mappings on fuzzy metric spaces," *Chaos, Solitons & Fractals*, vol. 42, no. 1, pp. 146–154, 2009.

[14] O. Hadzic and E. Pap, *Fixed Point Theory in Probabilistic Metric Spaces*, vol. 536, Springer Science & Business Media, 2013.

[15] S.-s. Chang, Y. J. Cho, and S.-m. Kang, *Nonlinear Operator Theory in Probablistic Metric Spaces*, Nova Publishers, 2001.

[16] D. Miheț, "A class of contractions in fuzzy metric spaces," *Fuzzy Sets and Systems*, vol. 161, no. 8, pp. 1131–1137, 2010.

[17] K. Fathi Vajargah, H. Mottaghi Golshan, and A. Arjomand Far, "Caristi's fixed point theorem in probabilistic metric spaces," *Kybernetika*, vol. 57, no. 1, pp. 46–59, 2021.

[18] T.-C. Lim, "On characterizations of Meir-Keeler contractive maps," *Nonlinear Analysis: Theory, Methods & Applications*, vol. 46, no. 1, pp. 113–120, 2001.

[19] T. Suzuki, "Fixed-point theorem for asymptotic contractions of Meir-Keeler type in complete metric spaces," *Nonlinear Analysis: Theory, Methods & Applications*, vol. 64, no. 5, pp. 971–978, 2006.

[20] D. W. Boyd and J. S. W. Wong, "On nonlinear contractions," *Proceedings of the American Mathematical Society*, vol. 20, no. 2, pp. 458–464, 1969.

[21] A. Meir and E. Keeler, "A theorem on contraction mappings," *Journal of Mathematical Analysis and Applications*, vol. 28, no. 2, pp. 326–329, 1969.

[22] A. Razani, "A contraction theorem in fuzzy metric spaces," *Fixed Point Theory and Applications*, vol. 2005, Article ID 427012, 2005.

[23] J. Rodríguez-López and S. Romaguera, "The Hausdorff fuzzy metric on compact sets," *Fuzzy Sets and Systems*, vol. 147, no. 2, pp. 273–283, 2004.

[24] B. Schweizer and A. Sklar, "Statistical metric spaces," *Pacific Journal of Mathematics*, vol. 10, no. 1, pp. 313–334, 1960.

Hindawi
Advances in Mathematical Physics
Volume 2021, Article ID 4275898, 4 pages
https://doi.org/10.1155/2021/4275898

Research Article

Blowing Up for the p-Laplacian Parabolic Equation with Logarithmic Nonlinearity

Asma Alharbi

Department of Mathematics, College of Sciences and Arts, ArRass, Qassim University, Saudi Arabia

Correspondence should be addressed to Asma Alharbi; ao.alharbi@qu.edu.sa

Received 9 May 2021; Accepted 17 July 2021; Published 27 July 2021

Academic Editor: Kamyar Hosseini

In this article, we are concerned with a problem for the p-Laplacian parabolic equation with logarithmic nonlinearity; the blow-up result of the solution is proven. This work is completed Boulaaras' work in Math. Methods Appl. Sci., (2020), where the author did not study the blowup of the solution.

1. Introduction

In the current manuscript, we consider the following initial-boundary value problem for a nonlinear p-Laplacian equation:

$$\begin{cases} u_t - \operatorname{div}\left(|\nabla u|^{p-2}\nabla u\right) + |u|^{p-2}u = |u|^{p-2}u \ln |u|, x \in \Omega, t > 0, \\ u(x,0) = u_0(x), x \in \Omega, \\ u(x,t) = 0, x \in \partial\Omega, t \geq 0, \end{cases} \tag{1}$$

where $\Omega \subset R^n$ is a bounded domain with smooth boundary $\partial\Omega$ and u_0 is the initial data p satisfying

$$\begin{cases} 2 < p < \infty, & \text{if } n \leq p, \\ 2 < p < \dfrac{np}{n-p}, & \text{if } n > p. \end{cases} \tag{2}$$

The terminology of nonlinear polynomials is among the work that researchers have focused on recently. For example, it is found in edge detection and optical elasticity, materials science, engineering, physics, and photonics. In addition, many works and problems in applied sciences have been designed and proposed by means of partial differential equations, including the modeling of some dynamic systems in physics and engineering ([1–13]).

The same is said for the evolutionary partial differential equations associated with $p(x)$-Laplacian (see [8, 14, 15]).

We also note that logarithmic nonlinearity has been concerned by many scientists and researchers, and it has introduced many issues, including the wave equation (see [3, 16–18]).

And for more information on some of the other works to which this term was introduced, we refer the reader to [13, 14, 16–24].

Later on, in [25], the authors by the multiplier method gave the energy decay of the solution of the following problem:

$$u_{tt} - \operatorname{div}\left(|\nabla u|^{p-2}\nabla u\right) - \Delta u_t + |u_t|^{q-1}u_t = |u|^{p-1}u. \tag{3}$$

In addition, the authors in [14] proved the decay rate of solutions (exponential and polynomial) by using the inequality of Nakao for the seminar problem (3).

On the other hand, for the Laplacian parabolic equation with the logarithmic source term in [21], Chen et al. studied the following problem:

$$u_t - \Delta u - \Delta u_t = u \ln u. \tag{4}$$

Then, in [23], the authors proved the global existence, the decay, and the blowup of the solutions of the problem:

$$u_t - \operatorname{div}\left(|\nabla u|^{p-2}\nabla u\right) - \Delta u_t = |u|^{p-2}u \ln |u|, \tag{5}$$

where $p > 2$.

Also, in [14], the authors established the global boundedness and the blowup of the solution of the problem (5) for $1 < p < 2$.

Motivated by the last recent mentioned works, here, we investigated problem (1) with the nonlinear diffusion $\Delta_p = \operatorname{div}(|\nabla u|^{p-2}\nabla u)$ and logarithmic nonlinearity $|u|^{p-2}u \ln |u|$ which extends problem in [14]. Our goal is to blow up solutions for problem (1) in order to put some preliminaries. More precisely, we give the blow-up result.

2. Preliminaries

As a starting point, we gave some essential definitions and lemmas.

$$\|u\|_p = \|u\|_{L^p(\Omega)}, \|u\|_{1,p} = \|u\|_{W_0^{1,p}(\Omega)} = \left(\|u\|_p + \|\nabla u\|_p\right)^{1/p}, \tag{6}$$

for $1 < p < \infty$, and we symbolize the positive constants by C and C_i $(i = 1, 2, \cdots)$.

Lemma 1 [7] (logarithmic Sobolev inequality). *Let u be all function $u \in W_0^{1,p}(R^n) \setminus \{0\}$. Then, for $p > 1$, $\mu > 0$,*

$$p\int_{R^n} u^p \ln\left(\frac{|u|}{\|u\|_{L^p(R^n)}}\right)dx \le \mu\int_{R^n}|\nabla u|^p dx - \frac{n}{p}\ln\left(\frac{p\mu e}{n\mathscr{L}_p}\right)\int_{R^n}|u|^p dx, \tag{7}$$

where

$$\mathscr{L}_p = \frac{p}{n}\left(\frac{p-1}{e}\right)^{p-1}\pi^{-p/2}\left[\frac{\Gamma((n/2)+1)}{\Gamma(n((p-1)/p)+1)}\right]^{p/n}. \tag{8}$$

Remark 2. Let $u \in W_0^{1,p}(\Omega) \setminus \{0\}$, and by defining $u(x) = 0$ for $x \in R^n \setminus \Omega$, we can write

$$p\int_{\Omega} u^p \ln\left(\frac{|u|}{\|u\|_{L^p(\Omega)}}\right)dx \le \mu\int_{\Omega}|\nabla u|^p dx - \frac{n}{p}\ln\left(\frac{p\mu e}{n\mathscr{L}_p}\right)\int_{\Omega}|u|^p dx. \tag{9}$$

3. Blowup

In this third section, we gave the proof of blowup of solution of our problem.

Theorem 3. *For any initial data $u_0 \in \mathscr{H}$, the problem (1) has a unique weak solution:*

$$u \in C([0, T]; \mathscr{H}), \tag{10}$$

for some $T > 0$.

First, we introduce the energy functional in the following lemma.

Lemma 4. *Let $u(t)$ be a solution of (1), then $E(t)$ is nonincreasing; that is,*

$$E(t) = \frac{1}{p}\|\nabla u\|_p^p - \frac{1}{p}\int_{\Omega}\ln|u|u^p dx + \frac{p+1}{p^2}\|u\|_p^p \tag{11}$$

satisfies

$$E'(t) = -\|u_t\|_2^2. \tag{12}$$

Proof. Multiplying (1) by u_t and integrating on Ω, we have

$$\begin{aligned} &-\int_{\Omega}\operatorname{div}\left(|\nabla u|^{p-2}\nabla u\right)u_t dx + \int_{\Omega}|u|^{p-2}uu_t dx + \int_{\Omega}u_t u_t dx \\ &\quad = \int_{\Omega}u^{p-2}u\ln|u|u_t dx, \\ &\frac{d}{dt}\left(\frac{1}{p}\|\nabla u\|_p^p + \frac{1}{p}\|u\|_p^p - \frac{1}{p}\int_{\Omega}\ln|u|u^p dx + \frac{1}{p^2}\|u\|_p^p\right) \\ &\quad = -\|u_t\|^2. \end{aligned} \tag{13}$$

Thus,

$$E'(t) = -\|u_t\|^2. \tag{14}$$

□

To get to our goal of proving the main result, we define the functional

$$H(t) = -E(t) = -\frac{1}{p}\|\nabla u\|_p^p + \frac{1}{p}\int_{\Omega}\ln|u|u^p dx - \frac{p+1}{p^2}\|u\|_p^p. \tag{15}$$

Theorem 5. *Assume that $E(0) < 0$, then the solution of problem (1) blows up in finite time.*

Proof. From (12), we have

$$E(t) \le E(0) \le 0. \tag{16}$$

Hence,

$$H'(t) = -E'(t) = \|u_t\|_2^2 \geq 0,$$
$$0 \leq H(0) \leq H(t) \leq \frac{1}{p}\int_\Omega \ln|u|u^p dx. \tag{17}$$

We set

$$\mathscr{K}(t) = H^{1-\alpha} + \frac{\varepsilon}{2}\int_\Omega u^2 dx, \tag{18}$$

where $\varepsilon > 0$ and

$$0 < \alpha < \frac{p-2}{p} < 1. \tag{19}$$

Multiplying (1) by u and the derivative of (18) gives

$$\mathscr{K}' - \alpha H'(t) - \varepsilon\|\nabla u\|_p^p - \varepsilon\|\nabla u\|_p^p + \varepsilon\int_\Omega |u|^p \ln|u| dx. \tag{20}$$

Adding and subtracting $\varepsilon\delta H(t)$ into (20) ($\delta > 0$), we obtain

$$\mathscr{K}' - \alpha H'(t) + \varepsilon\left(\frac{\delta - p}{p}\right)\|\nabla u\|_p^p + \varepsilon\left(\frac{\delta - p}{p} + \frac{1}{p^2}\right)\|u\|_p^p - \varepsilon\left(\frac{\delta - p}{p}\right)\int_\Omega \ln|u|u^p dx + \varepsilon\delta H(t). \tag{21}$$

Applying the logarithmic Sobolev inequality gives

$$\mathscr{K}' - \alpha H'(t) + \varepsilon\delta H(t) + \varepsilon\left(\frac{\delta - p}{p}\right)\left(1 - \frac{\mu}{p}\right)\|\nabla u\|_p^p + \varepsilon\left(\frac{\delta - p}{p}\right) \cdot \left[1 + \frac{\delta}{p(\delta - p)} - \ln\|u\|_p + \left(\frac{n}{p^2}\ln\left(\frac{p\mu e}{n\mathscr{L}_p}\right)\right)\right]\|u\|_p^p. \tag{22}$$

Setting $\mu = p/2$ and taking $\delta > p$ give

$$\left[1 + \frac{\delta}{p(\delta - p)} - \ln\|u\|_p + \left(\frac{n}{p^2}\ln\left(\frac{p^2 e}{2n\mathscr{L}_p}\right)\right)\right] > 0, \tag{23}$$

since

$$\|u\|_p > e^{\left(1+\frac{\delta}{p(\delta-p)}\right)}\left(\frac{p^2 e}{2n\mathscr{L}_p}\right)^{n/p^2}. \tag{24}$$

Consequently, for some $\beta > 0$, inequality (25) gives

$$\mathscr{K}'(t) \geq \beta\left\{H(t) + \|u\|_p^p + \|\nabla u\|_p^p\right\}, \tag{25}$$

$$\mathscr{K}(t) \geq \mathscr{K}(0) > 0, \quad t > 0. \tag{26}$$

Next, by (18), we have

$$\mathscr{K}(t) = H^{1-\alpha} + \frac{\varepsilon}{2}\int_\Omega u^2 dx \leq H^{1-\alpha} + \varepsilon C\|u\|_p^2 \leq H^{1-\alpha} + \varepsilon C\left(\|u\|_p^p\right)^{2/p}. \tag{27}$$

Therefore,

$$\mathscr{K}^{1/1-\alpha}(t) \leq H^{1-\alpha} + \varepsilon C\left(\|u\|_p^p\right)^{2/p(1-\alpha)}, \tag{28}$$

where $0 < 2/p(1-\alpha) < 1$,

$$\left(\|u\|_p^2\right)^{2/p(1-\alpha)} \leq C\left(\left(\|u\|_p^p\right)^p + H(t)\right). \tag{29}$$

Hence,

$$\mathscr{K}^{1/1-\alpha}(t) \leq C_1\left[H(t) + \|u\|_p^p\right] \leq C_1\left[H(t) + \|\nabla u\|_p^p + \|u\|_p^p\right]. \tag{30}$$

According to (25) and (30), we get

$$\mathscr{K}'(t) \geq \lambda\mathscr{K}^{1/1-\alpha}(t), \tag{31}$$

where $\lambda = C_1/\beta > 0$, depending only on β and C_1.

Finally, by integrating (31), we obtain

$$\mathscr{K}^{\alpha/1-\alpha}(t) \geq \frac{1}{\mathscr{K}^{-\alpha/(1-\alpha)}(0) - \lambda(\alpha/(1-\alpha))t}. \tag{32}$$

Hence, $\mathscr{K}(t)$ blows up in time:

$$T \leq T^* = \frac{1-\alpha}{\lambda\alpha\mathscr{K}^{\alpha/(1-\alpha)}(0)}. \tag{33}$$

As a result, the proof is completed. □

Data Availability

No data were used to support the study.

Conflicts of Interest

The author declares that he has no conflicts of interest.

Acknowledgments

The researcher would like to thank the Deanship of Scientific Research, Qassim University, for funding the publication of this project.

References

[1] S. Boulaaras and Y. Bouizem, "Blow up of solutions for a nonlinear viscoelastic system with general source term," *Quaestiones Mathematicae*, pp. 1–11, 2020.

[2] S. Boulaaras, A. Choucha, B. Cherif et al., "Blow up of solutions for a system of two singular nonlocal viscoelastic equations with damping, general source terms and a wide class of relaxation functions," *AIMS Mathematics*, vol. 6, no. 5, pp. 4664–4676, 2021.

[3] S. Boulaaras, "A well-posedness and exponential decay of solutions for a coupled Lamé system with viscoelastic term and logarithmic source terms," *Applicable Analysis*, vol. 100, no. 7, pp. 1514–1532, 2021.

[4] A. Choucha, D. Ouchenane, and S. Boulaaras, "Blow-up of a nonlinear viscoelastic wave equation with distributed delay combined with strong damping and source terms," *Journal of Nonlinear Functional Analysis*, vol. 2020, no. 1, 2020.

[5] A. Menaceur, S. Boulaaras, A. Makhlouf, K. Rajagobal, and M. Abdalla, "Limit cycles of a class of perturbed differential systems via the first-order averaging method," *Complexity*, vol. 2021, Article ID 5581423, 6 pages, 2021.

[6] D. Ouchenane, S. Boulaaras, A. Alharbi, and B. Cherif, "Blow up of coupled nonlinear Klein-Gordon system with distributed delay, strong damping, and source terms," *Journal of Function Spaces*, vol. 2020, Article ID 5297063, 9 pages, 2020.

[7] S. Boulaaras, "Existence of positive solutions for a new class of Kirchhoff parabolic systems," *The Rocky Mountain Journal of Mathematics*, vol. 50, no. 2, pp. 445–454, 2020.

[8] N. Ioku, "The Cauchy problem for heat equations with exponential nonlinearity," *Journal of Differential Equations*, vol. 251, no. 4-5, pp. 1172–1194, 2011.

[9] H. Yüksekkaya, E. Pişkin, S. M. Boulaaras, B. B. Cherif, and S. A. Zubair, "Existence, nonexistence, and stability of solutions for a delayed plate equation with the logarithmic source," *Advances in Mathematical Physics*, vol. 2021, Article ID 8561626, 11 pages, 2021.

[10] E. Piskin and H. Yuksekkaya, "Local existence and blow up of solutions for a logarithmic nonlinear viscoelastic wave equation with delay," *Computational Methods for Differential Equations*, vol. 9, no. 2, pp. 623–636, 2021.

[11] H. T. Song and D. S. Xue, "Blow up in a nonlinear viscoelastic wave equation with strong damping," *Nonlinear Analysis*, vol. 109, pp. 245–251, 2014.

[12] H. T. Song and C. K. Zhong, "Blow-up of solutions of a nonlinear viscoelastic wave equation," *Nonlinear Analysis: Real World Applications*, vol. 11, no. 5, pp. 3877–3883, 2010.

[13] S. Boulaaras, A. Choucha, D. Ouchenane, and B. Cherif, "Blow up of solutions of two singular nonlinear viscoelastic equations with general source and localized frictional damping terms," *Advances in Difference Equations*, vol. 2020, no. 1, 2020.

[14] E. Pişkin, S. Boulaaras, and N. Irkil, "Qualitative analysis of solutions for the p-Laplacian hyperbolic equation with logarithmic nonlinearity," *Mathematical Methods in the Applied Sciences*, vol. 44, no. 6, pp. 4654–4672, 2021.

[15] F. Ekinci, E. Pişkin, S. Boulaaras, and I. Mekawy, "Global existence and general decay of solutions for a quasilinear system with degenerate damping terms," *Journal of Function Spaces*, vol. 2021, Article ID 4316238, 10 pages, 2021.

[16] I. Bialynicki-Birula and J. Mycielski, "Wave equations with logarithmic nonlinearities," *Bulletin de l'Academie Polonaise des Sciences. Serie des Sciences, Mathematiques, Astronomiques et Physiques*, vol. 23, pp. 461–466, 1975.

[17] I. Bialynicki-Birula and J. Mycielski, "Nonlinear wave mechanics," *Annals of Physics*, vol. 100, no. 1–2, pp. 62–93, 1976.

[18] P. Gorka, "Logarithmic Klein–Gordon equation," *Acta Physica Polonica B*, vol. 40, pp. 59–66, 2009.

[19] A. Merah, F. Mesloub, S. Boulaaras, and B. Cherif, "A new result for a blow-up of solutions to a logarithmic flexible structure with second sound," *Advances in Mathematical Physics*, vol. 2021, Article ID 5555930, 7 pages, 2021.

[20] X. S. Han, "Global existence of weak solutions for a logarithmic wave equation arising from Q-ball dynamics," *Bulletin of the Korean Mathematical Society*, vol. 50, no. 1, pp. 275–283, 2013.

[21] S. Boulaaras, "Polynomial decay rate for a new class of viscoelastic Kirchhoff equation related with Balakrishnan-Taylor dissipation and logarithmic source terms," *Alexandria Engineering Journal*, vol. 59, no. 3, pp. 1059–1071, 2020.

[22] A. Choucha, S. Boulaaras, D. Ouchenane, and S. Beloul, "General decay of nonlinear viscoelastic Kirchhoff equation with Balakrishnan-Taylor damping, logarithmic nonlinearity and distributed delay terms," *Mathematicsl Methods in the Applied Sciences*, vol. 44, no. 7, pp. 5436–5457, 2021.

[23] C. N. Le and X. T. Le, "Global solution and blow up for a class of pseudo p-Laplacian evolution equations with logarithmic nonlinearity," *Computers & Mathematcs with Applications*, vol. 73, pp. 2076–2091, 2017.

[24] N. Mezouar and S. Boulaaras, "Global existence and exponential decay of solutions for generalized coupled non-degenerate Kirchhoff system with a time varying delay term," *Boundary Value Problems*, vol. 2020, no. 1, 2020.

[25] Y. Wu and X. Xue, "Uniform decay rate estimates for a class of quasilinear hyperbolic equations with nonlinear damping and source terms," *Applicable Analysis*, vol. 92, no. 6, pp. 1169–1178, 2013.

Hindawi
Advances in Mathematical Physics
Volume 2021, Article ID 5547804, 13 pages
https://doi.org/10.1155/2021/5547804

Research Article

A Semianalytical Approach to the Solution of Time-Fractional Navier-Stokes Equation

Zeeshan Ali,[1] **Shayan Naseri Nia**,[1] **Faranak Rabiei**,[1] **Kamal Shah**,[2,3] **and Ming Kwang Tan**[1]

[1]*School of Engineering, Monash University Malaysia, 47500 Selangor, Malaysia*
[2]*Department of Mathematics, University of Malakand, Dir(L), 18000 Khyber Pakhtunkhwa, Pakistan*
[3]*Department of Mathematics and General Sciences, Prince Sultan University, Saudi Arabia*

Correspondence should be addressed to Zeeshan Ali; zeeshan.ali@monash.edu

Received 12 February 2021; Revised 19 April 2021; Accepted 26 June 2021; Published 19 July 2021

Academic Editor: ZEA Fellah

In this manuscript, a semianalytical solution of the time-fractional Navier-Stokes equation under Caputo fractional derivatives using Optimal Homotopy Asymptotic Method (OHAM) is proposed. The above-mentioned technique produces an accurate approximation of the desired solutions and hence is known as the semianalytical approach. The main advantage of OHAM is that it does not require any small perturbations, linearization, or discretization and many reductions of the computations. Here, the proposed approach's reliability and efficiency are demonstrated by two applications of one-dimensional motion of a viscous fluid in a tube governed by the flow field by converting them to time-fractional Navier-Stokes equations in cylindrical coordinates using fractional derivatives in the sense of Caputo. For the first problem, OHAM provides the exact solution, and for the second problem, it performs a highly accurate numerical approximation of the solution compare with the exact solution. The presented simulation results of OHAM comparison with analytical and numerical approaches reveal that the method is an efficient technique to simulate the solution of time-fractional types of Navier-Stokes equation.

1. Introduction

Partial differential equations (PDEs) are utilized to mathematically formulate and thus help solve physical and other problems involving functions of several variables, such as the propagation of sound or heat, electrostatics, fluid flow, elasticity, and electrodynamics. In fluid mechanics, the Navier-Stokes equation is a PDE that illustrates incompressible fluids' flow. This equation is a generalization of the equation developed to illustrate the flow of frictionless and incompressible fluids by Euler in the eighteenth century. In 1821, Navier added the viscosity (friction) element to make viscous fluids more realistic and complex. The British physicist and mathematician Stokes improved it during the middle of the nineteenth century, though complete solutions were achieved only for simple two-dimensional flows [1]. That is why the equation is called the Navier-Stokes equation. The mathematical model of the above-mentioned equation is given by:

$$\frac{\partial \mathcal{U}(s,t)}{\partial t} + (\mathcal{U}(s,t)\cdot\nabla)\mathcal{U}(s,t) = -\frac{1}{\rho}\nabla \mathbf{p} + \vartheta\nabla^2\mathcal{U}(s,t), \quad (1)$$

where $\mathcal{U}$ is the velocity, t is the time, ρ is the density, s is the spatial variable, ϑ is the kinematics viscosity, p is the pressure, and ∇ denotes the gradient differential operator.

Fractional differential equations have proven to be a powerful tool for modeling real-world problems in the literature. It was noticed that time-fractional derivatives usually appear as infinitesimal generators of the time evolution when choosing a long-time scaling limit. Several essential phenomena in physics and polymer technology [2], electrical circuits [3], electrochemistry [4], electrodynamics

of complex medium [5], control theory [6], thermodynamics [7], viscoelasticity [8], aerodynamics [9], capacitor theory [10], biology [11], blood flow [12], and fitting of experimental data [13], are well described by the aforesaid equations. Equation (1) can be converted to time-fractional derivative of order $\alpha \in (0, 1]$, as given by:

$$\frac{\partial^{\alpha}\mathcal{U}(s,t)}{\partial t^{\alpha}} + (\mathcal{U}(s,t)\cdot\nabla)\mathcal{U}(s,t) = -\frac{1}{\rho}\nabla \mathbf{p} + \vartheta\nabla^{2}\mathcal{U}(s,t). \quad (2)$$

Here, $\partial^{\alpha}/\partial t^{\alpha}$ is the Caputo fractional derivative. As the equation mentioned above is nonlinear, there is no known general method for resolving it. There are very few cases where it is possible to achieve the exact solution of Equation (2), making some predictions about the fluid's state and a simple arrangement considered for the flow pattern; for detail, see [14].

Analytical and numerical techniques are extensively utilized to solve nonlinear differential equations modeling physical phenomena. This is because the exact solutions of the above-mentioned equations are challenging to achieve. In recent decades, a new variety of perturbation methods have developed, which is loosely based on Poincare's homotopy applied in topology. Liao [15] introduced the Homotopy Analysis Method (HAM) in 1992. In 1998, He [16] followed Liao's work and developed the Homotopy Perturbation Method (HPM). Both methods have been successfully implemented to the problems, which exist in engineering and science fields. For example, Ganji and Rafei [17] solved nonlinear Hirota-Satsuma coupled Korteweg-De Vries equation by HPM. Lu and Liu [18] solved the Korteweg-De Vries-Burgers equation via the help of HAM. Siddiqui et al. [19] utilized HPM and examined the irregular 2D flow of a viscous magnetohydrodynamics fluid within two parallel plates.

In [20], Marinca and Herisanu proposed a technique called OHAM. The benefit of the above-mentioned technique is in the built-in convergence criteria alike to HAM but extraflexible. The researchers have successfully implemented this approach to solving essential science problems and have also explained its reliability and effectiveness, for example, the dynamics of an electrical machine exhibiting nonlinear vibration [21], the oscillations of a particle that moves on a rotating parabola [22], the explicit solutions for some oscillators with discontinuities and a fractional power restoring force [23], and nonlinear equations arising in heat transfer [20], in an application to the steady flow of a fourth-grade fluid [24]. The above-mentioned technique is the HAM's modification, which is based on minimizing the residual error. In OHAM, the adjustment and control of the convergence region are provided conveniently.

In [14], Momani and Odibat considered unsteady one-dimensional motion of a viscous fluid in a tube. The equations of motion which govern the flow field in the tube are the Navier-Stokes equations in cylindrical coordinates. They converted Equation (2) to the operator form as:

$$\frac{\partial^{\alpha}\mathcal{U}(s,t)}{\partial t^{\alpha}} = \mathrm{P} + \vartheta\left(\frac{\partial^{2}\mathcal{U}(s,t)}{\partial s^{2}} + \frac{1}{s}\frac{\partial\mathcal{U}(s,t)}{\partial s}\right), \quad (3)$$

where $0 < \alpha \le 1$ is the fractional order derivative and $P = -\partial \mathbf{p}/\rho\partial z$. For $\alpha = 1$, we can get the standard Navier-Stokes equation. For the analytical solution, they have utilized the Adomian decomposition method. Lately, several powerful analytical techniques have been utilized to achieve the solution of Equation (3), such as the modified Laplace decomposition method [25], the q-homotopy analysis transform scheme [26], the new homotopy perturbation transform method [27], the iterative Elzaki transform method [28], the natural homotopy perturbation method [29], Elzaki transform with homotopy perturbation technique [30], and He's homotopy perturbation and variational iteration methods [31]. The aforementioned methods are called analytical, and no one has used the semianalytical technique for the solution of Equation (3) in the previous studies. Therefore, the objective of this manuscript is to present the semianalytical solution of Equation (3) by a semianalytical approach called OHAM.

The rest of the manuscript is structured as follows: in Section 2, we recall some definitions and properties of noninteger order operators. Section 3 is devoted to the basic formulation of OHAM. In Section 4, we apply the above-mentioned technique to time-fractional Navier-Stokes type of equations and discuss the method reliability through tables and plots. Section 5 is devoted to the conclusion.

2. Definitions and Properties

This section deals with some definitions and properties that are used in the manuscript.

Definition 1. A real function $\psi(t)$, $t > 0$ is supposed to be in the space C_{κ} $(\kappa > 0)$ if it can express as $\psi(t) = t^{p}\psi_{1}(t)$ for certain $p > \kappa$ where $\psi_{1}(t) \in C[0,\infty)$, and it is supposed to be in the space $\mathrm{C}_{\kappa}^{m} \Leftrightarrow \psi^{m} \in \mathrm{C}_{\kappa}, m \in \mathbb{N}$.

Definition 2 (see [32]). The $\alpha \ge 0$ order integral operator for a function $\psi \in C_{\kappa}$, $\kappa \ge -1$ in the Riemann-Liouville sense is defined as:

$$\mathbf{I}^{\alpha}\psi(t) = \frac{1}{\Gamma(\alpha)}\int_{0}^{\mathrm{t}}\frac{\psi(\theta)}{(t-\theta)^{1-\alpha}}d\theta. \quad (4)$$

Let $\psi \in C_{\kappa}$, $\kappa \ge -1$, $\alpha,\gamma \ge 0$, and $\mu > -1$, then we have the properties [32] given by:

$$\begin{aligned}\mathbf{I}^{\alpha}\mathbf{I}^{\gamma}\psi(t) &= \mathbf{I}^{\alpha+\gamma}\psi(t),\\ \mathbf{I}^{\alpha}\mathbf{I}^{\gamma}\psi(t) &= \mathbf{I}^{\gamma}\mathbf{I}^{\alpha}\psi(t),\\ \mathbf{I}^{\alpha}t^{\mu} &= \frac{\Gamma(\mu+1)}{\Gamma(\mu+\alpha+1)}t^{\mu+\alpha}.\end{aligned} \quad (5)$$

Definition 3 (see [32]). The $\alpha > 0$ order Caputo derivative operator for a function $\psi \in \mathrm{C}_{-1}^{m}, m \in \mathbb{N}$ is defined as:

$${}^{c}\mathbf{D}^{\alpha}\psi(t) = \frac{1}{\Gamma(n-\alpha)}\int_{0}^{t}\frac{\psi^{(n)}(\theta)}{(t-\theta)^{\alpha-n+1}}d\theta, \quad t > 0, \quad (6)$$

where $[\alpha]$ is the integer part of α and $n = [\alpha] + 1$. For ψ, $\phi \in C_{\kappa}^{m}$, $\kappa \geq -1$, we have the properties [32] given by:

$$
\begin{aligned}
{}^{c}\mathbf{D}^{\alpha}(a\psi(t) + b\phi(t)) &= a^{c}\mathbf{D}^{\alpha}\psi(t) + b^{c}\mathbf{D}^{\alpha}\phi(t), \quad a, b \in \mathrm{IR},\\
{}^{c}\mathbf{D}^{\alpha}\mathbf{I}^{\alpha}\psi(t) &= \psi(t),\\
\mathbf{I}^{\alpha}[{}^{c}\mathbf{D}^{\alpha}]\psi(t) &= \psi(t) - \sum_{j=0}^{k-1}\psi^{(j)}(0)\frac{x_j}{j!}.
\end{aligned}
\tag{7}
$$

3. Basic Formulation of the OHAM

We formulate OHAM for PDEs with boundary condition, in the steps given by [33]:

$$
\mathscr{L}(\mathscr{U}(s,t)) + \mathscr{N}(\mathscr{U}(s,t)) + \hbar(s,t) = 0, \mathscr{B}\left(\mathscr{U}, \frac{\partial \mathscr{U}}{\partial t}\right) = 0, \quad s \in \Upsilon,
\tag{8}
$$

where $\mathscr{L}$ and $\mathscr{N}$ are the linear and nonlinear operators, respectively. $\mathscr{U}(s,t)$ is an unknown function, the boundary operator denoted by $\mathscr{B}$, s and t denote spatial and time variables, respectively, $\hbar(s,t)$ is known function, and Υ is the domain of the problem.

By OHAM, we construct the homotopy $\omega(s,t;\wp)$: $\Upsilon \times J \longrightarrow R$, where $J = [0,1]$, which satisfies:

$$
\begin{aligned}
(1-\wp)\{\mathscr{L}(\omega(s,t;\wp)) + \hbar(s,t)\} &= \mathscr{H}(\wp)\{\mathscr{L}(\omega(s,t;\wp))\\
&\quad + \mathscr{N}(\omega(s,t;\wp)) + \hbar(s,t)\},
\end{aligned}
\tag{9}
$$

where $\wp \in J$ is an embedding parameter and $\mathscr{H}(\wp)$ is a nonzero auxiliary function for $\wp \neq 0$ and $\mathscr{H}(0) = 0$. Equation (9) is to be the optimal homotopy equation. Obviously,

$$
\begin{aligned}
&\wp = 0 \Rightarrow \mathscr{L}(\omega(s,t;\wp)) + \hbar(s,t) = 0,\\
&\wp = 1 \Rightarrow \mathscr{L}(\omega(s,t;\wp)) + \mathscr{N}(\omega(s,t;\wp)) + \hbar(s,t).
\end{aligned}
\tag{10}
$$

For $\wp = 0$, we can obtain $\omega(s,t;0) = \mathscr{U}_0(s,t)$, and for $\wp = 1$, we can get $\omega(s,t;1) = \mathscr{U}(s,t)$. Therefore, as $\wp$ extend from 0 to 1, then $\omega(s,t;\wp)$ moves from $\mathscr{U}_0(s,t)$ to $\mathscr{U}(s,t)$, where $\mathscr{U}_0(s,t)$ is got from Equation (9) for $\wp = 0$:

$$
\mathscr{L}(\mathscr{U}_0(s,t;\wp)) + \hbar(s,t) = 0, \mathscr{B}\left(\mathscr{U}_0, \frac{\partial \mathscr{U}_0}{\partial t}\right) = 0.
\tag{11}
$$

Now, we take $\mathscr{H}(\wp)$, which is called auxiliary function, in the following form:

$$
\mathscr{H}(\wp) = \wp C_1 + \wp^2 C_2 + \wp^3 C_3 + \cdots + \wp^m C_m.
\tag{12}
$$

For the numerical solution, we utilize Taylor's series about $\wp$ and expand $\omega(s,t;\wp,C_p)$ in the following way:

$$
\omega(s,t;\wp,C_p) = \mathscr{U}_0(s,t) + \sum_{q-1}^{\infty}\mathscr{U}_q(s,t;C_p)\wp^q, \quad p = 1,2,3,\cdots.
\tag{13}
$$

Plugging Equation (13) in Equation (9) and equating the coefficient of like powers of $\wp$, we get the problem of zerothorder; given in (11), the problems of the first and second order are given by the Equations (14) and (15), respectively, and the general governing equations for $\mathscr{U}_q(s,t)$ are given in Equation (16):

$$
\mathscr{L}(\mathscr{U}_1(s,t)) = C_1\mathscr{N}_0(\mathscr{U}_1(s,t)), \mathscr{B}\left(\mathscr{U}_1, \frac{\partial \mathscr{U}_1}{\partial t}\right) = 0,
\tag{14}
$$

$$
\begin{aligned}
&\mathscr{L}(\mathscr{U}_2(s,t)) - \mathscr{L}(\mathscr{U}_1(s,t)) = C_2\mathscr{N}_0(\mathscr{U}_0(s,t)) + C_1[\mathscr{L}(\mathscr{U}_1(s,t)) + \mathscr{N}_1(\mathscr{U}_0(s,t),\mathscr{U}_1(s,t))], \mathscr{B}\left(\mathscr{U}_2, \frac{\partial \mathscr{U}_2}{\partial t}\right) = 0,\\
&\quad\vdots
\end{aligned}
\tag{15}
$$

$$
\begin{aligned}
\mathscr{L}\left(\mathscr{U}_q(s,t)\right) - \mathscr{L}\left(\mathscr{U}_{q-1}(s,t)\right) &= C_q\mathscr{N}_0(\mathscr{U}_0(s,t)) + \sum_{p=1}^{q-1}C_p\left[\mathscr{L}\left(\mathscr{U}_{q-p}(s,t)\right)\right.\\
&\quad \left. + \mathscr{N}_{q-p}\left(\mathscr{U}_0(s,t),\mathscr{U}_1(s,t),\mathscr{U}_2(s,t),\cdots,\mathscr{U}_{q-p}(s,t)\right)\right], \mathscr{B}\left(\mathscr{U}_q, \frac{\partial \mathscr{U}_q}{\partial t}\right), \quad q = 2,3,\cdots,
\end{aligned}
\tag{16}
$$

where $\mathcal{N}_{q-p}(\mathcal{U}_0(s,t), \mathcal{U}_1(s,t), \cdots, \mathcal{U}_{q-p}(s,t))$ is the coefficient of $\wp^{q-p}$ in the expansion of $\mathcal{N}(\omega(s,t;\wp))$ about the embedding parameter $\wp$.

$$\mathcal{N}\left(\omega\left(s,t;\wp,C_p\right)\right) = \mathcal{N}_0(\mathcal{U}_0(s,t)) + \sum_{q\geq 1} \mathcal{N}_q\left(\mathcal{U}_0, \mathcal{U}_1, \cdots, \mathcal{U}_q\right)\wp^q. \tag{17}$$

Here, $\mathcal{U}_q$ for $q \geq 0$ is the set of linear equations with linear boundary conditions, which can be solved very easily.

The series in Equation (13) depends on $C_1, C_2, \cdots$. If it is convergent at $\wp = 1$, then:

$$\tilde{\mathcal{U}}\left(s,t\,;C_p\right) = \mathcal{U}_0(s,t) + \sum_{q=1}^{m} \mathcal{U}_q\left(s,t,C_p\right). \tag{18}$$

Putting Equation (18) in Equation (8), one can obtain the residual expression in the form:

$$\mathrm{R}\left(s,t\,;C_p\right) = \mathcal{L}\left(\tilde{\mathcal{U}}\left(s,t\,;C_p\right)\right) + \mathcal{N}\left(\tilde{\mathcal{U}}\left(s,t\,;C_p\right)\right) + \hbar(s,t). \tag{19}$$

If $\mathrm{R}(s,t\,;C_p) = 0$, then $\tilde{\mathcal{U}}(s,t\,;C_p)$ will be the exact solution. But generally, it is not possible in nonlinear problems.

For calculating the C_p, $p = 1, 2, \cdots, m$, one can utilize the least square technique as given by:

$$\Phi\left(C_p\right) = \int_0^t \int_\Upsilon R^2\left(s,t\,;C_p\right) ds dt, \tag{20}$$

where R is the residual given by Equation (19) and

$$\frac{\partial \Phi}{\partial C_1} = \frac{\partial \Phi}{\partial C_2} = \frac{\partial \Phi}{\partial C_3} = \cdots = \frac{\partial \Phi}{\partial C_m} = 0. \tag{21}$$

The convergence based on $C_1, C_2, C_3, \cdots$ can be identified and minimized optimally by Equation (21).

4. Numerical Examples

In this section, the fractional OHAM is utilized to get the solution of time-fractional Navier-Stokes equations.

Example 1. Suppose a time-fractional Navier-Stokes equation:

$$\frac{\partial^\alpha \mathcal{U}(s,t)}{\partial t^\alpha} = P + \frac{\partial^2 \mathcal{U}(s,t)}{\partial s^2} + \frac{1}{s}\frac{\partial \mathcal{U}(s,t)}{\partial s}, \tag{22}$$

with the initial condition:

$$\mathcal{U}(s,0) = 1 - s^2, \tag{23}$$

where $\partial^\alpha/\partial t^\alpha$ is Caputo fractional derivative and $0 < \alpha \leq 1$. The exact solution of Equation (22) is given by [14]:

$$\mathcal{U}(s,t) = 1 - s^2 + (P-4)t. \tag{24}$$

According to Section 3, we can set up the homotopy in the following way:

$$(1-\wp)\frac{\partial^\alpha \omega(s,t;\wp)}{\partial t^\alpha} = \mathcal{H}\left(\wp, C_p\right) \left[\frac{\partial^\alpha \omega(s,t;\wp)}{\partial t^\alpha} - P - \frac{\partial^2 \omega(s,t;\wp)}{\partial s^2} - \frac{1}{s}\frac{\partial \omega(s,t;\wp)}{\partial s}\right], \tag{25}$$

where

$$\omega(s,t;\wp) = \mathcal{U}_0(s,t) + \sum_{q=1}^{\infty} \mathcal{U}_q\left(s,t\,;C_p\right)\wp^q, \quad p = 1, 2, 3 \cdots, \tag{26}$$

$$\mathcal{H}\left(\wp, C_p\right) = \wp C_1 + \wp^2 C_2 + \wp^3 C_3 + \wp^4 C_4 + \cdots. \tag{27}$$

Plugging Equations (26) and (27) in (25) and equating the coefficient of the same powers of $\wp$, one can get the simpler problems, given as:

Zero-order problem:

$$\frac{\partial^\alpha \mathcal{U}_0(s,t)}{\partial t^\alpha} = 0, \quad \mathcal{U}_0(s,0) = 1 - s^2. \tag{28}$$

First-order problem:

$$\frac{\partial^\alpha \mathcal{U}_1(s,t\,;C_1)}{\partial t^\alpha} = (1+C_1)\frac{\partial^\alpha \mathcal{U}_0(s,t)}{\partial t^\alpha} - C_1 P - C_1 \frac{\partial^2 \mathcal{U}_0(s,t)}{\partial s^2} - \frac{C_1}{s}\frac{\partial \mathcal{U}_0(s,t)}{\partial s}, \quad \mathcal{U}_1(s,0) = 0. \tag{29}$$

Respective solutions of Equations (28) and (29) after apply fractional integral and initial condition are given:

$$\begin{aligned} \mathcal{U}_0(s,t) &= 1 - s^2, \\ \mathcal{U}_1(s,t\,;C_1) &= -\frac{C_1(P-4)t^\alpha}{\Gamma(1+\alpha)}. \end{aligned} \tag{30}$$

One can get the following expression:

$$\begin{aligned} \tilde{\mathcal{U}}(s,t) &= \mathcal{U}_0(s,t) + \mathcal{U}_1(s,t\,;C_1) + \mathcal{U}_2(s,t\,;C_1,C_2) + \cdots \\ &= 1 - s^2 - \frac{C_1(P-4)t^\alpha}{\Gamma(1+\alpha)}. \end{aligned} \tag{31}$$

We used the least square method after finding the residual and then got the auxiliary constant value for $\alpha = 1$; we have $C_1 = -1$. Putting the value of C_1 in Equation (31), we get

$$\tilde{\mathcal{U}}(s,t) = 1 - s^2 + \frac{(P-4)t^\alpha}{\Gamma(1+\alpha)}. \tag{32}$$

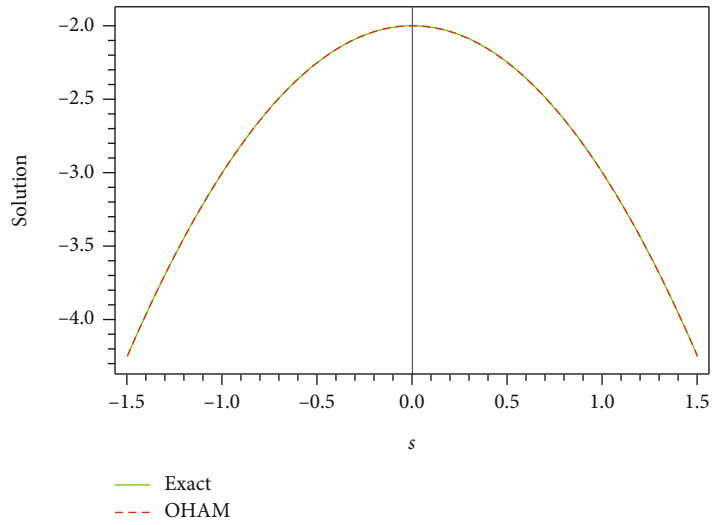

(a) Exact vs. OHAM solution

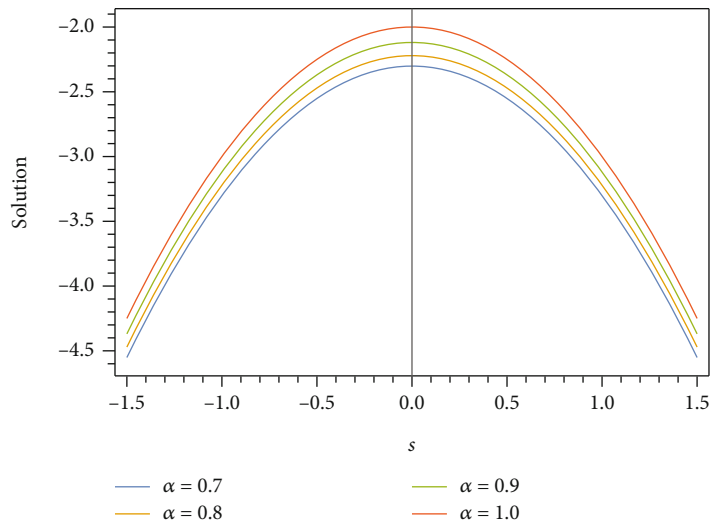

(b) Solution behavior for different values of α

FIGURE 1: Continued.

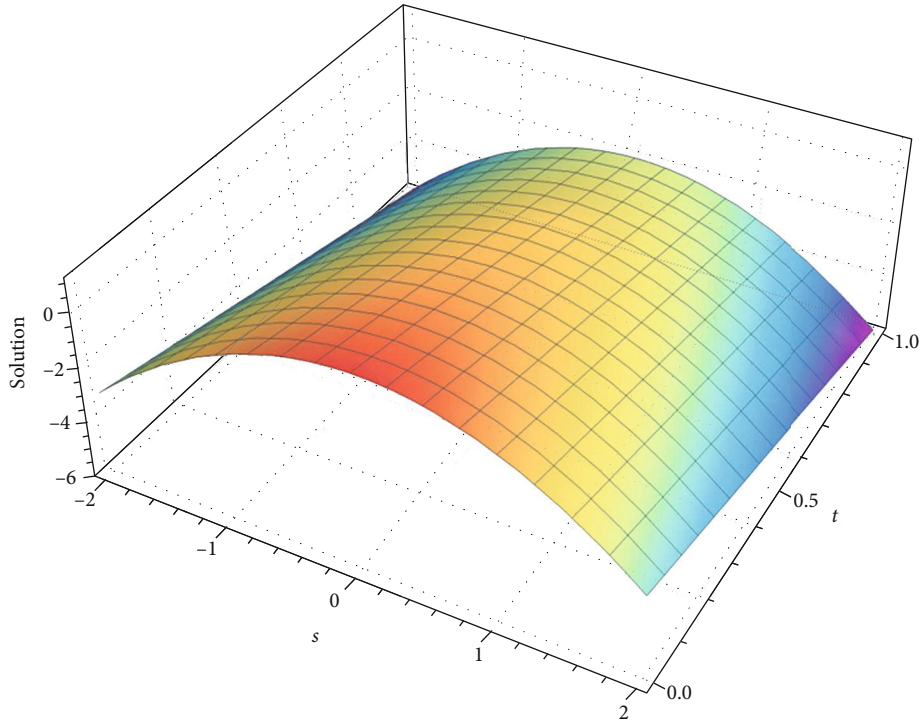

(c) Exact solution

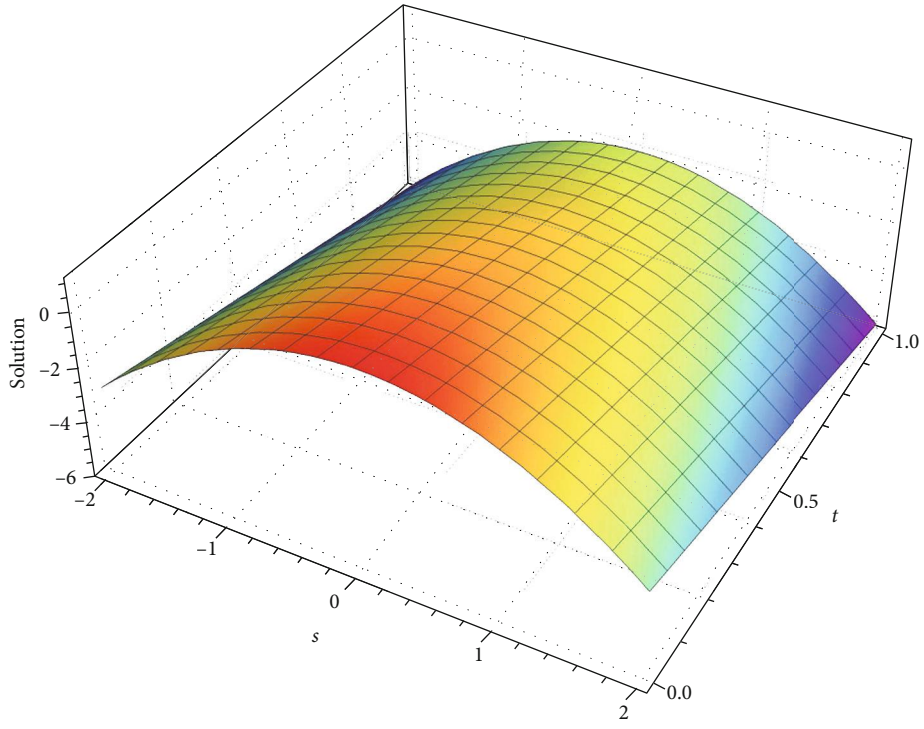

(d) OHAM solution for $\alpha = 1$

Figure 1: Continued.

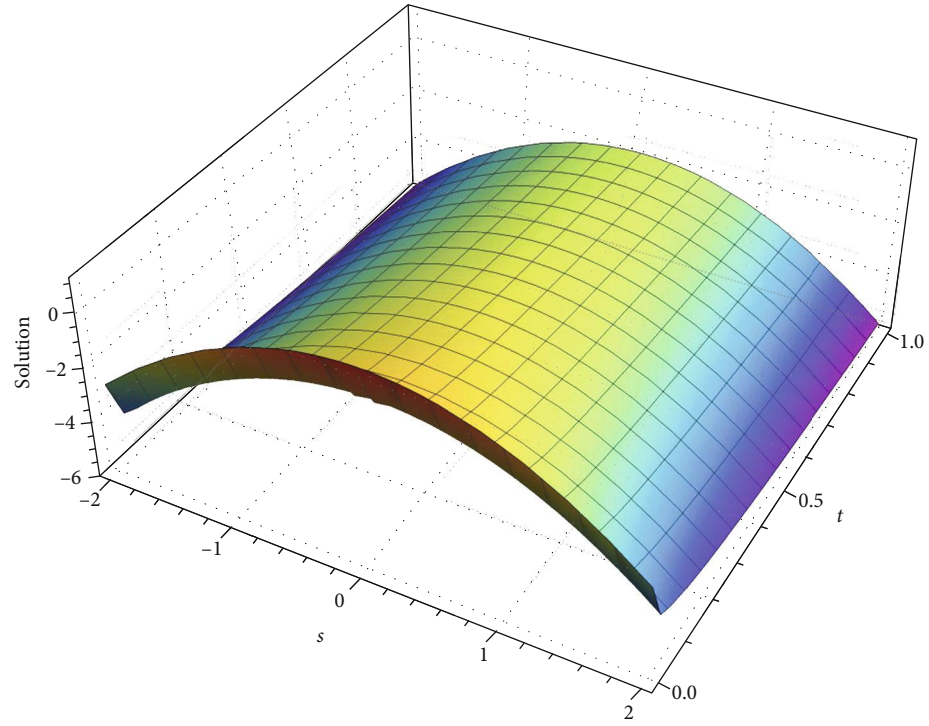

(e) Solution for $\alpha = 0.2$

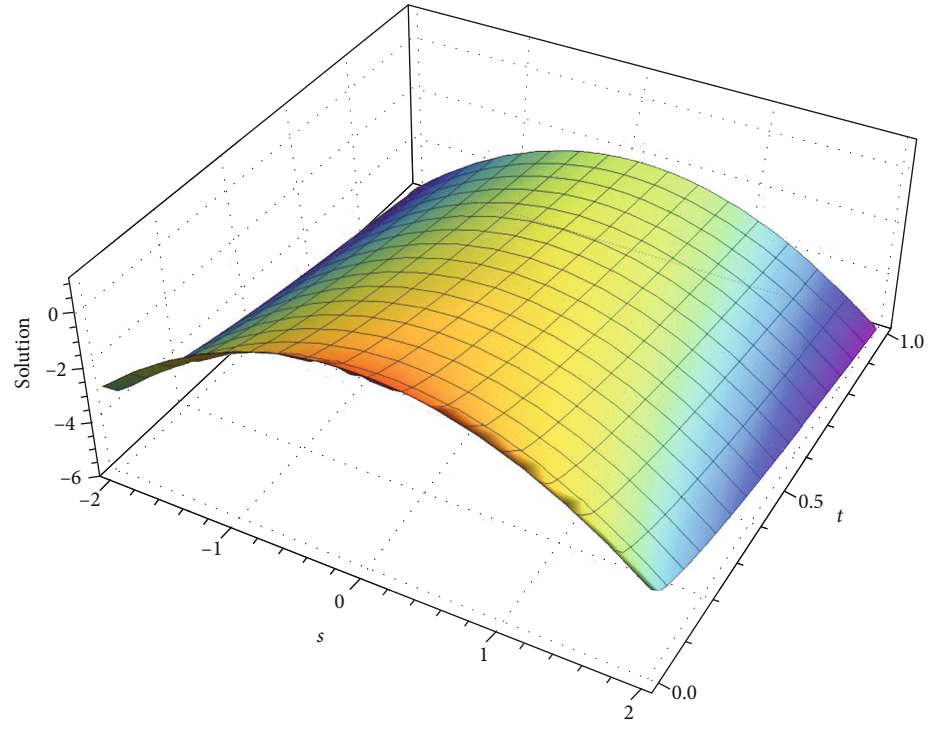

(f) Solution for $\alpha = 0.5$

Figure 1: Exact solution and OHAM solution behavior of Example 1.

The result (32) is in complete agreement with [14, 25–31]. Figure 1 shows the evaluation results of the semianalytical solution for Example 1 when $P = 1$ and show the dynamics of the obtained solution by OHAM for various noninteger order Brownian motions and for standard motions, i.e., for $\alpha = 1$. It can be seen that the solution acquired via the above-mentioned technique is decreasing very swiftly with the increase in t in Example 1, which is illustrated in Figure 1(b). Figure 1(a) shows the efficiency of the above-mentioned method. Figures 1(e) and 1(f) show the solution behavior for $\alpha = 0.2$ and $\alpha = 0.5$. Besides, we have obtained the exact solution by OHAM.

Example 2. Suppose a time-fractional Navier-Stokes equation:

$$\frac{\partial^{\alpha}\mathcal{U}(s,t)}{\partial t^{\alpha}} = \frac{\partial^{2}\mathcal{U}(s,t)}{\partial s^{2}} + \frac{1}{s}\frac{\partial\mathcal{U}(s,t)}{\partial s}, \tag{33}$$

with the initial condition

$$\mathcal{U}(s,0) = s, \tag{34}$$

where $\partial^{\alpha}/\partial t^{\alpha}$ is Caputo fractional derivative and $0 < \alpha \leq 1$. We consider the first four terms of the exact solution of (33) from [14] is given by:

$$\mathcal{U}(s,t) = s + \frac{t}{s} + \frac{t^{2}}{2s^{3}} + \frac{9t^{3}}{6s^{5}}. \tag{35}$$

According to Section 3, we can set up the homotopy in the following way:

$$(1-\wp)\frac{\partial^{\alpha}\omega(s,t;\wp)}{\partial t^{\alpha}} = \mathcal{H}(\wp,C_{p})\left[\frac{\partial^{\alpha}\omega(s,t;\wp)}{\partial t^{\alpha}} - \frac{\partial^{2}\omega(s,t;\wp)}{\partial s^{2}} - \frac{1}{s}\frac{\partial\omega(s,t;\wp)}{\partial s}\right], \tag{36}$$

where

$$\omega(s,t;\wp) = \mathcal{U}_{0}(s,t) + \sum_{q=1}^{\infty}\mathcal{U}_{q}(s,t;C_{p})\wp^{q}, \quad p = 1,2,3\cdots \tag{37}$$

$$\mathcal{H}(\wp,C_{p}) = \wp C_{1} + \wp^{2}C_{2} + \wp^{3}C_{3} + \wp^{4}C_{4} + \cdots. \tag{38}$$

Plugging Equations (37) and (38) in (36) and equating the coefficient of the same powers of $\wp$, one can get the simpler problems, given as:

Zero-order problem:

$$\frac{\partial^{\alpha}\mathcal{U}_{0}(s,t)}{\partial t^{\alpha}} = 0, \quad \mathcal{U}_{0}(s,0) = s. \tag{39}$$

First-order problem:

$$\frac{\partial^{\alpha}\mathcal{U}_{1}(s,t;C_{1})}{\partial t^{\alpha}} = (1+C_{1})\frac{\partial^{\alpha}\mathcal{U}_{0}(s,t)}{\partial t^{\alpha}} - C_{1}\frac{\partial^{2}\mathcal{U}_{0}(s,t)}{\partial s^{2}} - \frac{C_{1}}{s}\frac{\partial\mathcal{U}_{0}(s,t)}{\partial s}, \qquad \mathcal{U}_{1}(s,0) = 0. \tag{40}$$

Second-order problem:

$$\begin{aligned}\frac{\partial^{\alpha}\mathcal{U}_{2}(s,t;C_{1},C_{2})}{\partial t^{\alpha}} &= (1+C_{1})\frac{\partial^{\alpha}\mathcal{U}_{1}(s,t;C_{1})}{\partial t^{\alpha}} - C_{1}\frac{\partial^{2}\mathcal{U}_{1}(s,t;C_{1})}{\partial s^{2}} \\ &\quad - \frac{C_{1}}{s}\frac{\partial\mathcal{U}_{1}(s,t;C_{1})}{\partial s} + C_{2}\frac{\partial^{\alpha}\mathcal{U}_{0}(s,t)}{\partial t^{\alpha}} \\ &\quad - C_{2}\frac{\partial^{2}\mathcal{U}_{0}(s,t)}{\partial s^{2}} - \frac{C_{2}}{s}\frac{\partial\mathcal{U}_{0}(s,t)}{\partial s}, \quad \mathcal{U}_{2}(s,0) = 0.\end{aligned} \tag{41}$$

Table 1: C_1, C_2, C_3 for various values of α.

α	C_1	C_2	C_3
0.7	-1.036692817879	-0.001240278601	-4.24687×10^{-5}
0.8	-1.020447062606	-0.000376864638	-7.02931×10^{-6}
0.9	-1.010550021386	-0.000101578844	-9.88500×10^{-7}
0.10	-0.999953117565	-0.000040256679	3.30467×10^{-8}

Table 2: Comparison of exact and OHAM solution.

s	Exact	OHAM	Abs error
1.0	2.94735999	2.94736040	$4.04145499 \times 10^{-7}$
1.2	3.05262208	3.05262204	$3.73698401 \times 10^{-8}$
1.4	3.16486784	3.16486694	$8.94947017 \times 10^{-7}$
1.6	3.28483456	3.28483228	$2.27227761 \times 10^{-6}$
1.8	3.41325952	3.41325524	$4.27305321 \times 10^{-6}$
2.0	3.55088000	3.55087299	$7.00096540 \times 10^{-6}$

Third-order problem:

$$\begin{aligned}\frac{\partial^{\alpha}\mathcal{U}_{3}(s,t;C_{1},C_{2},C_{3})}{\partial t^{\alpha}} &= (1+C_{1})\frac{\partial^{\alpha}\mathcal{U}_{2}(s,t;C_{1},C_{2})}{\partial t^{\alpha}} - C_{1}\frac{\partial^{2}\mathcal{U}_{2}(s,t;C_{1},C_{2})}{\partial s^{2}} \\ &\quad - \frac{C_{1}}{s}\frac{\partial\mathcal{U}_{2}(s,t;C_{1},C_{2})}{\partial s} + C_{2}\frac{\partial^{\alpha}\mathcal{U}_{1}(s,t;C_{1})}{\partial t^{\alpha}} \\ &\quad - C_{2}\frac{\partial^{2}\mathcal{U}_{1}(s,t;C_{1})}{\partial s^{2}} - \frac{C_{2}}{s}\frac{\partial\mathcal{U}_{1}(s,t;C_{1})}{\partial s} \\ &\quad + C_{3}\frac{\partial^{\alpha}\mathcal{U}_{0}(s,t)}{\partial t^{\alpha}} - C_{3}\frac{\partial^{2}\mathcal{U}_{0}(s,t)}{\partial s^{2}} \\ &\quad - \frac{C_{3}}{s}\frac{\partial\mathcal{U}_{0}(s,t)}{\partial s}, \mathcal{U}_{3}(s,0) = 0.\end{aligned} \tag{42}$$

Respective solutions of Equations (39)–(42) after apply fractional integral and initial condition are given:

$$\begin{aligned}\mathcal{U}_{0}(s,t) &= s, \\ \mathcal{U}_{1}(s,t;C_{1}) &= -\frac{C_{1}t^{\alpha}}{s\Gamma(1+\alpha)}, \\ \mathcal{U}_{2}(s,t;C_{1},C_{2}) &= -\frac{(C_{1}+C_{1}^{2}+C_{2})t^{\alpha}}{s\Gamma(1+\alpha)} + \frac{C_{1}^{2}t^{2\alpha}}{s^{3}\Gamma(1+2\alpha)}, \\ \mathcal{U}_{3}(s,t;C_{1},C_{2},C_{3}) &= -\frac{(C_{1}+2C_{1}^{2}+C_{1}^{3}+2C_{1}C_{2}+C_{2}+C_{3})(t)^{\alpha}}{s\Gamma(1+\alpha)} \\ &\quad + \frac{2C_{1}(C_{1}+C_{1}^{2}+C_{2})t^{2\alpha}}{s^{3}\Gamma(1+2\alpha)} - \frac{9C_{1}^{3}t^{3\alpha}}{s^{5}\Gamma(1+3\alpha)}. \\ &\vdots\end{aligned} \tag{43}$$

One can calculate the next order problem solutions by above similar process. In the end, we can get the expression:

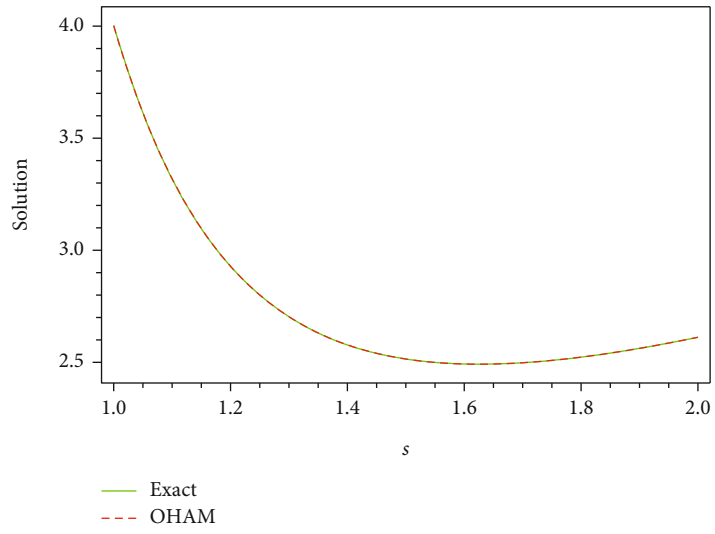

(a) Exact vs. OHAM solution

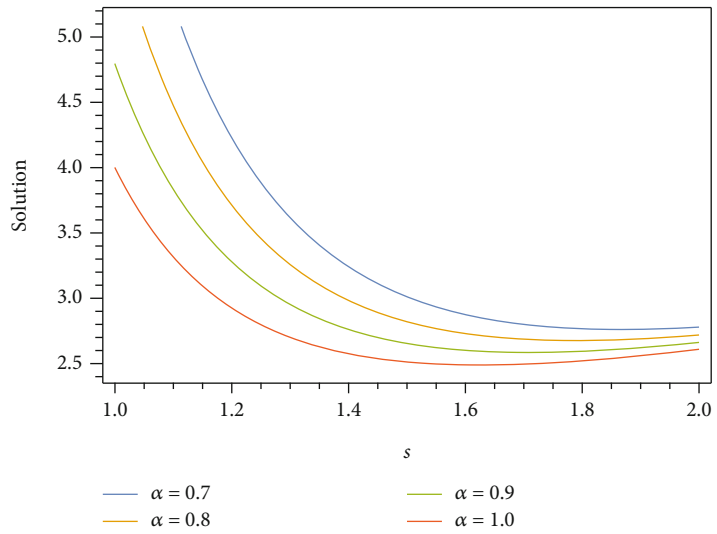

(b) Solution behavior for different values of α

Figure 2: Continued.

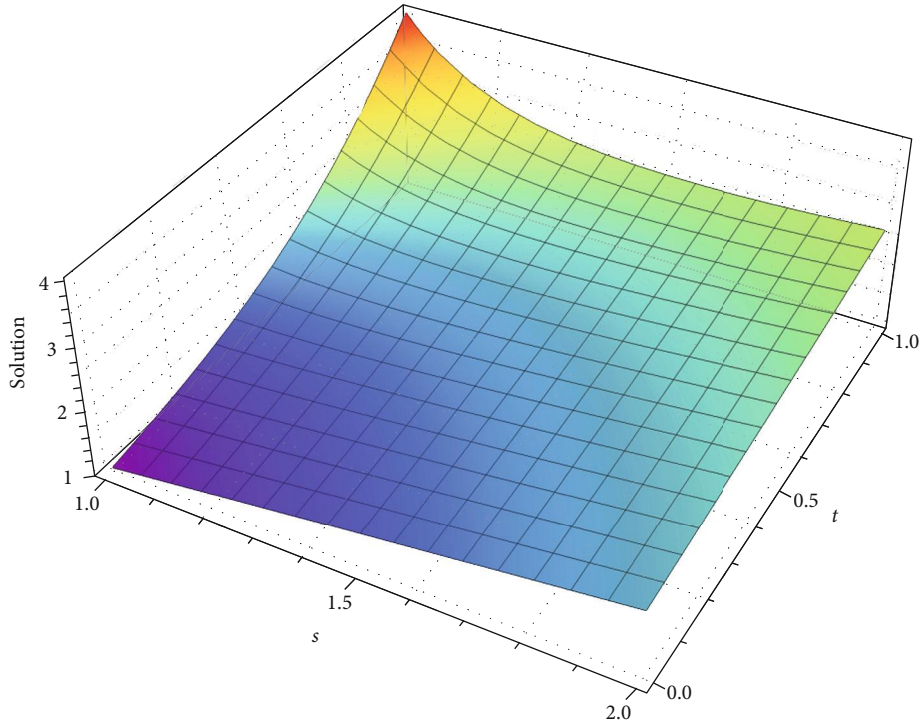

(c) Exact solution

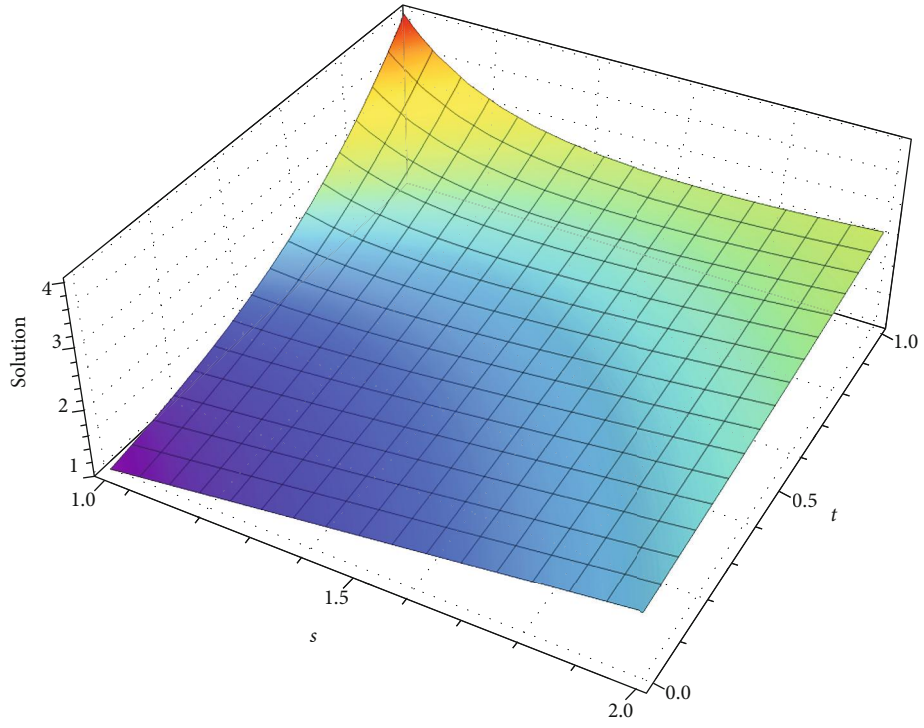

(d) OHAM solution for $\alpha = 1$

Figure 2: Continued.

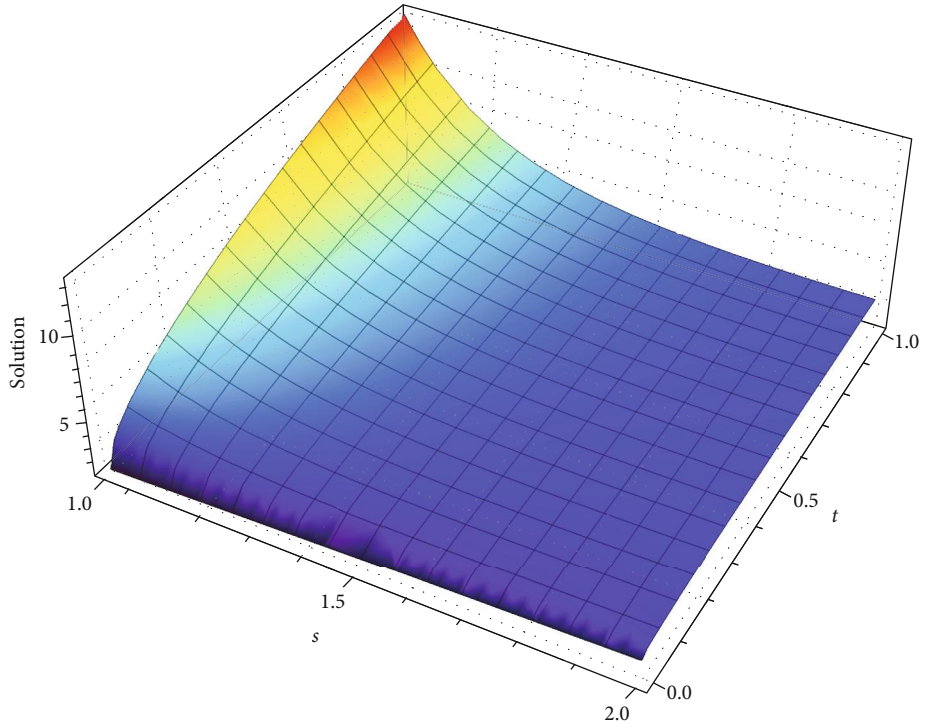

(e) Solution for $\alpha = 0.2$

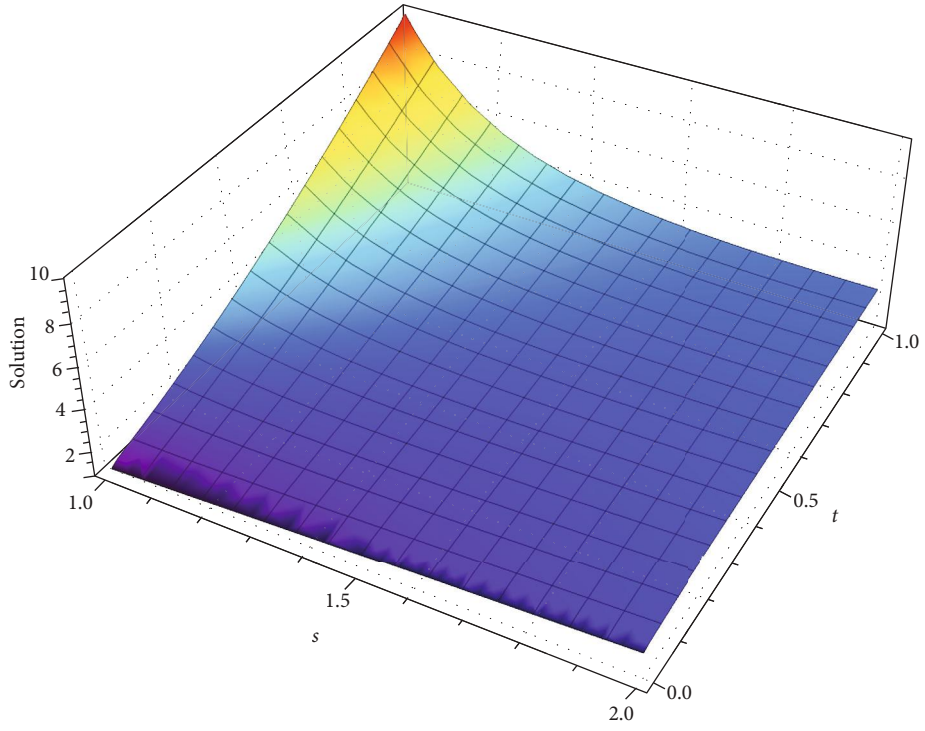

(f) Solution for $\alpha = 0.5$

Figure 2: Exact solution and OHAM solution behavior of Example 2.

$$\begin{aligned}\tilde{\mathcal{U}}(s,t) &= \mathcal{U}_0(s,t) + \mathcal{U}_1(s,t;C_1) + \mathcal{U}_2(s,t;C_1,C_2) \\ &\quad + \mathcal{U}_3(s,t;C_1,C_2,C_3)+\cdots \\ &= s - \frac{\left(3C_1 + 3C_1^2 + C_1^3 + 2C_2 + 2C_1C_2 + C_3\right)t^{\alpha}}{s\Gamma(1+\alpha)} \\ &\quad + \frac{C_1\left(3C_1 + 2C_1^2 + 2C_2\right)t^{2\alpha}}{s^3\Gamma(1+2\alpha)} - \frac{9C_1^3t^{3\alpha}}{s^5\Gamma(1+3\alpha)}\cdots.\end{aligned} \tag{44}$$

We used the least square method after finding the residual and then got the auxiliary constant value for α (see Table 1). The absolute error of both solutions can be seen in Table 2.

Putting the values of C_1, C_2, and C_3 for $\alpha = 1$ in Equation (44), we get

$$\tilde{\mathcal{U}}(s,t) = s + \frac{t^{\alpha}}{s\Gamma(1+\alpha)} + \frac{1.00008t^{2\alpha}}{s^3\Gamma(1+2\alpha)} + \frac{8.99873t^{3\alpha}}{s^5\Gamma(1+3\alpha)}. \tag{45}$$

Figure 2 shows the solution behavior of the time-fractional order Navier-Stokes equation by OHAM. In Figure 2(a), the solution curves are decreasing rapidly for higher fractional orders until we get the standard motion of fluid for $\alpha = 1$, and Figure 2(b) shows the proposed method's effectiveness and reliability. Figures 2(e) and 2(f) show the OHAM solution behavior for $\alpha = 0.2$ and $\alpha = 0.5$, respectively. The obtained results reveal that the method mentioned above is an efficient tool to study such types of fractional order fluid mechanics problems, which can be seen in Table 2.

5. Conclusion

In this study, fractional-order OHAM is successfully implemented to obtain the optimal solutions of time-fractional Navier-Stokes equation. From the acquired results, it can be seen that OHAM is an efficient and reliable semianalytical technique to approximate the solution of different fractional-order linear and nonlinear problems appearing in engineering and science. The above-mentioned technique provides a simple approach to control and adjust the convergence of the series solution utilizing the constants C_p's which are determined optimally. Two examples have been studied to illustrate the efficiency and versatility of this approach. The OHAM solution of the first example is the same as the exact solution, and for the OHAM solution of the second example, the obtained numerical approximation of the solution has a strong agreement with the exact solution. Besides, when the order of approximation increases, the error accuracy of the numerical solution decreases and becomes closer to the exact solutions. The proposed technique's fast accuracy and convergence are valid reasons for the researcher to use it for various problems in science and technology. It has been noted that the semianalytical solutions by extended formulation are in remarkable agreement with the exact solutions.

Data Availability

No real data were used to support this study.

Conflicts of Interest

This work does not have any conflicts of interest.

Authors' Contributions

The authors have contributed equally to this manuscript.

Acknowledgments

This research is studied at the School of Engineering, Monash University Malaysia.

References

[1] S. R. Bistafa, "On the development of the Navier-Stokes equation by Navier," *Revista Brasileira de Ensino de Física*, vol. 40, no. 2, p. 12, 2018.

[2] R. Hilfer, *Applications of Fractional Calculus in Physics*, World Scientific, Singapore, 2000.

[3] S. Das, *Functional Fractional Calculus*, Springer Berlin Heidelberg, Berlin, Heidelberg, 2011.

[4] K. Oldham, "Fractional differential equations in electrochemistry," *Advances in Engineering Software*, vol. 41, no. 1, pp. 9–12, 2010.

[5] V. E. Tarasov, *Fractional Dynamics: Applications of Fractional Calculus to Dynamics of Particles, Fields and Media*, Springer Science & Business Media, 2011.

[6] R. Matušu, "Application of fractional order calculus to control theory," *International Journal of Mathematical Models and Methods in Applied Sciences*, vol. 5, no. 7, pp. 1162–1169, 2011.

[7] R. P. Meilanov and R. A. Magomedov, "Thermodynamics in fractional calculus," *Journal of Engineering physics and thermophysics*, vol. 87, no. 6, pp. 1521–1531, 2014.

[8] F. Meral, T. Royston, and R. Magin, "Fractional calculus in viscoelasticity: an experimental study," *Communications in Nonlinear Science and Numerical Simulation*, vol. 15, no. 4, pp. 939–945, 2010.

[9] O. W. Abdulwahhab and N. H. Abbas, "A new method to tune a fractional-order PID controller for a twin rotor aerodynamic system," *Arabian Journal for Science and Engineering*, vol. 42, no. 12, pp. 5179–5189, 2017.

[10] Y. Jiang, B. Zhang, X. Shu, and Z. Wei, "Fractional-order autonomous circuits with order larger than one," *Journal of Advanced Research*, vol. 25, pp. 217–225, 2020.

[11] F. Liu and K. Burrage, "Novel techniques in parameter estimation for fractional dynamical models arising from biological systems," *Computers & Mathematcs with Applications*, vol. 62, no. 3, pp. 822–833, 2011.

[12] N. Ali Shah, D. Vieru, and C. Fetecau, "Effects of the fractional order and magnetic field on the blood flow in cylindrical domains," *Journal of Magnetism and Magnetic Materials*, vol. 409, pp. 10–19, 2016.

[13] N. H. Can, H. Jafari, and M. N. Ncube, "Fractional calculus in data fitting," *Alexandria Engineering Journal*, vol. 59, no. 5, pp. 3269–3274, 2020.

[14] S. Momani and Z. Odibat, "Analytical solution of a time-fractional Navier-Stokes equation by Adomian decomposition method," *Applied Mathematics and Computation*, vol. 177, no. 2, pp. 488–494, 2006.

[15] S. J. Liao, *On the Proposed Homotopy Analysis Technique for Nonlinear Problems and its Applications, [Ph.D. thesis]*, Shanghai Jio Tong University, Shanghai, China, 1992.

[16] J. He, "An approximate solution technique depending on an artificial parameter: a special example," *Communications in Nonlinear Science and Numerical Simulation*, vol. 3, no. 2, pp. 92–97, 1998.

[17] D. D. Ganji and M. Rafei, "Solitary wave solutions for a generalized Hirota-Satsuma coupled KdV equation by homotopy perturbation method," *Physics Letters A*, vol. 356, no. 2, pp. 131–137, 2006.

[18] D. Lu and J. Liu, "Application of the homotopy analysis method for solving the variable coefficient KdV-Burgers equation," *Abstract and Applied Analysis*, vol. 2014, Article ID 309420, 4 pages, 2014.

[19] A. M. Siddiqui, S. Irum, and A. R. Ansari, "A solution of the unsteady squeezing flow of a viscous fluid between parallel plates using the homotopy perturbation method," *Mathematical Modelling and Analysis*, vol. 13, no. 4, pp. 565–576, 2008.

[20] V. Marinca and N. Herisanu, "Application of optimal homotopy asymptotic method for solving nonlinear equations arising in heat transfer," *International Communications in Heat and Mass Transfer*, vol. 35, no. 6, pp. 710–715, 2008.

[21] N. Herisanu, V. Marinca, T. Dordea, and G. Madescu, "A new analytical approach to nonlinear vibration of an electrical machine," *Proceedings of the Romanian Academy, Series A*, vol. 9, no. 3, pp. 229–236, 2008.

[22] V. Marinca and N. Herisanu, "Determination of periodic solutions for the motion of a particle on a rotating parabola by means of the optimal homotopy asymptotic method," *Journal of Sound and Vibration*, vol. 329, no. 9, pp. 1450–1459, 2010.

[23] N. Herisanu and V. Marinca, "Accurate analytical solutions to oscillators with discontinuities and fractional-power restoring force by means of the optimal homotopy asymptotic method," *Computers & Mathematics with Applications*, vol. 60, no. 6, pp. 1607–1615, 2010.

[24] V. Marinca, N. Herişanu, C. Bota, and B. Marinca, "An optimal homotopy asymptotic method applied to the steady flow of a fourth- grade fluid past a porous plate," *Applied Mathematics Letters*, vol. 22, no. 2, pp. 245–251, 2009.

[25] S. Kumar, D. Kumar, S. Abbasbandy, and M. M. Rashidi, "Analytical solution of fractional Navier-Stokes equation by using modified Laplace decomposition method," *Ain Shams Engineering Journal*, vol. 5, no. 2, pp. 569–574, 2014.

[26] A. Prakash, D. G. Prakasha, and P. Veeresha, "A reliable algorithm for time-fractional Navier-Stokes equations via Laplace transform," *Nonlinear Engineering*, vol. 8, no. 1, pp. 695–701, 2019.

[27] D. Kumar, J. Singh, and S. Kumar, "A fractional model of Navier-Stokes equation arising in unsteady flow of a viscous fluid," *Journal of the Association of Arab Universities for Basic and Applied Sciences*, vol. 17, no. 1, pp. 14–19, 2015.

[28] K. Wang and S. Liu, "Analytical study of time-fractional Navier-Stokes equations by transform methods," *Advances in Difference Equations*, vol. 2016, no. 1, Article ID 61, 2016.

[29] S. Maitama, "Analytical solution of time-fractional Navier-Stokes equation by natural homotopy perturbation method," *Progress in Fractional Differentiation and Applications*, vol. 4, no. 2, pp. 123–131, 2018.

[30] B. K. Albuohimad, "Analytical technique of the fractional Navier-Stokes model by Elzaki transform and homotopy perturbation method," *AIP Conference Proceedings*, vol. 2144, article 050002, 2019.

[31] N. A. Khan, A. Ara, S. A. Ali, and A. Mahmood, "Analytical study of Navier-Stokes equation with fractional orders using He's homotopy perturbation and variational iteration methods," *International Journal of Nonlinear Sciences and Numerical Simulation*, vol. 10, no. 9, pp. 1127–1134, 2009.

[32] A. A. Kilbas, H. M. Srivastava, and J. J. Trujillo, *Theory and Applications of Fractional Differential Equations, North-Holland Mathematics Studies*, vol. 204, Elsevier, Amsterdam, 2006.

[33] S. Iqbal, M. Idrees, A. M. Siddiqui, and A. R. Ansari, "Some solutions of the linear and nonlinear Klein-Gordon equations using the optimal homotopy asymptotic method," *Applied Mathematics and Computation*, vol. 216, no. 10, pp. 2898–2909, 2010.

Hindawi
Advances in Mathematical Physics
Volume 2021, Article ID 5554280, 11 pages
https://doi.org/10.1155/2021/5554280

Research Article

Regarding New Traveling Wave Solutions for the Mathematical Model Arising in Telecommunications

Haci Mehmet Baskonus,[1] **Juan Luis García Guirao**,[2,3] **Ajay Kumar**,[4] **Fernando S. Vidal Causanilles**,[2] **and German Rodriguez Bermudez**[5]

[1]*Department of Mathematics and Science Education, Faculty of Education, Harran University, Sanliurfa, Turkey*
[2]*Departamento de Matemática Aplicada y Estadstica. Universidad Politécnica de Cartagena, Hospital de Marina, 30203 Cartagena, Región de Murcia, Spain*
[3]*Department of Mathematics, Faculty of Science, King Abdulaziz University, P.O. Box 80203, Jeddah 21589, Saudi Arabia*
[4]*Bakhtiyarpur College of Engineering (Department of Science and Technology, Govt. of Bihar), Patna 803212, India*
[5]*University Centre of Defence at the Spanish Air Force Academy, UPCT-MDE Calle Coronel Lopez Peña, s/n, Santiago de la Ribera, Murcia 30720, Spain*

Correspondence should be addressed to Juan Luis García Guirao; jlgarcia@kau.edu.sa

Received 24 February 2021; Accepted 19 June 2021; Published 14 July 2021

Academic Editor: Nikos E. Mastorakis

This research paper focuses on the application of the tanh function method to find the soliton solutions of the (2+1)-dimensional nonlinear electrical transmission line model. Materials used to form a transmitting line are very important to transmit electric charge. In this sense, we find some new voltage behaviors such as dark, trigonometric, and complex function solutions. Choosing some suitable values of parameters, we present some various surfaces of results obtained in this paper. These results play an important role in telecommunications lines used to stand for wave propagations.

1. Introduction

Nonlinear partial differential equations (NPDEs) are recently used to investigate the meanings of physical problems such as fluid dynamics, mathematics, physics and quantum field theory, and nonlinear fiber optics. Systems of NPDEs are also considered as a main tool to investigate in chemical and biological experiments. Some methods such as index the extended tanh method [1, 2], the sine cosine method [3], the inverse scattering transform method [4], finite difference method [5], tanh and extended tanh methods [6–8], Jacobi elliptic function expansion method [9], modified expansion method [10], generalized tanh method [11, 12], sine-Gordon expansion method [13], extended mean value theorem [14], and interval-valued fuzzy topsis method [15] to obtain various solutions of such NPDEs have been presented in the literatures. Cordero et al. have observed the stability analysis of the fourth-order iterative method in [16]. The (3 +1) Dimensional Boiti-Leon-Manna-Pempinelli equation has been deeply studied in [17]. Using time scale calculus, discrete normal vector field approximation has been presented in [18]. A Handy Technique has been handled in [19]. Classical Boussinesq equations have been immensely studied in [20]. Traveling wave solutions of nonlinear Klein Gordon equation were observed in [21] and so on [15, 17, 18, 22–43].

The contents of this paper are as follows. Section 2 presents the general properties of the tanh function method (TFM) [44]. This TFM has been proposed as a strong and creditable method for finding the solutions of the nonlinear models. Section 3 introduces some new complex dark, trigonometric, and hyperbolic soliton solutions to the nonlinear

electrical transmission line. To express physical properties in terms of mathematical dynamics, such as wave propagation of electrical transmission lines, has been presented by equation defined as [9]

$$v_{tt} - \alpha\left(v^2\right)_{tt} + \beta\left(v^3\right)_{tt} - w_0^2\delta_1^2 v_{xx} - w_0^2\frac{\delta_1^4}{12}v_{xxxx} - \omega_0^2\delta_2^2 v_{yy} - \omega_0^2\frac{\delta_2^2}{12}v_{yyyy} = 0, \tag{1}$$

where $v = v(x, y, t)$ is used to explain the tightness throughout the electrical line and x and y are interpreted like the promulgation distance. t is the period, and α and β are constants with nonzero. δ_1 is the space between two proximate sections in during longitudinally flank, while δ_2 is the space between two proximate sections in the transversal flank [9]. With the help of some computational programs, we are able to plot in terms of 2D, 3D, and contour surfaces of the results theoretically found. Finally, the main conclusions are given in the last section of the paper.

2. The Tanh Function Method

In this part of the paper, we present the general properties of the tanh function method in a detailed manner [45–48].

$$P\left(u, u_x, u_y, u_t, u_{xx}, uu_{xyt}, \cdots\right) = 0, \tag{2}$$

where P is a polynomial in the dependent variable u. Considering the traveling wave transformation as $u = u(x, y, t) = U(\xi)$, $\xi = k(x + y - ct)$, we obtain the following nonlinear ordinary differential equation

$$N\left(U, U^2, U', U'', U''', \cdots\right) = 0, \tag{3}$$

with N is a polynomial of $U = U(\xi)$. Now, finding the traveling wave solutions to Eq. (2) is equivalent to obtain the solution to reduced ordinary differential Eq. (3), and it can be introduced a new independent variable defined as

$$Y(\xi) = \mathrm{Tanh}(\xi). \tag{4}$$

We can find the following for some derivations as

$$\begin{aligned} \frac{d}{d\xi}(.) &= \left(1 - Y^2\right)\frac{d}{dY}(.), \\ \frac{d^2}{d\xi^2}(.) &= \left(1 - Y^2\right)\left[-2Y\frac{d}{dY}(.) + \left(1 - Y^2\right)\frac{d^2}{dY^2}(.)\right], \\ \frac{d^3}{d\xi^3}(.) &= \cdots, \\ &\vdots . \end{aligned} \tag{5}$$

As the last step, we present the tanh series as being

$$U(\xi) = S(Y) = \sum_{i=0}^{m} a_i Y^i, \tag{6}$$

where m is a positive integers. The values of m, generally, with the help of the balance principle can be determined.

3. Mathematical Analysis

In this part of the paper, we find some new complex dark, trigonometric, and hyperbolic function solutions of Eq. (1) by using TFM. First of all, we consider the traveling wave transformation defined as

$$v = V(\xi), \xi = k(x + y - ct), \tag{7}$$

where k, c are nonzero constants or complex-valued parameters. When considering Eq. (7) into Eq. (1), we find

$$\begin{aligned} &c^2 V_{\xi\xi} - \alpha c^2\left(V^2\right)_{\xi\xi} + \beta c^2\left(V^3\right)_{\xi\xi} - w_0^2\delta_1^2 V_{\xi\xi} \\ &\quad - k^2 w_0^2\frac{\delta_1^4}{12}V_{\xi\xi\xi\xi} - \omega_0^2\delta_2^2 V_{\xi\xi} - k^2\omega_0^2\frac{\delta_2^2}{12}V_{\xi\xi\xi\xi} = 0. \end{aligned} \tag{8}$$

Integrating Eq. (8) twice with regard to ξ, setting the constants of integrations to zero yields

$$12\left[c^2 - w_0^2\delta_1^2 - \omega_0^2\delta_2^2\right]V + 12\beta c^2 V^3 - 12\alpha c^2 V^2 - k^2\left[w_0^2\delta_1^4 + \omega_0^2\delta_2^4\right]V'' = 0. \tag{9}$$

According to the general properties of TFM, it can be considered as

$$V = S = \sum_{m=0}^{M} a_m Y^m, \tag{10}$$

Substituting Eqs. (5), (10) into Eq. (9) gives

$$\begin{aligned} &\left[12\left(c^2 - w_0^2\delta_1^2 - \omega_0^2\delta_2^2\right)S + 12\beta c^2 S^3 - 12\alpha c^2 S^2\right. \\ &\quad \left. - k^2\left(w_0^2\delta_1^4 + \omega_0^2\delta_2^4\right)\left(1 - Y^2\right)\left(-2Y\frac{dS}{dY} + \left(1 - Y^2\right)\frac{d^2S}{dY}\right)\right] = 0. \end{aligned} \tag{11}$$

Using the balance rule, M can be found as

$$M = 1, \tag{12}$$

which result in

$$S = a_0 + a_1 Y. \tag{13}$$

Substituting Eq. (13) into Eq. (11) by getting necessary derivations presents

$$\begin{aligned} &\left[12\left(c^2 - w_0^2\delta_1^2 - \omega_0^2\delta_2^2\right)(a_0 + a_1 Y) + 12\beta c^2(a_0 + a_1 Y)^3\right. \\ &\quad \left. - 12\alpha c^2(a_0 + a_1 Y)^2 - k^2\left(w_0^2\delta_1^4 + \omega_0^2\delta_2^4\right)\left(1 - Y^2\right)(-2a_1 Y)\right] = 0. \end{aligned} \tag{14}$$

After some calculations, it can be obtained as follows:

Y^0: $12\left(c^2 a_0 - w_0^2\delta_1^2 a_0 - \omega_0^2\delta_2^2 a_0\right) + 12\beta c^2 a_0^3 - 12\alpha c^2 a_0^2 = 0,$

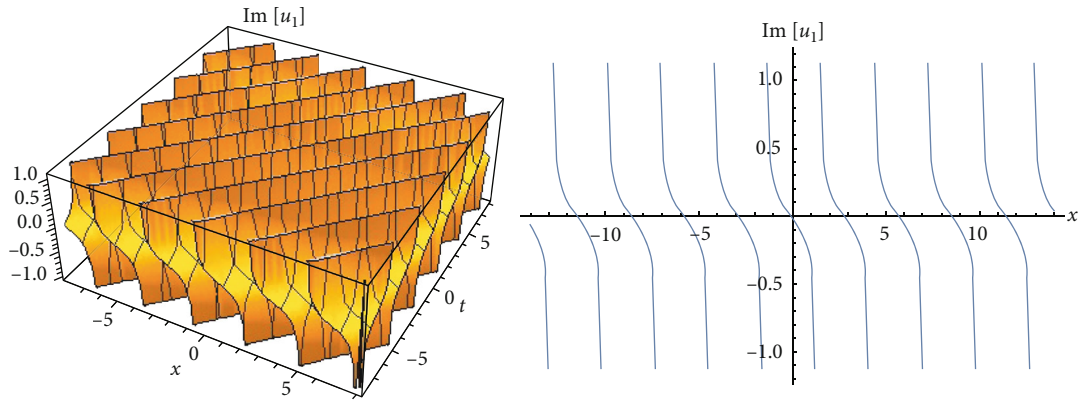

Figure 1: 2D and 3D surfaces of imaginary part of Eq. (16).

Y^1: $12(c^2a_1 - w_0^2\delta_1^2a_1 - \omega_0^2\delta_2^2a_1) + 36\beta c^2a_0^2a_1 - 24\alpha c^2a_0a_1 + 2k^2\omega_0^2\delta_2^4a_1 + 2k^2w_0^2\delta_1^4a_1 = 0$,

Y^2: $36\beta c^2a_0a_1^2 - 12c^2\alpha a_1^2 = 0$,

Y^3: $12\beta c^2a_1^3 - 2k^2\omega_0^2\delta_2^4a_1 - 2k^2w_0^2\delta_1^4a_1 = 0$.

Solving this system yields the following cases:

Case 1. When

$$a_0 = \frac{\alpha}{3\beta}\,; a_1 = \frac{\alpha}{3\beta}\,; k = \frac{i\sqrt{6}\sqrt{\alpha^2\left(w_0^2\delta_1^2 + \delta_2^2\omega_0^2\right)}}{\sqrt{\left(2\alpha^2 - 9\beta\right)\left(\delta_1^4w^2{}_0 - \delta_2^4\omega_0^2\right)}}\,; c = \frac{3i\sqrt{\beta\left(w_0^2\delta_1^2 + \delta_2^2\omega_0^2\right)}}{\sqrt{2\alpha^2 - 9\beta}}, \tag{15}$$

we get the following complex trigonometric function solution

$$v_1(x,y,t) = \frac{\alpha}{3\beta} + \frac{i\alpha}{3\beta}\tan\left[\frac{i\sqrt{6}\sqrt{\alpha^2\left(w_0^2\delta_1^2 + \delta_2^2\omega_0^2\right)}\left(x + y - \left(3i\sqrt{\beta\left(w_0^2\delta_1^2 + \delta_2^2\omega_0^2\right)}/\sqrt{2\alpha^2 - 9\beta}\right)t\right)}{\sqrt{\left(2\alpha^2 - 9\beta\right)\left(w_0^2\delta_1^4 + \delta_2^4\omega_0^2\right)}}\right], \tag{16}$$

in which α, β, δ_1, δ_2, and ω_0 are constant and nonzero. Choosing suitable values of coefficients in Eq. (16), we can observe some (Figures 1 and 2).

Case 2. Choosing as

$$a_0 = \frac{\alpha}{3\beta}\,; a_1 = \frac{\alpha}{3\beta}\,; c = \frac{3ik\delta_2\omega_0\sqrt{\beta\left(\delta_1^2 - \delta_2^2\right)}}{\sqrt{6\alpha^2 + k^2(2\alpha^2 - 9\beta)\delta_1^2}}, w_0 = \frac{i\delta_2\omega_0\sqrt{6\alpha^2 + k^2\delta_2^2(2\alpha^2 - 9\beta)}}{\sqrt{6\alpha^2\delta_1^2 + k^2(2\alpha^2 - 9\beta)\delta_1^4}}, \tag{17}$$

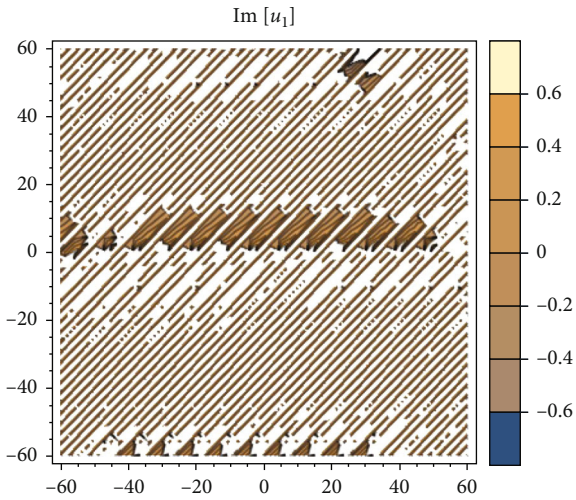

Figure 2: Contour surface of imaginary part of Eq. (16).

we get another new complex dark function solution

$$v_2(x,y,t) = \frac{\alpha}{3\beta} + \frac{\alpha}{3\beta}\tanh\left[kx + ky - \frac{3ik^2\delta_2\omega_0\sqrt{\beta\left(\delta_1^2 - \delta_2^2\right)}}{\sqrt{6\alpha^2 + k^2(2\alpha^2 - 9\beta)\delta_1^2}}t\right], \tag{18}$$

with strain conditions are $2\alpha^2 - 9\beta > 0$, $\beta(\delta_1^2 - \delta_2^2) > 0$, and also $\alpha, \beta, k, \delta_1, \omega_0, \delta_2$ are real constants and nonzero or complex-valued parameters. Considering some values of parameters under the strain conditions, different wave patterns can be observed from (Figures 3 and 4) for Eq. (18).

Case 3. Selecting

$$a_0 = \frac{\alpha}{3\beta}\,; a_1 = \frac{\alpha}{3\beta}\,; c = \frac{-3ik\delta_2\omega_0\sqrt{\beta\left(\delta_1^2 - \delta_2^2\right)}}{\sqrt{6\alpha^2 + k^2(2\alpha^2 - 9\beta)\delta_1^2}}, w_0 = \frac{-i\delta_2\omega_0\sqrt{6\alpha^2 + k^2\delta_2^2(2\alpha^2 - 9\beta)}}{\sqrt{6\alpha^2\delta_1^2 + k^2(2\alpha^2 - 9\beta)\delta_1^4}}, \tag{19}$$

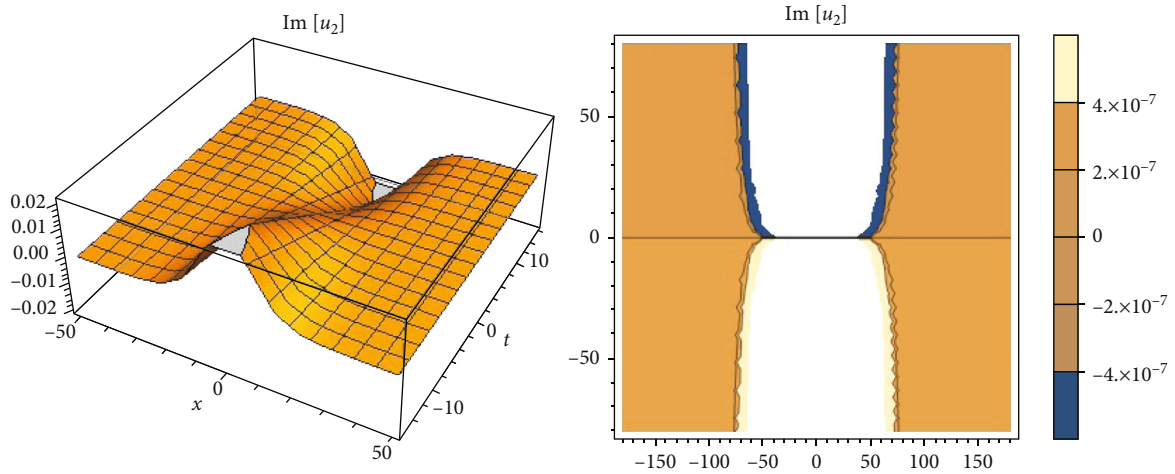

Figure 3: 3D and contour graphs of imaginary part of Eq. (18).

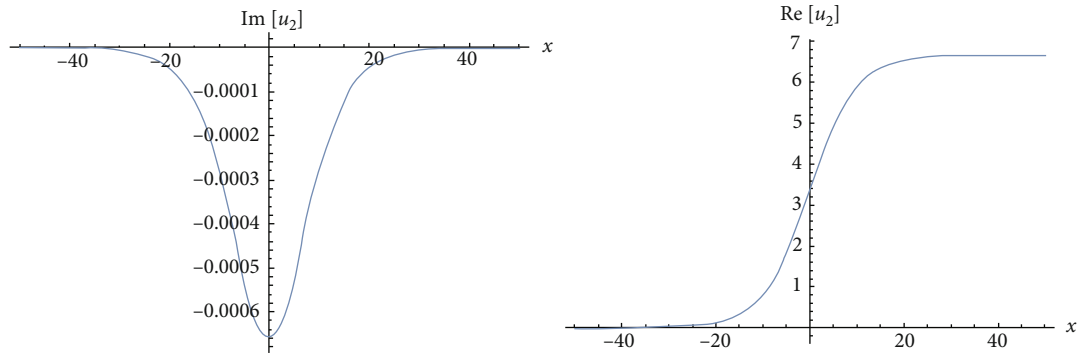

Figure 4: 2D figures of imaginary and real parts of Eq. (18).

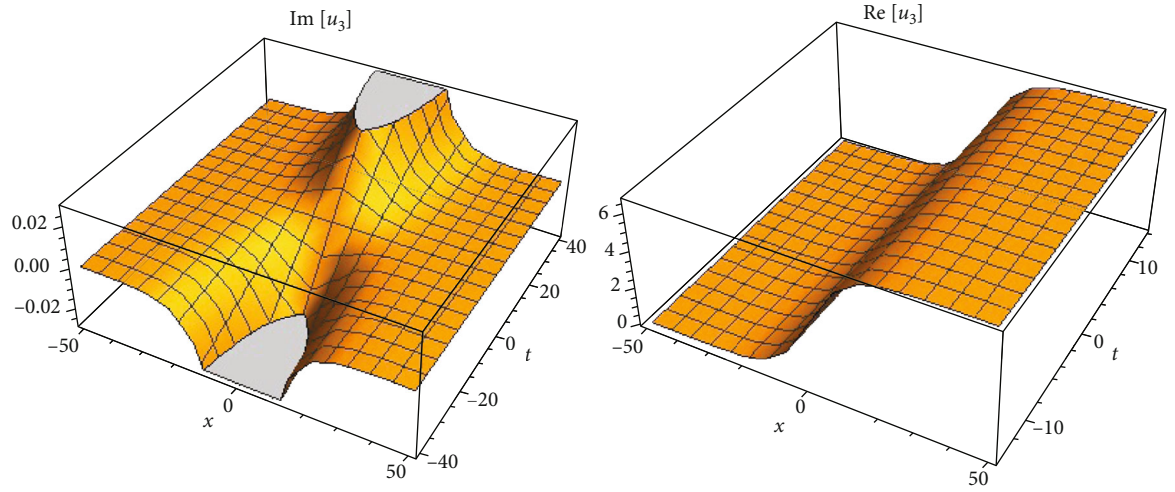

Figure 5: 3D graph of imaginary and real parts of Eq. (20).

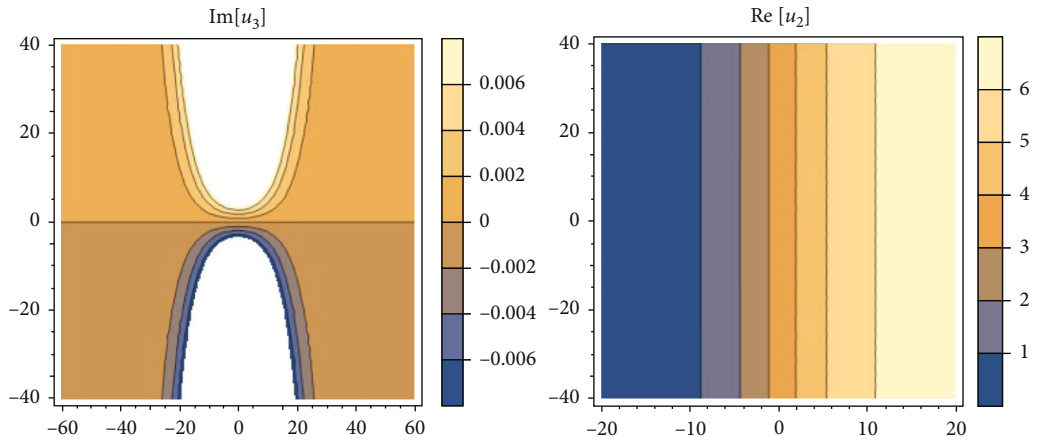

Figure 6: Contour figures of imaginary and real parts of Eq. (20).

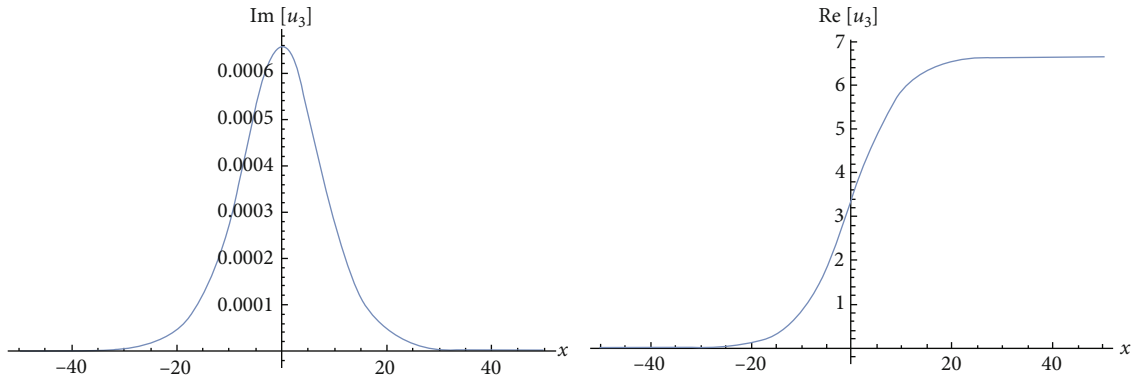

Figure 7: 2D figures of imaginary and real parts of Eq. (20).

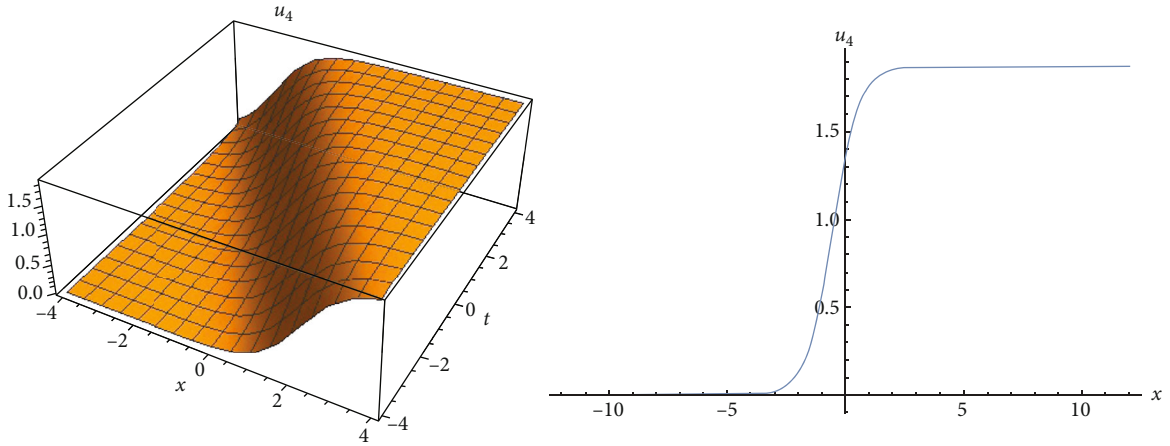

Figure 8: 2D and 3D simulations of Eq. (22).

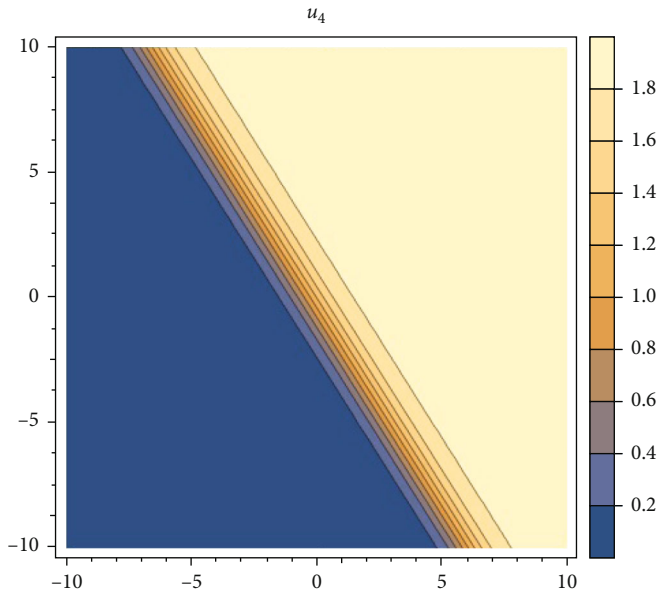

Figure 9: Contour graph of Eq. (22).

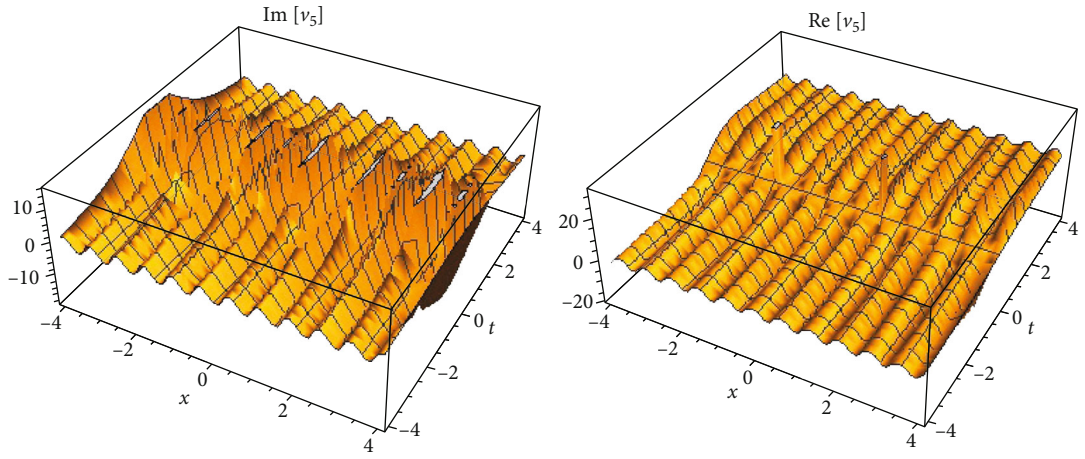

Figure 10: 3D figures of imaginary and real parts of Eq. (24).

we get conjugate new complex dark function solution as

$$v_3(x,y,t) = \frac{\alpha}{3\beta} + \frac{\alpha}{3\beta}\tanh\left[kx + ky + \frac{3ik^2\delta_2\omega_0\sqrt{\beta\left(\delta_1^2 - \delta_2^2\right)}}{\sqrt{6\alpha^2 + k^2(2\alpha^2 - 9\beta)\delta_1^2}}t\right], \tag{20}$$

with strain conditions are $2\alpha^2 - 9\beta > 0$, $\beta(\delta_1^2 - \delta_2^2) > 0$, and also $\alpha, \beta, k, \delta_1, \omega_0, \delta_2$ are real constants and nonzero or complex-valued parameters. 3D, 2D, and contour surfaces of Eq. (20) can be also seen (Figures 5–7) with the strain conditions.

Case 4. Choosing as

$$a_0 = a_1 = \frac{3k^2\left(w_0^2\delta_1^4 + \delta_2^4\omega_0^2\right)}{2\alpha\left(w_0^2\delta_1^2\left(3 + k^2\delta_1^2\right) + \delta_2^2\left(3 + k^2\delta_2^2\right)\right)}, c = \frac{-1}{\sqrt{3}}\sqrt{w_0^2\delta_1^2\left(3 + k^2\delta_1^2\right) + \delta_2^2\omega_0^2\left(3 + k^2\delta_2^2\right)},$$

$$\beta = \frac{2\alpha^2}{9k^2\left(w_0^2\delta_1^4 + \delta_2^4\omega_0^2\right)}\left(w_0^2\delta_1^2\left(3 + k^2\delta_1^2\right) + \delta_2^2\omega_0^2\left(3 + k^2\delta_2^2\right)\right), \tag{21}$$

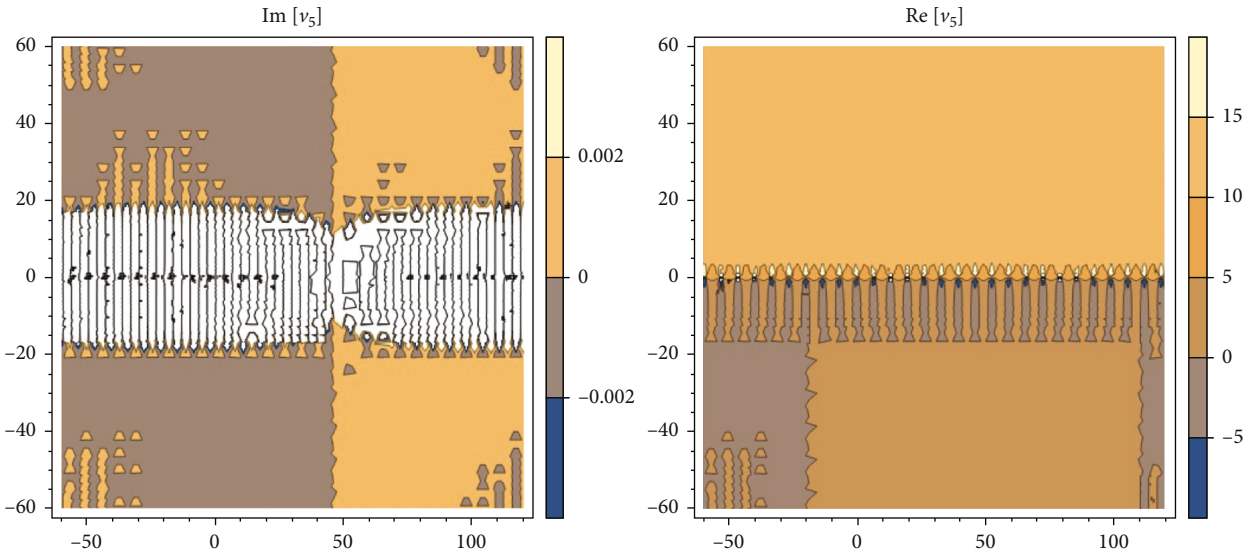

Figure 11: Contour figures of imaginary and real parts of Eq. (24).

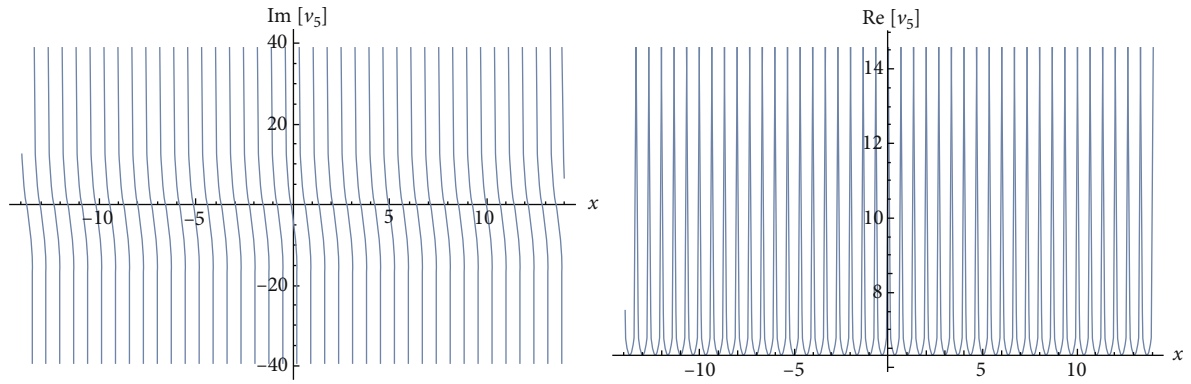

Figure 12: 2D figures of imaginary and real parts of Eq. (24).

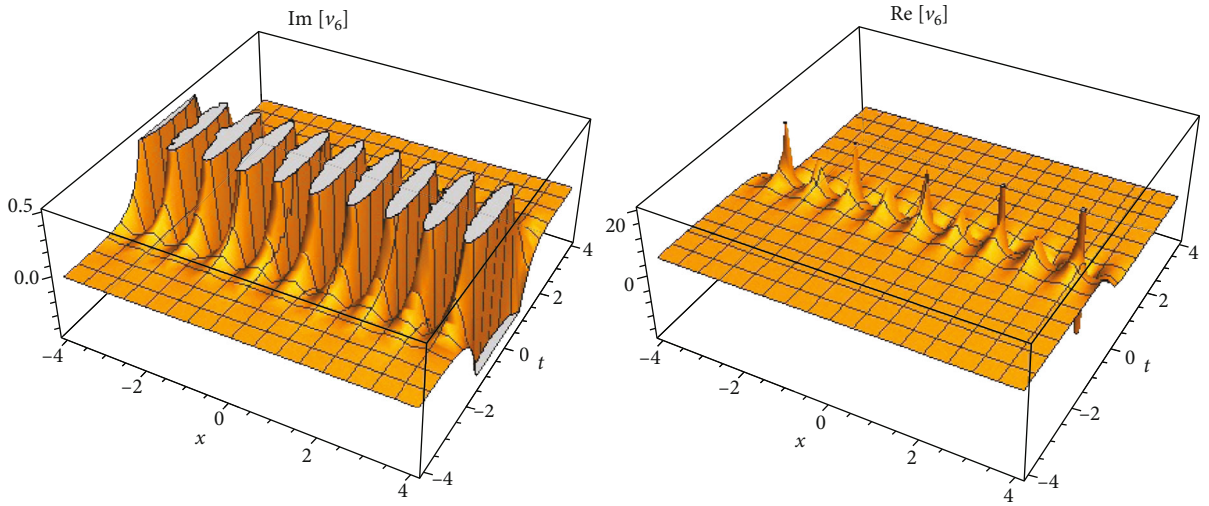

Figure 13: 2D and 3D of simulations of imaginary and real parts of Eq. (26).

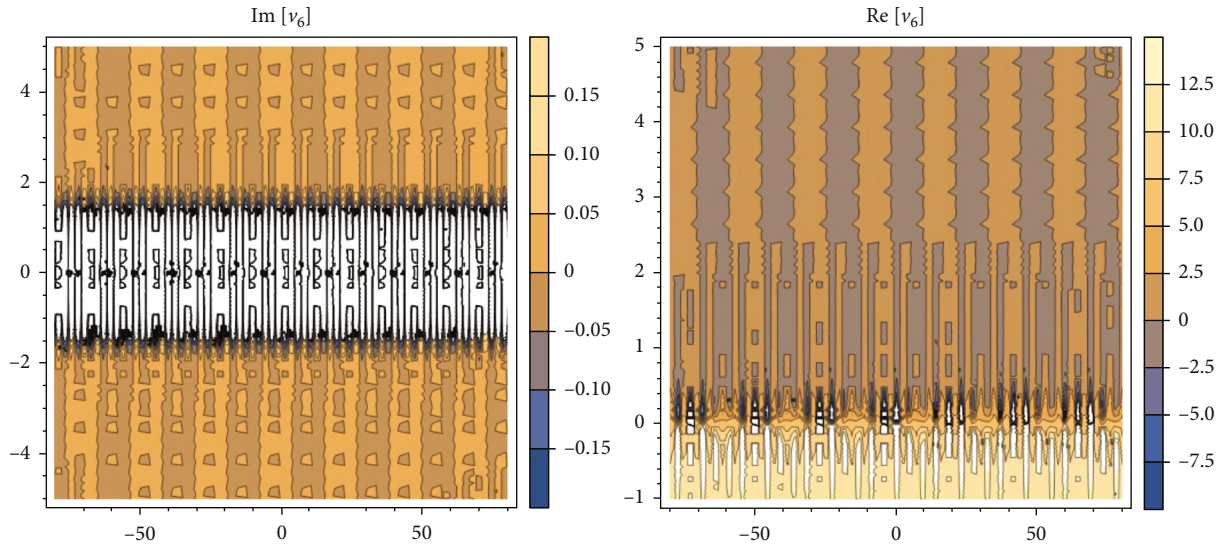

Figure 14: Contour surfaces of imaginary and real parts of Eq. (26).

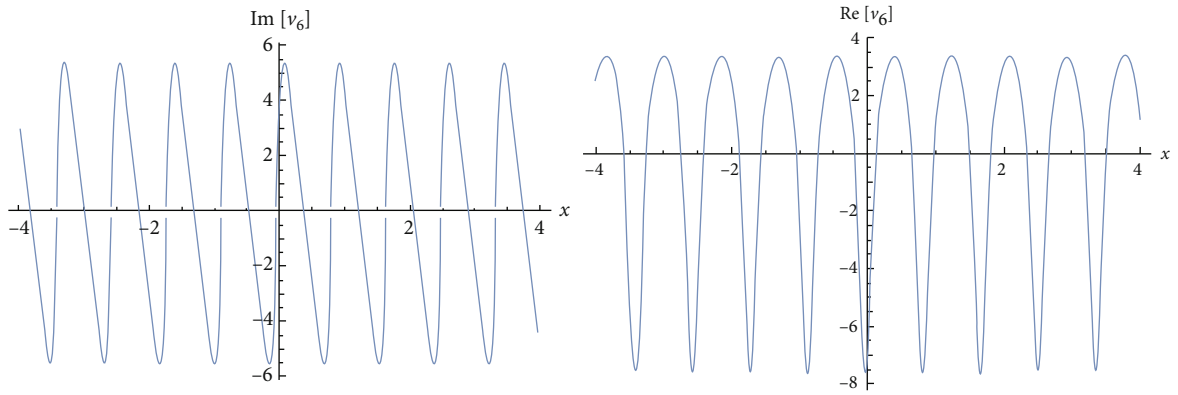

Figure 15: 2D figures of imaginary and real parts of Eq. (26).

produces the following dark soliton solution

$$v_4(x,y,t) = \frac{3k^2\left(w_0^2\delta_1^4 + \delta_2^4\omega_0^2\right)}{2\alpha\left(w_0^2\delta_1^2\left(3+k^2\delta_1^2\right) + \delta_2^2\left(3+k^2\delta_2^2\right)\right)} \cdot \left(1 + \tan h\left[kx + ky + \frac{k}{\sqrt{3}}\varpi t\right]\right) \tag{22}$$

in which $\varpi = \sqrt{w_0^2\delta_1^2(3+k^2\delta_1^2) + \delta_2^2\omega_0^2(3+k^2\delta_2^2)}$ and strain conditions are $\alpha, k, \delta_1, \omega_0, \delta_2$ are real constants and nonzero. 3D, 2D, and contour surfaces of Eq. (22) can be also observed (Figures 8 and 9).

Case 5. Taking as

$$a_0 = \frac{\alpha}{3\beta}, a_1 = \frac{\alpha}{3\beta}, k = \frac{-i\sqrt{6}\sqrt{\alpha^2\left(w_0^2\delta_1^2 + \delta_2^2\omega_0^2\right)}}{\sqrt{(2\alpha^2 - 9\beta)\left(\delta_1^4 w^2{}_0 + \delta_2^4\omega_0^2\right)}}, c = \frac{-3i\sqrt{\beta\left(w_0^2\delta_1^2 + \delta_2^2\omega_0^2\right)}}{\sqrt{2\alpha^2 - 9\beta}}, \tag{23}$$

produces another complex dark traveling wave solution to the governing model

$$v_5(x,y,t) = \frac{\alpha}{3\beta} - \frac{i\alpha}{3\beta}\tan\left[\frac{\sqrt{6}\sqrt{\alpha^2\left(w_0^2\delta_1^2 + \delta_2^2\omega_0^2\right)}\left(x + y + \left(3i\sqrt{\beta\left(w_0^2\delta_1^2 + \delta_2^2\omega_0^2\right)}/\sqrt{2\alpha^2 - 9\beta}\right)t\right)}{\sqrt{(2\alpha^2 - 9\beta)\left(w_0^2\delta_1^4 + \delta_2^4\omega_0^2\right)}}\right], \tag{24}$$

with strain conditions $\beta > 0, 2\alpha^2 > 9\beta$ and $\alpha, \beta, \omega_0, \delta_1, \delta_2$ are real constants and nonzero. 3D, 2D, and contour surfaces of Eq. (24) can be also observed in (Figures 10–12).

Case 6. Once we select other coefficients given as

$$a_0 = \frac{\alpha}{3\beta}, a_1 = \frac{\alpha}{3\beta}, k = \frac{-i\sqrt{6}\sqrt{\alpha^2\left(w_0^2\delta_1^2 + \delta_2^2\omega_0^2\right)}}{\sqrt{(2\alpha^2 - 9\beta)\left(\delta_1^4 w^2{}_0 + \delta_2^4\omega_0^2\right)}}, c = \frac{3i\sqrt{\beta\left(w_0^2\delta_1^2 + \delta_2^2\omega_0^2\right)}}{\sqrt{2\alpha^2 - 9\beta}}, \tag{25}$$

results in another complex dark traveling wave solution to the Eq. (1)

$$v_6(x,y,t) = \frac{\alpha}{3\beta} - \frac{i\alpha}{3\beta}\tan\left[\frac{\sqrt{6}\sqrt{\alpha^2\left(w_0^2\delta_1^2+\delta_2^2\omega_0^2\right)}\left(x+y-\left(3i\sqrt{\beta\left(w_0^2\delta_1^2+\delta_2^2\omega_0^2\right)}/\sqrt{2\alpha^2-9\beta}\right)t\right)}{\sqrt{\left(2\alpha^2-9\beta\right)\left(w_0^2\delta_1^4+\delta_2^4\omega_0^2\right)}}\right], \tag{26}$$

with strain conditions $\beta > 0, 2\alpha^2 > 9\beta$ and $\alpha, \beta, \omega_0, \delta_1, \delta_2$ are real constants and nonzero. Various surfaces of Eq. (26) with the considering suitable values of parameters can be also presented as (Figures 13–15).

4. Conclusions

In this manuscript, TFM being one of the powerful techniques has been successfully used to Eq. (1). Many new trigonometric, complex, and hyperbolic function solutions have been extracted, afterwards. The conditions which guarantee the existence of the valid solutions to this model are also given in a detailed manner. Considering the strain conditions of coefficients of results, various simulations have been also plotted by using some computational programs. These solutions are of various physical properties of the electrical transmission line. For example, the tanh function arises in gravitational potential as a dark structure [49]. Hence, it is estimated that the solution of v_4 is of such physical property. From (Figures 1–15), it can be also seen that the results simulate estimated wave behaviors. TFM used in this paper can be considered to solve other nonlinear problems arising in the theory of solitons and other areas of nonlinear science [50–56].

Data Availability

This work is not based on any data.

Conflicts of Interest

The authors declare that there is no conflict of interest.

Acknowledgments

This paper has been partially supported by Fundación Séneca (Spain), grant 20783/PI/18, and Ministerio de Ciencia, Innovación y Universidades (Spain), grant PGC2018-097198-B-I00. Secondly, the first author extends his special thanks to Harran University because this projected work was partially (not financial) supported by Harran University with the project HUBAP ID: 20124.

References

[1] A. R. Adem, "Symbolic computation on exact solutions of a coupled Kadomtsev-Petviashvili equation: lie symmetry analysis and extended tanh method," *Computers and Mathematics with Applications*, vol. 74, no. 8, pp. 1897–1902, 2017.

[2] A. M. Wazwaz, "New travelling wave solutions to the Boussinesq and the Klein Gordon equations," *Communications in Nonlinear Science and Numerical Simulation*, vol. 13, no. 5, pp. 889–901, 2008.

[3] A. M. Wazwaz, "The tanh method and the sine cosine method for solving the KP-MEW equation," *International Journal of Computer Mathematics*, vol. 82, no. 2, pp. 235–246, 2007.

[4] A. J. Morrison, E. J. Parkes, and V. O. Vakhnenko, "A Bäcklund transformation and the inverse scattering transform method for the generalised Vakhnenko equation," *Chaos, Solitons and Fractals*, vol. 17, pp. 683–692, 2003.

[5] A. Yokus and S. Gulbahar, "Numerical solutions with linearization techniques of the fractional Harry Dym equation," *Applied Mathematics and Nonlinear Sciences*, vol. 4, no. 1, pp. 35–42, 2019.

[6] D. M. T. Syed and B. Sadaf, "New traveling wave solutions of Drinefeld Sokolov Wilson Equation using Tanh and Extended Tanh methods," *Journal of the Egyptian Mathematical Society*, vol. 22, no. 3, pp. 517–523, 2014.

[7] E. Fan, "Extended tanh-function method and its applications to nonlinear equations," *Physics Letters A*, vol. 277, no. 4-5, pp. 212–218, 2000.

[8] E. J. Parkes and B. R. Duffy, "An automated tanh-function method for finding solitary wave solutions to nonlinear evolution equations," *Computer Physics Communications*, vol. 98, no. 3, pp. 288–300, 1998.

[9] E. M. E. Zayed and E. Tala-Tebue, "New Jacobi elliptic function solutions, solitons and other solutions for the (2+1)-dimensional nonlinear electrical transmission line equation," *European Physical Journal Plus*, vol. 314, no. 133, 2018.

[10] H. M. Baskonus, C. Cattani, and A. Ciancio, "Periodic, complex and kink-type solitons for the nonlinear model in microtubules," *Journal Applied Sciences*, vol. 21, pp. 34–45, 2019.

[11] G. Qingling, "A generalized tanh method and its application," *Applied Mathematical Sciences*, vol. 5, no. 76, pp. 3789–3800, 2011.

[12] H. Willy and W. Malfliet, "The tanh method: II. Perturbation technique for conservative systems," *Physica Scripta*, vol. 54, no. 6, pp. 569–575, 1996.

[13] H. M. Baskonus, "New acoustic wave behaviors to the Davey-Stewartson equation with power-law nonlinearity arising in fluid dynamics," *Nonlinear Dynamics*, vol. 86, no. 1, pp. 177–183, 2016.

[14] E. Ilhan and I. O. Kiymaz, "A generalization of truncated M-fractional derivative and applications to fractional differential equations," *Applied Mathematics and Nonlinear Sciences*, vol. 5, no. 1, pp. 171–188, 2020.

[15] N. M. Lanbaran, E. Celik, and M. Yigider, "Evaluation of investment opportunities with interval-valued fuzzy Topsis method," *Applied Mathematics and Nonlinear Sciences*, vol. 5, no. 1, pp. 461–474, 2020.

[16] A. Cordero, J. P. Jaiswal, and J. R. Torregrosa, "Stability analysis of fourth-order iterative method for finding multiple roots of non-linear equations," *Applied Mathematics and Nonlinear Sciences*, vol. 4, no. 1, pp. 43–56, 2019.

[17] G. Yel and T. Akturk, "A new approach to (3+1) dimensional Boiti-Leon-Manna-Pempinelli equation," *Applied Mathematics and Nonlinear Sciences*, vol. 5, no. 1, pp. 309–316, 2020.

[18] O. Akganduller and S. P. Atmaca, "Discrete normal vector field approximation via time scale calculus," *Applied Mathematics and Nonlinear Sciences*, vol. 5, no. 1, pp. 349–360, 2020.

[19] O. Ozer, "A handy technique for fundamental unit in specific type of real quadratic fields," *Applied Mathematics and Nonlinear Sciences*, vol. 5, no. 1, pp. 495–498, 2020.

[20] H. Roshid and M. A. Rahman, "The exp $(\Phi(\eta))$-expansion method with application in the (1+1)-dimensional classical Boussinesq equations," *Results in Physics*, vol. 4, pp. 150–155, 2014.

[21] H. Roshid, N. Rahman, and M. Ali Akbar, "Traveling waves solutions of nonlinear Klein Gordon equation by extended (G'/G)-expansion method," *Annals of Pure and Applied Mathematics*, vol. 3, no. 1, pp. 10–16, 2013.

[22] E. I. Eskitascioglu, M. B. Aktas, and H. M. Baskonus, "New complex and hyperbolic forms for Ablowitz-Kaup-Newell-Segur wave equation with fourth order," *Applied Mathematics and Nonlinear Sciences*, vol. 4, no. 1, pp. 105–112, 2019.

[23] M. S. Ullah, H. Roshid, M. Z. Ali et al., "Optical soliton polarization with Lakshmanan-Porsezian-Daniel model by unified approach," *Results in Physics*, vol. 22, p. 103958, 2021.

[24] H. Durur, O. Tasbozan, and A. K. de Griñó, "New analytical solutions of conformable time fractional bad and good modified Boussinesq equations," *Applied Mathematics and Nonlinear Sciences*, vol. 5, no. 1, pp. 447–454, 2020.

[25] M. S. Ullah, M. Z. Ali, H. Roshid, A. R. Seadawy, and D. Baleanu, "Collision phenomena among lump, periodic and soliton solutions to a (2+1)-dimensional Bogoyavlenskii's breaking soliton model," *Physics Letters A*, vol. 397, p. 127263, 2021.

[26] N. Y. Aksoy, "The solvability of first type boundary value problem for a Schrödinger equation," *Applied Mathematics and Nonlinear Sciences*, vol. 5, no. 1, pp. 211–220, 2020.

[27] W. Gao, G. Yel, H. M. Baskonus, and C. Cattani, "Complex solitons in the conformable (2+1)-dimensional Ablowitz-Kaup-Newell-Segur equation," *AIMS Mathematics*, vol. 5, no. 1, pp. 507–521, 2020.

[28] D. Arslan, "The comparison study of hybrid method with RDTM for solving Rosenau-Hyman equation," *Applied Mathematics and Nonlinear Sciences*, vol. 5, no. 1, pp. 267–274, 2020.

[29] H. Roshid and W. X. Ma, "Dynamics of mixed lump-solitary waves of an extended (2+1)-dimensional shallow water wave model," *Physics Letters A*, vol. 382, no. 45, pp. 3262–3268, 2018.

[30] H. Ismael, H. Bulut, and H. M. Baskonus, "Optical soliton solutions to the Fokas-Lenells equation via sine-Gordon expansion method and (m+G'/G)-expansion method," *Pramana-Journal of Physics*, vol. 94, no. 35, pp. 1–9, 2020.

[31] D. Arslan, "The numerical study of a hybrid method for solving telegraph equation," *Applied Mathematics and Nonlinear Sciences*, vol. 5, no. 1, pp. 293–302, 2020.

[32] W. Gao, H. F. Ismael, A. M. Husien, H. Bulut, and H. M. Baskonus, "Optical soliton solutions of the nonlinear Schrödinger and resonant nonlinear Schrödinger equation with parabolic law," *Applied Science*, vol. 10, no. 1, pp. 1–20, 2020.

[33] K. K. Ali, R. Yilmazer, H. M. Baskonus, and H. Bulut, "Modulation instability analysis and analytical solutions to the system of equations for the ion sound and Langmuir waves," *Physica Scripta*, vol. 95, no. 65602, pp. 1–10, 2020.

[34] F. Dusunceli, "New exact solutions for generalized (3+1) shallow water-like (SWL) equation," *Applied Mathematics and Nonlinear Sciences*, vol. 4, no. 2, pp. 365–370, 2019.

[35] G. Yel, C. Cattani, H. M. Baskonus, and W. Gao, "On the complex simulations with dark–bright to the Hirota-Maccari system," *Journal of Computational and Nonlinear Dynamics*, vol. 16, no. 6, 2021.

[36] D. Ziane, M. H. Cherif, C. Cattani, and K. Belghaba, "Yang-laplace decomposition method for nonlinear system of local fractional partial differential equations," *Applied Mathematics and Nonlinear Sciences*, vol. 4, no. 2, pp. 489–502, 2019.

[37] M. Zamir, F. Nadeem, T. Abdeljawad, and Z. Hammouch, "Threshold condition and non pharmaceuticalinterventions's control strategies for elimination of COVID-19," *Results in Physics*, vol. 20, p. 103698, 2021.

[38] A. Ullah, Z. Ullah, T. Abdeljawad, Z. Hammouch, and K. Shah, "A hybrid method for solving fuzzy Volterra integral equations of separable type kernels," *Journal of King SaudUniversity-Science*, vol. 33, no. 1, p. 101246, 2021.

[39] Y. M. Li, S. Rashid, Z. Hammouch, D. Baleanu, and Y. M. Chu, "New Newton's type estimates pertaining to local fractional integral via generalized p-convexity with applications," *Fractals*, 2021.

[40] P. Bigot and L. C. G. de Souza, "Design of non-linear controller for a flexiblerotatory beam using state-dependent Riccati equation (SDRE) control," *International Journal of Electrical Engineering and Computer Science (EEACS)*, vol. 1, pp. 56–63, 2019.

[41] A. Errachdi and M. Benrejeb, "Adaptive internal model neural networks control for nonlinear system," *International Journal of Electrical Engineering and Computer Science (EEACS)*, vol. 2, pp. 1–14, 2020.

[42] W.-J. Chang, S. Che-Lun, and K. Cheung-Chieh, "Robust fuzzy controller design with decay rate for nonlinear perturbed singular systems," *Engineering World*, vol. 1, pp. 4–8, 2019.

[43] A. Errachdi and M. Benrejeb, "Model reference adaptive control based-on neural networks for nonlinear time-varying system," *International Journal of Applied Mathematics, Computational Science and Systems Engineering*, vol. 1, pp. 6–10, 2019.

[44] J. D. Evans and R. K. Raslan, "The tanh function method for solving some important non-linear partial differential equations," *International Journal of Computer Mathematics*, vol. 82, no. 7, pp. 897–905, 2005.

[45] S. A. Muhannad, A. K. Khalid, and K. R. Raslana, "The modified extended tanh method with the Riccati equation for solving the space-time fractional EW and MEW equations," *Chaos, Solitons and Fractals*, vol. 103, pp. 404–409, 2017.

[46] A. M. Wazwaz, "The tanh function method for solving some important non-linear partial differential equations," *International Journal of Computer Mathematics*, vol. 82, no. 7, pp. 897–905, 2007.

[47] A. M. Wazwaz, "The extended tanh method for new solitons solutions for many forms of the fifth-order KdV equations," *Applied Mathematics and Computation*, vol. 184, no. 2, pp. 1002–1014, 2007.

[48] W. Malfliet, "The tanh method a tool for solving certain classes of nonlinear evolution and wave equations," *Journal of Computational and Applied Mathematics*, vol. 164, no. 165, pp. 529–541, 2004.

[49] E. W. Weisstein, *Concise Encyclopedia of Mathematics*, CRC Press, New York, 2nd edition, 2002.

[50] A. Kumar, E. Ilhan, A. Ciancio, G. Yel, and H. M. Baskonus, "Extractions of some new travelling wave solutions to the

conformable Date-JimboKashiwara-Miwa equation," *Aims Mathematics*, vol. 6, no. 5, pp. 4238–4264, 2021.

[51] A. Yokus and H. Bulut, "Numerical simulation of KdV equation by finite difference method," *Indian Journal of Physics*, vol. 92, no. 12, pp. 1571–1575, 2018.

[52] H. F. Ismael, H. Bulut, and H. M. Baskonus, "W-shaped surfaces to the nematic liquid crystals with three nonlinearity laws," *Soft Computing*, vol. 25, no. 6, pp. 4513–4524, 2021.

[53] G. Yel, "New wave patterns to the doubly dispersive equation in nonlinear dynamic elasticity," *Pramana*, vol. 94, no. 1, p. 79, 2020.

[54] M. Yavuz, "Dynamical behaviors of separated homotopy method defined by conformable operator," *Konuralp Journal of Mathematics*, vol. 7, no. 1, pp. 1–6, 2019.

[55] B. Gurbuz and M. Sezer, "Modified operational matrix method for second-order nonlinear ordinary differential equations with quadratic and cubic terms," *An International Journal of Optimization and Control: Theories and Applications*, vol. 10, no. 2, pp. 218–225, 2020.

[56] Z. Pinar, "Analytical studies on waves in nonlinear transmission line media," *An International Journal of Optimization and Control: Theories and Applications*, vol. 9, no. 2, pp. 100–104, 2019.

Hindawi
Advances in Mathematical Physics
Volume 2021, Article ID 9967368, 8 pages
https://doi.org/10.1155/2021/9967368

Research Article

Dimension Reduction Big Data Using Recognition of Data Features Based on Copula Function and Principal Component Analysis

Fazel Badakhshan Farahabadi,[1] **Kianoush Fathi Vajargah**,[2] **and Rahman Farnoosh**[3]

[1]*Department of Statistics, Islamic Azad University, Science and Research Branch, Tehran, Iran*
[2]*Department of Statistics, Islamic Azad University, Tehran North Branch, Iran*
[3]*School of Mathematics, Iran University of Science and Technology, Tehran 16844, Iran*

Correspondence should be addressed to Kianoush Fathi Vajargah; fathi_kia10@yahoo.com

Received 12 March 2021; Accepted 16 June 2021; Published 12 July 2021

Academic Editor: Sandro Wimberger

Nowadays, data are generated in the world with high speed; therefore, recognizing features and dimensions reduction of data without losing useful information is of high importance. There are many ways to dimension reduction, including principal component analysis (PCA) method, which is by identifying effective dimensions in an acceptable level, reducing dimension of data. In the usual method of principal component analysis, data are usually normal, or we normalize data; then, the principal component analysis method is used. Many studies have been done on the principal component analysis method as a step of data preparation. In this paper, we propose a method that improves the principal component analysis method and makes data analysis easier and more efficient. Also, we first identify the relationships between the data by fitting the multivariate copula function to data and simulate new data using the estimated parameters; then, we reduce the dimensions of new data by principal component analysis method; the aim is to improve the performance of the principal component analysis method to find effective dimensions.

1. Introduction

In many real-world programs, reduction of high-volume data is of high importance and necessity as a prestage of data processing. For example, in data mining programs, dimensionality reduction is considered one of the most important stages to remove data redundancy, to increase precision of measurement, and to improve decision making process. Analyzing high-volume data is intrinsically difficult via high-volume computations for many learning algorithms as well as data processing. In dimensionality reduction methods, extraction of data features is highly important. A highly used method to reduce dimension reduction of data in data mining and in the data preparing phase is the principal component analysis method. The PCA method can be used if the original variables are correlated, homogeneous, if each component is guaranteed to be independent and if the dataset is normally distributed [1, 2]. The critical issues for the majority of dimensionality reduction studies are how to provide a convenient way to generate correlated multivariate random variables without imposing constrain to specific types of marginal distributions. An appropriate approach to this problem is to use Copula's theory [3, 4]. In this paper, we first use the copula function to study the correlation and relationships between data to determine and eliminate irrelevant properties and simulate new data using the estimated parameter; then, by using the PCA method, we reduce the dimensions of data [4–6].

1.1. Principal Component Analysis (PCA). Principal component analysis method has been first developed by Karl Pearson in 1901. The analysis includes analyzing special

values of the covariance matrix. Analyzing principal components upon mathematics definition is an orthogonal transformation taking data to a new system of coordinates so that the largest data variance would be placed on the first coordinate axis; the second largest variance would be placed on the second coordinate axis and etc. Principal component analysis is aimed at transferring dataset X with m dimensions to data Y with l dimensions. Therefore, it is assumed that matrix X is formed of vectors $X_1, X_2, \cdots, X_n$ each of which placed in m column in matrix X. So, the data matrix would be in form of $m \times n$. Principal components are just related to covariance matrix Σ (correlation matrix p) of random variables $X_1, X_2, \cdots, X_n$ [7].

1.2. Calculating Empirical Mean and Covariance Matrix and Data Normalization. To calculate covariance matrix, data have to be normalized first. To do so, the primarily vector of empirical mean would be calculated as follows:

$$U_m = \frac{1}{n}\sum_{i=1}^{n} X_{[m,i]}. \tag{1}$$

Clearly, the empirical mean would be applied on matrix lines.

Then, the distance matrix to mean would be obtained as follows:

$$B = X - uh, \tag{2}$$

where h is a vector with size of $1 \times n$ and value equal to 1 in each of the entries.

Covariance matrix Σ with $m \times m$ dimensions would be obtained as follows:

$$\sum = E[B \otimes B] = E[B \cdot B^*] = \frac{1}{n} B \cdot B^*, \tag{3}$$

where E is arithmetic mean, $\bigotimes$ is an external coefficient, and B^* is the matrix B conjugate transpose.

Consider $X' = [X_1, X_2, \cdots, X_n]$ random vector and assume that this random vector has matrix covariance Σ with special values $\lambda_1 \geq \lambda_2 \geq \cdots \geq \lambda_n \geq 0$. Consider following linear compositions:

$$\begin{cases} Y_1 = l_1'X = l_{11}X_1 + l_{21}X_2 + \cdots + l_{n1}X_n, \\ Y_2 = l_2'X = l_{12}X_1 + l_{22}X_2 + \cdots + l_{n2}X_n, \\ \vdots \\ Y_n = l_n'X = l_{1n}X_1 + l_{2n}X_2 + \cdots + l_{nn}X_n. \end{cases} \tag{4}$$

Using relationship (4), we have

$$\text{var}\,(Y_i) = l_i' \sum l_i, \quad \text{cov}\,(Y_i, Y_k) = l_i' \sum l_k, \quad i, k = 1, 2, \cdots, n. \tag{5}$$

Its principal components are $Y_1, Y_2, \cdots, Y_n$ unrelated linear compositions; variances of which in relationship (5) would be large to the extent possible. The first principal component of a linear composition has maximum variance. Clearly, $\text{var}\,(Y_1) = l_1' \Sigma l_1$ can be maximized through multiplying each l_1 by a constant. That is, the first principal component of linear composition is $l_1'X$ which maximizes $\text{var}\,(Y_1)$ with consideration of $l_1' l_1' = 1$. The second principal component of linear composition is $l_2'X$ which maximizes $\text{var}\,(Y_2)$ with consideration of $l_2' l_2 = 1$ and $\text{cov}\,(l_1'X, l_2'X) = 0$, continuously to the n^{th} principal component.

According to relationship (5), we have

$$\sum_{i=1}^{n} \text{var}(X_i) = \sigma_{11} + \sigma_{22} + \cdots + \sigma_{nn} = \lambda_1 + \lambda_2 + \cdots + \lambda_n = \sum_{i=1}^{n} \text{var}(Y_i), \tag{6}$$

and ratio of total variance to K^{th} component $(k = 1, 2, \cdots, n)$ is

$$\left(\text{Total share of population variance related to principal } K^{\text{th}} \text{ component}\right) = \frac{\lambda_k}{\lambda_1 + \lambda_2 + \cdots + \lambda_n}. \tag{7}$$

If for large n, the highest maximum variance of total population (80 or 90%) could be attributed to the first several components; these components can be replaced by n primary variables, losing not much information [2, 8–10].

2. Copula Function

In general, the copula function is the link function of multivariate distributions and their marginal distributions. The copula function is a multivariate distribution, marginal distribution which follows uniform distribution of [0,1] interval [11–13].

2.1. Characteristics of Copula Function. Assume the following characteristics for $C : I^2 \longrightarrow I$:

(1) For every $u, v \in [0, 1]$, we will have

$$C(u, 0) = C(0, v) = 0, C(u, 1) = u, C(1, v) = v \tag{8}$$

(2) For every $0 \leq v_1 < v_2 \leq 1, 0 \leq u_1 < u_2 \leq 1$, we will have

$$C(U_2, v_2) + C(U_1, v_1) - C(U_1, v_2) - C(U_2, v_1) \geq 0 \tag{9}$$

Such function like C implied in the two above conditions is called the copula function [14].

2.2. Sklar's Theorem. It is indicated by Sklar's theorem that if joint distribution function like H would be available with marginal distributions F and G, then, there would be copula function C available. That is, for every $X_i, X_j \in \mathbb{R}$, we have

$$H(X_i, X_j) = C(F(X_i), G(X_j)), \tag{10}$$

and if F and G would be continuous, then, copula function C would be unique. Otherwise, C would be defined as unique on $\text{Rang}(F) \times \text{Rang}(G)$.

The most important application of the copula function is formulation of a proper method to produce distribution of random related multivariate variables and to provide a solution for the problem of density estimation transformation [15].

For reversible transformation of n continuous random variables $X_1, X_2, \cdots, X_n$ based on their distribution function to n independent variables with uniform distribution $U_1 = F_1(X_1)$, $U_2 = F_2(X_2), \cdots, U_n = F_n(X_n)$, the probability density function $X_1, X_2, \cdots, X_n$ would be equal to $f(X_1, \cdots, X_n)$ and joint probability density function $U_1, U_2, \cdots, U_n$ would be equal to $C(U_1, \cdots, U_n)$. Therefore, probability density function $f(X_1, \cdots, X_n)$ can provide a nonparametric form (unknown distribution). Here, probability density function $C(U_1, \cdots, U_n)$ for $U_1, U_2, \cdots, U_n$ would be estimated instead of $X_1, X_2, \cdots, X_n$, so that problem of density estimation becomes simpler. Then, it would be simulated so that random samples $X_1, X_2, \cdots, X_n$ would be obtained through reverse transformation $X_i = F^{-1}(U_i)$.

According to Sklar's theorem, one copula function with n unique dimensions C is available in $[0, 1]^n$ with uniform marginal distribution $U_1, U_2, \cdots, U_n$. That is, every function F with margins $F_1, F_2, \cdots, F_n$ can be written as follows:

$$\forall (X_1, \cdots, X_n) \in \mathbb{R}^n, F(X_1, \cdots, X_n) = C(F_1(X_1), \cdots, F_n(X_n)). \tag{11}$$

To evaluate a copula function selected via an estimated parameter and to avoid defining any hypothesis on distributions, empirical distribution function can be used. An empirical copula function is useful to study the dependence structure of multivariate random vectors. In general, empirical copula function is as follows:

$$C_{ij} = \frac{1}{n} \sum_{k=1}^{n} I_{\left(U_{kj} \leq U_{ij}\right)}, \tag{12}$$

where $I_{(\bullet)}$ would be an indicator function [16].

2.3. Gaussian Copula Function. Difference between Gaussian copula function and normal joint distribution function is that the first one authorizes various distribution functions to be used for joint distribution [14]. However, in probability theory and statistics, normal multivariate distribution is considered the generalization of one-dimensional normal distribution [17].

Gaussian copula function is defined as

$$C(\Phi(X_1), \cdots, \Phi(X_n)) = \frac{1}{|\sum|^{1/2}} \exp\left\{\frac{-1}{2} X^t \left(\sum^{-1} - I\right) X\right\}, \tag{13}$$

where $\Phi(X_i)$ is a standard Gaussian function and X_i has standard normal distribution and Σ is a correlation matrix. As a result, $C(U_1, \cdots U_n)$ copula function would be called a Gaussian copula function.

3. Methodology

In the research, a two-stage method would be used for dimensionality reduction. That is, primarily empirical copula function and fit of Gaussian copula function to data would be used to estimate parameter p for variables X_1, $X_2, \cdots, X_n$. Important advantages of using the copula function in multivariate distributions is that correlation between variables would be considered by these functions, and in fact, there would be no need for independence of variables; instead, the correlation structure between variables would be even considered by these functions [18]. For estimation purposes, generating function is available with dependence unscaled value available in it. The correlation coefficient value has to be specified. To do so, the Pearson correlation coefficient will be used and defined as follows for two X_i and X_j variables:

$$\rho = \frac{\text{cov}\left(X_i, X_j\right)}{\sigma_{X_i} \sigma_{X_j}}, \tag{14}$$

where σ_{X_i} and σ_{X_j} are standard deviations of X_i and X_j, respectively.

Then, those data with lower correlation compared to others would be eliminated and using estimated function and Gaussian copula function for $X_1, X_2, \cdots, X_m$, where m uniform variables $U_1 = F_1(X_1)$, $U_2 = F_2(X_2), \cdots, U_n = F_m(X_m)$ would be generated $(m \leq n)$ and placed instead of $X_1, X_2, \cdots, X_m$ in the principal component analysis method. After dimensionality reduction, the results would be compared through applying the method on raw data [16, 19].

4. Numerical Results

During past 30 years, increasing prevalence of urinary stone disease has been observed. About 80% of kidney stones are from calcium oxalate type. Here, 79 urine samples would be analyzed to see if some of physical features of urine are related to formation of calcium oxalate or not. These data include following columns (variables), which is available at https://cran.r-project.org/web/packages/cond.

Using Gaussian copula function, correlation values of variables would be obtained as follows:

Considering Table 1, it is observed that correlation of variable $X2$ is lower than other variables; so, it would be eliminated at the first stage. After estimation of parameters, new data would be generated. Figure 1 shows the copula function for main data and data generated by this method.

Now, data would be generated based on estimated parameters. To specify whether data are generated correctly or not, diagram QQPlot would be drawn.

Table 1: Estimation of parameter ρ for variables of urine.

	$X1$	$X2$	$X3$	$X4$	$X5$	$X6$
$X1$	1	-0.30856	0.83231	0.57256	0.81165	0.54872
$X2$		1	-0.25167	-0.09762	-0.27985	-0.12147
$X3$			1	0.77226	0.81012	0.58452
$X4$				1	0.45542	0.43444
$X5$					1	0.58813
$X6$						1

$X1$is urine gravity, $X2$ is urine pH, $X3$ is urine osmolarity (it is corresponding to unit of solute concentration), $X4$ is urine conductivity (it is corresponding to concentration of charged ions in solution), $X5$ is urea concentration (mM/liter), and $X6$ is calcium concentration (mM/liter).

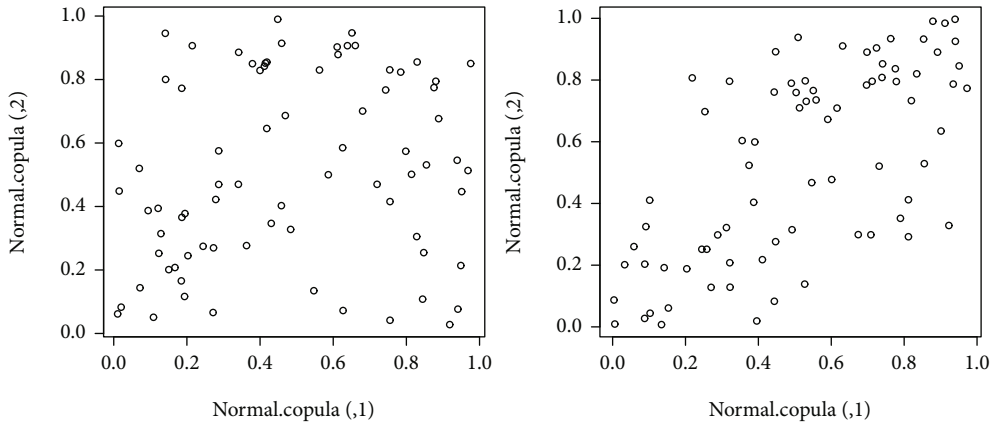

Figure 1: Diagram of copula function for generated data based on main and reduced data.

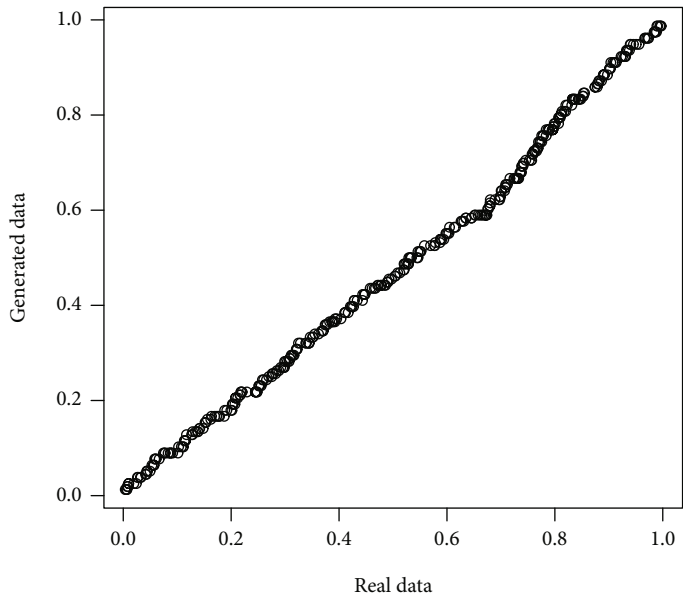

Figure 2: QQ Plot diagram of real and generated data for data of example 1.

Correct data generation is shown by Figure 2. In the second stage, after elimination of the $X2$ variable on data generated, principal component analysis would be done. In Figure 2, principal components for primary data and those generated by copula function are shown after reduction of the $X2$ variable. Figure 3 shows principal components for main data and the data generated.

Ratios of population variance related to principal components are provided in following table. Its screen plot is as follows.

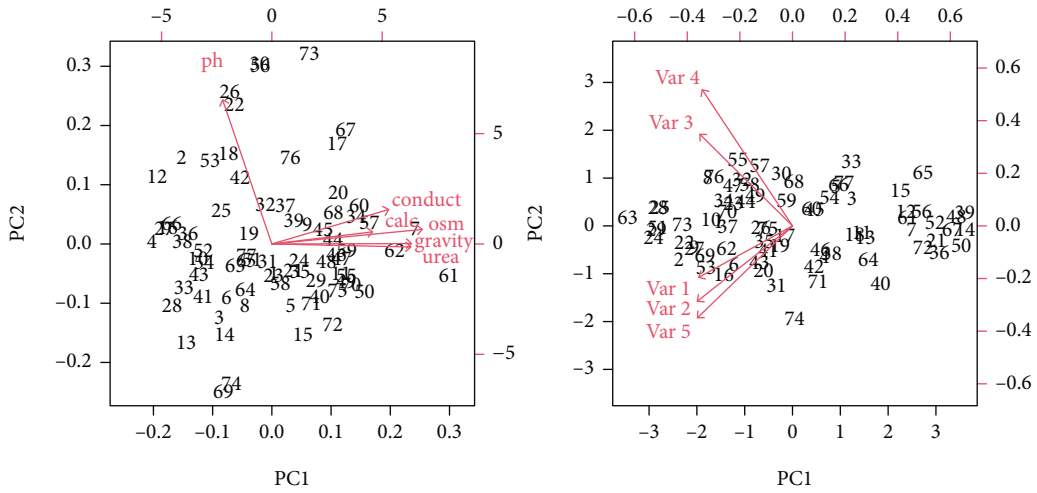

Figure 3: Diagram of principal components for raw and generated data through recommended method.

Table 2: Ratios of population variance related to principal components for main data.

PC1	PC2	PC3	PC4	PC5	PC6
0.61817360	0.15701415	0.11567297	0.07879801	0.02912841	0.00121285

Table 3: Ratios of population variance related to principal components for data generated through the recommended method.

PC1	PC2	PC3	PC4	PC5
0.73414280	0.07840848	0.07583399	0.06866719	0.04294755

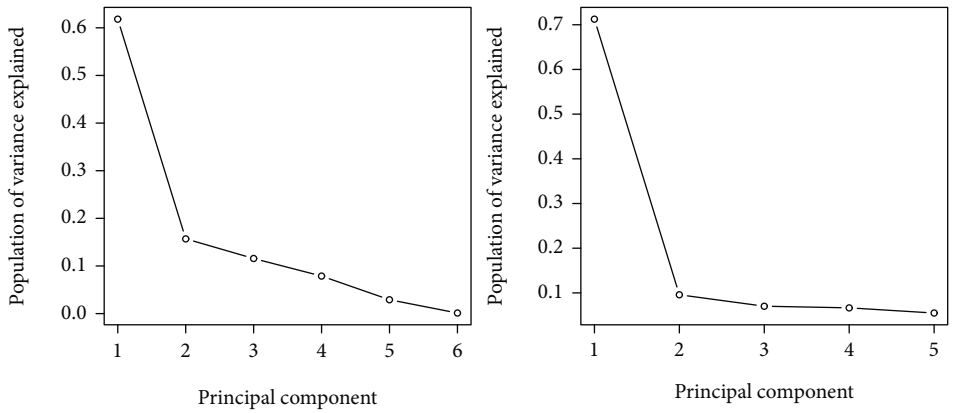

Figure 4: Diagram of population variance ration related to principal components for main data and generated data through recommended method.

Considering Tables 2 and 3 as well as Figure 4, it is observed that in dimensionality reduction method presented in the research, two first components include more than 80% of population variances and first component includes more than 70% of population.

Example 1. To recognize image resolution in a rectangular monitor, its display would be divided into different boxes and numbers of black and white dots in these boxes would be measured. Images of these characters have been made based on 20 different images, and each box from within these 20 boxes has been randomly selected. A file including 20000 unique simulators have been produced. Each stimulator has been transformed and scaled to 7 following numerical variables so that they would be placed within 0-15 range, (which is available at https://cran.r-project.org/web/packages/mlbench/index.html).

There are 2000 observations available from these variables.

Table 4: Estimation of parameter ρ for variables of resolution in a rectangular monitor.

	$X1$	$X2$	$X3$	$X4$	$X5$	$X6$	$X7$
$X1$	1	0,7960	0,8788	0,7439	0,7282	-0,0263	0,0296
$X2$		1	0,7044	0,8203	0,6148	0,0784	-0,0754
$X3$			1	0,7089	0,8156	0,0648	0.0119
$X4$				1	0.0119	0,0618	-0,0190
$X5$					1	0,1196	-0,0278
$X6$						1	-0,4227
$X7$							1

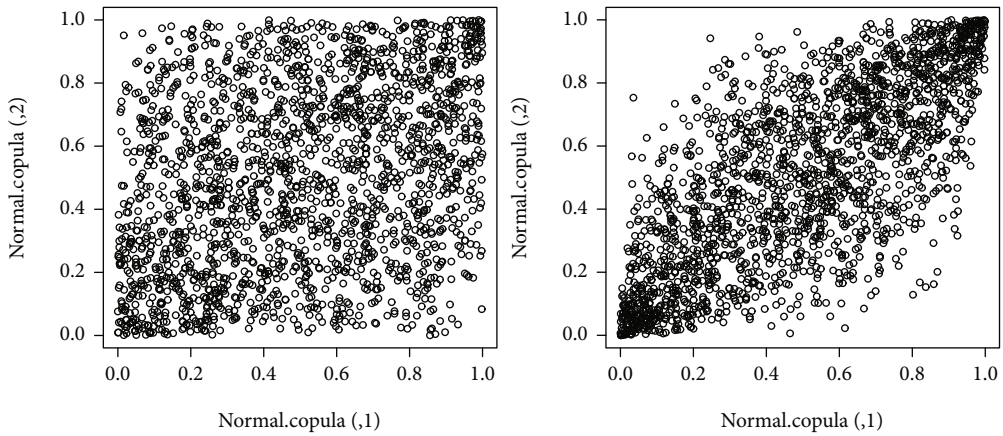

Figure 5: Diagram of copula function for main and reduced data.

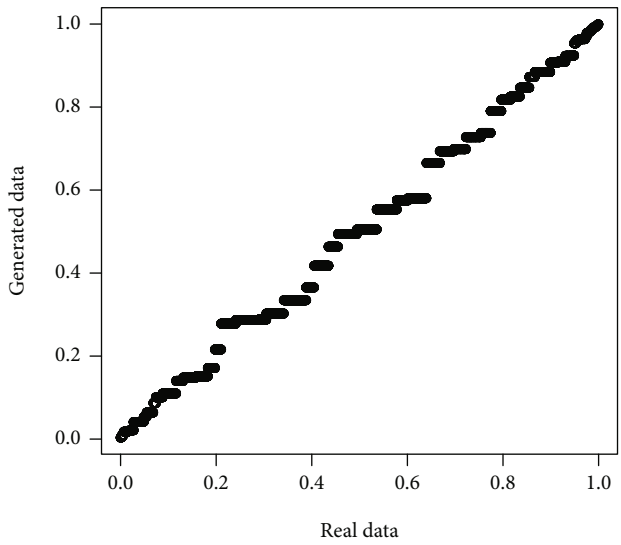

Figure 6: QQ Plot diagram of real and generated data for data of example 2.

Using Gaussian copula function, correlation values of variables would be obtained as follows:

X is the box. $X1$ is the horizontal location of box, $X2$ is the vertical location of box (y.box), $X3$is width of box (width), $X4$ is the height of box (height), $X5$ is the total numbers of dots in the box (onpix), $X6$ is the mean value of x in dots of the box (x .bar), and $X7$ is the mean value of y in dots of box (y.bar).

Considering Table 4, it is observed that correlation between variables $X6$ and $X7$ is less compared to other variables. So, these two would be eliminated at first stage and then Gaussian copula function would be fitted to reduced data and new data would be generated through estimated parameter, which is shown in Figure 5.

Now, data would be generated. QQPlot would be as follows.

Now, principal component analysis would be done on generated data. Diagrams of principal components are as follows (Figure 6).

Table 5: Ratio of population variance related to principal components for main data.

PC1	PC2	PC3	PC4	PC5	PC6
0.55123270	0.20018487	0.09008126	0.07169468	0.05074973	0.02071375

Table 6: Ratio of population variance related to principal components for data reduced through recommended method.

PC1	PC2	PC3	PC4	PC5
0.79028555	0.05470965	0.05363693	0.05154868	0.0498199

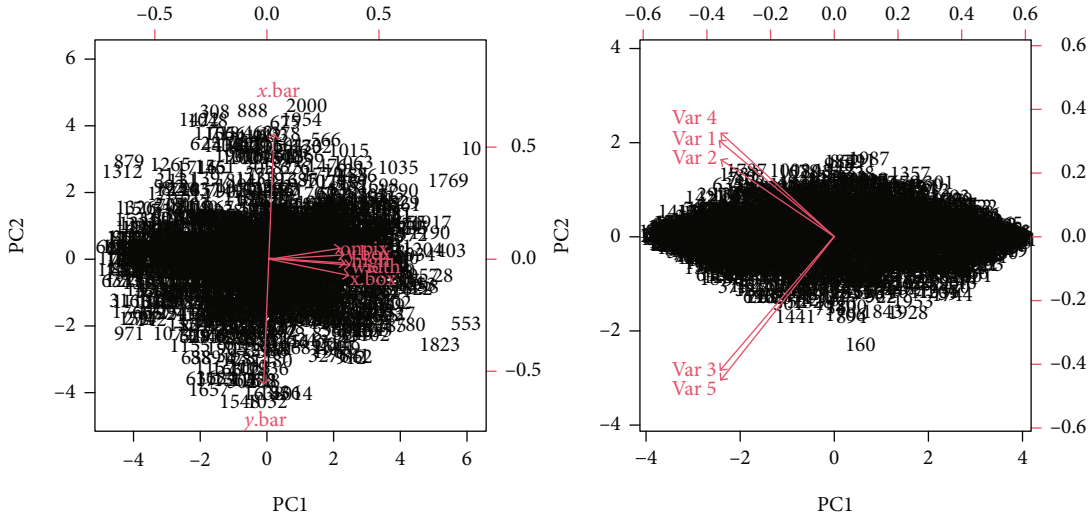

Figure 7: Diagrams of population variance ratios related to principal components for main data and recommended method.

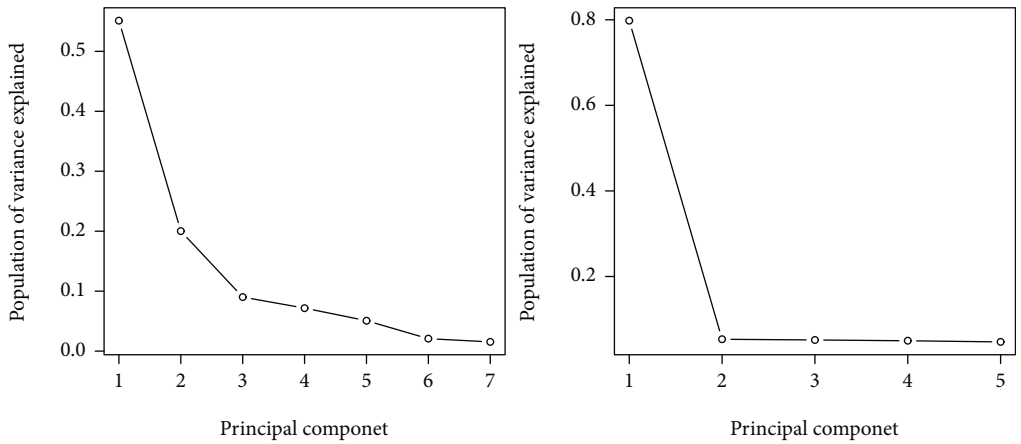

Figure 8: QQPlot diagram of real and generated data.

Screen plot of population variance ratio related to principal components for both methods are as follows.

According to Tables 5 and 6 as well as Figure 7, it is observed that ratio of population variance for the first two components in the recommended method includes almost 85% of population and the first component includes almost 80% of population, whereas, for main data, ratio of population variance for the three first components includes almost 85% of population.

5. Conclusion

Considering the two aforementioned examples, it has been observed that data generated according to the estimated parameters of the Gaussian copula distribution are consistent with the original data (see Figures 2 and 8) by using the recommended method in the research and copula function to recognize dependencies and structural dependence between variables in addition to elimination of redundant data will

increase efficiency of principal component analysis method as well as speed of obtaining analysis results (see Figures 4 and 7, Tables 2, 3, 5, and 6). Considering the point that nowadays data are generated with high-speed, appropriate, and efficient methods for dimensionality reduction without losing information are of high importance and necessity, and recommended method in the research is a useful one to do so. The recommended method in the research can be also used for other dimensionality reduction techniques so that data would be prepared for more analysis, for example in data mining.

Data Availability

The data that support the findings of this study are openly available at https://cran.r-project.org/web/packages/cond and https://cran.r-project.org/web/packages/mlbench/index.html.

Conflicts of Interest

The authors declare that they have no competing interests.

Authors' Contributions

All authors contributed equally. All authors read and approved the final manuscript.

References

[1] J. Forkman, J. Josse, and H.-P. Piepho, "Hypothesis tests for principal component analysis when variables are standardized," *Journal of Agricultural, Biological and Environmental Statistics*, vol. 24, no. 2, pp. 289–308, 2019.

[2] I. T. Jolliffe and J. Cadima, "Principal component analysis: a review and recent developments," *Philosophical Transactions of the Royal Society A: Mathematical, Physical and Engineering Sciences*, vol. 374, no. 2065, article 20150202, 2016.

[3] A. Colomé, G. Neumann, J. Peters, and C. Torras, "Dimensionality reduction for probabilistic movement primitives," in *2014 IEEE-RAS International Conference on Humanoid Robots*, pp. 794–800, Madrid, Spain, 2014.

[4] R. Fakoor and M. Huber, "A sampling-based approach to reducing the complexity of continuous state space pomdps by decomposition into coupled perceptual and decision processes," in *2012 11th International Conference on Machine Learning and Applications*, pp. 687–692, Boca Raton, FL, USA, 2012.

[5] I. M. Johnstone and A. Y. Lu, "On consistency and sparsity for principal components analysis in high dimensions," *Journal of the American Statistical Association*, vol. 104, no. 486, pp. 682–693, 2009.

[6] D. Paul and I. M. Johnstone, "Augmented sparse principal component analysis for high dimensional data," 2012, https://arxiv.org/abs/1202.1242.

[7] L. I. Smith, "A tutorial on principal components analysis," 2002, Computer Science Technical Report No. OUCS-2002-12), 2002, https://hdl.handle.net/10523/7534.

[8] I. T. Jolliffe, "Principal components in regression analysis," in *Principal Component Analysis*, pp. 129–155, Springer, 1986.

[9] P. P. Markopoulos, S. Kundu, S. Chamadia, and D. A. Pados, "Efficient l1-norm principal-component analysis via bit flipping," *IEEE Transactions on Signal Processing*, vol. 65, no. 16, pp. 4252–4264, 2017.

[10] M. Zhai, F. Shi, D. Duncan, and N. Jacobs, "Covariance-based PCA for multi-size data," in *2014 22nd International Conference on Pattern Recognition*, pp. 1603–1608, Stockholm, Sweden, 2014.

[11] E. W. Weisstein, "Mathworld–a wolfram web resource," 2004, https://mathworld.wolfram.com/Erf.html.

[12] D. Lopez-Paz, J. M. Hernández-Lobato, and G. Zoubin, "Gaussian process vine copulas for multivariate dependence," in *International Conference on Machine Learning*, pp. 10–18, Atlanta, Georgia, USA, 2013.

[13] D. MacKenzie and T. Spears, "'The formula that killed wall street': the gaussian copula and modelling practices in investment banking," *Social Studies of Science*, vol. 44, no. 3, pp. 393–417, 2014.

[14] R. B. Nelsen, *An Introduction to Copulas*, Springer Science & Business Media, 2007.

[15] F. Durante, J. Fernandez-Sanchez, and C. Sempi, "A topological proof of Sklar's theorem," *Applied Mathematics Letters*, vol. 26, no. 9, pp. 945–948, 2013.

[16] R. Houari, A. Bounceur, M.-T. Kechadi, A.-K. Tari, and R. Euler, "Dimensionality reduction in data mining: a Copula approach," *Expert Systems with Applications*, vol. 64, pp. 247–260, 2016.

[17] D. MacKenzie and T. Spears, *The Formula that Killed Wall Street? The Gaussian Copula and the Material Cultures of Modelling*, School of Social and Political Science, University of Edinburgh, 2012.

[18] A. Lipton and A. Rennie, *Credit Correlation: Life after Copulas*, World Scientific, 2008.

[19] F. R. Pirolla, M. T. Santos, J. C. Felipe, and M. X. Ribeiro, "Dimensionality reduction to improve contentbased image retrieval: a clustering approach," in *2012 IEEE International Conference on Bioinformatics and Biomedicine Workshops*, pp. 752-753, Philadelphia, PA, USA, 2012.

Hindawi
Advances in Mathematical Physics
Volume 2021, Article ID 8561626, 11 pages
https://doi.org/10.1155/2021/8561626

Research Article

Existence, Nonexistence, and Stability of Solutions for a Delayed Plate Equation with the Logarithmic Source

Hazal Yüksekkaya,[1] Erhan Pişkin,[1] Salah Mahmoud Boulaaras,[2,3] Bahri Belkacem Cherif,[2,4] and Sulima Ahmed Zubair[2,5]

[1]*Department of Mathematics, Dicle University, Diyarbakir, Turkey*
[2]*Department of Mathematics, College of Sciences and Arts, ArRas, Qassim University, Saudi Arabia*
[3]*Laboratory of Fundamental and Applied Mathematics of Oran (LMFAO), University of Oran 1, Oran, 31000 Oran, Algeria*
[4]*Preparatory Institute for Engineering Studies in Sfax, Tunisia*
[5]*Department of Mathematics, College of Education, Juba University, Sudan*

Correspondence should be addressed to Sulima Ahmed Zubair; sulimaa2021@gmail.com

Received 12 May 2021; Accepted 16 June 2021; Published 28 June 2021

Academic Editor: Kamyar Hosseini

In this work, we study a plate equation with time delay in the velocity, frictional damping, and logarithmic source term. Firstly, we obtain the local and global existence of solutions by the logarithmic Sobolev inequality and the Faedo-Galerkin method. Moreover, we prove the stability and nonexistence results by the perturbed energy and potential well methods.

1. Introduction

In this article, we consider a plate equation with frictional damping, delay, and logarithmic terms as follows:

$$\begin{cases} u_{tt} + \Delta^2 u + \alpha u_t(t) + \beta u_t(x, t-\tau) = u \ln |u|^{\gamma} & \text{for } (x,t) \in \Omega \times (0,\infty), \\ u(x,t) = \dfrac{\partial u(x,t)}{\partial \upsilon} = 0 & \text{for } (x,t) \in \partial\Omega \times (0,\infty), \\ u(x,0) = u_0(x), u_t(x,0) = u_1(x) & \text{for } x \in \Omega, \\ u_t(x,t) = j_0(x,t) & \text{for } (x,t) \in \Omega \times (-\tau, 0), \end{cases} \tag{1}$$

where $\Omega \subset R^N$, $N \geq 1$, is a bounded domain with smooth boundary $\partial\Omega$. $\tau > 0$ denotes time delay, and α, β, and γ are real numbers that will be specified later. Generally, logarithmic nonlinearity seems to be in supersymmetric field theories and in cosmological inflation. From quantum field theory, that kind of $(u|u|^{p-2} \ln |u|^k)$ logarithmic source term seems to be in nuclear physics, inflation cosmology, geophysics, and optics (see [1, 2]). Time delays often appear in various problems, such as thermal, economic, biological, chemical, and physical phenomena. Recently, partial differential equations have become an active area with time delay (see [3, 4]). In 1986, Datko et al. [5] indicated that, in boundary control, a small delay effect is a source of instability. Generally, a small delay can destabilize a system which is uniformly stable [6]. To stabilize hyperbolic systems with time delay, some control terms will be needed (see [7–9] and references therein).

For the literature review, firstly, we begin with the studies of Bialynicki-Birula and Mycielski [10, 11]. The authors investigated the equation with the logarithmic term as follows:

$$u_{tt} - u_{xx} + u - \varepsilon u \ln |u|^2 = 0, \tag{2}$$

where the authors proved that, in any number of dimensions, wave equations including the logarithmic term have localized, stable, soliton-like solutions.

In 1980, Cazenave and Haraux [12] studied the equation as follows:

$$u_{tt} - \Delta u = u \ln |u|^k, \tag{3}$$

where the authors in [12] proved the existence and uniqueness of the solutions for equation (3). Gorka [2] obtained the global existence results of solutions for one-dimensional equation (3). Bartkowski and Gŏrka [1] considered the weak solutions and obtained the existence results.

In [13], Hiramatsu et al. studied the equation as follows:

$$u_{tt} - \Delta u + u + u_t + \left|u^2\right|u = u \ \ln \ u. \tag{4}$$

In [14], Han established the global existence of solutions for equation (4).

In [15], Al-Gharabli and Messaoudi were concerned with the plate equation with the logarithmic term as follows:

$$u_{tt} + \Delta^2 u + u + h(u_t) = ku \ \ln |u|. \tag{5}$$

They established the existence results by the Galerkin method and obtained the explicit and decay of solutions utilizing the multiplier method for equation (5).

In [16], Liu introduced the plate equation with the logarithmic term as follows:

$$u_{tt} + \Delta^2 u + |u_t|^{m-2}u_t = |u|^{p-2}u \ \log |u|^k. \tag{6}$$

The author proved the local existence by the contraction mapping principle. Also, he studied the global existence and decay results. Moreover, under suitable conditions, the author proved the blow-up results with $E(0) < 0$.

In [17], Messaoudi studied the equation as follows:

$$u_{tt} + \Delta^2 u + |u_t|^{m-2}u_t = |u|^{p-2}u, \tag{7}$$

and obtained the existence results and obtained that, if $m \geq p$, the solution is global and blows up in finite time if $m < p$. Later, Chen and Zhou [18] extended this result. In the presence of the strong damping term $(-\Delta u_t)$, Pişkin and Polat [19] proved the global existence and decay of solutions for equation (7). For more results about plate problems, see [20–22].

In [7], Nicaise and Pignotti studied the equation as follows:

$$u_{tt} - \Delta u + a_0 u_t(x,t) + a u_t(x, t-\tau) = 0, \tag{8}$$

where $a_0, a > 0$. They proved that, under the condition $0 \leq a \leq a_0$, the system is exponentially stable. The authors obtained a sequence of delays that shows the solution is unstable in the case $a \geq a_0$. In the absence of delay, some other authors [23, 24] looked into exponential stability for equation (8). In [9], Xu et al., by using the spectral analysis approach, established the same result similar to [7] for the one space dimension.

In [25], Nicaise et al. studied the wave equation in one space dimension in the presence of time-varying delay. In this article, the authors showed the exponential stability results with the condition

$$a \leq \sqrt{1-d}\, a_0, \tag{9}$$

where d is a constant and

$$\tau'(t) \leq d < 1, \quad \forall t > 0. \tag{10}$$

In [26], Kafini and Messaoudi studied wave equations with delay and logarithmic terms as follows:

$$u_{tt} - \Delta u + \mu_1 u_t(x,t) + \mu_2 u_t(x, t-\tau) = |u|^{p-2}u \ \log |u|^k. \tag{11}$$

The authors proved the local existence and blow-up results for equation (11).

In [27], Park considered the equation with delay and logarithmic terms as follows:

$$u_{tt} - \Delta u + \alpha u_t(t) + \beta u_t(x, t-\tau) = u \ \ln |u|^\gamma. \tag{12}$$

The author showed the local and global existence results for equation (12). Also, the author investigated the decay and nonexistence results for equation (12). In recent years, some other authors investigate hyperbolic-type equations with delay terms (see [28–33]).

In this work, we studied the local existence, global existence, nonexistence, and stability results of plate equation (1) with delay and logarithmic terms, motivated by the above works. There is no research, to our best knowledge, related to plate equation (1) with the delay $(\beta u_t(x, t-\tau))$ term and logarithmic $(u \ln |u|^\gamma)$ source term; hence, our work is the generalization of the above studies.

This work consists of five sections in addition to the introduction. Firstly, in Section 2, we recall some assumptions and lemmas. Then, in Section 3, we obtain the local and global existence of solutions. Moreover, in Section 4, we establish the nonexistence results. Finally, in Section 5, we get the stability of solutions.

2. Preliminaries

In this part, we show the norm of X by $\|\cdot\|_X$ for a Banach space X. We give the scalar product in $L^2(\Omega)$ by $(\cdot, \cdot)$. We show $\|\cdot\|_2$ by $\|\cdot\|$, for brevity. Let B_1 be the constant of the embedding inequality

$$\|u\|^2 \leq B_1 \|\Delta u\|^2 \quad \text{for } u \in H_0^2(\Omega). \tag{13}$$

We have the following assumptions related to problem (1):

(H1). The weights of delay and dissipation satisfy

$$0 < |\beta| < \alpha. \tag{14}$$

(H2). The constant γ in (1) satisfies

$$0 < \gamma < \pi e^{(2(N+1))/N}. \tag{15}$$

To get the main result, we have the lemmas as follows.

Lemma 1 (see [34, 35]) (Logarithmic Sobolev inequality). *For any $u \in H_0^1(\Omega)$,*

$$\int_\Omega u^2 \ln |u| dx \le \frac{1}{2}\|u\|^2 \ln \|u\|^2 + \frac{k^2}{2\pi}\|\nabla u\|^2 - \frac{N}{2}(1+\ln\ k)\|u\|^2, \tag{16}$$

where k is a positive real number.

Corollary 2. *For any $u \in H_0^2(\Omega)$,*

$$\int_\Omega u^2 \ln |u| dx \le \frac{1}{2}\|u\|^2 \ln \|u\|^2 + \frac{k^2}{2\pi}\|\Delta u\|_2^2 - \frac{N}{2}(1+\ln\ k)\|u\|^2, \tag{17}$$

where k is a positive real number.

Remark 3. Assume that inequality (17) holds for all $k > 0$, and we choose the constant k that satisfies

$$\rho = \max\left\{e^{-(N+1)/N}, \mu^{1/N}\sqrt{\frac{\pi}{\gamma}}\right\} < k < \sqrt{\frac{\pi}{\gamma}}, \tag{18}$$

where μ is any real number with

$$0 < \mu < 1. \tag{19}$$

Lemma 4 (see [12]) (Logarithmic Gronwall inequality). *Suppose that $c > 0$ and $l \in L^1(0, T; R^+)$. If a function $f : [0, T] \longrightarrow [1,\infty)$ satisfies*

$$f(t) \le c\left(1 + \int_0^t l(s) f(s) \ln f(s) ds\right), \quad 0 \le t \le T, \tag{20}$$

then

$$f(t) \le c e^{c\int_0^t l(s)ds}, \quad 0 \le t \le T. \tag{21}$$

We define

$$J(v) = \frac{1}{2}\|\Delta v\|^2 - \frac{1}{2}\int_\Omega v^2 \ln |v|^\gamma dx + \frac{\gamma}{4}\|v\|^2, \tag{22}$$

$$I(v) = \|\Delta v\|^2 - \int_\Omega v^2 \ln |v|^\gamma dx, \tag{23}$$

for $v \in H_0^2(\Omega)$; then,

$$J(v) = \frac{1}{2}I(v) + \frac{\gamma}{4}\|v\|^2. \tag{24}$$

Suppose that

$$d = \inf_{v \in H_0^2(\Omega)\setminus\{0\}} \sup_{\lambda \ge 0} J(\lambda v). \tag{25}$$

Then, it satisfies (see, e.g., [36–38])

$$0 < d = \inf_{v \in \mathcal{N}} J(v), \tag{26}$$

where $\mathcal{N}$ is the well-known Nehari manifold, denoted by

$$\mathcal{N} = \left\{v \in H_0^2(\Omega) \setminus \{0\} \mid I(v) = 0\right\}. \tag{27}$$

Lemma 5. *I and J are the functions that satisfy*

$$I(\lambda v) = \lambda \frac{\partial J(\lambda v)}{\lambda v} \begin{cases} >0, 0 < \lambda < \lambda^*, \\ = 0, \lambda = \lambda^*, \\ <0, \lambda > \lambda^*, \end{cases} \tag{28}$$

for any $v \in H_0^2(\Omega)$ with $\|v\| \ne 0$, where

$$\lambda^* = \exp\left(\frac{\|\Delta v\|^2 - \int_\Omega v^2 \ln |v|^\gamma dx}{\gamma\|v\|^2}\right). \tag{29}$$

Proof. We obtain, for $\lambda \ge 0$,

$$\begin{aligned} \lambda \frac{\partial}{\partial \lambda} J(\lambda v) &= \lambda\left\{\lambda\|\Delta v\|^2 - \lambda\int_\Omega v^2 \ln |v|^\gamma dx + \frac{\gamma\lambda}{2}\|v\|^2 \right. \\ &\quad \left. -\lambda\int_\Omega v^2 \ln |\lambda|^\gamma dx - \frac{\gamma\lambda}{2}\int_\Omega v^2 dx\right\} \\ &= \lambda^2\left(\|\Delta v\|^2 - \int_\Omega v^2 \ln |v|^\gamma dx - \gamma \ln |\lambda| \int_\Omega v^2 dx\right) \\ &= I(\lambda v), \end{aligned} \tag{30}$$

and therefore, we obtain the desired result. □

Remark 6. $J(\lambda v)$ has the absolute maximum value at λ^*, such that

$$\sup_{\lambda \ge 0} J(\lambda v) = J(\lambda^* v) = \exp\left(\frac{2\|\Delta v\|^2 - 2\int_\Omega v^2 \ln |v|^\gamma dx}{\gamma\|v\|^2}\right)\frac{\gamma}{4}\|v\|^2, \tag{31}$$

for $v \in H_0^2(\Omega)$.

Lemma 7. *The potential depth d in (25) satisfies*

$$d \ge \frac{\gamma}{4} e^N \left(\frac{\pi}{\gamma}\right)^{N/2} = E_1. \tag{32}$$

Proof. By Corollary 2, (13), and (18), we have

$$I(v) \geq \left(1 - \frac{k^2\gamma}{2\pi}\right)\|\Delta v\|^2 + \frac{N\gamma}{2}(1 + \ln k)\|v\|^2 - \frac{\gamma}{2}\|v\|^2 \ln \|v\|^2 > \frac{N\gamma}{2}(1 + \ln k)\|v\|^2 - \frac{\gamma}{2}\|v\|^2 \ln \|v\|^2. \tag{33}$$

Taking the limit $k \longrightarrow \sqrt{\pi/\gamma}$, we obtain

$$I(v) \geq \left\{\frac{N\gamma}{2}\left(1 + \ln\sqrt{\frac{\pi}{\gamma}}\right) - \frac{\gamma}{2}\ln\|v\|^2\right\}\|v\|^2. \tag{34}$$

Taking into consideration this and (28), we get

$$0 = I(\lambda^* v) \geq \left\{\frac{N\gamma}{2}\left(1 + \ln\sqrt{\frac{\pi}{\gamma}}\right) - \frac{\gamma}{2}\ln\|\lambda^* v\|^2\|\lambda^* v\|^2\right\}, \tag{35}$$

and therefore,

$$\|\lambda^* v\|^2 \geq e^N\left(\frac{\pi}{\gamma}\right)^{N/2}. \tag{36}$$

Hence, we have by (24) and (31)

$$\sup_{\lambda\geq 0} J(\lambda v) = J(\lambda^* v) = \frac{1}{2}I(\lambda^* v) + \frac{\gamma}{4}\|\lambda^* v\|^2 = \frac{\gamma}{4}\|\lambda^* v\|^2 \geq \frac{\gamma}{4}e^N\left(\frac{\pi}{\gamma}\right)^{N/2}. \tag{37}$$

From the definition of d given in (25), we obtain the result. □

3. Existence

In this part, we have studied the local existence, global existence, nonexistence, and stability results of plate equation (1) with delay and logarithmic terms, motivated by the above works. There is no research, to our best knowledge, related to plate equation (1) with the delay ($\beta u_t(x, t-\tau)$) term and logarithmic ($u \ln |u|^\gamma$) source term; hence, our work is the generalization of the above studies. Firstly, we introduce the new function

$$y(x, \eta, t) = u_t(x, t - \eta\tau) \quad \text{for } (x, \eta, t) \in \Omega \times [0, 1] \times (0, \infty). \tag{38}$$

Hence, problem (1) takes the form

$$\begin{cases} u_{tt} + \Delta^2 u + \alpha u_t(x,t) + \beta y(x,1,t) = u \ln|u|^\gamma & \text{for } (x,t) \in \Omega \times (0,\infty), \\ \tau y_t(x,\eta,t) + y_\eta(x,\eta,t) = 0 & \text{for } (x,\eta,t) \in \Omega \times (0,1) \times (0,\infty), \\ u(x,t) = \dfrac{\partial u(x,t)}{\partial v} = 0 & \text{for } (x,t) \in \partial\Omega \times (0,\infty), \\ u(x,0) = u_0(x),\ u_t(x,0) = u_1(x) & \text{for } x \in \Omega, \\ y(x,\eta,0) = j_0(x,-\eta\tau) = y_0(x,\eta) & \text{for } (x,\eta) \in \Omega \times (0,1). \end{cases} \tag{39}$$

Definition 8. Assume that $T > 0$. (u, y) is a local solution of problem (39) if it satisfies

$$u \in C([0,T]; H_0^2(\Omega)) \cap C^1([0,T]; L^2(\Omega)) \cap C^2([0,T]; H^{-2}(\Omega)),$$

$$(u_{tt}, v) + (\Delta u, \Delta v) + \alpha(u_t(t), v) + \beta(y(1,t), v) = (u \ln|u|^\gamma, v) \quad \text{for any } v \in H_0^2(\Omega),$$

$$\tau\int_0^1 (y_t(\eta,t), \varphi(\eta))d\eta + \int_0^1 \left(y_\eta(\eta,t), \varphi(\eta)\right)d\eta = 0 \quad \text{for any } \varphi \in L^2(\Omega \times (0,1)),$$

$$u(0) = u_0 \quad \text{in } H_0^2(\Omega),$$

$$u_t(0) = u_1 \quad \text{in } L^2(\Omega),$$

$$y(0) = y_0 \quad \text{in } L^2(\Omega \times (0,1)). \tag{40}$$

3.1. Local Existence. In this part, we establish the local existence results similar to [8, 39].

Theorem 9. *Suppose that (H1) and (H2) are satisfied. Then, for the initial data $u_0 \in H_0^2(\Omega)$, $u_1 \in L^2(\Omega)$, and $y_0 \in L^2(\Omega \times (0,1))$, there exists a local solution (u, y) for problem (39).*

Proof. Let $\{v_i\}_{i\in N}$ be the orthogonal basis of $H_0^2(\Omega)$ that is orthonormal in $L^2(\Omega)$. Define $\varphi_i(x, 0) = v_i(x)$, and we extend $\varphi_i(x, 0)$ by $\varphi_i(x, \eta)$ over $L^2(\Omega \times (0, 1))$. We denote $V_n = \text{span}\{v_1, v_2, \cdots, v_n\}$ and $W_n = \text{span}\{\varphi_1, \varphi_2, \cdots, \varphi_n\}$ for $n \geq 1$. We consider the Faedo-Galerkin approximation solution $(u^n, y^n) \in V_n \times W_n$ of the form

$$u^n = \sum_{i=1}^n h_i^n(t)v_i(x), \qquad y^n(x,\eta,t) = \sum_{i=1}^n g_i^n(t)\varphi_i(x,\eta), \quad n = 1, 2, \cdots, \tag{41}$$

solving the approximate system

$$(u_{tt}^n, v) + (\Delta u^n, \Delta v) + \alpha(u_t^n(t), v) + \beta(y^n(1,t), v) = \int_\Omega u^n \ln|u^n|^\gamma v dx \quad \text{for } v \in V_n, \tag{42}$$

$$\tau\int_0^1 (y_t^n(\eta,t),\varphi(\eta))d\eta + \int_0^1 \left(y_\eta^n(\eta,t),\varphi(\eta)\right)d\eta = 0 \quad \text{for } \varphi \in W_n, \tag{43}$$

$$\begin{aligned} u^n(0) &= u_0^n, \\ u_t^n(0) &= u_1^n, \\ y^n(0) &= y_0^n, \end{aligned} \tag{44}$$

where

$$\begin{aligned} u_0^n &\longrightarrow u_0 \quad \text{in } H_0^2(\Omega), \\ u_1^n &\longrightarrow u_1 \quad \text{in } L^2(\Omega), \\ y_0^n &\longrightarrow y_0 \quad \text{in } L^2(\Omega\times(0,1)). \end{aligned} \tag{45}$$

Since problem (42)–(44) is a normal system of ordinary differential equations, there exists a solution (u^n, y^n) on the interval $[0, t_n)$, $t_n \in (0, T]$. The extension of that solution to the $[0, T)$ is a consequence of the estimate below.

By replacing v by $u_t^n(t)$ in (42) and by using the relation

$$\int_\Omega u^n \ln|u^n|^\gamma u_t^n dx = \frac{d}{dt}\left\{\frac{1}{2}\int_\Omega (u^n)^2 \ln|u^n|^\gamma dx - \frac{\gamma}{4}\|u^n\|^2\right\}, \tag{46}$$

we have

$$\begin{aligned} &\frac{d}{dt}\left\{\frac{1}{2}\|u_t^n\|^2 + \frac{1}{2}\|\Delta u^n\|^2 + \frac{\gamma}{4}\|u^n\|^2 - \frac{1}{2}\int_\Omega (u^n)^2 \ln|u^n|^\gamma dx\right\} \\ &\quad = -\alpha\|u_t^n(t)\|^2 - \beta(y^n(1,t), u_t^n(t)). \end{aligned} \tag{47}$$

By replacing φ by $\omega y^n(\eta, t)$ in (43), we see that

$$\frac{\omega\tau}{2}\frac{d}{dt}\int_\Omega\int_0^1 (y^n(x,\eta,t))^2 d\eta dx = -\frac{\omega}{2}\|y^n(1,t)\|^2 + \frac{\omega}{2}\|y^n(0,t)\|^2. \tag{48}$$

Summing (47) and (48), we obtain

$$\frac{d}{dt}E^n(t) = -\alpha\|u_t^n\|^2 - \beta(y^n(1,t), u_t^n(t)) - \frac{\omega}{2}\|y^n(1,t)\|^2 + \frac{\omega}{2}\|y^n(0,t)\|^2, \tag{49}$$

where

$$\begin{aligned} E^n(t) = {} & \frac{1}{2}\|u_t^n\|^2 + \frac{1}{2}\|\Delta u^n\|^2 + \frac{\gamma}{4}\|u^n\|^2 - \frac{1}{2}\int_\Omega (u^n)^2 \ln|u^n|^\gamma dx \\ & + \frac{\omega\tau}{2}\|y^n\|^2_{L^2(\Omega\times(0,1))}, \end{aligned} \tag{50}$$

where

$$|\beta| < \omega < 2\alpha - |\beta|. \tag{51}$$

Utilizing Young's inequality and the fact that $y^n(x, 0, t) = u_t^n(x, t)$, we obtain

$$\frac{d}{dt}E^n(t) \le -\left(\alpha - \frac{|\beta|}{2} - \frac{\omega}{2}\right)\|u_t^n\|^2 - \left(\frac{\omega}{2} - \frac{|\beta|}{2}\right)\|y^n(1,t)\|^2 \le 0, \tag{52}$$

$$E^n(t) + C_1\int_0^t \|u_t^n(s)\|^2 ds + C_2\int_0^t \|y^n(1,s)\|^2 ds \le E^n(0), \tag{53}$$

where

$$\begin{aligned} C_1 &= \alpha - \frac{|\beta|}{2} - \frac{\omega}{2} > 0, \\ C_2 &= \frac{\omega}{2} - \frac{|\beta|}{2} > 0. \end{aligned} \tag{54}$$

Taking into consideration this and Corollary 2, we have

$$\begin{aligned} &\|u_t^n\|^2 + \left(1 - \frac{\gamma k^2}{2\pi}\right)\|\Delta u^n\|^2 + \frac{\gamma}{2}(1 + N(1 + \ln k))\|u^n\|^2 \\ &\quad + 2C_1\int_0^t \|u_t^n(s)\|^2 ds + 2C_2\int_0^t \|y^n(1,s)\|^2 ds + \omega\tau\|y^n\|^2_{L^2(\Omega\times(0,1))} \\ &\quad \le 2E^n(0) + \frac{\gamma}{2}\|u^n\|^2 \ln\|u^n\|^2. \end{aligned} \tag{55}$$

By using (18), we obtain

$$\begin{aligned} 1 - \frac{\gamma k^2}{2\pi} &> 0, \\ \frac{\gamma}{2}(1 + N(1 + \ln k)) &> 0, \end{aligned} \tag{56}$$

and therefore,

$$\begin{aligned} &\|u_t^n\|^2 + \|\Delta u^n\|^2 + \|u^n\|^2 + \int_0^t \|u_t^n(s)\|^2 ds + \int_0^t \|y^n(1,s)\|^2 ds \\ &\quad + \|y^n\|^2_{L^2(\Omega\times(0,1))} \le c_1\left(1 + \|u^n\|^2 \ln\|u^n\|^2\right), \end{aligned} \tag{57}$$

where the sequel c_j, $j = 1, 2, \cdots$, shows a positive constant. Also, we know that

$$u^n(x,t) = u^n(x,0) + \int_0^t u_t^n(x,s) ds. \tag{58}$$

Utilizing Cauchy-Schwarz's inequality and (57), we obtain

$$\begin{aligned}\|u^n(t)\|^2 &= 2\|u^n(0)\|^2 + 2T\int_0^t \|u_t^n(s)\|^2 ds \\ &\le 2\|u^n(0)\|^2 + 2T\int_0^t c_1\left(1 + \|u^n(s)\|^2 \ln \|u^n(s)\|^2\right) ds \\ &\le c_2\left(1 + \int_0^t \|u^n(s)\|^2 \ln \|u^n(s)\|^2 ds\right).\end{aligned} \tag{59}$$

From Lemma 4, we arrive at

$$\|u^n(t)\|^2 \le c_3 e^{c_4 T}. \tag{60}$$

$f(s) = s \ln s$ is the function which is continuous on $(0, \infty)$, $\lim_{s\longrightarrow 0^+} f(s) = 0$, $\lim_{s\longrightarrow +\infty} f(s) = +\infty$, and f decreases on $(0, e^{-1})$ and increases on $(e^{-1}, +\infty)$; hence, we get by (57) and (60)

$$\begin{aligned}\|u_t^n\|^2 + \|\Delta u^n\|^2 + \|u^n\|^2 + \int_0^t \|u_t^n(s)\|^2 ds + \int_0^t \|y^n(1,s)\|^2 ds \\ + \|y^n\|^2_{L^2(\Omega\times(0,1))} \le c_5.\end{aligned} \tag{61}$$

Hence, there exists a subsequence of $\{(u^n, y^n)\}$, which we still denote $\{(u^n, y^n)\}$, such that

$$\begin{aligned} u^n &\longrightarrow u \quad \text{weakly star in } L^\infty\left(0, T; H_0^2(\Omega)\right), \\ u_t^n &\longrightarrow u_t \quad \text{weakly star in } L^\infty\left(0, T; L^2(\Omega)\right), \\ y^n &\longrightarrow y \quad \text{weakly star in } L^\infty\left(0, T; L^2(\Omega\times(0,1))\right), \\ y^n(1) &\longrightarrow y(1) \quad \text{weakly in } L^2\left(0, T; L^2(\Omega)\right). \end{aligned} \tag{62}$$

Utilizing the Aubin-Lions compactness theorem, we conclude that

$$\begin{aligned} u^n &\longrightarrow u \quad \text{strongly in } L^2\left(0, T; L^2(\Omega)\right), \\ u^n &\longrightarrow u \quad \text{a.e.in } \Omega\times(0,T). \end{aligned} \tag{63}$$

The function $s \longrightarrow s \ln |s|^\gamma$ is continuous on R; hence,

$$u^n \ln |u^n|^\gamma \longrightarrow u \ln |u|^\gamma \quad \text{a.e.in } \Omega\times(0,T). \tag{64}$$

Let

$$\begin{aligned} \Omega_1 &= \{x \in \Omega \mid |u^n| < 1\}, \\ \Omega_2 &= \{x \in \Omega \mid |u^n| \ge 1\}. \end{aligned} \tag{65}$$

Thus, we obtain

$$\begin{aligned}\int_\Omega (u^n \ln |u^n|^\gamma)^2 dx &= \gamma^2\left\{\int_{\Omega_1} (u^n \ln |u^n|)^2 dx + \int_{\Omega_2} (u^n \ln |u^n|)^2 dx\right\} \\ &\le \gamma^2\left\{e^{-2}|\Omega_1| + e^{-2}\left(\frac{2}{q-2}\right)^2 \int_{\Omega_2} (u^n)^q dx\right\} \quad \text{for any } q > 2,\end{aligned} \tag{66}$$

where we used

$$\begin{aligned} |s \ln s| &\le \frac{1}{e} \quad \text{for } 0 < s < 1, \\ s^{-\kappa} \ln s &\le \frac{1}{e\kappa} \quad \text{for } s \ge 1 \text{ and } \kappa > 0. \end{aligned} \tag{67}$$

By (57) and (66), we conclude that

$$\int_\Omega (u^n \ln |u^n|^\gamma)^2 dx \le \gamma^2\left\{e^{-2}|\Omega_1| + e^{-2}\left(\frac{2}{q-2}\right)^2 B_2^q \|\Delta u^n\|^q\right\} \le c_6, \tag{68}$$

where B_2 is the Sobolev imbedding constant of

$$H_0^2(\Omega) \subset L^q(\Omega) \quad \text{for } q > 2, \text{ if } N = 1, 2, 3, 4; 2 < q < \frac{2N}{N-4}, \text{ if } N \ge 5. \tag{69}$$

Therefore, we get from (68)

$$u^n \ln |u^n|^\gamma \quad \text{which is uniformly bounded in } L^\infty\left(0, T; L^2(\Omega)\right). \tag{70}$$

From the Lebesgue bounded convergence theorem, (64), and (70), we arrive at

$$u^n \ln |u^n|^\gamma \longrightarrow u \ln |u|^\gamma \quad \text{strongly in } L^2\left(0, T; L^2(\Omega)\right). \tag{71}$$

We pass the limit $m \longrightarrow \infty$ in (42) and (43). The remainder of the proof is standard and similar to [39, 40]. □

3.2. Global Existence. In this part, we obtain the global existence results for problem (39). For this goal, we define the energy functional of problem (39):

$$\begin{aligned}E(t) = \frac{1}{2}\|u_t\|^2 + \frac{1}{2}\|\Delta u\|^2 + \frac{\gamma}{4}\|u\|^2 - \frac{1}{2}\int_\Omega u^2 \ln |u|^\gamma dx \\ + \frac{\omega\tau}{2}\|y\|^2_{L^2(\Omega\times(0,1))},\end{aligned} \tag{72}$$

where ω is the positive constant given in (51). We see that

$$\begin{aligned}E(t) = \frac{1}{2}\|u_t\|^2 + J(u(t)) + \frac{\omega\tau}{2}\|y\|^2_{L^2(\Omega\times(0,1))} = \frac{1}{2}\|u_t\|^2 \\ + \frac{1}{2}I(u(t)) + \frac{\gamma}{4}\|u\|^2 + \frac{\omega\tau}{2}\|y\|^2_{L^2(\Omega\times(0,1))}.\end{aligned} \tag{73}$$

By the same arguments similar to (52), we infer that

$$\frac{d}{dt}E(t) \le -C_1\|u_t\|^2 - C_2\|y(1,t)\|^2 \le 0, \tag{74}$$

where C_1 and C_2, given in (54), are positive constants.

Lemma 10. *Suppose that (H1) and (H2) are satisfied. If $E(0) < d$ and $I(u_0) > 0$, then the solution u of problem (1) satisfies*

$$I(u(t)) > 0 \quad \text{for } t \in [0, T), \tag{75}$$

where T is the maximal existence time of the solutions.

Proof. We know that $I(u_0) > 0$ and u is continuous on $[0, T)$; hence, we have

$$I(u(t)) > 0 \quad \text{for some interval } [0, t_1) \in [0, T). \tag{76}$$

Let t_0 be the maximum of t_1 satisfying (76). Assume that $t_0 < T$; then, $I(u(t_0)) = 0$, that is,

$$u(t_0) \in \mathcal{N}. \tag{77}$$

Therefore, we obtain by (26)

$$J(u(t_0)) \ge \inf_{v\in\mathcal{N}} J(v) = d. \tag{78}$$

We see that this is in contradiction to the relation as follows:

$$J(u(t_0)) \le E(t_0) \le E(0) < d. \tag{79}$$

By (74) and Lemma 10, we see that $E(t)$ is a nonincreasing function. □

Theorem 11. *The solution u is global, under the conditions of Lemma 10.*

Proof. It suffices to show that $\|u_t\|^2 + \|\Delta u\|^2$ is bounded independent of t. By Lemma 10, (73), and (74), we get

$$\|u_t\|^2 \le \|u_t\|^2 + I(u(t)) \le 2E(t) \le 2E(0) < 2d. \tag{80}$$

In a similar way, we get

$$\|u\|^2 < \|u\|^2 + \frac{2}{\gamma}I(u(t)) = \frac{4}{\gamma}J(u(t)) \le \frac{4}{\gamma}E(t) \le \frac{4}{\gamma}E(0) < \frac{4d}{\gamma}. \tag{81}$$

By Corollary 2 and (23), we conclude that

$$\|\Delta u\|^2 = I(u(t)) + \gamma\int_\Omega u^2 \ln|u|dx \le 2E(t) + \frac{\gamma}{2}\|u\|^2 \ln\|u\|^2 + \frac{k^2\gamma}{2\pi}\|\Delta u\|^2 - \frac{N\gamma}{2}(1+\ln k)\|u\|^2. \tag{82}$$

By taking the limit $k \longrightarrow \rho^+$ in this inequality and from (81), we obtain

$$\begin{aligned}\left(1 - \frac{\rho^2\gamma}{2\pi}\right)\|\Delta u\|^2 &\le 2E(t) + \frac{\gamma}{2}\left(\ln\|u\|^2 - N(1+\ln\rho)\right)\|u\|^2 \\ &< 2d + \frac{\gamma}{2}\left(\ln\left(\frac{4d}{\gamma}\right)\right) - N(1+\ln\rho)\|u\|^2 \\ &= 2d + \frac{\gamma}{2}\left\{\ln\left(\frac{4d}{\gamma}e^{-N}\rho^{-N}\right)\right\}\|u\|^2.\end{aligned} \tag{83}$$

By Lemma 7 and (18), we get

$$\begin{aligned}\ln\left(\frac{4d}{\gamma}e^{-N}\rho^{-N}\right) &\ge \ln\left(\left(\frac{\pi}{\gamma}\right)^{N/2}\rho^{-N}\right) \\ &= \ln\left(\left(\sqrt{\frac{\pi}{\gamma}}\rho^{-1}\right)^N\right) \ln 1 = 0.\end{aligned} \tag{84}$$

Therefore, we see by (81) and (83) that

$$\left(1 - \frac{\rho^2\gamma}{2\pi}\right)\|\Delta u\|^2 \le 2d + 2d\ \ln\left(\frac{4d}{\gamma}e^{-N}\rho^{-N}\right). \tag{85}$$

Hence, we conclude that

$$\|\Delta u\|^2 < 2d\left(1 - \frac{\rho^2\gamma}{2\pi}\right)^{-1}\left(1 + \ln\left(\frac{4d}{\gamma}e^{-N}\rho^{-N}\right)\right). \tag{86}$$

Therefore, we complete the proof by (80) and (86). □

4. Nonexistence

In this part, similar to [41–43], we get the nonexistence results for problem (1). Firstly, we need the lemma as follows.

Lemma 12. *Assume that (H1) and (H2) are satisfied. If $E(0) < E_1$ and $I(u_0) < 0$, then the solution u of problem (1) satisfies*

$$I(u(t)) < 0 \quad \text{for } t \in [0, T), \tag{87}$$

$$\|u(t)\|^2 > \frac{4E_1}{\gamma} \quad \text{for } t \in [0, T), \tag{88}$$

where T is the maximal existence time of the solutions.

Proof. We know that $I(u_0) < 0$ and u is continuous on $[0, T)$; hence, we have

$$I(u(t)) < 0 \quad \text{for some interval } [0, t_1) \subset [0, T). \tag{89}$$

Let t_0 be the maximal time satisfying (89) and assume that $t_0 < T$; then, $I(u_0) = 0$, such that

$$u(t_0) \in \mathcal{N}. \tag{90}$$

Therefore, we obtain

$$d \le J(u(t_0)) = \frac{1}{2} I(u(t_0)) + \frac{\gamma}{4}\|u(t_0)\|^2 \le E(u(t_0)) \le E(0) < E_1. \tag{91}$$

This is in contradiction to Lemma 7. Thus, (87) is proved. By Lemma 7, (31), and (87), we conclude that

$$E_1 \le d \le J(\lambda^* u(t)) = \exp\left(\frac{2\|\Delta u\|^2 - 2\int_\Omega u^2 \ln |u|^\gamma dx}{\gamma \|u\|^2}\right) \frac{\gamma}{4}\|u\|^2 < \frac{\gamma}{4}\|u\|^2. \tag{92}$$

Therefore, the proof is completed. □

Theorem 13. *Suppose that (H1) and (H2) are satisfied. Let $E(0) < \zeta E_1$, where $0 < \zeta < 1$, and $I(u_0) < 0$. Then, the solution of problem (1) blows up at infinity.*

Proof. Firstly, we set

$$F(t) = \zeta E_1 - E(t). \tag{93}$$

By (74), we obtain

$$F'(t) = -E'(t) \ge C_1\|u_t\|^2 + C_2\|y(1,t)\|^2 \ge 0. \tag{94}$$

Utilizing (72), (88), and (94), we see that

$$0 < F(0) \le F(t) \le \zeta E_1 + \frac{1}{2}\int_\Omega u^2 \ln |u|^\gamma dx < \frac{\gamma}{4}\|u\|^2 + \frac{1}{2}\int_\Omega u^2 \ln |u|^\gamma dx. \tag{95}$$

We define

$$G(t) = F(t) + \varepsilon(u, u_t) + \frac{\varepsilon\alpha}{2}\|u\|^2. \tag{96}$$

By (39) and (72), we get

$$G'(t) = F'(t) + \varepsilon\|u_t\|^2 - \varepsilon\|\Delta u\|^2 - \varepsilon\beta(u, y(1,t)) + \varepsilon\int_\Omega u^2 \ln |u|^\gamma dx = F'(t) + 2\varepsilon\|u_t\|^2 - \varepsilon\beta(u, y(1,t)) - 2\varepsilon E(t) + \frac{\varepsilon\gamma}{2}\|u\|^2 + \omega\tau\|y\|^2_{L^2(\Omega\times(0,1))}. \tag{97}$$

Utilizing Young's inequality and (94), we obtain

$$\beta(u, y(1,t)) \le |\beta|\left(\delta\|u\|^2 + \frac{1}{4\delta}\|y(1,t)\|^2\right) \le \delta|\beta|\|u\|^2 + \frac{|\beta|}{4\delta C_2}F'(t). \tag{98}$$

By adapting this to (97) and from (88) and (93), we have

$$\begin{aligned} G'(t) &\ge \left(1 - \frac{\varepsilon|\beta|}{4\delta C_2}\right)F'(t) + 2\varepsilon\|u_t\|^2 + \left(\frac{\varepsilon\gamma}{2} - \varepsilon|\beta|\delta\right)\|u\|^2 \\ &\quad + 2\varepsilon F(t) - 2\varepsilon\zeta E_1 + \omega\tau\|y\|^2_{L^2(\Omega\times(0,1))} \\ &\ge \left(1 - \frac{\varepsilon|\beta|}{4\delta C_2}\right)F'(t) + 2\varepsilon\|u_t\|^2 + \varepsilon\left((1-\zeta)\frac{\gamma}{2} - |\beta|\delta\right)\|u\|^2 \\ &\quad + 2\varepsilon F(t) + \omega\tau\|y\|^2_{L^2(\Omega\times(0,1))}. \end{aligned} \tag{99}$$

Firstly, fix $\delta > 0$ such that $(1-\zeta)(\gamma/2) - |\beta|\delta > 0$ and then choose $\varepsilon > 0$ small enough so that $1 - (\varepsilon|\beta|/4\delta C_2) > 0$. Then, by (94), we get

$$G'(t) \ge c_8\left(F(t) + \|u_t\|^2 + \|u\|^2\right) \ge 0. \tag{100}$$

Also, we conclude that

$$G(t) \le c_9\left(F(t) + \|u_t\|^2 + \|u\|^2\right). \tag{101}$$

Taking $\varepsilon > 0$ small enough again, we obtain

$$G(0) = F(0) + \varepsilon(u_0, u_1) + \frac{\varepsilon\alpha}{2}\|u_0\|^2 > 0. \tag{102}$$

By (100) and (102), we get

$$G(t) \ge G(0) > 0. \tag{103}$$

Utilizing (100) and (101), we see that

$$G'(t) \ge c_{10}G(t), \tag{104}$$

and therefore,

$$G(t) \ge e^{c_{10}t}G(0) > 0. \tag{105}$$

Therefore, $G(t)$ blows up at infinity. Consequently, the proof is completed. □

5. Stability

In this part, we obtain the stability of global solutions. Firstly, we define the perturbed energy by

$$\Psi(t) = E(t) + \varepsilon\Phi(t) + \varepsilon\Xi(t), \tag{106}$$

where $\varepsilon > 0$, $\Phi(t) = (u_t, u)$, and $\Xi(t) = \int_\Omega\int_0^1 e^{-\tau\eta}y^2(x,\eta,t)d\eta\,dx$.

Lemma 14. *Under the conditions of Lemma 10, for $C_3, C_4 > 0$, we obtain*

$$C_3E(t) \le \Psi(t) \le C_4E(t). \tag{107}$$

Proof. Utilizing Lemma 10 and Young's inequality, we have

$$\begin{aligned}|\Phi(t)+\Xi(t)| &\le \frac{1}{2}\|u_t\|^2+\frac{1}{2}\|u\|^2+\|y\|^2_{L^2(\Omega\times(0,1))}\\ &\le \frac{1}{2}\|u_t\|^2+\frac{2}{\gamma}\left(\frac{\gamma}{4}\|u\|^2+\frac{1}{2}I(u(t))\right)\\ &\quad+\|y\|^2_{L^2(\Omega\times(0,1))}=\frac{1}{2}\|u_t\|^2+\frac{2}{\gamma}J(u(t))\\ &\quad+\|y\|^2_{L^2(\Omega\times(0,1))}\le c_7E(t).\end{aligned} \tag{108}$$

Taking $\varepsilon>0$ small enough, we complete the proof. □

Theorem 15. *Assume that (H1) and (H2) are satisfied. Suppose that $E(0)<E_1$ and $I(u_0)>0$. Hence, for $C_0, C_5>0$, we obtain*

$$0<E(t)\le C_0e^{-C_5t}\quad \text{for } t\ge 0. \tag{109}$$

Proof. From (39) and Young's inequality, we get

$$\begin{aligned}\Phi'(t) &= \|u_t\|^2-\|\Delta u\|^2-\alpha(u_t(t),u(t))-\beta(y(1,t),u(t))\\ &\quad+\int_\Omega u^2\ln|u|^\gamma dx\le\|u_t\|^2-\frac{1}{2}\|\Delta u\|^2+\alpha^2B_1\|u_t(t)\|^2\\ &\quad+\beta^2B_1\|y(1,t)\|^2+\int_\Omega u^2\ln|u|^\gamma dx.\end{aligned} \tag{110}$$

By using the second equation of (39) and the integration by parts, we obtain

$$\begin{aligned}\Xi'(t) &= -\frac{2}{\tau}\int_\Omega\int_0^1 e^{-\tau\eta}y(x,\eta,t)y_\eta(x,\eta,t)d\eta dx\\ &= -\frac{1}{\tau}\int_\Omega\int_0^1 e^{-\tau\eta}\frac{\partial}{\partial\eta}y^2(x,\eta,t)d\eta dx\\ &= -\frac{e^{-\tau}}{\tau}\|y(1,t)\|^2+\frac{1}{\tau}\|y(0,t)\|^2-\int_\Omega\int_0^1 e^{-\tau\eta}y^2(x,\eta,t)d\eta dx\\ &\le \frac{1}{\tau}\|u_t\|^2-e^{-\tau}\int_\Omega\int_0^1 y^2(x,\eta,t)d\eta dx.\end{aligned} \tag{111}$$

Summing these and (74), we obtain

$$\begin{aligned}\Psi'(t) &\le -\left(C_1-\varepsilon-\varepsilon\alpha^2B_1-\frac{\varepsilon}{\tau}\right)\|u_t\|^2-\frac{\varepsilon}{2}\|\Delta u\|^2\\ &\quad-\left(C_2-\varepsilon\beta^2B_1\right)\|y(1,t)\|^2+\varepsilon\int_\Omega u^2\ln|u|^\gamma dx\\ &\quad-\varepsilon e^{-\tau}\|y\|^2_{L^2(\Omega\times(0,1))}.\end{aligned} \tag{112}$$

Adding and subtracting $\xi E(t)$ with $0<\xi<2\varepsilon$, we get

$$\begin{aligned}\Psi'(t) &\le -\xi E(t)-\left(C_1-\varepsilon-\varepsilon\alpha^2B_1-\frac{\varepsilon}{\tau}-\frac{\xi}{2}\right)\|u_t\|^2\\ &\quad-\left(\frac{\varepsilon}{2}-\frac{\xi}{2}-\frac{\xi\gamma B_1}{4}\right)\|\Delta u\|^2-\left(C_2-\varepsilon\beta^2B_1\right)\|y(1,t)\|^2\\ &\quad+\left(\varepsilon-\frac{\xi}{2}\right)\int_\Omega u^2\ln|u|^\gamma dx-\left(\varepsilon e^{-\tau}-\frac{\xi\omega\tau}{2}\right)\|y\|^2_{L^2(\Omega\times(0,1))}.\end{aligned} \tag{113}$$

Utilizing the logarithmic Sobolev inequality, we have

$$\begin{aligned}\Psi'(t) &\le -\xi E(t)-\left(C_1-\varepsilon-\varepsilon\alpha^2B_1-\frac{\varepsilon}{\tau}-\frac{\xi}{2}\right)\|u_t\|^2\\ &\quad-\left\{\varepsilon\left(\frac{1}{2}-\frac{\gamma k^2}{2\pi}\right)-\frac{\xi}{2}\left(1-\frac{\gamma k^2}{2\pi}\right)-\frac{\xi\gamma B_1}{4}\right\}\|\Delta u\|^2\\ &\quad+\frac{\gamma}{2}\left(\varepsilon-\frac{\xi}{2}\right)\left\{\ln\|u\|^2-N(1+\ln k)\right\}\|u\|^2\\ &\quad-\left(C_2-\varepsilon\beta^2B_1\right)\|y(1,t)\|^2-\left(\varepsilon e^{-\tau}-\frac{\xi\omega\tau}{2}\right)\|y\|^2_{L^2(\Omega\times(0,1))}.\end{aligned} \tag{114}$$

Now, choose $\varepsilon>0$ small enough, such that

$$\begin{aligned}C_1-\varepsilon-\varepsilon\alpha^2B_1-\frac{\varepsilon}{\tau}&>0,\\ C_2-\varepsilon\beta^2B_1&>0.\end{aligned} \tag{115}$$

By taking $\xi>0$ sufficiently small and noting that $(1/2)-(\gamma k^2/2\pi)>0$ (see (18)), we infer that

$$\Psi'(t)\le -\xi E(t)+\frac{\gamma}{2}\left(\varepsilon-\frac{\xi}{2}\right)\left\{\ln\|u\|^2-N(1+\ln k)\right\}\|u\|^2, \tag{116}$$

where $0<E(0)<E_1$; therefore, there exists $0<\mu<1$, that is, $E(0)=\mu E_1$. Therefore, we obtain by (81)

$$\begin{aligned}\ln\|u\|^2 &< \ln\left(\frac{4}{\gamma}E(t)\right)\le\ln\left(\frac{4}{\gamma}E(0)\right)=\ln\left(\frac{4\mu E_1}{\gamma}\right)\\ &=\ln\left(\mu e^N\left(\frac{\pi}{\gamma}\right)^{N/2}\right).\end{aligned} \tag{117}$$

Hence, by (18), we arrive at

$$\begin{aligned}\ln\|u\|^2-N(1+\ln k) &\le \ln\left(\mu e^N\left(\frac{\pi}{\gamma}\right)^{N/2}\right)-N(1+\ln k)\\ &=N\ln\left(\mu^{1/N}\sqrt{\frac{\pi}{\gamma}}k^{-1}\right)<N\ln 1=0.\end{aligned} \tag{118}$$

Substituting this into (116), we arrive at

$$\Psi'(t) \leq -\xi E(t). \tag{119}$$

As a result, from Lemma 14, we completed the proof. □

6. Conclusions

Recently, there have been many published works related to wave equations with time delay. There were no local existence, global existence, nonexistence, and stability results of the plate equation with delay and logarithmic source terms, to the best of our knowledge. Firstly, we have obtained the local and global existence results. Then, we have obtained the nonexistence of solutions. Finally, we have proved stability results under sufficient conditions.

Data Availability

No data were used to support the study.

Conflicts of Interest

The authors declare that they have no competing interests.

Acknowledgments

The first and second authors are grateful to DUBAP (ZGEF.20.009) for research funds.

References

[1] K. Bartkowski and P. Gŏrka, "One-dimensional Klein-Gordon equation with logarithmic nonlinearities," *Journal of Physics A: Mathematical and Theoretical*, vol. 41, no. 35, article 355201, 2008.

[2] P. Gorka, "Logarithmic Klein-Gordon equation," *Acta Physica Polonica*, vol. B40, pp. 59–66, 2009.

[3] C. Abdallah, P. Dorato, J. Benitez-Read, and R. Byrne, "Delayed positive feedback can stabilize oscillatory system," A.C.C. San Francisco, 1993.

[4] I. H. Suh and Z. Bien, "Use of time-delay actions in the controller design," *IEEE Transactions on Automatic Control*, vol. 25, no. 3, pp. 600–603, 1980.

[5] R. Datko, J. Lagnese, and M. P. Polis, "An example on the effect of time delays in boundary feedback stabilization of wave equations," *SIAM Journal on Control and Optimization*, vol. 24, no. 1, pp. 152–156, 1986.

[6] M. Kafini and S. A. Messaoudi, "A blow-up result in a nonlinear wave equation with delay," *Mediterranean Journal of Mathematics*, vol. 13, no. 1, pp. 237–247, 2016.

[7] S. Nicaise and C. Pignotti, "Stability and instability results of the wave equation with a delay term in the boundary or internal feedbacks," *SIAM Journal on Control and Optimization*, vol. 45, no. 5, pp. 1561–1585, 2006.

[8] S. Nicaise and C. Pignotti, "Stabilization of the wave equation with boundary or internal distributed delay," *Differential and Integral Equations*, vol. 21, pp. 935–958, 2008.

[9] C. Q. Xu, S. P. Yung, and L. K. Li, "Stabilization of the wave system with input delay in the boundary control," *ESAIM*, vol. 12, pp. 770–785, 2006.

[10] I. Bialynicki-Birula and J. Mycielski, "Wave equations with logarithmic nonlinearities," *Bulletin de l'Academie Polonaise des Sciences. Serie des Sciences, Mathematiques, Astronomiques et Physiques*, vol. 23, no. 4, pp. 461–466, 1975.

[11] I. Bialynicki-Birula and J. Mycielski, "Nonlinear wave mechanics," *Annals of Physics*, vol. 100, no. 1-2, pp. 62–93, 1976.

[12] T. Cazenave and A. Haraux, "Équations d'évolution avec non linéarité logarithmique," *Annales de la Faculté des Sciences de Toulouse Mathématiques*, vol. 2, no. 1, pp. 21–51, 1980.

[13] T. Hiramatsu, M. Kawasaki, and F. Takahashi, "Numerical study of q-ball formation in gravity mediation," *Journal of Cosmology and Astroparticle Physics*, vol. 2010, no. 6, p. 8, 2010.

[14] X. Han, "Global existence of weak solutions for a logarithmic wave equation arising from q-ball dynamics," *Bulletin of the Korean Mathematical Society*, vol. 50, no. 1, pp. 275–283, 2013.

[15] M. M. Al-Gharabli and S. A. Messaoudi, "Existence and a general decay result for a plate equation with nonlinear damping and a logarithmic source term," *Journal of Evolution Equations*, vol. 18, no. 1, pp. 105–125, 2018.

[16] G. Liu, "The existence, general decay and blow-up for a plate equation with nonlinear damping and a logarithmic source term," *Electronic Research Archive*, vol. 28, no. 1, pp. 263–289, 2020.

[17] S. A. Messaoudi, "Global existence and nonexistence in a system of Petrovsky," *Journal of Mathematical Analysis and Applications*, vol. 265, no. 2, pp. 296–308, 2002.

[18] W. Chen and Y. Zhou, "Global nonexistence for a semilinear Petrovsky equation," *Nonlinear Analysis: Theory, Methods & Applications*, vol. 70, no. 9, pp. 3203–3208, 2009.

[19] E. Pişkin and N. Polat, "On the decay of solutions for a nonlinear Petrovsky equation," *Mathematical Sciences Letters*, vol. 3, no. 1, pp. 43–47, 2013.

[20] V. Komornik, "On the nonlinear boundary stabilization of Kirchhoff plates," *Nonlinear Differential Equations and Applications NoDEA*, vol. 1, no. 4, pp. 323–337, 1994.

[21] J. Lagnese, "Asymptotic energy estimates for Kirchhoff plates subject to weak viscoelastic damping," in *International Series of Numerical Mathematics*, vol. 91, Birhauser, Verlag, Bassel, 1989.

[22] J. Muñoz Rivera, E. C. Lapa, and R. Barreto, "Decay rates for viscoelastic plates with memory," *Journal of Elasticity*, vol. 44, no. 1, pp. 61–87, 1996.

[23] K. Liu, "Locally distributed control and damping for the conservative systems," *SIAM Journal on Control and Optimization*, vol. 35, no. 5, pp. 1574–1590, 1997.

[24] E. Zuazua, "Exponential decay for the semilinear wave equation with locally distributed damping," *Communications in Partial Differential Equations*, vol. 15, pp. 205–235, 1990.

[25] S. Nicaise, J. Valein, and E. Fridman, "Stability of the heat and of the wave equations with boundary time-varying delays," *Discrete & Continuous Dynamical Systems - S*, vol. 2, no. 3, pp. 559–581, 2009.

[26] M. Kafini and S. A. Messaoudi, "Local existence and blow up of solutions to a logarithmic nonlinear wave equation with delay," *Applicable Analysis*, vol. 99, pp. 530–547, 2019.

[27] S. H. Park, "Global existence, energy decay and blow-up of solutions for wave equations with time delay and logarithmic source," *Advances in Difference Equations*, vol. 2020, 17 pages, 2020.

[28] E. Pişkin and H. Yüksekkaya, "Nonexistence of solutions of a delayed wave equation with variable-exponents," *C-POST*, vol. 3, no. 1, pp. 97–101, 2020.

[29] E. Pişkin and H. Yüksekkaya, "Decay and blow up of solutions for a delayed wave equation with variable-exponents," *Conference Proceedings of Science and Technology*, vol. 3, no. 1, pp. 91–96, 2020.

[30] E. Pişkin and H. Yüksekkaya, "Local existence and blow up of solutions for a logarithmic nonlinear viscoelastic wave equation with delay," *Computational Methods for Differential Equations*, vol. 9, no. 2, pp. 623–636, 2021.

[31] E. Piskin and H. Yüksekkaya, "Nonexistence of global solutions of a delayed wave equation with variable-exponents," *Miskolc Math. Notes*, vol. 22, pp. 1–19, 2021.

[32] E. Pişkin and H. Yüksekkaya, "Decay of solutions for a nonlinear Petrovsky equation with delay term and variable exponents," *The Aligarh Bulletin Of Mathematics*, vol. 39, no. 2, pp. 63–78, 2020.

[33] E. Pişkin and H. Yüksekkaya, "Blow-up of solutions for a logarithmic quasilinear hyperbolic equation with delay term," *Journal of Mathematical Analysis and Applications*, vol. 12, no. 1, pp. 56–64, 2021.

[34] H. Chen, P. Luo, and G. W. Liu, "Global solution and blow-up of a semilinear heat equation with logarithmic nonlinearity," *Journal of Mathematical Analysis and Applications*, vol. 422, no. 1, pp. 84–98, 2015.

[35] L. Gross, "Logarithmic Sobolev inequalities," *American Journal of Mathematics*, vol. 97, no. 4, pp. 1061–1083, 1975.

[36] H. Chen and G. Liu, "Global existence and nonexistence for semilinear parabolic equations with conical degeneration," *Journal of Pseudo-Differential Operators and Applications*, vol. 3, no. 3, pp. 329–349, 2012.

[37] Y. Liu, "On potential wells and applications to semilinear hyperbolic equations and parabolic equations," *Nonlinear Analysis*, vol. 64, pp. 2665–2687, 2006.

[38] L. Payne and D. Sattinger, "Saddle points and instability of nonlinear hyperbolic equation," *Israel Journal of Mathematics*, vol. 226, pp. 273–303, 1975.

[39] M. M. Al-Gharabli and S. A. Messaoudi, "The existence and the asymptotic behavior of a plate equation with frictional damping and a logarithmic source term," *Journal of Mathematical Analysis and Applications*, vol. 454, no. 2, pp. 1114–1128, 2017.

[40] J. L. Lions, *Quelques Méthodes de Résolution des Problémes aux Limites Non Linéaires*, Dunod, Paris, 1969.

[41] W. J. Liu and J. Yu, "On decay and blow-up of the solution for a viscoelastic wave equation with boundary damping and source terms," *Nonlinear Analysis*, vol. 74, no. 6, pp. 2175–2190, 2011.

[42] S. A. Messaoudi, "Blow up and global existence in a nonlinear viscoelastic wave equation," *Mathematische Nachrichten*, vol. 260, no. 1, pp. 58–66, 2003.

[43] S. H. Park, M. J. Lee, and J. R. Kang, "Blow-up results for viscoelastic wave equations with weak damping," *Applied Mathematics Letters*, vol. 80, pp. 20–26, 2018.

Hindawi
Advances in Mathematical Physics
Volume 2021, Article ID 5211451, 18 pages
https://doi.org/10.1155/2021/5211451

Research Article

M-Breather, Lumps, and Soliton Molecules for the $(2+1)$-Dimensional Elliptic Toda Equation

Yuechen Jia, Yu Lu, Miao Yu, and Hasi Gegen

School of Mathematical Science, Inner Mongolia University, No. 235 West College Road, Hohhot, Inner Mongolia 010021, China

Correspondence should be addressed to Hasi Gegen; gegen@imu.edu.cn

Received 22 April 2021; Accepted 30 May 2021; Published 24 June 2021

Academic Editor: Mohammad Mirzazadeh

The $(2+1)$-dimensional elliptic Toda equation is a higher dimensional generalization of the Toda lattice and also a discrete version of the Kadomtsev-Petviashvili-1 (KP1) equation. In this paper, we derive the *M*-breather solution in the determinant form for the $(2+1)$-dimensional elliptic Toda equation via Bäcklund transformation and nonlinear superposition formulae. The lump solutions of the $(2+1)$-dimensional elliptic Toda equation are derived from the breather solutions through the degeneration process. Hybrid solutions composed of two line solitons and one breather/lump are constructed. By introducing the velocity resonance to the *N*-soliton solution, it is found that the $(2+1)$-dimensional elliptic Toda equation possesses line soliton molecules, breather-soliton molecules, and breather molecules. Based on the *N*-soliton solution, we also demonstrate the interactions between a soliton/breather-soliton molecule and a lump and the interaction between a soliton molecule and a breather. It is interesting to find that the KP1 equation does not possess a line soliton molecule, but its discrete version—the $(2+1)$-dimensional elliptic Toda equation—exhibits line soliton molecules.

1. Introduction

The Toda lattice is an integrable one-dimensional lattice model which originally describes the motion of a chain of particles due to nearest neighbor interaction through an exponential potential function [1]. The Toda equation takes the form

$$v_{tt}(n) = e^{v(n-1)-v(n)} - e^{v(n)-v(n+1)}, \quad n \in Z, \tag{1}$$

which is the equation of motion for the nth particle. Here, we denote $v(n,t)$ as $v(n)$ for simplicity. This equation also describes nonlinear wave propagation in many areas of physics such as ladder circuits [2], biophysics [3], and elementary particle physics [4]. The $(2+1)$-dimensional elliptic Toda lattice which is a natural dimensional generalization of the Toda lattice (1) reads

$$\Delta v(n) = e^{v(n-1)-v(n)} - e^{v(n)-v(n+1)}, \quad n \in Z, \tag{2}$$

where $\Delta = \partial_{xx} + \partial_{yy}$ is a two-dimensional Laplacian operator. It first appears in connection with Laplace-Darboux transformation for general second-order partial differential equations in the work of Darboux in 1887 [5]. In 1979, the integrability of the $(2+1)$-dimensional Toda lattice was established through the inverse scattering method [6, 7] and Lie group theory [8]. The $(2+1)$-dimensional Toda lattice and its relatives have important applications in 2D gravity [9, 10], string theory [11, 12], differential geometry [13], and random matrices and orthogonal polynomials [14, 15]. The Bessel-type solutions for the $(2+1)$-dimensional elliptic Toda lattice (1) were derived in [16], and its various classes of special solutions such as lump-type solutions, periodic solutions, and line solitons were investigated via the inverse scattering transform in [17]. In [18], the rational solution and breather solution for (2) were studied applying the Hirota bilinear method. Nakamura derived exact solutions for the $(2+1)$-dimensional cylindrical Toda equation and the $(3+1)$-dimensional elliptic Toda equation in [19, 20]. In [21], three classes of lump solutions for (2) were constructed through symbolic computation.

The study of the nonlinear localized waves such as solitons, breathers, lumps, and rough waves has attracted great attention due to their important applications in nonlinear

physical areas such as nonlinear optics, biophysics, oceanography, Bose-Einstein condensates, and plasma [22–27]. A breather is a special localized solitary wave that is periodic in space or time. Breathers have important applications in many physical areas such as optics, hydrodynamics, and quantized superfluid [28–30]. A lump solution is a kind of two-dimensional localized wave that decays algebraically in all directions [31]. Bäcklund transformation, which owes its origin to classical differential geometry in the 19th century, is an important tool in studying nonlinear integrable equations [32, 33]. The Bäcklund transformations and their associated nonlinear superposition formulae allow the generation of the various solutions of the nonlinear equations by purely algebraic procedures. In Hirota bilinear formalism, the original bilinear equation is bilinear in the dependent variables, whereas its bilinear Bäcklund transformations are linear in both the old and new dependent variables; therefore, one only needs to solve a set of linear partial differential equations to obtain new solutions from old ones [34]. Combining the bilinear Bäcklund transformation and associated nonlinear superposition formulae, we may derive an infinite sequence of solutions for nonlinear equations. In this paper, we derive an M-breather solution in the determinant form for the $(2+1)$-dimensional elliptic Toda equation (2) by applying the bilinear Bäcklund transformation and associated nonlinear superposition formulae. We also obtain its lump solutions by taking the infinite period of the breathers. Some bound states of solitons such as soliton molecules, breather molecules, and breather-soliton molecules have been theoretically and experimentally found in optics [35, 36] and Bose-Einstein condensation [37]. They are of great interest for applications in optical technologies because they would provide a doubling of the data-carrying capacity of the fiber [38, 39]. The velocity resonance mechanism has been proposed in [40] to study the soliton molecule. Many novel soliton molecules such as dark soliton molecules, dromion molecules, breather molecules, and breather-soliton molecules for continuous nonlinear wave equations have been found by utilizing this method [41–43]. However, the soliton molecules for the discrete nonlinear wave equations have not been reported yet. In this paper, we discuss the resonant structures for the solitons such as line soliton molecules, breather-soliton molecules, and breather molecules for the $(2+1)$-dimensional elliptic Toda equation via the velocity resonance.

The paper is organized as follows. In Section 2, the$M$-breather solution and hybrid solution composed of line solitons and breathers for the$(2+1)$-dimensional elliptic Toda equation are derived via the Bäcklund transformation and nonlinear superposition formulae. In addition, we analyze the dynamical properties of 1-breather and 2-breather. In Section 3, we derive the lump solutions for the $(2+1)$-dimensional elliptic Toda equation by taking the infinite period of the breathers. Furthermore, we construct hybrid solutions consisting of line solitons, breathers, and lumps. In Section 4, line soliton molecules, breather-soliton molecules, and breather molecules for the $(2+1)$-dimensional elliptic Toda equation are investigated through the velocity resonance mechanism, and interactions between soliton molecules and breathers/lumps are illustrated. A summary and discussion are given in Section 5.

2. M-Breather of the $(2+1)$-Dimensional Elliptic Toda Equation

By introducing $u(n) = e^{v(n-1)-v(n)}$, the $(2+1)$-dimensional elliptic Toda equation (2) can be written as

$$\left(\frac{\partial^2}{\partial x^2} + \frac{\partial^2}{\partial y^2}\right) \ln u(n) = u(n+1) - 2u(n) + u(n-1), \quad (3)$$

where we denote $u(n,x,y)$ as $u(n)$ for simplicity. Through the dependent variable transformation $u(n) = (f(n+1)f(n-1))/f(n)^2$, equation (3) can be transformed into the bilinear form

$$\left(D_x^2 + D_y^2\right) f(n)\cdot f(n) = \left(2e^{Dn} - 2\right) f(n)\cdot f(n). \quad (4)$$

The bilinear equation (4) admits the following Bäcklund transformation:

$$\begin{aligned} &\left(D_x + iD_y + \lambda^{-1}e^{-D_n} + \mu\right) f(n)\cdot g(n) = 0,\\ &\left(\left(D_x - iD_y\right)e^{-1/2D_n} - \lambda e^{1/2D_n} + \gamma e^{-1/2D_n}\right) f(n)\cdot g(n) = 0. \end{aligned} \quad (5)$$

Here, the bilinear operators $D_x^m D_t^n$ and e^{Dn} are defined by [44]

$$\begin{aligned} D_x^m D_t^n f\cdot g &= \frac{\partial^m}{\partial y^m}\frac{\partial^n}{\partial s^n} f(x+y,t+s)g(x-y,t-s)\Big|_{s=0,y=0},\\ e^{Dn} f(n)\cdot g(n) &= f(n+1)\cdot g(n-1),\\ e^{-Dn} f(n)\cdot g(n) &= f(n-1)\cdot g(n+1). \end{aligned} \quad (6)$$

If we take $f(n) = 1$, $\mu = -\lambda^{-1}$, and $\gamma = \lambda$ in equation (5), then we obtain $g(n) = 1 + e^{\eta}$, $\eta = px + qy + rn + \beta^0$, and $\lambda = (p - iq)/(1 - e^{-r})$ and the dispersion relation for the $(2+1)$-dimensional elliptic Toda equation (3):

$$p^2 + q^2 = 4\sinh^2\frac{r}{2}. \quad (7)$$

We apply the following nonlinear superposition formula presented in [45] to derive the 1-breather solution for equation (3).

Proposition 1. *Let $f_0(n)$ be a nonzero solution of equation (5) and suppose that $f_1(n)$ and $f_2(n)$ are solutions of (5) such that $f_0(n) \longrightarrow^{\lambda_i} f_i(n)(i = 1, 2)$; then, there exists the following nonlinear superposition formula:*

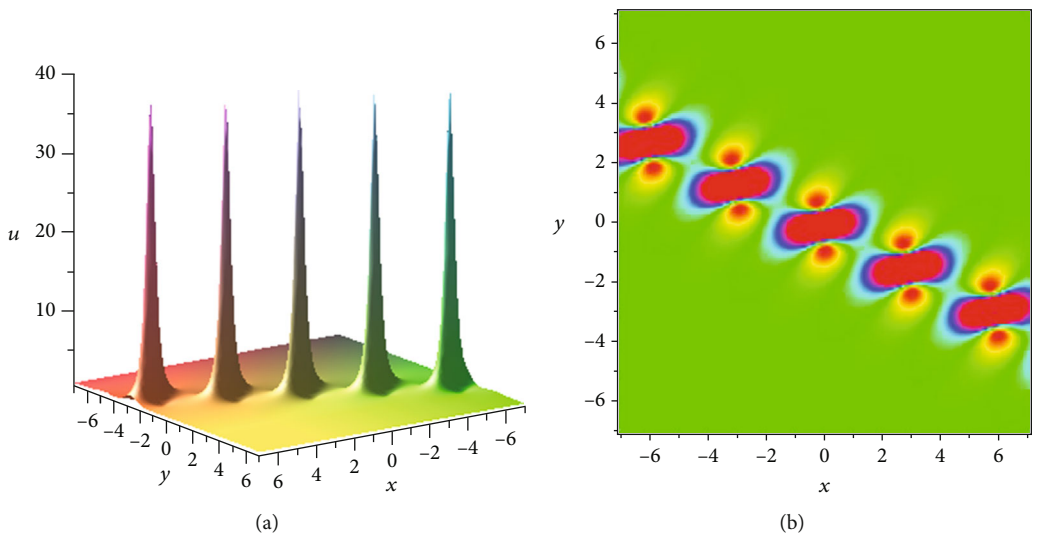

Figure 1: (a) 1-breather. (b) Density picture of 1-breather.

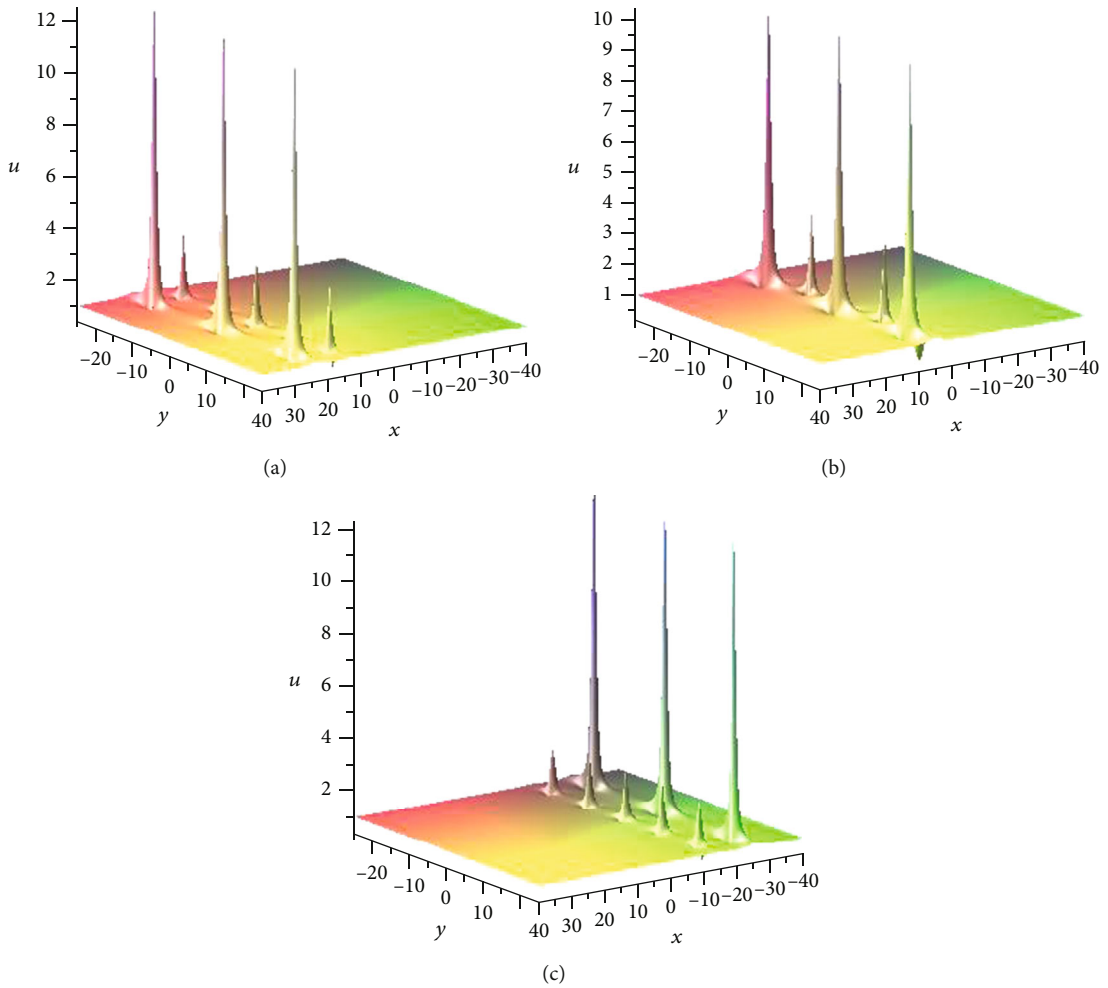

Figure 2: Propagation of 2-breather for $L_1L_2 > 0$ at different times: (a) $n = -30$, (b) $n = -8$, and (c) $n = 35$.

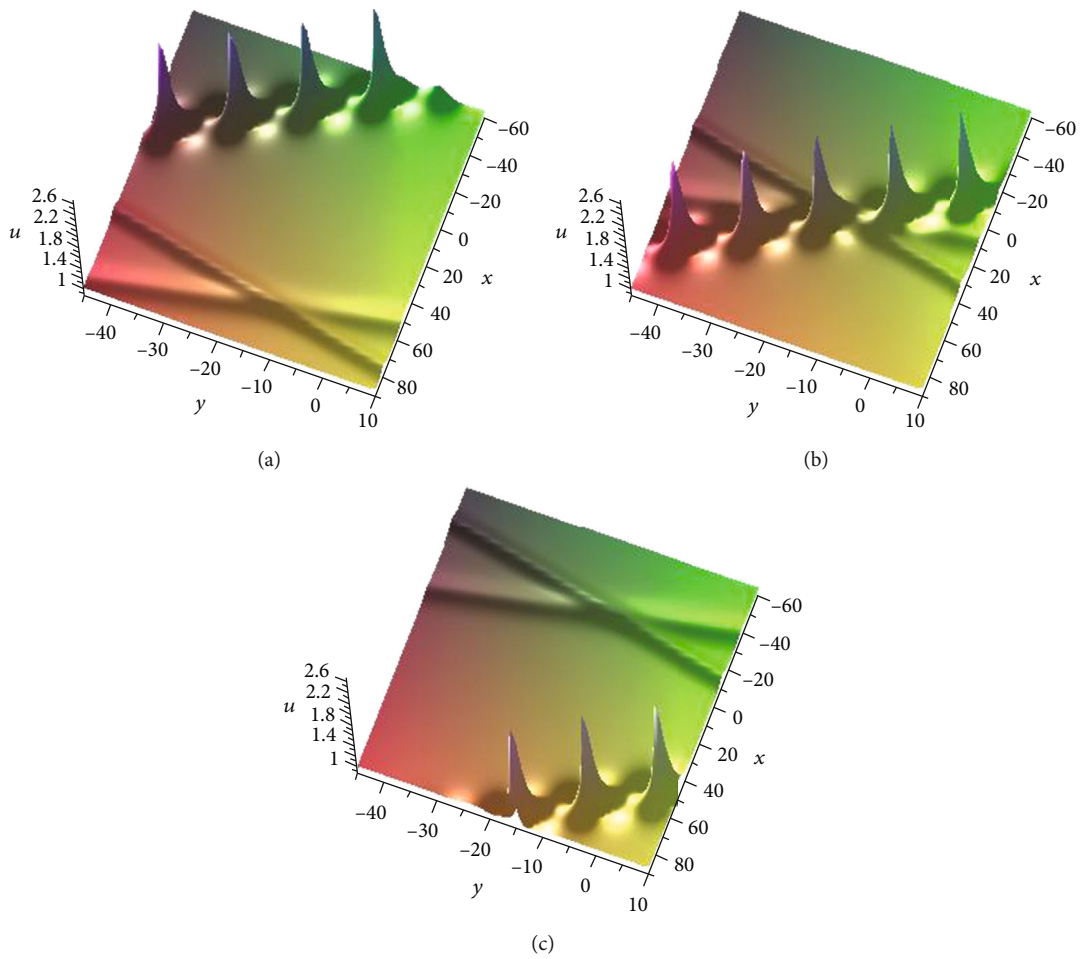

Figure 3: Propagation of hybrid solution composed of two line solitons and one breather at different times: (a) $n = -40$, (b) $n = 0$, and (c) $n = 40$.

$$e^{-1/2D_n} f_0(n) \cdot f_{12}(n) = c\left(\lambda_1 e^{-1/2D_n} - \lambda_2 e^{1/2D_n}\right) f_1(n) \cdot f_2(n), \tag{8}$$

where $f_{12}(n)$ is a new solution of (4) related to $f_1(n)$ and $f_2(n)$ with parameters λ_2 and λ_1, respectively. Here, c is a nonzero constant.

By taking $c = 1/(\lambda_1 - \lambda_2)$, $f_0(n) = 1$, and $f_i(n) = 1 + e^{\eta_i}$ $(i = 1, 2)$ in nonlinear superposition formula (8), we derive

$$f_{12}(n) = 1 + e^{\eta_1} + e^{\eta_2} + A_{12} e^{\eta_1 + \eta_2}, \tag{9}$$

where $\lambda_i = (p_i - iq_i)/(1 - e^{-r_i})$ and $\eta_i = p_i x + q_i y + r_i n + \beta_i^0$ $(i = 1, 2)$. According to dispersion relation (7), we may take $p_i = 2 \sinh k_i \cos l_i$, $q_i = 2 \sinh k_i \sin l_i$, and $r_i = 2k_i (i = 1, 2)$. Consequently,

$$A_{12} = \frac{\cos(l_1 - l_2) - \cosh(k_1 - k_2)}{\cos(l_1 - l_2) - \cosh(k_1 + k_2)}. \tag{10}$$

Furthermore, if we take $k_1 = k_2^* = \alpha_1 + \beta_1 i$, $l_1 = l_2^* = \gamma_1 + \delta_1 i$, $\beta_1^0 = \beta_2^{0*} = \ln(a/2) + i\theta_1$, and $e^{i\theta_1} = -(1/b^2) e^{\sigma_1 + i\theta_1}$ in equation (9), we get

$$f^{1b}(n) = 1 - \frac{a}{b^2} e^{R_1} \cos I_1 + \frac{A_{12} a^2}{4b^4} e^{2R_1}, \tag{11}$$

where

$$\begin{aligned}
R_1 &= 2\left(\widehat{a}_1 x + \widehat{b}_1 y + \alpha_1 n\right) + \sigma_1, \\
I_1 &= 2\left(\widehat{c}_1 x + \widehat{d}_1 y + \beta_1 n\right) + \theta_1, \\
\widehat{a}_1 &= (P_1 \cos \gamma_1 + Q_1 \sin \gamma_1), \\
\widehat{b}_1 &= (P_1 \sin \gamma_1 - Q_i \cos \gamma_1), \\
\widehat{c}_1 &= (\xi_1 \cos \gamma_1 - \zeta_1 \sin \gamma_1), \\
\widehat{d}_1 &= (\xi_1 \sin \gamma_1 + \zeta_1 \cos \gamma_1), \\
P_1 &= \sinh \alpha_1 \cosh \delta_1 \cos \beta_1, \\
Q_1 &= \cosh \alpha_1 \sinh \delta_1 \sin \beta_1, \\
\xi_1 &= \cosh \alpha_1 \cosh \delta_1 \sin \beta_1, \\
\zeta_1 &= \sinh \alpha_1 \sinh \delta_1 \cos \beta_1,
\end{aligned} \tag{12}$$

and α_1, β_1, γ_1, δ_1, σ_1, and θ_1 are arbitrary real-valued

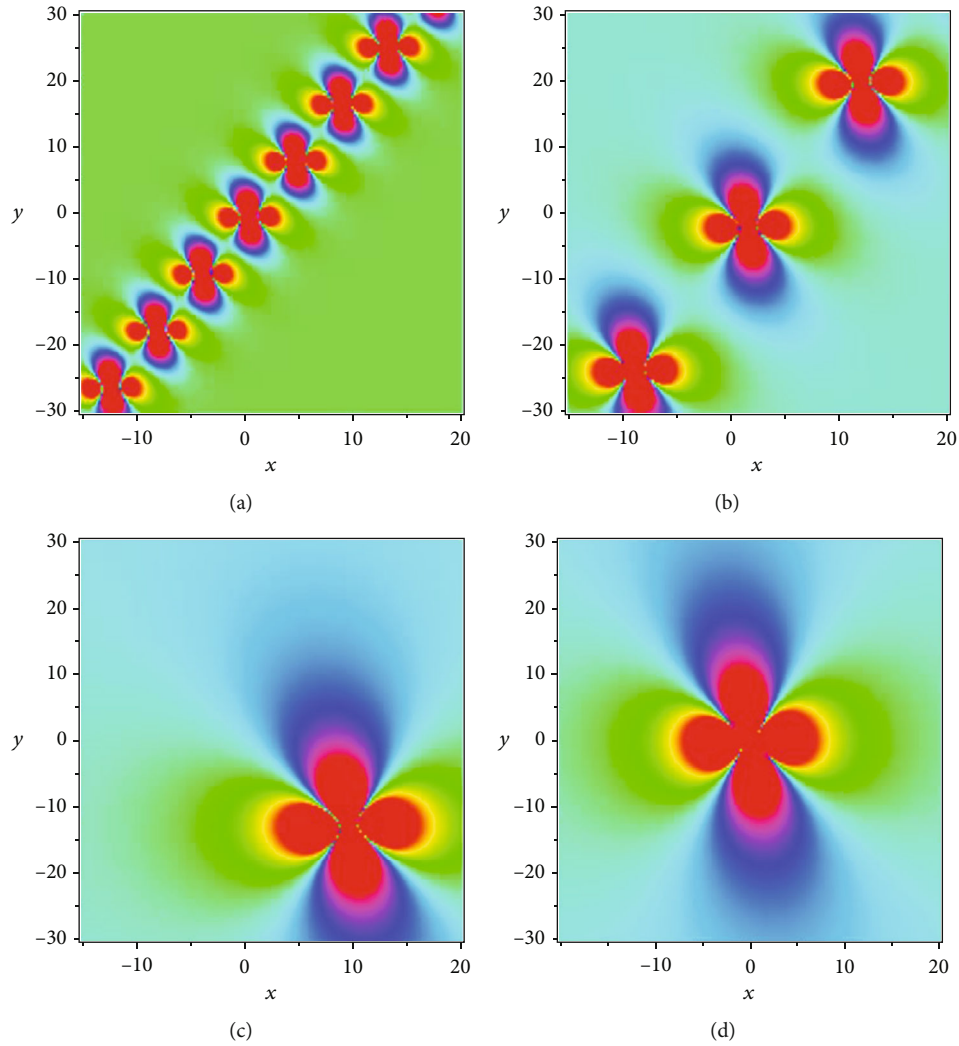

FIGURE 4: The degeneration of 1-breather (14) with $\gamma = 0.1$ and $\delta = 0.7$: (a) $\alpha = \beta = 1/4$, (b) $\alpha = \beta = 1/10$, (c) $\alpha = \beta = 1/60$, and (d) 1-lump.

constants. Since $k_1 = k_2^* = \alpha_1 + \beta_1 i$ *and* $l_1 = l_2^* = \gamma_1 + \delta_1 i$, *we can get*

$$A_{12} = \frac{\cosh 2\delta_1 - \cos 2\beta_1}{\cosh 2\delta_1 - \cos 2\alpha_1}. \tag{13}$$

By substituting equation (11) into $u(n) = (f(n+1)f(n-1))/f(n)^2$, *we derive the 1-breather solution for equation (3) as follows:*

$$u(n)^{1b} = \frac{A_{12}\left(\cosh^2(R_1+\varepsilon) + \sinh^2 2\alpha_1\right) + \cos^2 I_1 - \sin^2 2\beta_1 - 2\sqrt{A_{12}}\kappa}{\left(\sqrt{A_{12}}\cosh(R_1+\varepsilon) - \cos I_1\right)^2}, \tag{14}$$

where $\kappa = \cos 2\beta_1 \cosh 2\alpha_1 \cos I_1 \cosh(R_1+\varepsilon) + \sin 2\beta_1 \sinh 2\alpha_1 \sin I_1 \sinh(R_1+\varepsilon)$ *and* $\varepsilon = \ln(a\sqrt{A_{12}}/2b^2)$.

To obtain the nonsingular solution, we impose the condition $A_{12} > 1$. Figure 1 shows the 1-breather (14) with $\alpha_1 = 0.5$, $\beta_1 = 0.5$, $\gamma_1 = 5$, $\delta_1 = 1$, $n = 0$, $a = 1$, $b = 1$, $\sigma = 0$, and $\theta = 0$. Its top trace is a line l_1 on the (x, y)-plane for a given time n (see Figure 1(b)), which is defined by $l_1 : 2(\widehat{a}_1 x + \widehat{b}_1 y + \alpha_1 n) + \sigma_1 + \varepsilon = 0$. The period of 1-breather (14) is $T_{[x]} = (Q_1 \cos\gamma_1 - P_1 \sin\gamma_1)\pi/W$ along the x-direction and $T_{[y]} = (P_1 \cos\gamma_1 + Q_1 \sin\gamma_1)\pi/W$ for the y-direction, where $W = \sinh\delta_1 \cosh\delta_1(\sinh^2\alpha_1 \cos^2\beta_1 + \cosh^2\alpha_1 \sin^2\beta_1)$. Then, the distance of two neighboring peaks in 1-breather (14) is

$$T = \frac{\pi\sqrt{P_1^2 + Q_1^2}}{W}. \tag{15}$$

Note that T is the period of 1-breather $u(n)^{1b}$.

Proposition 2. *The elliptic Toda equation admits the general nonlinear superposition formula [45]*

$$e^{-1/2D_n} f_{N-1}(n) \cdot f_{N+1}(n) = c_N\left(\lambda_N e^{-1/2D_n} - \lambda_{N+1} e^{1/2D_n}\right) f_N(n) \cdot \widehat{f}_N(n), \tag{16}$$

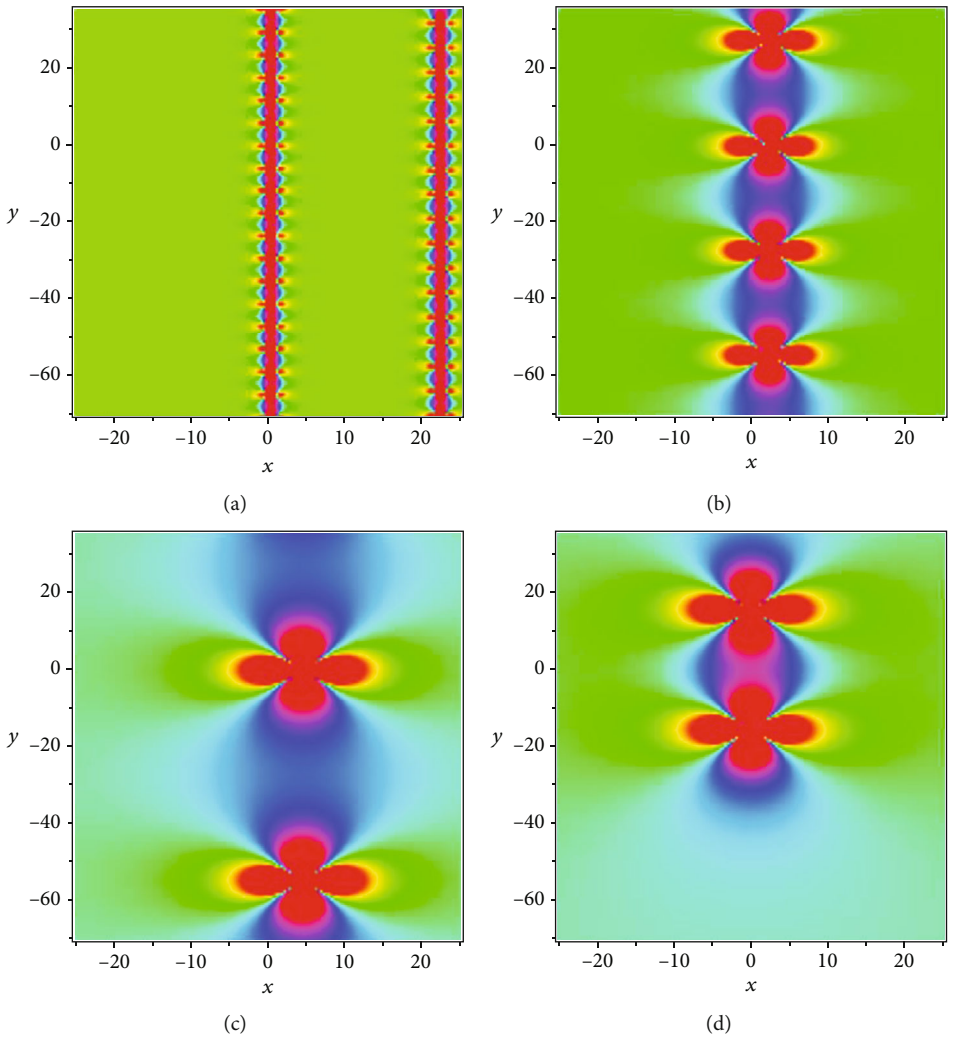

Figure 5: The degeneration of 2-breather (23) with $\beta_1 = \beta_2 = 0, \gamma_1 = \gamma_2 = 0, \delta_1 = 1.7/\sqrt{3}$, and $\delta_2 = 1.6/\sqrt{3}$: (a) $\alpha_1 = \alpha_2 = 0.45$, (b) $\alpha_1 = \alpha_2 = 0.1$, (c) $\alpha_1 = \alpha_2 = 0.05$, and (d) 2-lump.

where

$$f_N := c_N |1(n), \cdots, N(n)|, \tag{17}$$

$$\widehat{f}_N(n) = |1(n), \cdots, N-1(n), N+1(n)|, \tag{18}$$

$$j(n) = \left(\varphi_j(n), \cdots, (-\lambda_j)^{N-1}\varphi_j(n-N+1)\right)^T. \tag{19}$$

If we take $c_N = \prod_{1\le i<j\le N} 1/(\lambda_j - \lambda_i)$, $\varphi_j(n) = 1 + e^{\eta_j}$, $\lambda_j = (p_j - iq_j)/(1 - e^{-r_j})$, *and* $\eta_j = p_j x + q_j y + r_j n + \beta_j^0 = 2 \sinh k_j \cos l_j x + 2 \sinh k_j \sin l_j y + 2k_j n + \beta_j^0$ $(j = 1, 2, \cdots, N)$ *in nonlinear superposition formula (17), we derive N-soliton as*

$$f = \sum_{\mu=0,1} \exp\left(\sum_{i<j}^{N} \mu_i \mu_j A_{ij} + \sum_{i=1}^{N} \mu_i \eta_i\right), \tag{20}$$

where $e^{A_{ij}} \triangleq A_{ij} = (\cos(l_i - l_j) - \cosh(k_i - k_j))/(\cos(l_i - l_j) - \cosh(k_i + k_j))$, $\sum_{\mu=0,1}$ *implies the summation over all possible combinations of* $\mu_1 = 0.1, \mu_2 = 0.1, \cdots, \mu_N = 0.1$, *and* $\sum_{j<m}^{(N)}$ *indicates the summation over all possible pairs chosen from N elements.*

By taking $N = 2M$, $c_N = \prod_{1\le i<j\le N} 1/(\lambda_j - \lambda_i)$, $\varphi_j(n) = 1 + e^{\eta_j}$, $k_{j+M} = k_j^*$, $l_{j+M} = l_j^*$, *and* $\beta_{j+M}^0 = \beta_j^{0*}$ $(j = 1, 2, \cdots, M)$ *in equation (17), we derive the determinant form of M-breather for the (2 + 1)-dimensional elliptic Toda equation (3) under certain nonsingular conditions. When M = 2, we derive the following 2-breather for equation (3):*

$$\begin{aligned} f = 1 &- \frac{e^{R_1}\cos I_1}{b_1^2} - \frac{e^{R_2}\cos I_2}{b_2^2} + \frac{K_1}{4b_1^4}e^{2R_1} + \frac{K_2}{4b_2^4}e^{2R_2} \\ &+ \frac{K_1K_2(L_1^2 + M_1^2)(L_2^2 + M_2^2)}{16b_1^4b_2^4}e^{2R_1+2R_2} \\ &+ \frac{e^{R_1+R_2}}{2b_1^2b_2^2}(L_1\cos(I_1 + I_2) - M_1\sin(I_1 + I_2)) \\ &+ \frac{e^{R_1+R_2}}{2b_1^2b_2^2}(L_2\cos(I_1 - I_2) - M_2\sin(I_1 - I_2)) \end{aligned}$$

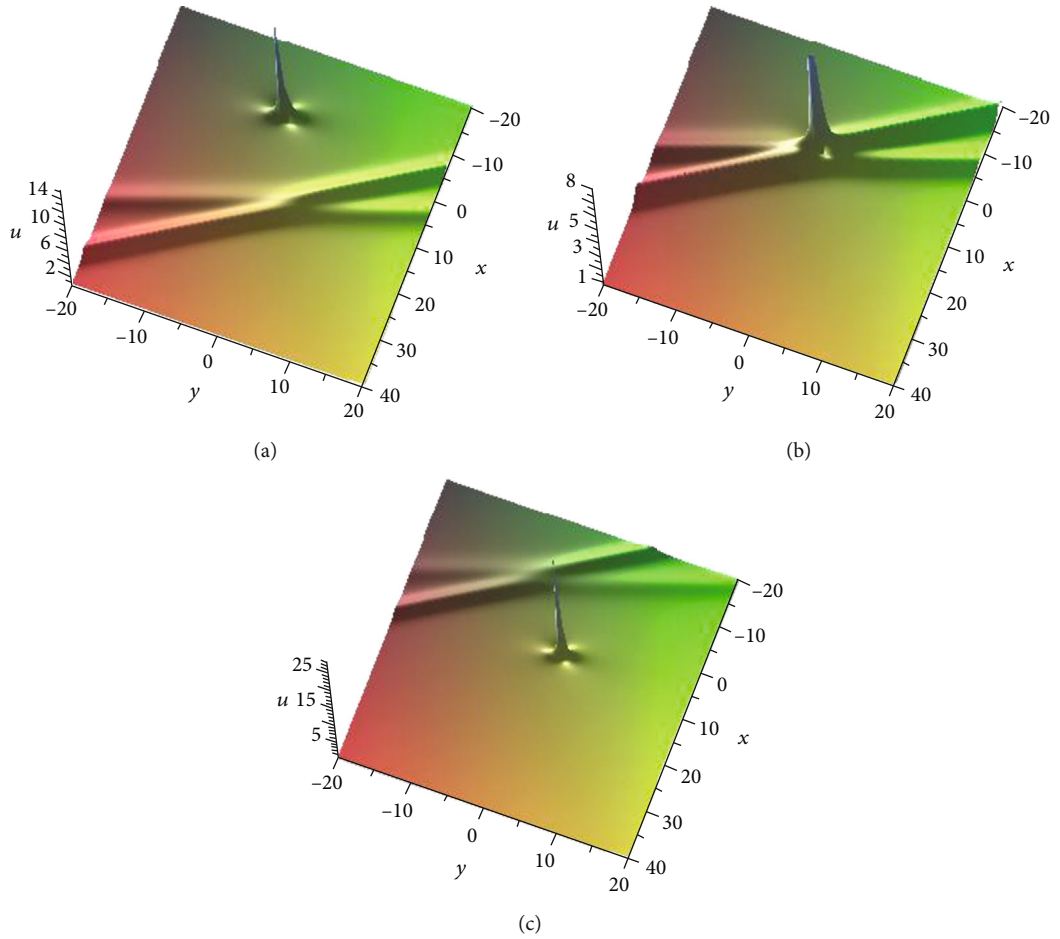

Figure 6: Propagation of hybrid solution composed of two line solitons and one lump at different times: (a) $n = -10$, (b) $n = 0$, and (c) $n = 10$.

$$-\frac{K_1 e^{2R_1+R_2}}{4b_1^4 b_2^2}\left((L_1L_2+M_1M_2)\cos I_2-(L_2M_1-L_1M_2)\sin I_2\right)$$

$$-\frac{K_2 e^{R_1+2R_2}}{4b_1^2 b_2^4}\left((L_1L_2-M_1M_2)\cos I_1-(L_2M_1+L_1M_2)\sin I_1\right), \tag{21}$$

where

$$R_i = 2\left(\widehat{a}_i x+\widehat{b}_i y+\alpha_i n\right)+\sigma_i,$$

$$I_i = 2\left(\widehat{c}_i x+\widehat{d}_i y+\beta_i n\right)+\theta_i,$$

$$\widehat{a}_i = (P_i\cos\gamma_i+Q_i\sin\gamma_i),$$

$$\widehat{b}_i = (P_i\sin\gamma_i-Q_i\cos\gamma_i),$$

$$\widehat{c}_i = (\xi_i\cos\gamma_i-\zeta_i\sin\gamma_i),$$

$$\widehat{d}_i = (\xi_i\sin\gamma_i+\zeta_i\cos\gamma_i),$$

$$P_i = \sinh\alpha_i\cosh\delta_i\cos\beta_i,$$

$$Q_i = \cosh\alpha_i\sinh\delta_i\sin\beta_i,$$

$$\xi_i = \cosh\alpha_i\cosh\delta_i\sin\beta_i,$$

$$\zeta_i = \sinh\alpha_i\sinh\delta_i\cos\beta_i \quad (i=1,2),$$

$$L_1 = \mathrm{Re}\,(A_{12}),$$

$$L_2 = \mathrm{Re}\,(A_{14}),$$

$$K_1 = A_{13},$$

$$K_2 = A_{24},$$

$$M_1 = \mathrm{Im}\,(A_{12}),$$

$$M_2 = \mathrm{Im}\,(A_{14}), \tag{22}$$

and α_i, β_i, γ_i, δ_i, σ_i, and $\theta_i (i = 1, 2)$ are arbitrary real-valued constants.

Now, we show that the interaction of two breathers is elastic and calculate their phase shift before and after the interaction. We consider y-periodic 2-breather-soliton (i.e.,

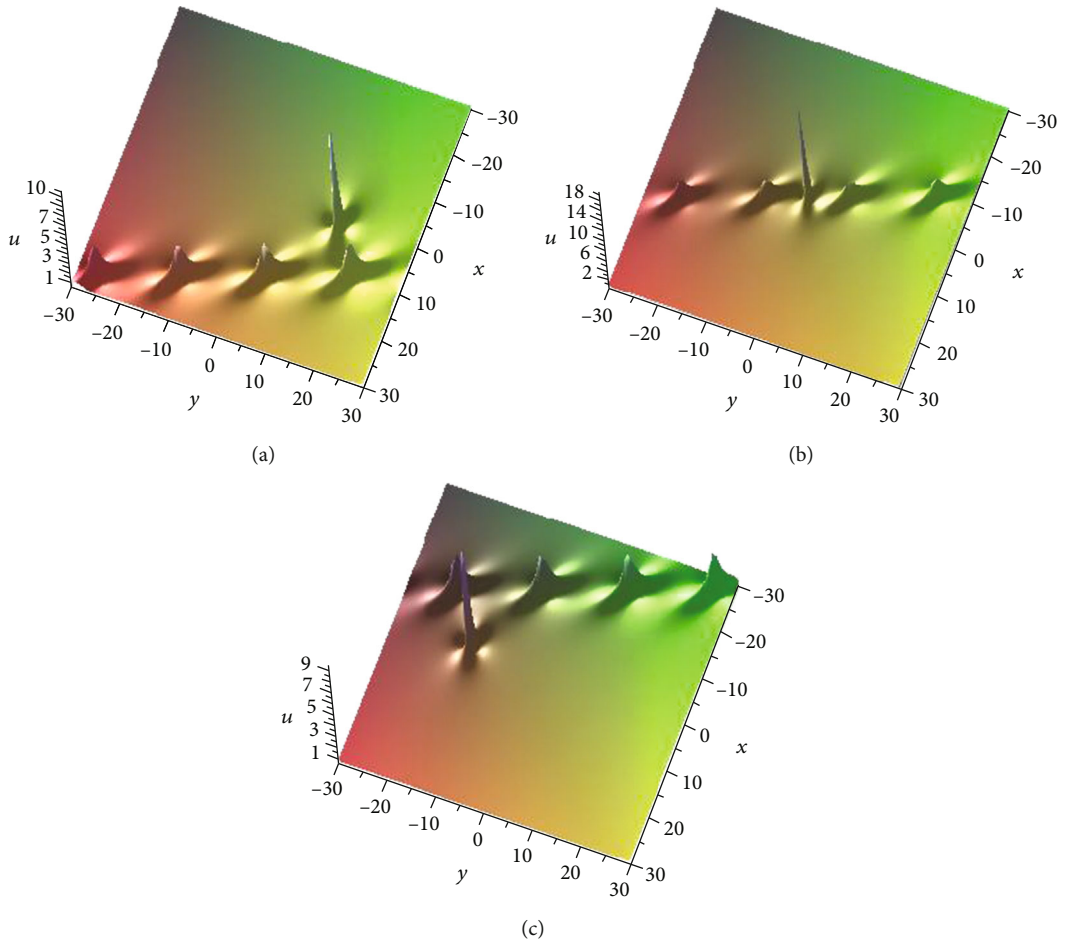

Figure 7: Propagation of hybrid solution composed of a breather and a lump at different times: (a) $n = -20$, (b) $n = 0$, and (c) $n = 20$.

$\beta_i = \gamma_i = 0$ $(i = 1, 2)$ in equation (21)):

$$\begin{aligned} f = 1 &+ \frac{K_1}{4b_1^4} e^{2R_1} + \frac{K_2}{4b_2^4} e^{2R_2} + \frac{K_1 K_2 L_1^2 L_2^2}{16 b_1^4 b_2^4} e^{2R_1+2R_2} \\ &- \frac{e^{R_1} \cos I_1}{b_1^2} \left(\frac{L_1 L_2 K_2}{4b_2^4} e^{2R_2} + 1 \right) \\ &- \frac{e^{R_2} \cos I_2}{b_2^2} \left(\frac{L_1 L_2 K_1}{4b_1^4} e^{2R_1} + 1 \right) \\ &+ \frac{e^{R_1+R_2}}{2b_1^2 b_2^2} \left(L_1 \cos (I_1 + I_2) + L_2 \cos (I_1 - I_2) \right), \end{aligned} \tag{23}$$

where

$$L_1 = \frac{\cosh(\delta_1 - \delta_2) - \cosh(\alpha_1 - \alpha_2)}{\cosh(\delta_1 - \delta_2) - \cosh(\alpha_1 + \alpha_2)},$$

$$L_2 = \frac{\cosh(\delta_1 + \delta_2) - \cosh(\alpha_1 - \alpha_2)}{\cosh(\delta_1 + \delta_2) - \cosh(\alpha_1 + \alpha_2)},$$

$$K_1 = \frac{\cosh 2\delta_1 - 1}{\cosh 2\delta_1 - \cosh 2\alpha_1},$$

$$K_2 = \frac{\cosh 2\delta_2 - 1}{\cosh 2\delta_2 - \cosh 2\alpha_2},$$

$$u_{pj} = 2b_j^2 K_j \frac{1 - \left(1/\sqrt{K_j}\right) \cosh R_j \cos I_j}{\left(\sqrt{K_j} \cosh R_j - \cos I_j\right)^2} \quad (j = 1, 2). \tag{24}$$

Assuming that $\alpha_1 > 0$, $\alpha_2 > 0$, and $\alpha_1/\sinh \alpha_1 \cosh \delta_1 > \alpha_2/\sinh \alpha_2 \cosh \delta_2$, we show that the interaction of two breathers is elastic and obtain the phase shift between two breathers after the interaction:

(1) Before interaction $(n \longrightarrow -\infty)$

Breather 1 (R_1 is finite, and $R_2 \longrightarrow -\infty$):

$$f_1(R_1, I_1) = 1 + \frac{K_1}{4b_1^4} e^{2R_1} - \frac{1}{b_1^2} e^{R_1} \cos I_1. \tag{25}$$

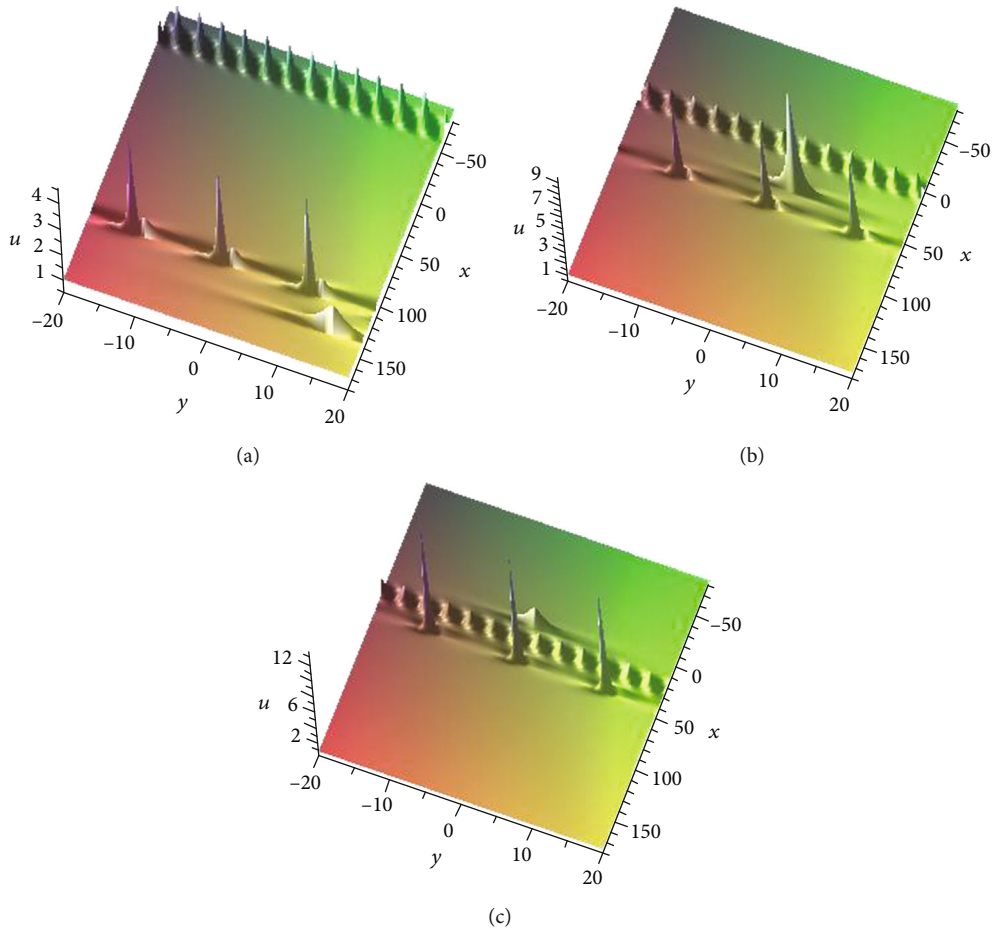

Figure 8: Propagation of hybrid solution composed of two breathers and a lump at different times: (a) $n = -180$, (b) $n = -50$, and (c) $n = -10$.

Breather 2 ($R_1 \longrightarrow -\infty$, and R_2 is finite):

$$f_2(R_2, I_2) = \frac{K_1}{4b_1^4} e^{2R_1} \left(1 + \frac{K_2 L_1^2 L_2^2}{4b_2^4} e^{2R_2} - \frac{L_1 L_2 \cos I_2}{b_2^2} e^{R_2}\right). \tag{26}$$

(2) After interaction ($n \longrightarrow \infty$)

Breather 1 (R_1 is finite, and $R_2 \longrightarrow \infty$):

$$f_1(R_2, I_1) = \frac{K_2}{4b_2^4} e^{2R_2} \left(1 + \frac{K_1 L_1^2 L_2^2}{4b_2^4} e^{2R_1} - \frac{L_1 L_2 \cos I_1}{b_2^2} e^{R_1}\right). \tag{27}$$

Breather 2 ($R_1 \longrightarrow \infty$, and R_2 is finite):

$$f_2(R_2, I_2) = 1 + \frac{K_2}{4b_2^4} e^{2R_2} - \frac{1}{b_2^2} e^{R_2} \cos I_2. \tag{28}$$

Taking into account $u_j(n) = (f_j(n+1) f_j(n-1))/f_j(n)^2$ ($j = 1, 2$), we find that the two separated breathers before and after the interaction are of the form

$$\begin{aligned} &[u_1(R_1, I_1), u_2(R_2 + \ln|L_1 L_2|, I_2)] \\ &\quad \longrightarrow [u_1(R_1 + \ln|L_1 L_2|, I_1), u_2(R_2, I_2)], \qquad L_1 L_2 > 0, \\ &\longrightarrow [u_1(R_1 + \ln|L_1 L_2|, I_1 + \pi), u_2(R_2, I_2 - \pi)], \quad L_1 L_2 < 0. \end{aligned} \tag{29}$$

From the above expression, we conclude that whether $L_1 L_2 > 0$ or $L_1 L_2 < 0$, the interaction of two breathers in 2-breather (23) is elastic. The interaction of 2-breather solution (23) for $L_1 L_2 > 0$ is depicted in Figure 2 by taking $\alpha_1 = 0.2$, $\alpha_2 = 0.15$, $\beta_1 = 0$, $\beta_2 = 0$, $\gamma_1 = 0$, $\gamma_2 = 0$, $\delta_1 = 0.75$, $\delta_2 = 1.5$, $\sigma_1 = 0$, $\sigma_2 = 0$, $\theta_1 = 0$, and $\theta_2 = 0$. The sequence of snapshots of Figure 2 shows the interaction between two y-periodic breathers under the case $\beta_1 = \gamma_1 = 0$ or $\beta_2 = \gamma_2 = 0$, while the two y-periodic breathers propagate in the negative direction of the x-coordinate. The humps of the second breather pass through between the humps of the first breather as shown in Figure 2(b). After that, they begin to separate and recover the initial shapes and velocities in Figure 2(c).

Now, we construct a hybrid solution composed of two line solitons and one breather. By taking $N = 4$, $k_3 = k_4^*$, $l_3 = l_4^*$, and $\beta_3^0 = \beta_4^{0*}$ in N-soliton (20), we obtain the hybrid

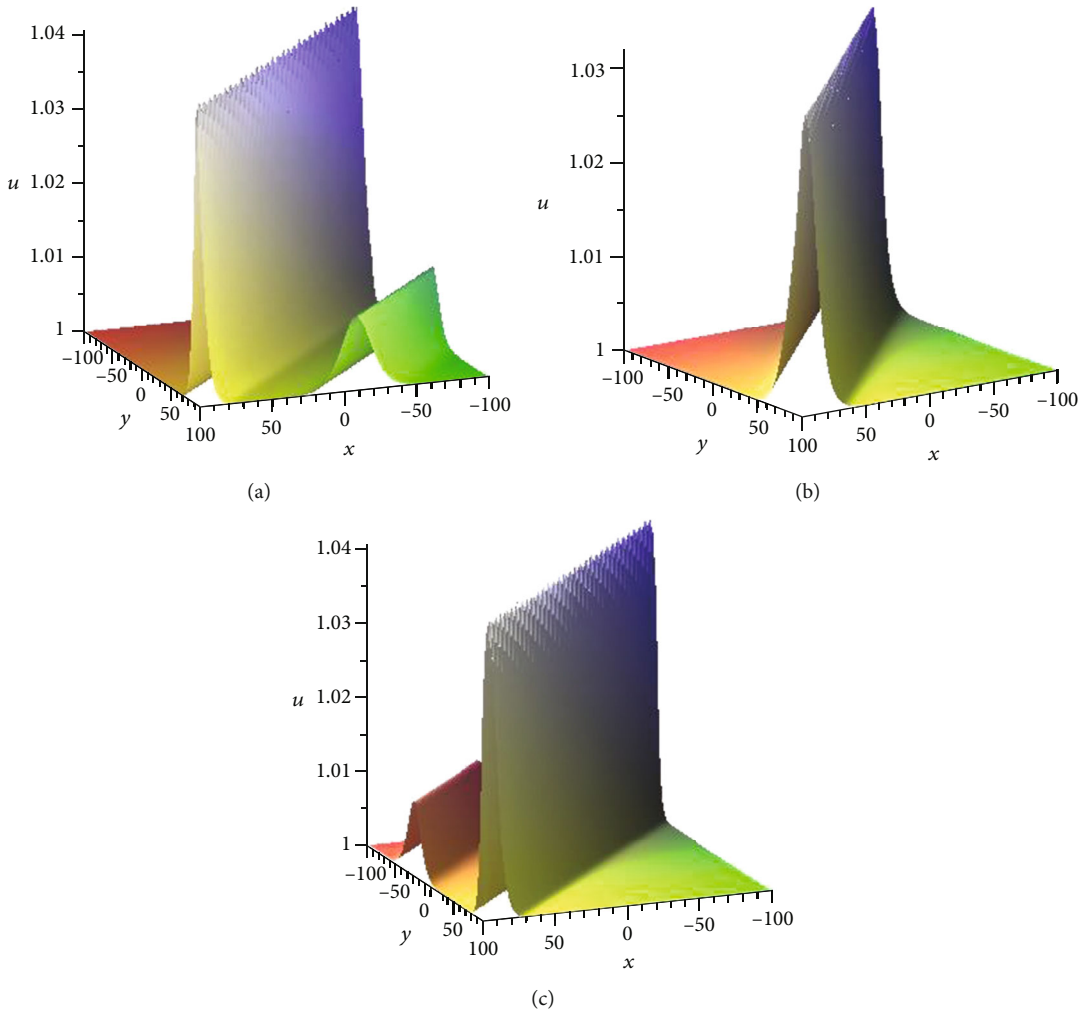

FIGURE 9: (a) Soliton molecule in $\beta_1^0 = 15$ and $\beta_2^0 = 0$. (b) Asymmetric soliton in $\beta_1^0 = 0$ and $\beta_2^0 = 0$. (c) Soliton molecule in $\beta_1^0 = -15$ and $\beta_2^0 = 0$.

solution of two line solitons and one breather which is shown in Figure 3 with $k_1 = 0.2, k_2 = 0.3, k_3 = k_4^* = 0.2 + 0.2i, l_1 = 0.5$, $l_2 = -0.5$, $l_3 = l_4^* = 4.5 + 0.4i$, $\beta_1^0 = -5$, $\beta_2^0 = 15$, $\beta_3^0 = 0$, and $\beta_4^0 = 0$. In addition, we find that two line solitons propagate along the negative direction of the x-coordinate; then, the 1-breather propagates along the positive direction of the x-coordinate. In Figure 3(a) at $n = -40$, two line solitons are in front of the 1-breather. Then, the 1-breather overtakes and collides with two line solitons in Figure 3(b) at $n = 0$. After that, they become farther and farther without changing their shapes and directions of movement in Figure 3(c) at $n = 40$.

3. Degeneration of Breathers

In this section, we derive lump solutions for the $(2+1)$-dimensional elliptic Toda equation (3) by taking the limit of an infinitely large period of breathers derived in the previous section. We also construct the hybrid solution composed of two line solitons and one lump and the hybrid solution composed of one breather and one lump.

By taking the limits $\alpha_1 \longrightarrow 0$ and $\beta_1 \longrightarrow 0$ in the 1-breather (14), the period (15) of 1-breather tends to infinity. Under these limits, 1-breather (14) has degenerated into 1-lump which is given by

$$u_l^{[1]} = \frac{f_l^{[1]}(n+1) \cdot f_l^{[1]}(n-1)}{\left(f_l^{[1]}(n)\right)^2} = \frac{\left((1/(\cosh 2\delta_1 - 1)) + 4\omega^2 + \nu^2 + 4\right)^2 - 64\omega^2}{\left((1/(\cosh 2\delta_1 - 1)) + 4\omega^2 + \nu^2\right)^2}, \tag{30}$$

where $f_l^{[1]}(n) = (1/(\cosh 2\delta_1 - 1)) + 4\omega^2 + 4\nu^2$, $\omega = \cosh \delta_1 (\cos \gamma_1 x + \sin \gamma_1 y) + n$, and $\nu = \sinh \delta_1 (\sin \gamma_1 x - \cos \gamma_1 y)$.

Figures 4(a)–4(c) show the degeneration process of 1-breather (14) along the line $l_1 : 2(\widehat{a}_1 x + \widehat{b}_1 y + \alpha_1 n) + \sigma_1 + \varepsilon = 0$ at $n = 0$. Figure 4 shows the density pictures of the degeneration process of 1-breather (14) by taking the parameters $\gamma = 0.1$, $\delta = 0.7$, $a = 1$, $b = 1$, $\sigma = \theta = 0$, and $n = 0$. The degeneration of the 1-breather given in Figure 4(c) is very similar to that of the 1-lump (30) depicted in Figure 4(d) with the parameter selection of $\gamma = 0.1$, $\delta = 0.7$, and $n = 0$, and thus, the former is a good approximation of the latter.

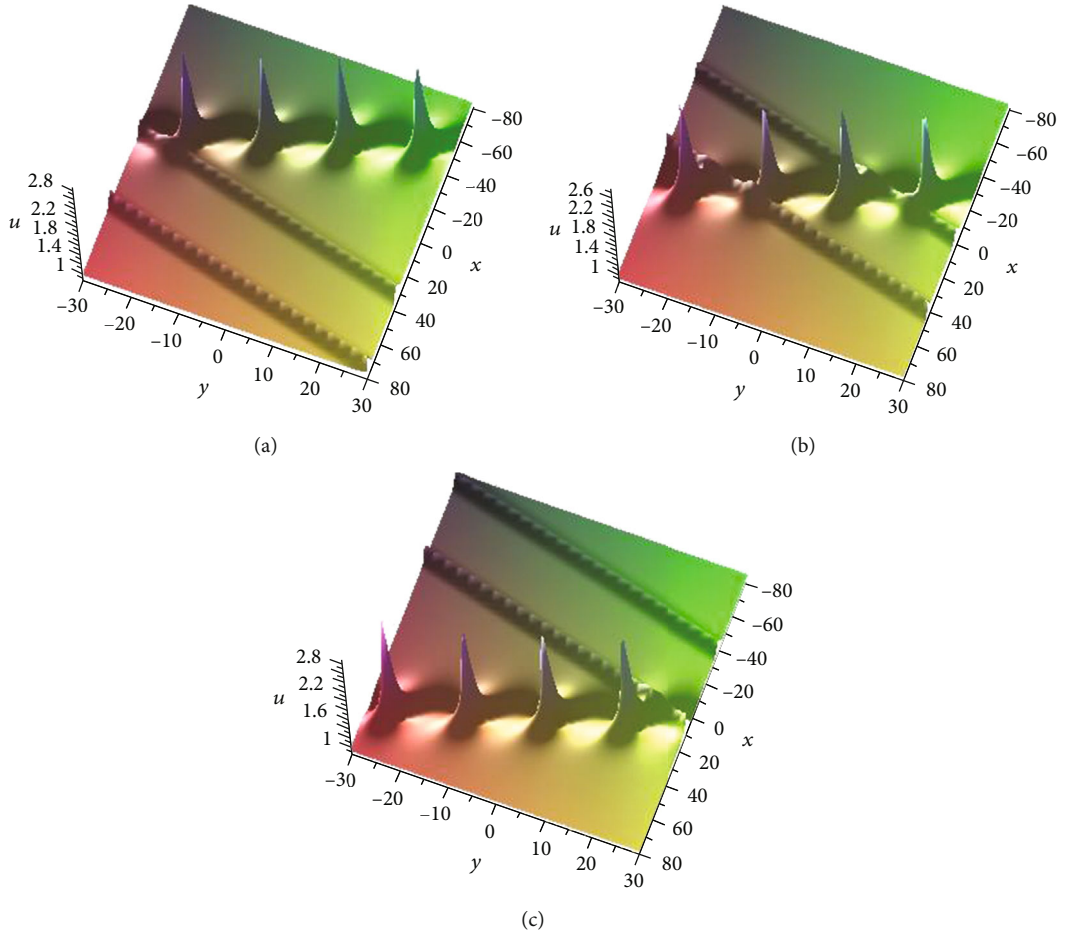

Figure 10: Propagation of hybrid solution composed of a soliton molecule and a breather at different times: (a) $n = -30$, (b) $n = 0$, and (c) $n = 30$.

Similarly, if we let $\alpha_1, \alpha_2 \longrightarrow 0$ and $\beta_1, \beta_2 \longrightarrow 0$ in 2-breather (21), we obtain the following 2-lump solution for (3):

$$f = \left(\omega_1^2 + \nu_1^2\right)\left(\omega_2^2 + \nu_2^2\right) + \frac{\omega_2^2 + \nu_2^2}{2\cosh\delta_1 - 2} + \frac{\omega_1^2 + \nu_1^2}{2\cosh\delta_2 - 2} + \frac{1 + 2H}{2Q_1} + \frac{1 + 2h}{2Q_2} + \frac{1}{(2\cosh\delta_1 - 2)(2\cosh\delta_2 - 2)}, \tag{31}$$

where

$$\omega_j = \cosh\delta_j\left(\cos\gamma_j x + \sin\gamma_j y\right) + n,$$

$$\nu_j = \sinh\delta_j\left(\sin\gamma_j x - \cos\gamma_j y\right) \quad (j = 1, 2),$$

$$Q_1 = \cos 2(\gamma_1 - \gamma_2) + \cosh 2(\delta_1 - \delta_2) - 4\cos(\gamma_1 - \gamma_2)\cosh(\delta_1 - \delta_2) + 2,$$

$$Q_2 = \cos 2(\gamma_1 - \gamma_2) + \cosh 2(\delta_1 + \delta_2) - 4\cos(\gamma_1 - \gamma_2)\cosh(\delta_1 + \delta_2) + 2,$$

$$\begin{aligned} h = {} & 2((x\cos\gamma_1 + y\sin\gamma_1)(x\cos\gamma_2 + y\sin\gamma_2)\cosh\delta_2 \\ & + (x\cos\gamma_2 + y\sin\gamma_2)n\cosh\delta_2 \\ & - \sinh\delta_1\sinh\delta_2 y(x\sin\gamma_2 - y\cos\gamma_2)\cos\gamma_1 \\ & + \sin\gamma_1\sin\gamma_2\sinh\delta_1\sinh\delta_2 x^2 \\ & - \sin\gamma_1\cos\gamma_2\sinh\delta_1\sinh\delta_2 xy + n^2)\cosh(\delta_1 + \delta_2) \\ & \cdot \cos(\gamma_1 - \gamma_1) - 2\sinh(\delta_1 + \delta_2)(-x\sinh\delta_2\sin\gamma_1 \\ & - y\cos\gamma_2)(x\cos\gamma_1 + y\sin\gamma_1)\cosh\delta_2 \\ & + n(x\sin\gamma_1\sinh\delta_1 - y(\sinh\delta_1\cos\gamma_1 - \sinh\delta_2\cos\gamma_2) \\ & - \sin\gamma_2\sinh\delta_2))\sin(\gamma_1 - \gamma_2) - 2(y\sin\gamma_1 + x\cos\gamma_1) \\ & \cdot ((y\sin\gamma_2 + x\cos\gamma_2)\cosh\delta_2 + n)\cosh\delta_1 \\ & - 2n(x\cos\gamma_2 + y\sin\gamma_2)\cosh\delta_2 \\ & + 2y\sinh\delta_1\sinh\delta_2(x\sin\gamma_2 - y\cos\gamma_2)\cos\gamma_1 \\ & - 2\sin\gamma_1\sin\gamma_2\sinh\delta_1\sinh\delta_2 x^2 \\ & + 2\sin\gamma_1\cos\gamma_2\sinh\delta_1\sinh\delta_2 xy - 2n^2, \end{aligned}$$

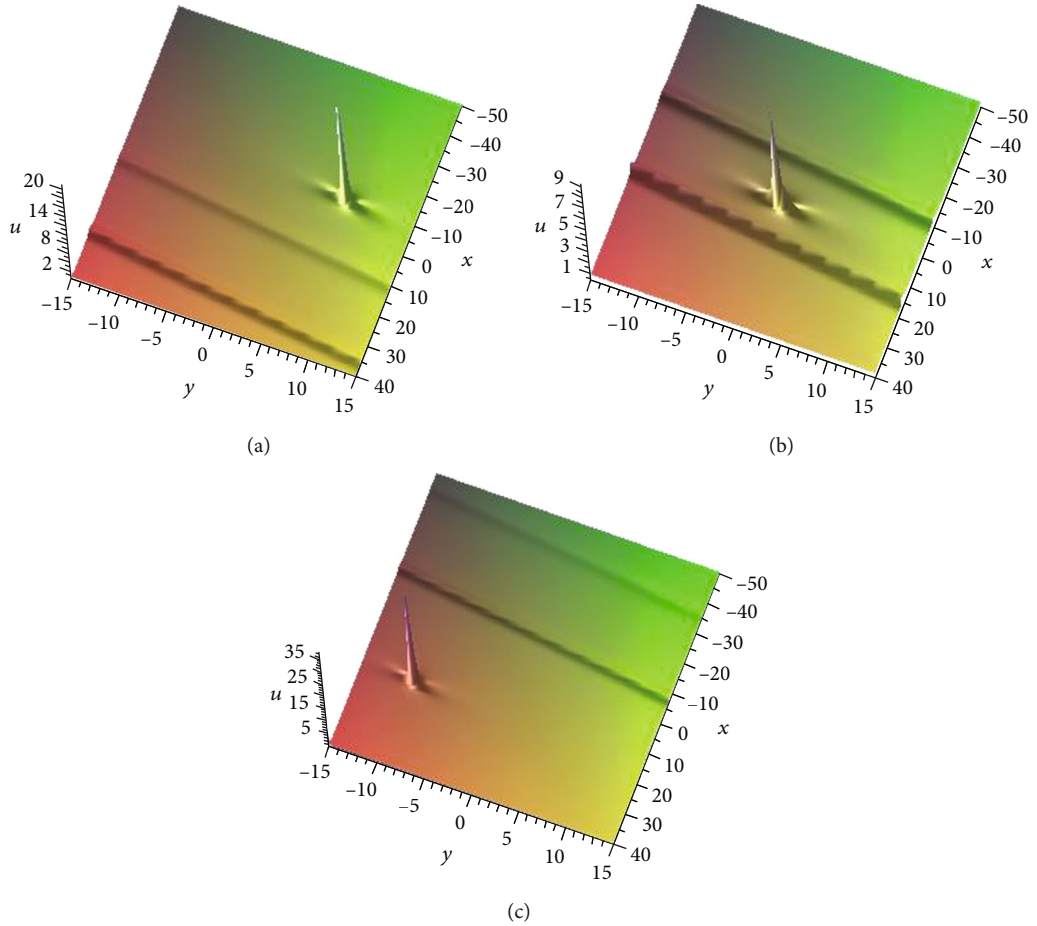

Figure 11: Propagation of hybrid solution composed of a soliton molecule and a lump at different times: (a) $n = -20$, (b) $n = 0$, and (c) $n = 25$.

$$
\begin{aligned}
H = {} & 2\cos(\gamma_1 - \gamma_2)((x\cos\gamma_1 + y\sin\gamma_1)((x\cos\gamma_2 \\
& + y\sin\gamma_2)\cosh\delta_2 + n)\cosh\delta_1 + n(x\cos\gamma_2 \\
& + y\sin\gamma_2)\cosh\delta_2 + y\sinh\delta_1\sinh\delta_2(x\sin\gamma_2 \\
& + y\cos\gamma_2)\cos\gamma_1 - \sin\gamma_1\sin\gamma_2\sinh\delta_1\sinh\delta_2 x^2 \\
& + \sin\gamma_1\cos\gamma_1\sinh\delta_1\sinh\delta_2 xy + n^2)\cosh(\delta_1 - \delta_2) \\
& - 2(\sinh\delta_2(x\cos\gamma_2 - y\sin\gamma_2)(x\cos\gamma_1 + y\sin\gamma_1) \\
& \cdot \cosh\delta_1 + \sinh\delta_1(x\cos\gamma_2 + y\sin\gamma_2)(x\sin\gamma_1 \\
& - y\cos\gamma_1)\cosh\delta_2 + n(x(\sin\gamma_1\sinh\delta_1) \\
& + \sin\gamma_2\sinh\delta_2 - y(\sinh\delta_1\cos\gamma_1 + \sinh\delta_2\cos\gamma_2) \\
& + \sin\gamma_2\sinh\delta_2)\sin(\gamma_1 - \gamma_2)\sinh(\delta_1 - \delta_2) \\
& - 2(x\cos\gamma_1 + y\sin\gamma_1)(x\cos\gamma_2\cosh\delta_2 + y\sin\gamma_2 + n) \\
& - 2n(x\cos\gamma_2 + y\sin\gamma_2)\cosh\delta_2 \\
& - 2y\sinh\delta_1\sinh\delta_2(x\sin\gamma_2 + y\cos\gamma_2)\cos\gamma_1 \\
& + 2x^2\sin\gamma_1\sin\gamma_2\sinh\delta_1\sinh\delta_2 \\
& - 2xy\sin\gamma_1\cos\gamma_2\sinh\delta_1\sinh\delta_2 - 2n^2.
\end{aligned}
\tag{32}
$$

Here, we take the parameters $\beta_1 = \beta_2 = 0$, $\gamma_1 = \gamma_2 = 0$, $\delta_1 = 1.7/\sqrt{3}$, $\delta_2 = 1.6/\sqrt{3}$, $\theta_1 = 0$, $\theta_2 = \pi$, and $n = 0$ in y-periodic 2-breather (23) and show the degeneration process of the 2-breather in Figures 5(a)–5(c). The degeneration of the 2-breather given in Figure 5(c) is very similar to that of the 2-lump (31) depicted in Figure 5(d) with the parameter selection of $\gamma_1 = 0$, $\gamma_2 = 0$, $\delta_1 = 1.7/\sqrt{3}$, $\delta_2 = 1.6/\sqrt{3}$, and $n = 0$, and thus, the former is a good approximation of the latter. Therefore, we find that an M-lump can be degenerated from an M-breather in the same way.

By taking $\alpha_i \longrightarrow 0$ and $\beta_i \longrightarrow 0 (i = 1, 2)$ in the 4-soliton solution ($N = 4$ for (20)), we derive the hybrid solution composed of two line solitons and one lump:

$$
\begin{aligned}
f = {} & \left(\frac{B_{12}}{2} + \theta_1\theta_2\right)(1 + e^{\eta_3} + e^{\eta_4} + A_{34}e^{\eta_3+\eta_4}) \\
& + (M_{33} + N_{23}\theta_1 + N_{13}\theta_2)e^{\eta_3} \\
& + (M_{44} + N_{24}\theta_1 + N_{14}\theta_2)e^{\eta_4} \\
& + (G_{34} + N_{234}\theta_1 + N_{134}\theta_2)A_{34}e^{\eta_3+\eta_4},
\end{aligned}
\tag{33}
$$

where $B_{12} = 1/(\cos(l_1 - l_2) - 1)$, $B_{13} = 1/(\cos(l_1 - l_3) - \cosh(k_3))$, $B_{14} = 1/(\cos(l_1 - l_4) - \cosh(k_4))$, $B_{23} = 1/(\cos(l_2 - l_3) - \cosh(k_3))$, $B_{24} = 1/(\cos(l_2 - l_4) - \cosh(k_4))$, $\theta_m = \sin(l_m)x + \cos(l_m)y + n$, $M_{ij} = \sinh(k_i)\sinh(k_j)B_{1i}B_{2j}$, $N_{mi} = \sinh(k_i)B_{mi}$, $N_{mij} = \sinh(k_i)B_{mi} + \sinh(k_j)B_{mj}$, and $G_{34} =$

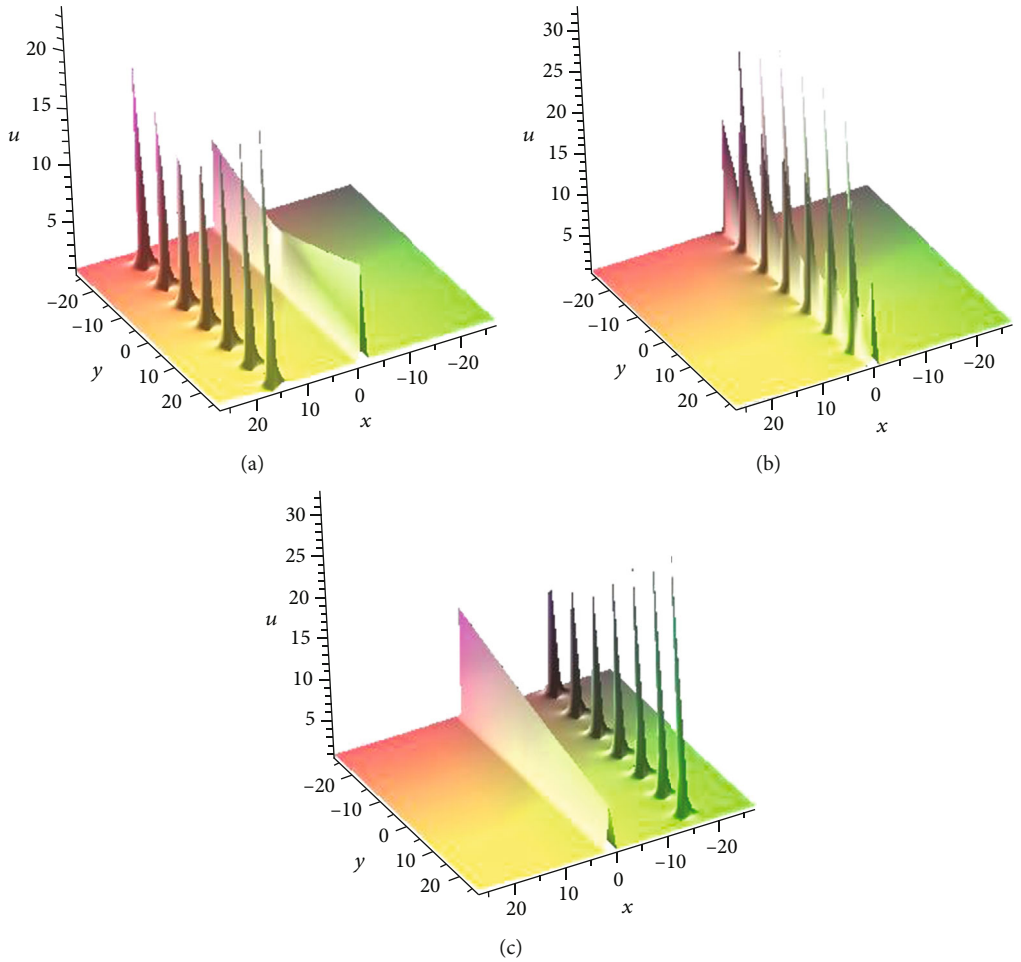

FIGURE 12: (a) Breather-soliton molecule in $\beta_1^0 = -10$, $\beta_2^0 = -10$, and $\beta_3^0 = 10$. (b) Breather-soliton molecule in $\beta_1^0 = 0$, $\beta_2^0 = 0$, and $\beta_3^0 = 10$. (c) Breather-soliton molecule in $\beta_1^0 = 10$, $\beta_2^0 = 10$, and $\beta_3^0 = -10$.

$M_{33} + M_{34} + M_{43} + M_{44}(i, j = 3, 4, m = 1, 2)$. As shown in Figure 6, a 4-soliton solution exhibits the interaction between two line solitons and one lump under the longwave limits with the parameter selection of $l_1 = l_2^* = 3.5 + i$, $k_3 = 0.5$, $k_4 = 0.8$, $l_3 = 0.5$, $l_4 = 0.75$, and $\beta_3 = \beta_4 = 0$ in (33). At first, they move toward each other at $n = -10$ in Figure 6(a); then, the lump is collided and swallowed by two line solitons at $n = 0$ in Figure 6(b). After that, they keep moving forward without changing their shapes and directions of movement.

The hybrid solution of one breather and one lump was constructed by equation (33) with the conjugation of two solitons by taking $k_3 = k_4^*$, $l_3 = l_4^*$, and $\beta_3^0 = \beta_4^{0*}$. Figure 7 depicts the hybrid solution of one breather and one lump from equation (33) with the parameter selection of $l_1 = l_2^* = 1.5 + 0.85i$, $l_3 = l_4^* = 0.8 + 0.5i$, $k_3 = k_4^* = 0.2 + 0.2i$, and $\beta_3^0 = \beta_4^{0*} = 0$. In Figure 7, we find that both the breather and the lump propagate along the negative direction of the x-coordinate. They start to interact and become in a line at $n = 0$ in Figure 7(b). Then, they form a separate state and keep initial directions of movement and shapes at $n = 20$ in Figure 7(c).

In the same way of obtaining equation (33), we construct the hybrid solution composed of three line solitons and one lump:

$$
\begin{aligned}
f = {} & \left(\frac{B_{12}}{2} + \theta_1\theta_2\right)\left(\sum_{\mu=0,1} \exp\left(\sum_{3\le j<m\le 5} A_{jm}\mu_j\mu_m + \sum_{j=3}^{5}\mu_j\eta_j\right)\right) \\
& + \sum_{3\le j\le 5}\left(M_{jj} + N_{2j}\theta_1 + N_{1j}\theta_2\right)e^{\eta_j} + \sum_{3\le i<j\le 5}\left(G_{ij} + N_{2ij}\theta_1 + N_{1ij}\theta_2\right)A_{ij}e^{\eta_i+\eta_j} \\
& + \left(G_{345} + N_{2345}\theta_1 + N_{1345}\theta_2\right)\prod_{3\le i<j\le 5} A_{ij}e^{\eta_3+\eta_4+\eta_5},
\end{aligned}
\tag{34}
$$

and we also construct the hybrid solution of four line solitons and one lump:

$$
\begin{aligned}
f = {} & \left(\frac{B_{12}}{2} + \theta_1\theta_2\right)\left(\sum_{\mu=0,1} \exp\left(\sum_{3\le j<m\le 6} A_{jm}\mu_j\mu_m + \sum_{j=3}^{6}\mu_j\eta_j\right)\right) \\
& + \sum_{j=3}^{6}\left(M_{jj} + N_{2j}\theta_1 + N_{1j}\theta_2\right)e^{\eta_j} + \sum_{3\le i<j\le 6}\left(G_{ij} + N_{2ij}\theta_1 + N_{1ij}\theta_2\right)A_{ij}e^{\eta_i+\eta_j} \\
& + \sum_{3\le i<j<l\le 6}\left(G_{ijl} + N_{2ijl}\theta_1 + N_{1ijl}\theta_2\right)A_{ij}A_{il}A_{jl}e^{\eta_i+\eta_j+\eta_l} \\
& + \left(G_{3456} + N_{23456}\theta_1 + N_{13456}\theta_2\right)\prod_{3\le i<j\le 6} A_{ij}e^{\eta_3+\eta_4+\eta_5+\eta_6},
\end{aligned}
\tag{35}
$$

where

$$\theta_m = \sin(l_m)x + \cos(l_m)y + n,$$
$$M_{ij} = \sinh(k_i)\sinh(k_j)B_{1i}B_{2j},$$
$$G_{ij} = \sum_{\cdot=i,j}\sum_{\cdot=i,j} M_{\cdot\cdot},$$
$$N_{mi} = \sinh(k_i)B_{mi},$$
$$N_{mij} = N_{mi} + N_{mj},$$
$$G_{ijl} = \sum_{\cdot=i,j,l}\sum_{\cdot=i,j,l} M_{\cdot\cdot},$$
$$N_{m3456} = \sum_{3\le i\le 6} N_{mi},$$
$$N_{mijl} = N_{mi} + N_{mj} + N_{ml},$$
$$G_{3456} = \sum_{\cdot=3,4,5,6}\sum_{\cdot=3,4,5,6} M_{\cdot\cdot} \quad (i,j,l = 3,4,5,6,\ m = 1,2),$$
$$B_{sn} = \frac{1}{\cos(l_s - l_n) - \cosh(k_s + k_n)} \quad (s,n = 1,2,3,4,5,6,\ k_1 = k_2 = 0). \tag{36}$$

Figure 8 describes the interaction between two breathers and one lump in (35) by taking the parameters $k_3 = k_4^* = 0.828 + 0.2i$, $k_5 = k_6^* = 0.134 + 5i$, $l_1 = l_2^* = 0.1 + 0.7i$, $l_3 = l_4^* = 1 + 0.750i$, $l_5 = l_6^* = 8 + 0.275i$, $\beta_3^0 = -15$, $\beta_4^0 = -15$, $\beta_5^0 = 15$, and $\beta_6^0 = 15$. It can be observed in Figure 8 that the two breathers move in opposite directions on the x-coordinate and the lump propagates in the negative direction of the x-coordinate; then, the direction of two breathers becomes smaller. Figure 8(a) depicts the lump gradually approaching the two breathers at $n = -180$; then, they collide at $n = -50$ in Figure 8(b), and Figure 8(c) shows their separation with initial structures at $n = -10$.

4. Soliton Molecules and Breather Molecules

In this section, we investigate the soliton molecules, the breather-soliton molecules, the breather molecules, the interaction between soliton/breather-soliton molecules and lumps, and the interaction between soliton molecules and breathers for the $(2+1)$-dimensional elliptic Toda equation (3) via the velocity resonant method and degeneration of breathers.

Case 1. Soliton molecule. The soliton molecule is constructed by imposing the velocity resonance condition on a 2-soliton solution ($N = 2$ in (20)). The velocity resonance condition for 2-soliton is

$$\frac{r_1}{p_1} = \frac{r_2}{p_2}, \qquad \frac{r_1}{q_1} = \frac{r_2}{q_2}, \tag{37}$$

where $p_i = 2\sinh k_i \cos l_i$, $q_i = 2\sinh k_i \sin l_i$, and $r_i = 2k_i$ $(i = 1,2)$.

The 2-soliton solution ($N = 2$ in (20)) exhibits one soliton molecule shape under the velocity resonance (37) in Figure 9 with the parameter selection of $k_1 = 0.1$, $k_2 = 0.2$, $l_1 = \arcsin(k_1\sinh(k_2)) - \pi/4$, $l_2 = \arcsin(k_2\sinh(k_1)) - \pi/4$, and $n = 0$. It can be observed in Figures 9(a)–9(c) that the sizes of the soliton molecule depend on the parameters β_1^0 and β_2^0. In addition, the two line solitons in the soliton molecule are different because of $k_1 \neq k_2$ and $l_1 \neq l_2$, although the velocities of the two solitons are the same. Comparing Figures 9(a)–9(c), we can find that an asymmetric soliton can be obtained by changing the size decided by parameters β_1^0 and β_2^0 in the molecule. The height of the asymmetric soliton (see in Figure 9(b)) is between the heights of the two solitons, and the wave width of the asymmetric soliton is widened.

Now, we describe the interaction between a soliton molecule and a breather under the velocity resonance condition (37) and the conjugation of two solitons ($k_3 = k_4^*$, $l_3 = l_4^*$, and $\beta_3^0 = \beta_4^{0*}$) in 4-soliton ($N = 4$ in (20)). Figure 10 depicts the hybrid solution composed of a soliton molecule and a breather with $k_1 = 0.5$, $k_2 = 0.4$, $k_3 = k_4^* = 0.1 + 0.2i$, $l_1 = \arcsin(k_1\sinh(k_2)) - \pi/4$, $l_2 = \arcsin(k_2\sinh(k_1)) - \pi/4$, $l_3 = l_4^* = 4.5 + 0.4i$, $\beta_1^0 = -15$, $\beta_2^0 = 15$, and $\beta_3^0 = \beta_4^{0*} = 0$ in 4-soliton. As the breather is approaching the soliton molecule in Figure 10(a), we can see that the four humps of the breather collide with the soliton molecule in Figure 10(b); then, the breather and the soliton molecule still propagate in their original directions and keep their original shapes after they separated in Figure 10(c).

If two solitons satisfy the velocity resonance condition (37) in equation (33), we can get a hybrid solution composed of a soliton molecule and a lump in Figure 11 with $k_3 = 0.8$, $k_4 = 0.5$, $l_1 = l_2^* = 2.5 + i$, $l_3 = \arcsin(k_3\sinh(k_4)) - \pi/4$, $l_4 = \arcsin(k_4\sinh(k_3)) - \pi/4$, $\beta_3^0 = 15$, and $\beta_4^0 = 15$. At first, they move toward each other at $n = -20$ in Figure 11(a), and then, the lump collided with the soliton molecule at $n = 0$ in Figure 11(b). After that, they have not changed the directions of movement and shapes at $n = 25$ in Figure 11(c).

Case 2. Breather-soliton molecule. The breather-soliton molecule is constructed by imposing the velocity resonance condition on a 3-soliton solution ($N = 3$ in (20)). The velocity resonance condition for 3-soliton is

$$\frac{\mathrm{Re}(r_1)}{\mathrm{Re}(p_1)} = \frac{r_3}{p_3}, \qquad \frac{\mathrm{Re}(r_1)}{\mathrm{Re}(q_1)} = \frac{r_3}{q_3}, \tag{38}$$

where $p_i = 2\sinh k_i \cos l_i$, $q_i = 2\sinh k_i \sin l_i$, and $r_i = 2k_i$ $(i = 1,2,3)$. To derive the breather-soliton molecule in Figure 12, we need to take $N = 3$ in (20) and choose the parameters $k_1 = k_2^* = 0.1 + 0.25i$, $l_1 = l_2^* = 1.1 + i$, $k_3 = 2.117$, $l_3 = \mathrm{Re}(\sinh(k_1)\sin(1_1)/\mathrm{Re}(\sinh k_1)\cos(1_1)$, and $n = 0$. Similarly, it can be observed that the size of the breather-

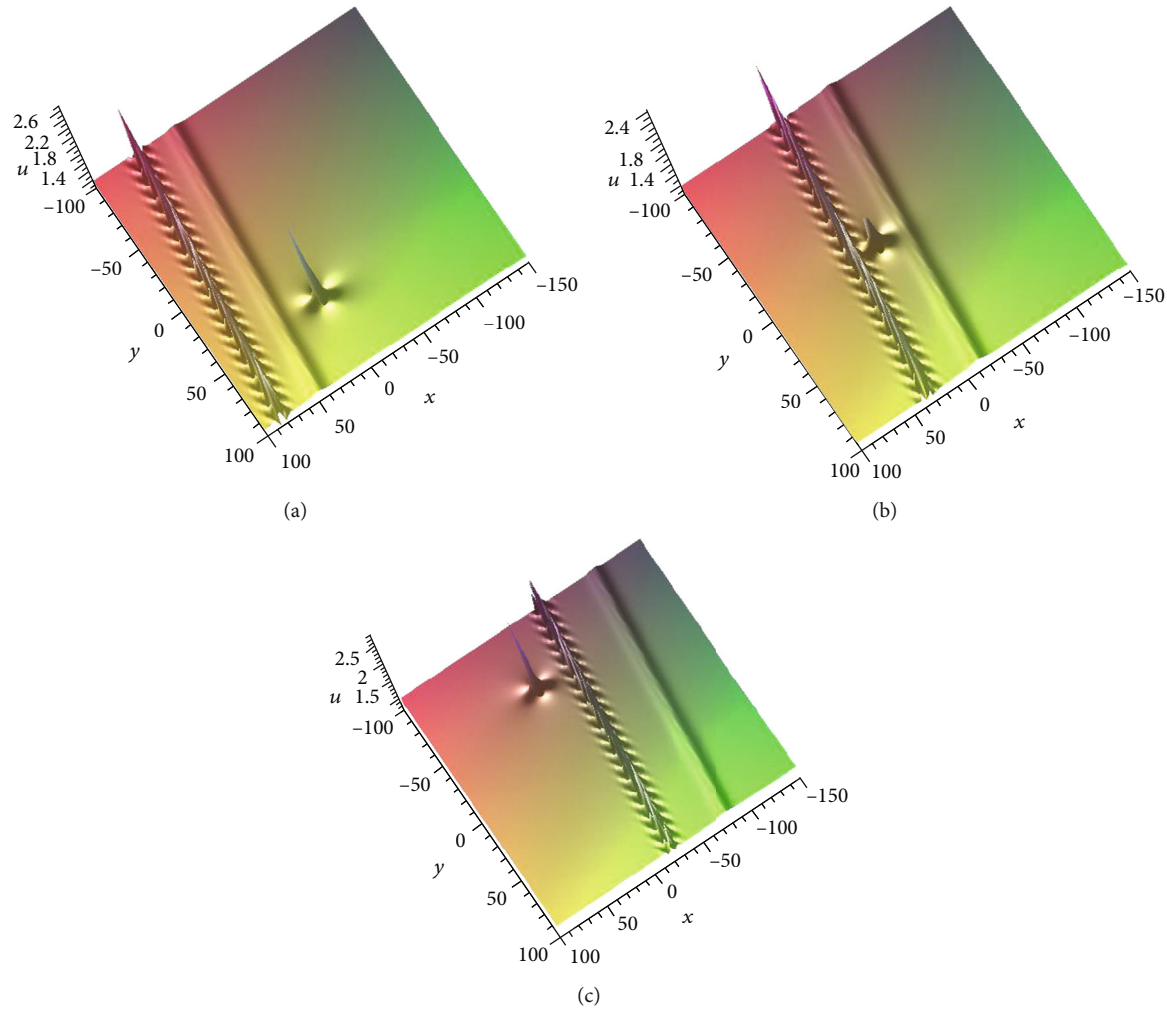

FIGURE 13: Propagation of hybrid solution composed of a breather-soliton molecule and a lump at different times: (a) $n = -60$, (b) $n = 0$, and (c) $n = 65$.

soliton molecule is controlled by the parameters β_1^0, β_2^0, and β_3^0. Figures 12(a) and 12(c) are breather-soliton molecules of different sizes, and Figure 12(b) can be regarded as a collision between a soliton and a breather.

The hybrid solution of a breather-soliton molecule and a lump can be constructed by the condition of velocity resonance (38) in equation (34). The interaction between a breather-soliton molecule and a lump can be obtained, which is depicted in Figure 13 with $k_3 = k_4^* = 0.2 + 0.4i$, $k_5 = 0.2$, $l_1 = l_2 = 1.5 + 0.7i$, $l_3 = l_4^* = 0.5 + 0.35i$, $l_5 = \mathrm{Re}(\sinh(k_3)\sin(1_3)/\mathrm{Re}(\sinh k_3)\cos(1_3)$, $\beta_3^0 = -10$, $\beta_4^0 = -10$, and $\beta_5^0 = 10$. As time n goes on, the breather-soliton molecule and the lump move closer both along the negative direction of the x-coordinate; then, they interact with each other at $n = 0$ in Figure 13(b). Finally, they move apart, keeping their shapes and directions of movement, but the size of the breather-soliton molecule becomes larger.

Case 3. Breather-breather molecule. The breather-breather molecule is constructed by imposing the velocity resonance condition on a 4-soliton solution ($N = 4$ in (20)). The velocity resonance condition for 4-soliton is

$$\frac{\mathrm{Re}(k_1)}{\mathrm{Re}(\sinh k_1 \cos l_1)} = \frac{\mathrm{Re}(k_3)}{\mathrm{Re}(\sinh k_3 \cos l_3)},$$
$$\frac{\mathrm{Re}(k_1)}{\mathrm{Re}(\sinh k_1 \sin l_1)} = \frac{\mathrm{Re}(k_3)}{\mathrm{Re}(\sinh k_3 \sin l_3)}, \tag{39}$$

where $p_i = 2\sinh k_i \cos l_i$, $q_i = 2\sinh k_i \sin l_i$, and $r_i = 2k_i$ $(i = 1, 2, 3, 4)$. Figure 14 illustrates a breather-breather molecule with the parameter selection of $k_1 = k_2^* = -0.0326551718 + 0.2i$, $k_3 = k_4^* = 0.1340192245 + 5i$, $l_1 = l_2^* = 1.8 + 0.848416875i$, $l_3 = l_4^* = 8 + 0.2746749837i$, and $n = 0$ in a 4-soliton solution. Similarly, Figures 14(a)–14(c), respectively, show the breather-breather molecules with different sizes depending on β_1^0, β_2^0, β_3^0, and β_4^0. In Figure 14(b), two breathers of the breather-breather molecule become in line and also can be regarded as a collision between a breather and a breather.

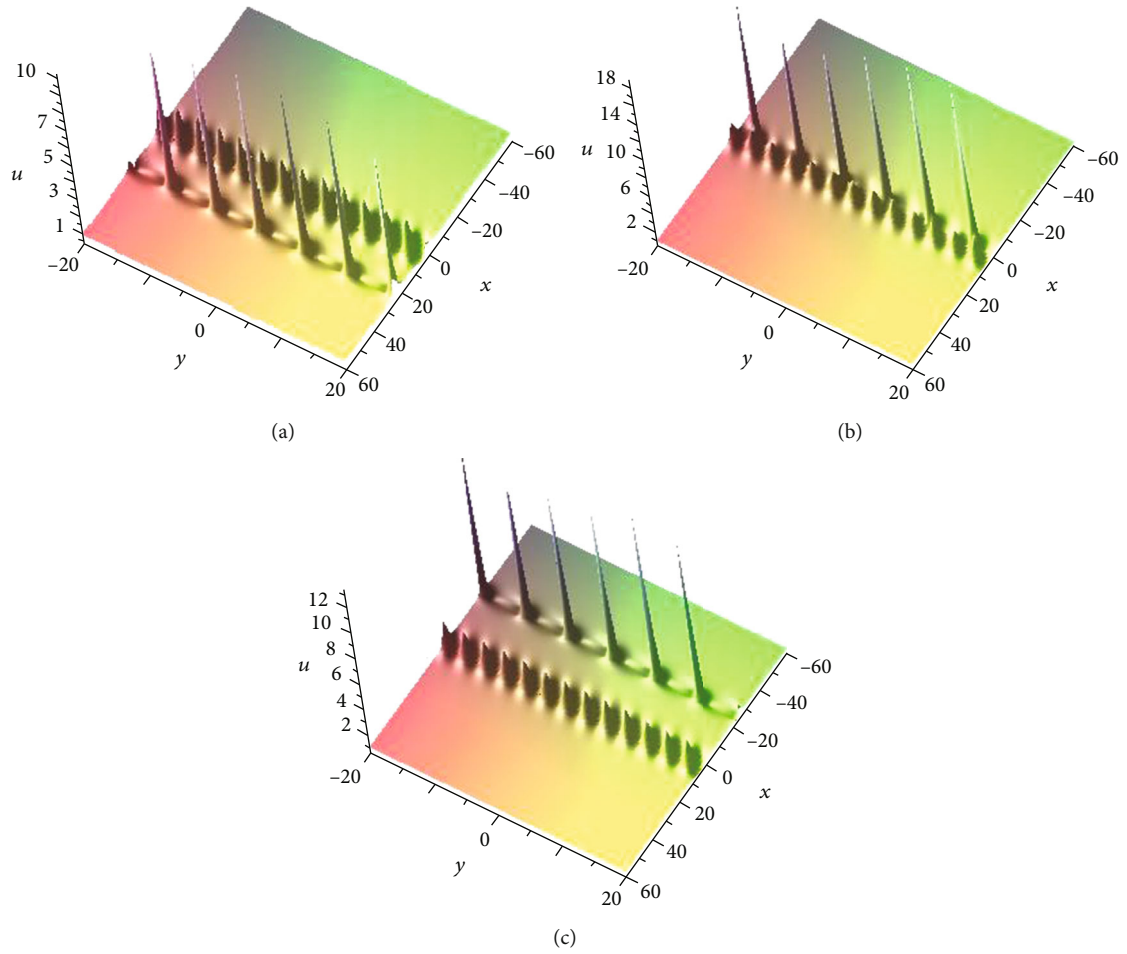

FIGURE 14: (a) Breather-breather molecule in $\beta_1^0 = -15$, $\beta_2^0 = -15$, $\beta_3^0 = 0$, and $\beta_4^0 = 0$. (b) Breather-breather molecule in $\beta_1^0 = 0$, $\beta_2^0 = 0$, $\beta_3^0 = 0$, and $\beta_4^0 = 0$. (c) Breather-breather molecule in $\beta_1^0 = 15$, $\beta_2^0 = 15$, $\beta_3^0 = 0$, and $\beta_4^0 = 0$.

5. Conclusion and Discussion

In this paper, we have considered a variety of solutions for the $(2+1)$-dimensional elliptic Toda equation. This equation is investigated to search for M-breather, lumps, possible molecules constructed by solitons and breathers, and hybrid solutions of them. It is interesting to find that the $(2+1)$ -dimensional elliptic Toda equation possesses the line soliton molecules, but its continuous version KP1 does not exhibit soliton molecule structures. This shows that the discrete nonlinear wave equations have more diverse molecule structures than their continuous counterparts. We expect that the method of bilinear Bäcklund transformation and nonlinear superposition formulae can be applied to more continuous and discrete nonlinear wave equations to investigate various nonlinear wave phenomena.

Data Availability

The data used to support the findings of this study are included within the article.

Conflicts of Interest

The authors declare that they have no conflicts of interest.

Acknowledgments

We would like to express our sincere thanks to Prof. Xing-Biao Hu for stimulating discussions and helpful comments. This work was supported by the National Natural Science Foundation of China (Grant Nos. 12061051 and 11965014).

References

[1] M. Toda, "Vibration of a chain with nonlinear interaction," *Journal of the Physical Society of Japan*, vol. 22, no. 2, pp. 431–436, 1967.

[2] R. Hirota and K. Suzuki, "Studies on lattice solitons by using electrical networks," *Journal of the Physical Society of Japan*, vol. 28, no. 5, pp. 1366-1367, 1970.

[3] S. Akio, H. Masamitsu, and U. Yoshihisa, "Pressure pulse wave for blood flow in the aorta from the viewpoint of the nonlinear Toda lattice," *Physics Letters A*, vol. 221, pp. 395–399.

[4] A. N. Leznov and M. V. Saveliev, "Spherically symmetric equations in gauge theories for an arbitrary semisimple compact Lie group," *Physics Letters B*, vol. 79, no. 3, pp. 294–296, 1978.

[5] G. Darboux, *Leçons sur la théorie générale des surfaces*, Gauthiers-Villars, Paris, France, 1887.

[6] A. V. Mikhailov, "Intergrability of a two-dimensional generalization of the Toda chain," *JETP Letters*, vol. 30, pp. 414–418, 1979.

[7] A. V. Mikhailov, "The reduction problem and the inverse scattering method," *Physica D*, vol. 3, no. 1-2, pp. 73–117, 1981.

[8] A. V. Leznov and M. V. Saveliev, "Representation of zero curvature for the system of nonlinear partial differential equations $x_{\alpha,z\bar{z}} = \exp(kx)_\alpha$ and its integrability," *Letters in Mathematical Physics*, vol. 3, pp. 489–494, 1979.

[9] E. J. Martinec, "On the origin of integrability in matrix models," *Communications in Mathematical Physics*, vol. 138, no. 3, pp. 437–449, 1991.

[10] A. Gerasimov, A. Marshakov, A. Mironov, A. Morozov, and A. Orlov, "Matrix models of two-dimensional gravity and Toda theory," *Nuclear Physics B*, vol. 357, no. 2-3, pp. 565–618, 1991.

[11] T. Eguchi and H. Kanno, "Toda lattice hierarchy and the topological description of the _c_ = 1 string theory," *Physics Letters B*, vol. 331, no. 3-4, pp. 330–334, 1994.

[12] K. Takasaki, "Toda lattice hierarchy and generalized string equations," *Communications in Mathematical Physics*, vol. 181, no. 1, pp. 131–156, 1996.

[13] A. V. Razumov and M. V. Saveliev, "Differential geometry of Toda systems," *Communications in Analysis and Geometry*, vol. 2, no. 3, pp. 461–511, 1994.

[14] M. Adler and P. van Moerbeke, "Matrix integrals, Toda symmetries, Virasoro constraints and orthogonal polynomials," *Duke Mathematical Journal*, vol. 80, pp. 863–911, 1995.

[15] M. Adler and P. van Moerbeke, "Integrals over classical groups, random permutations, Toda and Toeplitz lattices," *Communications on Pure and Applied Mathematics*, vol. 54, no. 2, pp. 153–205, 2001.

[16] A. Nakamura, "Exact Bessel type solution of the two-dimensional Toda lattice equation," *Journal of the Physical Society of Japan*, vol. 52, no. 2, pp. 380–387, 1983.

[17] J. Villarroel and M. J. Ablowitz, "Solutions to the 2+1 Toda equation," *Journal of Physics A: Mathematical and General*, vol. 27, no. 3, pp. 931–941, 1994.

[18] K. Narita, "Rational and *N*-breather solutions for the 2D Toda lattice equation," *Journal of Mathematical Analysis and Applications*, vol. 281, no. 2, pp. 757–760, 2003.

[19] A. Nakamura, "Solitons in higher dimensions," *Progress of Theoretical Physics Supplement*, vol. 94, pp. 195–209, 1988.

[20] A. Nakamura, "The 3+1 dimensional Toda equation and its exact solutions," *Journal of the Physical Society of Japan*, vol. 56, no. 10, pp. 3491–3498, 1987.

[21] Y. L. Sun, W. X. Ma, and J. P. Yu, "Lump solutions of the 2D Toda equation," *Mathematical Methods in the Applied Sciences*, vol. 43, no. 10, pp. 6276–6282, 2020.

[22] A. Chowdury, D. J. Kedziora, and A. Ankiewicz, "Breather solutions of the integrable quintic nonlinear Schrödinger equation and their interactions," *Physical Review E*, vol. 91, no. 2, article 022919, 2015.

[23] L. Kaur and A. M. Wazwaz, "Dynamical analysis of lump solutions for (3 + 1) dimensional generalized KP-Boussinesq equation and its dimensionally reduced equations," *Physica Scripta*, vol. 93, no. 7, article 075203, 2018.

[24] L. Kaur and A. M. Wazwaz, "Bright - dark optical solitons for Schrodinger-Hirota equation with variable coefficients," *Optik*, vol. 179, pp. 479–484, 2019.

[25] L. C. Zhao, S. C. Li, and L. Ling, "W-shaped solitons generated from a weak modulation in the Sasa-Satsuma equation," *Physical Review E*, vol. 93, no. 3, article 032215, 2016.

[26] L. Kaur and A. M. Wazwaz, "Lump, breather and solitary wave solutions to new reduced form of the generalized BKP equation," *International Journal of Numerical Methods for Heat & Fluid Flow*, vol. 29, no. 2, pp. 569–579, 2019.

[27] S. Xu, J. He, and K. Porsezian, "Double degeneration on second-order breather solutions of Maxwell-Bloch equation," *Wave Motion*, vol. 80, pp. 82–90, 2018.

[28] A. Chabchoub, B. Kibler, J. M. Dudley, and N. Akhmediev, "Hydrodynamics of periodic breathers," *Philosophical Transactions of the Royal Society A*, vol. 372, pp. 4152–4160, 2014.

[29] B. Kibler, J. Fatome, C. Finot et al., "Observation of Kuznetsov-Ma soliton dynamics in optical fibre," *Scientific Reports*, vol. 2, no. 1, pp. 463–467, 2012.

[30] B. Frisquet, B. Kibler, and G. Millot, "Collision of Akhmediev breathers in nonlinear fiber optics," *Physical Review X*, vol. 3, no. 4, article 041032, 2013.

[31] J. Satsuma and M. J. Ablowitz, "Two-dimensional lumps in nonlinear dispersive systems," *Journal of Mathematical Physics*, vol. 20, no. 7, pp. 1496–1503, 1979.

[32] C. Rogers and W. F. Shadwick, *Bäcklund Transformations and Their Applications*, Academic Press, New York, 1982.

[33] C. Rogers and W. Schief, *Bäcklund and Darboux Transformations-Geometry and Modern Applications in Soliton Theory*, Cambridge University Press, Cambridge, UK, 2002.

[34] R. Hirota, "A new form of Backlund transformations and its relation to the inverse scattering problem," *Progress of Theoretical Physics*, vol. 52, no. 5, pp. 1498–1512, 1974.

[35] G. Herink, F. Kurtz, B. Jalali, D. R. Solli, and C. Ropers, "Real-time spectral interferometry probes the internal dynamics of femtosecond soliton molecules," *Science*, vol. 356, no. 6333, pp. 50–54, 2017.

[36] G. Xu, "Breather wave molecules," *Physical Review Letters*, vol. 122, no. 8, article 084101, 2019.

[37] K. Lakomy, R. Nath, and L. Santos, "Faraday patterns in coupled one-dimensional dipolar condensates," *Physical Review A*, vol. 86, article 013610, 2012.

[38] P. Rohrmann, A. Hause, and F. Mitschke, "Solitons beyond binary: possibility of fibre-optic transmission of two bits per clock period," *Scientific Reports*, vol. 2, no. 1, pp. 866–869, 2012.

[39] F. Mitschke, A. Hause, and C. Mahnke, "Soliton molecules for advanced optical telecommunications," *The European Physical Journal Special Topics*, vol. 225, no. 13-14, pp. 2453–2464, 2016.

[40] S. Y. Lou, "Soliton molecules and asymmetric solitons in three fifth order systems via velocity resonance," *Journal of Physics Communications*, vol. 4, no. 4, article 041002, 2020.

[41] D. H. Xu and S. Y. Lou, "Dark soliton molecules in nonlinear optics," *Acta Physica Sinica*, vol. 69, no. 1, article 014208, 2020.

[42] J. C. Cui, X. Y. Tang, and Y. J. Cui, "New variable separation solutions and wave interactions for the $(3+1)$-dimensional

Boiti-Leon-Manna-Pempinelli equation," *Applied Mathematics Letters*, vol. 102, pp. 106–109, 2020.

[43] M. Jia, J. Lin, and S. Y. Lou, "Soliton and breather molecules in few-cycle-pulse optical model," *Nonlinear Dynamics*, vol. 100, no. 4, pp. 3745–3757, 2020.

[44] R. Hirota, *Direct Methods in Soliton Theory*, Cambridge University Press, 2014.

[45] X. B. Hu Gegenhasi, S. H. Li, and B. Wang, "Nonsingular rational solutions to integrable models," in *Asymptotic, Algebraic and Geometric Aspects of Integrable Systems*, F. Nijhoff, Y. Shi, and D. J. Zhang, Eds., pp. 79–100, Springer, Berlin, 2020.

Hindawi
Advances in Mathematical Physics
Volume 2021, Article ID 9998553, 7 pages
https://doi.org/10.1155/2021/9998553

Research Article

General Traveling Wave Solutions of Nonlinear Conformable Fractional Sharma-Tasso-Olever Equations and Discussing the Effects of the Fractional Derivatives

Kai Fan,[1,2,3,4] **Rui Wang**,[2,5] **and Cunlong Zhou**[2,3]

[1]*Engineering Research Center of Heavy Machinery Ministry of Education, Taiyuan University of Science and Technology, Taiyuan 030024, China*
[2]*School of Mechanical Engineering, Taiyuan University of Science and Technology, Taiyuan 030024, China*
[3]*Shanxi Provincial Key Laboratory of Metallurgical Device Design Theory and Technology, Taiyuan University of Science and Technology, Taiyuan 030024, China*
[4]*School of Applied Science, Taiyuan University of Science and Technology, Taiyuan 030024, China*
[5]*School of Mechanical and Equipment Engineering, Hebei University of Engineering, Handan 056107, China*

Correspondence should be addressed to Kai Fan; 2014279@tyust.edu.cn, Rui Wang; wr1396595@163.com, and Cunlong Zhou; zcunlong@tyust.edu.cn

Received 16 March 2021; Revised 25 April 2021; Accepted 11 May 2021; Published 25 May 2021

Academic Editor: Kamyar Hosseini

The exact traveling wave solution of the fractional Sharma-Tasso-Olever equation can be obtained by using the function expansion method, but the general traveling wave solution cannot be obtained. After transforming it into the Sharma-Tasso-Olever equation of the integer order by the fractional complex transformation, the general solution of its traveling wave is obtained by a specific function transformation. Through parameter setting, the solution of the kinked solitary wave is found from the general solution of the traveling wave, and it is found that when the two fractional derivatives become smaller synchronically, the waveform becomes more smooth, but the position is basically unchanged. The reason for this phenomenon is that the kink solitary wave reaches equilibrium in the counterclockwise and clockwise rotation, and the stretching phenomenon is accompanied in the process of reaching equilibrium. This is a further development of our previous work, and this kind of detailed causative analysis is rare in previous papers.

1. Introduction

Because of many phenomena, integer-order differential equations cannot be well described, which makes fractional nonlinear differential equations have research significance. As an effective mathematical modeling tool, it is widely used in the mathematical modeling of nonlinear phenomena in biology, physics, signal processing, control theory, system recognition, and other scientific fields. The widely studied fractional Sharma-Tasso-Olever (STO) equation in space and time [1–4]

$$\frac{\partial^\alpha u}{\partial t^\alpha} + 3\rho u^2 \frac{\partial^\beta u}{\partial x^\beta} + 3\rho\left(\left[\frac{\partial^\beta u}{\partial x^\beta}\right]^2 + u\frac{\partial^{2\beta} u}{\partial x^{2\beta}}\right) + \rho\frac{\partial^{3\beta} u}{\partial x^{3\beta}} = 0, 0 < \alpha \le 1, 0 < \beta \le 1. \tag{1}$$

In equation (1), if $\alpha = \beta$, we get [5]

$$\frac{\partial^\alpha u}{\partial t^\alpha} + 3\rho u^2 \frac{\partial^\alpha u}{\partial x^\alpha} + 3\rho\left(\left[\frac{\partial^\alpha u}{\partial x^\alpha}\right]^2 + u\frac{\partial^{2\alpha} u}{\partial x^{2\alpha}}\right) + \rho\frac{\partial^{3\alpha} u}{\partial x^{3\alpha}} = 0. \tag{2}$$

In equation (1), if $\beta = 1$, we get the time-fractional STO equation [6, 7]

$$D_t^\alpha u + 3\rho u^2 u_x + 3\rho u u_x^2 + 3\rho u u_{xx} + \rho u_{xxx} = 0, 0 < \alpha \le 1. \tag{3}$$

In equations (1)–(3), $u = u(x, t)$ is the function to be solved, ρ is an arbitrary real parameter, and α, β are conformable fractional derivatives.

Recently, we have looked at some papers that obtain the exact solutions of the traveling wave of fractional-order equations and have illustrated some solitary wave solutions contained in the exact traveling wave solutions. These articles used different methods to obtain a large number of accurate traveling wave solutions in various forms. In order to better understand our work, we present the definitions and properties of the conformable fractional derivative as follows.

Given a function $f : [0,\infty] \to R$. Then, the conformable fractional derivative of f of order $0 < \alpha < 1$ is defined as [8]

$$T_\alpha(f)(t) = \lim_{\varepsilon \to 0} \frac{f\left(t + \varepsilon t^{1-\alpha}\right) - f(t)}{\varepsilon}. \tag{4}$$

The conformable derivative is a fractal derivative [9]. According to the fractal derivative theory, the influence of environmental abnormal fluctuation on physical behavior is equivalent to the influence of fractal space-time transformation [10, 11]. Several properties of conformable fractional derivative definition are as follows:

$$\begin{aligned} &T_\alpha(af + bg) = aT_\alpha(f) + bT_\alpha(g), \text{ for all } a, b \in R, \\ &T_\alpha(C) = 0, \\ &T_\alpha\left(t^b\right) = bt^{b-\alpha}, \text{ for all } b \in R, \\ &T_\alpha(fg) = gT_\alpha(f) + \mathrm{f}\Gamma_\alpha(g), \\ &\text{if } f \text{ is differentiable, } T_\alpha(f)(t) = t^{1-a}\frac{df}{dt}(t). \end{aligned} \tag{5}$$

These properties have been proved in literature [8], and there is no need to repeat them here. The physical interpretation of the conformable fractional derivative can be found in the literature [12].

According to Theorem 2.11 (chain Rule) in literature [13], we show the following properties of consistent fractional derivatives.

$$T_\alpha^t f(g(t)) = f'_g(g(t))g'(t)t^{1-\alpha}. \tag{6}$$

For more detailed knowledge, refer to literature [13]. Formula (6) is briefly proved as follows.

Proof. Set $u = t + \varepsilon t^{1-\alpha}$ in the definition, and you get

$$\begin{aligned} T_\alpha^t f(g(t)) &= \lim_{u \to t} \frac{f(g(u)) - f(g(t))}{u - t} t^{1-\alpha} \\ &= \lim_{u \to t} \frac{f(g(u)) - f(g(t))}{g(u) - g(t)} \cdot \lim_{u \to t} \frac{g(u) - g(t)}{u - t} t^{1-\alpha} \\ &= \lim_{g(u) \to g(t)} \frac{f(g(u)) - f(g(t))}{g(u) - g(t)} \cdot \lim_{u \to t} \frac{g(u) - g(t)}{u - t} t^{1-\alpha} \\ &= f'_g(g(t))g'(t)t^{1-\alpha}. \end{aligned} \tag{7}$$

Now, let us look at some of the work with the STO equation of fractional order to find the exact traveling wave solution.

In literature [1], the author used fractional complex transformation for equation (1) and then used the exp-function method to obtain its precise traveling wave solution.

In literature [2], the author used fractional complex transformation on equation (1) and then used (G'/G^2)-expansion method to obtain the precise traveling wave solution of equation (1).

In literature [3], the author used fractional complex transformation on equation (1) and then used the novel (G'/G)-expansion method to obtain the exact traveling wave solution of equation (1); the generalized Kudryashov method was also used to obtain the precise traveling wave solution of equation (1).

In literature [4], the author used the improved (G'/G)-expansion method to get the exact traveling wave solution of equation (1) after using the complex fractional transformation.

In literature [5], the author used fractional complex transformation for equation (2), and then extended tanh-coth method was used to obtain the precise traveling wave solution of equation (2).

In literature [6], the author used fractional complex transformation for equation (3) and then used the Riccadi function expansion method to obtain the exact traveling wave solution of fractional-order equation (3).

In literature [7], the author used fractional complex transformation in equation (3) and then used a new generalized (G'/G)-expansion method to obtain the precise traveling wave solution of the fractal equation (3).

Here, we have just listed some of the articles on the accurate line-wave solution to the STO equation of fractional order. It can be seen from literature [1–7] that the first step of these authors was to reduce the STO equation of the fractional order to a nonlinear ordinary differential equation by using fractional complex transformation and then to solve the reduced equation by various methods to obtain the solution of the original fractional-order equation. In addition to the methods provided in literature [1–7], there are other techniques that can be used to obtain wave solutions of different structures [14–19]. It can be seen from equations (1)–(3) that the most general equation is equation (1), so we only discuss the accurate general traveling wave solution of equation (1).

For equation (1), α, β are conformable fractional derivatives and the fractional complex transformation used is [20]

$$u(x,t) = U(\xi), \xi = \frac{ct^\alpha}{\alpha} + \frac{kx^\beta}{\beta}, \tag{8}$$

where c, k are parameters to be determined. Through equation (8), equation (1) can be transformed into

$$cU' + 3k^2\rho\left(U'\right)^2 + 3k^2\rho UU'' + 3k\rho U^2U' + k^3\rho U''' = 0. \tag{9}$$

In literature [1–7], some articles integrate equation (13) once and then assume that the integral constant is zero,

which will lead to the exact solution obtained being less general than its original one [21, 22]. Equation (9) is a third-order differential equation, and in general, its general solution should contain three arbitrary constants. From this perspective, the exact line-wave solutions obtained in the article [1–7] we mentioned are not general solutions, but only partial solutions. In this paper, we consider the integrability of equation (9) and combine with the fractional complex transformation to obtain the general traveling wave solution of the fractional STO equation, which is different from the exact solution obtained by using the function expansion method in known literature. As we all know, from the exact solutions of traveling waves, various forms of solutions can be obtained by choosing appropriate parameters, such as soliton solutions and periodic wave solutions. This conclusion can be obtained by bifurcation analysis of the first integral equation of equation (9) [23]. If the reader wants to know how the exact linear wave solutions of equation (9) are bifurcated and how the exact traveling wave solutions correspond to different forms of solutions, please refer to [23]. We selected from the general solution of traveling wave a kink solitary wave to fractional-order parameter change on the influence of the waveform, found that when two fractional-order parameters decrease at the same time, the kink soliton will become more smooth, but the location remains the same basic phenomenon, through the analysis found that the cause of this phenomenon is a kink soliton in the clockwise and counterclockwise to balance. Papers with such detailed analysis are rare.

2. The General Solution of the Fractional STO Equation in Space and Time in the Traveling Wave

Substituting equation (8) into equation (1) for transformation, we get

$$cU' + 3k^2\rho\left(U'\right)^2 + 3k^2\rho UU'' + 3k\rho U^2U' + k^3\rho U''' = 0. \tag{10}$$

Integrate equation (10) once, and we get

$$cU + 3k^2\rho UU' + k\rho U^3 + k^3\rho U'' + C_0 = 0, \tag{11}$$

where $''U'' = dU/d\xi$, C_0 is the integral constant.

Considering the specific function transformation,

$$U = \frac{kF'}{F}, \tag{12}$$

where $''F'' = dF/d\xi, F = F(\xi)$, we can easily get the following equation.

$$\begin{aligned} U' &= k\frac{F''F - \left(F'\right)^2}{F^2}, \\ UU' &= k^2\frac{F''F'F - \left(F'\right)^3}{F^3}, \end{aligned} \tag{13}$$

$$U'' = k\frac{\left(F'''F + F''F' - 2F'F''\right)F - \left(F''F - \left(F'\right)^2\right)2F'}{F^3}. \tag{14}$$

Substituting equations (13) and (14) into equation (11), we get

$$\begin{aligned} ck\frac{F'}{F} + 3k^4\rho\frac{F''F'F - \left(F'\right)^3}{F^3} + \rho k^4\frac{\left(F'\right)^3}{F^3} \\ + \rho k^4\frac{\left(F'''F + F''F' - 2F'F''\right)F - \left(F''F - \left(F'\right)^2\right)2F'}{F^3} \\ + C_0 = 0. \end{aligned} \tag{15}$$

Arrange equation (15) to get

$$k\frac{F'}{F} + \rho k^4\frac{F'''}{F} + C_0 = 0 \Rightarrow F''' + \frac{c}{\rho k^3}F' + \frac{C_0}{\rho k^4}F = 0 \tag{16}$$

Equation (16) is a familiar three-differential equation, and its general solution can be easily obtained, denoted as $p = c/\rho k^3 \neq 0$, $q = C_0/\rho k^4$; then, equation (16) has a characteristic equation

$$r^3 + pr + q = 0 \tag{17}$$

The three roots of equation (17) can be obtained by Cardin formula in the following order:

$$r_1 = \sqrt[3]{-\frac{q}{2} + \sqrt{\left(\frac{q}{2}\right)^2 + \left(\frac{p}{3}\right)^3}} + \sqrt[3]{-\frac{q}{2} - \sqrt{\left(\frac{q}{2}\right)^2 + \left(\frac{p}{3}\right)^3}}, \tag{18}$$

$$r_2 = \omega\sqrt[3]{-\frac{q}{2} + \sqrt{\left(\frac{q}{2}\right)^2 + \left(\frac{p}{3}\right)^3}} + \omega^2\sqrt[3]{-\frac{q}{2} - \sqrt{\left(\frac{q}{2}\right)^2 + \left(\frac{p}{3}\right)^3}}, \tag{19}$$

$$r_3 = \omega^2\sqrt[3]{-\frac{q}{2} + \sqrt{\left(\frac{q}{2}\right)^2 + \left(\frac{p}{3}\right)^3}} + \omega\sqrt[3]{-\frac{q}{2} - \sqrt{\left(\frac{q}{2}\right)^2 + \left(\frac{p}{3}\right)^3}}, \tag{20}$$

where $\omega = (-1 + \sqrt{3}i)/2$.

(1) When discriminant $\Delta = (q/2)^2 + (p/3)^3 = 0$, that is, $(C_0)^2 = 4c^3/27\rho k$, the three roots of equation (17) are reduced to

$$r_1 = 2\sqrt[3]{-\frac{q}{2}}, r_2 = r_3 = \sqrt[3]{\frac{q}{2}}. \tag{21}$$

equation (16) has the following general solution:

$$F(\xi) = C_1 e^{2\sqrt[3]{-(q/2)}\xi} + (C_2 + C_3\xi)e^{\sqrt[3]{(q/2)}\xi}, \tag{22}$$

where C_1, C_2, and C_3 are arbitrary constants

Without loss of generality, we can assume C_1 is not equal to zero. By substituting equation (22) into equation (12) and combining with complex transformation equation (8), the general traveling wave solution of the original equation (1) is expressed as

$$\begin{aligned} U &= k\frac{C_1 2\sqrt[3]{-(q/2)}e^{2\sqrt[3]{-(q/2)}\xi} + \left(C_2\sqrt[3]{q/2} + C_3\sqrt[3]{(q/2)}\xi + C_3\right)e^{\sqrt[3]{(q/2)}\xi}}{C_1 e^{2\sqrt[3]{-(q/2)}\xi} + (C_2 + C_3\xi)e^{\sqrt[3]{(q/2)}\xi}} \\ &= k\frac{2\sqrt[3]{-(q/2)}e^{2\sqrt[3]{-(q/2)}\xi} + \left(C_2/C_1\sqrt[3]{q/2} + C_3/C_1\sqrt[3]{(q/2)}\xi + (C_3/C_1)\right)e^{\sqrt[3]{(q/2)}\xi}}{e^{2\sqrt[3]{-(q/2)}\xi} + ((C_2/C_1) + (C_3/C_1)\xi)e^{\sqrt[3]{(q/2)}\xi}}. \end{aligned} \tag{23}$$

In equation (23), there are only two arbitrary constants, which is caused by the fixed arbitrary constant C_0. Without loss of generality, we could write$C_4 = C_2/C_1$, $C_5 = C_3/C_1$.

(2) When discriminant $\Delta = (q/2)^2 + (p/3)^3 \neq 0$, equation (19) has the following general solution:

$$F(\xi) = C_1 e^{r_1\xi} + C_2 e^{r_2\xi} + C_3 e^{r_3\xi}, \tag{24}$$

where C_1, C_2, and C_3 are arbitrary constants

Without loss of generality, we can assume C_1 is not equal to zero. By substituting equation (24) into equation (12) and combining with complex transformation equation (8), the general traveling wave solution of the original equation (1) is expressed as

$$\begin{aligned} U &= k\frac{C_1 r_1 e^{r_1\xi} + C_2 r_2 e^{r_2\xi} + C_3 r_3 e^{r_3\xi}}{C_1 e^{r_1\xi} + C_2 e^{r_2\xi} + C_3 e^{r_3\xi}} \\ &= k\frac{r_1 e^{r_1\xi} + (C_2/C_1)r_2 e^{r_2\xi} + (C_e/C_1)r_3 e^{r_3\xi}}{e^{r_1\xi} + (C_2/C_1)e^{r_2\xi} + (C_3/C_1)e^{r_3\xi}}. \end{aligned} \tag{25}$$

Without loss of generality, we could write $C_4 = C_2/C_1$, $C_5 = C_3/C_1$, and we have an arbitrary constant C_0 hidden in the parameter q.

3. The Discussion and Explanation

We observed some articles about the STO equation of fractional order and found that they more or less ignored the properties of the equation itself in the solution process, and the exact solution of the traveling wave obtained by various function expansion methods was not the general solution. Because in general, it makes sense that the precise general solution to equation (10) should contain three arbitrary constants. In the following part, we will find the kinked solitary wave solution from the general solution obtained in this paper and analyze the influence of the synchronous change of two fractional derivatives on the kinked solitary wave solution waveform and the reasons for this phenomenon.

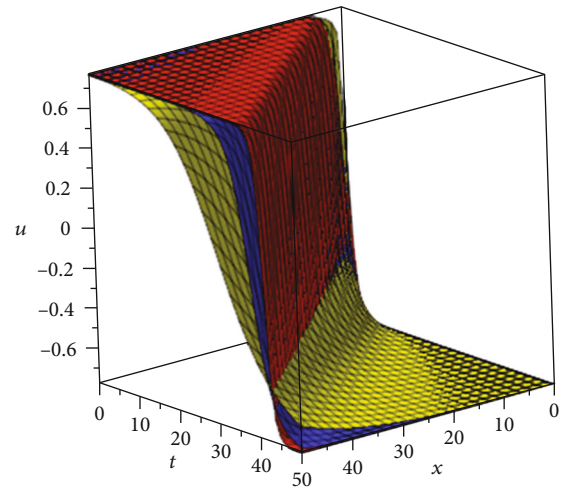

Solution (27) red: $\alpha = \beta = 1$, blue: $\alpha = \beta = 0.7$, yellow: $\alpha = \beta = 0.4$

Figure 1: 3D plot of solution (27) for various values of $\alpha = \beta$, and $k = 1, \rho = 2, c = -1.2, C_4 = C_5 = 1$.

Let ξ in equation (25) be the expression in equation (8), namely,

$$\xi = \frac{ct^\alpha}{\alpha} + \frac{kx^\beta}{\beta}. \tag{26}$$

We take the integral constant C_0 in equation (11) as zero; then, r_1, r_2, and r_3 in equation (25) are valued as $r_1 = 0, r_2 = \sqrt{-p} = \sqrt{-c/\rho k^3}, r_3 = -\sqrt{-p} = -\sqrt{-c/\rho k^3}$; then, equation (25) is rewritten as

$$\begin{aligned} U &= k\frac{r_1 e^{r_1\xi} + (C_2/C_1)r_2 e^{r_2\xi} + (C_3/C_1)r_3 e^{r_3\xi}}{e^{r_1\xi} + (C_2/C_1)e^{r_2\xi} + (C_3/C_1)e^{r_3\xi}} \\ &= k\frac{C_4 r_2 e^{r_2\xi} + C_5 r_3 e^{r_3\xi}}{1 + C_4 e^{r_2\xi} + C_5 e^{r_3\xi}} \\ &= k\frac{C_4\sqrt{-c/\rho k^3}\,e^{\sqrt{-c/\rho k^3}\left((ct^\alpha/\alpha)+\left(kx^\beta/\beta\right)\right)} - C_5\sqrt{-c/\rho k^3}\,e^{-\sqrt{-c/\rho k^3}\left((ct^\alpha/\alpha)+\left(kx^\beta/\beta\right)\right)}}{1 + C_4 e^{\sqrt{-c/\rho k^3}\left((ct^\alpha/\alpha)+\left(kx^\beta/\beta\right)\right)} + C_5 e^{-\sqrt{-c/\rho k^3}\left((ct^\alpha/\alpha)+\left(kx^\beta/\beta\right)\right)}}. \end{aligned} \tag{27}$$

In equation (27), take $k = 1, \rho = 2, c = -1.2, C_4 = C_5 = 1$; then, the diagram of solution (27) of equation (1) changing with $\alpha = \beta$ is shown in Figure 1. This is the kink solitary wave solution, which is a particular solution of the general solution (25) of equation (1). When $\alpha = \beta = 1$, the fractional-order STO equation degenerates into an equation of integer order. At this point, the diagram of

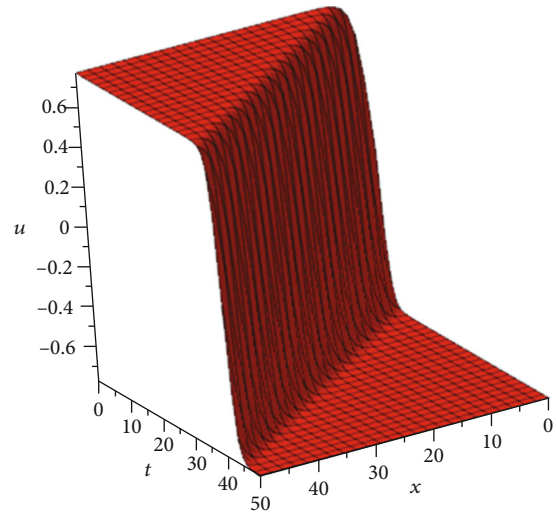

Figure 2: 3D plot of solution (27) for values of $\alpha = \beta = 1$, and $k = 1$, $\rho = 2$, $c = -1.2$, $C_4 = C_5 = 1$.

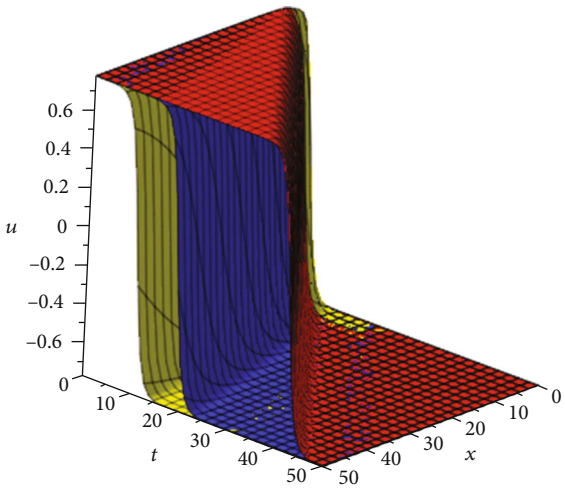

$\alpha = 1$; solution (27) red: $\beta = 1$, blue: $\beta = 0.7$, yellow: $\beta = 0.4$

Figure 3: 3D plot of solution (27) for various values of β, and $k = 1$, $\rho = 2$, $c = -1.2$, $C_4 = C_5 = 1$.

equation (27) is taken from Figure 1, as shown in Figure 2. After setting values for other parameters, Figure 1 explains the perspective view of the solution (27), when the values of $\alpha = \beta$ are 1, 0.7, and 0.4 in turn.

As can be seen from Figure 1, as the fractional derivative α and β become smaller synchronically, the twist of the kink solitary wave becomes smoothed, but the position of the twist of the kink solitary wave basically remains at the straight line $x = t$ on the t-x plane. In order to further explain this phenomenon and promote our previous work [24], this paper conducts a more detailed study of the influence of fractional derivative on the shape of kink solitary wave in two steps. First, the value of the time fractional derivative α is fixed, and only the change of the spatial fractional derivative β is observed. The result is shown in Figure 3. It can be seen from Figure 3 that the spatial fractional derivative β values 1, 0.7, and 0.4 in turn, and the kinked solitary wave rotates at the

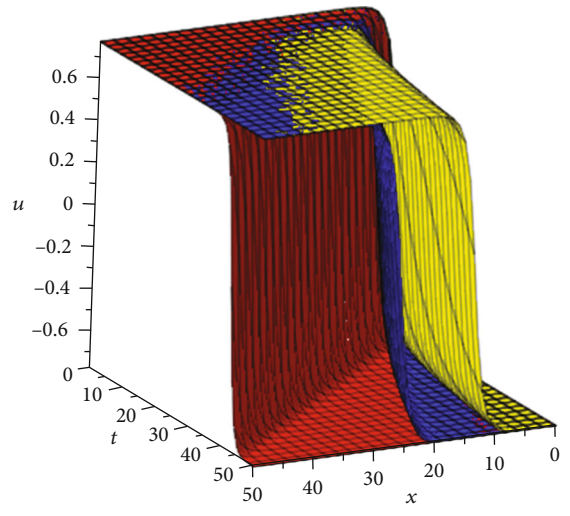

$\beta = 1$; solution (27) red: $\alpha = 1$, blue: $\alpha = 0.7$, yellow: $\alpha = 0.4$

Figure 4: 3D plot of solution (27) for various values of α, and $k = 1$, $\rho = 2$, $c = -1.2$, $C_4 = C_5 = 1$.

kinked position in the t-x plane, and the direction of rotation is close to the line $t = 0$ inside the t-x plane. Secondly, the value of the spatial fractional derivative β is fixed, and only the change of the time fractional derivative α is observed. The result is shown in Figure 4. It can be seen from Figure 4 that the time fractional derivative α is 1, 0.7, and 0.4 in turn, and the kinking position of the kink solitary wave in the t-x plane also rotates, with the direction approaching the line $x = 0$ in the x-t plane.

By comparing Figures 3 and 4, it is found that the spatial fractional derivative β becomes smaller, making the kink of the kink isolated wave as shown in the figure rotate clockwise in the t-x plane, while the time fractional derivative α becomes smaller, making the kink of the kink isolated wave as shown in the figure rotate counterclockwise in the t-x plane. When the fractional derivatives change synchronically, the kinks of the isolated wave in Figure 1 reach a balance in the clockwise rotation and counterclockwise rotation, and the position of the kinks almost stays the same. Meanwhile, the kinks of the isolated wave stretch together in the clockwise and counterclockwise rotation, which makes the kinks of the isolated wave smoothen.

4. Conclusion

The exact traveling wave solutions obtained by the function expansion method are usually not the general traveling wave solutions of fractional-order nonlinear partial differential equations. In this paper, the fractional-order STO equation is transformed into an integer-order STO equation through the complex fractional-order transformation, and then, the general traveling wave solution of the fractional-order STO equation is obtained through the transformation of a specific function, which will make our understanding of the traveling wave solution of the fractional-order STO equation more comprehensive. By setting parameters, a kinked solitary wave solution is extracted from the general traveling wave solution,

and the influence of the fractional derivative on the kinked solitary wave is analyzed in detail. It is found that the kinked solitary wave becomes more smooth when the fractional-order parameters are synchronized, but the position of the kinked solitary wave is basically unchanged. The position of the kinked solitary wave is basically unchanged because we have two fractional-order parameters, one of which becomes smaller so that the kinked waveform rotates clockwise, and the other fractional-order parameter becomes smaller so that the kinked waveform rotates counterclockwise. Such clockwise rotation and counterclockwise rotation achieve a balance. The kink solitary wave becomes smoother because of the tugging phenomenon that accompanies the process of reaching equilibrium.

Data Availability

No data were used to support this study.

Conflicts of Interest

The authors declare that they have no conflicts of interest.

Authors' Contributions

All authors read and approved the final manuscript.

Acknowledgments

This research was supported by the Shanxi Provincial Key Research and Development Project (CN) (20181101008, 20181102015).

References

[1] H. Ç. Yaslan and A. Girgin, "Exp-function method for the conformable space-time fractional STO, ZKBBM and coupled Boussinesq equations," *Arab Journal of Basic and Applied Sciences*, vol. 26, no. 1, pp. 163–170, 2019.

[2] S. Bibi, S. T. Mohyud-Din, R. Ullah, N. Ahmed, and U. Khan, "Exact solutions for STO and $(3+1)$-dimensional KdV-ZK equations using $G'G2$-expansion method," *Results in Physics*, vol. 7, pp. 4434–4439, 2017.

[3] S. Sirisubtawee, S. Koonprasert, and S. Sungnul, "New exact solutions of the conformable space-time Sharma–Tasso–Olver equation using two reliable methods," *Symmetry*, vol. 12, no. 4, p. 644, 2020.

[4] Y. W. Zhang, "Solving STO And KD equations with modified Riemann-Liouville derivative using improved (G'/G)-expansion function method," *IAENG International Journal of Applied Mathematics*, vol. 45, no. 1, pp. 16–22, 2015.

[5] A. Cesar and S. Gómez, "A nonlinear fractional Sharma-Tasso-Olver equation: new exact solutions," *Applied Mathematics and Computation*, vol. 266, pp. 385–389, 2015.

[6] H. Rezazadeh and F. S. Khodadad, "New structure for exact solutions of nonlinear time fractional Sharma-Tasso-Olver equation via conformable fractional derivative," *Applications and Applied Mathematics: An International Journal*, vol. 12, no. 1, pp. 405–414, 2017.

[7] R. Roy, M. A. Akbar, and A. M. Wazwaz, "Exact wave solutions for the nonlinear time fractional Sharma–Tasso–Olver equation and the fractional Klein–Gordon equation in mathematical physics," *Optical and Quantum Electronics*, vol. 50, no. 1, pp. 1–19, 2018.

[8] R. Khalil, M. al Horani, A. Yousef, and M. Sababheh, "A new definition of fractional derivative," *Journal of Computational and Applied Mathematics*, vol. 264, pp. 65–70, 2014.

[9] A. Atangana, D. Baleanu, and A. Alsaedi, "New properties of conformable derivative," *Open Mathematics*, vol. 13, no. 1, pp. 889–898, 2015.

[10] W. Chen, "Time-space fabric underlying anomalous diffusion," *Chaos, Solitons and Fractals*, vol. 28, no. 4, pp. 923–929, 2006.

[11] W. Cai, W. Chen, and W. Xu, "Characterizing the creep of viscoelastic materials by fractal derivative models," *International Journal of Non–Linear Mechanics*, vol. 87, pp. 58–63, 2016.

[12] D. Z. Zhao and M. Luo, "General conformable fractional derivative and its physical interpretation," *Calcolo*, vol. 54, no. 3, pp. 903–917, 2017.

[13] T. Abdeljawad, "On conformable fractional calulus," *Journal of Computational and Applied Mathematics*, vol. 264, pp. 65–70, 2015.

[14] M. N. Alam and M. S. Osman, "New structures for closed-form wave solutions for the dynamical equations model related to the ion sound and Langmuir waves," *Communications in Theoretical Physics*, vol. 73, no. 3, article 035001, 2021.

[15] M. N. Alam, E. Bonyah, M. Fayz-al-Asad, M. S. Osman, and K. M. Abualnaja, "Stable and functional solutions of the Klein-Fock-Gordon equation with nonlinear physical phenomena," *Physica Scripta*, vol. 96, no. 5, article 055207, 2021.

[16] F. S. Bayones, K. S. Nisar, K. A. Khan et al., "Magneto-hydrodynamics (MHD) flow analysis with mixed convection moves through a stretching surface," *AIP Advances*, vol. 11, no. 4, article 45001, 2021.

[17] M. Yang, M. S. Osman, and J. G. Liu, "Abundant lump-type solutions for the extended (3+1)-dimensional Jimbo-Miwa equation," *Results in Physics*, vol. 23, article 104009, 2021.

[18] S. Kumar, B. Kour, S. W. Yao, M. Inc, and M. S. Osman, "Invariance analysis, exact solution and conservation laws of $(2+1)$ dim fractional Kadomtsev-Petviashvili (KP) system," *Symmetry*, vol. 13, no. 3, p. 477, 2021.

[19] M. Akher Chowdhury, M. Mamun Miah, H. M. Shahadat Ali, Y. M. Chu, and M. S. Osman, "An investigation to the nonlinear $(2+1)$-dimensional soliton equation for discovering explicit and periodic wave solutions," *Results in Physics*, vol. 23, p. 104013, 2021.

[20] S. Javeed, S. Saif, A. Waheed, and D. Baleanu, "Exact solutions of fractional mBBM equation and coupled system of fractional Boussinesq-Burgers," *Results in Physics*, vol. 9, pp. 1275–1281, 2018.

[21] N. A. Kudryashov, "Seven common errors in finding exact solutions of nonlinear differential equations," *Communications in Nonlinear Science and Numerical Simulation*, vol. 14, no. 9-10, pp. 3507–3529, 2009.

[22] N. A. Kudryashov, "On "new travelling wave solutions" of the KdV and the KdV-Burgers equations," *Communications in Nonlinear Science and Numerical Simulation*, vol. 14, no. 5, pp. 1891–1900, 2009.

[23] M. N. Ali, S. M. Husnine, A. Saha, S. K. Bhowmik, S. Dhawan, and T. Ak, "Exact solutions, conservation laws, bifurcation of nonlinear and supernonlinear traveling waves for Sharma–Tasso–Olver equation," *Nonlinear Dynamics*, vol. 94, no. 3, pp. 1791–1801, 2018.

[24] K. Fan and C. Zhou, "Mechanical solving a few fractional partial differential equations and discussing the effects of the fractional order," *Advances in Mathematical Physics*, vol. 2020, Article ID 3758353, 17 pages, 2020.

Hindawi
Advances in Mathematical Physics
Volume 2021, Article ID 6696895, 12 pages
https://doi.org/10.1155/2021/6696895

Research Article

The New Scramble for Faure Sequence Based on Irrational Numbers

Ali Mogharrabi O.,[1] **Behrooz Fathi V.**,[2] **M. H. Behzadi**,[1] **and R. Farnoosh**[3]

[1]*Department of Statistics, Science and Research Branch, Islamic Azad University, Tehran, Iran*
[2]*Department of Statistics, University of Guilan, Rasht, Iran*
[3]*Department of Mathematics, Iran University of Science and Technology, Tehran, Iran*

Correspondence should be addressed to Behrooz Fathi V.; fathi@guilan.ac.ir

Received 24 December 2020; Revised 11 January 2021; Accepted 10 March 2021; Published 28 April 2021

Academic Editor: Leopoldo Greco

This article intends to review quasirandom sequences, especially the Faure sequence to introduce a new version of scrambled of this sequence based on irrational numbers, as follows to prove the success of this version of the random number sequence generator and use it in future calculations. We introduce this scramble of the Faure sequence and show the performance of this sequence in employed numerical codes to obtain successful test integrals. Here, we define a scrambling matrix so that its elements are irrational numbers. In addition, a new form of radical inverse function has been defined, which by combining it with our new matrix, we will have a sequence that not only has a better close uniform distribution than the previous sequences but also is a more accurate and efficient tool in estimating test integrals.

1. Introduction

It is well known that Monte Carlo calculations are based on the generation of random numbers on interval (0,1). Therefore, the generation of random numbers that have more uniformity on (0,1) guarantees better approximations in these calculations. In recent years, some researchers have employed quasirandom sequences instead of random numbers to aim producing extra uniformity of the randomly generated numbers on (0,1). Due to the breadth and complexity of some problems that are mostly unsolvable by classical mathematical methods or solving them with classical methods is associated with more time and computational cost, the stochastic solving of such cases with numerical methods and using the Monte Carlo method plays a key role. The quasirandom sequences are common in Monte Carlo calculations such as Faure, Halton, Niederreiter, and Sobol sequences, but due to the lack of complete success of these sequences in Monte Carlo computation, we use scrambled versions of them, all of which are designed to increase the uniformity of randomly (quasirandom) generated numbers on (0,1), so that we can estimate the obtained solution to the desired unknown solution of the problem.

To resolve this problem, researchers are competing on the use of scrambled quasirandom generators based on their version of random number generation to provide more accurate results in Monte Carlo calculations.

Today, Monte Carlo and quasi-Monte Carlo methods are widely used to solve the computations of physical and mathematical problems. Quasi-Monte Carlo (QMC) methods play an alternative role for Monte Carlo methods. The advantage of these methods is that they use numbers to provide extera uniformity on unit hypercube. This feature has led to the use of these methods to estimate high-dimensional integrals (Niederreiter, 1992; Spanier and Maize, 1994) [1].

So far, several quasirandom sequences (or low discrepancy sequences) have been introduced for the QMC method. Such as the Faure sequence, the Halton sequence, and the Sobol sequence. Despite the fact that among these three sequences, the Faure sequence has better features in terms of discrepancy bound, but in practice, it is less used. Because, the convergence rate of this class of sequences is not so good

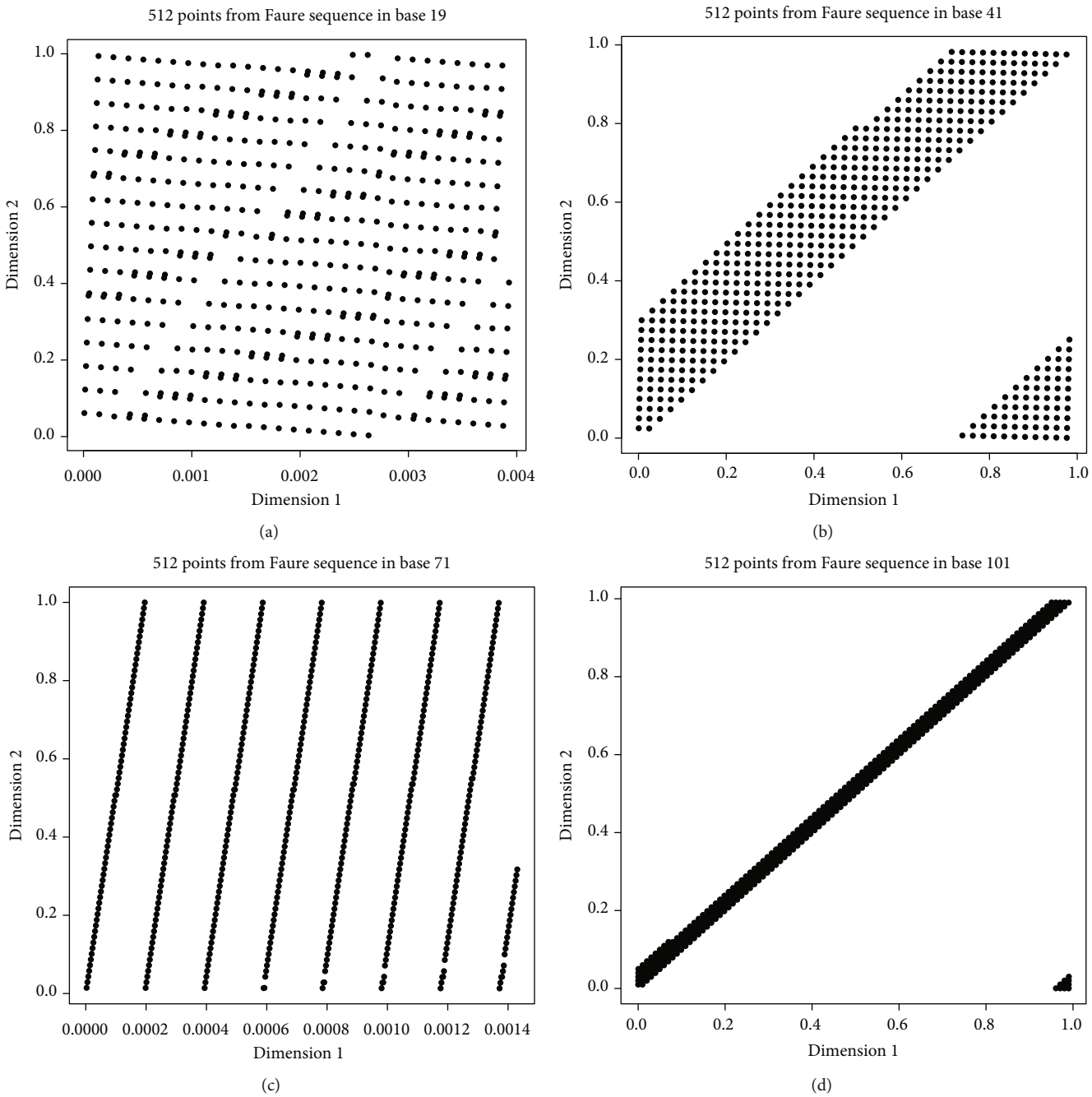

Figure 1: 512 points from the original Faure sequence in several bases.

compared with the other sequences [2]. In addition, due to the correlation between the different dimensions of the Faure sequence, the distribution of the sequence points is not very favorable, and we see poor two-dimensional projections (Figure 1). To overcome this problem, many scrambling methods have been proposed for the Faure sequence (see [3]). In almost all of these scrambles, there are attempts to define a new matrix by shifting numbers in the generating matrix or the placement of the elements, and there has been less talk about the properties of irrational numbers. The matrix that we introduce in this paper has been selected from several proposed matrices. Because it has good two-dimensional projections and it is also at a very high level in terms of integral estimation.

In the next section, the structure of the original Faure sequence is given. We then briefly list the scramblers that have already been introduced in Section 3. In Section 4, we have brought our proposed matrix. Sections 5 and 6 give the evaluation criteria for the quality of the sequence generated by our proposed matrix and compare it with previous sequences, and in Section 7, the conclusion is stated.

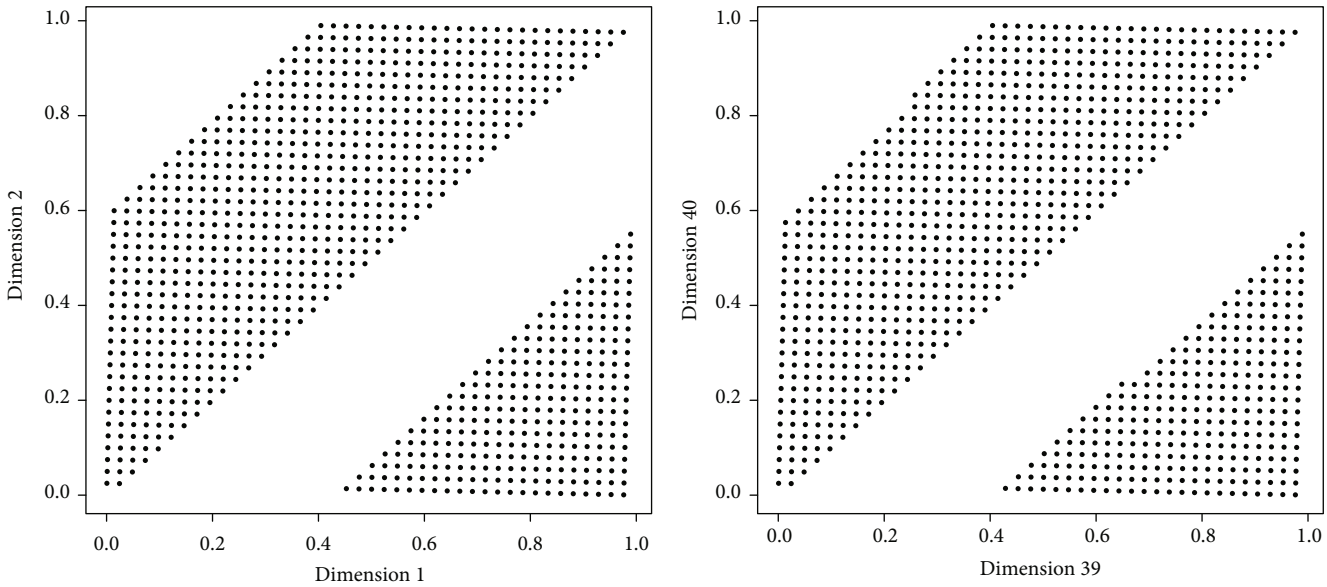

(a) (b)

Figure 2: 1000 points from the original Faure sequence.

2. The Faure Sequence

Suppose $p \geq 2$ is a prime number, and suppose N is the number of points we want to generate, and $\boldsymbol{n} = (a_0, a_1, \cdots, a_{m-1})^T$ is a vector of integers whose components are from the expansion of the number $\boldsymbol{n}$ on the base p, where $0 \leq a_j \leq p$ and $m = \lceil \log_p N \rceil$. We define the radical inverse function, $\phi_p(\boldsymbol{n})$, as

$$\phi_p(\boldsymbol{n}) = \frac{a_0}{p} + \frac{a_1}{p^2} + \cdots + \frac{a_{m-1}}{p^m}. \tag{1}$$

For the Faure sequence, we define a different generator matrix for each dimension. If $\boldsymbol{P}$ be the *Pascal matrix*, then for a s-dimensional Faure sequence the generator matrix of the jth dimension is $\boldsymbol{C}^{(j)} = \boldsymbol{P}^{j-1}$, $1 \leq j \leq s$, where the member on the row c and the column r is defined as follows:

$$\boldsymbol{P}^{j-1} = \binom{c-1}{r-1} (j-1)^{c-r} (\text{mod } p), c \geq 1, r \geq 1. \tag{2}$$

Thus, let $x_n^{(j)}$ be represents the number n in the dimension j in the Faure sequence, then

$$x_n^{(j)} = \phi_p\left(\boldsymbol{P}^{j-1}\boldsymbol{n}\right), \tag{3}$$

and so the $\boldsymbol{s}$-dimensional Faure sequence is $(\boldsymbol{\phi_p}(\boldsymbol{P^0 n}), \boldsymbol{\phi_p}(\boldsymbol{P^1 n}), \cdots, \boldsymbol{\phi_p}(\boldsymbol{P^{s-1} n}))$.

3. Scrambling the Faure Sequence

Since the introduction of the Faure sequence, several methods were proposed to scramble it. In this section, we give an overview of some of such scrambles.

3.1. The Generalized Faure Sequence. Tezuka [2] proposed the generalized Faure sequence, GFaure, with the jth dimension generator matrix $\boldsymbol{C}^{(j)} = \boldsymbol{A}^{(j)}\boldsymbol{P}^{j-1}$ and the $\boldsymbol{A}^{(j)}$ for $j = 1, 2, \cdots, s$ are arbitrary nonsingular lower triangular matrices over $\mathbb{F}_p$. A special case for $A^{(j)}$ is that all members are one for all dimensions [4].

3.2. Random Linear (Digit) Scrambling. After reviewing different versions of the Owen's method, Matoušek introduced a scramble matrix and a transfer vector for various dimensions [5]. The sequences obtained by Matoušek have the following general form:

$$\mathrm{x}_n = \left(\phi_p\left(\mathrm{A}^{(1)}\boldsymbol{P}^0\boldsymbol{n} + \boldsymbol{g}_1\right), \phi_p\left(\mathrm{A}^{(2)}\boldsymbol{P}^1\boldsymbol{n} + \boldsymbol{g}_2\right), \cdots, \phi_p\left(\mathrm{A}^{(s)}\boldsymbol{P}^{s-1}\boldsymbol{n} + \boldsymbol{g}_s\right)\right). \tag{4}$$

For the random linear scrambling, the matrices $A^{(j)}$ and the vectors $\boldsymbol{g}_j$ for $j = 1, \cdots, s$ are of the form

$$\boldsymbol{A}^{(j)} = \begin{pmatrix} h_{1,1} & 0 & 0 & 0 \\ h_{2,1} & h_{2,2} & 0 & 0 \\ h_{3,1} & h_{3,2} & h_{3,3} & 0 \\ \vdots & \vdots & \vdots & \ddots \\ & & & \end{pmatrix}, \boldsymbol{g}_j = \begin{pmatrix} g_1 \\ g_2 \\ g_3 \\ \vdots \\ \end{pmatrix}, \tag{5}$$

where the g_j's and the $h_{i,j}$ with $i \geq j$ are chosen randomly and independently from $\{0, 1, \cdots, b_1\}$, the $h_{j,j}$'s are chosen randomly and independently from $\{1, 2, \cdots, p-1\}$.

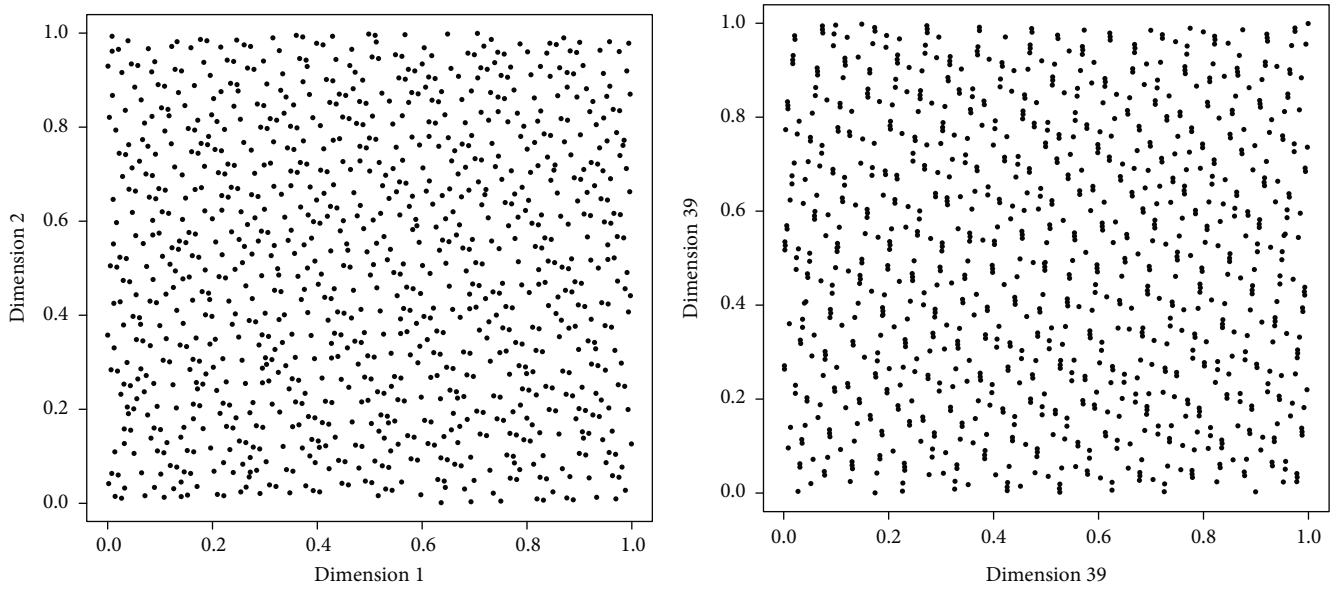

Figure 3: 1000 points from our scrambled Faure sequence.

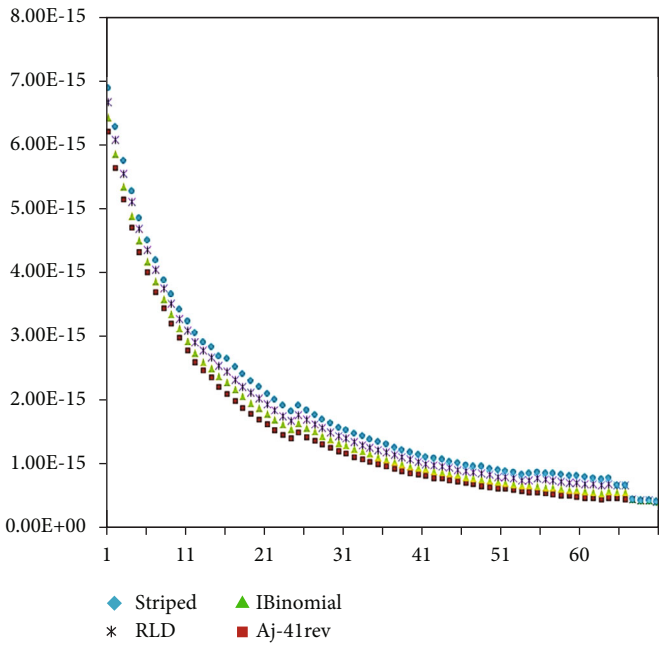

Figure 4: L_2-discrepancy for various randomized scramblings of a 40-dimensional Faure sequence.

Random linear digit method is the basis of other scrambles that will follow. Even the GFaure method is a subset of this method in which the members of the shift vectors are all zero.

3.3. I-Binomial Scrambling. A subset of the family of random linear scrambling methods is called left I-binomial scrambling [6]. Here, the $\boldsymbol{A}^{(j)}$ is defined as

$$\boldsymbol{A}^{(j)} = \begin{pmatrix} h_1 & 0 & 0 & 0 & 0 \\ h_2 & h_1 & 0 & 0 & 0 \\ h_3 & h_2 & h_1 & 0 & 0 \\ h_4 & h_3 & h_2 & h_1 & 0 \\ \ddots & \ddots & \ddots & \ddots & \ddots \end{pmatrix}, \tag{6}$$

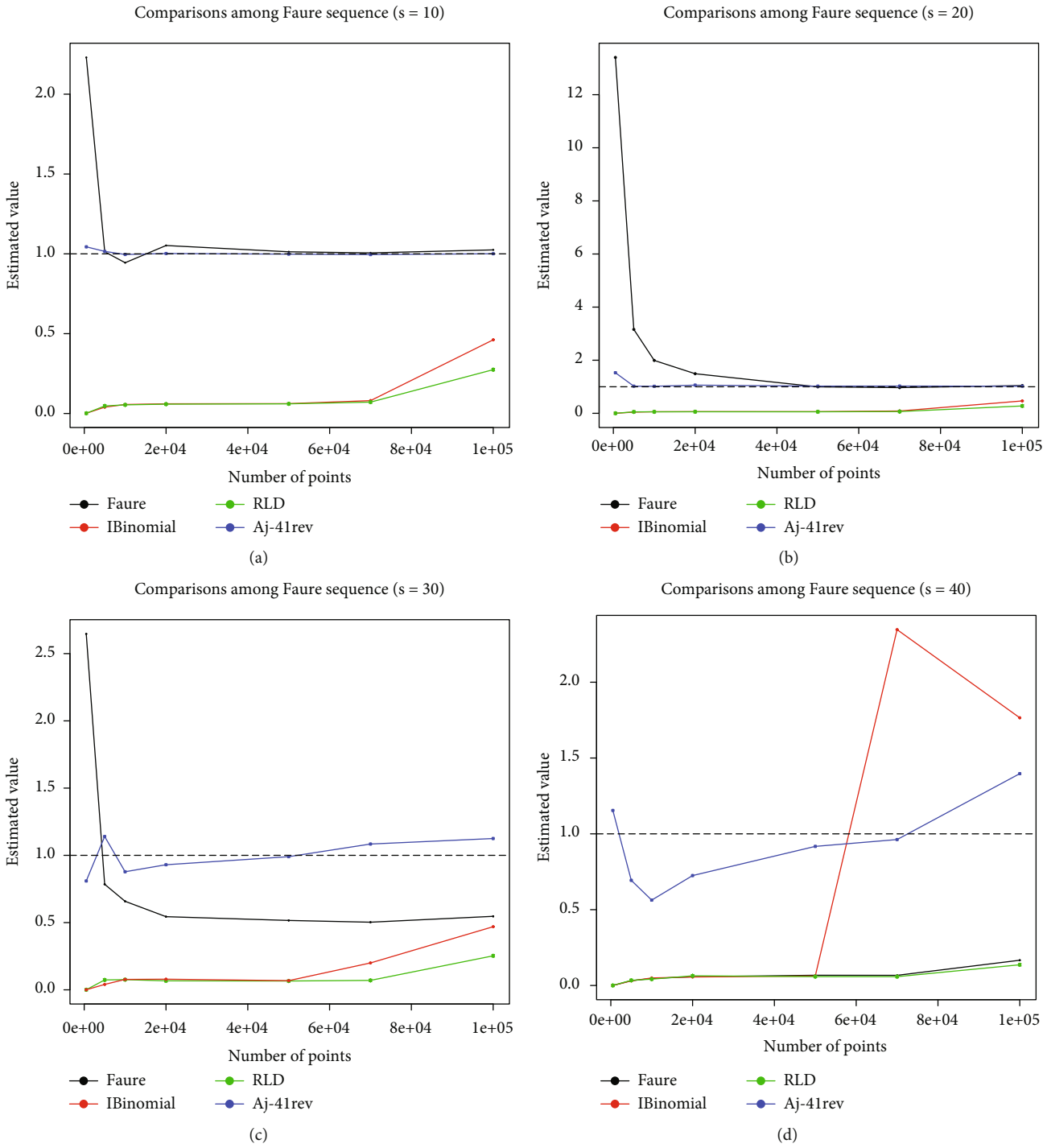

FIGURE 5: Estimates of the integral $I_1(f)$ by using various Faure sequences.

where h_1 is chosen randomly and independently from $\{1, 2, \cdots, p-1\}$ and also h_i's $(i > 1)$ are chosen randomly and independently from $\{0, 1, \cdots, p-1\}$.

3.4. Striped Matrix Scrambling. The scrambling matrix $\boldsymbol{A}^{(j)}$ for Striped Matrix Scrambling method, has the following form:

$$\boldsymbol{A}^{(j)} = \begin{pmatrix} h_1 & 0 & 0 & 0 & 0 \\ h_1 & h_2 & 0 & 0 & 0 \\ h_1 & h_2 & h_3 & 0 & 0 \\ h_1 & h_2 & h_3 & h_4 & 0 \\ \vdots & \vdots & \vdots & \vdots & \vdots \end{pmatrix}, \tag{7}$$

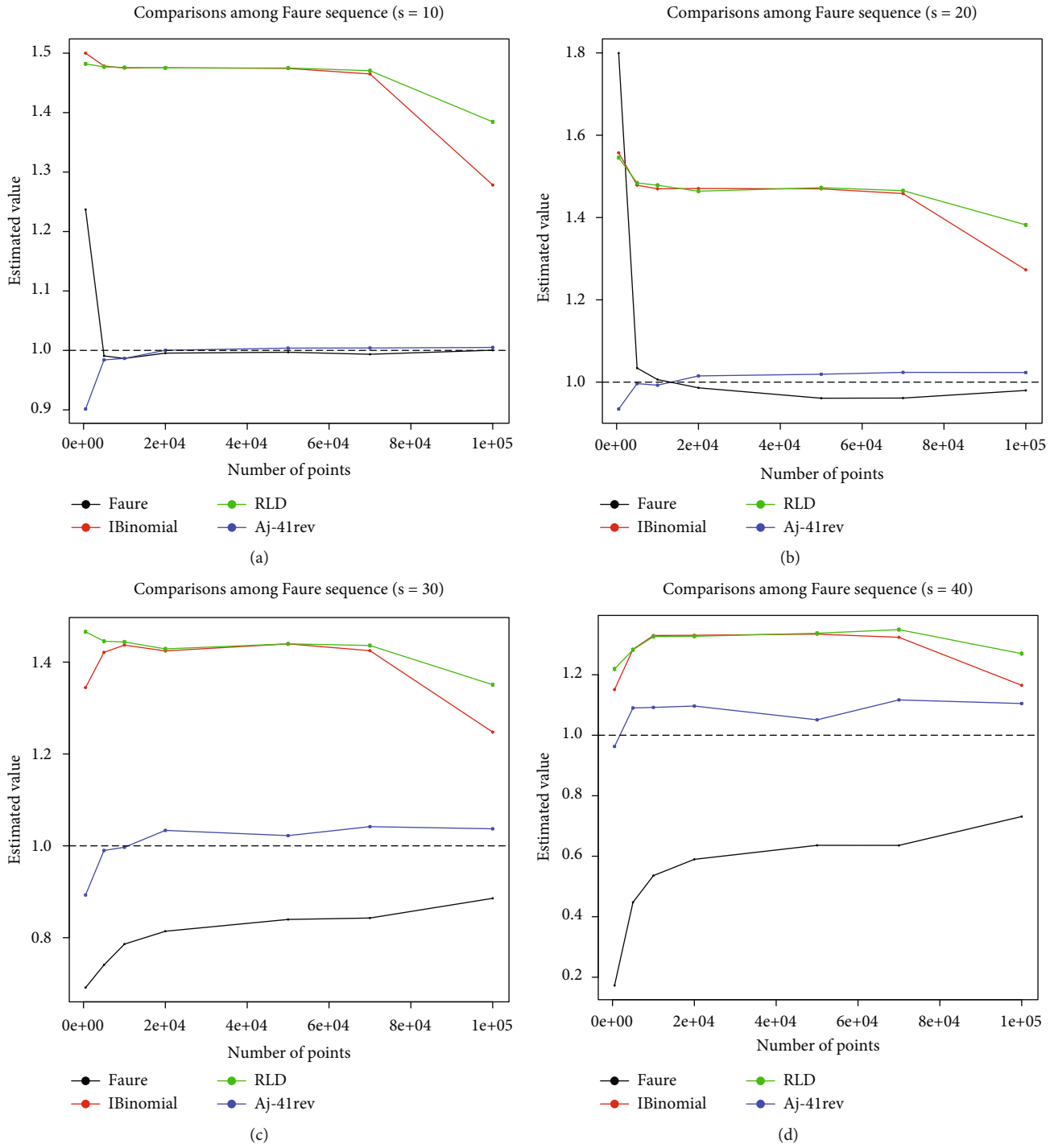

FIGURE 6: Estimates of the integral $I_2(f)$ with $a_i = 1$ by using various Faure sequences.

where the h_i's are chosen randomly and independently from $\{1, 2, \cdots, p-1\}$. The different types of this scramble are examined in [7], only for problems in the first dimension. Of course, it does not say what changes should be made to the matrix for higher dimensions.

3.5. Chi's Optimal Scramble. When we use the I-binomial method to scramble the Faure sequence, the value of (number) h_1 causes all the expansion digits of each number to be replaced (permuted). Now, if we leave out the first digit, the value of (number) h_2 causes all the remaining digits to be replaced (permuted).

So by cleverly selecting these two members, we can achieve better Faure sequences.

In [8], Chi has shown that the best choice for these two values can be obtained based on the primitive roots of the p. Finally, the Chi's optimal scramble matrix is as follows:

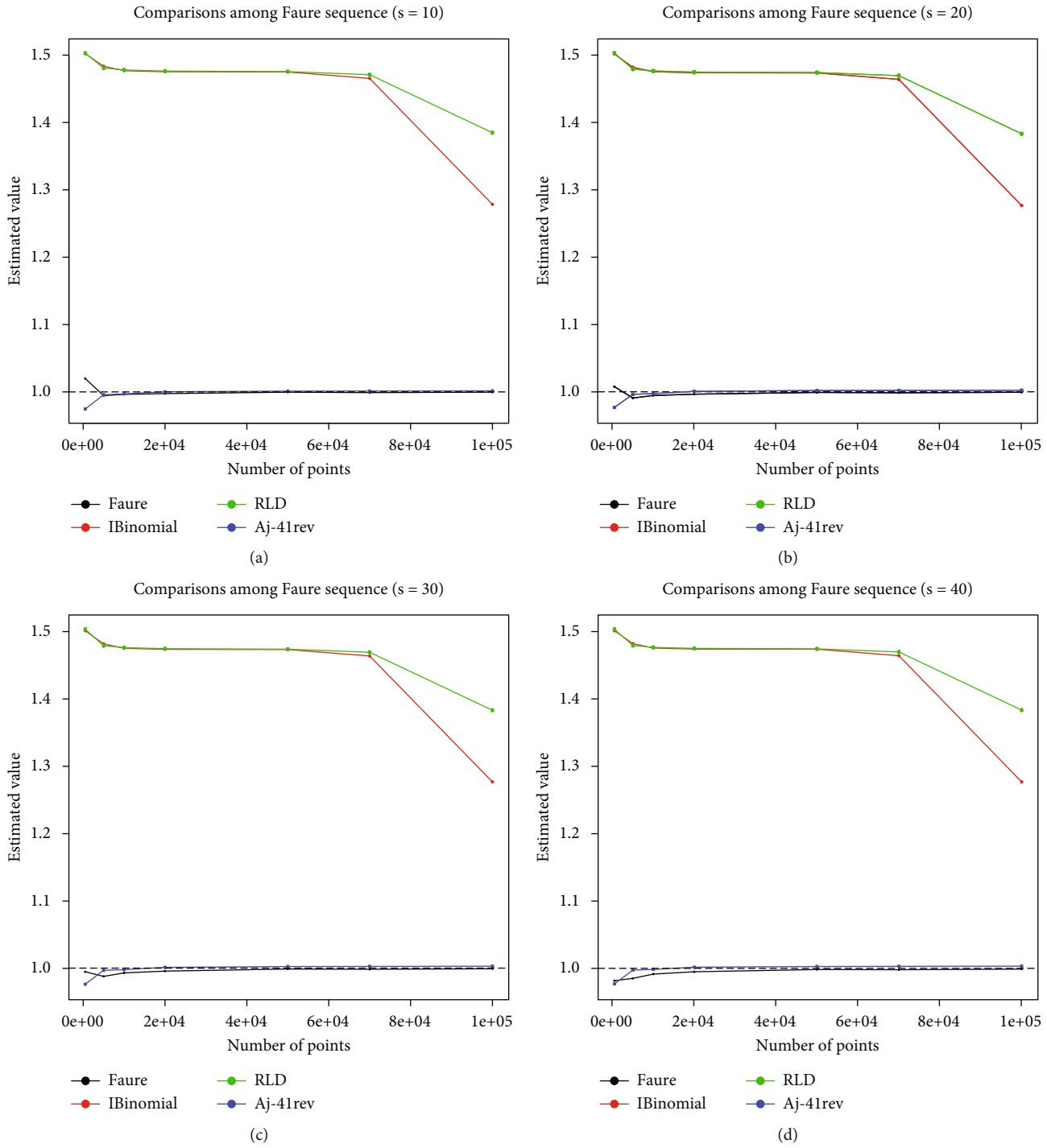

FIGURE 7: Estimates of the integral $I_2(f)$ with $a_i = i$ by using various Faure sequences.

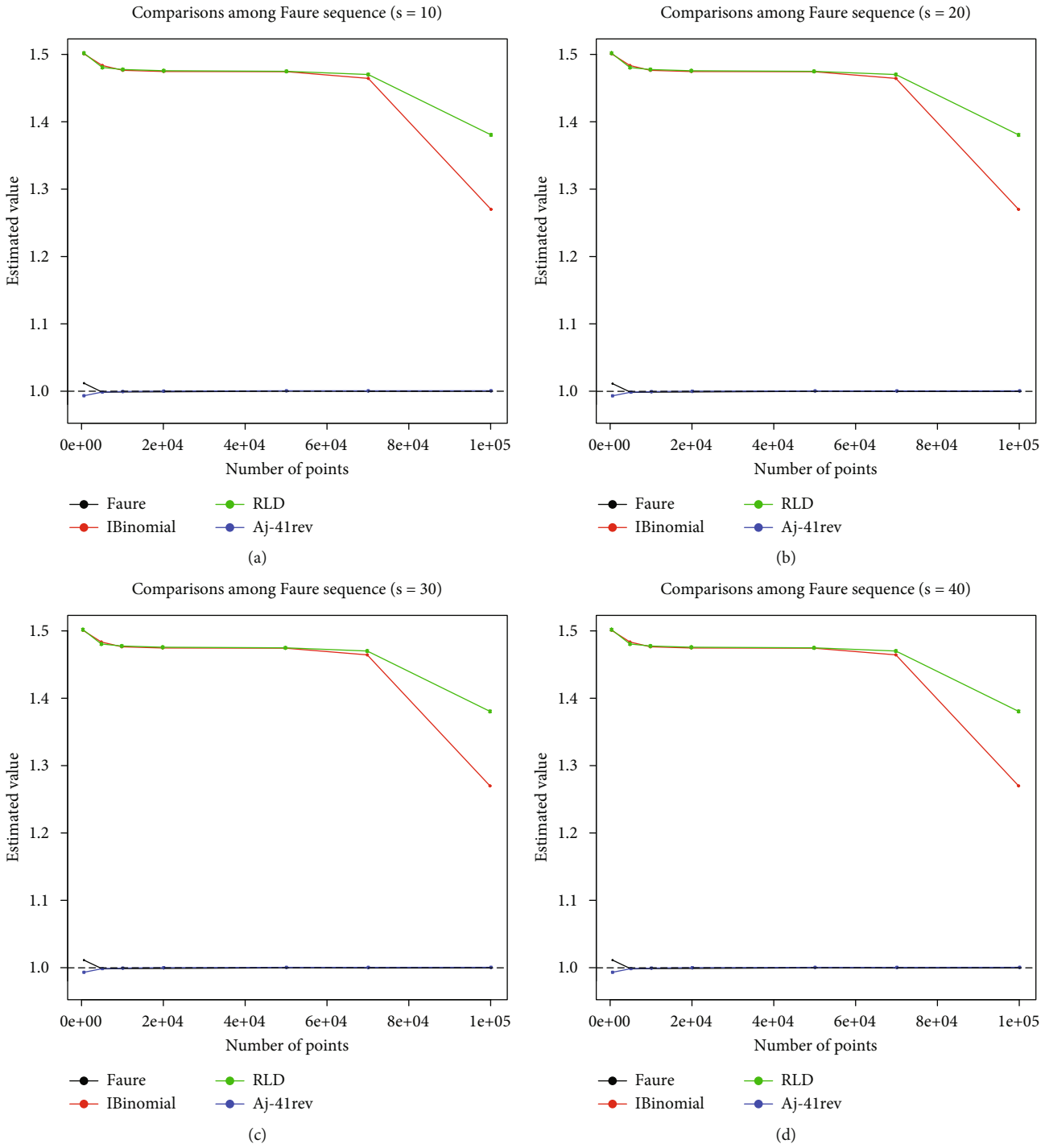

Figure 8: Estimates of the integral $I_2(f)$ with $a_i = i^2$ by using various Faure sequences.

$$\boldsymbol{A}^{(j)} = \begin{pmatrix} h_1^{j-1} & 0 & 0 & 0 \\ h_2 & h_1^{j-1} & 0 & 0 \\ 0 & h_2 & h_1^{j-1} & 0 \\ 0 & 0 & h_2 & h_1^{j-1} \\ \vdots & \vdots & \vdots & \ddots \end{pmatrix}, \tag{8}$$

3.6. Inverse Scrambling. Fathi and Eskandari [9] adapted Chi's optimal matrix and introduced two kind of matrix $\boldsymbol{A}^{(j)}$ as follows:

$$\boldsymbol{A}_1^{(j)} = \begin{pmatrix} d^{j-1} & 0 & 0 & 0 \\ 0 & d^{j-1} & 0 & 0 \\ 0 & 0 & d^{j-1} & 0 \\ \vdots & \vdots & \vdots & \ddots \end{pmatrix}, \quad \boldsymbol{A}_2^{(j)} = \begin{pmatrix} d^{j-1} & 0 & 0 & 0 \\ 0 & d^{j} & 0 & 0 \\ 0 & 0 & d^{j+1} & 0 \\ \vdots & \vdots & \vdots & \ddots \end{pmatrix}, \tag{9}$$

where d is chosen from $\{1, 2, \cdots, p-1\}$ for $j = 1, \cdots, s$.

Based on nonlinear congruential method, they proposed another scrambling method for the Faure sequence for which the jth coordinate of the nth point has the general form

$$x_n^{(j)} = \phi_p\left(\Phi^{-1}\left(\boldsymbol{A}^{(j)}\Psi\left(\boldsymbol{P}^{j-1}\boldsymbol{n}\right) + \boldsymbol{g}_j\right)\right), \tag{10}$$

where $\Phi(\boldsymbol{x})$ and $\Psi(\boldsymbol{x})$ are bijections that map a digit vector $\boldsymbol{x}$ to another digit vector.

4. Scrambling Matrix with Irrational Members

In this section, corresponding to the method of random linear digits, we introduce a scrambling matrix that its members are a function of square root of base p (that is, they are irrational numbers).

After testing many functions, we found the following function that has the most performance:

$$\boldsymbol{A}^{(j)} = \begin{pmatrix} \sqrt{p}-1 & 0 & 0 & 0 \\ \sqrt{p}-1 & \sqrt{p}-1 & 0 & 0 \\ \sqrt{p}-1 & \sqrt{p}-1 & \sqrt{p}-1 & 0 \\ \sqrt{p}-1 & \sqrt{p}-1 & \sqrt{p}-1 & \sqrt{p}-1 \end{pmatrix}. \tag{11}$$

In (1), we introduced the common form of radical inverse function ϕ for base p. Now, we define a new form of this function as follows:

$$\phi_p'(\boldsymbol{n}) = \frac{a_0}{p^m} + \frac{a_1}{p^{m-1}} + \cdots + \frac{a_{m-1}}{p}. \tag{12}$$

Table 1: Estimates of $I_1(f)$ by using Faure sequences.

Generator	N	$s = 5$	$s = 10$	$s = 20$	$s = 30$	$s = 40$
Faure	500	1.2175	2.2301	13.402	2.6464	0.0001
IB	500	0.0017	0.0016	0.0014	0.0006	0.0002
RLD	500	0.0013	0.0013	0.0011	0.0006	0.0001
Aj-41rev	500	1.0392	1.0439	1.5286	0.8095	1.1542
Faure	5000	0.9803	1.0128	3.1585	0.7848	0.0314
IB	5000	0.0340	0.0397	0.0443	0.0402	0.0306
RLD	5000	0.0469	0.0475	0.0548	0.0737	0.0341
Aj-41rev	5000	1.0015	1.0154	1.0219	1.1401	0.6935
Faure	10000	0.9584	0.9445	1.9919	0.6583	0.0464
IB	10000	0.0569	0.0564	0.0593	0.0774	0.0496
RLD	10000	0.0539	0.0541	0.0566	0.0758	0.0418
Aj-41rev	10000	0.9992	0.9959	1.0182	0.8780	0.5630
Faure	20000	0.9943	1.0522	1.4909	0.5440	0.0575
IB	20000	0.0610	0.0607	0.0628	0.0791	0.0561
RLD	20000	0.0583	0.0585	0.0592	0.0670	0.0637
Aj-41rev	20000	0.9999	1.0021	1.0614	0.9301	0.7249
Faure	50000	0.9965	1.0127	0.9972	0.5159	0.0674
IB	50000	0.0617	0.0618	0.0621	0.0683	0.0628
RLD	50000	0.0604	0.0605	0.0582	0.0657	0.0587
Aj-41rev	50000	0.9984	0.9983	1.0241	0.9901	0.9173
Faure	70000	0.9964	1.0058	0.9680	0.5029	0.0669
IB	70000	0.0809	0.0806	0.0877	0.2000	2.3467
RLD	70000	0.0711	0.0713	0.0671	0.0702	0.0583
Aj-41rev	70000	0.9985	0.9954	1.0260	1.0841	0.9623
Faure	100000	1.0008	1.0248	1.0459	0.5466	0.1665
IB	100000	0.4610	0.4616	0.4667	0.4694	1.7654
RLD	100000	0.2742	0.2746	0.2772	0.2529	0.1366
Aj-41rev	100000	0.9979	1.0007	1.0215	1.1251	1.3969

We call this as *reverse radical inverse function*, and we denote the sequences that are made in this way, with the suffix "rev." Therefore, by combining the matrix $\boldsymbol{A}^{(j)}$ and function ϕ', the general form of number n in dimension j will be as follows:

$$x_n^{(j)} = \phi'_p\left(\boldsymbol{A}^{(j)}\boldsymbol{P}^{j-1}\boldsymbol{n}\right). \tag{13}$$

So, for example, we denote the 40-dimensional Faure sequence generated on the base 41 by the scrambled matrix $\boldsymbol{A}^{(j)}$ and the function ϕ' with $\boldsymbol{A}^{(j)}$.41rev.

In the following sections, we have examined (studied) the quality of this sequence along with its performance compared to other sequences.

5. Investigation of the Uniformity of Generated Sequences

5.1. Two-Dimensional Projections. The first step in evaluating the performance of a sequence is to see how the points in the 2D projections are distributed. From Figure 2, in these designs, the Faure sequence points are located within parallel

Table 2: Estimates of $I_2(f)$ with $a_i = 1$ by using Faure sequences.

Generator	N	$s = 5$	$s = 10$	$s = 20$	$s = 30$	$s = 40$
Faure	500	1.0759	1.2370	1.7994	0.6913	0.1727
IB	500	1.5015	1.5000	1.5572	1.3445	1.1510
RLD	500	1.5123	1.4820	1.5456	1.4661	1.2191
Aj-41rev	500	0.9879	0.9014	0.9347	0.8930	0.9629
Faure	5000	0.9963	0.9908	1.0342	0.7406	0.4475
IB	5000	1.4836	1.4785	1.4787	1.4212	1.2841
RLD	5000	1.4807	1.4770	1.4840	1.4455	1.2824
Aj-41rev	5000	0.9976	0.9840	0.9964	0.9898	1.0902
Faure	10000	0.9935	0.9864	1.0062	0.7860	0.5359
IB	10000	1.4769	1.4750	1.4697	1.4370	1.3296
RLD	10000	1.4779	1.4759	1.4784	1.4438	1.3261
Aj-41rev	10000	0.9990	0.9865	0.9925	0.9968	1.0920
Faure	20000	0.9945	0.9954	0.9861	0.8140	0.5897
IB	20000	1.4753	1.4755	1.4706	1.4244	1.3306
RLD	20000	1.4763	1.4752	1.4640	1.4288	1.3271
Aj-41rev	20000	1.0000	1.0002	1.0151	1.0336	1.0965
Faure	50000	0.9992	0.9969	0.9609	0.8397	0.6360
IB	50000	1.4750	1.4744	1.4697	1.4397	1.3342
RLD	50000	1.4755	1.4751	1.4725	1.4398	1.3372
Aj-41rev	50000	1.0015	1.0039	1.0192	1.0222	1.0509
Faure	70000	0.9983	0.9935	0.9613	0.8428	0.6458
IB	70000	1.4654	1.4650	1.4582	1.4249	1.3238
RLD	70000	1.4710	1.4705	1.4653	1.4362	1.3491
Aj-41rev	70000	1.0020	1.0040	1.0237	1.0418	1.1168
Faure	100000	0.9997	1.0003	0.9798	0.8856	0.7312
IB	100000	1.2785	1.2783	1.2727	1.2476	1.1649
RLD	100000	1.3848	1.3844	1.3821	1.3508	1.2698
Aj-41rev	100000	1.0027	1.0050	1.0233	1.0371	1.1048

Table 3: Estimates of $I_2(f)$ with $a_i = i$ by using Faure sequences.

Generator	N	$s = 5$	$s = 10$	$s = 20$	$s = 30$	$s = 40$
Faure	500	1.0243	1.0200	1.0077	0.9945	0.9817
IB	500	1.5010	1.5022	1.5031	1.5030	1.5023
RLD	500	1.5055	1.5029	1.5043	1.5051	1.5045
Aj-41rev	500	0.9951	0.9746	0.9768	0.9761	0.9770
Faure	5000	0.9972	0.9944	0.9908	0.9877	0.9851
IB	5000	1.4837	1.4835	1.4833	1.4833	1.4832
RLD	5000	1.4810	1.4809	1.4807	1.4806	1.4804
Aj-41rev	5000	0.9990	0.9957	0.9963	0.9968	0.9974
Faure	10000	0.9977	0.9964	0.9946	0.9929	0.9915
IB	10000	1.4770	1.4769	1.4768	1.4768	1.4766
RLD	10000	1.4781	1.4780	1.4779	1.4778	1.4777
Aj-41rev	10000	0.9998	0.9971	0.9973	0.9977	0.9984
Faure	20000	0.9979	0.9977	0.9965	0.9956	0.9949
IB	20000	1.4752	1.4753	1.4753	1.4752	1.4752
RLD	20000	1.4764	1.4763	1.4763	1.4762	1.4762
Aj-41rev	20000	1.0002	1.0002	1.0007	1.0012	1.0017
Faure	50000	0.9999	0.9996	0.9991	0.9987	0.9983
IB	50000	1.4750	1.4750	1.4750	1.4750	1.4749
RLD	50000	1.4755	1.4755	1.4755	1.4755	1.4755
Aj-41rev	50000	1.0009	1.0012	1.0019	1.0024	1.0027
Faure	70000	0.9993	0.9989	0.9986	0.9983	0.9980
IB	70000	1.4654	1.4654	1.4654	1.4654	1.4653
RLD	70000	1.4710	1.4710	1.4709	1.4709	1.4709
Aj-41rev	70000	1.0011	1.0013	1.0021	1.0026	1.0029
Faure	100000	0.9997	0.9996	0.9993	0.9990	0.9989
IB	100000	1.2785	1.2785	1.2785	1.2785	1.2784
RLD	100000	1.3848	1.3848	1.3848	1.3848	1.3848
Aj-41rev	100000	1.0013	1.0016	1.0024	1.0028	1.0032

lines, which shows that there is a linear correlation between points in successive dimensions. Also in these designs, we see a lot of empty spaces. Therefore, the distribution of good points has not been done. In Figure 3, we draw the same designs using the by $\boldsymbol{A}^{(j)}$.41rev.

These figures show that two-dimensional projections of $\boldsymbol{A}^{(j)}$.41rev sequence are better than two-dimensional projections of the original Faure sequence.

5.2. Discrepancy. One way to measure the quality of a sequence is to calculate its discrepancy [10]. Warnock shows that

$$(T_N)^2 = \frac{1}{N^2}\sum_{k=1}^{N}\sum_{m=1}^{N}\prod_{i=1}^{s}\left(1 - \max\left(x_k^{(i)}, x_m^{(i)}\right)\right) - \frac{2^{1-s}}{N}\sum_{k=1}^{N}\prod_{i=1}^{s}\left(1 - x_k^{(i)^2}\right) + 3^{-s}. \tag{14}$$

where $x_k^{(i)}$ is the ith component of the point $\boldsymbol{x}_k$.

Figure 4 compares T_N between the original Faure sequence and the some scrambled Faure sequences that introduced in Section 3. From Figure 4, we see that the discrepancy p diagram for our new sequence is at all points below the other sequences. This is a good indication of the high quality of our sequence points.

6. Numerical Integration

Another way to compare the quality of sequences is to use them to solve high-dimensional integration problems with numerical methods. Consider the following test integrals:

$$I_1(f) = \int_0^1 \cdots \int_0^1 \prod_{i=1}^{s} \frac{\pi}{2} \sin(\pi x_i) dx_1 \cdots dx_s = 1, \tag{15}$$

$$I_2(f) = \int_0^1 \cdots \int_0^1 \prod_{i=1}^{s} \frac{|4x_i - 2| + a_i}{1 + a_i} dx_1 \cdots dx_s = 1, \tag{16}$$

where the a_i are parameters. There are four choices of parameters as follows:

(1) $a_i = 0$ for $1 \le i \le s$

(2) $a_i = 1$ for $1 \le i \le s$

Table 4: Estimates of $I_2(f)$ with $a_i = i^2$ by using Faure sequences.

Generator	N	$s = 5$	$s = 10$	$s = 20$	$s = 30$	$s = 40$
Faure	500	1.0125	1.0115	1.0110	1.0108	1.0106
IB	500	1.5003	1.5005	1.5006	1.5006	1.5006
RLD	500	1.5017	1.5015	1.5015	1.5015	1.5015
Aj-41rev	500	0.9966	0.9936	0.9936	0.9936	0.9936
Faure	5000	0.9988	0.9986	0.9985	0.9984	0.9984
IB	5000	1.4838	1.4838	1.4838	1.4838	1.4838
RLD	5000	1.4810	1.4810	1.4810	1.4810	1.4810
Aj-41rev	5000	0.9993	0.9989	0.9989	0.9989	0.9989
Faure	10000	0.9991	0.9990	0.9989	0.9989	0.9988
IB	10000	1.4770	1.4770	1.4770	1.4770	1.4770
RLD	10000	1.4781	1.4781	1.4781	1.4781	1.4781
Aj-41rev	10000	1.0000	0.9996	0.9996	0.9996	0.9996
Faure	20000	0.9992	0.9991	0.9991	0.9991	0.9991
IB	20000	1.4753	1.4753	1.4753	1.4753	1.4753
RLD	20000	1.4764	1.4764	1.4764	1.4764	1.4764
Aj-41rev	20000	1.0003	1.0002	1.0003	1.0003	1.0003
Faure	50000	1.0000	1.0000	1.0000	1.0000	1.0000
IB	50000	1.4750	1.4750	1.4750	1.4750	1.4750
RLD	50000	1.4755	1.4755	1.4755	1.4755	1.4755
Aj-41rev	50000	1.0006	1.0006	1.0007	1.0007	1.0007
Faure	70000	0.9998	0.9997	0.9997	0.9997	0.9997
IB	70000	1.4655	1.4655	1.4655	1.4655	1.4655
RLD	70000	1.4710	1.4710	1.4710	1.4710	1.4710
Aj-41rev	70000	1.0006	1.0006	1.0007	1.0007	1.0007
Faure	100000	0.9998	0.9998	0.9998	0.9998	0.9998
IB	100000	1.2785	1.2785	1.2785	1.2785	1.2785
RLD	100000	1.3848	1.3848	1.3848	1.3848	1.3848
Aj-41rev	100000	1.0007	1.0007	1.0007	1.0008	1.0008

(3) $a_i = i$ for $1 \le i \le s$

(4) $a_i = i^2$ for $1 \le i \le s$

Note that the most difficult case is when $a = 0$. Because in this case, the importance of all variables is the same and the superposition dimension is approximately the same as the truncation dimension. It is important to know that the larger a_i, the less important the variables are, and therefore, the effective dimension becomes smaller. The last three choices of the parameters will be considered here [11].

In numerical solution of problems with qMC methods, an accepted procedure is to omit the starting points of the sequence. For example, Fox [12] has suggested that we consider the starting point of the sequence as $n = QS^4 - 1$. Although, this may lead to better results, note that with this selection, a large amount of points must be omitted. For example, for $s = 40$, we have to skip the initial 2825760 points with this formula, which is practically impossible. We found in our research that if we select the p as the starting point, it will significantly improve the results. We will probably get the best result when we start from the $(p^2 + 1)$th point.

Therefore, we skip the first 41 points and start $n = 42$ in our calculations. For comparison purposes, we present numerical results for original Faure (Faure), our sequence (Aj-41rev), and two types of scrambled Faure sequences, I-binomial (IB) and random linear digits (RLD).

Now, we compare the numerical results of different scrambled Faure sequences presented in this paper. The estimated values for the test functions are given in Figures 5–8. These figures show that our proposed scramble has a very acceptable convergence compared to other scrambles.

An observation is that estimated values by the matrix Aj-41rev very close to the actual value. This can be seen in Tables 1–4. The estimation error obtained with this scramble in dimension 40, for the function (16) with parameters $a_i = 1$, $a_i = i$, and $a_i = i^2$ are at most 11.68%, 0.32%, and 0.64%, respectively. However, there are some exceptions. For example, in the first function, when the number of dimensions increases, the accuracy of the estimation decreases. So that, for the dimension 40, the maximum estimated relative error value is 43.7%.

7. Conclusion

We studied the original Faure sequence and some of its recent years introduced scrambles. Then, we introduced a new scrambling matrix based on irrational numbers that its elements are function of square root of base p. In Figures 5–8, we have shown that this modified scrambled Faure sequence provides better results than the previous versions of its scrambles. Also, we presented that this modified scrambled Faure sequence has greatly improved the distribution of points. The 2D designs confirm this claim, good two-dimensional projections in successive dimensions. As mentioned in the previous section, using this scramble leads to very small estimated relative errors that can often be ignored. In our next research, we will use deterministic scrambling matrices based on another irrational numbers and primitive roots. The results proved the improvements of accuracy using our new scramble.

Data Availability

The data is contained in the article itself.

Conflicts of Interest

The authors declares that there is no conflict of interest regarding the publication of this paper.

References

[1] A. B. Owen, "Monte Carlo, quasi-Monte Carlo, and randomized quasi-Monte Carlo," in *Monte Carlo and Quasi-Monte Carlo Methods*, H. Niederreiter and J. Spanier, Eds., pp. 86–97, Springer-Verlag, Berlin Heidelberg, 1998.

[2] S. Tezuka, "A generalization of Faure sequences and its efficient implementation," Technical Report RT0105, IBM. Tokyo Research Laboratory, 1994.

[3] B. Vandewoestyne, H. Chi, and R. Cools, "Computational investigations of scrambled Faure sequences," *Mathematics and Computers in Simulation*, vol. 81, pp. 522–535, 2003.

[4] H. Faure, "Variations on (0, s)-sequences," *Journal of Complexity*, vol. 17, no. 4, pp. 741–753, 2015.

[5] J. Matouˇsek's, "On the L2-discrepancy for anchored boxes," *Journal of Complexity*, vol. 14, pp. 527–556, 1998.

[6] S. Tezuka and H. Faure, "I-binomial scrambling of digital nets and sequences," *Journal of Complexity*, vol. 19, no. 6, pp. 744–757, 2003.

[7] P. Bratley, B. L. Fox, and H. Niederreiter, "Implementation and tests of low-discrepancy sequences," *ACM Transactions on Modeling and Computer Simulation*, vol. 2, no. 3, pp. 195–213, 1992.

[8] H. Chi, *Scrambled Quasirandom Sequences and their Applications, [Ph.D. thesis]*, Florida State University, Tallahassee, FL, USA, 2004.

[9] B. Fathi Vajargah and A. Eskandari Chechaglou, "New modified scrambled faure sequences," *Communications in Statistics - Simulation and Computation*, vol. 44, no. 3, pp. 666–682, 2012.

[10] B. Vandewoestyne, *Quasi-Monte Carlo Techniques for the Approximation of High-Dimensional Integrals, [Ph.D. theses]*, Advisor Ronald Cools, 2008.

[11] X. Wang and K. T. Fang, "The effective dimension and quasi-Monte Carlo integration," *Journal of Complexity*, vol. 19, no. 2, pp. 101–124, 2003.

[12] B. L. Fox, "Algorithm 647: implementation and relative efficiency of quasirandom sequence generators," *ACM Transactions on Mathematical Software*, vol. 12, no. 4, pp. 362–376, 1986.

Hindawi
Advances in Mathematical Physics
Volume 2021, Article ID 6672819, 9 pages
https://doi.org/10.1155/2021/6672819

Research Article

On the Exact Solitary Wave Solutions to the New (2 + 1) and (3 + 1)-Dimensional Extensions of the Benjamin-Ono Equations

Lan Wu,[1] **Xiao Zhang**,[1] **and Jalil Manafian**[2]

[1]*School of Mathematical Sciences, Peking University, Beijing, China*
[2]*Department of Applied Mathematics, Faculty of Mathematical Sciences, University of Tabriz, Tabriz, Iran*

Correspondence should be addressed to Jalil Manafian; j_manafianheris@tabrizu.ac.ir

Received 11 November 2020; Revised 26 December 2020; Accepted 20 March 2021; Published 21 April 2021

Academic Editor: Sergey Shmarev

In this paper, the Kudryashov method to construct the new exact solitary wave solutions for the newly developed (2 + 1)-dimensional Benjamin-Ono equation is successfully employed. In the same vein, also the new (2 + 1)-dimensional Benjamin-Ono equation to (3 + 1)-dimensional spaces is extended and then analyzed and investigated. Different forms of exact solitary wave solutions to this new equation were also determined. Graphical illustrations for certain solutions in both equations are provided. We alternatively offer that the determining method is general, impressive, outspoken, and powerful and can be exerted to create exact solutions of various kinds of nonlinear models originated in mathematical physics and engineering.

1. Introduction

Nonlinear evolution equations have been known for their vital roles in many fields of engineering and nonlinear sciences for long. A lot of these equations are famous in fluid flow problems and shallow water waves applications. A very good example for such equations is the Benjamin-Ono equation [1] that describes inner waves of deep-stratified fluids that reads

$$u_{tt} + \alpha\left(u^2\right)_{xx} + \beta u_{xxxx} = 0, \tag{1}$$

where α and β are nonzero constants for monitoring the nonlinear term and depth of the fluid, respectively. Further, different studies have been carried out on this important model ranging from analytical solution, numerical solution, stability, and well-posedness among others. For instance, the multisoliton solution and time-periodic solutions of the Benjamin-Ono equation were presented by Matsuno [2] and Ambrose and Wilkening [3], respectively (see also Angulo et al. [4] for the stability, Tutiya and Shiraishi [5] for discrete solutions, and [6–11] for other related studies).

Additionally, the (2 + 1)-dimensional version of Benjamin-Ono equation Eq. (1) was recently introduced by Wazwaz [12]. The new equations has the form

$$u_{tt} + \alpha\left(u^2\right)_{xx} + \beta u_{xxxx} + \gamma u_{yyyy} = 0, \tag{2}$$

where α, β, and γ are nonzero constants. Note that γ should not be zero; otherwise, we recover Eq. (1). In [12], the Hirota bilinear method and certain ansatzs methods have been used to construct a variety of multiple and complex soliton solutions and also checked the Painlevé integrality condition.

However, in this paper, we further extend the new (2 + 1)-dimensional Benjamin-Ono equation [12] given in Eq. (2) to (3 + 1)-dimensional spaces and call it the (3 + 1)-dimensional Benjamin-Ono equation given by

$$u_{tt} + \alpha\left(u^2\right)_{xx} + \beta u_{xxxx} + \gamma u_{yyyy} + \delta u_{zzzz} = 0, \tag{3}$$

where α, β, γ, and δ are nonzero constants. Furthermore, to present more new solitary wave solutions for the (2 + 1)-dimensional Benjamin-Ono equation in Eq. (2) and also to study the (3 + 1)-dimensional Benjamin-Ono equation, we developed Eq. (3), to employ the Kudryashov method [13, 14] as a powerful integration method for

treating various nonlinear evolution equations (see also [15–23] for other methods). The Kudryashov method and its modified versions have been investigated by capable authors in the plenty of nonlinear models such as the nonlinear differential equations [24], higher-order local and nonlocal nonlinear equations in optical fibers [25], some (2 + 1)-dimensional nonlinear evolution equations [26], exact traveling wave solutions of the PHI-four equation, and the Fisher equation [27]. As we all know, some novel and important developments for searching the analytical solitary wave solutions for PDE were investigated. Hence, there are fascinating results on some models in which are presented in research works containing the new iterative projection method for approximating fixed point problems and variational inequality problems [28], weighted inequalities for the Dunkl fractional maximal function and Dunkl fractional integrals [29], the Painlevé analysis, soliton molecule, and lump solution of the higher-order Boussinesq equation [30], and the Darboux solutions of the classical Painlevé second equation [31]. The structure of this paper is as follows: the analysis of the method has been summed up in "Analysis of the Method." In "Applications," the applications of "Analysis of the Method" for considered equation are investigated. Also, in "Some Graphical Illustrations," the graphical illustrations for nonlinear equations will be used. In "Conclusion," the conclusions have been given.

2. Analysis of the Method

To illustrate the idea of the Kudryashov method [13, 14], we consider the following system of nonlinear differential equations:

$$F(u, T_x u, T_{xx} u, T_{tt} u, T_{xxxx} u, \cdots) = 0. \tag{4}$$

Applying the transformation

$$u(x,t) = f(\xi), \xi = ax - ct - x_0, \tag{5}$$

where a and c are nonzero constants and x_0 is arbitrary constant, converts Eq. (4) to a nonlinear ordinary differential equations as follows

$$H\left(f', f'', f''', \cdots\right) = 0, \tag{6}$$

where the derivatives are with respect to ξ. It is assumed that the solutions of Eq. (6) are presented as a finite series, say

$$f(\xi) = a_0 + \sum_{i=1}^{N} a_i \Phi^i(\xi), \tag{7}$$

where $a_i,\ i = 1, 2, \cdots, N\ (a_N \neq 0)$, are constants to be computed, and $\Phi(\xi)$ is given by the following function:

$$\Phi(\xi) = \frac{1}{1 + we^{\xi}}, \tag{8}$$

which satisfies the ordinary differential equation

$$\Phi'(\xi) = \Phi(\xi)(\Phi(\xi) - 1). \tag{9}$$

Also, the value of N is determined by homogenous balancing method (see [13, 14]). Substituting Eq. (7) and its necessary derivatives like

$$\begin{aligned} f' &= \sum_{i=1}^{N} a_i \Phi^i(\Phi - 1), \\ f'' &= \sum_{i=1}^{N} a_i \Phi^i(\Phi - 1)((1+i)\Phi - i), \\ &\vdots \end{aligned} \tag{10}$$

into Eq. (6) gives

$$P(\Phi(\xi)) = 0, \tag{11}$$

where $P(\Phi(\xi))$ is a polynomial in $\Phi(\xi)$. Equating the coefficient of each power of $\Phi(\xi)$ in Eq. (11) to zero, a system of algebraic equations will be obtained whose solution yields the exact solutions of Eq. (4).

3. Applications

In this section, some new solitary wave solutions of the (2 + 1)-dimensional and (3 + 1)-dimensional Benjamin-Ono equations are constructed using the Kudryashov method presented above.

3.1. The (2 + 1)-Dimensional Benjamin-Ono Equation. In this section, we will study the (2 + 1)-dimensional Benjamin-Ono equation given by Eq. (2)

$$u_{tt} + \alpha\left(u^2\right)_{xx} + \beta u_{xxxx} + \gamma u_{yyyy} = 0, \tag{12}$$

where $u(x, y, t)$ is a sufficiently often a differentiable function and α, β, and γ are nonzero parameters.

To determine certain solitary wave solutions, we first substitute

$$u(x, y, t) = f(\xi), \xi = ax + by - ct - x_0, \tag{13}$$

into Eq. (12) where

$$\begin{aligned} T_{tt} u = c^2 f'(\xi), T_x u = a f'(\xi), T_{xx} u = a^2 f''(\xi), \\ T_{xxxx} u = a^4 f''''(\xi), T_{yyyy} u = b^4 f''''(\xi), \end{aligned} \tag{14}$$

and convert Eq. (12) to a nonlinear ordinary differential equation given below:

$$c^2 f'' + \alpha a^2 \left(f^2\right)'' + \beta a^4 f'''' + \gamma b^4 f'''' = 0. \tag{15}$$

Integrating Eq. (15) twice with respect to ξ, yields

$$c^2 f + \alpha a^2 \left(f^2\right) + \beta a^4 f'' + \gamma b^4 f'' = 0, \tag{16}$$

where the integrating constant is considered zero. Balancing

f^2 and f'' in Eq. (12) gives $2N = N + 2$, so $N = 2$. We integrate Eq. (15) with

$$f(\xi) = a_0 + a_1\Phi(\xi) + a_2\Phi^2(\xi). \tag{17}$$

Substituting Eq. (17) into Eq. (16) and equating the coefficient of each power of $\Phi(\xi)$ to zero, we get a system of algebraic equations given below:

$$\begin{aligned}
&c^2a_0 + a^2\alpha a_0^2 = 0,\\
&c^2a_1 + a^4\beta a_1 + b^4\gamma a_1 + 2a^2\alpha a_0 a_1 = 0,\\
&-3a^4\beta a_1 - 3b^4\gamma a_1 + a^2\alpha a_1^2 + c^2a_2\\
&\quad + 4a^4\beta a_2 + 4b^4\gamma a_2 + 2a^2\alpha a_0 a_2 = 0,\\
&2a^4\beta a_1 + 2b^4\gamma a_1 - 10a^4\beta a_2 - 10b^4\gamma a_2 + 2a^2\alpha a_1 a_2 = 0,\\
&6a^4\beta a_2 + 6b^4\gamma a_2 + a^2\alpha a_2^2 = 0.
\end{aligned} \tag{18}$$

Solving the above nonlinear algebraic system, the following results will be concluded as follows.

Case 1.

$$a_0 = 0, a_1 = -\frac{6c^2}{a^2\alpha}, a_2 = \frac{6c^2}{a^2\alpha}, b = \mp\frac{\left(-c^2 - a^4\beta\right)^{1/4}}{\gamma^{1/4}}. \tag{19}$$

Hence, the solution is formed as

$$u_{1,2}(x,y,t) = -\frac{6c^2/a^2\alpha}{1+we^{\xi}} + \frac{6c^2/a^2\alpha}{\left(1+we^{\xi}\right)^2},\ \xi = ax + by - ct - x_0. \tag{20}$$

Case 2.

$$a_0 = -\frac{c^2}{a^2\alpha}, a_1 = \frac{6c^2}{a^2\alpha}, a_2 = -\frac{6c^2}{a^2\alpha}, b = \mp\frac{\left(c^2 - a^4\beta\right)^{1/4}}{\gamma^{1/4}}. \tag{21}$$

Hence, the solution is formed as

$$\begin{aligned}
u_{3,4}(x,y,t) = &-\frac{c^2}{a^2\alpha} + \frac{6c^2/a^2\alpha}{1+we^{\xi}} - \frac{6c^2/a^2\alpha}{\left(1+we^{\xi}\right)^2},\ \xi\\
&= ax + by - ct - x_0.
\end{aligned} \tag{22}$$

Case 3.

$$a_0 = 0, a_1 = -\frac{6c^2}{a^2\alpha}, a_2 = \frac{6c^2}{a^2\alpha}, b = \mp\frac{i\left(-c^2 - a^4\beta\right)^{1/4}}{\gamma^{1/4}}. \tag{23}$$

Hence, the solution is formed as

$$u_{5,6}(x,y,t) = -\frac{6c^2/a^2\alpha}{1+we^{\xi}} + \frac{6c^2/a^2\alpha}{\left(1+we^{\xi}\right)^2},\ \xi = ax + by - ct - x_0. \tag{24}$$

Case 4.

$$a_0 = -\frac{c^2}{a^2\alpha}, a_1 = \frac{6c^2}{a^2\alpha}, a_2 = -\frac{6c^2}{a^2\alpha}, b = \mp\frac{i\left(c^2 - a^4\beta\right)^{1/4}}{\gamma^{1/4}}. \tag{25}$$

Hence, the solution is formed as:

$$\begin{aligned}
u_{7,8}(x,y,t) = &-\frac{c^2}{a^2\alpha} + \frac{6c^2/a^2\alpha}{1+we^{\xi}} - \frac{6c^2/a^2\alpha}{\left(1+we^{\xi}\right)^2},\ \xi\\
&= ax + by - ct - x_0.
\end{aligned} \tag{26}$$

The corresponding dynamic characteristics of the periodic wave solution are plotted in Figures 1 and 2 and arise at spaces $y = -1$, $y = 0$, and $y = 1$, in Figure 3, they arise at spaces $y = -10$, $y = -7$, and $y = 1$, and also in Figure 4, they arise at spaces $y = -10$, $y = 0$, and $y = 1$ with the following special parameters:

$$a = 2, \alpha = 2, \beta = -3, c = 2, \gamma = 2, r = 1, w = 0.3, t = 20, \tag{27}$$

with considering time $t = 20$.

3.2. The (3 + 1)-Dimensional Benjamin-Ono Equation. In this section, we will study the (3 + 1)-dimensional Benjamin-Ono equation which we give as

$$u_{tt} + \alpha\left(u^2\right)_{xx} + \beta u_{xxxx} + \gamma u_{yyyy} + \delta u_{zzzz} = 0, \tag{28}$$

where $u(x,y,z,t)$ is a sufficiently often differentiable function and α, β, γ and δ are nonzero parameters. Also to determine some soliton solutions, we first substitute the transformation

$$u(x,y,z,t) = f(\xi), \xi = ax + by + dz - ct - x_0, \tag{29}$$

into Eq. (28) where

$$\begin{aligned}
&T_{tt}u = c^2f'(\xi), T_xu = af'(\xi), T_{xx}u = a^2f''(\xi),\\
&T_{xxxx}u = a^4f''''(\xi), T_{yyyy}u = b^4f''''(\xi), T_{zzzz}u = d^4f''''(\xi),
\end{aligned} \tag{30}$$

which converts Eq. (28) into a nonlinear ordinary differential equation as follows:

$$c^2f'' + \alpha a^2\left(f^2\right)'' + \beta a^4f'''' + \gamma b^4f'''' + \delta d^4f'''' = 0. \tag{31}$$

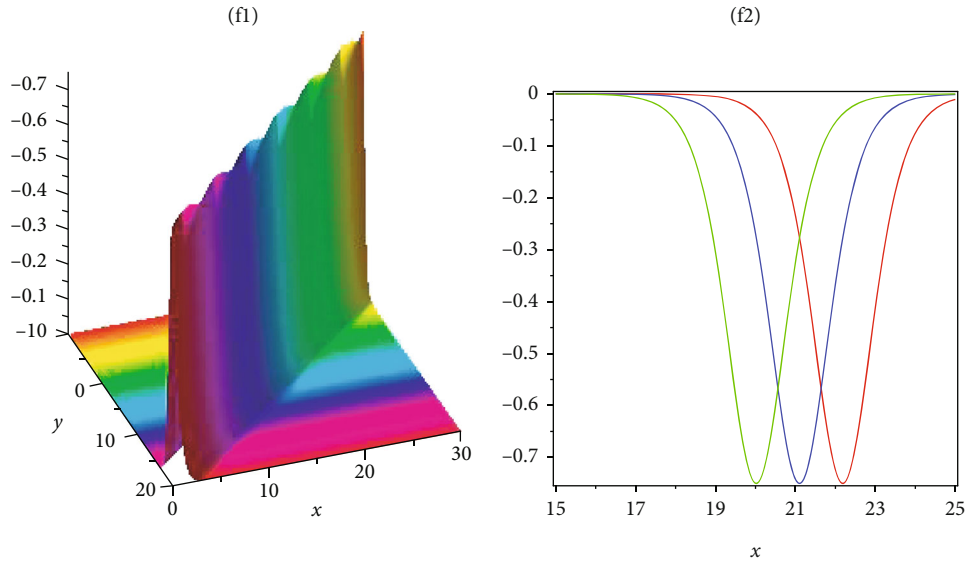

FIGURE 1: Graph of Eq. (20) for the (2 + 1)-dimensional Benjamin-Ono equation at $a = 2$, $\alpha = 2$, $\beta = -3$, $c = 2$, $\gamma = 2$, $r = 1$, $w = 0.3$, $t = 20$ and for 2 plot spaces $y = -1, 0, 1$.

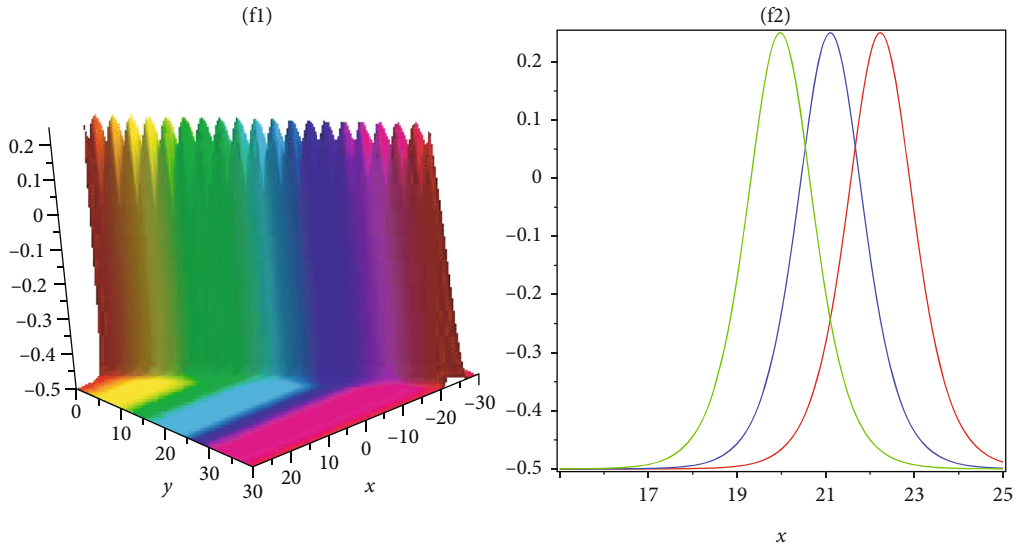

FIGURE 2: Graph of Eq. (22) for the (2 + 1)-dimensional Benjamin-Ono equation at $a = 2$, $\alpha = 2$, $\beta = -3$, $c = 2$, $\gamma = 2$, $r = 1$, $w = 0.3$, $t = 20$ and for 2 plot spaces $y = -1, 0, 1$.

Integrating (31) once with respect to ξ and setting the integrating constant zero yield

$$c^2 f + \alpha a^2 \left(f^2\right) + \beta a^4 f'' + \gamma b^4 f'' + \delta d^4 f'' = 0. \tag{32}$$

Balancing f^2 and f'' in Eq. (32) results to $2N = N + 2$, so $N = 2$. This offers a truncated series as the following form:

$$f(\xi) = a_0 + a_1 \Phi(\xi) + a_2 \Phi^2(\xi). \tag{33}$$

Substituting Eq. (33) into Eq. (32) and equating the coefficient of each power of $\Phi(\xi)$ to zero, we get the following system of algebraic equations:

$$c^2 a_0 + a^2 \alpha a_0^2 = 0,$$

$$c^2 a_1 + a^4 \beta a_1 + b^4 \gamma a_1 + d^4 \delta a_1 + 2a^2 \alpha a_0 a_1 = 0,$$

$$-3a^4 \beta a_1 - 3b^4 \gamma a_1 - 3d^4 \delta a_1 + a^2 \alpha a_1^2 + c^2 a_2 + 4a^4 \beta a_2 + 4b^4 \gamma a_2 + 4d^4 \delta a_2 + 2a^2 \alpha a_0 a_2 = 0,$$

$$2a^4 \beta a_1 + 2b^4 \gamma a_1 + 2d^4 \delta a_1 - 10a^4 \beta a_2 - 10b^4 \gamma a_2 - 10d^4 \delta a_2 + 2a^2 \alpha a_1 a_2 = 0,$$

$$6a^4 \beta a_2 + 6b^4 \gamma a_2 + 6d^4 \delta a_2 + a^2 \alpha a_2^2 = 0. \tag{34}$$

Solving the above system, yields the following.

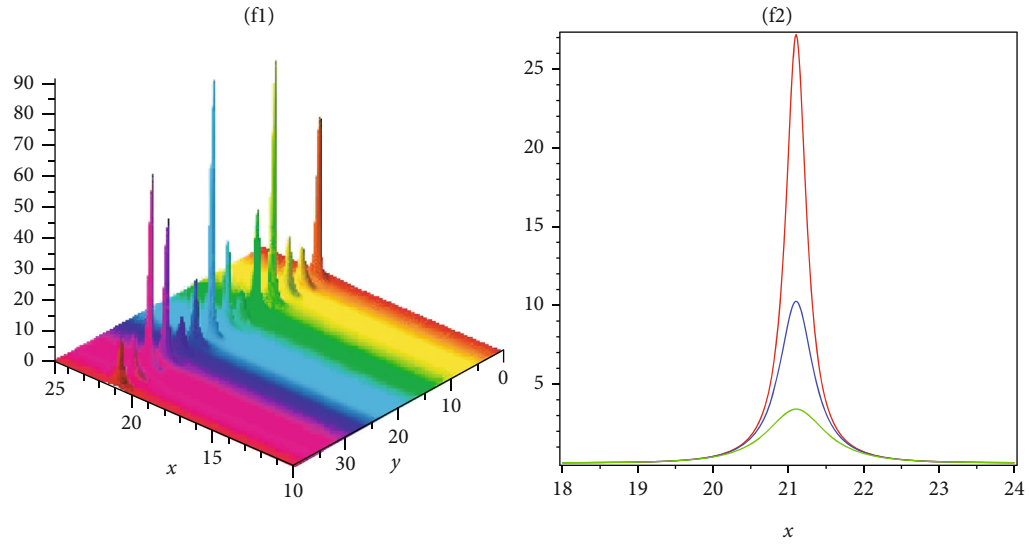

Figure 3: Graph of the absolute value of Eq. (24) for the (2 + 1)-dimensional Benjamin-Ono equation at $a = 2, \alpha = 2, \beta = -3, c = 2, \gamma = 2, r = 1, w = 0.3, t = 20$ and for 2 plot spaces $y = -10, -7, 1$.

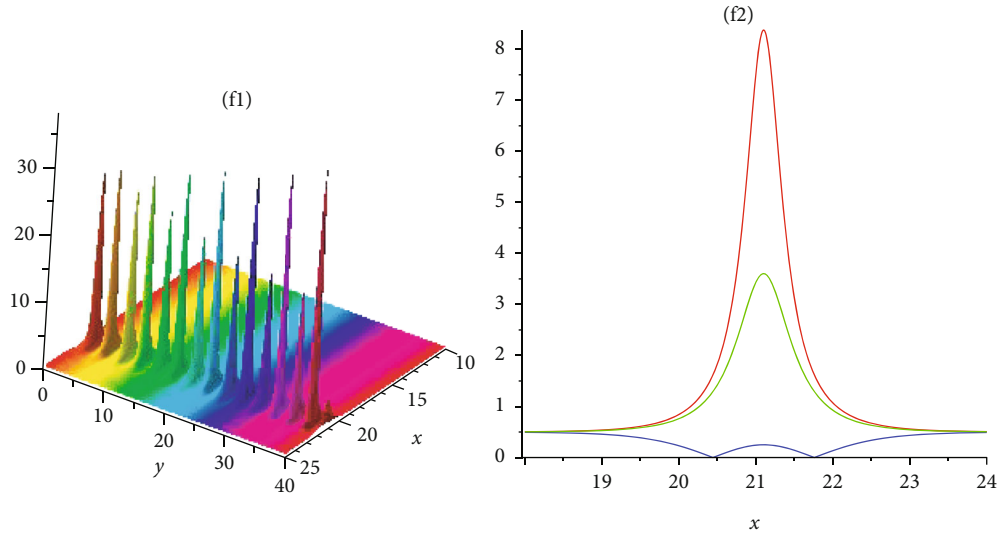

Figure 4: Graph of the absolute value of Eq. (42) for the (2 + 1)-dimensional Benjamin-Ono equation at $a = 2, \alpha = 2, \beta = -3, c = 2, \gamma = 2, r = 1, w = 0.3, t = 20$ and for 2 plot spaces $y = -10, 0, 1$.

Case 1.

$$a_0 = 0, a_1 = -\frac{6c^2}{a^2\alpha}, a_2 = \frac{6c^2}{a^2\alpha}, b = \mp\frac{\left(-c^2 - a^4\beta - d^4\delta\right)^{1/4}}{\gamma^{1/4}}. \tag{35}$$

Hence, the solution is formed as

$$u_{1,2}(x, y, z, t) = -\frac{6c^2/a^2\alpha}{1 + we^{\xi}} + \frac{6c^2/a^2\alpha}{\left(1 + we^{\xi}\right)^2}, \xi = ax + by + dz - ct - x_0. \tag{36}$$

Case 2.

$$a_0 = -\frac{c^2}{a^2\alpha}, a_1 = \frac{6c^2}{a^2\alpha}, a_2 = -\frac{6c^2}{a^2\alpha}, b = \mp\frac{\left(c^2 - a^4\beta - d^4\delta\right)^{1/4}}{\gamma^{1/4}}. \tag{37}$$

Hence, the solution is formed as

$$u_{3,4}(x, y, t) = -\frac{c^2}{a^2\alpha} + \frac{6c^2/a^2\alpha}{1 + we^{\xi}} - \frac{6c^2/a^2\alpha}{\left(1 + we^{\xi}\right)^2}, \xi = ax + by + dz - ct - x_0. \tag{38}$$

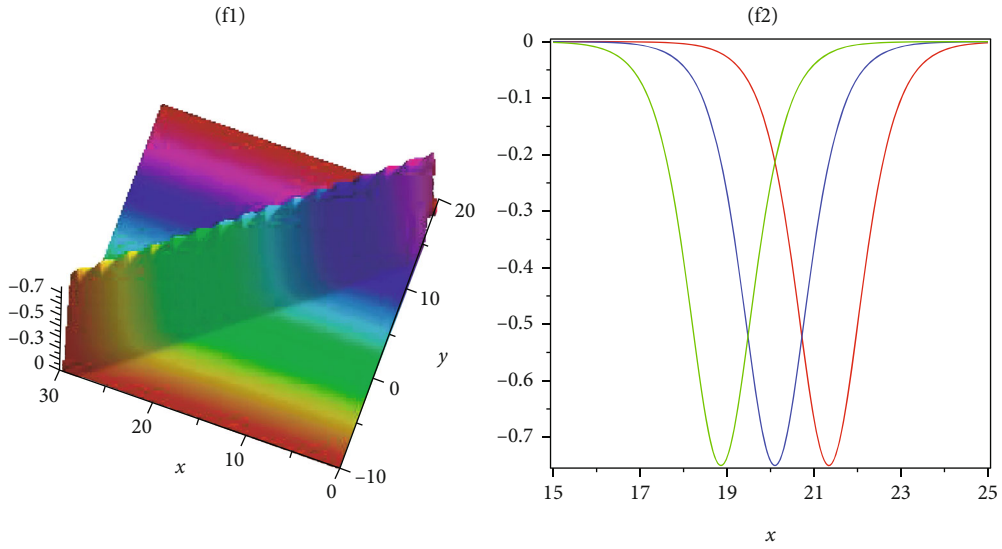

Figure 5: Graph of Eq. (36) for the (2 + 1)-dimensional Benjamin-Ono equation at $a = 2, \alpha = 2, \beta = -3, c = 2, \gamma = 2, r = 1, w = 0.3, d = 2, \delta = -2, z = 1, t = 20$ and for 2 plot spaces $y = -1, 0, 1$.

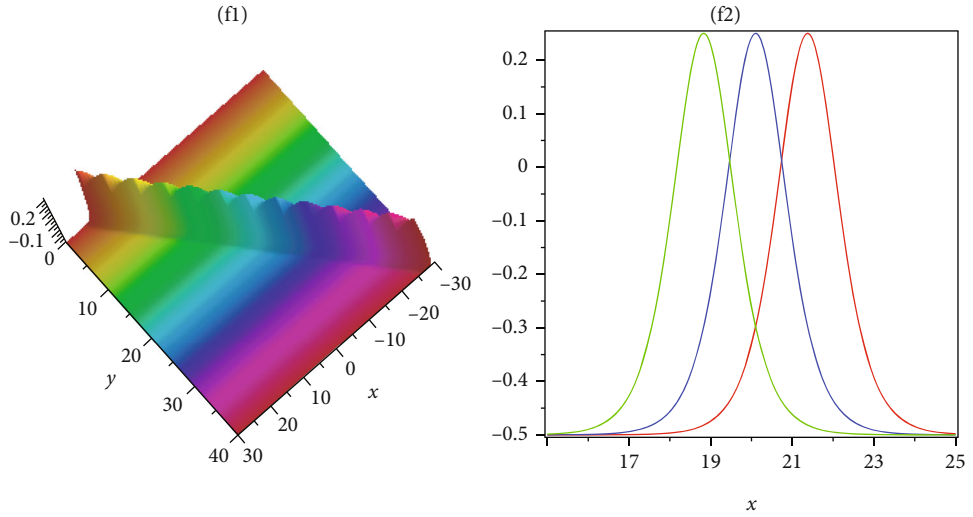

Figure 6: Graph of Eq. (38) for the (2 + 1)-dimensional Benjamin-Ono equation at $a = 2, \alpha = 2, \beta = -3, c = 2, \gamma = 2, r = 1, w = 0.3, d = 2, \delta = -2, z = 1, t = 20$ and for 2 plot spaces $y = -1, 0, 1$.

Case 3.

$$a_0 = 0, a_1 = -\frac{6c^2}{a^2\alpha}, a_2 = \frac{6c^2}{a^2\alpha}, b = \mp\frac{i\left(-c^2 - a^4\beta - d^4\delta\right)^{1/4}}{\gamma^{1/4}}. \tag{39}$$

Hence, the solution is formed as

$$u_{5,6}(x, y, t) = -\frac{6c^2/a^2\alpha}{1 + we^{\xi}} + \frac{6c^2/a^2\alpha}{\left(1 + we^{\xi}\right)^2}, \xi = ax + by + dz - ct - x_0. \tag{40}$$

Case 4.

$$a_0 = -\frac{c^2}{a^2\alpha}, a_1 = \frac{6c^2}{a^2\alpha}, a_2 = -\frac{6c^2}{a^2\alpha}, b = \mp\frac{i\left(c^2 - a^4\beta - d^4\delta\right)^{1/4}}{\gamma^{1/4}}. \tag{41}$$

Hence, the solution is formed as

$$u_{7,8}(x, y, t) = -\frac{c^2}{a^2\alpha} + \frac{6c^2/a^2\alpha}{1 + \mathrm{we}(\xi)} - \frac{6c^2/a^2\alpha}{\left(1 + we^{\xi}\right)^2}, \xi = ax + by + dz - ct - x_0. \tag{42}$$

The corresponding dynamic characteristics of the periodic wave solution are plotted in Figures 5 and 6 and arise at spaces $y = -1$, $y = 0$, and $y = 1$, in Figure 7, they arise at

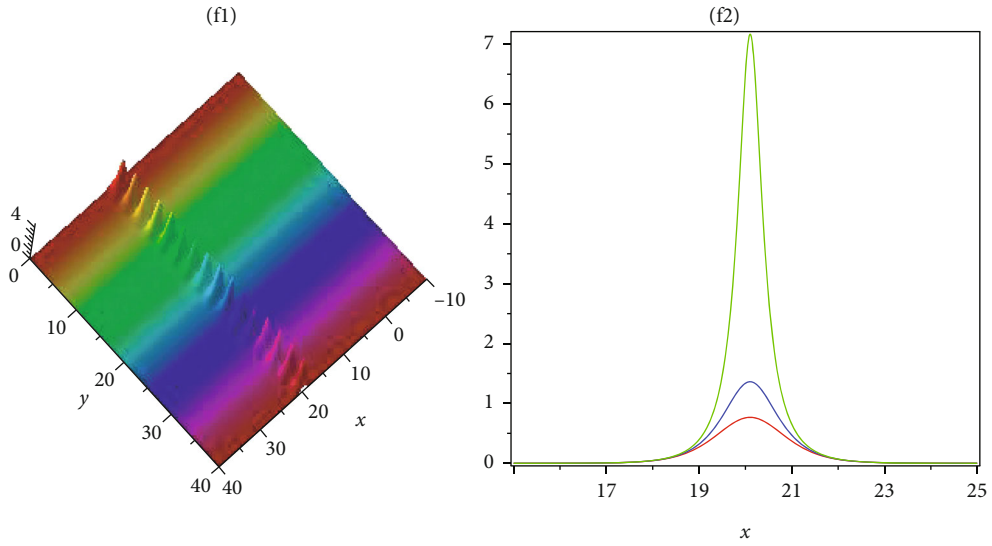

Figure 7: Graph of the absolute value of Eq. (40) for the (2 + 1)-dimensional Benjamin-Ono equation at $a = 2, \alpha = 2, \beta = -3, c = 2, \gamma = 2, r = 1, w = 0.3, d = 2, \delta = -2, z = 1, t = 20$ and for 2 plot spaces $y = -10, -7, 1$.

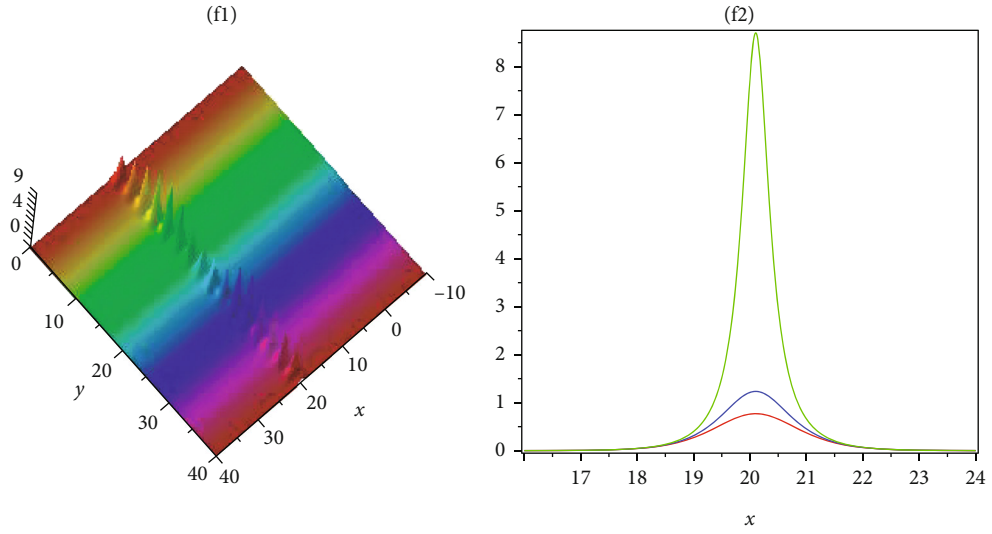

Figure 8: Graph of the absolute value of Eq. (42) for the (2 + 1)-dimensional Benjamin-Ono equation at $a = 2, \alpha = 2, \beta = -3, c = 2, \gamma = 2, r = 1, w = 0.3, d = 2, \delta = -2, z = 1, t = 20$ and for 2 plot spaces $y = -10, -3, 1$.

spaces $y = -10$, $y = -7$, and $y = 1$, and also in Figure 4, they arise at spaces $y = -10$, $y = 0$, and $y = 1$ with the following special parameters:

$$a = 2, \alpha = 2, \beta = -3, c = 2, \gamma = 2, r = 1, w = 0.3, d = 2, \delta = -2, \tag{43}$$

considering space and time $z = 1, t = 20$.

4. Some Graphical Illustrations

We depict in this section some graphical illustrations of the obtained solutions for the (2 + 1)- and (3 + 1)-dimensional extensions of the Benjamin-Ono equations, both the two and three dimensional plots for the solutions are plotted. Figures 1 and 4 show the graph of the solutions (20)–(26) for the (2 + 1)-dimensional Benjamin-Ono equation, respectively. Figures 5 and 8 show the behavior of the solutions (36)–(42) for the (3 + 1)-dimensional Benjamin-Ono equation, respectively.

5. Conclusion

In conclusion, we have presented new solitary wave solutions for the (2 + 1)-dimensional Benjamin-Ono equation introduced recently by Wazwaz and also extended it to (3 + 1)-dimensional spaces called the (3 + 1)-dimensional Benjamin-Ono equation. While constructing the solitary wave solutions, we make use of the Kudryashov method

being one of the powerful integration methods for treating various nonlinear evolution equations and construct various exponential solutions to both equations. The development of offered method may allow the extensions of the Benjamin-Ono equations to be used in more general configurations. The solutions are all verified by putting them back into the original equations with the aid of the Maple symbolic computation package 18.

Data Availability

The data used to support the findings of this study are available from the corresponding author upon request.

Conflicts of Interest

The authors declare that they have no conflict of interest.

Acknowledgments

Lan Wu and Xiao Zhang contributed equally to this work.

References

[1] T. B. Benjamin, "Internal waves of permanent form in fluids of great depth," *Journal of Fluid Mechanics*, vol. 29, no. 3, pp. 559–592, 1967.

[2] Y. Matsuno, "Exact multi-soliton solution of the Benjamin-Ono equation," *Journal of Physics A: Mathematical and General*, vol. 12, no. 4, pp. 619–621, 1979.

[3] D. M. Ambrose and J. J. Wilkening, "Computation of time-periodic solutions of the Benjamin–Ono equation," *Journal of Nonlinear Science*, vol. 20, no. 3, pp. 277–308, 2010.

[4] J. Angulo, M. Scialom, and C. Banquet, "The regularized Benjamin-Ono and BBM equations: well-posedness and nonlinear stability," *Journal of Differential Equations*, vol. 250, no. 11, pp. 4011–4036, 2011.

[5] Y. Tutiya and J. Shiraishi, "On some special solutions to periodic Benjamin-Ono equation with discrete Laplacian," *Mathematics and Computers in Simulation*, vol. 82, no. 7, pp. 1341–1347, 2012.

[6] L. Song, W. Chen, Z. Xu, and H. Chen, "Rogue wave for the Benjamin Ono equation," *Advances in Pure Mathematics*, vol. 5, no. 2, pp. 82–87, 2015.

[7] Y. K. Liu and B. Li, "Dynamics of rogue waves on multisoliton background in the Benjamin Ono equation," *Pramana-Journal of Physics*, vol. 88, no. 4, p. 57, 2017.

[8] M. J. Ablowitz, A. Demirci, and Y. P. Ma, "Dispersive shock waves in the Kadomtsev-Petviashvili and two dimensional Benjamin-Ono equations," *Physica D: Nonlinear Phenomena*, vol. 333, pp. 84–98, 2016.

[9] A. Esfahani and S. Levandosky, "Solitary waves of the rotation-generalized Benjamin-Ono equation," 2011, https://arxiv.org/abs/1105.5369.

[10] C. Muñoz and G. Ponce, "On the asymptotic behavior of solutions to the Benjamin-Ono equation," *Proceedings of the American Mathematical Society*, vol. 147, pp. 5303–5312, 2019.

[11] W. Tan and Z. Dai, "Spatiotemporal dynamics of lump solution to the (1+1)-dimensional Benjamin-Ono equation," *Nonlinear Dynamics*, vol. 89, no. 4, pp. 2723–2728, 2017.

[12] A. Wazwaz, "A $(2+1)$-dimensional extension of the Benjamin-Ono equation," *International Journal of Numerical Methods Heat Fluid and Flow*, vol. 28, no. 11, pp. 2681–2687, 2018.

[13] A. A. Gaber, A. F. Aljohani, A. Ebaid, and J. T. Machado, "The generalized Kudryashov method for nonlinear space-time fractional partial differential equations of Burgers type," *Nonlinear Dynamics*, vol. 95, no. 1, pp. 361–368, 2019.

[14] S. Tuluce Demiray, Y. Pandir, and H. Bulut, "Generalized Kudryashov method for time-fractional differential equations," *Abstract and Applied Analysis*, vol. 2014, Article ID 901540, 13 pages, 2014.

[15] J. Manafian and M. Lakestani, "Optical solitons with Biswas-Milovic equation for Kerr law nonlinearity," *The European Physical Journal Plus*, vol. 130, article 61, 2015.

[16] J. Manafian and S. Heidari, "Periodic and singular kink solutions of the Hamiltonian amplitude equation," *Advanced Mathematical Models & Applications*, vol. 4, pp. 134–149, 2019.

[17] H. M. Baskonus, D. A. Koç, and H. Bulut, "New travelling wave prototypes to the nonlinear Zakharov-Kuznetsov equation with power law nonlinearity," *Nonlinear Science Letters A*, vol. 7, pp. 67–76, 2016.

[18] M. Dehghan, J. Manafian, and A. Saadatmandi, "Solving nonlinear fractional partial differential equations using the homotopy analysis method," *Numerical Methods for Partial Differential Equations*, vol. 26, no. 2, pp. 448–479, 2010.

[19] M. Dehghan, J. Manafian, and A. Saadatmandi, "Analytical treatment of some partial differential equations arising in mathematical physics by using the Exp-function method," *International Journal of Modern Physics B*, vol. 25, pp. 2965–2981, 2011.

[20] J. Manafian, "Novel solitary wave solutions for the (3+1)-dimensional extended Jimbo-Miwa equations," *Computers & Mathematics with Applications*, vol. 76, no. 5, pp. 1246–1260, 2018.

[21] A. R. Seadawy and J. Manafian, "New soliton solution to the longitudinal wave equation in a magneto-electro-elastic circular rod," *Results in Physics*, vol. 8, pp. 1158–1167, 2018.

[22] J. Manafian, S. A. Mohammed, A. Alizadeh, H. M. Baskonus, and W. Gao, "Investigating lump and its interaction for the third-order evolution equation arising propagation of long waves over shallow water," *European Journal of Mechanics - B/Fluids*, vol. 84, pp. 289–301, 2020.

[23] M. Eslami and H. Rezazadeh, "The first integral method for Wu-Zhang system with conformable time-fractional derivative," *Calcolo*, vol. 53, no. 3, pp. 475–485, 2016.

[24] N. A. Kudryashov, "One method for finding exact solutions of nonlinear differential equations," *Communications in Nonlinear Science and Numerical Simulation*, vol. 17, no. 6, pp. 2248–2253, 2012.

[25] S. Garai, A. G. Choudhury, and J. Dan, "On the solution of certain higher-order local and nonlocal nonlinear equations in optical fibers using Kudryashov's approach," *Optik*, vol. 222, p. 165312, 2020.

[26] M. M. Hassan, M. A. Abdel-Razek, and A. A. H. Shoreh, "New exact solutions of some (2 + 1)-dimensional nonlinear evolution equations via extended Kudryashov method," *Reports on Mathematical Physics*, vol. 74, no. 3, pp. 347–358, 2014.

[27] F. Mahmud, M. Samsuzzoh, and M. A. Akbar, "The generalized Kudryashov method to obtain exact traveling wave

solutions of the PHI-four equation and the Fisher equation," *Results in Physics*, vol. 7, pp. 4296–4302, 2017.

[28] I. Karahan and M. Ozdemir, "A new iterative projection method for approximating fixed point problems and variational inequality problems," *Proceedings of the Institute of Mathematics and Mechanics*, vol. 40, pp. 68–79, 2014.

[29] Y. Y. Mammadov, "Weighted inequalities for Dunkl fractional maximal function and Dunkl fractional integrals," *Proceedings of the Institute of Mathematics and Mechanics*, vol. 40, pp. 93–103, 2014.

[30] B. Ren, "Painlevé analysis, soliton molecule, and lump solution of the higher-order Boussinesq equation," *Advances in Mathematical Physics*, vol. 2021, Article ID 6687632, 6 pages, 2021.

[31] I. Mahmood and M. Waseem, "Lax representation and Darboux solutions of the classical Painlevé second equation," *Advances in Mathematical Physics*, vol. 2021, Article ID 8851043, 5 pages, 2021.

Hindawi
Advances in Mathematical Physics
Volume 2021, Article ID 5545984, 7 pages
https://doi.org/10.1155/2021/5545984

Research Article

Characteristics of the Soliton Molecule and Lump Solution in the $(2+1)$-Dimensional Higher-Order Boussinesq Equation

Bo Ren

Institute of Nonlinear Science, Shaoxing University, Shaoxing 312000, China

Correspondence should be addressed to Bo Ren; renbosemail@163.com

Received 1 February 2021; Revised 19 March 2021; Accepted 25 March 2021; Published 10 April 2021

Academic Editor: Mohammad Mirzazadeh

The soliton molecules, as bound states of solitons, have attracted considerable attention in several areas. In this paper, the $(2+1)$-dimensional higher-order Boussinesq equation is constructed by introducing two high-order Hirota operators in the usual $(2+1)$-dimensional Boussinesq equation. By the velocity resonance mechanism, the soliton molecule and the asymmetric soliton of the higher-order Boussinesq equation are constructed. The soliton molecule does not exist for the usual $(2+1)$-dimensional Boussinesq equation. As a special kind of rational solution, the lump wave is localized in all directions and decays algebraically. The lump solution of the higher-order Boussinesq equation is obtained by using a quadratic function. This lump wave is just the bright form by some detail analysis. The graphics in this study are carried out by selecting appropriate parameters. The results in this work may enrich the variety of the dynamics of the high-dimensional nonlinear wave field.

1. Introduction

The $(2+1)$-dimensional Boussinesq equation can describe the propagation of small-amplitude long waves in shallow water. The physical and dynamical structures of the $(2+1)$-dimensional Boussinesq equation are investigated by using various methods [1–4]. The $(2+1)$-dimensional Boussinesq equation reads

$$u_{tt} + \gamma u_{xx} + 3\gamma\left(u^2\right)_{xx} - \alpha u_{xxxx} + \mu u_{yy} = 0, \tag{1}$$

where α, γ, and μ are arbitrary constants. It can be transformed into the Hirota form:

$$\left(D_t^2 + \gamma D_x^2 - \alpha D_x^4 + \mu D_y^2\right) f \cdot f = 0, \tag{2}$$

with the dependent variable transformation:

$$u = 2(\ln f)_{xx}. \tag{3}$$

The $(2+1)$-dimensional Boussinesq equation reduces the $(1+1)$-dimensional Boussinesq form with $\mu = 0$. The $(1+1)$-dimensional Boussinesq equation includes the "good" Boussinesq form and "bad" Boussinesq form with $\alpha < 0$ and $\alpha > 0$, respectively [5]. Investigating deeper into properties of this model (1), the extended $(2+1)$-dimensional Boussinesq equations are introduced based on the usual Boussinesq equation (1) [6, 7]. The topological kink-type soliton solutions of the extended $(2+1)$-dimensional Boussinesq equation are obtained by the sine-Gordon expansion method [6]. The modified exponential expansion method is applied to the coupled Boussinesq equation [7]. The multisoliton solutions, breather solutions, and rogue waves of the generalized Boussinesq equation are obtained via the symbolic computation method [8] and the polynomial functions in the bilinear form [9]. Generally, seeking exact solutions to nonlinear evolution equations is a vital task in soliton theory. Many methods have been proved effective in finding the exact solutions of the soliton equation [10–12]. By using the extended auxiliary equation method and the extended

direct algebraic method, the solitary traveling wave solutions and the stability of these solutions are analyzed [10–12]. In this work, we shall study the soliton molecule and lump wave of the higher-order Boussinesq equation by solving the bilinear form of the higher-order Boussinesq equation.

The soliton molecule which is formed by the balance of repulsive and attractive forces between solitons is treated as a boundary state [13]. It was first predicted within the framework of the nonlinear Schrödinger-Ginzburg-Landau equation [14]. Many effects including nonlinear and dispersive effects are a key role in the soliton molecule. The soliton molecule has become a focus of intense research in both experiment and simulation [13–17]. The theoretical frameworks to address the soliton molecule have been introduced [18, 19]. Recently, Lou proposed the velocity resonance mechanism to construct the soliton molecules of the $(1+1)$-dimensional nonlinear systems [20]. The velocity resonance mechanism is one of the useful methods to form the soliton molecule [20]. To balance the nonlinear effects, the high-order dispersive terms may play a key role in the velocity resonance mechanism [21]. The soliton molecule of a variety of integrable systems has been verified with the velocity resonance mechanism: the fifth-order Korteweg-de Vries (KdV) equation [22, 23], the modified KdV equation [24, 25], the $(3+1)$-dimensional Boiti-Leon-Manna-Pempinelli equation [26], and so on [27]. The dynamics between soliton molecules and breather solutions and between soliton molecules and dromions are presented by the velocity resonance mechanism, the Darboux transformation, and the variable separation approach [25–28].

In this paper, we try to construct the $(2+1)$-dimensional higher-order Boussinesq equation which possesses the soliton molecule. The soliton molecule is absent in the usual $(2+1)$-dimensional Boussinesq equation. This paper is organized as follows. In Section 2, the soliton molecule and the asymmetric soliton of the $(2+1)$-dimensional higher-order Boussinesq equation are constructed by the velocity resonance condition. In Section 3, the lump solution of the higher-order Boussinesq equation is obtained by solving the corresponding Hirota bilinear form. Finally, the conclusions of this paper follow in the last section.

2. Soliton Molecule for the $(2+1)$-Dimensional Higher-Order Boussinesq Equation

Based on the bilinear form of the $(2+1)$-dimensional Boussinesq equation, we can construct the higher-order form by introducing the high-order Hirota operators (D_x^6 and D_y^4):

$$\left(D_t^2+\gamma D_x^2-\alpha D_x^4-\beta D_x^6+\mu D_y^2+\nu D_y^4\right)f\cdot f=0, \tag{4}$$

where D is the bilinear derivative operator [29]:

$$\begin{aligned} D_x^l D_y^n D_t^m (f\cdot g)=&\left(\frac{\partial}{\partial x}-\frac{\partial}{\partial x'}\right)^l\left(\frac{\partial}{\partial y}-\frac{\partial}{\partial y'}\right)^n\\ &\left(\frac{\partial}{\partial t}-\frac{\partial}{\partial t'}\right)^m f(x,y,t)\\ &\cdot g\left(x',y',t'\right)\Big|_x{}^{\prime=x,y=y',t\prime=t}. \end{aligned} \tag{5}$$

Two-soliton solution of the higher-order Boussinesq equation can be calculated as

$$f=1+\exp(\eta_1)+\exp(\eta_2)+a_{12}\exp(\eta_1+\eta_2), \tag{6}$$

where $\eta_i=k_ix+l_iy+\omega_it+c_i\,(i=1,2)$. By substituting (6) into (4), the phase shift a_{12} and the dispersion relation are written as

$$\begin{aligned} a_{12}&=\frac{2\gamma k_1k_2+2\mu l_1l_2+2\nu l_1l_2(2L-3l_1l_2)-2\alpha k_1k_2(2K-3k_1k_2)-k_1k_2\left(6K^2-15k_1k_2K+8k_1^2k_2^2\right)+2\omega_1\omega_2}{2\gamma k_1k_2+2\mu l_1l_2+2\nu l_1l_2(2L+3l_1l_2)-2\alpha k_1k_2(2K+3k_1k_2)-k_1k_2\left(6K^2+15k_1k_2K+8k_1^2k_2^2\right)+2\omega_1\omega_2},\\ K&=k_1^2+k_2^2,\\ L&=l_1^2+l_2^2,\\ \omega_i^2&+\gamma k_i^2-\alpha k_i^4-\beta k_i^6+\mu l_i^2+\nu l_i^4=0. \end{aligned} \tag{7}$$

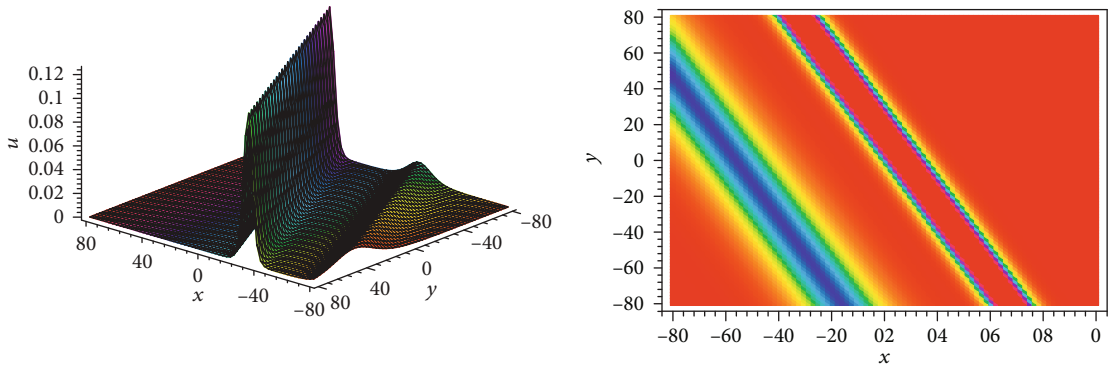

(a) (b)

Figure 1: (a) Soliton molecule of the $(2+1)$-dimensional higher-order Boussinesq equation. (b) Density plot of the corresponding soliton molecule.

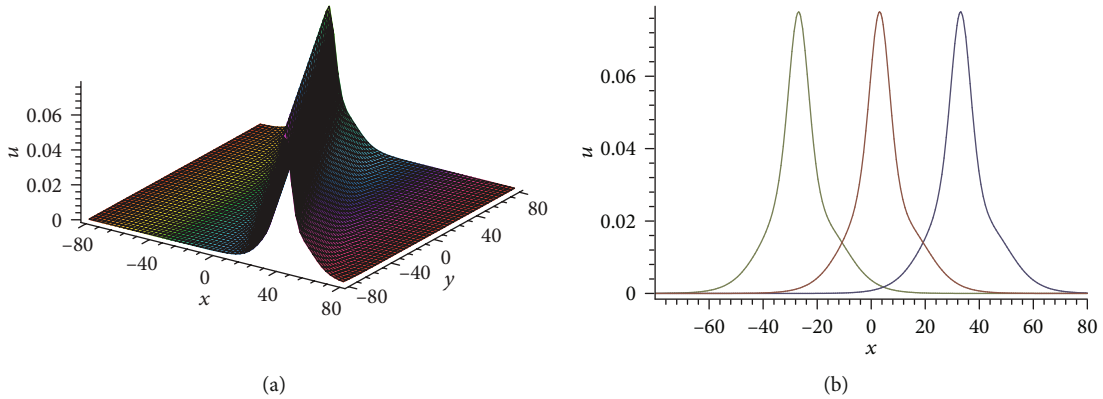

(a) (b)

Figure 2: (a) Asymmetric soliton of the $(2+1)$-dimensional higher-order Boussinesq equation. (b) The wave propagation pattern along the x-axis by selecting different times $t = 60$, $t = 0$, and $t = -60$ (from left to right).

The soliton molecule can be constructed with the velocity resonance condition [30]. The velocity resonance condition $(k_i \neq k_j)$ reads

$$\frac{k_i}{k_j} = \frac{l_i}{l_j} = \frac{\omega_i}{\omega_j} = \frac{\sqrt{\alpha k_i^4 + \beta k_i^6 - \gamma k_i^2 - \mu l_i^2 - \nu l_i^4}}{\sqrt{\alpha k_j^4 + \beta k_j^6 - \gamma k_j^2 - \mu l_j^2 - \nu l_j^4}}. \tag{8}$$

By solving condition (8), the velocity resonant condition becomes

$$k_j = \pm \frac{\sqrt{\beta\left(\nu l_i^4 - \alpha k_i^4 - \beta k_i^6\right)}}{k_i^2},$$
$$l_j = \pm \frac{l_i\sqrt{\beta\left(\nu l_i^4 - \alpha k_i^4 - \beta k_i^6\right)}}{k_i^3}. \tag{9}$$

Above velocity resonant condition (9) cannot be obtained while equation (4) is absent in the high-order Hirota operators D_x^6 and D_y^4. A soliton molecule and an asymmetric soliton can be constructed by selecting appropriate parameters in (8) or (9). These phenomena are shown in Figures 1 and 2. We select the same parameters and different phases for Figures 1 and 2. The parameters are

$$k_1 = \frac{1}{2},$$
$$k_2 = \frac{\sqrt{2}}{8},$$
$$l_1 = \frac{1}{4},$$
$$l_2 = \frac{\sqrt{2}}{16},$$
$$\alpha = -\frac{1}{4},$$
$$\beta = 1,$$
$$\gamma = -1,$$
$$\mu = 1,$$
$$\nu = \frac{1}{2}. \tag{10}$$

The phases of Figures 1 and 2 are $c_1 = 0$, $c_2 = 10$ and c_1

$= 0, c_2 = 1$, respectively. The soliton molecule and the asymmetric soliton are described in Figures 1 and 2. The soliton molecule and the asymmetric soliton can be transformed with each other by selecting different parameters. Two solitons in the molecule have different amplitudes, while two solitons in the molecule possess the same velocity.

3. Lump Solution of the $(2+1)$-Dimensional Higher-Order Boussinesq Equation

Lump solutions, which can be considered a kind of rational function solutions, decay polynomially in all directions of space [31–36]. One can construct lump solutions by the Hirota bilinear method and the Darboux transformation [37–45]. Lump waves of the high-dimensional nonlinear systems are constructed by solving the Hirota bilinear method [46–49]. A symbolic computation approach is one of the useful methods to search the lump wave [31]. The interaction between the lump waves and other complicated waves is presented by the symbolic computation approach [38–43]. In this section, we shall study the dynamics of lump waves by using the symbolic computation approach.

To obtain the lump solution of the $(2+1)$-dimensional higher-order Boussinesq equation, a quadratic function of f is shown as

$$f = (a_1x + a_2y + a_3t)^2 + (a_4x + a_5y + a_6t)^2 + a_7, \tag{11}$$

where $a_i\,(i = 1, 2, \cdots, 7)$ are arbitrary constants. By substituting (11) into the Hirota bilinear form (4) and balancing the different powers of x, y, and t, the parameters are constrained as the following three cases.

Case 1.

$$\begin{aligned} a_1 &= \sqrt{\frac{\mu a_5^2 + a_6^2}{\gamma}}, \\ a_2 &= \frac{a_3 a_5}{a_6}, \\ a_4 &= \frac{a_3}{a_6}\sqrt{\frac{\mu a_5^2 + a_6^2}{\gamma}}, \\ a_7 &= -\frac{3\nu a_5^4\left(a_3^2 + a_6^2\right)}{a_6^2\left(\mu a_5^2 + a_6^2\right)} + \frac{3\alpha\left(a_3^2 + a_6^2\right)\left(\mu a_5^2 + a_6^2\right)}{\gamma^2 a_6^2}. \end{aligned} \tag{12}$$

The solution of u can be localized in the (x, y)-plane with the parameters satisfying

$$\begin{aligned} &\mu\nu > 0, \\ &a_7 > 0. \end{aligned} \tag{13}$$

Case 2.

$$\begin{aligned} a_1 &= \frac{-\mu a_5^2 + a_6^2}{\gamma}, \\ a_2 &= -a_5, \\ a_4 &= \frac{-\mu a_5^2 + a_6^2}{\gamma}, \\ a_7 &= \frac{6\alpha\left(\mu a_5^2 - a_6^2\right)^2}{\gamma^2 a_6^2} - \frac{6\nu a_5^4}{a_6^2}. \end{aligned} \tag{14}$$

Case 3.

$$\begin{aligned} a_1 &= \frac{-\mu a_5^2 + a_6^2}{\gamma}, \\ a_3 &= -a_6, \\ a_4 &= \frac{-\mu a_5^2 + a_6^2}{\gamma}, \\ a_7 &= \frac{6\alpha\left(\mu a_5^2 - a_6^2\right)^2}{\gamma^2 a_6^2} - \frac{6\nu a_5^4}{a_6^2}. \end{aligned} \tag{15}$$

In order to localize the solution of u in the (x, y)-plane for Cases 2 and 3, the parameters should be satisfied:

$$\alpha\left(\mu a_5^2 - a_6^2\right)^2 - \nu\gamma^2 a_5^4 > 0. \tag{16}$$

Take Case 1 as an example to describe the dynamics of lump waves. By substituting (11) into (3), the lump wave of the $(2+1)$-dimensional higher-order Boussinesq equation in Case 1 is generated:

$$u = \frac{4\left(a_3^2 + a_6^2\right)\left(\mu a_5^2 + a_6^2\right)}{\gamma a_6^2 f} - \frac{8\left(a_3^2 + a_6^2\right)^2\left(\mu a_5^2 + a_6^2\right)^2 x^2}{\gamma^2 a_6^4 f^2}. \tag{17}$$

To describe the lump wave of the $(2+1)$-dimensional higher-order Boussinesq equation, the parameters are selected as

$$\begin{aligned} \alpha &= 1, \\ \gamma &= 1, \\ a_3 &= 1, \\ a_5 &= 3, \\ a_6 &= 2, \\ \mu &= 1, \\ \nu &= \frac{1}{2}. \end{aligned} \tag{18}$$

The spatiotemporal structure and the density of a lump wave are described in Figures 3(a) and 3(b), respectively.

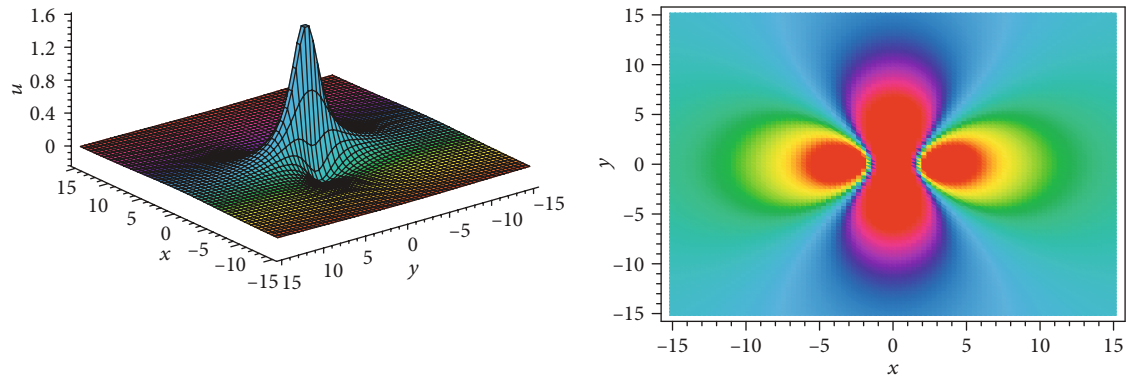

Figure 3: (a) The three-dimensional plot of a lump wave of the $(2+1)$-dimensional higher-order Boussinesq equation with the parameters in (18). (b) The corresponding density plot.

The critical points of the lump wave are solved:

$$\frac{\partial u(x,y,t)}{\partial x} = 0, \qquad \frac{\partial u(x,y,t)}{\partial y} = 0. \tag{19}$$

By solving above condition (19), we find that the function u reaches the maximum value at the point $(0,-(a_6/a_5)t)$ and the minimum values at two points $(\pm(3\sqrt{\alpha(\mu a_5^2+a_6^2)^2-\nu\gamma^2 a_5^2})/(\sqrt{\gamma}(\mu a_5^2+a_6^2)),-(a_6/a_5)t)$. By substituting above three points values into (17), the maximum and minimum values of the function u are $(4\gamma(\mu a_5^2+a_6^2)^2)/(3(\alpha(\mu a_5^2+a_6^2)^2-\nu\gamma^2 a_5^2))$ and $-(\gamma(\mu a_5^2+a_6^2)^2)/(6(\alpha(\mu a_5^2+a_6^2)^2-\nu\gamma^2 a_5^2))$, respectively. The value of the maximum point is bigger than zero due to $a_7>0$. The ratio between the maximum and minimum amplitudes is 8. The lump wave of the higher-order Boussinesq equation is just the bright form by the above detail analysis.

4. Conclusion

In summary, the soliton molecule and lump solution of the $(2+1)$-dimensional higher-order Boussinesq equation are studied by solving the Hirota bilinear form (4). The soliton molecule and the asymmetric soliton are obtained by the velocity resonance mechanism. The lump solution can be derived by using a positive quadratic function. The lump wave of the higher-order Boussinesq equation is just the bright form after some detail analysis. Figures 1–3 show the dynamics of the soliton molecule and lump wave by putting suitable parameters. The soliton molecule and the asymmetric soliton can be transformed with each other by selecting different phases. The soliton molecule and the asymmetric soliton cannot be derived in the $(2+1)$-dimensional Boussinesq equation (1).

In this paper, the $(2+1)$-dimensional higher-order Boussinesq equation is constructed by introducing the high-order Hirota bilinear operators D_x^6 and D_y^4 based on the usual $(2+1)$-dimensional Boussinesq equation. Similar to introducing the high-order Hirota bilinear operator procedure, we propose one equation

$$\left(D_t^2+\gamma D_x^2-\sum_{i=1}^{n}\left(\alpha_i D_x^{2+2i}\right)+\sum_{j=1}^{m}\left(\beta_j D_y^{2j}\right)\right) f\cdot f=0, \tag{20}$$

with α_i and β_j being arbitrary constants. The soliton molecule and lump wave of (20) are worthy of study by the velocity resonance mechanism and the symbolic computation approach. Rogue waves are unexpectedly high-amplitude single waves that have been reported by using the Hirota bilinear method [50, 51]. These nonlinear excitations of (20) are valuable to increase understanding of the phenomena between different nonlinear waves.

Data Availability

The datasets supporting the conclusions of this article are included in the article.

Conflicts of Interest

The authors declare that they have no conflict of interest.

Acknowledgments

This work is supported by the National Natural Science Foundation of China (No. 11775146).

References

[1] F. Özpinar, H. M. Baskonus, and H. Bulut, "On the complex and hyperbolic structures for the (2+1)-dimensional Boussinesq water equation," *Entropy*, vol. 17, no. 12, pp. 8267–8277, 2015.

[2] H. Zhang, X. Meng, J. Li, and B. Tian, "Soliton resonance of the -dimensional Boussinesq equation for gravity water waves," *Nonlinear Analysis: Real World Applications*, vol. 9, no. 3, pp. 920–926, 2008.

[3] A. S. A. Rady, E. S. Osman, and M. Khalfallah, "On soliton solutions of the (2 + 1)-dimensional Boussinesq equation," *Applied Mathematics and Computation*, vol. 219, no. 8, pp. 3414–3419, 2012.

[4] X. B. Wang, S. F. Tian, C. Y. Qin, and T. T. Zhang, "Characteristics of the breathers, rogue waves and solitary waves in a generalized (2+1)-dimensional Boussinesq equation," *Europhysics Letters*, vol. 115, no. 1, article 10002, 2016.

[5] J. G. Rao, Y. B. Liu, C. Qian, and J. S. He, "Rogue waves and hybrid solutions of the Boussinesq equation," *Zeitschrift Fur Naturforschung Section A*, vol. 72, no. 4, pp. 307–314, 2017.

[6] J. L. García Guirao, H. M. Baskonus, and A. Kumar, "Regarding new wave patterns of the newly extended nonlinear (2+1)-dimensional Boussinesq equation with fourth order," *Mathematics*, vol. 8, no. 3, p. 341, 2020.

[7] T. A. Sulaiman, H. Bulut, A. Yokus, and H. M. Baskonus, "On the exact and numerical solutions to the coupled Boussinesq equation arising in ocean engineering," *Indian Journal of Physics*, vol. 93, no. 5, pp. 647–656, 2019.

[8] Y. L. Ma, "N-solitons, breathers and rogue waves for a generalized Boussinesq equation," *International Journal of Computer Mathematics*, vol. 97, no. 8, pp. 1648–1661, 2020.

[9] Y. L. Ma and B. Q. Li, "Analytic rogue wave solutions for a generalized fourth-order Boussinesq equation in fluid mechanics," *Mathematical Methods in the Applied Sciences*, vol. 42, no. 1, pp. 39–48, 2019.

[10] A. R. Seadawy, "Stability analysis for two-dimensional ion-acoustic waves in quantum plasmas," *Physics of Plasmas*, vol. 21, no. 5, article 052107, 2014.

[11] A. R. Seadawy, "Travelling-wave solutions of a weakly nonlinear two-dimensional higher-order Kadomtsev-Petviashvili dynamical equation for dispersive shallow-water waves," *The European Physical Journal Plus*, vol. 132, no. 29, pp. 1–13, 2017.

[12] Y. S. Özkan, E. Yaşar, and A. R. Seadawy, "A third-order nonlinear Schrödinger equation: the exact solutions, group-invariant solutions and conservation laws," *Journal of Taibah University for Science*, vol. 14, no. 1, pp. 585–597, 2020.

[13] L. Gui, P. Wang, Y. Ding et al., "Soliton molecules and multi-soliton states in ultrafast fibre lasers: intrinsic complexes in dissipative systems," *Applied Sciences*, vol. 8, no. 2, p. 201, 2018.

[14] B. A. Malomed, "Bound solitons in the nonlinear Schrödinger-Ginzburg-Landau equation," *Physical Review A*, vol. 44, no. 10, pp. 6954–6957, 1991.

[15] B. Ortaç, A. Zaviyalov, C. K. Nielsen et al., "Observation of soliton molecules with independently evolving phase in a mode-locked fiber laser," *Optics Letters*, vol. 35, no. 10, pp. 1578–1580, 2010.

[16] M. Stratmann, T. Pagel, and F. Mitschke, "Experimental observation of temporal soliton molecules," *Physical Review Letters*, vol. 95, no. 14, article 143902, 2005.

[17] K. Krupa, K. Nithyanandan, U. Andral, P. Tchofo-Dinda, and P. Grelu, "Real-time observation of internal motion within ultrafast dissipative optical soliton molecules," *Physical Review Letters*, vol. 118, no. 24, article 243901, 2017.

[18] U. Al Khawaja, "Stability and dynamics of two-soliton molecules," *Physical Review E*, vol. 81, no. 5, article 056603, 2010.

[19] L. C. Crasovan, Y. V. Kartashov, D. Mihalache, L. Torner, Y. S. Kivshar, and V. M. Pérez-García, "Soliton molecules: robust clusters of spatiotemporal optical solitons," *Physical Review E*, vol. 67, no. 4, article 046610, 2003.

[20] S. Y. Lou, "Soliton molecules and asymmetric solitons in three fifth order systems via velocity resonance," *Journal Physiscs Communications*, vol. 4, no. 4, article 041002, 2020.

[21] D. H. Xu and S. Y. Lou, "Dark soliton molecules in nonlinear optics," *Acta Physica Sinica*, vol. 69, no. 1, article 014208, 2020.

[22] Z. Zhang, S. X. Yang, and B. Li, "Soliton molecules, asymmetric solitons and hybrid solutions for (2+1)-dimensional fifth-order KdV equation," *Chinese Physics Letters*, vol. 36, no. 12, article 120501, 2019.

[23] B. Ren and J. Lin, "Soliton molecules, nonlocal symmetry and CRE method of the KdV equation with higher-order corrections," *Physica Scripta*, vol. 95, no. 7, article 075202, 2020.

[24] B. Ren, J. Lin, and P. Liu, "Soliton molecules and the CRE method in the extended mKdV equation," *Communications in Theoretical Physics*, vol. 72, no. 5, article 055005, 2020.

[25] Z. Zhang, X. Yang, and B. Li, "Soliton molecules and novel smooth positons for the complex modified KdV equation," *Applied Mathematics Letters*, vol. 103, article 106168, 2020.

[26] C. J. Cui, X. Y. Tang, and Y. J. Cui, "New variable separation solutions and wave interactions for the (3+1)-dimensional Boiti-Leon-Manna-Pempinelli equation," *Applied Mathematics Letters*, vol. 102, article 106109, 2020.

[27] B. Ren, "Painlevé analysis, soliton molecule, and lump solution of the higher-order Boussinesq equation," *Advances in Mathematical Physics*, vol. 2021, Article ID 6687632, 6 pages, 2021.

[28] Z. Yan and S. Lou, "Soliton molecules in Sharma-Tasso-Olver-Burgers equation," *Applied Mathematics Letters*, vol. 104, article 106271, 2020.

[29] R. Hirota, *The Direct Method in Soliton Theory*, Cambridge University Press, Cambridge, 2004.

[30] B. Ren and J. Lin, "D'Alembert wave and soliton molecule of the modified Nizhnik-Novikov-Veselov equation," *The European Physical Journal Plus*, vol. 136, no. 1, p. 123, 2021.

[31] W. X. Ma, "Lump solutions to the Kadomtsev-Petviashvili equation," *Physics Letters A*, vol. 379, no. 36, pp. 1975–1978, 2015.

[32] Y. F. Hua, B. L. Guo, W. X. Ma, and X. Lü, "Interaction behavior associated with a generalized (2+1)-dimensional Hirota bilinear equation for nonlinear waves," *Applied Mathematical Modelling*, vol. 74, pp. 184–198, 2019.

[33] X. W. Jin and J. Lin, "Rogue wave, interaction solutions to the KMM system," *Journal of Magnetism and Magnetic Materials*, vol. 502, article 166590, 2020.

[34] C. Y. Qin, S. F. Tian, X. B. Wang, and T. T. Zhang, "On breather waves, rogue waves and solitary waves to a generalized (2+1)-dimensional Camassa-Holm-Kadomtsev-Petviashvili equation," *Communications in Nonlinear Science and Numerical Simulation*, vol. 62, pp. 378–385, 2018.

[35] X. W. Yan, S. F. Tian, M. J. Dong, L. Zhou, and T. T. Zhang, "Characteristics of solitary wave, homoclinic breather wave and rogue wave solutions in a (2+1)-dimensional generalized breaking soliton equation," *Computers Mathematics with Applications*, vol. 76, no. 1, pp. 179–186, 2018.

[36] C. Q. Dai, J. Liu, Y. Fan, and D. G. Yu, "Two-dimensional localized Peregrine solution and breather excited in a variable-coefficient nonlinear Schrödinger equation with partial nonlocality," *Nonlinear Dynamics*, vol. 88, no. 2, pp. 1373–1383, 2017.

[37] S. Lou and J. Lin, "Rogue waves in nonintegrable KdV-type systems," *Chinese Physics Letters*, vol. 35, no. 5, article 050202, 2018.

[38] B. Ren, W. X. Ma, and J. Yu, "Rational solutions and their interaction solutions of the (2+1)-dimensional modified dispersive water wave equation," *Computers Mathematics with Applications*, vol. 77, no. 8, pp. 2086–2095, 2019.

[39] B. Ren, W. X. Ma, and J. Yu, "Characteristics and interactions of solitary and lump waves of a (2+1)-dimensional coupled nonlinear partial differential equation," *Nonlinear Dynamics*, vol. 96, no. 1, pp. 717–727, 2019.

[40] X. Zhang, Y. Chen, and X. Tang, "Rogue wave and a pair of resonance stripe solitons to KP equation," *Computers Mathematics with Applications*, vol. 76, no. 8, pp. 1938–1949, 2018.

[41] L. Huang, Y. Yue, and Y. Chen, "Localized waves and interaction solutions to a (3+1)-dimensional generalized KP equation," *Computers Mathematics with Applications*, vol. 76, no. 4, pp. 831–844, 2018.

[42] J. P. Yu and Y. L. Sun, "Lump solutions to dimensionally reduced Kadomtsev-Petviashvili-like equations," *Nonlinear Dynamics*, vol. 87, no. 2, pp. 1405–1412, 2017.

[43] B. Ren, J. Lin, and Z. M. Lou, "Consistent Riccati expansion and rational solutions of the Drinfel'd-Sokolov- Wilson equation," *Applied Mathematics Letters*, vol. 105, article 106326, 2020.

[44] N. Akhmediev, A. Ankiewicz, and J. M. Soto-Crespo, "Rogue waves and rational solutions of the nonlinear Schrödinger equation," *Physical Review E*, vol. 80, no. 2, article 026601, 2009.

[45] L. Kaur and A. M. Wazwaz, "Lump, breather and solitary wave solutions to new reduced form of the generalized BKP equation," *International Journal of Numerical Methods for Heat Fluid Flow*, vol. 29, no. 2, pp. 569–579, 2019.

[46] K. Hosseini, M. Samavat, M. Mirzazadeh, W. X. Ma, and Z. Hammouch, "A new (3+1)-dimensional Hirota bilinear equation: its Bäcklund transformation and rational-type solutions," *Regular and Chaotic Dynamics*, vol. 25, no. 4, pp. 383–391, 2020.

[47] K. Hosseini, R. Ansari, R. Pouyanmehr, F. Samadani, and M. Aligoli, "Kinky breather-wave and lump solutions to the (2+1)-dimensional Burgers equations," *Analysis and Mathematical Physics*, vol. 10, no. 65, p. 120, 2020.

[48] Y. L. Ma and B. Q. Li, "Mixed lump and soliton solutions for a generalized (3+1)-dimensional Kadomtsev-Petviashvili equation," *AIMS Mathematics*, vol. 5, no. 2, pp. 1162–1176, 2020.

[49] L. Kaur and A. M. Wazwaz, "Dynamical analysis of lump solutions for (3 + 1) dimensional generalized KP-Boussinesq equation and its dimensionally reduced equations," *Physica Scripta*, vol. 93, no. 7, article 075203, 2018.

[50] Y. L. Ma and B. Q. Li, "Interactions between soliton and rogue wave for a (2+1)-dimensional generalized breaking soliton system: hidden rogue wave and hidden soliton," *Computers Mathematics with Applications*, vol. 78, no. 3, pp. 827–839, 2019.

[51] Y. L. Ma, "Interaction and energy transition between the breather and rogue wave for a generalized nonlinear Schrödinger system with two higher-order dispersion operators in optical fibers," *Nonlinear Dynamics*, vol. 97, no. 1, pp. 95–105, 2019.

Hindawi
Advances in Mathematical Physics
Volume 2021, Article ID 5532691, 17 pages
https://doi.org/10.1155/2021/5532691

Research Article

The Galerkin Method for Fourth-Order Equation of the Moore–Gibson–Thompson Type with Integral Condition

Ahlem Mesloub,[1] Abderrahmane Zaraï,[1] Fatiha Mesloub,[1] Bahri-Belkacem Cherif,[2,3] and Mohamed Abdalla[4,5]

[1]*Laboratory of mathematics, Informatics and Systems (LAMIS), Department of Mathematics and Computer Science, Larbi Tebessi University, 12002 Tebessa, Algeria*
[2]*Preparatory Institute for Engineering Studies in Sfax, Sfax, Tunisia*
[3]*Department of Mathematics, College of Sciences and Arts, Qassim University, Ar Rass, Saudi Arabia*
[4]*Mathematics Department, College of Science, King Khalid University, Abha, Saudi Arabia*
[5]*Mathematics Department, Faculty of Science, South Valley University, Qena 83523, Egypt*

Correspondence should be addressed to Bahri-Belkacem Cherif; bahi1968@yahoo.com

Received 25 February 2021; Revised 14 March 2021; Accepted 24 March 2021; Published 7 April 2021

Academic Editor: Kamyar Hosseini

In this manuscript, we consider the fourth order of the Moore–Gibson–Thompson equation by using Galerkin's method to prove the solvability of the given nonlocal problem.

1. Introduction

Research on the nonlinear propagation of sound in a situation of high amplitude waves has shown literature on physically well-founded partial differential models (see, e.g., [1–23]). This still very active field of research is carried by a wide range of applications such as the medical and industrial use of high-intensity ultrasound in lithotripsy, thermotherapy, ultrasound cleaning, and sonochemistry. The classical models of nonlinear acoustics are Kuznetsov's equation, the Westervelt equation, and the KZK (Kokhlov-Zabolotskaya-Kuznetsov) equation. For a mathematical existence and uniqueness analysis of several types of initial boundary value problems for these nonlinear second order in time PDEs, we refer to [24–44]. Focusing on the study of the propagation of acoustic waves, it should be noted that the MGT equation is one of the equations of nonlinear acoustics describing acoustic wave propagation in gases and liquids. The behavior of acoustic waves depends strongly on the medium property related to dispersion, dissipation, and nonlinear effects. It arises from modeling high-frequency ultrasound (HFU) waves (see [10, 12, 34]). The derivation of the equation, based on continuum and fluid mechanics, takes into account viscosity and heat conductivity as well as effect of the radiation of heat on the propagation of sound. The original derivation dates back to [44]. This model is realized through the third-order hyperbolic equation:

$$\tau u_{ttt} + u_{tt} - c^2 \Delta u - b \Delta u_t = 0. \tag{1}$$

The unknown function $u = u(x, t)$ denotes the scalar acoustic velocity, c denotes the speed of sound, and τ denotes the thermal relaxation. Besides, the coefficient $b = \beta c^2$ is related to the diffusively of the sound with $\beta \in (0, \tau]$. In [44], Chen and Palmieri studied the blow-up result for the semilinear Moore–Gibson–Thompson equation with nonlinearity of derivative type in the conservative case defined as follows:

$$\beta u_{ttt} + u_{tt} - \Delta u - \beta \Delta u_t = |u_t|^p, x \in \mathbb{R}^n, t > 0. \tag{2}$$

This paper is related to the following works (see [16, 39]). Now, when we talk about the (MGT) equation with memory term, we have Lasieka and Wang in [17] who studied the exponential decay of the energy of the temporally third-order (Moore–Gibson–Thompson) equation with a memory term as follows:

$$\tau u_{ttt} + \alpha u_{tt} - c^2 Au - bAu_t - \int_0^t g(t-s)Aw(s)ds = 0, \quad (3)$$

where τ, α, b, c^2 are physical parameters and A is a positive self-adjoint operator on a Hilbert space H. The convolution term $\int_0^t g(t-s)Aw(s)ds$ reflects the memory effects of materials due to viscoelasticity. In [18], Lasieka and Wang studied the general decay of solution of same problem above. The Moore–Gibson–Thompson equation with a nonlocal condition is a new posed problem. Existence and uniqueness of the generalized solution are established by using the Galerkin method. These problems can be encountered in many scientific domains and many engineering models (see previous works [5, 25–32, 35, 36, 40, 41]). Mesloub and Mesloub in [33] have applied the Galerkin method to a higher dimension mixed with nonlocal problem for a Boussinesq equation, while Boulaaras et al. investigated the Moore–Gibson–Thompson equation with the integral condition in [4]. Motivated by these outcomes, we improve the existence and uniqueness by the Galerkin method of the fourth-order equation of the Moore–Gibson–Thompson type with integral condition; this problem was cited by the work of Dell'Oro and Pata in [9].

We define the problem as follows:

$$\begin{cases} u_{tttt} + \alpha u_{ttt} + \beta u_{tt} - \rho\Delta u - \delta\Delta u_t - \gamma\Delta u_{tt} = 0, \\ u(x,0) = u_0(x),\ u_t(x,0) = u_1(x), u_{tt}(x,0) = u_2(x), u_{ttt}(x,0) = u_3(x) \\ \dfrac{\partial u}{\partial \eta} = \displaystyle\int_0^t \int_\Omega u(\xi,\tau)d\xi d\tau, x \in \partial\Omega. \end{cases} \quad (4)$$

The aim of this manuscript is to consider the following nonlocal mixed boundary value problem for the Moore–Gibson–Thompson (MGT) equation for all $(x;t) \in Q_T = (0,T)$, where $\Omega \subset \mathbb{R}^n$ is a bounded domain with sufficiently smooth boundary $\partial\Omega$. solution of the posed problem.

We divide this paper into the following: In "Preliminaries," some definitions and appropriate spaces have been given. Then in "Solvability of the Problem," we use Galerkin's method to prove the existence, and in "Uniqueness of Solution," we demonstrate the uniqueness.

2. Preliminaries

Let $V(Q_T)$ and $W(Q_T)$ be the set spaces defined, respectively, by

$$V(Q_T) = \left\{u \in W_2^1(Q_T):\ u_t \in W_2^1(Q_T):\ u_{tt} \in W_2^1(Q_T)\right\},$$
$$W(Q_T) = \left\{u \in V(Q_T):\ u(x,T) = 0\right\}. \quad (5)$$

Consider the equation

$$(u_{tttt}, v)_{L^2(Q_T)} + \alpha(u_{ttt}, v)_{L^2(Q_T)} + \beta(u_{tt}, v)_{L^2(Q_T)} - \varrho(\Delta u, v)_{L^2(Q_T)} - \delta(\Delta u_t, v)_{L^2(Q_T)}\gamma(\Delta u_{tt}, v)_{L^2(Q_T)} = 0, \quad (6)$$

where $(.,.)_{L^2(Q_T)}$ depend on the inner product in $L^2(Q_T)$, u is supposed to be a solution of (1), and $v \in W(Q_T)$. Upon using (6) and (1), we find

$$\begin{aligned} &-(u_{ttt}, v_t)_{L^2(Q_T)} - \alpha(u_{tt}, v_t)_{L^2(Q_T)} - \beta(u_t, v_t)_{L^2(Q_T)} + \varrho(\nabla u, \nabla v)_{L^2(Q_T)} \\ &\quad + \delta(\nabla u_t, \nabla v)_{L^2(Q_T)} - \gamma(\nabla u_t, \nabla v_t)_{L^2(Q_T)} \\ &= \varrho\int_0^T\int_{\partial\Omega} v\left(\int_0^t\int_\Omega u(\xi,\tau)d\xi d\tau\right)ds_x dt + \delta\int_0^T\int_{\partial\Omega} v\int_\Omega u(\xi,t)d\xi ds_x dt \\ &\quad - \delta\int_0^T\int_{\partial\Omega} v\int_\Omega u_0(\xi)d\xi ds_x dt - \gamma\int_0^T\int_{\partial\Omega} v_t\left(\int_0^t\int_\Omega u_\tau(\xi,\tau)d\xi d\tau\right)ds_x dt \\ &\quad + (u_3(x), v(x,0))_{L^2(\Omega)} + \alpha(u_2(x), v(x,0))_{L^2(\Omega)} + \beta(u_1(x), v(x,0))_{L^2(\Omega)} \\ &\quad - \gamma(\Delta u_1, v(x,0))_{L^2(\Omega)}. \end{aligned} \quad (7)$$

Now, we give two useful inequalities:

(i) Gronwall inequality: if for any $t \in I$, we have

$$y(t) \le h(t) + c\int_0^t y(s)ds, \quad (8)$$

where $h(t)$ and $y(t)$ are two nonnegative integrable functions on the interval I with $h(t)$ nondecreasing and c is constant, then

$$y(t) \le h(t)\ \exp\ (ct) \quad (9)$$

(ii) Trace inequality: when $w \in W_1^2(\Omega)$, we have

$$\|w\|^2_{L^2(\partial\Omega)} \le \varepsilon\|\nabla w\|^2_{L^2(\Omega)} + l(\varepsilon)\|w\|^2_{L^2(\Omega)}, \quad (10)$$

where Ω is a bounded domain in $\mathbb{R}^n$ with smooth boundary $\partial\Omega$, and $l(\varepsilon)$ is a positive constant.

Definition 1. If a function $u \in V(Q_T)$ satisfies Equation (3), each $v \in W(Q_T)$ is called a generalized solution of problem (1).

3. Solvability of the Problem

Here, by using Galerkin's method, we give the existence of problem (1).

Theorem 2. *If $u_0 \in$, $u_1 \in$ and $u_2 \in$, $u_3 \in$, then there is at least one generalized solution in $V(Q_T)$ to problem (1).*

Proof. Let $\{Z_k(x)\}_{k\ge1}$ be a fundamental system in $W_2^1(\Omega)$, such that $(Z_k, Z_l)_{L^2(\Omega)} = \delta_{k,l}$. Now, we will find an approximate solution of the problem (1) in the form

$$u^N(x,t) = \sum_{k=1}^N C_k(t)Z_k(x), \quad (11)$$

where the constants $C_k(t)$ are defined by the conditions

$$C_k(t) = \left(u^N(x,t), Z_k(x)\right)_{L^2(\Omega)}, k = 1, \cdots, N, \tag{12}$$

and can be determined from the relations

$$\begin{aligned}
&\left(u^N_{tttt}, Z_l(x)\right)_{L^2(\Omega)} + \alpha\left(u^N_{ttt}, Z_l(x)\right)_{L^2(\Omega)} + \beta\left(u^N_{tt}, Z_l(x)\right)_{L^2(\Omega)} \\
&\quad + \varrho\left(\nabla u^N, \nabla Z_l(x)\right)_{L^2(\Omega)} + \delta\left(\nabla u^N_t, \nabla Z_l(x)\right)_{L^2(\Omega)} + \gamma\left(\nabla u^N_{tt}, \nabla Z_l(x)\right)_{L^2(\Omega)} \\
&= \varrho\int_{\partial\Omega} Z_l(x)\left(\int_0^t\int_\Omega u^N(\xi,\tau)d\xi d\tau\right)ds_x + \delta\int_{\partial\Omega} Z_l(x)\left(\int_0^t\int_\Omega u^N_\tau(\xi,\tau)d\xi d\tau\right)ds_x \\
&\quad + \gamma\int_{\partial\Omega} Z_l(x)\left(\int_0^t\int_\Omega u^N_{\tau\tau}(\xi,\tau)d\xi d\tau\right)ds_x.
\end{aligned} \tag{13}$$

Invoking to (11) in (6) gives for $l = 1, \cdots, N$.

$$\begin{aligned}
&\int_\Omega \sum_{k=1}^N \Big\{ C''_k(t)Z_k(x)Z_l(x) + \alpha C''_k(t)Z_k(x)Z_l(x) + \beta C'_k(t)Z_k(x)Z_l(x) \\
&\quad + \varrho C_k(t)\nabla Z_k(x).\nabla Z_l(x) + \delta C'_k(t)\nabla Z_k(x).\nabla Z_l(x) + \gamma C''_k(t)\nabla Z_k.\nabla Z_l \Big\}dx \\
&= \varrho\sum_{k=1}^N\int_0^t C_k(\tau)\left(\int_{\partial\Omega} Z_l(x)\int_\Omega Z_k(\xi)d\xi ds_x\right)d\tau + \delta\sum_{k=1}^N\int_0^t C'_k(\tau) \\
&\quad \times \left(\int_{\partial\Omega} Z_l(x)\int_\Omega Z_k(\xi)d\xi ds_x\right)d\tau + \gamma\sum_{k=1}^N\int_0^t\left(C'_k(\tau)\int_{\partial\Omega} Z_l(x)\int_\Omega Z_k(\xi)d\xi ds_x\right)d\tau.
\end{aligned} \tag{14}$$

From (7), it follows that

$$\begin{aligned}
&\sum_{k=1}^N C''_k(t)\left(Z_k(x), Z_l(x)\right)_{L^2(\Omega)} + \alpha C''_k(t)\left(Z_k(x), Z_l(x)\right)_{L^2(\Omega)} \\
&\quad + \beta C'_k(t)\left(Z_k(x), Z_l(x)\right)_{L^2(\Omega)} + \varrho C_k(t)\left(\nabla Z_k, \nabla Z_l\right)_{L^2(\Omega)} \\
&\quad + \delta C'_k(t)\left(\nabla Z_k(x), \nabla Z_l(x)\right)_{L^2(\Omega)} + \gamma C''_k(t)\left(\nabla Z_k(x), \nabla Z_l(x)\right)_{L^2(\Omega)} \\
&= \varrho\sum_{k=1}^N\int_0^t C_k(\tau)\left(\int_{\partial\Omega} Z_l(x)\int_\Omega Z_k(\xi)d\xi ds_x\right)d\tau \\
&\quad + \delta\sum_{k=1}^N\int_0^t C'_k(\tau)\left(\int_{\partial\Omega} Z_l(x)\int_\Omega Z_k(\xi)d\xi ds_x\right)d\tau \\
&\quad + \gamma\sum_{k=1}^N\int_0^t\left(C'_k(\tau)\int_{\partial\Omega} Z_l(x)\int_\Omega Z_k(\xi)d\xi ds\right)d\tau, l = 1, \cdots, N.
\end{aligned} \tag{15}$$

Let

$$\begin{aligned}
\left(Z_k, Z_l\right)_{L^2(\Omega)} &= \delta_{kl} = \begin{cases} 1, & k = l \\ 0, & k \neq l, \end{cases} \\
\left(\nabla Z_k, \nabla Z_l\right)_{L^2(\Omega)} &= \gamma_{kl}, \\
\int_{\partial\Omega} Z_l(x)\int_\Omega Z_k(\xi)d\xi ds &= \chi_{kl}.
\end{aligned} \tag{16}$$

Then (8) can be written as

$$\begin{aligned}
&\sum_{k=1}^N C''_k(t)\delta_{kl} + \alpha C''_k(t)\delta_{kl} + C'_k(t)(\beta\delta_{kl} + \gamma\gamma_{kl}) + \delta C'_k(t)\gamma_{kl} \\
&\quad + \varrho C_k(t)\gamma_{kl} - \int_0^t\Big(\varrho C_k(\tau)\chi_{kl} + \delta C'_k(\tau)\chi_{kl} + \gamma C''_k(\tau)\chi_{kl} = 0.
\end{aligned} \tag{17}$$

A differentiation with respect to t yields

$$\begin{aligned}
&\sum_{k=1}^N C'''_k(t)\delta_{kl} + \alpha C'''_k(t)\delta_{kl} + C''_k(t)(\beta\delta_{kl} + \gamma\gamma_{kl}) + C'_k(t)(\delta\gamma_{kl} - \gamma\chi_{kl}) + C'_k(t)(\varrho\gamma_{kl} - \delta\chi_{kl})\gamma_{kl} - \varrho C_k(t)\chi_{kl} = 0, \\
&\begin{cases}
\sum_{k=1}^N\left[C'''_k(0)\delta_{kl} + \alpha C''_k(0)\delta_{kl} + C''_k(0)(\beta\delta_{kl} + \gamma\gamma_{kl}) + \delta C'_k(0)\gamma_{kl} + \varrho C_k(0)\gamma_{kl}\right] = 0 \\
C_k(0) = \left(Z_k, u_0\right)_{L^2(\Omega)},\ C'_k(0) = \left(Z_k, u_1(x)\right)_{L^2(\Omega)},\ C''_k(t) = \left(Z_k, u_2(x)\right)_{L^2(\Omega)}, C'''_k(t) = \left(Z_k, u_3(x)\right)_{L^2(\Omega)}.
\end{cases}
\end{aligned} \tag{18}$$

Thus, for every n, there exists a function $u^N(x)$ satisfying (6). Now, we will demonstrate that the sequence u^N is bounded. To do this, we multiply each equation of (6) by the appropriate $C_k{}'(t)$ summing over k from 1 to N then integrating the resultant equality with respect to t from 0 to τ, with $\tau \leq T$, which yields

$$\begin{aligned}
&\left(u^N_{tttt}, u^N_t\right)_{L^2(Q_\tau)} + \alpha\left(u^N_{ttt}, u^N_t\right)_{L^2(Q_\tau)} + \beta\left(u^N_{tt}, u^N_t\right)_{L^2(Q_\tau)} + \varrho\left(\nabla u^N, \nabla u^N_t\right)_{L^2(Q_\tau)} \\
&\quad + \delta\left(\nabla u^N_t, \nabla u^N_t\right)_{L^2(Q_\tau)} + \gamma\left(\nabla u^N_{tt}, \nabla u^N_t\right)_{L^2(Q_\tau)} = \varrho\int_0^\tau\int_{\partial\Omega} u^N_t(x,t) \\
&\quad \times \left(\int_0^t\int_\Omega u^N(\xi,\eta)d\xi d\eta\right)ds_x dt + \delta\int_0^\tau\int_{\partial\Omega} u^N_t(x,t)\left(\int_0^t\int_\Omega u^N_t(\xi,\eta)d\xi d\eta\right)ds_x dt \\
&\quad + \gamma\int_0^\tau\int_{\partial\Omega} u^N_t(x,t)\left(\int_0^t\int_\Omega u^N_{tt}(\xi,\eta)d\xi d\eta\right)ds_x dt.
\end{aligned} \tag{19}$$

After simplification of the LHS of (19), we observe that

$$\begin{aligned}
\left(u^N_{tttt}, u^N_t\right)_{L^2(Q_\tau)} &= -\int_0^\tau\left(u^N_{ttt}, u^N_{tt}\right)_{L^2(\Omega)}dt \\
&\quad + \left(u^N_{\tau\tau\tau}(x,\tau), u^N_\tau(x,\tau)\right)_{L^2(\Omega)} \\
&\quad - \left(u^N_{ttt}(x,0), u^N_t(x,0)\right)_{L^2(\Omega)},
\end{aligned} \tag{20}$$

$$\begin{cases}
\alpha\left(u^N_{ttt}, u^N_t\right)_{L^2(Q_\tau)} = \alpha\left(u^N_{\tau\tau}(x,\tau), u^N_\tau(x,\tau)\right)_{L^2(\Omega)} - \left(u^N_{tt}(x,0), u^N_t(x,0)\right)_{L^2(\Omega)} \\
-\alpha\int_0^\tau \|u_{tt}(x,t)\|^2_{L^2(\Omega)}dt,
\end{cases} \tag{21}$$

$$\beta\left(u_{tt}^N, u_t^N\right)_{L^2(Q_\tau)} = \frac{\beta}{2}\left\|u_\tau^N(x,\tau)\right\|_{L^2(\Omega)}^2 - \frac{\beta}{2}\left\|u_t^N(x,0)\right\|_{L^2(\Omega)}^2, \tag{22}$$

$$\varrho\left(\nabla u^N, \nabla u_t^N\right)_{L^2(Q_\tau)} = \frac{\varrho}{2}\left\|\nabla u^N(x,\tau)\right\|_{L^2(\Omega)}^2 - \frac{\varrho}{2}\left\|\nabla u^N(x,0)\right\|_{L^2(\Omega)}^2, \tag{23}$$

$$\delta\left(\nabla u_t^N, \nabla u_t^N\right)_{L^2(Q_\tau)} = \delta\int_0^\tau \left\|\nabla u_t^N(x,t)\right\|_{L^2(\Omega)}^2 dt, \tag{24}$$

$$\gamma\left(\nabla u_{tt}^N, \nabla u_t^N\right)_{L^2(Q_\tau)} = \frac{\gamma}{2}\left\|\nabla u_\tau^N(x,\tau)\right\|_{L^2(\Omega)}^2 - \frac{\gamma}{2}\left\|\nabla u_t^N(x,0)\right\|_{L^2(\Omega)}^2, \tag{25}$$

$$\varrho\int_0^\tau\int_{\partial\Omega} u_t^N\left(\int_0^t\int_\Omega u^N(\xi,\eta)d\xi d\eta\right)ds_x dt = \varrho\int_{\partial\Omega} u^N(x,\tau)\int_0^\tau\int_\Omega u^N(\xi,t)d\xi dt ds_x - \varrho\int_{\partial\Omega}\int_0^\tau u^N(x,t)\int_\Omega u^N(\xi,t)d\xi dt ds_x, \tag{26}$$

$$\begin{aligned}\delta\int_0^\tau\int_{\partial\Omega} u_t^N\left(\int_0^t\int_\Omega u_t^N(\xi,\eta)d\xi d\eta\right)ds_x dt &= \delta\int_{\partial\Omega}\int_0^\tau u_t^N(x,t)\int_\Omega u^N(\xi,t)d\xi dt ds_x \\ &\quad - \delta\int_{\partial\Omega}\int_0^\tau u_t^N(x,t)\int_\Omega u^N(\xi,0)d\xi dt ds_x,\end{aligned} \tag{27}$$

$$\begin{aligned}&\gamma\int_0^\tau\int_{\partial\Omega} u_t^N(x,t)\left(\int_0^t\int_\Omega u_{tt}^N(\xi,\eta)d\xi d\eta\right)ds_x dt \\ &\quad = \gamma\int_0^\tau\int_{\partial\Omega} u_t^N(x,t)\left(\int_\Omega u_t^N(\xi,t)d\xi\right)ds_x dt \\ &\qquad - \gamma\int_0^\tau\int_{\partial\Omega} u_t^N(x,t)\left(\int_\Omega u_t^N(\xi,0)d\xi\right)ds_x dt.\end{aligned} \tag{28}$$

Taking into account the equalities (20) and (21) in (12), we obtain

$$\begin{aligned}&\left(u_{\tau\tau\tau}^N(x,\tau), u_\tau^N(x,\tau)\right)_{L^2(\Omega)} + \alpha\left(u_{\tau\tau}^N(x,\tau), u_\tau^N(x,\tau)\right)_{L^2(\Omega)} \\ &\quad + \frac{\beta}{2}\left\|u_\tau^N(x,\tau)\right\|_{L^2(\Omega)}^2 + \frac{\varrho}{2}\left\|\nabla u^N(x,\tau)\right\|_{L^2(\Omega)}^2 + \frac{\gamma}{2}\left\|\nabla u_\tau^N(x,\tau)\right\|_{L^2(\Omega)}^2 \\ &\quad = \left(u_{ttt}^N(x,0), u_t^N(x,0)\right)_{L^2(\Omega)} + \alpha\left(u_{tt}^N(x,0), u_t^N(x,0)\right)_{L^2(\Omega)} \\ &\quad\quad + \frac{\beta}{2}\left\|u_t^N(x,0)\right\|_{L^2(\Omega)}^2 + \frac{\varrho}{2}\left\|\nabla u^N(x,0)\right\|_{L^2(\Omega)}^2 + \frac{\gamma}{2}\left\|\nabla u_t^N(x,0)\right\|_{L^2(\Omega)}^2 \\ &\quad\quad + \int_0^\tau\left(u_{ttt}^N, u_{tt}^N\right)_{L^2(\Omega)}dt + \alpha\int_0^\tau\left\|u_{tt}(x,t)\right\|_{L^2(\Omega)}^2 dt - \delta\int_0^\tau\left\|\nabla u_t^N(x,t)\right\|_{L^2(\Omega)}^2 dt \\ &\quad\quad + \varrho\int_{\partial\Omega} u^N(x,\tau)\int_0^\tau\int_\Omega u^N(\xi,t)d\xi dt ds_x - \varrho\int_{\partial\Omega}\int_0^\tau u^N(x,t)\int_\Omega u^N(\xi,t)d\xi dt ds_x \\ &\quad\quad + \delta\int_{\partial\Omega}\int_0^\tau u_t^N(x,t)\int_\Omega u^N(\xi,t)d\xi dt ds_x - \delta\int_{\partial\Omega}\int_0^\tau u_t^N(x,t)\int_\Omega u^N(\xi,0)d\xi dt ds_x \\ &\quad\quad + \gamma\int_0^\tau\int_{\partial\Omega} u_t^N(x,t)\left(\int_\Omega u_t^N(\xi,t)d\xi\right)ds_x dt - \gamma\int_0^\tau\int_{\partial\Omega} u_t^N(x,t) \\ &\quad\quad \times\left(\int_\Omega u_t^N(\xi,0)d\xi\right)ds_x dt.\end{aligned} \tag{29}$$

Now, multiplying each equation of (6) by the appropriate $C_k'(t)$, we add them up from 1 to N and then integrate with respect to t from 0 to τ, with $\tau \le T$, and we obtain

$$\begin{aligned}&\left(u_{tttt}^N, u_{tt}^N\right)_{L^2(Q_\tau)} + \alpha\left(u_{ttt}^N, u_{tt}^N\right)_{L^2(Q_\tau)} + \beta\left(u_{tt}^N, u_{tt}^N\right)_{L^2(Q_\tau)} \\ &\quad + \varrho\left(\nabla u^N, \nabla u_{tt}^N\right)_{L^2(Q_\tau)} + \delta\left(\nabla u_t^N, \nabla u_{tt}^N\right)_{L^2(Q_\tau)} + \gamma\left(\nabla u_{tt}^N, \nabla u_{tt}^N\right)_{L^2(Q_\tau)} \\ &\quad = \varrho\int_0^\tau\int_{\partial\Omega} u_{tt}^N(x,t)\left(\int_0^t\int_\Omega u^N(\xi,\eta)d\xi d\eta\right)ds_x dt \\ &\quad\quad + \delta\int_0^\tau\int_{\partial\Omega} u_{tt}^N(x,t)\left(\int_0^t\int_\Omega u_t^N(\xi,\eta)d\xi d\eta\right)ds_x dt \\ &\quad\quad + \gamma\int_0^\tau\int_{\partial\Omega} u_{tt}^N(x,t)\left(\int_0^t\int_\Omega u_{tt}^N(\xi,\eta)d\xi d\eta\right)ds_x dt.\end{aligned} \tag{30}$$

With the same reasoning in (12), we find

$$\left(u_{tttt}^N, u_{tt}^N\right)_{L^2(Q_\tau)} = -\int_0^\tau\left\|u_{ttt}^N(x,t)\right\|_{L^2(\Omega)}^2 dt + \left(u_{\tau\tau\tau}^N(x,\tau), u_{\tau\tau}^N(x,\tau)\right)_{L^2(\Omega)} - \left(u_{ttt}^N(x,0), u_{tt}^N(x,0)\right)_{L^2(\Omega)}, \tag{31}$$

$$\alpha\left(u_{ttt}^N, u_{tt}^N\right)_{L^2(Q_\tau)} = \frac{\alpha}{2}\left\|u_{\tau\tau}^N(x,\tau)\right\|_{L^2(\Omega)}^2 - \frac{\alpha}{2}\left\|u_{tt}^N(x,0)\right\|_{L^2(\Omega)}^2, \tag{32}$$

$$\beta\left(u_{tt}^N, u_{tt}^N\right)_{L^2(Q_\tau)} = \beta\int_0^\tau\left\|u_{tt}^N(x,t)\right\|_{L^2(\Omega)}^2 dt, \tag{33}$$

$$\begin{aligned}\varrho\left(\nabla u^N, \nabla u_{tt}^N\right)_{L^2(Q_\tau)} &= \varrho\left(\nabla u^N(x,\tau), \nabla u_\tau^N(x,\tau)\right)_{L^2(Q_\tau)} \\ &\quad - \varrho\left(\nabla u^N(x,0), \nabla u_t^N(x,0)\right)_{L^2(\Omega)} \\ &\quad - \varrho\int_0^\tau\left\|\nabla u_t^N(x,t)\right\|_{L^2(\Omega)}^2 dt,\end{aligned} \tag{34}$$

$$\delta\left(\nabla u_t^N, \nabla u_{tt}^N\right)_{L^2(Q_\tau)} = \frac{\delta}{2}\left\|\nabla u_\tau^N(x,\tau)\right\|_{L^2(\Omega)}^2 - \frac{\delta}{2}\left\|\nabla u_t^N(x,0)\right\|_{L^2(\Omega)}^2, \tag{35}$$

$$\gamma\left(\nabla u_{tt}^N, \nabla u_{tt}^N\right)_{L^2(Q_\tau)} = \gamma\int_0^\tau\left\|\nabla u_{tt}^N(x,t)\right\|_{L^2(\Omega)}^2 dt, \tag{36}$$

$$\begin{aligned}&\varrho\int_0^\tau\int_{\partial\Omega} u_{tt}^N\left(\int_0^t\int_\Omega u^N(\xi,\eta)d\xi d\eta\right)ds_x dt \\ &\quad = \varrho\int_{\partial\Omega} u_\tau^N(x,\tau)\int_0^\tau\int_\Omega u^N(\xi,t)d\xi dt ds_x \\ &\quad\quad - \varrho\int_{\partial\Omega}\int_0^\tau u_t^N(x,t)\int_\Omega u^N(\xi,t)d\xi dt ds_x,\end{aligned} \tag{37}$$

$$\begin{aligned}&\delta\int_0^\tau\int_{\partial\Omega} u_{tt}^N(x,t)\left(\int_0^t\int_\Omega u_t^N(\xi,\eta)d\xi d\eta\right)ds_x dt \\ &\quad = \delta\int_{\partial\Omega} u_\tau^N(x,\tau)\int_\Omega u^N(\xi,\tau)d\xi ds_x - \delta\int_{\partial\Omega} u_\tau^N(x,\tau)\int_\Omega u^N(\xi,0)d\xi ds_x \\ &\quad\quad - \delta\int_{\partial\Omega}\int_0^\tau u_t^N(x,t)\int_\Omega u_t^N(\xi,t)d\xi dt ds,\end{aligned} \tag{38}$$

$$\gamma\int_0^\tau\int_{\partial\Omega} u_{tt}^N(x,t)\left(\int_0^t\int_\Omega u_{tt}^N(\xi,\eta)d\xi d\eta\right)ds_x dt = \gamma\int_{\partial\Omega} u_\tau^N(x,\tau)\int_\Omega u_\tau^N(\xi,\tau)d\xi ds_x - \gamma\int_{\partial\Omega} u_\tau^N(x,\tau)\int_\Omega u_t^N(\xi,0)d\xi ds_x - \gamma\int_{\partial\Omega}\int_0^\tau u_t^N(x,t)\int_\Omega u_{tt}^N(\xi,t)d\xi dt ds, \tag{39}$$

Upon using (31) and (32) into (23), we have

$$\begin{aligned}&\left(u_{\tau\tau\tau}^N(x,\tau), u_{\tau\tau}^N(x,\tau)\right)_{L^2(\Omega)} + \frac{\alpha}{2}\left\|u_{\tau\tau}^N(x,\tau)\right\|_{L^2(\Omega)}^2 + \frac{\delta}{2}\left\|\nabla u_\tau^N(x,\tau)\right\|_{L^2(\Omega)}^2\\ &+ \varrho\left(\nabla u^N(x,\tau),\nabla u_\tau^N(x,\tau)\right)_{L^2(\Omega)} = \int_0^\tau\left\|u_{ttt}^N(x,t)\right\|_{L^2(\Omega)}^2 dt\\ &+ \left(u_{ttt}^N(x,0), u_{tt}^N(x,0)\right)_{L^2(\Omega)} + \frac{\alpha}{2}\left\|u_{tt}^N(x,0)\right\|_{L^2(\Omega)}^2 - \beta\int_0^\tau\left\|u_{tt}^N(x,t)\right\|_{L^2(\Omega)}^2 dt\\ &+ \varrho\left(\nabla u^N(x,0),\nabla u_t^N(x,0)\right)_{L^2(\Omega)} + \varrho\int_0^\tau\left\|\nabla u_t(x,t)\right\|_{L^2(\Omega)}^2 dt\\ &+ \frac{\delta}{2}\left\|\nabla u_t^N(x,0)\right\|_{L^2(\Omega)}^2 - \gamma\int_0^\tau\left\|\nabla u_{tt}^N(x,t)\right\|_{L^2(\Omega)}^2 dt\\ &+ \varrho\int_{\partial\Omega} u_\tau^N(x,\tau)\int_0^\tau\int_\Omega u^N(\xi,t)d\xi dt ds_x\\ &- \varrho\int_{\partial\Omega}\int_0^\tau u_t^N(x,t)\int_\Omega u^N(\xi,t)d\xi dt ds_x + \delta\int_{\partial\Omega} u_\tau^N(x,\tau)\int_\Omega u^N(\xi,\tau)d\xi ds_x\\ &- \delta\int_{\partial\Omega} u_\tau^N(x,\tau)\int_\Omega u^N(\xi,0)d\xi ds_x - \delta\int_{\partial\Omega}\int_0^\tau u_t^N(x,t)\int_\Omega u_t^N(\xi,t)d\xi dt ds_x\\ &+ \gamma\int_{\partial\Omega} u_\tau^N(x,\tau)\int_\Omega u_\tau^N(\xi,\tau)d\xi ds_x - \gamma\int_{\partial\Omega} u_\tau^N(x,\tau)\int_\Omega u_t^N(\xi,0)d\xi ds_x\\ &- \gamma\int_{\partial\Omega}\int_0^\tau u_t^N(x,t)\int_\Omega u_{tt}^N(\xi,t)d\xi dt ds_x.\end{aligned} \tag{40}$$

Now, multiplying each equation of (6) by the appropriate $C_k'(t)$, we add them up from 1 to N and then integrate with respect to t from 0 to τ, with $\tau \le T$, and we obtain

$$\begin{aligned}&\left(u_{tttt}^N, u_{ttt}^N\right)_{L^2(Q_\tau)} + \alpha\left(u_{ttt}^N, u_{ttt}^N\right)_{L^2(Q_\tau)} + \beta\left(u_{tt}^N, u_{ttt}^N\right)_{L^2(Q_\tau)} + \varrho\left(\nabla u^N,\nabla u_{ttt}^N\right)_{L^2(Q_\tau)}\\ &+ \delta\left(\nabla u_t^N,\nabla u_{ttt}^N\right)_{L^2(Q_\tau)} + \gamma\left(\nabla u_{tt}^N,\nabla u_{ttt}^N\right)_{L^2(Q_\tau)}\\ &= \varrho\int_0^\tau\int_{\partial\Omega} u_{ttt}^N(x,t)\left(\int_0^t\int_\Omega u^N(\xi,\eta)d\xi d\eta\right)ds_x dt\\ &+ \delta\int_0^\tau\int_{\partial\Omega} u_{ttt}^N(x,t)\left(\int_0^t\int_\Omega u_t^N(\xi,\eta)d\xi d\eta\right)ds_x dt\\ &+ \gamma\int_0^\tau\int_{\partial\Omega} u_{ttt}^N(x,t)\left(\int_0^t\int_\Omega u_{tt}^N(\xi,\eta)d\xi d\eta\right)ds_x dt.\end{aligned} \tag{41}$$

With the same reasoning in (12), we find

$$\left(u_{tttt}^N, u_{ttt}^N\right)_{L^2(Q_\tau)} = \frac{1}{2}\left\|u_{\tau\tau\tau}^N(x,\tau)\right\|_{L^2(\Omega)}^2 - \frac{1}{2}\left\|u_{ttt}^N(x,0)\right\|_{L^2(\Omega)}^2, \tag{42}$$

$$\alpha\left(u_{ttt}^N, u_{ttt}^N\right)_{L^2(Q_\tau)} = \alpha\int_0^\tau\left\|u_{ttt}^N(x,t)\right\|_{L^2(\Omega)}^2, \tag{43}$$

$$\beta\left(u_{tt}^N, u_{ttt}^N\right)_{L^2(Q_\tau)} = \frac{\beta}{2}\left\|u_{\tau\tau}^N(x,\tau)\right\|_{L^2(\Omega)}^2 - \frac{\beta}{2}\left\|u_{tt}^N(x,0)\right\|_{L^2(\Omega)}^2, \tag{44}$$

$$\begin{aligned}\varrho\left(\nabla u^N,\nabla u_{ttt}^N\right)_{L^2(Q_\tau)} &= \varrho\left(\nabla u^N(x,\tau),\nabla u_{\tau\tau}^N(x,\tau)\right)_{L^2(\Omega)}\\ &\quad - \varrho\left(\nabla u^N(x,0),\nabla u_{tt}^N(x,0)\right)_{L^2(\Omega)}\\ &\quad - \varrho\int_0^\tau\left(\nabla u_t^N,\nabla u_{tt}^N\right)_{L^2(\Omega)}dt,\end{aligned} \tag{45}$$

$$\begin{aligned}\delta\left(\nabla u_t^N,\nabla u_{ttt}^N\right)_{L^2(Q_\tau)} &= -\delta\int_0^\tau\left\|\nabla u_{tt}^N(x,t)\right\|_{L^2(\Omega)}^2 dt + \delta\left(\nabla u_\tau^N(x,\tau),\nabla u_{\tau\tau}^N(x,\tau)\right)_{L^2(\Omega)}\\ &\quad - \delta\left(\nabla u_t^N(x,0),\nabla u_{tt}^N(x,0)\right)_{L^2(\Omega)},\end{aligned} \tag{46}$$

$$\gamma\left(\nabla u_{tt}^N,\nabla u_{ttt}^N\right)_{L^2(Q_\tau)} = \frac{\gamma}{2}\left\|\nabla u_{\tau\tau}^N(x,\tau)\right\|_{L^2(\Omega)}^2 - \frac{\gamma}{2}\left\|\nabla u_{tt}^N(x,0)\right\|_{L^2(\Omega)}^2, \tag{47}$$

$$\begin{aligned}&\varrho\int_0^\tau\int_{\partial\Omega} u_{ttt}^N\left(\int_0^t\int_\Omega u^N(\xi,\eta)d\xi d\eta\right)ds_x dt\\ &= \varrho\int_{\partial\Omega} u_{\tau\tau}^N(x,\tau)\int_0^\tau\int_\Omega u^N(\xi,t)d\xi dt ds_x\\ &\quad - \varrho\int_{\partial\Omega}\int_0^\tau u_{tt}^N(x,t)\int_\Omega u^N(\xi,t)d\xi dt ds_x,\end{aligned} \tag{48}$$

$$\begin{aligned}&\delta\int_0^\tau\int_{\partial\Omega} u_{ttt}^N(x,t)\left(\int_0^t\int_\Omega u_t^N(\xi,\eta)d\xi d\eta\right)ds_x dt\\ &= \delta\int_{\partial\Omega} u_{\tau\tau}^N(x,\tau)\int_\Omega u^N(\xi,\tau)d\xi ds_x - \delta\int_{\partial\Omega} u_{\tau\tau}^N(x,\tau)\int_\Omega u^N(\xi,0)d\xi ds_x\\ &\quad - \delta\int_{\partial\Omega}\int_0^\tau u_{tt}^N(x,t)\int_\Omega u_t^N(\xi,t)d\xi dt ds,\end{aligned} \tag{49}$$

$$\begin{aligned}&\gamma\int_0^\tau\int_{\partial\Omega} u_{ttt}^N(x,t)\left(\int_0^t\int_\Omega u_{tt}^N(\xi,\eta)d\xi d\eta\right)ds_x dt\\ &= \gamma\int_{\partial\Omega} u_{\tau\tau}^N(x,\tau)\int_\Omega u_\tau^N(\xi,\tau)d\xi ds_x - \gamma\int_{\partial\Omega} u_{\tau\tau}^N(x,\tau)\int_\Omega u_t^N(\xi,0)d\xi ds_x\\ &\quad - \gamma\int_{\partial\Omega}\int_0^\tau u_{tt}^N(x,t)\int_\Omega u_{tt}^N(\xi,t)d\xi dt ds,\end{aligned} \tag{50}$$

A substitution of equalities (42) and (43) in (34) gives

$$\begin{aligned}&\frac{1}{2}\left\|u_{\tau\tau\tau}^N(x,\tau)\right\|_{L^2(\Omega)}^2 + \frac{\beta}{2}\left\|u_{\tau\tau}^N(x,\tau)\right\|_{L^2(\Omega)}^2 + \varrho\left(\nabla u^N(x,\tau),\nabla u_{\tau\tau}^N(x,\tau)\right)_{L^2(\Omega)}\\ &+\delta\left(\nabla u_\tau^N(x,\tau),\nabla u_{\tau\tau}^N(x,\tau)\right)_{L^2(\Omega)} + \frac{\gamma}{2}\left\|\nabla u_{\tau\tau}^N(x,\tau)\right\|_{L^2(\Omega)}^2\\ &= \frac{1}{2}\left\|u_{ttt}^N(x,0)\right\|_{L^2(\Omega)}^2 - \alpha\int_0^\tau\left\|u_{ttt}^N(x,t)\right\|_{L^2(\Omega)}^2 - \frac{\beta}{2}\left\|u_{tt}^N(x,0)\right\|_{L^2(\Omega)}^2\\ &+\varrho\left(\nabla u^N(x,0),\nabla u_{tt}^N(x,0)\right)_{L^2(\Omega)} + \varrho\int_0^\tau\left(\nabla u_t^N,\nabla u_{tt}^N\right)_{L^2(\Omega)}dt\\ &+\delta\int_0^\tau\left\|\nabla u_{tt}^N(x,t)\right\|_{L^2(\Omega)}^2 dt + \delta\left(\nabla u_t^N(x,0),\nabla u_{tt}^N(x,0)\right)_{L^2(\Omega)} - \frac{\gamma}{2}\left\|\nabla u_{tt}^N(x,0)\right\|_{L^2(\Omega)}^2\\ &+\varrho\int_{\partial\Omega} u_{\tau\tau}^N(x,\tau)\int_0^\tau\int_\Omega u^N(\xi,t)d\xi dt ds_x - \varrho\int_{\partial\Omega}\int_0^\tau u_{tt}^N(x,t)\int_\Omega u^N(\xi,t)d\xi dt ds_x\\ &+\delta\int_{\partial\Omega} u_{\tau\tau}^N(x,\tau)\int_\Omega u^N(\xi,\tau)d\xi ds_x - \delta\int_{\partial\Omega} u_{\tau\tau}^N(x,\tau)\int_\Omega u^N(\xi,0)d\xi ds_x\end{aligned}$$

$$-\delta\int_{\partial\Omega}\int_0^\tau u_{tt}^N(x,t)\int_\Omega u_t^N(\xi,t)d\xi dtds\gamma+\int_{\partial\Omega}u_{\tau\tau}^N(x,\tau)\int_\Omega u_\tau^N(\xi,\tau)d\xi ds_x$$
$$-\gamma\int_{\partial\Omega}u_{\tau\tau}^N(x,\tau)\int_\Omega u_t^N(\xi,0)d\xi ds_x-\gamma\int_{\partial\Omega}\int_0^\tau u_{tt}^N(x,t)\int_\Omega u_{tt}^N(\xi,t)d\xi dtds. \tag{51}$$

Multiplying (22) by λ_1, (33) by λ_2, and (44) by λ_3, we get

$$\lambda_1\left(u_{\tau\tau\tau}^N(x,\tau),u_\tau^N(x,\tau)\right)_{L^2(\Omega)}+\lambda_1\alpha\left(u_{\tau\tau}^N(x,\tau),u_\tau^N(x,\tau)\right)_{L^2(\Omega)}+\frac{\lambda_1\beta}{2}\left\|u_\tau^N(x,\tau)\right\|_{L^2(\Omega)}^2$$
$$+\frac{\lambda_1\varrho}{2}\left\|\nabla u^N(x,\tau)\right\|_{L^2(\Omega)}^2+\left(\frac{\lambda_1\gamma}{2}+\frac{\lambda_2\delta}{2}\right)\left\|\nabla u_\tau^N(x,\tau)\right\|_{L^2(\Omega)}^2+\lambda_2\left(u_{\tau\tau\tau}^N(x,\tau),u_{\tau\tau}^N(x,\tau)\right)_{L^2(\Omega)}$$
$$+\left(\frac{\lambda_2\alpha}{2}+\frac{\lambda_3\beta}{2}\right)\left\|u_{\tau\tau}^N(x,\tau)\right\|_{L^2(\Omega)}^2+\lambda_2\varrho\left(\nabla u^N(x,\tau),\nabla u_\tau^N(x,\tau)\right)_{L^2(\Omega)}+\frac{\lambda_3}{2}\left\|u_{\tau\tau\tau}^N(x,\tau)\right\|_{L^2(\Omega)}^2$$
$$+\lambda_3\varrho\left(\nabla u^N(x,\tau),\nabla u_{\tau\tau}^N(x,\tau)\right)_{L^2(\Omega)}+\lambda_3\delta\left(\nabla u_\tau^N(x,\tau),\nabla u_{\tau\tau}^N(x,\tau)\right)_{L^2(\Omega)}+\frac{\lambda_3\gamma}{2}\left\|\nabla u_{\tau\tau}^N(x,\tau)\right\|_{L^2(\Omega)}^2$$
$$=\lambda_1\left(u_{ttt}^N(x,0),u_t^N(x,0)\right)_{L^2(\Omega)}+\lambda_1\alpha\left(u_{tt}^N(x,0),u_t^N(x,0)\right)_{L^2(\Omega)}+\frac{\lambda_1\beta}{2}\left\|u_t^N(x,0)\right\|_{L^2(\Omega)}^2$$
$$+\frac{\lambda_1\varrho}{2}\left\|\nabla u^N(x,0)\right\|_{L^2(\Omega)}^2+\left(\frac{\lambda_1\gamma}{2}+\frac{\lambda_2\delta}{2}\right)\left\|\nabla u_t^N(x,0)\right\|_{L^2(\Omega)}^2+\lambda_1\int_0^\tau\left(u_{ttt}^N,u_{tt}^N\right)_{L^2(\Omega)}dt$$
$$+(\lambda_1\alpha-\lambda_2\beta)\int_0^\tau\left\|u_{tt}(x,t)\right\|_{L^2(\Omega)}^2dt+(\lambda_2\varrho-\lambda_1\delta)\int_0^\tau\left\|\nabla u_t^N(x,t)\right\|_{L^2(\Omega)}^2dt$$
$$+(\lambda_2-\lambda_3\alpha)\int_0^\tau\left\|u_{ttt}^N(x,t)\right\|_{L^2(\Omega)}^2dt+\lambda_2\left(u_{ttt}^N(x,0),u_{tt}^N(x,0)\right)_{L^2(\Omega)}+\left(\frac{\lambda_2\alpha}{2}-\frac{\lambda_3\beta}{2}\right)\left\|u_{tt}^N(x,0)\right\|_{L^2(\Omega)}^2$$
$$+\lambda_2\varrho\left(\nabla u^N(x,0),\nabla u_t^N(x,0)\right)_{L^2(\Omega)}+(\lambda_3\delta-\lambda_2\gamma)\int_0^\tau\left\|\nabla u_{tt}^N(x,t)\right\|_{L^2(\Omega)}^2dt+\frac{\lambda_3}{2}\left\|u_{ttt}^N(x,0)\right\|_{L^2(\Omega)}^2$$
$$+\lambda_3\varrho\left(\nabla u^N(x,0),\nabla u_{tt}^N(x,0)\right)_{L^2(\Omega)}+\lambda_3\varrho\int_0^\tau\left(\nabla u_t^N,\nabla u_{tt}^N\right)_{L^2(\Omega)}dt,$$
$$+\lambda_3\delta\left(\nabla u_t^N(x,0),\nabla u_{tt}^N(x,0)\right)_{L^2(\Omega)}-\frac{\lambda_3\gamma}{2}\left\|\nabla u_{tt}^N(x,0)\right\|_{L^2(\Omega)}^2$$
$$+\lambda_1\varrho\int_{\partial\Omega}u^N(x,\tau)\int_0^\tau\int_\Omega u^N(\xi,t)d\xi dtds_x-\lambda_1\varrho\int_{\partial\Omega}\int_0^\tau u^N(x,t)\cdot\int_\Omega u^N(\xi,t)d\xi dtds_x$$
$$+(\lambda_1\delta-\lambda_2\varrho)\int_{\partial\Omega}\int_0^\tau u_t^N(x,t)\int_\Omega u^N(\xi,t)d\xi dtds_x-\lambda_1\delta\int_{\partial\Omega}\int_0^\tau u_t^N(x,t)\cdot\int_\Omega u^N(\xi,0)d\xi dtds_x$$
$$+(\lambda_1\gamma-\lambda_2\delta)\int_0^\tau\int_{\partial\Omega}u_t^N(x,t)\left(\int_\Omega u_t^N(\xi,t)d\xi\right)ds_xdt-\lambda_1\gamma\int_0^\tau\int_{\partial\Omega}u_t^N(x,t)\cdot\left(\int_\Omega u_t^N(\xi,0)d\xi\right)ds_xdt.$$
$$+\lambda_2\varrho\int_{\partial\Omega}u_\tau^N(x,\tau)\int_0^\tau\int_\Omega u^N(\xi,t)d\xi dtds_x+\lambda_2\delta\int_{\partial\Omega}u_\tau^N(x,\tau)\int_\Omega u^N(\xi,\tau)d\xi ds_x$$
$$-\lambda_2\delta\int_{\partial\Omega}u_\tau^N(x,\tau)\int_\Omega u^N(\xi,0)d\xi ds_x+\lambda_2\gamma\int_{\partial\Omega}u_\tau^N(x,\tau)\int_\Omega u_\tau^N(\xi,\tau)d\xi ds_x$$
$$-\lambda_2\gamma\int_{\partial\Omega}u_\tau^N(x,\tau)\int_\Omega u_t^N(\xi,0)d\xi ds_x-\lambda_2\gamma\int_{\partial\Omega}\int_0^\tau u_t^N(x,t)\int_\Omega u_{tt}^N(\xi,t)d\xi dtds_x$$
$$+\lambda_3\varrho\int_{\partial\Omega}u_{\tau\tau}^N(x,\tau)\int_0^\tau\int_\Omega u^N(\xi,t)d\xi dtds_x-\lambda_3\varrho\int_{\partial\Omega}\int_0^\tau u_{tt}^N(x,t)\int_\Omega u^N(\xi,t)d\xi dtds_x$$
$$+\lambda_3\delta\int_{\partial\Omega}u_{\tau\tau}^N(x,\tau)\int_\Omega u^N(\xi,\tau)d\xi ds_x-\lambda_3\delta\int_{\partial\Omega}u_{\tau\tau}^N(x,\tau)\int_\Omega u^N(\xi,0)d\xi ds_x$$
$$-\lambda_3\delta\int_{\partial\Omega}\int_0^\tau u_{tt}^N(x,t)\int_\Omega u_t^N(\xi,t)d\xi dtds+\lambda_3\gamma\int_{\partial\Omega}u_{\tau\tau}^N(x,\tau)\int_\Omega u_\tau^N(\xi,\tau)d\xi ds_x$$
$$-\lambda_3\gamma\int_{\partial\Omega}u_{\tau\tau}^N(x,\tau)\int_\Omega u_t^N(\xi,0)d\xi ds_x-\lambda_3\gamma\int_{\partial\Omega}\int_0^\tau u_{tt}^N(x,t)\int_\Omega u_{tt}^N(\xi,t)d\xi dtds. \tag{52}$$

We can estimate all the terms in the right-hand side of (45) as follows:

$$\lambda_1\varrho\int_{\partial\Omega}u^N(x,\tau)\int_0^\tau\int_\Omega u^N(\xi,t)d\xi dtds_x$$
$$\le\frac{\lambda_1\varrho}{2\varepsilon_1}\left(\varepsilon\left\|\nabla u^N(x,\tau)\right\|_{L^2(\Omega)}^2+l(\varepsilon)\left\|u^N(x,\tau)\right\|_{L^2(\Omega)}^2\right)+\frac{\lambda_1\varrho}{2}\varepsilon_1T|\Omega||\partial\Omega|\int_0^\tau\left\|u^N(x,t)\right\|_{L^2(\Omega)}^2dt,$$
$$-\lambda_1\varrho\int_{\partial\Omega}\int_0^\tau u^N(x,t)\int_\Omega u^N(\xi,t)d\xi dtds_x$$
$$\le\frac{\lambda_1\varrho}{2}\varepsilon\int_0^\tau\left\|\nabla u^N(x,t)\right\|_{L^2(\Omega)}^2dt+\frac{\lambda_1\varrho}{2}\left(l(\varepsilon)+|\Omega||\partial\Omega|\right)\int_0^\tau\left\|u^N(x,t)\right\|_{L^2(\Omega)}^2dt,$$
$$(\lambda_1\delta-\lambda_2\varrho)\int_{\partial\Omega}\int_0^\tau u_t^N(x,t)\int_\Omega u^N(\xi,t)d\xi dtds_x$$
$$\le\underline{(\lambda_1\delta+\lambda_2\varrho)}$$
$$2\left(\varepsilon\int_0^\tau\left\|\nabla u_t^N(x,t)\right\|_{L^2(\Omega)}^2dt+l(\varepsilon)\int_0^\tau\left\|u_t^N(x,t)\right\|_{L^2(\Omega)}^2dt\right)$$

$$+\frac{(\lambda_1\delta+\lambda_2\varrho)}{2}|\Omega||\partial\Omega|\int_0^\tau\left\|u^N(x,t)\right\|^2_{L^2(\Omega)}dt,$$

$$-\lambda_1\delta\int_{\partial\Omega}\int_0^\tau u_t^N(x,t)\int_\Omega u^N(\xi,0)d\xi dtds_x$$

$$\le\frac{\lambda_1\delta}{2}\left(\varepsilon\int_0^\tau\left\|\nabla u_t^N(x,t)\right\|^2_{L^2(\Omega)}dt+l(\varepsilon)\int_0^\tau\left\|u_t^N(x,t)\right\|^2_{L^2(\Omega)}dt\right)$$

$$+\frac{\lambda_1\delta}{2}|\Omega||\partial\Omega|T\left\|u^N(x,0)\right\|^2_{L^2(\Omega)},$$

$$\lambda_2\varrho\int_{\partial\Omega}u_\tau^N(x,\tau)\int_0^\tau\int_\Omega u^N(\xi,t)d\xi dtds_x$$

$$\le\frac{\lambda_2\varrho}{2}\left(\frac{\varepsilon}{\varepsilon_2}\left\|\nabla u_\tau^N(x,\tau)\right\|^2_{L^2(\Omega)}+\frac{l(\varepsilon)}{\varepsilon_2}\left\|u_\tau^N(x,\tau)\right\|^2_{L^2(\Omega)}\right)$$

$$+\frac{\lambda_2\varrho}{2}\varepsilon_2|\Omega||\partial\Omega|T\int_0^\tau\left\|u^N(x,t)\right\|^2_{L^2(\Omega)}dt,$$

$$\lambda_2\delta\int_{\partial\Omega}u_\tau^N(x,\tau)\int_\Omega u^N(\xi,\tau)d\xi ds_x$$

$$\le\frac{\lambda_2\delta}{2\varepsilon_3}\left(\varepsilon\left\|\nabla u_\tau^N(x,\tau)\right\|^2_{L^2(\Omega)}+l(\varepsilon)\left\|u_\tau^N(x,\tau)\right\|^2_{L^2(\Omega)}\right)$$

$$+\frac{\lambda_2\delta}{2}\varepsilon_3|\Omega||\partial\Omega|\left\|u^N(x,\tau)\right\|^2_{L^2(\Omega)},$$

$$-\lambda_2\delta\int_{\partial\Omega}u_\tau^N(x,\tau)\int_\Omega u^N(\xi,0)d\xi ds_x$$

$$\le\frac{\lambda_2\delta}{2\varepsilon_4}\left(\varepsilon\left\|\nabla u_\tau^N(x,\tau)\right\|^2_{L^2(\Omega)}+l(\varepsilon)\left\|u_\tau^N(x,\tau)\right\|^2_{L^2(\Omega)}\right)$$

$$+\frac{\lambda_2\delta}{2}\varepsilon_4|\Omega||\partial\Omega|\left\|u^N(x,0)\right\|^2_{L^2(\Omega)},$$

$$(\lambda_1\gamma-\lambda_2\delta)\int_{\partial\Omega}\int_0^\tau u_t^N(x,t)\int_\Omega u_t^N(\xi,t)d\xi dtds_x$$

$$\le\frac{(\lambda_1\gamma+\lambda_2\delta)}{2}\varepsilon\int_0^\tau\left\|\nabla u_t^N(x,t)\right\|^2_{L^2(\Omega)}dt$$

$$+\frac{(\lambda_1\gamma+\lambda_2\delta)}{2}(l(\varepsilon)+|\Omega||\partial\Omega|)\int_0^\tau\left\|u_t^N(x,t)\right\|^2_{L^2(\Omega)}dt,\quad(53)$$

$$-\lambda_1\gamma\int_0^\tau\int_{\partial\Omega}u_t^N(x,t)\left(\int_\Omega u_t^N(\xi,0)d\xi\right)ds_xdt$$

$$\le\frac{\lambda_1\gamma}{2}\left(\varepsilon\int_0^\tau\left\|\nabla u_t^N(x,t)\right\|^2_{L^2(\Omega)}dt+l(\varepsilon)\int_0^\tau\left\|u_t^N(x,t)\right\|^2_{L^2(\Omega)}dt\right)$$

$$+\frac{\lambda_1\gamma}{2}|\Omega||\partial\Omega|T\left\|u_t^N(x,0)\right\|^2_{L^2(\Omega)},$$

$$\lambda_2\gamma\int_{\partial\Omega}u_\tau^N(x,\tau)\int_\Omega u_\tau^N(\xi,\tau)d\xi ds_x$$

$$\le\frac{\lambda_2\gamma}{2\varepsilon_5}\left(\varepsilon\left\|\nabla u_\tau^N(x,\tau)\right\|^2_{L^2(\Omega)}+l(\varepsilon)\left\|u_\tau^N(x,\tau)\right\|^2_{L^2(\Omega)}\right)$$

$$+\frac{\lambda_2\gamma}{2}\varepsilon_5|\Omega||\partial\Omega|\left\|u_\tau^N(x,\tau)\right\|^2_{L^2(\Omega)},-\lambda_2\gamma\int_{\partial\Omega}u_\tau^N(x,\tau)\int_\Omega u_t^N(\xi,0)d\xi ds_x$$

$$\le\frac{\lambda_2\gamma}{2\varepsilon_6}\left(\varepsilon\left\|\nabla u_\tau^N(x,\tau)\right\|^2_{L^2(\Omega)}+l(\varepsilon)\left\|u_\tau^N(x,\tau)\right\|^2_{L^2(\Omega)}\right)$$

$$+\frac{\lambda_2\gamma}{2}\varepsilon_6|\Omega||\partial\Omega|\left\|u_t^N(x,0)\right\|^2_{L^2(\Omega)},$$

$$-\lambda_2\gamma\int_{\partial\Omega}\int_0^\tau u_t^N(x,t)\int_\Omega u_{tt}^N(\xi,t)d\xi dtds_x$$

$$\le\frac{\lambda_2\gamma}{2}\varepsilon\int_0^\tau\left\|\nabla u_t^N(x,t)\right\|^2_{L^2(\Omega)}dt+\frac{\lambda_2\gamma}{2}l(\varepsilon)\int_0^\tau\left\|u_t^N(x,t)\right\|^2_{L^2(\Omega)}dt$$

$$+\frac{\lambda_2\gamma}{2}|\Omega||\partial\Omega|\int_0^\tau\left\|u_{tt}^N(x,t)\right\|^2_{L^2(\Omega)}dt,$$

$$\lambda_3\varrho\int_{\partial\Omega}u_{\tau\tau}^N(x,\tau)\int_0^\tau\int_\Omega u^N(\xi,t)d\xi dtds_x$$

$$\le\frac{\lambda_3\varrho}{2}\left(\frac{\varepsilon}{\varepsilon_7}\left\|\nabla u_{\tau\tau}^N(x,\tau)\right\|^2_{L^2(\Omega)}+\frac{l(\varepsilon)}{\varepsilon_7}\left\|u_{\tau\tau}^N(x,\tau)\right\|^2_{L^2(\Omega)}\right)$$

$$+\frac{\lambda_3\varrho}{2}\varepsilon_7|\Omega||\partial\Omega|T\int_0^\tau\left\|u^N(x,t)\right\|^2_{L^2(\Omega)}dt,$$

$$-\lambda_3\varrho\int_{\partial\Omega}\int_0^\tau u_{tt}^N(x,t)\int_\Omega u^N(\xi,t)d\xi dtds_x$$

$$\le\frac{\lambda_3\varrho}{2}\left(\varepsilon\int_0^\tau\left\|\nabla u_{tt}^N(x,t)\right\|^2_{L^2(\Omega)}dt+l(\varepsilon)\int_0^\tau\left\|u_{tt}^N(x,t)\right\|^2_{L^2(\Omega)}dt\right)$$

$$+\frac{\lambda_3\varrho}{2}|\Omega||\partial\Omega|\int_0^\tau\left\|u^N(x,t)\right\|^2_{L^2(\Omega)}dt,$$

$$\lambda_3\delta\int_{\partial\Omega}u_{\tau\tau}^N(x,\tau)\int_\Omega u^N(\xi,\tau)d\xi ds_x$$

$$\le\frac{\lambda_3\delta}{2\varepsilon_8}\left(\varepsilon\left\|\nabla u_{\tau\tau}^N(x,\tau)\right\|^2_{L^2(\Omega)}+l(\varepsilon)\left\|u_{\tau\tau}^N(x,\tau)\right\|^2_{L^2(\Omega)}\right)$$

$$+\frac{\lambda_3\delta}{2}\varepsilon_8|\Omega||\partial\Omega|\left\|u^N(x,\tau)\right\|^2_{L^2(\Omega)},\quad(54)$$

$$-\lambda_3\delta\int_{\partial\Omega}u_{\tau\tau}^N(x,\tau)\int_\Omega u^N(\xi,0)d\xi ds_x$$

$$\le\frac{\lambda_3\delta}{2\varepsilon_9}\left(\varepsilon\left\|\nabla u_{\tau\tau}^N(x,\tau)\right\|^2_{L^2(\Omega)}+l(\varepsilon)\left\|u_{\tau\tau}^N(x,\tau)\right\|^2_{L^2(\Omega)}\right)$$

$$+\frac{\lambda_3\delta}{2}\varepsilon_9|\Omega||\partial\Omega|\left\|u^N(x,0)\right\|^2_{L^2(\Omega)},\quad(55)$$

$$-\lambda_3\delta\int_{\partial\Omega}\int_0^\tau u_{tt}^N(x,t)\int_\Omega u_t^N(\xi,t)d\xi dtds_x$$

$$\le\frac{\lambda_3\delta}{2}\left(\varepsilon\int_0^\tau\left\|\nabla u_{tt}^N(x,t)\right\|^2_{L^2(\Omega)}dt+l(\varepsilon)\int_0^\tau\left\|u_{tt}^N(x,t)\right\|^2_{L^2(\Omega)}dt\right)$$

$$+\frac{\lambda_3\delta}{2}|\Omega||\partial\Omega|\int_0^\tau\left\|u_t^N(x,t)\right\|^2_{L^2(\Omega)}dt,$$

$$\begin{aligned}
&\lambda_3\gamma\int_{\partial\Omega}u_{\tau\tau}^N(x,\tau)\int_\Omega u_\tau^N(\xi,\tau)d\xi ds_x\\
&\quad\le\frac{\lambda_3\gamma}{2\varepsilon_{10}}\left(\varepsilon\left\|\nabla u_{\tau\tau}^N(x,\tau)\right\|_{L^2(\Omega)}^2+l(\varepsilon)\left\|u_{\tau\tau}^N(x,\tau)\right\|_{L^2(\Omega)}^2\right)\\
&\qquad+\frac{\lambda_3\gamma}{2}\varepsilon_{10}|\Omega||\partial\Omega|\left\|u_\tau^N(x,\tau)\right\|_{L^2(\Omega)}^2,
\end{aligned}\tag{56}$$

$$\begin{aligned}
&-\lambda_3\gamma\int_{\partial\Omega}u_{\tau\tau}^N(x,\tau)\int_\Omega u_t^N(\xi,0)d\xi ds_x\\
&\quad\le\frac{\lambda_3\gamma}{2\varepsilon_{11}}\left(\varepsilon\left\|\nabla u_{\tau\tau}^N(x,\tau)\right\|_{L^2(\Omega)}^2+l(\varepsilon)\left\|u_{\tau\tau}^N(x,\tau)\right\|_{L^2(\Omega)}^2\right)\\
&\qquad+\frac{\lambda_3\gamma}{2}\varepsilon_{11}|\Omega||\partial\Omega|\left\|u_t^N(x,0)\right\|_{L^2(\Omega)}^2,
\end{aligned}$$

$$\begin{aligned}
&-\lambda_3\gamma\int_{\partial\Omega}\int_0^\tau u_{tt}^N(x,t)\int_\Omega u_{tt}^N(\xi,t)d\xi dt ds_x\\
&\quad\le\frac{\lambda_3\gamma}{2}\varepsilon\int_0^\tau\left\|\nabla u_{tt}^N(x,t)\right\|_{L^2(\Omega)}^2dt\\
&\qquad+\frac{\lambda_3\gamma}{2}\left(l(\varepsilon)+|\Omega||\partial\Omega|\right)\int_0^\tau\left\|u_{tt}^N(x,t)\right\|_{L^2(\Omega)}^2dt,
\end{aligned}$$

$$\begin{aligned}
&-\frac{\lambda_1}{2}\left\|u_{\tau\tau\tau}^N(x,\tau)\right\|_{L^2(\Omega)}^2-\frac{\lambda_1}{2}\left\|u_\tau^N(x,\tau)\right\|_{L^2(\Omega)}^2\\
&\quad\le\lambda_1\left(u_{\tau\tau\tau}^N(x,\tau),u_\tau^N(x,\tau)\right)_{L^2(\Omega)},
\end{aligned}\tag{57}$$

$$\begin{aligned}
&-\frac{\lambda_2}{2}\left\|u_{\tau\tau\tau}^N(x,\tau)\right\|_{L^2(\Omega)}^2-\frac{\lambda_2}{2}\left\|u_{\tau\tau}^N(x,\tau)\right\|_{L^2(\Omega)}^2\\
&\quad\le\lambda_2\left(u_{\tau\tau\tau}^N(x,\tau),u_{\tau\tau}^N(x,\tau)\right)_{L^2(\Omega)},
\end{aligned}$$

$$\begin{aligned}
&-\frac{\lambda_1\alpha}{2}\left\|u_{\tau\tau}^N(x,\tau)\right\|_{L^2(\Omega)}^2-\frac{\lambda_1\alpha}{2}\left\|u_\tau^N(x,\tau)\right\|_{L^2(\Omega)}^2\\
&\quad\le\lambda_1\alpha\left(u_{\tau\tau}^N(x,\tau),u_\tau^N(x,\tau)\right)_{L^2(\Omega)},
\end{aligned}$$

$$\begin{aligned}
&-\frac{\lambda_2\varrho\varepsilon_{12}}{2}\left\|\nabla u^N(x,\tau)\right\|_{L^2(\Omega)}^2-\frac{\lambda_2\varrho}{2\varepsilon_{12}}\left\|\nabla u_\tau^N(x,\tau)\right\|_{L^2(\Omega)}^2\\
&\quad\le\lambda_2\varrho\left(\nabla u^N(x,\tau),\nabla u_\tau^N(x,\tau)\right)_{L^2(\Omega)},
\end{aligned}$$

$$\begin{aligned}
&-\frac{\lambda_2\varrho\varepsilon_{13}}{2}\left\|\nabla u^N(x,\tau)\right\|_{L^2(\Omega)}^2-\frac{\lambda_2\varrho}{2\varepsilon_{13}}\left\|\nabla u_{\tau\tau}^N(x,\tau)\right\|_{L^2(\Omega)}^2\\
&\quad\le\lambda_3\varrho\left(\nabla u^N(x,\tau),\nabla u_{\tau\tau}^N(x,\tau)\right)_{L^2(\Omega)},
\end{aligned}$$

$$\begin{aligned}
&-\frac{\lambda_3\delta\varepsilon_{14}}{2}\left\|\nabla u_\tau^N(x,\tau)\right\|_{L^2(\Omega)}^2-\frac{\lambda_3\delta\varepsilon_{14}}{2}\left\|\nabla u_{\tau\tau}^N(x,\tau)\right\|_{L^2(\Omega)}^2\\
&\quad\le\lambda_3\delta\left(\nabla u_\tau^N(x,\tau),\nabla u_{\tau\tau}^N(x,\tau)\right)_{L^2(\Omega)},
\end{aligned}$$

$$\begin{aligned}
&\lambda_1\left(u_{ttt}^N(x,0),u_t^N(x,0)\right)_{L^2(\Omega)}\\
&\quad\le\frac{\lambda_1}{2}\left\|u_{ttt}^N(x,0)\right\|_{L^2(\Omega)}^2+\frac{\lambda_1}{2}\left\|u_t^N(x,0)\right\|_{L^2(\Omega)}^2,
\end{aligned}$$

$$\begin{aligned}
&\lambda_1\alpha\left(u_{tt}^N(x,0),u_t^N(x,0)\right)_{L^2(\Omega)}\\
&\quad\le\frac{\lambda_1\alpha}{2}\left\|u_{tt}^N(x,0)\right\|_{L^2(\Omega)}^2+\frac{\lambda_1\alpha}{2}\left\|u_t^N(x,0)\right\|_{L^2(\Omega)}^2,
\end{aligned}$$

$$\begin{aligned}
&\lambda_2\left(u_{ttt}^N(x,0),u_{tt}^N(x,0)\right)_{L^2(\Omega)}\\
&\quad\le\frac{\lambda_2}{2}\left\|u_{ttt}^N(x,0)\right\|_{L^2(\Omega)}^2+\frac{\lambda_2}{2}\left\|u_{tt}^N(x,0)\right\|_{L^2(\Omega)}^2,
\end{aligned}$$

$$\begin{aligned}
&\lambda_2\varrho\left(\nabla u^N(x,0),\nabla u_t^N(x,0)\right)_{L^2(\Omega)}\\
&\quad\le\frac{\lambda_2}{2}\varrho\left\|\nabla u^N(x,0)\right\|_{L^2(\Omega)}^2+\frac{\lambda_2}{2}\varrho\left\|\nabla u_t^N(x,0)\right\|_{L^2(\Omega)}^2,
\end{aligned}$$

$$\begin{aligned}
&\lambda_3\varrho\left(\nabla u^N(x,0),\nabla u_{tt}^N(x,0)\right)_{L^2(\Omega)}\\
&\quad\le\frac{\lambda_3}{2}\varrho\left\|\nabla u^N(x,0)\right\|_{L^2(\Omega)}^2+\frac{\lambda_3}{2}\varrho\left\|\nabla u_{tt}^N(x,0)\right\|_{L^2(\Omega)}^2,
\end{aligned}$$

$$\begin{aligned}
&\lambda_3\delta\left(\nabla u_t^N(x,0),\nabla u_{tt}^N(x,0)\right)_{L^2(\Omega)}\\
&\quad\le\frac{\lambda_3}{2}\delta\left\|\nabla u_t^N(x,0)\right\|_{L^2(\Omega)}^2+\frac{\lambda_3}{2}\delta\left\|\nabla u_{tt}^N(x,0)\right\|_{L^2(\Omega)}^2,
\end{aligned}\tag{58}$$

$$\begin{aligned}
&\lambda_1\int_0^\tau\left(u_{ttt}^N,u_{tt}^N\right)_{L^2(\Omega)}dt\le\frac{\lambda_1}{2}\int_0^\tau\left\|u_{ttt}^N(x,t)\right\|_{L^2(\Omega)}^2dt\\
&\qquad+\frac{\lambda_1}{2}\int_0^\tau\left\|u_{tt}^N(x,t)\right\|_{L^2(\Omega)}^2dt,
\end{aligned}\tag{59}$$

$$\begin{aligned}
&\lambda_3\varrho\int_0^\tau\left(\nabla u_t^N,\nabla u_{tt}^N\right)_{L^2(\Omega)}dt\le\frac{\lambda_3\varrho}{2}\int_0^\tau\left\|\nabla u_t^N(x,t)\right\|_{L^2(\Omega)}^2dt\\
&\qquad+\frac{\lambda_3\varrho}{2}\int_0^\tau\left\|u_{tt}^N(x,t)\right\|_{L^2(\Omega)}^2dt.
\end{aligned}\tag{60}$$

Combining inequalities (46)–(79) and equality (45) and making use of the following inequality:

$$\begin{aligned}
&m_1\left\|u^N(x,\tau)\right\|_{L^2(\Omega)}^2\le m_1\left\|u^N(x,t)\right\|_{L^2(Q_\tau)}^2+m_1\left\|u_t^N(x,t)\right\|_{L^2(Q_\tau)}^2\\
&\qquad+m_1\left\|u^N(x,0)\right\|_{L^2(\Omega)}^2,
\end{aligned}$$

$$\begin{aligned}
&m_2\left\|u_\tau^N(x,\tau)\right\|_{L^2(\Omega)}^2\le m_2\left\|u_t^N(x,t)\right\|_{L^2(Q_\tau)}^2+m_2\left\|u_{tt}^N(x,t)\right\|_{L^2(Q_\tau)}^2\\
&\qquad+m_2\left\|u_t^N(x,0)\right\|_{L^2(\Omega)}^2,
\end{aligned}$$

$$\begin{aligned}
&m_3\left\|u_{\tau\tau}^N(x,\tau)\right\|_{L^2(\Omega)}^2\le m_3\left\|u_{tt}^N(x,t)\right\|_{L^2(Q_\tau)}^2+m_3\left\|u_{ttt}^N(x,t)\right\|_{L^2(Q_\tau)}^2\\
&\qquad+m_3\left\|u_{tt}^N(x,0)\right\|_{L^2(\Omega)}^2,
\end{aligned}$$

$$\begin{aligned}
&m_4\left\|\nabla u^N(x,\tau)\right\|_{L^2(\Omega)}^2\le m_4\left\|\nabla u^N(x,t)\right\|_{L^2(Q_\tau)}^2\\
&\qquad+m_4\left\|\nabla u_t^N(x,t)\right\|_{L^2(Q_\tau)}^2+m_4\left\|\nabla u^N(x,0)\right\|_{L^2(\Omega)}^2,
\end{aligned}$$

$$\begin{aligned}
&m_5\left\|\nabla u_\tau^N(x,\tau)\right\|_{L^2(\Omega)}^2\le m_5\left\|\nabla u_t^N(x,t)\right\|_{L^2(Q_\tau)}^2\\
&\qquad+m_5\left\|\nabla u_{tt}^N(x,t)\right\|_{L^2(Q_\tau)}^2+m_5\left\|\nabla u_t^N(x,0)\right\|_{L^2(\Omega)}^2,
\end{aligned}\tag{61}$$

where

$$m_1 = \frac{\lambda_2\delta}{2}\varepsilon_3|\Omega||\partial\Omega| + \frac{\lambda_3\delta}{2}\varepsilon_8|\Omega||\partial\Omega|,$$

$$m_2 = \frac{\lambda_2\varrho}{2}\frac{l(\varepsilon)}{\varepsilon_2} + \frac{\lambda_2\delta}{2}\frac{l(\varepsilon)}{\varepsilon_3} + \frac{\lambda_2\delta}{2}\frac{l(\varepsilon)}{\varepsilon_4} + \frac{\lambda_2\gamma}{2}\left(\frac{l(\varepsilon)}{\varepsilon_5} + \varepsilon_5|\Omega||\partial\Omega|\right) + \frac{\lambda_2\gamma}{2}\frac{l(\varepsilon)}{\varepsilon_6} + \frac{\lambda_3\gamma}{2}\varepsilon_{10}|\Omega||\partial\Omega| + \frac{\lambda_1}{2},$$

$$m_3 = \frac{\lambda_3\varrho}{2}\frac{l(\varepsilon)}{\varepsilon_7} + \frac{\lambda_3\delta}{2}\frac{l(\varepsilon)}{\varepsilon_8} + \frac{\lambda_3\delta}{2}\frac{l(\varepsilon)}{\varepsilon_9} + \frac{\lambda_3\gamma}{2}\frac{l(\varepsilon)}{\varepsilon_{10}} + \frac{\lambda_3\gamma}{2}\frac{l(\varepsilon)}{\varepsilon_{11}} + \frac{\lambda_2}{2} + \frac{\lambda_1\alpha}{2},$$

$$m_4 = \frac{\lambda_1\varrho}{2\varepsilon_1}\varepsilon + \frac{\lambda_2\varrho}{2}\varepsilon_{12} + \frac{\lambda_2\varrho}{2}\varepsilon_{13},$$

$$m_5 = \frac{\lambda_2\varrho}{2}\frac{\varepsilon}{\varepsilon_2} + \frac{\lambda_2\delta}{2}\frac{\varepsilon}{\varepsilon_3} + \frac{\lambda_2\delta}{2}\frac{\varepsilon}{\varepsilon_4} + \frac{\lambda_2\gamma}{2}\frac{\varepsilon}{\varepsilon_5} + \frac{\lambda_2\gamma}{2}\frac{\varepsilon}{\varepsilon_6} + \frac{\lambda_2\varrho}{2\varepsilon_{12}} + \frac{\lambda_3\delta\varepsilon_{14}}{2}, \tag{62}$$

we have

$$\begin{aligned}
&\frac{\lambda_1\varrho}{2\varepsilon_1}l(\varepsilon)\left\|u^N(x,\tau)\right\|^2_{L^2(\Omega)} + \frac{\lambda_1\beta}{2}\left\|u^N_\tau(x,\tau)\right\|^2_{L^2(\Omega)} \\
&\quad + \left(\frac{\lambda_2\alpha}{2} + \frac{\lambda_3\beta}{2}\right)\left\|u^N_{\tau\tau}(x,\tau)\right\|^2_{L^2(\Omega)} \\
&\quad + \left\{\frac{\lambda_3}{2} - \frac{\lambda_1}{2} - \frac{\lambda_2}{2}\right\}\left\|u^N_{\tau\tau\tau}(x,\tau)\right\|^2_{L^2(\Omega)} + \frac{\lambda_1\varrho}{2}\left\|\nabla u^N(x,\tau)\right\|^2_{L^2(\Omega)} \\
&\quad + \left\{\frac{\lambda_1\gamma}{2} + \frac{\lambda_2\delta}{2}\right\}\left\|\nabla u^N_\tau(x,\tau)\right\|^2_{L^2(\Omega)} \\
&+ \left\{-\frac{\lambda_3\varrho}{2}\frac{\varepsilon}{\varepsilon_7} - \frac{\lambda_3\delta}{2}\frac{\varepsilon}{\varepsilon_8} - \frac{\lambda_3\delta}{2}\frac{\varepsilon}{\varepsilon_9} - \frac{\lambda_3\gamma}{2}\frac{\varepsilon}{\varepsilon_{10}} - \frac{\lambda_3\gamma}{2}\frac{\varepsilon}{\varepsilon_{11}} - \frac{\lambda_2\varrho}{2\varepsilon_{13}} - \frac{\lambda_3\delta}{2\varepsilon_{14}} + \frac{\lambda_3\gamma}{2}\right\} \\
&\quad \cdot \left\|\nabla u^N_{\tau\tau}(x,\tau)\right\|^2_{L^2(\Omega)} \\
&\le \left\{\frac{\lambda_1\delta}{2}|\Omega||\partial\Omega|T + \frac{\lambda_2\delta}{2}\varepsilon_4|\Omega||\partial\Omega| + \frac{\lambda_3\delta}{2}\varepsilon_9|\Omega||\partial\Omega| + m_1\right\} \\
&\quad \cdot \left\|u^N(x,0)\right\|^2_{L^2(\Omega)} \\
&\left\{\frac{\lambda_1\gamma}{2}|\Omega||\partial\Omega|T + \frac{\lambda_2\gamma}{2}\varepsilon_6|\Omega||\partial\Omega| + \frac{\lambda_3\gamma}{2}\varepsilon_{11}|\Omega||\partial\Omega| + \frac{\lambda_1}{2} + \frac{\lambda_1\alpha}{2} + \frac{\lambda_1\beta}{2} + m_2\right\} \\
&\quad \cdot \left\|u^N_t(x,0)\right\|^2_{L^2(\Omega)} \\
&\quad + \left\{\frac{\lambda_2}{2} + \frac{\lambda_1\alpha}{2} + \left(\frac{\lambda_2\alpha}{2} - \frac{\lambda_3\beta}{2}\right) + m_3\right\}\left\|u^N_{tt}(x,0)\right\|^2_{L^2(\Omega)} \\
&\quad + \left\{\frac{\lambda_1}{2} + \frac{\lambda_2}{2} + \frac{\lambda_3}{2}\right\}\left\|u^N_{ttt}(x,0)\right\|^2_{L^2(\Omega)} \\
&\quad + \left\{\frac{\lambda_1\varrho}{2} + \frac{\lambda_2\varrho}{2} + \frac{\lambda_3\varrho}{2} + m_4\right\}\left\|\nabla u^N(x,0)\right\|^2_{L^2(\Omega)} \\
&\quad + \left\{\frac{\lambda_2\varrho}{2} + \frac{\lambda_3\delta}{2} + \frac{\lambda_1\gamma}{2} + \frac{\lambda_2\delta}{2} + m_5\right\}\left\|\nabla u^N_t(x,0)\right\|^2_{L^2(\Omega)}, \\
&\quad + \left\{\frac{\lambda_3\varrho}{2} + \frac{\lambda_3\delta}{2} - \frac{\lambda_3\gamma}{2}\right\}\left\|\nabla u^N_{tt}(x,0)\right\|^2_{L^2(\Omega)} \\
&\quad + (\gamma_1 + m_1)\int_0^\tau \left\|u^N(x,t)\right\|^2_{L^2(\Omega)}dt \\
&\quad + (\gamma_2 + m_1 + m_2)\int_0^\tau \left\|u^N_t(x,t)\right\|^2_{L^2(\Omega)}dt + (\gamma_3 + m_2 + m_3)\int_0^\tau \\
&\quad \cdot \left\|u^N_{tt}(x,t)\right\|^2_{L^2(\Omega)}dt \\
&\quad + \left\{\frac{\lambda_1}{2} + \lambda_2 - \lambda_3\alpha + m_3\right\}\int_0^\tau \left\|u^N_{ttt}(x,t)\right\|^2_{L^2(\Omega)}dt \\
&\quad + \left\{\frac{\lambda_1\varrho}{2}\varepsilon + m_4\right\}\int_0^\tau \left\|\nabla u^N(x,t)\right\|^2_{L^2(\Omega)}dt \\
&\quad + (\gamma_4 + m_4 + m_5)\int_0^\tau \left\|\nabla u^N_t(x,t)\right\|^2_{L^2(\Omega)}dt \\
&\quad + (\gamma_5 + m_5)\int_0^\tau \left\|\nabla u^N_{tt}(x,t)\right\|^2_{L^2(\Omega)}dt,
\end{aligned} \tag{63}$$

where

$$\gamma_1 = \frac{\lambda_1\varrho}{2}\varepsilon_1 T|\Omega||\partial\Omega| + \frac{\lambda_1\varrho}{2}(l(\varepsilon) + |\Omega||\partial\Omega|) + \left(\frac{\lambda_1\delta + \lambda_2\varrho}{2}\right)|\Omega||\partial\Omega| + \frac{\lambda_2\varrho}{2}\varepsilon_2 T|\Omega||\partial\Omega| + \frac{\lambda_3\varrho}{2}\varepsilon_7 T|\Omega||\partial\Omega| + \frac{\lambda_3\varrho}{2}|\Omega||\partial\Omega|,$$

$$\gamma_2 = \left(\frac{\lambda_1\delta + \lambda_2\varrho}{2}\right)l(\varepsilon) + \frac{\lambda_1\delta}{2}l(\varepsilon) + \left(\frac{\lambda_1\gamma + \lambda_2\delta}{2}\right)(l(\varepsilon) + |\Omega||\partial\Omega|) + \frac{\lambda_1\gamma}{2}l(\varepsilon) + \frac{\lambda_2\gamma}{2}l(\varepsilon) + \frac{\lambda_3\delta}{2}|\Omega||\partial\Omega|,$$

$$\gamma_3 = \frac{\lambda_2\gamma}{2}|\Omega||\partial\Omega| + \frac{\lambda_3\varrho}{2}l(\varepsilon) + \frac{\lambda_3\delta}{2}l(\varepsilon) + \frac{\lambda_3\gamma}{2}(l(\varepsilon) + |\Omega||\partial\Omega|) + \frac{\lambda_1}{2} + (\lambda_1\alpha - \lambda_2\beta),$$

$$\gamma_4 = \left(\frac{\lambda_1\delta + \lambda_2\varrho}{2}\right)\varepsilon + \frac{\lambda_1\delta}{2}\varepsilon + \left(\frac{\lambda_1\gamma + \lambda_2\delta}{2}\right)\varepsilon + \frac{\lambda_1\gamma}{2}\varepsilon + \frac{\lambda_2\gamma}{2}\varepsilon + \frac{\lambda_3\varrho}{2} + (\lambda_2\rho - \lambda_1\delta),$$

$$\gamma_5 = \frac{\lambda_3\delta}{2}\varepsilon + \frac{\lambda_3\gamma}{2}\varepsilon + \frac{\lambda_3\varrho}{2} + (\lambda_3\delta - \lambda_2\gamma). \tag{64}$$

Choosing ε_7, ε_8, $\varepsilon_9, \varepsilon_{10}$, ε_{11}, ε_{113}, and ε_{14} sufficiently large

$$\frac{\lambda_3\varrho}{2}\frac{\varepsilon}{\varepsilon_7}+\frac{\lambda_3\delta}{2}\frac{\varepsilon}{\varepsilon_8}+\frac{\lambda_3\delta}{2}\frac{\varepsilon}{\varepsilon_9}+\frac{\lambda_3\gamma}{2}\frac{\varepsilon}{\varepsilon_{10}}+\frac{\lambda_3\gamma}{2}\frac{\varepsilon}{\varepsilon_{11}}+\frac{\lambda_3\delta}{2\varepsilon_{14}}+\frac{\lambda_2\varrho}{2\varepsilon_{13}}<\frac{\lambda_3\gamma}{2}, \tag{65}$$

the relation (80) reduces to

$$\begin{aligned}&\left\{\left\|u^N(x,\tau)\right\|^2_{L^2(\Omega)}+\left\|\nabla u^N(x,\tau)\right\|^2_{L^2(\Omega)}+\left\|u^N_\tau(x,\tau)\right\|^2_{L^2(\Omega)}\right.\\&\quad\left.+\left\|\nabla u^N_\tau(x,\tau)\right\|^2_{L^2(\Omega)}\right.\\&\left.+\left\|u^N_{\tau\tau}(x,\tau)\right\|^2_{L^2(\Omega)}+\left\|\nabla u^N_{\tau\tau}(x,\tau)\right\|^2_{L^2(\Omega)}+\left\|u^N_{\tau\tau\tau}(x,\tau)\right\|^2_{L^2(\Omega)}\right\}\\&\le D\int_0^\tau\left\{\left\|u^N(x,t)\right\|^2_{L^2(\Omega)}+\left\|\nabla u^N(x,t)\right\|^2_{L^2(\Omega)}+\left\|u^N_t(x,t)\right\|^2_{L^2(\Omega)}\right.\\&\quad+\left\|\nabla u^N_t(x,t)\right\|^2_{L^2(\Omega)}+\left\|u^N_{tt}(x,t)\right\|^2_{L^2(\Omega)}+\left\|\nabla u^N_{tt}(x,t)\right\|^2_{L^2(\Omega)}\\&\quad\left.+\left\|u^N_{ttt}(x,t)\right\|^2_{L^2(\Omega)}\right\}dt\\&+D\left\{\left\|u^N(x,0)\right\|^2_{W^1_2(\Omega)}+\left\|u^N_t(x,0)\right\|^2_{W^1_2(\Omega)}\right.\\&\left.+\left\|u^N_{tt}(x,0)\right\|^2_{W^1_2(\Omega)}+\left\|u^N_{ttt}(x,0)\right\|^2_{L^2(\Omega)}\right\},\end{aligned} \tag{66}$$

where

$$\begin{aligned}D:=\frac{\max\left\{(\lambda_1\delta/2)|\Omega||\partial\Omega|T+(\lambda_2\delta/2)\varepsilon_4|\Omega||\partial\Omega|+(\lambda_3\delta/2)\varepsilon_9|\Omega||\partial\Omega|+m_1,(\lambda_1\gamma/2)|\Omega||\partial\Omega|T+(\lambda_2\gamma/2)\varepsilon_6|\Omega||\partial\Omega|\right.}{\min\left\{(\lambda_1\varrho/2\varepsilon_1)l(\varepsilon),(\lambda_1\beta/2),(\lambda_2\alpha/2)+(\lambda_3\beta/2),\right.}\\\frac{+(\lambda_3\gamma/2)\varepsilon_{11}|\Omega||\partial\Omega|+(\lambda_1/2)+(\lambda_1\alpha/2)+(\lambda_1\beta/2)+m_2,(\lambda_2/2)+(\lambda_1\alpha/2)+(\lambda_2\alpha/2)-(\lambda_3\beta/2)+m_3,(\lambda_1/2)+(\lambda_2/2)+(\lambda_3/2)}{\lambda_3/2-\lambda_1/2-\lambda_2/2,\lambda_1\varrho/2,(\lambda_1\gamma/2)+(\lambda_2\delta/2),}\\\frac{(\lambda_1\varrho/2)+(\lambda_2\varrho/2)+(\lambda_3\varrho/2)+m_4,(\lambda_2\varrho/2)+(\lambda_3\delta/2)+(\lambda_1\gamma/2)+(\lambda_2\delta/2)+m_5,(\lambda_3\varrho/2)+(\lambda_3\delta/2)-\lambda_3\gamma/2,}{\left.,-(\lambda_3\varrho/2)(\varepsilon/\varepsilon_7)-(\lambda_3\delta/2)(\varepsilon/\varepsilon_8)-(\lambda_3\delta/2)(\varepsilon/\varepsilon_9)-(\lambda_3\gamma/2)(\varepsilon/\varepsilon_{10})-(\lambda_3\gamma/2)(\varepsilon/\varepsilon_{11})-\lambda_2\varrho/2\varepsilon_{13}-\lambda_3\delta/2\varepsilon_{14}-\lambda_3\gamma/2\right\}}\\\frac{\gamma_1+m_1,\gamma_2+m_1+m_2,\gamma_3+m_2+m_3,(\lambda_1/2)+\lambda_2-\lambda_3\alpha+m_3,}{(\lambda_1\varrho/2)\varepsilon+m_4,\gamma_4+m_4+m_5,\gamma_5+m_5\}}.\end{aligned} \tag{67}$$

Applying the Gronwall inequality to (60) and then integrating from 0 to τ, it appears that

$$\begin{aligned}&\left\{\left\|u^N(x,t)\right\|^2_{W^1_2(Q_\tau)}+\left\|u^N_t(x,t)\right\|^2_{W^1_2(Q_\tau)}+\left\|u^N_{tt}(x,t)\right\|^2_{W^1_2(Q_\tau)}\right.\\&\left.\le De^{DT}\left\{\|u_0(x)\|^2_{W^1_2(\Omega)}+\|u_1(x)\|^2_{W^1_2(\Omega)}+\|u_2(x)\|^2_{L^2(\Omega)}+\|u_3(x)\|^2_{L^2(\Omega)}\right\}.\right.\end{aligned} \tag{68}$$

We deduce from (84) that

$$\left\|u^N(x,t)\right\|^2_{w^1_2(Q_\tau)}+\left\|u^N_t(x,t)\right\|^2_{w^1_2(Q_\tau)}+\left\|u^N_{tt}(x,t)\right\|^2_{w^1_2(Q_\tau)}\le A. \tag{69}$$

Therefore, the sequence $\{u^N\}_{N\ge1}$ is bounded in $V(Q_T)$, and we can extract from it a subsequence for which we use the same notation which converges weakly in $V(Q_T)$ to a limit function $u(x,t)$; we have to show that $u(x,t)$ is a generalized solution of (4). Since $u^N(x,t)\to u(x,t)$ in $L^2(Q_T)$ and $u^N(x,0)\to\zeta(x)$ in $L^2(\Omega)$, then $u(x,0)=\zeta(x)$.

Now to prove that (3) holds, we multiply each relation in (15) by a function $p_l(t)\in W^1_2(0,T)$, $p_l(t)=0$, then add up the obtained equalities ranging from $l=1$ to $l=N$, and integrate over t on $(0,T)$. If we let $\eta^N=\sum_{k=1}^N p_k(t)Z_k(x)$, then we have

$$\begin{aligned}&-\left(u^N_{ttt},\eta^N_t\right)_{L^2(Q_T)}-\alpha\left(u^N_{tt},\eta^N_t\right)_{L^2(Q_T)}-\beta\left(u^N_t,\eta^N_t\right)_{L^2(Q_T)}\\&+\varrho\left(\nabla u^N,\nabla\eta^N\right)_{L^2(Q_T)}+\delta\left(\nabla u^N_t,\nabla\eta^N\right)_{L^2(Q_T)}-\gamma\left(\nabla u^N_t,\nabla\eta^N_t\right)_{L^2(Q_T)}\\&=\varrho\int_{\partial\Omega}\int_0^T\eta^N(x,t)\left(\int_0^t\int_\Omega u^N(\xi,\tau)d\xi d\tau\right)dtds_x\\&\quad+\delta\int_{\partial\Omega}\int_0^T\eta^N(x,t)\int_\Omega u^N(\xi,t)d\xi dtds_x\\&\quad-\delta\int_{\partial\Omega}\int_0^T\eta^N(x,t)\int_\Omega u^N(\xi,0)d\xi dtds_x\\&\quad-\gamma\int_0^T\int_{\partial\Omega}\eta^N_t\left(\int_\Omega u^N(\xi,t)d\xi\right)ds_xdt\\&\quad+\gamma\int_0^T\int_{\partial\Omega}\eta^N_t\left(\int_\Omega u^N(\xi,0)d\xi\right)ds_xdt\\&\quad-\gamma\left(\Delta u^N_t(x,0),\eta^N(0)\right)_{L^2(\Omega)}\end{aligned}$$

$$+\left(u_{ttt}^{N}(x,0),\eta^{N}(0)\right)_{L^2(\Omega)}+\alpha\left(u_{tt}^{N}(x,0),\eta^{N}(0)\right)_{L^2(\Omega)}+\beta\left(u_{tt}^{N}(x,0),\eta^{N}(0)\right)_{L^2(\Omega)}, \tag{70}$$

for all η^N of the form $\sum_{k=1}^{N}p_l(t)Z_k(x)$.

Since

$$\int_0^t\int_\Omega\left(\left(u^N(\xi,\tau)-u(\xi,\tau)\right)d\xi d\tau\le\sqrt{T|\Omega|}\left\|u^N-u\right\|_{L^2(Q_T)},$$

$$\int_0^T\eta^N(x,t)\int_\Omega\left(u_t^N(\xi,t)-u_t(\xi,t)\right)d\xi dt\le\sqrt{|\Omega|}\left(\int_0^T\left(\eta^N(x,t)\right)^2dt\right)^{1/2}\left\|u_t^N-u_t\right\|_{L^2(Q_T)},$$

$$\int_0^T\eta^N(x,t)\int_\Omega\left(u\left({}^N(\xi,0)-u(\xi,0)\right)d\xi dt\le\sqrt{|\Omega|}\left(\int_0^T\left(\eta^N(x,t)\right)^2\right)^{1/2}\left\|u^N(x,0)\right\|_{L^2(Q_T)},$$

$$\left\|u^N-u\right\|_{L^2(Q_T)}\to0,\ \text{as}N\to\infty, \tag{71}$$

therefore, we have

$$\begin{aligned}
&\varrho\int_{\partial\Omega}\int_0^T\eta^N(x,t)\int_0^t\int_\Omega u^N(\xi,\tau)d\xi d\tau dt ds_x,\\
&\to\varrho\int_{\partial\Omega}\int_0^T\eta(x,t)\int_0^t\int_\Omega u(\xi,\tau)d\xi d\tau dt ds_x,\\
&\delta\int_{\partial\Omega}\int_0^T\eta^N(x,t)\int_\Omega u^N(\xi,t)d\xi dt ds_x,\\
&\to\delta\int_{\partial\Omega}\int_0^T\eta(x,t)\int_\Omega u(\xi,t)d\xi dt ds_x,\\
&-\delta\int_{\partial\Omega}\int_0^T\eta^N(x,t)\int_\Omega u^N(\xi,0)d\xi dt ds,\\
&\to-\delta\int_{\partial\Omega}\int_0^T\eta(x,t)\int_\Omega u(\xi,0)d\xi dt ds,\\
&-\gamma\int_0^T\int_{\partial\Omega}\eta_t^N\left(\int_\Omega u^N(\xi,t)d\xi\right)ds_x dt,\\
&\to-\gamma\int_0^T\int_{\partial\Omega}\eta_t\left(\int_\Omega u(\xi,t)d\xi\right)ds_x dt,\\
&\gamma\int_0^T\int_{\partial\Omega}\eta_t^N\left(\int_\Omega u^N(\xi,0)d\xi\right)ds_x dt,\\
&\to\gamma\int_0^T\int_{\partial\Omega}\eta_t\left(\int_\Omega u(\xi,0)d\xi\right)ds_x dt.
\end{aligned} \tag{72}$$

Thus, the limit function u satisfies (3) for every $\eta^N=\sum_{k=1}^{N}p_l(t)Z_k(x)$. We denote by $\mathbb{Q}_N$ the totality of all functions of the form $\eta^N=\sum_{k=1}^{N}p_l(t)Z_k(x)$, with $p_l(t)\in W_2^1(0,T)$, $p_l(t)=0$.

But $\cup_{l=1}^{N}\mathbb{Q}_N$ is dense in $W(Q_T)$, and then relation (3) holds for all $u\in W(Q_T)$. Thus, we have shown that the limit function $u(x,t)$ is a generalized solution of problem (4) in $V(Q_T)$.

4. Uniqueness of Solution

Theorem 3. *The problem (4) cannot have more than one generalized solution in $V(Q_T)$.*

Proof. Suppose that there exist two different generalized solutions $u_1\in V(Q_T)$ and $u_2\in V(Q_T)$ for the problem (1). Then, the difference $U=u_1-u_2$ solves

$$\begin{cases}U_{tttt}+\alpha U_{ttt}+\beta U_{tt}-\varrho\Delta U-\delta\Delta U_t-\gamma\Delta U_{tt}=0,\\ U(x,0)=U_t(x,0)=U_{tt}(x,0)=U_{ttt}(x,0)=0\\ \dfrac{\partial u}{\partial\eta}=\displaystyle\int_0^t\int_\Omega u(\xi,\tau)d\xi d\tau,x\in\partial\Omega,\end{cases} \tag{73}$$

and (3) gives

$$\begin{aligned}
&-(U_{ttt},v_t)_{L^2(Q_T)}-\alpha(U_{tt},v_t)_{L^2(Q_T)}-\beta(U_t,v_t)_{L^2(Q_T)}\\
&+\varrho(\nabla U,\nabla v)_{L^2(Q_T)}+\delta(\nabla U_t,\nabla v)_{L^2(Q_T)}-\gamma(\nabla U_t,\nabla v_t)_{L^2(Q_T)}\\
&=\varrho\int_0^T\int_{\partial\Omega}v\left(\int_0^t\int_\Omega u(\xi,\tau)d\xi d\tau\right)ds_x dt\\
&+\delta\int_0^T\int_{\partial\Omega}v\int_\Omega u(\xi,t)d\xi ds_x dt-\gamma\int_0^T\int_{\partial\Omega}v_t\left(\int_\Omega u_\tau(\xi,t)d\xi dt\right)ds_x dt.
\end{aligned} \tag{74}$$

Consider the function

$$v(x,t)=\begin{cases}\displaystyle\int_t^\tau U(x,s)ds, & 0\le t\le\tau,\\ 0, & \tau\le t\le T.\end{cases} \tag{75}$$

It is obvious that $v\in W(Q_T)$ and $v_t(x,t)=-U(x,t)$ for all $t\in[0,\tau]$. Integration by parts in the left hand side of (75) gives

$$-(U_{ttt},v_t)_{L^2(Q_T)}=(U_{\tau\tau}(x,\tau),U(x,\tau))_{L^2(\Omega)}-\frac{1}{2}\|U_\tau(x,\tau)\|_{L^2(\Omega)}^2, \tag{76}$$

$$-\alpha(U_{tt},v_t)_{L^2(Q_T)}=\alpha(U_\tau(x,\tau),U(x,\tau))_{L^2(\Omega)}-\alpha\int_0^\tau\|U_t(x,t)\|_{L^2(\Omega)}^2dt, \tag{77}$$

$$-\beta(U_t,v_t)_{L^2(Q_T)}=\frac{\beta}{2}\|U(x,\tau)\|_{L^2(\Omega)}^2, \tag{78}$$

$$\varrho(\nabla U,\nabla v)_{L^2(Q_T)} = \frac{\varrho}{2}\|\nabla v(x,0)\|^2_{L^2(\Omega)}, \tag{79}$$

$$\delta(\nabla U_t,\nabla v)_{L^2(Q_T)} = \delta\int_0^\tau \|\nabla v_t(x,t)\|^2_{L^2(\Omega)}dt, \tag{80}$$

$$-\gamma(\nabla U_t,\nabla v_t)_{L^2(Q_T)} = \frac{\gamma}{2}\|\nabla U(x,\tau)\|^2_{L^2(\Omega)}, \tag{81}$$

Plugging (76)–(95) into (88), we obtain

$$\begin{aligned}
&(U_{\tau\tau}(x,\tau), U(x,\tau))_{L^2(\Omega)} + \alpha(U_\tau(x,\tau), U(x,\tau))_{L^2(\Omega)}\\
&\quad + \frac{\beta}{2}\|U(x,\tau)\|^2_{L^2(\Omega)} + \frac{\varrho}{2}\|\nabla v(x,0)\|^2_{L^2(\Omega)}\\
&\quad + \frac{\gamma}{2}\|\nabla U(x,\tau)\|^2_{L^2(\Omega)} - \frac{1}{2}\|U_\tau(x,\tau)\|^2_{L^2(\Omega)}\\
&= \alpha\int_0^\tau \|U_t(x,t)\|^2_{L^2(\Omega)}dt - \delta\int_0^\tau \|\nabla v_t(x,t)\|^2_{L^2(\Omega)}dt\\
&\quad + \varrho\int_0^T\int_{\partial\Omega} v\left(\int_0^t\int_\Omega U(\xi,\tau)d\xi d\tau\right)ds_x dt\\
&\quad + \delta\int_0^T\int_{\partial\Omega} v\int_\Omega U(\xi,t)d\xi ds_x dt\\
&\quad - \gamma\int_0^T\int_{\partial\Omega} v_t\left(\int_\Omega U(\xi,t)d\xi\right)dsdt.
\end{aligned} \tag{82}$$

Now, since

$$v^2(x,t) = \left(\int_t^\tau U(x,s)ds\right)^2 \le \tau\int_0^\tau U^2(x,s)ds, \tag{83}$$

then

$$\|v\|^2_{L^2(Q_\tau)} \le \tau^2\|U\|^2_{L^2(Q_\tau)} \le T^2\|U\|^2_{L^2(Q_\tau)}. \tag{84}$$

Using the trace inequality, the right-hand side of (96) can be estimated as follows:

$$\begin{aligned}
&\varrho\int_0^T\int_{\partial\Omega} v\left(\int_0^t\int_\Omega U(\xi,\tau)d\xi d\tau\right)ds_x dt\\
&\quad \le \frac{\varrho}{2}T^2\{l(\varepsilon) + |\Omega||\partial\Omega|\}\int_0^\tau \|U(x,t)\|^2_{L^2(\Omega)}dt + \frac{\varrho}{2}\varepsilon\int_0^\tau \|\nabla v(x,t)\|^2_{L^2(\Omega)}dt,
\end{aligned}$$

$$\begin{aligned}
\delta\int_0^T\int_{\partial\Omega} v\int_\Omega U(\xi,t)d\xi ds_x dt &\le \frac{\delta}{2}\left\{T^2 l(\varepsilon) + |\Omega||\partial\Omega|\right\}\int_0^\tau \|U(x,t)\|^2_{L^2(\Omega)}dt\\
&\quad + \frac{\delta}{2}\varepsilon\int_0^\tau \|\nabla v(x,t)\|^2_{L^2(\Omega)}dt,
\end{aligned}$$

$$\begin{aligned}
-\gamma\int_0^T\int_{\partial\Omega} v_t\left(\int_\Omega U(\xi,t)d\xi\right)dsdt &= \gamma\int_0^T\int_{\partial\Omega} v\left(\int_\Omega U_t(\xi,t)d\xi\right)dsdt\\
&= \gamma\int_0^\tau\int_{\partial\Omega} v\left(\int_\Omega U_t(\xi,t)d\xi\right)dsdt \le \frac{\gamma|\Omega||\partial\Omega|}{2}\|U_t\|^2_{L^2(Q_\tau)}\\
&\quad + \frac{\eta^2}{2}\varepsilon\|\nabla v\|^2_{L^2(Q_\tau)} + \frac{\gamma}{2}l(\varepsilon)T^2\|U\|^2_{L^2(Q_\tau)}.
\end{aligned} \tag{85}$$

Combining the relations (98)-(101) and (96), we get

$$\begin{aligned}
&(U_{\tau\tau}(x,\tau), U(x,\tau))_{L^2(\Omega)} + \alpha(U_\tau(x,\tau), U(x,\tau))_{L^2(\Omega)}\\
&\quad + \frac{\beta}{2}\|U(x,\tau)\|^2_{L^2(\Omega)}\\
&+ \frac{\varrho}{2}\|\nabla v(x,0)\|^2_{L^2(\Omega)} + \frac{\gamma}{2}\|\nabla U(x,\tau)\|^2_{L^2(\Omega)} - \frac{1}{2}\|U_\tau(x,\tau)\|^2_{L^2(\Omega)}\\
&\le\left\{\frac{\varrho}{2}T^2(l(\varepsilon) + |\Omega||\partial\Omega|) + \frac{\delta}{2}\left(T^2 l(\varepsilon) + |\Omega||\partial\Omega|\right) + \frac{\gamma}{2}l(\varepsilon)T^2\right\}\\
&\quad \cdot\int_0^\tau \|U(x,t)\|^2_{L^2(\Omega)}dt\\
&+\left(\alpha + \frac{\gamma|\Omega||\partial\Omega|}{2}\right)\int_0^\tau \|U_t(x,t)\|^2_{L^2(\Omega)}dt + \frac{1}{2}\int_0^\tau \|U_{tt}(x,t)\|^2_{L^2(\Omega)}dt\\
&+\left(\frac{\varrho+\delta+\gamma}{2}\right)\varepsilon\int_0^\tau \|\nabla v(x,t)\|^2_{L^2(\Omega)}dt.
\end{aligned} \tag{86}$$

Next, multiplying the differential equation in (73) by U_{ttt} and integrating over $Q_\tau = \Omega\times(0,\tau)$, we obtain

$$\begin{aligned}
&(U_{tttt}, U_{ttt})_{L^2(Q_\tau)} + \alpha(U_{ttt}, U_{ttt})_{L^2(Q_\tau)} + \beta(U_{tt}, U_{ttt})_{L^2(Q_\tau)}\\
&\quad - \varrho(\Delta U, U_{ttt})_{L^2(Q_\tau)} - \delta(\Delta U_t, U_{ttt})_{L^2(Q_\tau)} - \gamma(\Delta U_t, U_{ttt})_{L^2(Q_\tau)} = 0.
\end{aligned} \tag{87}$$

An integration by parts in (102) yields

$$(U_{tttt}, U_{ttt})_{L^2(Q_\tau)} = \frac{1}{2}\|U_{\tau\tau\tau}(x,\tau)\|^2_{L^2(\Omega)}, \tag{88}$$

$$\alpha(U_{ttt}, U_{ttt})_{L^2(Q_\tau)} = \alpha\int_0^\tau \|U_{ttt}(x,t)\|^2_{L^2(\Omega)}dt, \tag{89}$$

$$\beta(U_{tt}, U_{ttt})_{L^2(Q_\tau)} = \frac{\beta}{2}\|U_{\tau\tau}(x,\tau)\|^2_{L^2(\Omega)}, \tag{90}$$

$$\begin{aligned}
-\varrho(\Delta U, U_{ttt})_{L^2(Q_\tau)} &= \varrho\nabla U(x,\tau),\nabla U_{\tau\tau}(x,\tau)_{L^2(\Omega)}\\
&\quad - \frac{\varrho}{2}\|\nabla U_\tau(x,\tau)\|^2_{L^2(\Omega)} - \varrho\int_{\partial\Omega} U_{\tau\tau}(x,\tau)\\
&\quad \cdot\left(\int_0^\tau\int_\Omega U(\xi,\eta)d\xi d\eta\right)ds_x\\
&\quad + \varrho\int_{\partial\Omega}\int_0^\tau U_{tt}(x,t)\int_\Omega U(\xi,t)d\xi dtds_x,
\end{aligned} \tag{91}$$

$$\begin{aligned}
-\delta(\Delta U_t, U_{ttt})_{L^2(Q_\tau)} &= \delta(\nabla U_\tau(x,\tau),\nabla U_{\tau\tau}(x,\tau))_{L^2(\Omega)}\\
&\quad - \delta\int_0^\tau \|\nabla U_{tt}(x,)\|^2_{L^2(\Omega)}dt - \delta\int_{\partial\Omega} U_{\tau\tau}(x,\tau)\\
&\quad \cdot\int_\Omega U(\xi,\tau)d\xi ds_x + \delta\int_0^\tau\int_{\partial\Omega} U_{tt}(x,t)\\
&\quad \cdot\int_\Omega U_t(\xi,t)d\xi ds_x dt,
\end{aligned} \tag{92}$$

$$-\gamma(\Delta U_{tt}, U_{ttt})_{L^2(Q_\tau)} = \frac{\gamma}{2}\|\nabla U_{\tau\tau}(x,\tau)\|^2_{L^2(\Omega)} - \gamma\int_{\partial\Omega} U_{\tau\tau}(x,\tau) \cdot \int_\Omega U_\tau(\xi,\tau)d\xi ds_x + \gamma\int_0^\tau\int_{\partial\Omega} U_{tt}(x,t) \cdot \int_\Omega U_{tt}(\xi,t)d\xi ds_x dt. \tag{93}$$

Substituting (88)–(108) into (102), we get the equality

$$\begin{aligned}
&\frac{1}{2}\|U_{\tau\tau\tau}(x,\tau)\|^2_{L^2(\Omega)} + \frac{\beta}{2}\|U_{\tau\tau}(x,\tau)\|^2_{L^2(\Omega)} + \varrho(\nabla U(x,\tau),\nabla U_{\tau\tau}(x,\tau))_{L^2(\Omega)} \\
&+\delta(\nabla U_\tau(x,\tau),\nabla U_{\tau\tau}(x,\tau))_{L^2(\Omega)} + \frac{\gamma}{2}\|\nabla U_{\tau\tau}(x,\tau)\|^2_{L^2(\Omega)} - \frac{\varrho}{2}\|\nabla U_\tau(x,\tau)\|^2_{L^2(\Omega)} \\
&= -\alpha\int_0^\tau \|U_{ttt}(x,t)\|^2_{L^2(\Omega)}dt + \delta\int_0^\tau \|\nabla U_{tt}(x,)\|^2_{L^2(\Omega)}dt \\
&+\varrho\int_{\partial\Omega} U_{\tau\tau}(x,\tau)\left(\int_0^\tau\int_\Omega U(\xi,\eta)d\xi d\eta\right)ds_x - \varrho\int_{\partial\Omega}\int_0^\tau U_{tt}(x,t)\int_\Omega U(\xi,t)d\xi dt ds_x \\
&+\delta\int_{\partial\Omega} U_{\tau\tau}(x,\tau)\int_\Omega U(\xi,\tau)d\xi ds_x - \delta\int_0^\tau\int_{\partial\Omega} U_{tt}(x,t)\int_\Omega U_t(\xi,t)d\xi ds_x dt \\
&+\gamma\int_{\partial\Omega} U_{\tau\tau}(x,\tau)\int_\Omega U_\tau(\xi,\tau)d\xi ds_x - \gamma\int_0^\tau\int_{\partial\Omega} U_{tt}(x,t)\int_\Omega U_{tt}(\xi,t)d\xi ds_x dt.
\end{aligned} \tag{94}$$

The right-hand side of (109) can be bounded as follows:

$$\begin{aligned}
&\varrho\int_{\partial\Omega} U_{\tau\tau}(x,\tau)\left(\int_0^\tau\int_\Omega U(\xi,\eta)d\xi d\eta\right)ds_x \\
&\quad\le \frac{\varrho}{2\varepsilon_1'}\left(\varepsilon\|\nabla U_{\tau\tau}(x,\tau)\|^2_{L^2(\Omega)} + l(\varepsilon)\|U_{\tau\tau}(x,\tau)\|^2_{L^2(\Omega)}\right) \\
&\qquad + \frac{\varrho}{2}\varepsilon_1' T|\partial\Omega||\Omega|\int_0^\tau \|U(x,t)\|^2_{L^2(\Omega)}dt,
\end{aligned}$$

$$\begin{aligned}
&-\varrho\int_{\partial\Omega}\int_0^\tau U_{tt}(x,t)\int_\Omega U(\xi,t)d\xi dt ds_x \\
&\quad\le \frac{\varrho}{2}\int_0^\tau\left\{\varepsilon\|\nabla U_{tt}(x,t)\|^2_{L^2(\Omega)} + l(\varepsilon)\|U_{tt}(x,t)\|^2_{L^2(\Omega)}\right\}dt \\
&\qquad + \frac{\varrho}{2}|\Omega||\partial\Omega|\int_0^\tau \|U(x,t)\|^2_{L^2(\Omega)}dt,
\end{aligned}$$

$$\begin{aligned}
&\delta\int_{\partial\Omega} U_{\tau\tau}(x,\tau)\int_\Omega U(\xi,\tau)d\xi ds_x \\
&\quad\le \frac{\delta}{2\varepsilon_2'}\left(\varepsilon\|\nabla U_{\tau\tau}(x,\tau)\|^2_{L^2(\Omega)} + l(\varepsilon)\|U_{\tau\tau}(x,\tau)\|^2_{L^2(\Omega)}\right) \\
&\qquad + \frac{\delta}{2}\varepsilon_2' T|\Omega||\partial\Omega|\|U(x,\tau)\|^2_{L^2(\Omega)},
\end{aligned}$$

$$\begin{aligned}
&-\delta\int_0^\tau\int_{\partial\Omega} U_{tt}(x,t)\int_\Omega U_t(\xi,t)d\xi ds_x dt \\
&\quad\le \frac{\delta}{2}\varepsilon\int_0^\tau \|\nabla U_{tt}(x,t)\|^2_{L^2(\Omega)}dt + \frac{\delta}{2}l(\varepsilon)\int_0^\tau \|U_{tt}(x,t)\|^2_{L^2(\Omega)}dt \\
&\qquad + \frac{\delta}{2}T|\Omega||\partial\Omega|\int_0^\tau \|U_t(x,t)\|^2_{L^2(\Omega)}dt,
\end{aligned}$$

$$\begin{aligned}
&\gamma\int_{\partial\Omega} U_{\tau\tau}(x,\tau)\int_\Omega U_\tau(\xi,\tau)d\xi ds_x \\
&\quad\le \frac{\gamma}{2\varepsilon_3'}\left(\varepsilon\|\nabla U_{\tau\tau}(x,\tau)\|^2_{L^2(\Omega)} + l(\varepsilon)\|U_{\tau\tau}(x,\tau)\|^2_{L^2(\Omega)}\right) \\
&\qquad + \frac{\gamma}{2}\varepsilon_3' T|\Omega||\partial\Omega|\|U_\tau(x,\tau)\|^2_{L^2(\Omega)},
\end{aligned}$$

$$\begin{aligned}
&-\gamma\int_0^\tau\int_{\partial\Omega} U_{tt}(x,t)\int_\Omega U_{tt}(\xi,t)d\xi ds_x dt \\
&\quad\le \frac{\gamma}{2}l(\varepsilon)\int_0^\tau \|U_{tt}(x,t)\|^2_{L^2(\Omega)}dt + \frac{\gamma}{2}\varepsilon\int_0^\tau \|\nabla U_{tt}(x,t)\|^2_{L^2(\Omega)}dt \\
&\qquad + \frac{\gamma}{2}T|\Omega||\partial\Omega|\int_0^\tau \|U_{tt}(x,t)\|^2_{L^2(\Omega)}dt.
\end{aligned} \tag{95}$$

So, combining inequalities (110)–(115) and equality (109), we obtain

$$\begin{aligned}
&\frac{1}{2}\|U_{\tau\tau\tau}(x,\tau)\|^2_{L^2(\Omega)} + \left\{\frac{\beta}{2} - \frac{\varrho}{2\varepsilon_1'}l(\varepsilon) - \frac{\delta}{2\varepsilon_2'}l(\varepsilon) - \frac{\delta}{2}\varepsilon(\varepsilon)\right\}\|U_{\tau\tau}(x,\tau)\|^2_{L^2(\Omega)} \\
&-\frac{\gamma}{2}\varepsilon_3' T|\Omega||\partial\Omega|\|U_\tau(x,\tau)\|^2_{L^2(\Omega)} - \frac{\delta}{2}\varepsilon_2' T|\Omega||\partial\Omega|\|U(x,\tau)\|^2_{L^2(\Omega)} \\
&+\left\{\frac{\gamma}{2} - \frac{\varrho}{2\varepsilon_1'}\varepsilon - \frac{\delta}{2\varepsilon_2'}\varepsilon - \frac{\gamma}{2\varepsilon_3'}\varepsilon\right\}\|\nabla U_{\tau\tau}(x,\tau)\|^2_{L^2(\Omega)} - \frac{\varrho}{2}\|\nabla U_\tau(x,\tau)\|^2_{L^2(\Omega)} \\
&+\varrho(\nabla U(x,\tau),\nabla U_{\tau\tau}(x,\tau))_{L^2(\Omega)} + \delta(\nabla U_\tau(x,\tau),\nabla U_{\tau\tau}(x,\tau))_{L^2(\Omega)} \\
&\le -\alpha\int_0^\tau \|U_{ttt}(x,t)\|^2_{L^2(\Omega)}dt + \left\{\frac{\varrho}{2}l(\varepsilon) + \frac{\delta}{2}l(\varepsilon) + \frac{\gamma}{2}l(\varepsilon) + \frac{\gamma}{2}T|\Omega||\partial\Omega|\right\} \\
&\quad\cdot\int_0^\tau \|U_{tt}(x,t)\|^2_{L^2(\Omega)}dt \\
&+\left\{\frac{\varrho}{2}\varepsilon_1' T|\partial\Omega||\Omega| + \frac{\varrho}{2}|\Omega||\partial\Omega|\right\}\int_0^\tau \|U(x,t)\|^2_{L^2(\Omega)}dt \\
&+\frac{\delta}{2}T|\Omega||\partial\Omega|\int_0^\tau \|U_t(x,t)\|^2_{L^2(\Omega)}dt \\
&+\left\{\delta + \frac{\varrho}{2}\varepsilon + \frac{\delta}{2}\varepsilon + \frac{\gamma}{2}\varepsilon\right\}\int_0^\tau \|\nabla U_{tt}(x,)\|^2_{L^2(\Omega)}dt.
\end{aligned} \tag{96}$$

Adding side to side (101) and (116), we obtain

$$\begin{aligned}
&\left\{\frac{\beta}{2} - \frac{\delta}{2}\varepsilon_2' T|\Omega||\partial\Omega|\right\}\|U(x,\tau)\|^2_{L^2(\Omega)} + \left\{-\frac{1}{2} - \frac{\gamma}{2}\varepsilon_3' T|\Omega||\partial\Omega|\right\} \\
&\quad\cdot\|U_\tau(x,\tau)\|^2_{L^2(\Omega)} \\
&+\left\{\frac{\beta}{2} - \frac{\varrho}{2\varepsilon_1'}l(\varepsilon) - l(\varepsilon)\frac{\delta}{2\varepsilon_2'} - \frac{\gamma}{2\varepsilon_3'}l(\varepsilon)\right\}\|U_{\tau\tau}(x,\tau)\|^2_{L^2(\Omega)} \\
&+\frac{1}{2}\|U_{\tau\tau\tau}(x,\tau)\|^2_{L^2(\Omega)} \\
&+(U_{\tau\tau}(x,\tau), U(x,\tau))_{L^2(\Omega)} + \alpha(U_\tau(x,\tau), U(x,\tau))_{L^2(\Omega)} \\
&+\frac{\varrho}{2}\|\nabla v(x,0)\|^2_{L^2(\Omega)}
\end{aligned}$$

$$
\begin{aligned}
&+\varrho(\nabla U(x,\tau),\nabla U_{\tau\tau}(x,\tau))_{L^2(\Omega)}\\
&+\delta(\nabla U_\tau(x,\tau),\nabla U_{\tau\tau}(x,\tau))_{L^2(\Omega)}
\end{aligned}
$$

$$
\begin{aligned}
&+\frac{\gamma}{2}\|\nabla U(x,\tau)\|^2_{L^2(\Omega)}-\frac{\varrho}{2}\|\nabla U_\tau(x,\tau)\|^2_{L^2(\Omega)}\\
&+\left\{\frac{\gamma}{2}-\frac{\varrho}{2\varepsilon_1'}\varepsilon-\frac{\delta}{2\varepsilon_2'}-\frac{\gamma}{2\varepsilon_3'}\varepsilon\right\}\|\nabla U_{\tau\tau}(x,\tau)\|^2_{L^2(\Omega)}
\end{aligned}
$$

$$
\begin{aligned}
\le&\left\{\frac{\varrho}{2}\varepsilon_1'T|\partial\Omega||\Omega|+\frac{\varrho}{2}|\Omega||\partial\Omega|+\frac{\varrho}{2}T^2(l(\varepsilon)+|\Omega||\partial\Omega|)\right.\\
&\left.+\frac{\delta}{2}\left(T^2l(\varepsilon)+|\Omega||\partial\Omega|\right)\right.\\
&\left.+\frac{\gamma}{2}l(\varepsilon)T^2\right\}\int_0^\tau\|U(x,t)\|^2_{L^2(\Omega)}dt
\end{aligned}
$$

$$
+\left(\alpha+\frac{\gamma|\Omega||\partial\Omega|}{2}+\frac{\delta}{2}T|\Omega||\partial\Omega|\right)\int_0^\tau\|U_t(x,t)\|^2_{L^2(\Omega)}dt
$$

$$
\begin{aligned}
&+\left\{\frac{1}{2}+l(\varepsilon)\frac{\varrho}{2}+\frac{\delta}{2}l(\varepsilon)+\frac{\gamma}{2}l(\varepsilon)+\frac{\gamma}{2}T|\Omega||\partial\Omega|\right\}\int_0^\tau\\
&\cdot\|U_{tt}(x,t)\|^2_{L^2(\Omega)}dt-\alpha\int_0^\tau\|U_{ttt}(x,t)\|^2_{L^2(\Omega)}dt
\end{aligned}
$$

$$
\begin{aligned}
&+\left\{\frac{\delta}{2}\varepsilon+\frac{\gamma}{2}\varepsilon+\varepsilon\frac{\varrho}{2}+\delta\right\}\int_0^\tau\|\nabla U_{tt}(x,t)\|^2_{L^2(\Omega)}dt\\
&+\left(\frac{\varrho+\delta+\gamma}{2}\right)\varepsilon\int_0^\tau\|\nabla v(x,t)\|^2_{L^2(\Omega)}dt.
\end{aligned}
\tag{97}
$$

Now, to deal with the last term on the right-hand side of (117), we define the function $\theta(x,t)$ by the relation

$$
\theta(x,t):=\int_0^t U(x,s)ds. \tag{98}
$$

Hence, using (89), it follows that

$$
v(x,t)=\theta(x,\tau)-\theta(x,t),\ \nabla v(x,0)=\nabla\theta(x,\tau),
$$

$$
\begin{aligned}
\|\nabla v\|^2_{L^2(Q_\tau)}&=\|\nabla\theta(x,\tau)-\nabla\theta(x,t)\|^2_{L^2(\Omega)}\\
&\le 2\left(\tau\|\nabla\theta(x,\tau)\|^2_{L^2(\Omega)}+\|\nabla\theta(x,t)\|^2_{L^2(Q_\tau)}\right).
\end{aligned}
\tag{99}
$$

And we make use of the following inequality:

$$
\begin{aligned}
-\frac{\alpha}{2}\|U_\tau(x,\tau)\|^2_{L^2(\Omega)}-\frac{\alpha}{2}\|U(x,\tau)\|^2_{L^2(\Omega)}&\le\alpha(U_\tau(x,\tau),U(x,\tau))_{L^2(\Omega)},\\
-\frac{1}{2}\|U_{\tau\tau}(x,\tau)\|^2_{L^2(\Omega)}-\frac{1}{2}\|U(x,\tau)\|^2_{L^2(\Omega)}&\le(U_{\tau\tau}(x,\tau),U(x,\tau))_{L^2(\Omega)},\\
-\frac{\varrho}{2\varepsilon_4'}\|\nabla U_{\tau\tau}(x,\tau)\|^2_{L^2(\Omega)}-\frac{\varrho}{2}\varepsilon_4'\|\nabla U(x,\tau)\|^2_{L^2(\Omega)}&\le\varrho(\nabla U(x,\tau),\nabla U_{\tau\tau}(x,\tau))_{L^2(\Omega)},\\
-\frac{\delta}{2\varepsilon_5'}\|\nabla U_{\tau\tau}(x,\tau)\|^2_{L^2(\Omega)}-\frac{\delta}{2}\varepsilon_5'\|\nabla U_\tau(x,\tau)\|^2_{L^2(\Omega)}&\le\delta(\nabla U_\tau(x,\tau),\nabla U_{\tau\tau}(x,\tau))_{L^2(\Omega)},\\
m_1\|U(x,\tau)\|^2_{L^2(\Omega)}&\le m_1\|U(x,t)\|^2_{L^2(Q_\tau)}+m_1\|U_t(x,t)\|^2_{L^2(Q_\tau)},\\
m_2\|U_\tau(x,\tau)\|^2_{L^2(\Omega)}&\le m_2\|U_t(x,t)\|^2_{L^2(Q_\tau)}+m_2\|U_{tt}(x,t)\|^2_{L^2(Q_\tau)},\\
m_3\|U_{\tau\tau}(x,\tau)\|^2_{L^2(\Omega)}&\le m_3\|U_{tt}(x,t)\|^2_{L^2(Q_\tau)}+m_3\|U_{ttt}(x,t)\|^2_{L^2(Q_\tau)},\\
m_4\|\nabla U(x,\tau)\|^2_{L^2(\Omega)}&\le m_4\|\nabla U(x,t)\|^2_{L^2(Q_\tau)}+m_4\|\nabla U_t(x,t)\|^2_{L^2(Q_\tau)},\\
m_5\|\nabla U_\tau(x,\tau)\|^2_{L^2(\Omega)}&\le m_5\|\nabla U_t(x,t)\|^2_{L^2(Q_\tau)}+m_5\|\nabla U_{tt}(x,t)\|^2_{L^2(Q_\tau)}.
\end{aligned}
\tag{100}
$$

Let

$$
\begin{cases}
m_1:=\dfrac{1}{2}+\dfrac{\delta}{2}\varepsilon_2'T|\Omega||\partial\Omega|+\dfrac{\alpha}{2}\\[2ex]
m_2:=1+\dfrac{\gamma}{2}\varepsilon_3'T|\Omega||\partial\Omega|+\dfrac{\alpha}{2}\\[2ex]
m_3:=\dfrac{\varrho}{2\varepsilon_1'}l(\varepsilon)+l(\varepsilon)\dfrac{\delta}{2\varepsilon_2'}+\dfrac{\gamma}{2\varepsilon_3'}l(\varepsilon)+\dfrac{1}{2}\\[2ex]
m_4:=\dfrac{\varrho}{2}\varepsilon_4'\\[2ex]
m_5:=1+\dfrac{\varrho}{2}+\dfrac{\delta}{2\varepsilon_5'},
\end{cases}
\tag{101}
$$

choosing ε_1', ε_2', ε_3', ε_4', and ε_5' sufficiently large:

$$
\frac{\varrho}{2\varepsilon_1'}\varepsilon+\frac{\delta}{2\varepsilon_2'}+\frac{\gamma}{2\varepsilon_3'}\varepsilon+\frac{\varrho}{2\varepsilon_4'}+\frac{\delta}{2\varepsilon_5'}<\frac{\gamma}{2}. \tag{102}
$$

Since τ is arbitrary, we get that $\varrho/2-\tau\varepsilon(\varrho+\delta+\gamma)>0$; thus, inequality (117) takes the form

$$
\begin{aligned}
&\frac{\beta}{2}\|U(x,\tau)\|^2_{L^2(\Omega)}+\frac{1}{2}\|U_\tau(x,\tau)\|^2_{L^2(\Omega)}+\frac{\beta}{2}\|U_{\tau\tau}(x,\tau)\|^2_{L^2(\Omega)}\\
&\quad+\frac{1}{2}\|U_{\tau\tau\tau}(x,\tau)\|^2_{L^2(\Omega)}
\end{aligned}
$$

$$
\begin{aligned}
&+\left\{\frac{\varrho}{2}-\tau\varepsilon(\varrho+\delta+\gamma)\right\}\|\nabla\theta(x,\tau)\|^2_{L^2(\Omega)}+\frac{\gamma}{2}\|\nabla U(x,\tau)\|^2_{L^2(\Omega)}\\
&+\|\nabla U_\tau(x,\tau)\|^2_{L^2(\Omega)}
\end{aligned}
$$

$$
+\left\{\frac{\gamma}{2}-\frac{\varrho}{2\varepsilon_1'}\varepsilon-\frac{\delta}{2\varepsilon_2'}-\frac{\gamma}{2\varepsilon_3'}\varepsilon-\frac{\varrho}{2\varepsilon_4'}-\frac{\delta}{2\varepsilon_5'}\right\}\|\nabla U_{\tau\tau}(x,\tau)\|^2_{L^2(\Omega)}
$$

$$
\begin{aligned}
&\leq \left\{\gamma_1' + m_1\right\} \int_0^\tau \|U(x,t)\|_{L^2(\Omega)}^2 dt + \left(\gamma_2' + m_1 + m_2\right) \int_0^\tau \\
&\quad \cdot \|U_t(x,t)\|_{L^2(\Omega)}^2 dt \\
&+ \left\{\gamma_3' + m_2 + m_3\right\} \int_0^\tau \|U_{tt}(x,t)\|_{L^2(\Omega)}^2 dt + (m_3 - \alpha) \int_0^\tau \\
&\quad \cdot \|U_{ttt}(x,t)\|_{L^2(\Omega)}^2 dt \\
&+ \varepsilon(\varrho + \delta + \gamma) \int_0^\tau \|\nabla\theta(x,t)\|_{L^2(\Omega)}^2 dt \\
&+ m_4 \int_0^\tau \|\nabla U(x,t)\|_{L^2(\Omega)}^2 dt + (m_4 + m_5) \int_0^\tau \|\nabla U_t(x,t)\|_{L^2(\Omega)}^2 dt \\
&+ \left\{\frac{\delta}{2}\varepsilon + \frac{\gamma}{2}\varepsilon + \varepsilon\frac{\varrho}{2} + \delta + m_5\right\} \int_0^\tau \|\nabla U_{tt}(x,t)\|_{L^2(\Omega)}^2 dt, \quad (103)
\end{aligned}
$$

where

$$
\begin{cases}
\gamma_1' \coloneqq \dfrac{\varrho}{2}\varepsilon_1' T|\partial\Omega||\Omega| + \dfrac{\varrho}{2}|\Omega||\partial\Omega| + \dfrac{\varrho}{2}T^2(l(\varepsilon) + |\Omega||\partial\Omega|) + \dfrac{\delta}{2}\left(T^2 l(\varepsilon) + |\Omega||\partial\Omega|\right) + \dfrac{\gamma}{2}l(\varepsilon)T^2 \\
\gamma_2' \coloneqq \alpha + \dfrac{\gamma|\Omega||\partial\Omega|}{2} + \dfrac{\delta}{2}T|\Omega||\partial\Omega| \\
\gamma_3' \coloneqq \dfrac{1}{2} + l(\varepsilon)\dfrac{\varrho}{2} + \dfrac{\delta}{2}l(\varepsilon) + \dfrac{\gamma}{2}l(\varepsilon) + \dfrac{\gamma}{2}T|\Omega||\partial\Omega|.
\end{cases} \quad (104)
$$

We obtain

$$
\begin{aligned}
&\|U(x,\tau)\|_{L^2(\Omega)}^2 + \|U_\tau(x,\tau)\|_{L^2(\Omega)}^2 + \|U_{\tau\tau}(x,\tau)\|_{L^2(\Omega)}^2 + \|U_{\tau\tau\tau}(x,\tau)\|_{L^2(\Omega)}^2 \\
&\quad + \|\nabla U(x,\tau)\|_{L^2(\Omega)}^2 + \|\nabla U_\tau(x,\tau)\|_{L^2(\Omega)}^2 + \|\nabla U_{\tau\tau}(x,\tau)\|_{L^2(\Omega)}^2 \\
&\quad + \|\nabla\theta(x,\tau)\|_{L^2(\Omega)}^2 \leq D\int_0^\tau \Big\{\|U(x,t)\|_{L^2(\Omega)}^2 + \|U_t(x,t)\|_{L^2(\Omega)}^2 + \|U_{tt}(x,t)\|_{L^2(\Omega)}^2 \\
&\quad + \|U_{ttt}(x,t)\|_{L^2(\Omega)}^2 + \|\nabla U(x,t)\|_{L^2(\Omega)}^2 + \|\nabla U_t(x,t)\|_{L^2(\Omega)}^2 + \|\nabla U_{tt}(x,t)\|_{L^2(\Omega)}^2 \\
&\quad + \|\nabla\theta(x,t)\|_{L^2(\Omega)}^2\Big\} dt,
\end{aligned} \quad (105)
$$

where

$$
\begin{aligned}
D \coloneqq \frac{\max\left\{\left(\gamma_1' + m_1\right), \left(\gamma_2' + m_1 + m_2\right)_4, \gamma_3' + m_2 + m_3, m_3 - \alpha, m_4\right.}{\min\left\{(\beta/2), 1/2, ,(\gamma/2), \left\{\gamma/2 - \left(\varrho/2\varepsilon_1'\right)\varepsilon - \delta/2\varepsilon_2' - \left(\gamma/2\varepsilon_3'\right)\varepsilon - \varrho/2\varepsilon_4' - \delta/2\varepsilon_5'\right\},\right.} \\
\left., m_4 + m_5, (\delta/2)\varepsilon + (\gamma/2)\varepsilon + \varepsilon(\varrho/2) + \delta + m_5, \varepsilon(\varrho + \delta + \gamma)\right\} \\
\left., \left\{\varrho/2 - \tau\varepsilon(\varrho + \delta + \gamma)\right\}\right\}
\end{aligned}. \quad (106)
$$

Further, applying Gronwall's lemma to (133), we deduce that

$$
\begin{aligned}
&\|U(x,\tau)\|_{L^2(\Omega)}^2 + \|U_\tau(x,\tau)\|_{L^2(\Omega)}^2 + \|U_{\tau\tau}(x,\tau)\|_{L^2(\Omega)}^2 + \|U_{\tau\tau\tau}(x,\tau)\|_{L^2(\Omega)}^2 \\
&+ \|\nabla U(x,\tau)\|_{L^2(\Omega)}^2 + \|\nabla U_\tau(x,\tau)\|_{L^2(\Omega)}^2 + \|\nabla U_{\tau\tau}(x,\tau)\|_{L^2(\Omega)}^2 + \|\nabla\theta(x,\tau)\|_{L^2(\Omega)}^2 \\
&\leq 0, \forall\tau \in \left[0, \frac{\varrho}{2\varepsilon(\rho + \delta + \gamma)}\right].
\end{aligned} \quad (107)
$$

We proceed in the same way for the intervals $\tau \in [((m-1)\varrho/2\varepsilon(\varrho + \delta + \gamma)), (m\varrho/2\varepsilon(\varrho + \delta + \gamma))]$ to cover the whole interval $[0, T]$, and thus proving that $U(x,\tau) = 0$, for all τ in $[0, T]$. Thus, the uniqueness is proved.

5. Conclusion

In the study of the propagation of acoustic waves, it should be noted that the Moore–Gibson–Thompson equation is one of the equations of nonlinear acoustics describing acoustic wave

propagation in gases and liquids. The behavior of acoustic waves depends strongly on the medium property related to dispersion, dissipation, and nonlinear effects. It arises from modeling high-frequency ultrasound (HFU) waves (see [10, 12, 34]). In this work, we have studied the solvability of the nonlocal mixed boundary value problem for the fourth order of the Moore–Gibson–Thompson equation. Galerkin's method was the main used tool for proving the solvability of the given nonlocal problem. In the next work, we will try to use the same method with the Hall-MHD equations which are nonlinear partial differential equation that arises in hydrodynamics and some physical applications. It was subsequently applied to problems in the percolation of water in porous subsurface strata (see for example [45–48]) by using some famous algorithms (see [49–51])

Data Availability

No data were used to support the study.

Conflicts of Interest

This work does not have any conflicts of interest.

Acknowledgments

The fifth author extend their appreciation to the Deanship of Scientific Research at King Khalid University for funding this work through research group program under grant (R.G.P.1/3/42).

References

[1] S. Adhikari, *Structural Dynamic Analysis with Generalized Damping Models: Analysis*, Wiley, Germany, 2013.

[2] F. Alabau-Boussouira, P. Cannarsa, and D. Sforza, "Decay estimates for second order evolution equations with memory," *Journal of Functional Analysis*, vol. 254, pp. 1342–1372, 2008.

[3] S. Toualbia, A. Zara, and S. Boulaaras, "Decay estimate and non-extinction of solutions of p-Laplacian nonlocal heat equations," *AIMS Mathematics*, vol. 5, no. 3, pp. 1663–1679, 2020.

[4] S. Boulaaras, A. Zaraï, and A. Draifia, "Galerkin method for nonlocal mixed boundary value problem for the Moore-Gibson-Thompson equation with integral condition," *Mathematical Methods in the Applied Sciences*, vol. 42, pp. 2664–2679, 2019.

[5] Y. S. Choi and K. Y. Chan, "A parabolic equation with nonlocal boundary conditions arising from electrochemistry," *Nonlinear Analysis*, vol. 18, no. 4, pp. 317–331, 1992.

[6] S. Boulaaras, "Solvability of the Moore-Gibson-Thompson equation with viscoelastic memory term and integral condition via Galerkin method," *Fractals*, vol. 29, 2021.

[7] K. Hosseini, M. Mirzazadeh, F. Rabieic, H. M. Baskonus, and G. Yel, "Dark optical solitons to the Biswas-Arshed equation with high order dispersions and absence of the self-phase modulation," *Optik*, vol. 209, p. 164576, 2020.

[8] H. Bulut, T. A. Sulaiman, H. M. Baskonus, H. Rezazadeh, M. Eslami, and M. Mirzazadeh, "Optical solitons and other solutions to the conformable space-time fractional Fokas-Lenells equation," *Optik*, vol. 172, pp. 20–27, 2018.

[9] F. Dell'Oro and V. Pata, "On a fourth-order equation of Moore–Gibson–Thompson type," *Milan Journal of Mathematics*, vol. 85, no. 2, pp. 215–234, 2017.

[10] S. Boulaaras and N. Mezouar, "Global existence and decay of solutions of a singular nonlocal viscoelastic system with a nonlinear source term, nonlocal boundary condition, and localized damping term," *Mathematical Methods in the Applied Sciences*, vol. 43, no. 10, pp. 6140–6164, 2020.

[11] V. P. Kuznetsov, "Equations of nonlinear acoustics," *Soviet Physics Acoustics*, vol. 16, pp. 467–AS470, 1971.

[12] N. Doudi and S. Boulaaras, "Global existence combined with general decay of solutions for coupled Kirchhoff system with a distributed delay term," *Revista de la Real Academia de Ciencias Exactas, Físicas y Naturales. Serie A. Matemáticas*, vol. 114, no. 4, p. 204, 2020.

[13] S. M. Boulaaras, A. Choucha, A. Zara, M. Abdalla, and B.-B. Cheri, "Global existence and decay estimates of energy of solutions for a new class of -Laplacian heat equations with logarithmic nonlinearity," *Journal of Function Spaces*, vol. 2021, Article ID 5558818, 11 pages, 2021.

[14] A. Choucha, S. Boulaaras, and D. Ouchenane, "Exponential decay of solutions for a viscoelastic coupled Lame system with logarithmic source and distributed delay terms," *Mathematical Methods in the Applied Sciences*, vol. 44, no. 6, pp. 4858–4880, 2021.

[15] A. Choucha, S. Boulaaras, D. Ouchenane, and S. Beloul, "General decay of nonlinear viscoelastic Kirchhoff equation with Balakrishnan-Taylor damping, logarithmic nonlinearity and distributed delay terms," *Mathematical Methods in the Applied Sciences*, 2020.

[16] B. Kaltenbacher, I. Lasiecka, and R. Marchand, "Wellposedness and exponential decay rates for the Moore Gibson-Thompson equation arising in high intensity ultrasound," *Control and Cybernetics*, vol. 40, no. 4, pp. 971–988, 2011.

[17] I. Lasiecka and X. Wang, "Moore-Gibson-Thompson equation with memory, part I: exponential decay of energy," *Zeitschrift für angewandte Mathematik und Physik*, vol. 67, no. 2, 2016.

[18] S. Boulaaras and N. Doudi, "Global existence and exponential stability of coupled Lamé system with distributed delay and source term without memory term," *Boundary Value Problems*, vol. 2020, no. 1, 2020.

[19] N. Mezouar and S. Boulaaras, "Global existence and decay of solutions of a singular nonlocal viscoelastic system with damping terms," *Topological Methods in Nonlinear Analysis*, vol. 56, no. 1, pp. 1–312, 2020.

[20] A. Choucha, S. M. Boulaaras, D. Ouchenane, and A. Allahem, "Global existence for two singular one-dimensional nonlinear viscoelastic equations with respect to distributed delay term," *Journal of Function Spaces*, vol. 2021, Article ID 6683465, 18 pages, 2021.

[21] A. Merah, F. Mesloub, S. M. Boulaaras, and B. B. Cherif, "A new result for a blow-up of solutions to a logarithmic flexible structure with second sound," *Advances in Mathematical Physics*, vol. 2021, Article ID 5555930, 7 pages, 2021.

[22] S. Boulaaras, A. Choucha, B. Cherif, A. Alharbi, and M. Abdalla, "Blow up of solutions for a system of two singular nonlocal viscoelastic equations with damping, general source terms and a wide class of relaxation functions," *AIMS Mathematics*, vol. 6, no. 5, pp. 4664–4676, 2021.

[23] S. Boulaaras and Y. Bouizem, "Blow up of solutions for a nonlinear viscoelastic system with general source term," *Quaestiones Mathematicae*, pp. 1–11, 2020.

[24] N. Mezouar and S. Boulaaras, "Global existence and exponential decay of solutions for generalized coupled non-degenerate Kirchhoff system with a time varying delay term," *Boundary Value Problems*, vol. 2020, no. 1, 2020.

[25] S. Mesloub and A. Bouziani, "On a class of singular hyperbolic equation with a weighted integral condition," *International Journal of Mathematics and Mathematical Sciences*, vol. 22, no. 3, p. 519, 1999.

[26] S. Mesloub and A. Bouziani, "Mixed problem with a weighted integral condition for a parabolic equation with Bessel operator," *Journal of Applied Mathematics and Stochastic Analysis*, vol. 15, no. 3, pp. 291–300, 2002.

[27] S. Mesloub and S. A. Messaoudi, "Global existence, decay, and blow up of solutions of a singular nonlocal viscoelastic problem," *Acta Applicandae Mathematicae*, vol. 110, no. 2, pp. 705–724, 2010.

[28] A. Choucha, S. Boulaaras, D. Ouchenane, S. Alkhalaf, I. Mekawy, and M. Abdalla, "On the system of coupled nondegenerate kirchhoff equations with distributed delay: global existence and exponential decay," *Journal of Function Spaces*, vol. 2021, Article ID 5577277, 13 pages, 2021.

[29] S. Mesloub and N. Lekrine, "On a nonlocal hyperbolic mixed problem," *Acta Scientiarum Mathematicarum*, vol. 70, pp. 65–75, 2004.

[30] S. Mesloub, "On a singular two dimensional nonlinear evolution equation with nonlocal conditions," *Nonlinear Analysis: Theory, Methods & Applications*, vol. 68, no. 9, pp. 2594–2607, 2008.

[31] S. Mesloub, "A nonlinear nonlocal mixed problem for a second order pseudoparabolic equation," *Journal of Mathematical Analysis and Applications*, vol. 316, no. 1, pp. 189–209, 2006.

[32] S. Mesloub and F. Mesloub, "On the higher dimension Boussinesq equation with nonclassical condition," *Mathematicsl Methods in the Applied Sciences*, vol. 34, no. 5, pp. 578–586, 2011.

[33] F. K. Moore and W. E. Gibson, "Propagation of weak disturbances in a gas subject to relaxation effects," *Journal of the Aerospace Sciences*, vol. 27, no. 2, pp. 117–127, 1960.

[34] L. S. Pulkina, "A nonlocal problem with integral conditions for hyperbolic equations," *Electronic Journal of Differential Equations*, vol. 45, pp. 1–6, 1999.

[35] L. S. Pulkina, "On solvability in l2 of nonlocal problem with integral conditions for a hyperbolic equation," *Differentsial'nye Uravneniya*, vol. 36, pp. 316–318, 2000.

[36] R. Racke and B. Said-Houari, "Global well-posedness of the Cauchy problem for the Jordan-Moore-Gibson Thompson equation," *Konstanzer Schriften in Mathematik*, vol. 38, 2019.

[37] S. Rashid, S. Parveen, H. Ahmad, and Y. M. Chu, "New quantum integral inequalities for some new classes of generalized convex functions and their scope in physical systems," *Open Physics*, vol. 19, no. 1, 2021.

[38] S. Rashid, S. I. Butt, S. Kanwal, H. Ahmad, and M.-K. Wang, "Quantum integral inequalities with respect to Raina's function via coordinated generalized -convex functions with applications," *Journal of Function Spaces*, vol. 2021, 16 pages, 2021.

[39] P. Shi and M. Shillor, "Design of contact patterns in one dimensional thermoelasticity," in *Theoretical Aspects of Industrial Design*, pp. 76–82, SIAM, Philadelphia, 1992.

[40] P. Shi, "Weak solution to an evolution problem with a nonlocal constraint," *SIAM Journal on Mathematical Analysis*, vol. 24, no. 1, pp. 46–58, 1993.

[41] P. Stokes, "XXXVIII. An examination of the possible effect of the radiation of heat on the propagation of sound," *The London, Edinburgh, and Dublin Philosophical Magazine and Journal of Science*, vol. 4, pp. 305–317, 1851.

[42] S. S. Zhou, S. Rashid, S. Parveen, A. O. Akdemir, and Z. Hammouch, "New computations for extended weighted functionals within the Hilfer generalized proportional fractional integral operators," *AIMS Mathematics*, vol. 6, no. 5, pp. 4507–4525, 2021.

[43] Q. Zhou, M. Ekici, A. Sonmezoglu, and M. Mirzazadeh, "Optical solitons with Biswas-Milovic equation by extended G'/G-expansion method," *Optik*, vol. 127, no. 16, pp. 6277–6290, 2016.

[44] W. Chen and A. Palmieri, "A blow–up result for the semilinear Moore–Gibson–Thompson equation with nonlinearity of derivative type in the conservative case," *Evolution Equations & Control Theory*, 2019.

[45] R. P. Agarwal, S. Gala, and M. A. Ragusa, "A regularity criterion in weak spaces to Boussinesq equations," *Mathematics*, vol. 8, no. 6, p. 920, 2020.

[46] A. Barbagallo, S. Gala, M. A. Ragusa, and M. Théra, "On the regularity of weak solutions of the Boussinesq equations in Besov spaces," *Vietnam Journal of Mathematics*, 2020.

[47] R. P. Agarwal, A. M. A. Alghamdi, S. Gala, and M. A. Ragusa, "On the continuation principle of local smooth solution for the Hall-MHD equations," *Applicable Analysis*, pp. 1–9, 2020.

[48] R. P. Agarwal, S. Gala, and M. A. Ragusa, "A regularity criterion of the 3D MHD equations involving one velocity and one current density component in Lorentz space," *Zeitschrift für Angewandte Mathematik und Physik*, vol. 71, no. 3, p. 95, 2020.

[49] S. Boulaaras and M. Haiour, "L^{∞}-asymptotic behavior for a finite element approximation in parabolic quasi-variational inequalities related to impulse control problem," *Applied Mathematics and Computation*, vol. 217, no. 14, pp. 6443–6450, 2011.

[50] S. Boulaaras and M. Haiourc, "A new proof for the existence and uniqueness of the discrete evolutionary HJB equations," *Applied Mathematics and Computation*, vol. 262, pp. 42–55, 2015.

[51] S. Boulaaras, "Some new properties of asynchronous algorithms of theta scheme combined with finite elements methods for an evolutionary implicit 2-sided obstacle problem," *Mathematical Methods in the Applied Sciences*, vol. 40, no. 18, pp. 7231–7239, 2017.

Hindawi
Advances in Mathematical Physics
Volume 2021, Article ID 5538516, 7 pages
https://doi.org/10.1155/2021/5538516

Research Article

Solitary Wave Solutions to the Multidimensional Landau–Lifshitz Equation

Ahmad Neirameh

Department of Mathematics, Faculty of Sciences, Gonbad Kavous University, Gonbad, Iran

Correspondence should be addressed to Ahmad Neirameh; neirameh.edu@gmail.com

Received 23 January 2021; Revised 20 February 2021; Accepted 19 March 2021; Published 31 March 2021

Academic Editor: F. Rabiei

In this paper, we study the different types of new soliton solutions to the Landau–Lifshitz equation with the aid of the auxiliary equation method. Then, we get some special soliton solutions for this equation. Without the Gilbert damping term, we present a travelling wave solution with a finite energy in the initial time. The parameters of the soliton envelope are obtained as a function of the dependent model coefficients.

1. Introduction

Nonlinear partial differential equations have different types of equations; one of them is the Landau–Lifshitz equation that is relevant to the classical and quantum mechanics. Nonlinear evolution equations (NEEs) which describe many physical phenomena are often illustrated by nonlinear partial differential equations. So, the exact solutions of NLPDE are explored in detail in order to understand the physical structure of natural phenomena that are described by such equations. A variety of powerful methods have been used to study the nonlinear evolution equations, for the analytic and numerical solutions. Some of these methods, the Riccati Equation method [1], Hirota's bilinear operators [2], exponential rational function method [3], the Jacobi elliptic function expansion [4], the homogeneous balance method [5], the tanh-function expansion [6], first integral method [7, 8], the subequation method [9], the exp-function method [10], the Backlund transformation, and similarity reduction [11–29], are used to obtain the exact solutions of NLPDE.

In physics, the Landau–Lifshitz–Gilbert equation, named for Lev Landau, Evgeny Lifshitz, and T. L. Gilbert, is a name used for a differential equation describing the processional motion of magnetization M in a solid. It is a modification by Gilbert of the original equation of LLG equation (see [30]) can be written down as

$$\frac{\partial}{\partial t}S = \alpha S\Lambda\Delta S - \beta S\Lambda(S\Lambda\Delta S), \tag{1}$$

here, $S = (S_1(t, \vec{x}), S_2(t, \vec{x}), S_3(t, \vec{x})) \in S^2 \hookrightarrow R^3$, $\alpha \geq 0$, $\alpha^2 + \beta^2 = 1$, Λ denotes the cross product. The term multiplying with α represents the exchange interaction, while the β term denotes the Gilbert damping term. Especially, two extreme cases of (1) ($\beta = 0$ and $\alpha = 0$, respectively) include as special cases the well-known Schrödinger map equation and harmonic map heat flow, respectively. The well-posedness problem of the LL(G) equation are intensively studied in mathematics, to list a few, in 1986, of the weak solution of the LL(G) equation. Under the small initial value, the global existence of the solution in different spaces [31–33] was proved. The first progress on the existence of partially regular solutions to the LLG equation was found [30, 33–36]. Even for the small initial data, the exact form of the solution is still unknown. On the other hand, whether the LLG equation admits a global solution will develop a finite time singularity from the large initial data is an open equation.

2. Auxiliary Equation Method

Let us consider a typical nonlinear PDE for $q = q(x, t)$, given by

$$U(q_x, q_t, \cdots.) = 0. \tag{2}$$

Under the wave transformations of $q(x, t) = Q(\xi)$ and $\xi = \sigma x - lt$, Equation (2) becomes an ordinary differential equation given by

$$U\left(Q, \sigma Q', -lQ', \cdots.\right) = 0. \tag{3}$$

We assume that the solution $\phi(\xi)$ of the nonlinear Equation (18) can be presented as

$$Q(\xi) = \sum_{i=0}^{M} A_i \Upsilon^i(\xi), \tag{4}$$

in which $A_i (i = 0, \cdots, n)$ are all real constants to be determined, the balancing number M is a positive integer which can be determined by balancing the highest order derivative terms with the highest power nonlinear terms in Equation (2) and $\Upsilon^i(\xi)$ expresses the solutions of the following auxiliary ordinary differential equation:

$$\left(\frac{d\Upsilon}{d\xi}\right)^2 = s_1 \Upsilon^2(\xi) + s_2 \Upsilon^3(\xi) + s_3 \Upsilon^4(\xi), \tag{5}$$

where s_1, s_2, and s_3 are real parameters. Equations (6), (7), (8), (9), (10), (11), (12), (13), (14), (15), (16), (17), (18), and (19) with $\Delta = s_2^2 - 4s_1 s_3$ give the following solutions:

Case 1. For $s_1 > 0$,

$$\frac{-s_1 s_2 \operatorname{sech}^2\left(\sqrt{(s_1/2)}\xi\right)}{s_2^2 - s_1 s_3\left(1 + \xi \tanh\left(\sqrt{(s_1/2)}\xi\right)\right)}. \tag{6}$$

Case 2. For $s_1 > 0$,

$$\frac{-s_1 s_2 \operatorname{csch}^2\left(\sqrt{(s_1/2)}\xi\right)}{s_2^2 - s_1 s_3\left(1 + \xi \tanh\left(\sqrt{(s_1/2)}\xi\right)\right)}. \tag{7}$$

Case 3. For $s_1 > 0, \Delta > 0$,

$$\frac{2s_1 \operatorname{sech}\left(\sqrt{s_1}\xi\right)}{\varepsilon\sqrt{\Delta} - s_2 \operatorname{sech}\left(\sqrt{s_1}\xi\right)}. \tag{8}$$

Case 4. For $s_1 < 0, \Delta > 0$,

$$\frac{2s_1 \sec\left(\sqrt{-s_1}\xi\right)}{\varepsilon\sqrt{\Delta} - s_2 \sec\left(\sqrt{-s_1}\xi\right)}. \tag{9}$$

Case 5. For $s_1 > 0, \Delta < 0$,

$$\frac{2s_1 \operatorname{csch}\left(\sqrt{s_1}\xi\right)}{\varepsilon\sqrt{-\Delta} - s_2 \operatorname{csch}\left(\sqrt{s_1}\xi\right)}. \tag{10}$$

Case 6. For $s_1 < 0, \Delta > 0$,

$$\frac{2s_1 \csc\left(\sqrt{-s_1}\xi\right)}{\varepsilon\sqrt{\Delta} - s_2 \csc\left(\sqrt{-s_1}\xi\right)}. \tag{11}$$

Case 7. For $s_1 > 0, s_3 > 0$

$$\frac{-s_1 \operatorname{sech}^2\left(\left(\sqrt{s_1}/2\right)\xi\right)}{s_2 + 2\xi\sqrt{s_1 s_3} \tanh\left(\left(\sqrt{s_1}/2\right)\xi\right)}. \tag{12}$$

Case 8. For $s_1 < 0, s_3 > 0$,

$$\frac{-s_1 \sec^2\left(\left(\sqrt{-s_1}/2\right)\xi\right)}{s_2 + 2\xi\sqrt{-s_1 s_3} \tan\left(\left(\sqrt{-s_1}/2\right)\xi\right)}. \tag{13}$$

Case 9. For $s_1 > 0, s_3 > 0$

$$\frac{s_1 \operatorname{csch}^2\left(\left(\sqrt{s_1}/2\right)\xi\right)}{s_2 + 2\xi\sqrt{s_1 s_3} \coth\left(\left(\sqrt{s_1}/2\right)\xi\right)}. \tag{14}$$

Case 10. For $s_1 < 0, s_3 > 0$,

$$\frac{-s_1 \csc^2\left(\left(\sqrt{-s_1}/2\right)\xi\right)}{s_2 + 2\xi\sqrt{-s_1 s_3} \cot\left(\left(\sqrt{-s_1}/2\right)\xi\right)}. \tag{15}$$

Case 11. For $s_1 > 0, \Delta = 0$,

$$-\frac{s_1}{s_2}\left(1 + \xi \tanh\left(\frac{\sqrt{s_1}}{2}\xi\right)\right). \tag{16}$$

Case 12. For $s_1 > 0, \Delta = 0$,

$$-\frac{s_1}{s_2}\left(1 + \xi \coth\left(\frac{\sqrt{s_1}}{2}\xi\right)\right). \tag{17}$$

Case 13. For $s_1 > 0$,

$$\frac{4s_1 e^{\varepsilon\sqrt{s_1}\xi}}{\left(e^{\varepsilon\sqrt{s_1}\xi} - s_2\right)^2 - 4s_1 s_2}. \tag{18}$$

Case 14. For $s_1 > 0, s_2 = 0$,

$$\frac{\pm 4s_1 \varepsilon e^{\varepsilon\sqrt{s_1}\xi}}{1 - 4s_1 s_3 e^{2\varepsilon\sqrt{s_1}\xi}}. \tag{19}$$

Stage 2: substituting Equations (4) and (5) into Equation (3) and collecting all terms with the same order of Υ^j together, we convert the left-hand side of Equation (3) into a polynomial in Υ^j. Setting each coefficient of each polynomial to zero, we derive a set of algebraic equations for A_0,

A_1, and A_2. By solving these algebraic equations, we obtain several cases of variables solutions [15, 37]

Stage 3: by substituting the obtained solutions in stage 2 into Equation (4) along with general solutions of Equations (6), (7), (8), (9), (10), (11), (12), (13), (14), (15), (16), (17), (18), and (19), it finally generates new exact solutions for the nonlinear PDE (1)

3. Travelling Wave Solutions of the LL Equation via Aem

In this section, we construct a travelling wave solution without the Gilbert term [30]. Under the condition of the auxiliary equation method, we consider the following wave transformations:

$$W_{c,w}(t,\bar{r}) = e^{-iwt}\phi(\bar{r}-ct)e^{i\psi(\bar{r}-ct)}, \tag{20}$$

where c and w are constants undetermined.

Here, we assume $-c^2+4w>0$. Substitute (5) into (1) [30], the separate real and the virtual parts, respectively, as

$$\begin{aligned}&\phi(\xi)\left(w-2(\xi)^2+c\psi'(\xi)-\psi'(\xi)^2\right)\\&\quad+\phi(\xi)^3\left(w+c\psi'(\xi)+\psi'(\xi)^2\right)+\phi(\xi)^2\phi''(\xi)=0,\end{aligned} \tag{21}$$

$$\begin{aligned}&\phi'(\xi)\left(-c+2\psi'(\xi)\right)-\phi(\xi)^2\phi'(\xi)\left(c+2\psi'(\xi)\right)\\&\quad+\phi(\xi)\psi''(\xi)+\phi(\xi)^3\psi''(\xi)=0,\end{aligned} \tag{22}$$

where $\xi=\bar{r}-ct$. (21) and (22) are the nonlinear constant coefficients of ordinary differential equation system with the variable ξ. According to (22), we can obtain a relationship between ψ and ϕ:

$$\psi'(\xi)=\frac{\left(1+\phi(\xi)^2\right)\left(-c+2C_1+2C_1(\xi)^2\right)}{2\phi(\xi)^2}, \tag{23}$$

where C_1 is the arbitrary constant. If we set C_1=0, we have

$$\psi'(\xi)=-\frac{c\left(1+\phi(\xi)^2\right)}{2\phi(\xi)^2}. \tag{24}$$

Substituting (24) into (21), we get

$$\begin{aligned}&c^2+3c^2\phi(\xi)^2+\left(c^2-4w\right)\phi(\xi)^6+\phi(\xi)^2\left(3c^2-4w+8\phi'(\xi)^2\right)\\&\quad-4\phi(\xi)^3\left(1+\phi(\xi)^2\right)\phi''(\xi)=0.\end{aligned} \tag{25}$$

4. Results

By the auxiliary equation method, the solution of (25) is assumed as

$$\phi(\xi)=A_1\Upsilon(\xi)+A_0. \tag{26}$$

From (5), we have

$$\begin{aligned}\left(\Upsilon'\right)^2&=s_1\Upsilon^2(\xi)+s_2\Upsilon^3(\xi)+s_3\Upsilon^4(\xi),\\\Upsilon''&=\frac{1}{2}\left(s_1\Upsilon(\xi)+3s_2\Upsilon^2(\xi)+4s_3\Upsilon^3(\xi)\right),\end{aligned} \tag{27}$$

where A_1 and A_0 are constants. Substituting (26) into (25) along with (27) and comparing the coefficients of alike powers of $\Upsilon(\xi)$ provides an algebraic system of equations, and solving this set of algebraic equations by used of the Maple, we obtain several case solutions. For example is as follows.

Set 1:

$$\begin{aligned}A_1&=-\frac{20}{3}s_3\left(\frac{3s_1-12s_2}{240s_3-4w}\right),\\A_0&=\frac{3s_1-12s_2}{240s_3-4w},\\s_2&=0,\\c&=\frac{1}{30}\left(\sqrt{10\sqrt{25s_3(3s_1)^2+(-3120w-10800s_3)s_3(3s_1)+144(w+90s_3)^2}+(150s_1-10800)s_3+480w}\right).\end{aligned} \tag{28}$$

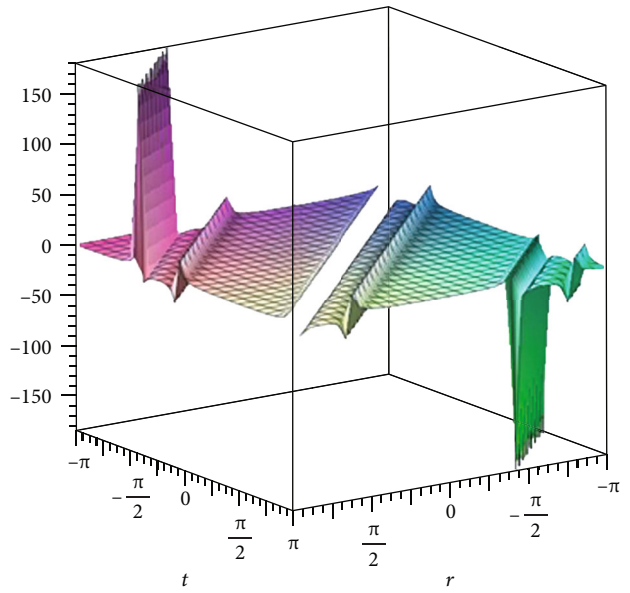

Figure 1: Graphical behavior for $\phi_1(\bar{r}, t)$, for $\bar{r}, t = -\pi..\pi, s_1 = -1$, $s_3 = 1$, and $w = 1$.

From set 1 and Eq. (26), we have

$$\phi(\xi) = -\frac{20}{3}s_3\left(\frac{3s_1}{240s_3 - 4w}\right)\Upsilon(\xi) + \frac{3s_1}{240s_3 - 4w}. \quad (29)$$

So, solutions of Equation (5) are obtained in (6), (7), (8), (9), (10), (11), (12), (13), (14), (15), (16), (17), (18), and (19), we have final solutions of Equation (1) and Equation (25) as follows:

$$\phi_1(\bar{r}, t) = -\frac{20}{3}s_3\left(\frac{3s_1}{240s_3 - 4w}\right) \times \frac{-s_1\csc^2\left(\left(\sqrt{-s_1}/2\right)(\bar{r} - ct)\right)}{2\varepsilon\sqrt{-s_1 s_3}\cot\left(\left(\sqrt{-s_1}/2\right)(\bar{r} - ct)\right)} + \frac{3s_1 - 12s_2}{240s_3 - 4w}. \quad (30)$$

In Figure 1, the graphical behavior of solutions ϕ_1 for $s_1 = -1, s_3 = 1$, and $w = 1$ in different values of $\bar{r}$ and t is illustrated.

$$\phi_2(\bar{r}, t) = -\frac{20}{3}s_3\left(\frac{3s_1}{240s_3 - 4w}\right) \times \frac{2s_1\sec\left(\sqrt{-s_1}(\bar{r} - ct)\right)}{\varepsilon\sqrt{-4s_1 s_3}} + \frac{3s_1 - 12s_2}{240s_3 - 4w}. \quad (31)$$

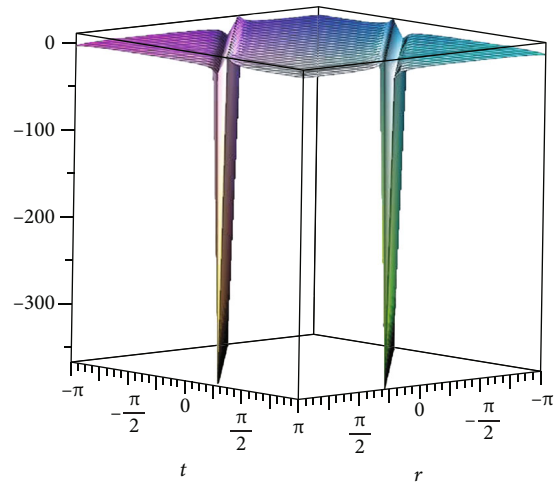

Figure 2: Graphical behavior for $\phi_2(\bar{r}, t)$, for $\bar{r}, t = -\pi..\pi, s_1 = -1$, $s_3 = 1$, and $w = 1$.

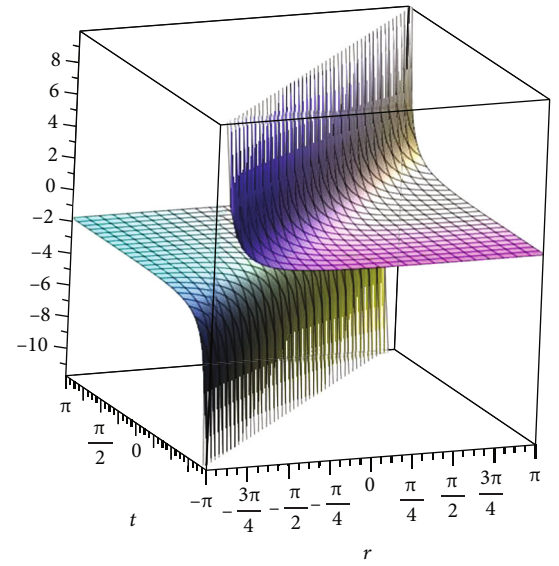

Figure 3: Graphical behavior for $\phi_3(\bar{r}, t)$, for $\bar{r}, t = -\pi..\pi, s_1 = 1$, $s_3 = 1$, and $w = 1$.

In Figure 2, the graphical behavior of solutions ϕ_2 for $s_1 = -1, s_3 = 1$, and $w = 1$ in different values of $\bar{r}$ and t is illustrated.

$$\phi_3(\bar{r}, t) = -\frac{20}{3}s_3\left(\frac{3s_1}{240s_3 - 4w}\right) \times \frac{s_1\operatorname{csch}^2\left(\left(\sqrt{s_1}/2\right)(\bar{r} - ct)\right)}{2\varepsilon\sqrt{s_1 s_3}\coth\left(\left(\sqrt{s_1}/2\right)(\bar{r} - ct)\right)} + \frac{3s_1}{240s_3 - 4w}. \quad (32)$$

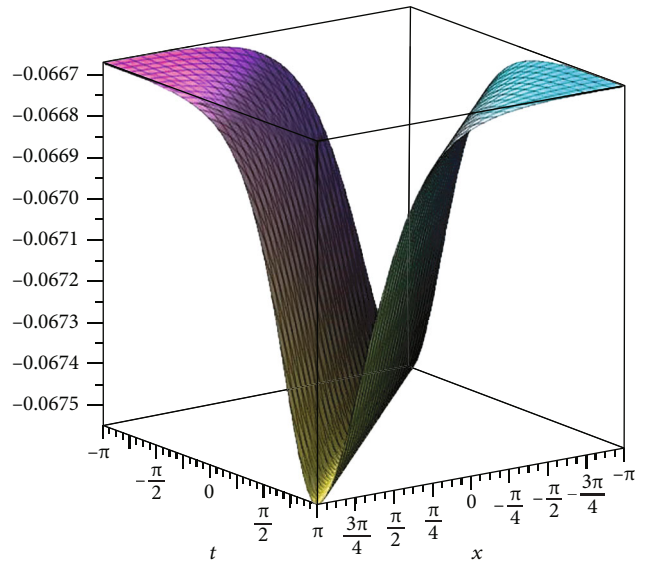

Figure 4: Graphical behavior for $\phi_6(\bar{r}, t)$, for $\bar{r}, t = -\pi..\pi, s_1 = 1$, and $s_2 = 1$.

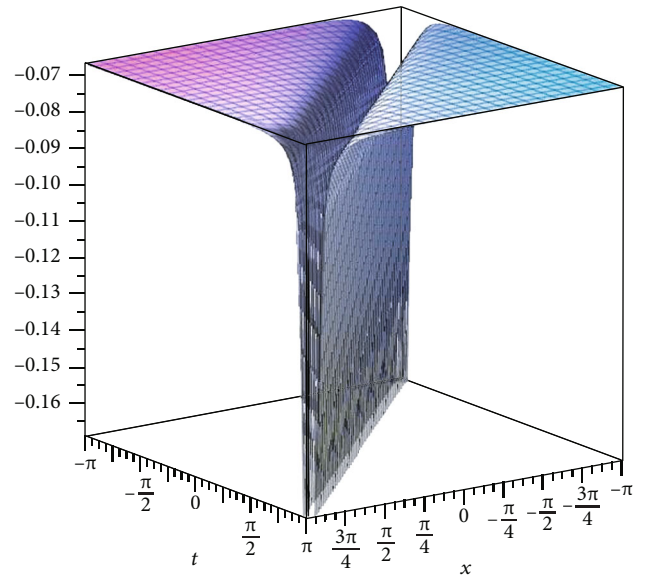

Figure 5: Graphical behavior for $\phi_7(\bar{r}, t)$, for $\bar{r}, t = -\pi..\pi, s_1 = 1$, and $s_2 = 1$

In Figure 3, the graphical behavior of solutions ϕ_3 for $s_1 = 1, s_3 = 1$, and $w = 1$ in different values of $\bar{r}$ and t is illustrated.

$$\phi_4(\bar{r}, t) = -\frac{20}{3}s_3\left(\frac{3s_1}{240s_3 - 4w}\right) \times \frac{4s_1 e^{\varepsilon\sqrt{s_1}(\bar{r}-ct)}}{\left(e^{\varepsilon\sqrt{s_1}(\bar{r}-ct)}\right)^2} + \frac{3s_1}{240s_3 - 4w},$$

$$\phi_5(\bar{r}, t) = -\frac{20}{3}s_3\left(\frac{3s_1}{240s_3 - 4w}\right) \times \frac{\pm 4s_1 \varepsilon e^{\varepsilon\sqrt{s_1}(\bar{r}-ct)}}{1 - 4s_1 s_3 e^{2\varepsilon\sqrt{s_1}(\bar{r}-ct)}} + \frac{3s_1}{240s_3 - 4w}, \tag{33}$$

$$W_{c,w}(t, \bar{r}) = e^{-iwt}\phi(\bar{r} - ct)e^{i\psi(\bar{r}-ct)},$$

$$\psi'(\xi) = -\frac{c\left(1 + \phi(\xi)^2\right)}{2\phi(\xi)^2} \text{ so } \psi(\xi) = -\int \frac{c\left(1 + \phi(\xi)^2\right)}{2\phi(\xi)^2} d\xi,$$

$$c = \frac{1}{30}\left(\sqrt{10\sqrt{25s_3(3s_1)^2 + (-3120w - 10800s_3)s_3(3s_1) + 144(w + 90s_3)^2} + (150s_1 - 10800)s_3 + 480w}\right). \tag{34}$$

Set 2:

$$A_1 = \frac{-{s_1}^2\left({s_1}^2 + 225{s_2}^2\right)(-90s_2 + s_1)}{12w(2{s_1}^4 - 75{s_1}^3 s_2 + 118125{s_2}^4)},$$

$$A_0 = -\frac{1}{15}\frac{s_1}{s_2},$$

$$s_3 = 0, \tag{35}$$

$$c = \sqrt{\left(\frac{4}{15}\frac{s_1}{s_2} + 4\right)w / \left(6 - \frac{1}{15}\frac{s_1}{s_2}\right)}.$$

From set 2 and Eq. (26), we have

$$\phi(\xi) = \frac{-{s_1}^2\left({s_1}^2 + 225{s_2}^2\right)(-90s_2 + s_1)}{12w(2{s_1}^4 - 75{s_1}^3 s_2 + 118125{s_2}^4)}\,\Upsilon(\xi) - \frac{1}{15}\frac{s_1}{s_2}. \tag{36}$$

So, solutions of Equation (5) are obtained in (6), (7), (8), (9), (10), (11), (12), (13), (14), (15), (16), (17), (18), and (19), we have final solutions of Equation (1) and Equation (25) as follows:

$$\phi_6(\bar{r},t)=\frac{-{s_1}^2\left({s_1}^2+225{s_2}^2\right)\left(-90s_2+s_1\right)}{12w\left(2{s_1}^4-75{s_1}^3s_2+118125{s_2}^4\right)}\times\frac{-s_1s_2\,\operatorname{sech}^2\left(\sqrt{s_1/2}(\bar{r}-ct)\right)}{s_2^2}-\frac{1}{15}\frac{s_1}{s_2}.\tag{37}$$

In Figure 4, the graphical behavior of solutions ϕ_6 for $s_1=1, s_2=1$ in different values of $\bar{r}$ and t is illustrated.

$$\phi_7(\bar{r},t)=\frac{-{s_1}^2\left({s_1}^2+225{s_2}^2\right)\left(-90s_2+s_1\right)}{12w\left(2{s_1}^4-75{s_1}^3s_2+118125{s_2}^4\right)}\times\frac{-s_1s_2\,\operatorname{csch}^2\left(\sqrt{s_1/2}(\bar{r}-ct)\right)}{s_2^2}-\frac{1}{15}\frac{s_1}{s_2}.\tag{38}$$

In Figure 5, the graphical behavior of solutions ϕ_7 for $s_1=1, s_3=1$ in different values of $\bar{r}$ and t is illustrated.

$$\phi_8(\bar{r},t)=\frac{-{s_1}^2\left({s_1}^2+225{s_2}^2\right)\left(-90s_2+s_1\right)}{12w\left(2{s_1}^4-75{s_1}^3s_2+118125{s_2}^4\right)}\times\frac{2s_1\,\operatorname{sech}\left(\sqrt{s_1}(\bar{r}-ct)\right)}{\varepsilon s_2-s_2\,\operatorname{sech}\left(\sqrt{s_1}(\bar{r}-ct)\right)}-\frac{1}{15}\frac{s_1}{s_2},$$

$$\phi_9(\bar{r},t)=\frac{-{s_1}^2\left({s_1}^2+225{s_2}^2\right)\left(-90s_2+s_1\right)}{12w\left(2{s_1}^4-75{s_1}^3s_2+118125{s_2}^4\right)}\times\frac{4s_1e^{\varepsilon\sqrt{s_1}(\bar{r}-ct)}}{\left(e^{\varepsilon\sqrt{s_1}(\bar{r}-ct)}-s_2\right)^2-4s_1s_2}-\frac{1}{15}\frac{s_1}{s_2},\tag{39}$$

$$W_{c,w}(t,\bar{r})=e^{-iwt}\phi(\bar{r}-ct)e^{i\psi(\bar{r}-ct)},$$

$$\psi'(\xi)=-\frac{c\left(1+\phi(\xi)^2\right)}{2\phi(\xi)^2}\ \text{so}\ \psi(\xi)=-\int\frac{c\left(1+\phi(\xi)^2\right)}{2\phi(\xi)^2}d\xi,$$

$$c=\sqrt{\left(\frac{4}{15}\frac{s_1}{s_2}+4\right)w/\left(6-\frac{1}{15}\frac{s_1}{s_2}\right)}.\tag{40}$$

For more convenience and understanding, the graphical behavior of the answers is considered (see Figures 1–5).

5. Conclusions

This paper derived new optical soliton solutions of the Landau–Lifshitz equation, which describe the propagation of ultrashort pulses in nonlinear optical fibers by using the auxiliary equation method. We boldly say that the work here is valuable and may be beneficial for studying in other nonlinear science. The exact solutions obtained from the model equations provide important insight into the dynamics of solitary waves. The solutions obtained in this paper have not been reported in the old research.

Data Availability

No data were used to support this study.

Conflicts of Interest

The authors declare that they have no conflicts of interest.

References

[1] A. Neirameh and M. Eslami, "New travelling wave solutions for plasma model of extended K–dV equation," *Afrika Matematika*, vol. 30, no. 1-2, pp. 335–344, 2019.

[2] R. Hirota, "Exact N-soliton solutions of the wave equation of long waves in shallow-water and in nonlinear lattices," *Journal of Mathematical Physics*, vol. 14, no. 7, pp. 810–814, 1973.

[3] B. Ghanbari, A. Yusuf, M. Inc, and D. Baleanu, "The new exact solitary wave solutions and stability analysis for the (2+1)-dimensional Zakharov–Kuznetsov equation," *Advances in Difference Equations*, vol. 2019, 2019.

[4] S. Liu, Z. Fu, S. Liu, and Q. Zhao, "Jacobi elliptic function expansion method and periodic wave solutions of nonlinear wave equations," *Physics Letters A*, vol. 289, no. 1-2, pp. 69–74, 2001.

[5] M. Wang, "Solitary wave solutions for variant Boussinesq equations," *Physics Letters A*, vol. 199, no. 3-4, pp. 169–172, 1995.

[6] E. J. Parkes and B. R. Duffy, "An automated tanh-function method for finding solitary wave solutions to non- linear evolution equations," *Computer Physics Communications*, vol. 98, no. 3, pp. 288–300, 1996.

[7] Y. He, S. Li, and Y. Long, "Exact solutions of the modified Benjamin-Bona-Mahoney (mBBM) equation by using the first integral method," *Differential Equations and Dynamical Systems*, vol. 21, no. 3, pp. 199–204, 2013.

[8] K. Hosseini and P. Gholamin, "Feng's first integral method for analytic treatment of two higher dimensional nonlinear partial differential equations," *Differential Equations and Dynamical Systems*, vol. 23, no. 3, pp. 317–325, 2015.

[9] B. Zheng, "A new Bernoulli sub-ODE method for constructing traveling wave solutions for two nonlinear equations with any order," *UPB Scientific Bulletin, Series A*, vol. 73, pp. 85–94, 2011.

[10] J. H. He, "Some asymptotic methods for strongly nonlinear equations," *International Journal of Modern Physics B*, vol. 22, pp. 3487–3578, 2008.

[11] M. Eslami and A. Neirameh, "New solitary and double periodic wave solutions for a generalized sinh-Gordon equation," *The European Physical Journal Plus*, vol. 129, no. 4, p. 54, 2014.

[12] A. Neirameh and M. Eslami, "An analytical method for finding exact solitary wave solutions ofthe coupled (2 1)-dimensional Painlevé Burgers equation," *Scientia Iranica*, vol. 24, no. 2, pp. 715–726, 2017.

[13] H. Rezazadeh, D. Kumar, A. Neirameh, M. Eslami, and M. Mirzazadeh, "Applications of three methods for obtaining optical soliton solutions for the Lakshmanan–Porsezian–Daniel model with Kerr law nonlinearity," *Pramana*, vol. 94, no. 1, p. 39, 2019.

[14] H. Rezazadeh, A. Neirameh, M. Eslami, A. Bekir, and A. Korkmaz, "A sub-equation method for solving the cubic–quartic NLSE with the Kerr law nonlinearity," *Modern Physics Letters B*, vol. 33, no. 18, pp. 195–197, 2019.

[15] H. Rezazadeh, A. Neirameh, N. Raza, and M. Eslami, "Exact solutions of nonlinear diffusive predator-prey system by new

extension of tanh method," *Journal of Computational and Theoretical Nanoscience*, vol. 15, pp. 3195–3200, 2019.

[16] K. Munusamy, C. Ravichandran, K. Sooppy Nisar, and B. Ghanbari, "Existence of solutions for some functional integrodifferential equations with nonlocal conditions," *Journal of Mathematical Methods in the Applied Sciences*, vol. 43, no. 17, pp. 10319–10331, 2020.

[17] B. Ghanbari, "On novel nondifferentiable exact solutions to local fractional Gardner's equation using an effective technique," *Journal of Mathematical Methods in the Applied Sciences*, vol. 44, no. 6, pp. 4673–4685, 2021.

[18] H. M. Srivastava, D. Baleanu, J. A. T. Machado et al., "Traveling wave solutions to nonlinear directional couplers by modified Kudryashov method," *Physica Scripta*, vol. 95, no. 7, article 075217, 2020.

[19] H. Rezazadeh, "New solitons solutions of the complex Ginzburg-Landau equation with Kerr law nonlinearity," *Optik*, vol. 167, pp. 218–227, 2018.

[20] H. Rezazadeh, Mustafa Inc, and D. Baleanu, "New solitary wave solutions for variants of (3+1)-dimensional Wazwaz-Benjamin-Bona-Mahony equations," *Frontiers in Physics*, vol. 8, 2020.

[21] Q. Ding, "Explicit blow-up solutions to the Schrodinger maps from R2 to the hyperbolic 2-space H2," *Journal of Mathematical Physics*, vol. 50, no. 10, article 103507, p. 17, 2009.

[22] B. Ghanbari, "On the nondifferentiable exact solutions to Schamel's equation with local fractional derivative on Cantor sets," *Numerical Methods for Partial Differential Equations*, vol. 29D, 2020.

[23] S. Ding and B. Guo, "Existence of partially regular weak solutions to Landau-Lifshitz-Maxwell equations," *Differential Equations*, vol. 244, no. 10, pp. 2448–2472, 2008.

[24] B. Guo and M. Hong, "The Landau-Lifshitz equations of the ferromagnetic spin chain and harmonic maps," *Calculus of Variations and Partial Differential Equations*, vol. 1, no. 3, pp. 311–334, 1993.

[25] S. Gutiérrez and A. de Laire, "Self-similar solutions of the one-dimensional Landau-Lifshitz-Gilbert equation," *Nonlinearity*, vol. 28, no. 5, pp. 1307–1350, 2015.

[26] S. Gutiérrez and A. de Laire, "The Cauchy problem for the Landau-Lifshitz-Gilbert equation in BMO and self-similar solutions," *Nonlinearity*, vol. 32, no. 7, pp. 2522–2563, 2019.

[27] B. Guo and G. Yang, "Some exact nontrivial global solutions with values in unit sphere for two-dimensional Landau-Lifshitz equations," *Journal of Mathematical Physics*, vol. 42, no. 11, pp. 5223–5227, 2001.

[28] H. Huh, "Blow-up solutions of modified Schrödinger maps," *Communications in Partial Differential Equations*, vol. 33, no. 2, pp. 235–243, 2008.

[29] B. Ghanbari, Mustafa Inc, and L. Rada, "Solitary wave solutions to the Tzitzéica type equations obtained by a new efficient approach," *Journal of Applied Analysis & Computation*, vol. 9, no. 2, pp. 568–589, 2019.

[30] L. D. Landau and E. M. Lifshitz, "On the theory of the dispersion of magnetic permeability in ferromagnetic bodies," in *Z. Sowjetunion 8. Reproduced in Collected Papers of L. D. Landau*, pp. 101–114, Pergamon, New York, NY, USA, 1965.

[31] I. Bejenaru, A. D. Ionescu, C. E. Kenig, and D. Tataru, "Global Schrödinger maps in dimensions d>=2: small data in the critical Sobolev spaces," *Annals of Mathematics*, vol. 173, no. 3, pp. 1443–1506, 2011.

[32] B. Ghanbari, K. Sooppy Nisar, and M. Aldhaifallah, "Abundant solitary wave solutions to an extended nonlinear Schrödinger's equation with conformable derivative using an efficient integration method," *Advances in Difference Equations*, vol. 2020, no. 1, 2020.

[33] A. Nahmod, A. Stefanov, and K. Uhlenbeck, "On Schrödinger maps," *Communications on Pure and Applied Mathematics*, vol. 56, no. 1, pp. 114–151, 2003.

[34] X. Liu, "Partial regularity for Landau-Lifshitz system of ferromagnetic spin chain," *Calculus of Variations and Partial Differential Equations*, vol. 20, no. 2, pp. 153–173, 2004.

[35] H. McGahagan, "An approximation scheme for Schrödinger maps," *Communications in Partial Differential Equations*, vol. 32, no. 3, pp. 375–400, 2007.

[36] J. Tjon and J. Wright, "Solitons in the continuous Heisenberg spin chain," *Physical Review B*, vol. 15, no. 7, pp. 3470–3476, 1977.

[37] L. G. de Azevedo, M. A. de Moura, C. Cordeiro, and B. Zeks, "Solitary waves in a 1D isotropic Heisenberg ferromagnet," *Journal of Physics C: Solid State Physics*, vol. 15, no. 36, pp. 7391–7396, 1982.

Hindawi
Advances in Mathematical Physics
Volume 2021, Article ID 6669287, 20 pages
https://doi.org/10.1155/2021/6669287

Review Article

An Efficient Explicit Decoupled Group Method for Solving Two–Dimensional Fractional Burgers' Equation and Its Convergence Analysis

N. Abdi,[1] H. Aminikhah ,[1,2] A. H. Refahi Sheikhani ,[3] J. Alavi,[1] and M. Taghipour[1]

[1]*Department of Applied Mathematics and Computer Science, Faculty of Mathematical Sciences, University of Guilan, P.O. Box 1914, Rasht 41938, Iran*
[2]*Center of Excellence for Mathematical Modelling, Optimization and Combinational Computing (MMOCC), University of Guilan, P.O. Box 1914, Rasht 41938, Iran*
[3]*Department of Applied Mathematics, Faculty of Mathematical Sciences, Lahijan Branch, Islamic Azad University, Lahijan, Iran*

Correspondence should be addressed to H. Aminikhah; aminikhah@guilan.ac.ir

Received 17 November 2020; Revised 10 December 2020; Accepted 22 February 2021; Published 16 March 2021

Academic Editor: Manuel De León

In this paper, the Crank–Nicolson (CN) and rotated four-point fractional explicit decoupled group (EDG) methods are introduced to solve the two-dimensional time–fractional Burgers' equation. The EDG method is derived by the Taylor expansion and 45° rotation of the Crank–Nicolson method around the x and y axes. The local truncation error of CN and EDG is presented. Also, the stability and convergence of the proposed methods are proved. Some numerical experiments are performed to show the efficiency of the presented methods in terms of accuracy and CPU time.

1. Introduction

Fractional calculus is a generalization of the integration and derivation of integer order operators to fractional order that allows us to describe a real system more accurately than integers. Although the fractional order of a real system may be low, it is yet considered as a fractional system. An important feature of fractional calculus is its nonlocality. The fractional derivative (and integrals) of a function is given by a definite integral, thus, it depends on the value of the function over the entire interval [1]. Researchers confirm the existence of interesting phenomena in nature, which cannot be modeled by classical differential equations. To cope with this problem, the nonlocality property of fractional derivative could be a beneficial tool to study our considered system. Fractional calculus has recently been used in various scientific and engineering fields [2–4]. Some fractional calculus applications in modeling and design of control systems are introduced in [5]. The most recent developments and trends in the use of fractional calculus in biomedicine and biology are presented by Ionescu et al. [6]. Based on the fractional calculate, Tang et al. [7] proposed a new four-element creep model; this model accords well with the experimental data of Changshan rock salt. Fractional calculus has an extraordinary potential in signal denoising [8]. Gong et al. discussed the generation conditions of chaotic behavior and proposed the adaptive synchronization control method for a class of fractional-order financial system [9]. Numerous definitions of fractional derivative have been introduced in the literature, amongst are Riemann–Liouville, Caputo, and Caputo–Fabrizio [10]. The Caputo–Fabrizio fractional derivative on the contrary of other derivatives has a nonsingular kernel. Hence, it has been considered by many researchers [11–15]. Since to obtain the exact solution of fractional differential equations is very difficult and sometimes impossible, it is usually approximated by a numerical method such as finite difference method [16–18], finite volume methods [19], and spectral method [20].

Burgers' equation as a nonlinear partial differential equation is widely used in various areas such as fluid mechanics, gas dynamics, and traffic flow which combine nonlinear propagation effects with diffusive one.

In this paper, we consider the following two dimensional time-fractional Burgers' equation:

$$\frac{\partial^\alpha u}{\partial t^\alpha} + u\left(\frac{\partial u}{\partial x} + \frac{\partial u}{\partial y}\right) = \nu\left(\frac{\partial^2 u}{\partial x^2} + \frac{\partial^2 u}{\partial y^2}\right) + f(x, y, t), \quad (x, y) \in \Omega, 0 < t < T, \tag{1}$$

with the initial condition

$$u(x, y, 0) = u_0(x, y), (x, y) \in \Omega, \tag{2}$$

and the boundary condition

$$u(x, y, t) = 0, (x, y) \in \partial\Omega, 0 \le t \le T, \tag{3}$$

where $\nu = 1/\mathrm{Re}$, Re is Reynolds number characterizing the strength of viscosity, $\Omega = (0, 1) \times (0, 1)$, $0 < \alpha < 1$, and the term $\partial^\alpha u/\partial t^\alpha$ denotes the α order Caputo-Fabrizio fractional derivative of the function $u(x, y, t)$ defined as:

$$\frac{\partial^\alpha u(x, y, t)}{\partial t^\alpha} = \frac{M(\alpha)}{1 - \alpha}\int_0^t \frac{\partial u(x, y, s)}{\partial s} e^{-\frac{\alpha}{1-\alpha}(t-s)} ds, \tag{4}$$

where $M(\alpha)$ is a normalization function such that $M(0) = M(1) = 1$.

We apply the finite difference method to solve Equations (1)–(3). In finite difference, to find the value corresponding to each grid point, it is used natural ordering (indexing the grid of point from left to right and bottom to top by point to point) or group to group. There are several different methods to order the interior mesh point such as natural ordering, diagonal ordering, and alternating diagonal ordering [21]. Different linear systems would be produced by different arrangements of the grid points.

We propose two finite difference schemes. The first scheme is given by the Crank–Nicolson difference method (by natural ordering). In this scheme, to obtain a more accurate numerical solution, we should use a smaller mesh size, which requires more storage space and computing time. In order to fix this problem and accelerate the convergence, we use the explicit decoupled group (EDG) method introduced by Abdullah in 1990 [22]. Many studies have been done in reference to the EDG method for examples [23–26]. The EDG method is based on rotating the Crank–Nicolson difference scheme and group ordering of grid points. Applying the EDG method to the Crank–Nicolson difference scheme result in a new scheme in which the dimension of the system is half of the dimension of the system generated by the Crank–Nicolson difference scheme. On this account, half of the grid points are obtained and the rest can be calculated directly. Consequently, the EDG method can be favourably used to reduce the computational cost. In addition, it is worth to notice that we can take advantage of parallel computers to run it.

The rest of the paper is organized as follows. In Section 2, the Crank–Nicolson difference scheme will be applied to Equations (1)–(3), and also, we give the truncation error. In Section 3, we describe the formulation of the EDG method. The stability of these schemes is discussed in Section 4. In Section 5, we analyze the convergence of these schemes. Numerical examples are carried out to verify the high efficiency of our method in Section 6. Finally, the paper ends with a brief conclusion in Section 7.

2. Ù'The Crank–Nicolson Difference Scheme

For the numerical solution of Equations (1)–(3), we introduce a uniform grid of mesh points (x_i, y_j, t_n) with $x_i = i\Delta x$, $i = 0, 1, \cdots, I$, $y_j = j\Delta y$, $j = 0, 1, \cdots, J$, and $t_n = n\Delta t$, $n = 0, 1, \cdots, N$.

Using the Crank–Nicolson approximation to Equations (1)–(3), we have

$$\left(\frac{\partial^\alpha u}{\partial t^\alpha}\right)_{i,j}^{n+1/2} + \frac{(uu_x)_{i,j}^{n+1} + (uu_x)_{i,j}^{n}}{2} + \frac{(uu_y)_{i,j}^{n+1} + (uu_y)_{i,j}^{n}}{2} = \nu\left(\frac{(u_{xx})_{i,j}^{n+1} + (u_{xx})_{i,j}^{n}}{2} + \frac{(u_{yy})_{i,j}^{n+1} + (u_{yy})_{i,j}^{n}}{2}\right) + f_{i,j}^{n+1/2}. \tag{5}$$

We use the following linearization technique for nonlinear term $(uu_x)^{n+1}$ and $(uu_y)^{n+1}$ [27]

$$\begin{aligned}(uu_x)^{n+1} &\approx u^{n+1}u_x^n + u^n u_x^{n+1} - u^n u_x^n,\\ (uu_y)^{n+1} &\approx u^{n+1}u_y^n + u^n u_y^{n+1} - u^n u_y^n.\end{aligned} \tag{6}$$

Substituting the above approximation into Equation (5), we yield

$$\left(\frac{\partial^\alpha u}{\partial t^\alpha}\right)_{i,j}^{n+1/2} + \frac{u_{i,j}^{n+1}(u_x)_{i,j}^{n} + u_{i,j}^{n}(u_x)_{i,j}^{n+1}}{2} + \frac{u_{i,j}^{n+1}(u_y)_{i,j}^{n} + u_{i,j}^{n}(u_y)_{i,j}^{n+1}}{2} = \nu\left(\frac{(u_{xx})_{i,j}^{n+1} + (u_{xx})_{i,j}^{n}}{2} + \frac{(u_{yy})_{i,j}^{n+1} + (u_{yy})_{i,j}^{n}}{2}\right) + f_{i,j}^{n+1/2}. \tag{7}$$

A discrete approximation to the ${}_0^{CF}D_t^\alpha u(x, y, t)$ at $(x_i, y_j, t_{n+1/2})$ can be obtained by the following approximation

$$\begin{aligned}
\frac{\partial^\alpha u\left(x_i,y_j,t_{n+1/2}\right)}{\partial t^\alpha} &= \frac{1}{1-\alpha}\int_0^{t_{n+\frac{1}{2}}}\frac{\partial u\left(x_i,y_j,s\right)}{\partial s}e^{-\frac{\alpha}{1-\alpha}\left(t_{n+\frac{1}{2}}-s\right)}ds \\
&= \frac{1}{1-\alpha}\left[\int_0^{t_n}\frac{\partial u\left(x_i,y_j,s\right)}{\partial s}e^{-\frac{\alpha}{1-\alpha}\left(t_{n+\frac{1}{2}}-s\right)}ds+\int_{t_n}^{t_{n+\frac{1}{2}}}\frac{\partial u\left(x_i,y_j,s\right)}{\partial s}e^{-\frac{\alpha}{1-\alpha}\left(t_{n+\frac{1}{2}}-s\right)}ds\right] \\
&= \frac{1}{1-\alpha}\left[\sum_{k=1}^{n}\int_{t_{k-1}}^{t_k}\left(\frac{u_{i,j}^k-u_{i,j}^{k-1}}{\Delta t}+\left(s-t_{k-\frac{1}{2}}\right)u_{tt}\left(x_i,y_j,c_k\right)\right)e^{-\frac{\alpha}{1-\alpha}\left(t_{n+\frac{1}{2}}-s\right)}ds\right. \\
&\quad \left.+\int_{t_n}^{t_{n+\frac{1}{2}}}\left(\frac{u_{i,j}^{n+1/2}-u_{i,j}^n}{\Delta t/2}+O(\Delta t)\right)e^{-\frac{\alpha}{1-\alpha}\left(t_{n+\frac{1}{2}}-s\right)}ds\right] \\
&= \frac{1}{1-\alpha}\left[\sum_{k=1}^{n}\int_{t_{k-1}}^{t_k}\left(\frac{u_{i,j}^k-u_{i,j}^{k-1}}{\Delta t}+\left(s-t_{k-\frac{1}{2}}\right)u_{tt}\left(x_i,y_j,c_k\right)\right)e^{-\frac{\alpha}{1-\alpha}\left(t_{n+\frac{1}{2}}-s\right)}ds\right. \\
&\quad \left.+\int_{t_n}^{t_{n+\frac{1}{2}}}\left(\frac{u_{i,j}^{n+1}+u_{i,j}^n/2-u_{i,j}^n}{\Delta t/2}+O(\Delta t)\right)e^{-\frac{\alpha}{1-\alpha}\left(t_{n+\frac{1}{2}}-s\right)}ds\right],
\end{aligned} \tag{8}$$

where $c_k \in (t_{k-1}, t_k)$. Then,

$$\begin{aligned}
\frac{\partial^\alpha u\left(x_i,y_j,t_{n+1/2}\right)}{\partial t^\alpha} &= \frac{1}{1-\alpha}\sum_{k=1}^{n}\int_{t_{k-1}}^{t_k}\frac{u_{i,j}^k-u_{i,j}^{k-1}}{\Delta t}e^{-\frac{\alpha}{1-\alpha}\left(t_{n+\frac{1}{2}}-s\right)}ds \\
&\quad+\frac{1}{1-\alpha}\sum_{k=1}^{n}\int_{t_{k-1}}^{t_k}\left(s-t_{k-\frac{1}{2}}\right)u_{tt}\left(x_i,y_j,c_k\right)e^{-\frac{\alpha}{1-\alpha}\left(t_{n+\frac{1}{2}}-s\right)}ds \\
&\quad+\frac{1}{1-\alpha}\int_{t_n}^{t_{n+\frac{1}{2}}}\left(\frac{u_{i,j}^{n+1}-u_{i,j}^n}{\Delta t}+O(\Delta t)\right)e^{-\frac{\alpha}{1-\alpha}\left(t_{n+\frac{1}{2}}-s\right)}ds \\
&= \frac{1}{\alpha\Delta t}\left\{\left(u_{i,j}^{n+1}-u_{i,j}^n\right)\left(1-e^{-\frac{\alpha}{1-\alpha}\left(\frac{1}{2}\right)\Delta t}\right)+\sum_{k=1}^{n}\left[u_{i,j}^k-u_{i,j}^{k-1}\right]\right. \\
&\quad\left.\cdot\left[e^{-\frac{\alpha}{1-\alpha}\left(n-k+\frac{1}{2}\right)\Delta t}-e^{-\frac{\alpha}{1-\alpha}\left(n-k+\frac{3}{2}\right)\Delta t}\right]\right\}+R_1+R_2,
\end{aligned} \tag{9}$$

which

$$R_1 = \frac{1}{1-\alpha}\sum_{k=1}^{n}\int_{t_{k-1}}^{t_k}\left(s-t_{k-\frac{1}{2}}\right)u_{tt}\left(x_i,y_j,c_k\right)e^{-\frac{\alpha}{1-\alpha}\left(t_{n+\frac{1}{2}}-s\right)}ds, \tag{10}$$

and

$$R_2 = \frac{1}{\alpha}\left(1-e^{-\frac{\alpha}{1-\alpha}\left(\frac{1}{2}\right)\Delta t}\right)O(\Delta t). \tag{11}$$

Therefore, we have

$$\begin{aligned}
R_1 &= \frac{1}{1-\alpha}\sum_{k=1}^{n}\int_{t_{k-1}}^{t_k}\left(s-t_{k-\frac{1}{2}}\right)u_{tt}\left(x_i,y_j,c_k\right)e^{-\frac{\alpha}{1-\alpha}\left(t_{n+\frac{1}{2}}-s\right)}ds \\
&= \frac{1}{1-\alpha}\sum_{k=1}^{n}u_{tt}\left(x_i,y_j,c_k\right)\int_{t_{k-1}}^{t_k}\left(s-t_{k-\frac{1}{2}}\right)e^{-\frac{\alpha}{1-\alpha}\left(t_{n+\frac{1}{2}}-s\right)}ds \\
&\le \frac{\max\left|u_{tt}\left(x_i,y_j,c_k\right)\right|\Delta t}{2(1-\alpha)}\sum_{k=1}^{n}\int_{t_{k-1}}^{t_k}e^{-\frac{\alpha}{1-\alpha}\left(t_{n+\frac{1}{2}}-s\right)}ds \\
&= \frac{\max\left|u_{tt}\left(x_i,y_j,c_k\right)\right|\Delta t}{2\alpha}\sum_{k=1}^{n}\left(e^{-\frac{\alpha}{1-\alpha}\left(n-k+\frac{1}{2}\right)\Delta t}-e^{-\frac{\alpha}{1-\alpha}\left(n-k+\frac{3}{2}\right)\Delta t}\right) \\
&= \frac{\max\left|u_{tt}\left(x_i,y_j,c_k\right)\right|\Delta t}{2\alpha}\left(e^{-\frac{\alpha}{1-\alpha}\left(\frac{1}{2}\right)\Delta t}-e^{-\frac{\alpha}{1-\alpha}\left(n+\frac{1}{2}\right)\Delta t}\right) \\
&\approx \frac{\max\left|u_{tt}\left(x_i,y_j,c_k\right)\right|\Delta t}{2\alpha}\left(\frac{\alpha}{1-\alpha}\left(n+\frac{1}{2}-\frac{1}{2}\right)\Delta t\right) \\
&= \frac{\max\left|u_{tt}\left(x_i,y_j,c_k\right)\right|\Delta t}{2(1-\alpha)}n\Delta t \\
&= \frac{\max\left|u_{tt}\left(x_i,y_j,c_k\right)\right|T\Delta t}{2(1-\alpha)} = O(\Delta t).
\end{aligned} \tag{12}$$

By setting

$$w_k = e^{-\frac{\alpha}{1-\alpha}\left(k-\frac{1}{2}\right)\Delta t}-e^{-\frac{\alpha}{1-\alpha}\left(k+\frac{1}{2}\right)\Delta t}, \tag{13}$$

finally, we obtain

$$\begin{aligned}
\frac{\partial^\alpha u\left(x_i,y_j,t_{n+1/2}\right)}{\partial t^\alpha} &= \frac{1}{\alpha\Delta t}\left[-w_n u_{i,j}^0+\sum_{k=1}^{n-1}\left(w_{n-k+1}-w_{n-k}\right)u_{i,j}^k\right. \\
&\quad\left.+w_1u_{i,j}^n+\left(u_{i,j}^{n+1}-u_{i,j}^n\right)\left(1-e^{-\frac{\alpha}{1-\alpha}\left(\frac{1}{2}\right)\Delta t}\right)\right] \\
&\quad+O(\Delta t).
\end{aligned} \tag{14}$$

Besides, utilizing the Taylor expansion, we have

$$\begin{aligned}
\frac{\partial^2 u\left(x_i,y_j,t_{n+1/2}\right)}{\partial x^2} &= \frac{1}{2}\left[\frac{u_{i+1,j}^{n+1}-2u_{i,j}^{n+1}+u_{i-1,j}^{n+1}}{(\Delta x)^2}+\frac{u_{i+1,j}^n-2u_{i,j}^n+u_{i-1,j}^n}{(\Delta x)^2}\right] \\
&\quad+O\left(\Delta t^2+\Delta x^2\right),
\end{aligned} \tag{15}$$

$$\begin{aligned}
\frac{\partial^2 u\left(x_i,y_j,t_{n+1/2}\right)}{\partial y^2} &= \frac{1}{2}\left[\frac{u_{i,j+1}^{n+1}-2u_{i,j}^{n+1}+u_{i,j-1}^{n+1}}{(\Delta y)^2}+\frac{u_{i,j+1}^n-2u_{i,j}^n+u_{i,j-1}^n}{(\Delta y)^2}\right] \\
&\quad+O\left(\Delta t^2+\Delta y^2\right),
\end{aligned} \tag{16}$$

$$u\left(x_i, y_j, t_{n+\frac{1}{2}}\right)\frac{\partial u\left(x_i, y_j, t_{k+1/2}\right)}{\partial x} = \frac{1}{4\Delta x}\left[u_{i,j}^{n}\left(u_{i+1,j}^{n+1} - u_{i-1,j}^{n+1}\right) + u_{i,j}^{n+1}\left(u_{i+1,j}^{n} - u_{i-1,j}^{n}\right)\right] + O\left(\Delta t^2 + \Delta x^2\right), \tag{17}$$

$$u\left(x_i, y_j, t_{n+\frac{1}{2}}\right)\frac{\partial u\left(x_i, y_j, t_{n+1/2}\right)}{\partial y} = \frac{1}{4\Delta y}\left[u_{i,j}^{n}\left(u_{i,j+1}^{n+1} - u_{i,j-1}^{n+1}\right) + u_{i,j}^{n+1}\left(u_{i,j+1}^{n} - u_{i,j-1}^{n}\right)\right] + O\left(\Delta t^2 + \Delta y^2\right). \tag{18}$$

Using the Equations (14)–(18), we derive the following difference scheme which is accurate of the order $O(\Delta t + \Delta x^2 + \Delta y^2)$,

$$\begin{aligned}
&\frac{1}{\alpha\Delta t}\left[-w_n U_{i,j}^{0} + \sum_{k=1}^{n-1}(w_{n-k+1} - w_{n-k})U_{i,j}^{k} + w_1 U_{i,j}^{n} + \left(U_{i,j}^{n+1} - U_{i,j}^{n}\right)D_0\right] \\
&= \frac{\nu}{2}\left[\frac{U_{i+1,j}^{n+1} - 2U_{i,j}^{n+1} + U_{i-1,j}^{n+1}}{(\Delta x)^2} + \frac{U_{i+1,j}^{n} - 2U_{i,j}^{n} + U_{i-1,j}^{n}}{(\Delta x)^2}\right] \\
&\quad + \frac{\nu}{2}\left[\frac{U_{i,j+1}^{n+1} - 2U_{i,j}^{n+1} + U_{i,j-1}^{n+1}}{(\Delta y)^2} + \frac{U_{i,j+1}^{n} - 2U_{i,j}^{n} + U_{i,j-1}^{n}}{(\Delta y)^2}\right] \\
&\quad - \frac{1}{4\Delta x}\left[U_{i,j}^{n}\left(U_{i+1,j}^{n+1} - U_{i-1,j}^{n+1}\right) + U_{i,j}^{n+1}\left(U_{i+1,j}^{n} - U_{i-1,j}^{n}\right)\right] \\
&\quad - \frac{1}{4\Delta y}\left[U_{i,j}^{n}\left(U_{i,j+1}^{n+1} - U_{i,j-1}^{n+1}\right) + U_{i,j}^{n+1}\left(U_{i,j+1}^{n} - U_{i,j-1}^{n}\right)\right] \\
&\quad + f\left(x_i, y_j, t_{n+\frac{1}{2}}\right),
\end{aligned} \tag{19}$$

where $D_0 = (1 - e^{-(\alpha/1-\alpha)(1/2)\Delta t})$ and $U_{i,j}^{n}$ represents the approximate solution of Equation (1).

After simplification, we obtain

$$\begin{aligned}
&\left(D_0 + \frac{\alpha\Delta t}{4\Delta x}\left(U_{i+1,j}^{n} - U_{i-1,j}^{n}\right) + \frac{\alpha\Delta t}{4\Delta y}\left(U_{i,j+1}^{n} - U_{i,j-1}^{n}\right) + \frac{\alpha\Delta t\nu}{(\Delta x)^2} + \frac{\alpha\Delta t\nu}{(\Delta y)^2}\right)U_{i,j}^{n+1} \\
&\quad - \left(\frac{\alpha\Delta t\nu}{2(\Delta x)^2} - U_{i,j}^{n}\frac{\alpha\Delta t}{4\Delta x}\right)U_{i+1,j}^{n+1} - \left(\frac{\alpha\Delta t\nu}{2(\Delta x)^2} + U_{i,j}^{n}\frac{\alpha\Delta t}{4\Delta x}\right)U_{i-1,j}^{n+1} \\
&\quad - \left(\frac{\alpha\Delta t\nu}{2(\Delta y)^2} - U_{i,j}^{n}\frac{\alpha\Delta t}{4\Delta y}\right)U_{i,j+1}^{n+1} - \left(\frac{\alpha\Delta t\nu}{2(\Delta y)^2} + U_{i,j}^{n}\frac{\alpha\Delta t}{4\Delta y}\right)U_{i,j-1}^{n+1} \\
&= \left(D_0 - \frac{\alpha\Delta t\nu}{(\Delta x)^2} - \frac{\alpha\Delta t\nu}{(\Delta y)^2} - w_1\right)U_{i,j}^{n} + \frac{\alpha\Delta t\nu}{2(\Delta x)^2}U_{i+1,j}^{n} + \frac{\alpha\Delta t\nu}{2(\Delta x)^2}U_{i-1,j}^{n} \\
&\quad + \frac{\alpha\Delta t\nu}{2(\Delta y)^2}U_{i,j+1}^{n} + \frac{\alpha\Delta t\nu}{2(\Delta y)^2}U_{i,j-1}^{n} + w_n U_{i,j}^{0} - \sum_{k=1}^{n-1}(w_{n-k+1} - w_{n-k})U_{i,j}^{k} + (\alpha\Delta t)f_{i,j}^{n+\frac{1}{2}}.
\end{aligned} \tag{20}$$

3. Fractional Explicit Decoupled Group Method

Another approximate formula for Equation (1) is obtained by Taylor's expansion and rotating Equation (20), 45° degrees clockwise around the $x - y$ axis. The Crank–Nicolson rotation formula for Equation (1) is as follows

$$\begin{aligned}
&\frac{1}{\alpha\Delta t}\left[-w_n U_{i,j}^{0} + \sum_{k=1}^{n-1}(w_{n-k+1} - w_{n-k})U_{i,j}^{k} + w_1 U_{i,j}^{n} + \left(U_{i,j}^{n+1} - U_{i,j}^{n}\right)D_0\right] \\
&= \frac{\nu}{4}\left[\frac{U_{i-1,j+1}^{n+1} - 2U_{i,j}^{n+1} + U_{i+1,j-1}^{n+1}}{h^2} + \frac{U_{i-1,j+1}^{n} - 2U_{i,j}^{n} + U_{i+1,j-1}^{n}}{h^2}\right] \\
&\quad + \frac{\nu}{4}\left[\frac{U_{i+1,j+1}^{n+1} - 2U_{i,j}^{n+1} + U_{i-1,j-1}^{n+1}}{h^2} + \frac{U_{i+1,j+1}^{n} - 2U_{i,j}^{n} + U_{i-1,j-1}^{n}}{h^2}\right] \\
&\quad - \frac{1}{4h}\left[\frac{U_{i,j}^{n}}{2}\left(\left(U_{i+1,j+1}^{n+1} + U_{i+1,j-1}^{n+1}\right) - \left(U_{i-1,j-1}^{n+1} + U_{i-1,j+1}^{n+1}\right)\right)\right. \\
&\quad \left. + \frac{U_{i,j}^{n+1}}{2}\left(\left(U_{i+1,j+1}^{n} + U_{i+1,j-1}^{n}\right) - \left(U_{i-1,j-1}^{n} + U_{i-1,j+1}^{n}\right)\right)\right] \\
&\quad - \frac{1}{4h}\left[\frac{U_{i,j}^{n}}{2}\left(\left(U_{i-1,j+1}^{n+1} + U_{i+1,j+1}^{n+1}\right) - \left(U_{i-1,j-1}^{n+1} + U_{i+1,j-1}^{n+1}\right)\right)\right. \\
&\quad \left. + \frac{U_{i,j}^{n+1}}{2}\left(\left(U_{i-1,j+1}^{n} + U_{i+1,j+1}^{n}\right) - \left(U_{i-1,j-1}^{n} + U_{i+1,j-1}^{n}\right)\right)\right] \\
&\quad + f\left(x_i, y_j, t_{n+\frac{1}{2}}\right),
\end{aligned} \tag{21}$$

where $h = \Delta x = \Delta y$. Similarly, the above-rotated difference scheme is accurate of order $O(\Delta t + \Delta x^2 + \Delta y^2)$. On simplification with $r_x = \alpha\Delta t/4h$ and $r_{xx} = \alpha\Delta t\nu/2h^2$, the following equation is obtained

$$\begin{aligned}
&\left(D_0 + r_x\left(U_{i+1,j+1}^{n} - U_{i-1,j-1}^{n}\right) + 2r_{xx}\right)U_{i,j}^{n+1} - \frac{r_{xx}}{2}U_{i+1,j-1}^{n+1} \\
&\quad - \frac{r_{xx}}{2}U_{i-1,j+1}^{n+1} - \left(\frac{r_{xx}}{2} - r_x U_{i,j}^{n}\right)U_{i+1,j+1}^{n+1} - \left(\frac{r_{xx}}{2} + r_x U_{i,j}^{n}\right)U_{i-1,j-1}^{n+1} \\
&= (D_0 - 2r_{xx} - w_1)U_{i,j}^{n} + \frac{r_{xx}}{2}U_{i+1,j-1}^{n} + \frac{r_{xx}}{2}U_{i-1,j+1}^{n} + \frac{r_{xx}}{2}U_{i+1,j+1}^{n} \\
&\quad + \frac{r_{xx}}{2}U_{i-1,j-1}^{n} + w_n U_{i,j}^{0} - \sum_{k=1}^{n-1}(w_{n-k+1} - w_{n-k})U_{i,j}^{k} + (\alpha\Delta t)f_{i,j}^{n+1/2}.
\end{aligned} \tag{22}$$

Utilizing Equation (22) to any group of four points on the solution domain gives a (4×4) system as follows

$$\begin{bmatrix} a_{i,j} & -c_{i,j} & 0 & 0 \\ -d_{i+1,j+1} & a_{i+1,j+1} & 0 & 0 \\ 0 & 0 & a_{i+1,j} & -b \\ 0 & 0 & -b & a_{i,j+1} \end{bmatrix}\begin{bmatrix} U_{i,j}^{n+1} \\ U_{i+1,j+1}^{n+1} \\ U_{i+1,j}^{n+1} \\ U_{i,j+1}^{n+1} \end{bmatrix} = \begin{bmatrix} rhs_{i,j} \\ rhs_{i+1,j+1} \\ rhs_{i+1,j} \\ rhs_{i,j+1} \end{bmatrix}, \tag{23}$$

where

$$\begin{aligned}
a_{i,j} &= D_0 + r_x\left(U_{i+1,j+1}^{n} - U_{i-1,j-1}^{n}\right) + 2r_{xx}, c_{i,j} = \frac{r_{xx}}{2} - r_x U_{i,j}^{n}, d_{i,j} \\
&= \frac{r_{xx}}{2} + r_x U_{i,j}^{n}, b = \frac{r_{xx}}{2},
\end{aligned} \tag{24}$$

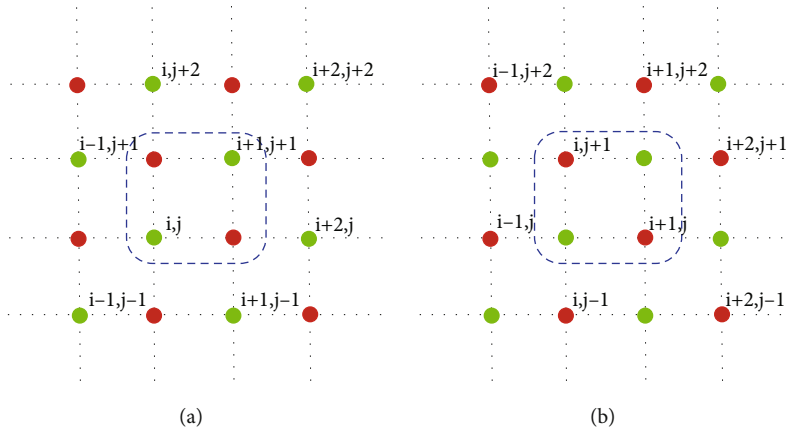

Figure 1: Grid point on $x-y$ plane. Computational molecule of Equation (27) (a) and computational molecule of Equation (28) (b).

with

$$\begin{bmatrix} rhs_{i,j} \\ rhs_{i+1,j+1} \\ rhs_{i+1,j} \\ rhs_{i,j+1} \end{bmatrix} = \begin{bmatrix} \left(b\left(U_{i+1,j-1}^{n+1}+U_{i-1,j+1}^{n+1}\right)+d_{i,j}U_{i-1,j-1}^{n+1}\right)+(D_0-2r_{xx}-w_1)U_{i,j}^{n}+b\left(U_{i+1,j-1}^{n}+U_{i-1,j+1}^{n}+U_{i+1,j+1}^{n}+U_{i-1,j-1}^{n}\right)+\tau_{i,j} \\ \left(b\left(U_{i+2,j}^{n+1}+U_{i,j+2}^{n+1}\right)+c_{i+1,j+1}U_{i+2,j+2}^{n+1}\right)+(D_0-2r_{xx}-w_1)U_{i+1,j+1}^{n}+b\left(U_{i+2,j}^{n}+U_{i,j+2}^{n}+U_{i+2,j+2}^{n}+U_{i,j}^{n}\right)+\tau_{i+1,j+1} \\ \left(bU_{i+2,j-1}^{n+1}+c_{i+1,j}U_{i+2,j+1}^{n+1}+d_{i+1,j}U_{i,j-1}^{n+1}\right)+(D_0-2r_{xx}-w_1)U_{i+1,j}^{n}+b\left(U_{i+2,j-1}^{n}+U_{i,j+1}^{n}+U_{i+2,j+1}^{n}+U_{i,j-1}^{n}\right)+\tau_{i+1,j} \\ \left(bU_{i-1,j+2}^{n+1}+c_{i,j+1}U_{i+1,j+2}^{n+1}+d_{i,j+1}U_{i-1,j}^{n+1}\right)+(D_0-2r_{xx}-w_1)U_{i+1,j}^{n}+b\left(U_{i+1,j}^{n}+U_{i-1,j+2}^{n}+U_{i+1,j+2}^{n}+U_{i-1,j}^{n}\right)+\tau_{i,j+1} \end{bmatrix}, \tag{25}$$

and

$$\begin{bmatrix} \tau_{i,j} \\ \tau_{i+1,j+1} \\ \tau_{i+1,j} \\ \tau_{i,j+1} \end{bmatrix} = \begin{bmatrix} w_n U_{i,j}^{0}-\sum_{k=1}^{n-1}(w_{n-k+1}-w_{n-k})U_{i,j}^{k}+(\alpha\Delta t)f_{i,j}^{n+\frac{1}{2}} \\ w_n U_{i+1,j+1}^{0}-\sum_{k=1}^{n-1}(w_{n-k+1}-w_{n-k})U_{i+1,j+1}^{k}+(\alpha\Delta t)f_{i+1,j+1}^{n+\frac{1}{2}} \\ w_n U_{i+1,j}^{0}-\sum_{k=1}^{n-1}(w_{n-k+1}-w_{n-k})U_{i+1,j}^{k}+(\alpha\Delta t)f_{i+1,j}^{n+\frac{1}{2}} \\ w_n U_{i,j+1}^{0}-\sum_{k=1}^{n-1}(w_{n-k+1}-w_{n-k})U_{i,j+1}^{k}+(\alpha\Delta t)f_{i,j+1}^{n+\frac{1}{2}} \end{bmatrix}. \tag{26}$$

Equation (23) leads to a decoupled system of 2×2 equations in explicit form

$$\begin{bmatrix} a_{i,j} & -c_{i,j} \\ -d_{i+1,j+1} & a_{i+1,j+1} \end{bmatrix} \begin{bmatrix} U_{i,j}^{n+1} \\ U_{i+1,j+1}^{n+1} \end{bmatrix} = \begin{bmatrix} rhs_{i,j} \\ rhs_{i+1,j+1} \end{bmatrix}, \tag{27}$$

and

$$\begin{bmatrix} a_{i+1,j} & -b \\ -b & a_{i,j+1} \end{bmatrix} \begin{bmatrix} U_{i+1,j}^{n+1} \\ U_{i,j+1}^{n+1} \end{bmatrix} = \begin{bmatrix} rhs_{i+1,j} \\ rhs_{i,j+1} \end{bmatrix}. \tag{28}$$

The computational molecule of Equations (27) and (28) is shown in Figure 1.

From Figure 1(a), it can be seen that Equation (27) is executed only by considering the green dots. On the contrary, Equation (28) only runs with red dots. Therefore, the implementation of these two equations is independent of each other, which makes the solution of Equation (1) consume less time.

In the EDG method, the grid points are divided into several groups. Each group consists of only two points of the grid (shown in Figure 2). We apply one of the Equation (27) or Equation (28) for each group in Figure 2. Therefore, half of the grid points (green dots) are calculated by the rotated finite-difference Equation (22). Before going to the next time level, we obtain other points of the grid (red dots) directly once by taking the Equation (20).

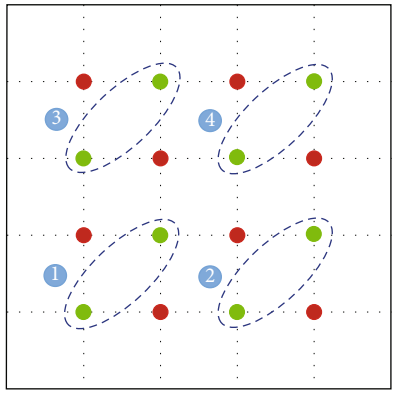

Figure 2: Group ordering for EDG method for $N = 5$.

4. Stability Analysis

In this section, the stability of the finite difference method is investigated with the Von-Neumann analysis. We first give a lemma about w_j, which will be used in the stability analysis.

Lemma 1 (see [28]). *The coefficients w_j in Equation (13) satisfy the following properties.*

$$0 \le w_j \le C\Delta t, \tag{29}$$

and

$$0 \le w_j - w_{j+1} \le C\Delta t w_j. \tag{30}$$

To investigate the stability of the difference scheme, the nonlinear term $u(u_x + u_y)$ in Equations (1)–(3) has been linearized by making the quantity u to a local constant. Thus, the nonlinear term in Equation (1) converts into $\hat{u}(u_x + u_y)$, and Equation (1) becomes:

$$\frac{\partial^\alpha u}{\partial t^\alpha} + \hat{u}\left(\frac{\partial u}{\partial x} + \frac{\partial u}{\partial y}\right) = \nu\left(\frac{\partial^2 u}{\partial x^2} + \frac{\partial^2 u}{\partial y^2}\right) + f(x, y, t). \tag{31}$$

Let $\tilde{U}^n_{i,j}$ and $\bar{U}^n_{i,j}$ be the approximate solutions of Equations (20) and (22), respectively, and define

$$\rho^n_{i,j} = U^n_{i,j} - \tilde{U}^n_{i,j}, \tag{32}$$

$$\phi^n_{i,j} = U^n_{i,j} - \bar{U}^n_{i,j}, 1 \le i \le I, 1 \le j \le J, 1 \le n \le N. \tag{33}$$

Then, by substituting Equation (32) into Equation (20), we have

$$\begin{aligned}
&\left(\frac{\nu\alpha\Delta t}{(\Delta x)^2} + \frac{\nu\alpha\Delta t}{(\Delta y)^2} + D_0\right)\rho^{n+1}_{i,j} + \left(\frac{\alpha\Delta t\hat{u}}{4\Delta x} - \frac{\nu\alpha\Delta t}{2(\Delta x)^2}\right)\rho^{n+1}_{i+1,j} \\
&+ \left(-\frac{\alpha\Delta t\hat{u}}{4\Delta x} - \frac{\nu\alpha\Delta t}{2(\Delta x)^2}\right)\rho^{n+1}_{i-1,j} + \left(\frac{\alpha\Delta t\hat{u}}{4\Delta y} - \frac{\nu\alpha\Delta t}{2(\Delta y)^2}\right)\rho^{n+1}_{i,j+1} \\
&+ \left(-\frac{\alpha\Delta t\hat{u}}{4\Delta y} - \frac{\nu\alpha\Delta t}{2(\Delta x)^2}\right)\rho^{n+1}_{i,j-1} = \left(-\frac{\nu\alpha\Delta t}{(\Delta x)^2} - \frac{\nu\alpha\Delta t}{(\Delta y)^2} - w_1 + D_0\right)\rho^n_{i,j} \\
&+ \left(-\frac{\alpha\Delta t\hat{u}}{4\Delta x} + \frac{\nu\alpha\Delta t}{2(\Delta x)^2}\right)\rho^n_{i+1,j} + \left(\frac{\alpha\Delta t\hat{u}}{4\Delta x} + \frac{\nu\alpha\Delta t}{2(\Delta x)^2}\right)\rho^n_{i-1,j} \\
&+ \left(-\frac{\alpha\Delta t\hat{u}}{4\Delta y} + \frac{\nu\alpha\Delta t}{2(\Delta y)^2}\right)\rho^n_{i,j+1} + \left(\frac{\alpha\Delta t\hat{u}}{4\Delta y} + \frac{\nu\alpha\Delta t}{2(\Delta y)^2}\right)\rho^n_{i,j-1} + w_n\rho^0_{i,j} \\
&- \sum_{k=1}^{n-1}(w_{n-k+1} - w_{n-k})\rho^k_{i,j}.
\end{aligned} \tag{34}$$

Also by putting Equation (33) in Equation (22), we get

$$\begin{aligned}
&(D_0 + 2r_{xx})\phi^{n+1}_{i,j} - \frac{r_{xx}}{2}\left(\phi^{n+1}_{i+1,j-1} - \phi^{n+1}_{i-1,j+1}\right) - \left(\frac{r_{xx}}{2} - \hat{u}r_x\right)\phi^{n+1}_{i+1,j+1} \\
&- \left(\frac{r_{xx}}{2} + \hat{u}r_x\right)\phi^{n+1}_{i-1,j-1} = (D_0 - w_1 + 2r_{xx})\phi^n_{i,j} \\
&+ \frac{r_{xx}}{2}\left(\phi^n_{i+1,j-1} + \phi^n_{i-1,j+1}\right) + \left(\frac{r_{xx}}{2} - \hat{u}r_x\right)\phi^n_{i+1,j+1} \\
&+ \left(\frac{r_{xx}}{2} + \hat{u}r_x\right)\phi^n_{i-1,j-1} + w_n\phi^0_{i,j} - \sum_{k=1}^{n-1}(w_{n-k+1} - w_{n-k})\phi^k_{i,j}.
\end{aligned} \tag{35}$$

The Fourier series for $\rho^n(x, y)$ and $\phi^n(x, y)$ is

$$\begin{aligned}
\rho^n(x, y) &= \sum_{m_2=-\infty}^{\infty}\sum_{m_1=-\infty}^{\infty}\xi_n(m_1, m_2)e^{\iota 2\pi\{m_1x + m_2y\}}, \\
\phi^n(x, y) &= \sum_{m_2=-\infty}^{\infty}\sum_{m_1=-\infty}^{\infty}\eta_n(m_1, m_2)e^{\iota 2\pi\{m_1x + m_2y\}},
\end{aligned} \tag{36}$$

where $\iota = \sqrt{-1}$ and the amplication factors ξ_n and η_n are defined by

$$\xi_n(m_1, m_2) = \int_0^1\int_0^1 e^{-\iota 2\pi\{m_1\tau + m_2\varepsilon\}}\rho^n(\tau, \varepsilon)d\tau d\varepsilon, \tag{37}$$

$$\eta_n(m_1, m_2) = \int_0^1\int_0^1 e^{-\iota 2\pi\{m_1\tau + m_2\varepsilon\}}\phi^n(\tau, \varepsilon)d\tau d\varepsilon. \tag{38}$$

Introducing the following norm

$$\begin{aligned}
\|\rho^n\|_2 &= \left(\sum_{j=1}^{J-1}\sum_{i=1}^{I-1}\Delta x\Delta y\left|\rho^n_{i,j}\right|^2\right)^{1/2} = \left(\int_0^1\int_0^1\left|\rho^n_{i,j}\right|^2 d\tau d\varepsilon\right)^{1/2}, \\
\|\phi^n\|_2 &= \left(\sum_{j=1}^{J-1}\sum_{i=1}^{I-1}\Delta x\Delta y\left|\phi^n_{i,j}\right|^2\right)^{1/2} = \left(\int_0^1\int_0^1\left|\phi^n_{i,j}\right|^2 d\tau d\varepsilon\right)^{1/2}.
\end{aligned} \tag{39}$$

By applying the Parseval's equality

$$\int_0^1\int_0^1 |\rho^n(\tau,\varepsilon)|^2 d\tau d\varepsilon = \sum_{m_2=-\infty}^{\infty}\sum_{m_1=-\infty}^{\infty} |\xi_n(m_1,m_2)|^2,$$
$$\int_0^1\int_0^1 |\phi^n(\tau,\varepsilon)|^2 d\tau d\varepsilon = \sum_{m_2=-\infty}^{\infty}\sum_{m_1=-\infty}^{\infty} |\eta_n(m_1,m_2)|^2, \tag{40}$$

we obtain

$$\|\rho^n\|_2^2 = \sum_{m_2=-\infty}^{\infty}\sum_{m_1=-\infty}^{\infty} |\xi_n(m_1,m_2)|^2,$$
$$\|\phi^n\|_2^2 = \sum_{m_2=-\infty}^{\infty}\sum_{m_1=-\infty}^{\infty} |\eta_n(m_1,m_2)|^2. \tag{41}$$

According to the above analysis, we can suppose that the solution of Equations (34) and (35) has the following form

$$\rho_{i,j}^n = \xi_n e^{\iota\left(\sigma_x i\Delta x+\sigma_y j\Delta y\right)},$$
$$\phi_{i,j}^n = \eta_n e^{\iota\left(\sigma_x i\Delta x+\sigma_y j\Delta y\right)}, \tag{42}$$

where $\sigma_x = 2m_1\pi, \sigma_y = 2m_2\pi$.

Lemma 2. *If* $w_1 \le D_0$ *in Equation (20) and* $\alpha \in (0,1)$, *then we have*

$$|\xi_n| \le |\xi_0|, n = 1, 2, \cdots, N, \tag{43}$$

where ξ_n is defined in Equation (37).

Proof. Substituting $\rho_{i,j}^n = \xi_n e^{\iota(\sigma_x i\Delta x+\sigma_y j\Delta y)}$ into Equation (34), we have

$$\begin{aligned}
&\left(\frac{\nu\alpha\Delta t}{(\Delta x)^2}+\frac{\nu\alpha\Delta t}{(\Delta y)^2}+D_0\right)\xi_{n+1}e^{\iota\left(\sigma_x i\Delta x+\sigma_y j\Delta y\right)}\\
&\quad+\left(\frac{\alpha\Delta t\hat{u}}{4\Delta x}-\frac{\nu\alpha\Delta t}{2\Delta x^2}\right)\xi_{n+1}e^{\iota\left(\sigma_x (i+1)\Delta x+\sigma_y j\Delta y\right)}\\
&\quad+\left(-\frac{\alpha\Delta t\hat{u}}{4\Delta x}-\frac{\nu\alpha\Delta t}{2\Delta x^2}\right)\xi_{n+1}e^{\iota\left(\sigma_x (i-1)\Delta x+\sigma_y j\Delta y\right)}\\
&\quad+\left(\frac{\alpha\Delta t\hat{u}}{4\Delta y}-\frac{\nu\alpha\Delta t}{2\Delta y^2}\right)\xi_{n+1}e^{\iota\left(\sigma_x i\Delta x+\sigma_y (j+1)\Delta y\right)}\\
&\quad+\left(-\frac{\alpha\Delta t\hat{u}}{4\Delta y}-\frac{\nu\alpha\Delta t}{2\Delta y^2}\right)\xi_{n+1}e^{\iota\left(\sigma_x i\Delta x+\sigma_y (j-1)\Delta y\right)}\\
&=\left(-\frac{\nu\alpha\Delta t}{(\Delta x)^2}-\frac{\nu\alpha\Delta t}{(\Delta y)^2}-w_1+D_0\right)\xi_n e^{\iota\left(\sigma_x i\Delta x+\sigma_y j\Delta y\right)}\\
&\quad+\left(-\frac{\alpha\Delta t\hat{u}}{4\Delta x}+\frac{\nu\alpha\Delta t}{2(\Delta x)^2}\right)\xi_n e^{\iota\left(\sigma_x (i+1)\Delta x+\sigma_y j\Delta y\right)}\\
&\quad+\left(\frac{\alpha\Delta t\hat{u}}{4\Delta x}+\frac{\nu\alpha\Delta t}{2(\Delta x)^2}\right)\xi_n e^{\iota\left(\sigma_x (i-1)\Delta x+\sigma_y j\Delta y\right)}\\
&\quad+\left(-\frac{\alpha\Delta t\hat{u}}{4\Delta y}+\frac{\nu\alpha\Delta t}{2(\Delta y)^2}\right)\xi_n e^{\iota\left(\sigma_x i\Delta x+\sigma_y (j+1)\Delta y\right)}\\
&\quad+\left(\frac{\alpha\Delta t\hat{u}}{4\Delta y}+\frac{\nu\alpha\Delta t}{2(\Delta y)^2}\right)\xi_n e^{\iota\left(\sigma_x i\Delta x+\sigma_y (j-1)\Delta y\right)}\\
&\quad+w_n\xi_0 e^{\iota\left(\sigma_x i\Delta x+\sigma_y j\Delta y\right)}\\
&\quad-\sum_{k=1}^{n-1}(w_{n-k+1}-w_{n-k})\xi_k e^{\iota\left(\sigma_x i\Delta x+\sigma_y j\Delta y\right)},
\end{aligned} \tag{44}$$

after simplifications, we can get

$$\begin{aligned}
&\xi_{n+1}\left[-\nu\alpha\Delta t\left(-\frac{1}{(\Delta x)^2}-\frac{1}{(\Delta y)^2}+\frac{\cos(\sigma_x\Delta x)}{(\Delta x)^2}+\frac{\cos(\sigma_y\Delta y)}{(\Delta y)^2}\right)\right.\\
&\quad\left.+D_0+\iota\frac{\alpha\Delta t\hat{u}}{2}\left(\frac{\sin(\sigma_x\Delta x)}{\Delta x}+\frac{\sin(\sigma_y\Delta y)}{\Delta y}\right)\right]\\
&=\xi_n\left[\nu\alpha\Delta t\left(-\frac{1}{(\Delta x)^2}-\frac{1}{(\Delta y)^2}+\frac{\cos(\sigma_x\Delta x)}{(\Delta x)^2}+\frac{\cos(\sigma_y\Delta y)}{(\Delta y)^2}\right)\right.\\
&\quad\left.+D_0-w_1-\iota\frac{\alpha\Delta t\hat{u}}{2}\left(\frac{\sin(\sigma_x\Delta x)}{\Delta x}+\frac{\sin(\sigma_y\Delta y)}{\Delta y}\right)\right]\\
&\quad+w_n\xi_0-\sum_{k=1}^{n-1}(w_{n-k+1}-w_{n-k})\xi_k.
\end{aligned} \tag{45}$$

First, letting $n = 0$ in Equation (45), we obtain

$$|\xi_1| = |\gamma||\xi_0|, \tag{46}$$

where

$$\gamma = \frac{\nu\alpha\Delta t A + D_0 - \iota(\alpha\Delta t\hat{u}/2)B}{-\nu\alpha\Delta t A + D_0 + \iota(\alpha\Delta t\hat{u}/2)B},$$
$$A = -\frac{1}{(\Delta x)^2}-\frac{1}{(\Delta y)^2}+\frac{\cos(\sigma_x\Delta x)}{(\Delta x)^2}+\frac{\cos(\sigma_y\Delta y)}{(\Delta y)^2},$$
$$B = \frac{\sin(\sigma_x\Delta x)}{\Delta x}+\frac{\sin(\sigma_y\Delta y)}{\Delta y}. \tag{47}$$

In the above expression, it is clear that the real part of the numerator is smaller than the real part of the denominator. Thus, the magnitude of the numerator is smaller than the denominator. So we have

$$|\xi_1| \le |\xi_0|. \tag{48}$$

Now, suppose that we have proved that $|\xi_n| \le |\xi_0|, n = 1, 2, \cdots, m$.

We should prove this for $n = m + 1$. Using Equation (45), we get

$$|\xi_{m+1}| \le \left|\frac{\nu\alpha\Delta tA + D_0 - w_1 - \iota(\alpha\Delta t\widehat{u}/2)B}{-\nu\alpha\Delta tA + D_0 + \iota(\alpha\Delta t\widehat{u}/2)B}\right||\xi_0| + \left|\frac{w_m - \sum_{k=1}^{m-1}(w_{m-k+1} - w_{m-k})}{-\nu\alpha\Delta tA + D_0 + \iota(\alpha\Delta t\widehat{u}/2)B}\right||\xi_0|. \tag{49}$$

Using Lemma 1, we have

$$|\xi_{m+1}| \le \frac{|\nu\alpha\Delta tA + D_0 - w_1 - \iota(\alpha\Delta t\widehat{u}/2)B| + w_1}{|-\nu\alpha\Delta tA + D_0 + \iota(\alpha\Delta t\widehat{u}/2)B|}|\xi_0|. \tag{50}$$

Consider the following two cases:

Case 3. If $\nu\alpha\Delta tA + D_0 - w_1 > 0$, then, we have

$$|\xi_{m+1}| \le \left(\frac{\nu\alpha\Delta tA + D_0}{-\nu\alpha\Delta tA + D_0}\right)|\xi_0| \le |\xi_0|. \tag{51}$$

Case 4. If $\nu\alpha\Delta tA + D_0 - w_1 \le 0$, then, we have

$$|\xi_{m+1}| \le \left(\frac{2w_1 - \nu\alpha\Delta tA - D_0}{-\nu\alpha\Delta tA + D_0}\right)|\xi_0|. \tag{52}$$

Therefore,

$$\frac{2w_1 - \nu\alpha\Delta tA - D_0}{-\nu\alpha\Delta tA + D_0} \le 1, \tag{53}$$

That is, $w_1 \le D_0$, or $|\xi_{m+1}| \le |\xi_0|$.
By mathematical induction, we finish the proof.

Theorem 5. *For $\alpha \in (0, 1)$, the finite difference scheme Equation (20) is stable if $w_1 \le D_0$.*

Proof. Let $w_1 \le D_0$, using Lemma 2 and Parseval's equality, we get

$$\begin{aligned}\|\rho^n\|_2 &= \sum_{j=1}^{J-1}\sum_{i=1}^{I-1}\Delta y\Delta x\left|\rho_{i,j}^n\right|^2 = \Delta y\Delta x\sum_{j=1}^{J-1}\sum_{i=1}^{I-1}\left|\xi_n e^{\iota\left(\sigma_x i\Delta x+\sigma_y j\Delta y\right)}\right|^2 \\ &= \Delta y\Delta x\sum_{j=1}^{J-1}\sum_{i=1}^{I-1}|\xi_n|^2 \le \Delta y\Delta x\sum_{j=1}^{J-1}\sum_{i=1}^{I-1}|\xi_0|^2 \\ &= \Delta y\Delta x\sum_{j=1}^{J-1}\sum_{i=1}^{I-1}\left|\xi_0 e^{\iota\left(\sigma_x i\Delta x+\sigma_y j\Delta y\right)}\right|^2 = \left\|\rho^0\right\|_2.\end{aligned} \tag{54}$$

So the difference scheme Equation (20) is conditionally stable.

Lemma 6. *If $w_1 \le D_0$ in Equation (22) and $\alpha \in (0, 1)$, then, we have*

$$|\eta_n| \le |\eta_0|, n = 1, 2, \cdots, N, \tag{55}$$

where η_n is defined in Equation (38).

Proof. Substituting $\phi_{i,j}^n = \eta_n e^{\iota(\sigma_x i\Delta x+\sigma_y j\Delta y)}$ into Equation (35), we have

$$\begin{aligned}&(D_0 + 2r_{xx})\eta_{n+1}e^{\iota\left(\sigma_x i\Delta x+\sigma_y j\Delta y\right)} - \frac{r_{xx}}{2}\eta_{n+1}e^{\iota\left(\sigma_x (i+1)\Delta x+\sigma_y (j-1)\Delta y\right)} \\ &\quad - \frac{r_{xx}}{2}\eta_{n+1}e^{\iota\left(\sigma_x (i-1)\Delta x+\sigma_y (j+1)\Delta y\right)} \\ &\quad - \left(\frac{r_{xx}}{2} - \widehat{u}r_x\right)\eta_{n+1}e^{\iota\left(\sigma_x (i+1)\Delta x+\sigma_y (j+1)\Delta y\right)} \\ &\quad - \left(\frac{r_{xx}}{2} + \widehat{u}r_x\right)\eta_{n+1}e^{\iota\left(\sigma_x (i-1)\Delta x+\sigma_y (j-1)\Delta y\right)} \\ &= (D_0 - w_1 - 2r_{xx})\eta_n e^{\iota\left(\sigma_x i\Delta x+\sigma_y j\Delta y\right)} + \frac{r_{xx}}{2}\eta_n e^{\iota\left(\sigma_x (i+1)\Delta x+\sigma_y (j-1)\Delta y\right)} \\ &\quad + \frac{r_{xx}}{2}\eta_n e^{\iota\left(\sigma_x (i-1)\Delta x+\sigma_y (j+1)\Delta y\right)} + \left(\frac{r_{xx}}{2} - \widehat{u}r_x\right)\eta_n e^{\iota\left(\sigma_x (i+1)\Delta x+\sigma_y (j+1)\Delta y\right)} \\ &\quad + \left(\frac{r_{xx}}{2} + \widehat{u}r_x\right)\eta_n e^{\iota\left(\sigma_x (i-1)\Delta x+\sigma_y (j-1)\Delta y\right)} + w_n\eta_0 e^{\iota\left(\sigma_x i\Delta x+\sigma_y j\Delta y\right)} \\ &\quad - \sum_{k=1}^{n-1}(w_{n-k+1} - w_{n-k})\eta_k e^{\iota\left(\sigma_x i\Delta x+\sigma_y j\Delta y\right)},\end{aligned} \tag{56}$$

by simple computation and noticing that $e^{\iota\beta} + e^{-\iota\beta} = 2\cos(\beta)$ and $e^{\iota\beta} - e^{-\iota\beta} = 2\iota sin(\beta)$, we can get

$$\begin{aligned}\eta_{n+1}(D_0 + r_{xx}(2 - A) + 2\iota\widehat{u}r_x B) &= \eta_n(D_0 - w_1 - r_{xx}(2 - A) - 2\iota\widehat{u}r_x B) \\ &\quad + w_n\eta_0 + \sum_{k=1}^{n-1}(w_{n-k} - w_{n-k+1})\eta_k,\end{aligned} \tag{57}$$

where

$$\begin{aligned}A &= \cos\left(\sigma_x\Delta x - \sigma_y\Delta y\right) + \cos\left(\sigma_x\Delta x + \sigma_y\Delta y\right), \\ B &= \sin\left(\sigma_x\Delta x + \sigma_y\Delta y\right).\end{aligned} \tag{58}$$

First, setting $n = 0$ in Equation (57), we obtain

$$\begin{aligned}|\eta_1| &= \left|\frac{D_0 - r_{xx}(2 - A) - 2\iota\widehat{u}r_x B}{D_0 + r_{xx}(2 - A) + 2\iota\widehat{u}r_x B}\right||\eta_0| \\ &= \sqrt{\frac{(D_0 - r_{xx}(2 - A))^2 + (2u\wedge r_x B)^2}{(D_0 + r_{xx}(2 - A))^2 + (2u\wedge r_x B)^2}}|\eta_0| \le |\eta_0|.\end{aligned} \tag{59}$$

Now, assume that we have proved that $|\eta_n| \le |\eta_0|$, $n = 1, 2, \cdots, m$.

We should prove this for $n = m + 1$. Utilizing Equation (57), we obtain

$$|\eta_{m+1}| \le \left|\frac{D_0 - w_1 - r_{xx}(2-A) - 2\iota\hat{u}r_xB}{D_0 + r_{xx}(2-A) + 2\iota\hat{u}r_xB}\right||\eta_0| + \left|\frac{w_m + \sum_{k=1}^{m-1}(w_{m-k} - w_{m-k+1})}{D_0 + r_{xx}(2-A) + 2\iota\hat{u}r_xB}\right||\eta_0|. \tag{60}$$

According to Lemma 1, we have

$$|\eta_{m+1}| \le \frac{|D_0 - w_1 - r_{xx}(2-A) - 2\iota\hat{u}r_xB| + w_1}{|D_0 + r_{xx}(2-A) + 2\iota\hat{u}r_xB|}|\eta_0|. \tag{61}$$

Consider the following two cases:

Case 7. If $D_0 - w_1 - r_{xx}(2-A) > 0$, then, we have

$$|\eta_{m+1}| \le \left(\frac{D_0 - r_{xx}(2-A)}{D_0 + r_{xx}(2-A)}\right)|\eta_0| \le |\eta_0|. \tag{62}$$

Case 8. If $D_0 - w_1 - r_{xx}(2-A) \le 0$, then, we have

$$|\eta_{m+1}| \le \left(\frac{2w_1 - D_0 + r_{xx}(2-A)}{D_0 + r_{xx}(2-A)}\right)|\eta_0|. \tag{63}$$

So that,

$$\frac{2w_1 - D_0 + r_{xx}(2-A)}{D_0 + r_{xx}(2-A)} \le 1, \tag{64}$$

This means $w_1 \le D_0$, or $|\eta_{m+1}| \le |\eta_0|$.
By mathematical induction, the proof is complete.

Theorem 9. *For $\alpha \in (0, 1)$, the finite difference scheme Equation (22) is stable if $w_1 \le D_0$.*

Proof. Suppose $w_1 \le D_0$, from Lemma 6 and Parseval's equality, we get

$$\begin{aligned}\|\phi^n\|_2 &= \sum_{j=1}^{J-1}\sum_{i=1}^{I-1}\Delta y\Delta x\left|\phi_{i,j}^n\right|^2 = \Delta y\Delta x\sum_{j=1}^{J-1}\sum_{i=1}^{I-1}\left|\eta_n e^{\iota\left(\sigma_x i\Delta x + \sigma_y j\Delta y\right)}\right|^2 \\ &= \Delta y\Delta x\sum_{j=1}^{J-1}\sum_{i=1}^{I-1}|\eta_n|^2 \le \Delta y\Delta x\sum_{j=1}^{J-1}\sum_{i=1}^{I-1}|\eta_0|^2 \\ &= \Delta y\Delta x\sum_{j=1}^{J-1}\sum_{i=1}^{I-1}\left|\eta_0 e^{\iota\left(\sigma_x i\Delta x + \sigma_y j\Delta y\right)}\right|^2 = \left\|\phi^0\right\|_2.\end{aligned} \tag{65}$$

So the difference scheme Equation (22) is conditionally stable.

5. Convergence Analysis

We first introduce some notations and lemmas which will be used in the convergence analysis.

$$\delta_x^2 v_{i,j}^n = \frac{v_{i+1,j}^n - 2v_{i,j}^n + v_{i-1,j}^n}{(\Delta x)^2}, \delta_y^2 v_{i,j}^n = \frac{v_{i,j+1}^n - 2v_{i,j}^n + v_{i,j-1}^n}{(\Delta y)^2},$$

$$\Delta_x^0 v_{i,j}^n = \frac{v_{i+1,j}^n - v_{i-1,j}^n}{2\Delta x}, \Delta_y^0 v_{i,j}^n = \frac{v_{i,j+1}^n - v_{i,j-1}^n}{2\Delta y},$$

$$(\mathbf{v}, \mathbf{w}) = \Delta x\Delta y\sum_{j=1}^{J-1}\sum_{i=1}^{I-1}v_{ij}w_{ij}, \|\mathbf{v}\| = \left[\Delta x\Delta y\sum_{j=1}^{J-1}\sum_{i=1}^{I-1}\left(v_{ij}\right)^2\right]^{1/2},$$

$$c_0 = \max_{(x,y,t)\in[0,L]\times[0,L]\times(0,T)}\left\{|u(x,y,t)|, \left|\frac{\partial u}{\partial x}(x,y,t)\right|, \left|\frac{\partial u}{\partial y}(x,y,t)\right|\right\}. \tag{66}$$

It is straightforward to show

$$\left|\Delta_x^0 v, v\right| = 0, \left|\Delta_y^0 v, v\right| = 0. \tag{67}$$

Notice that in this section we suppose C stands for a positive constant independent of $\Delta t, \Delta x, \Delta y, i, j$, and n, which may take different values at different places.

Lemma 10. *(Discrete Gronwall's inequality [29]).*
Suppose d be a nonnegetive constant, $\{z_n\}$ and $\{f_n\}$ are nonnegative sequences. Let

$$z_n \le d + \sum_{0\le k<n} f_k z_k, n \ge 0, \tag{68}$$

then

$$z_n \le d\ \exp\left(\sum_{0\le j<n} f_j\right), n \ge 0. \tag{69}$$

Theorem 11. *The Crank–Nicolson scheme Equation (20) is convergent and the order of convergence is $O(\Delta t + \Delta x^2 + \Delta y^2)$.*

Proof. Let $e_{i,j}^n$ be the error at (x_i, y_j, t_n) as defined below

$$\begin{aligned}e_{i,j}^n &= u\left(x_i, y_j, t_n\right) - U_{i,j}^n \\ &= u_{i,j}^n - U_{i,j}^n, 1 \le j \le J, 1 \le i \le I, 1 \le n \le N.\end{aligned} \tag{70}$$

Substituting Equation (70) in Equation (19), we get the following error equations

Table 1: Absolute errors of Example 13 at $T = 1$ for Re = 10, $\Delta t = 0.01$, $\alpha = 0.1$, and $\alpha = 0.3$.

N	$\alpha = 0.1$				$\alpha = 0.3$			
	CN	Time	EDG	Time	CN	Time	EDG	Time
9	$4.2593e-03$	0.75	$6.1387e-03$	0.74	$3.9001e-03$	0.22	$6.0143e-03$	0.11
19	$9.8379e-04$	0.93	$1.6263e-03$	0.69	$9.0356e-04$	1.01	$1.6124e-03$	0.51
49	$1.9672e-04$	9.82	$2.6073e-04$	4.69	$1.8465e-04$	10.61	$2.6040e-04$	4.73
99	$9.1297e-05$	123.15	$9.7575e-05$	39.87	$8.8260e-05$	118.02	$9.3869e-05$	42.01

Table 2: Absolute errors of Example 13 at $T = 1$ for Re = 10, $\Delta t = 0.01$, $\alpha = 0.7$, and $\alpha = 0.9$.

N	$\alpha = 0.7$				$\alpha = 0.9$			
	CN	Time	EDG	Time	CN	Time	EDG	Time
9	$2.7474e-03$	0.16	$5.6163e-03$	0.12	$1.8409e-03$	0.17	$5.2940e-03$	0.12
19	$6.6801e-04$	0.84	$1.5736e-03$	0.60	$4.8985e-04$	0.86	$1.5707e-03$	0.59
49	$1.5163e-04$	10.26	$2.5934e-04$	5.68	$1.4882e-04$	10.38	$2.5869e-04$	5.35
99	$8.2965e-05$	119.25	$8.6473e-05$	41.44	$1.0295e-04$	121.48	$1.0451e-04$	42.37

$$
\begin{aligned}
&-w_n e_{ij}^0 + \sum_{k=1}^{n-1}(w_{n-k+1} - w_{n-k})e_{ij}^k + w_1 e_{ij}^n + \left(e_{ij}^{n+1} - e_{ij}^n\right)D_0 \\
&\quad = \frac{\nu\alpha\Delta t}{2}\left(\delta_x^2\left(e_{i,j}^{n+1} + e_{i,j}^n\right) + \delta_y^2\left(e_{i,j}^{n+1} + e_{i,j}^n\right)\right) \\
&\qquad - \frac{\alpha\Delta t}{2}(\sigma_4 + \sigma_5) + \alpha\Delta t R_{i,j}^{n+\frac{1}{2}}, \\
&\qquad 1 \le j \le J-1, 1 \le i \le I-1, 1 \le n \le N, \\
&\quad e_{0,j}^n = e_{I,j}^n = 0, 1 \le n \le N, 0 \le j \le J, \\
&\quad e_{i,0}^n = e_{i,J}^n = 0, 1 \le n \le N, 0 \le i \le I, \\
&\quad e_{i,j}^0 = 0, 0 \le j \le J, 1 \le i \le I,
\end{aligned} \tag{71}
$$

where

$$
\begin{aligned}
R_{i,j}^{n+\frac{1}{2}} &= O\left(\Delta t + \Delta x^2 + \Delta y^2\right), \\
\sigma_4 &= e_{i,j}^n \Delta_x^0 u_{i,j}^{n+1} + u_{i,j}^n \Delta_x^0 e_{i,j}^{n+1} + e_{i,j}^{n+1}\Delta_x^0 u_{i,j}^n + u_{i,j}^{n+1}\Delta_x^0 e_{i,j}^n, \\
\sigma_5 &= e_{i,j}^n \Delta_y^0 u_{i,j}^{n+1} + u_{i,j}^n \Delta_y^0 e_{i,j}^{n+1} + e_{i,j}^{n+1}\Delta_y^0 u_{i,j}^n + u_{i,j}^{n+1}\Delta_y^0 e_{i,j}^n.
\end{aligned} \tag{72}
$$

Multiplying Equation (71) by $\Delta x \Delta y(e_{i,j}^{n+1} + e_{i,j}^n)$ and summing up for i from 1 to I − 1 and j from 1 to $J - 1$, we obtain

$$
\begin{aligned}
&\left|\sum_{k=1}^{n-1}(w_{n-k+1} - w_{n-k})e^k + w_1 e^n + \left(e^{n+1} - e^n\right)D_0, e^{n+1} + e^n\right| \\
&= \frac{\nu\alpha\Delta t}{2}\left(\left|\delta_x^2\left(e^{n+1} + e^n\right), e^{n+1} + e^n\right| + \left|\delta_y^2\left(e^{n+1} + e^n\right), e^{n+1} + e^n\right|\right) \\
&\quad - \frac{\alpha\Delta t}{2}\left|\sigma_4 + \sigma_5, e^{n+1} + e^n\right| + \alpha\Delta t\left|R^{n+\frac{1}{2}}, e^{n+1} + e^n\right|, 1 \le n \le N.
\end{aligned} \tag{73}
$$

It is clear that $|\delta_x^2(e^{n+1} + e^n), e^{n+1} + e^n| \le 0$ and $|\delta_y^2(e^{n+1} + e^n), e^{n+1} + e^n| \le 0$, so we have

$$
\begin{aligned}
D_0\left\|e^{n+1}\right\|^2 &\le (D_0 - w_1)\|e^n\|^2 + w_1\left|\left|e^{n+1}, e^n\right|\right| \\
&\quad + \left|\sum_{k=1}^{n-1}(w_{n-k} - w_{n-k+1})e^k, e^{n+1} + e^n\right| \\
&\quad + \frac{\alpha\Delta t}{2}\left|\left|\sigma_4 + \sigma_5, e^{n+1} + e^n\right|\right| \\
&\quad + \alpha\Delta t\left|R^{n+\frac{1}{2}}, e^{n+1} + e^n\right|, 1 \le n \le N.
\end{aligned} \tag{74}
$$

Now, we estimate the third, fourth, and fifth terms of the right-hand side of Equation (74), respectively

$$
\begin{aligned}
&\left|\sum_{k=1}^{n-1}(w_{n-k} - w_{n-k+1})e^k, e^{n+1} + e^n\right| \\
&\quad = \sum_{k=1}^{n-1}(w_{n-k} - w_{n-k+1})\left|e^k, e^{n+1}\right| + \sum_{k=1}^{n-1}(w_{n-k} - w_{n-k+1})\left|e^k, e^n\right|.
\end{aligned} \tag{75}
$$

Using Young inequality $ab \le \varepsilon a^2 + (1/4\varepsilon)b^2$, $a, b \in \mathbb{R}$, and Lemma 1, we have

$$
\begin{aligned}
&\left|\sum_{k=1}^{n-1}(w_{n-k} - w_{n-k+1})e^k, e^{n+1} + e^n\right| \le C\Delta t^2\sum_{k=1}^{n-1}\left\|e^k\right\|^2 \\
&\quad + C\Delta t\left(\|e^n\|^2 + \left\|e^{n+1}\right\|^2\right).
\end{aligned} \tag{76}
$$

For the fourth term, utilizing Young inequality and Equation (67), we obtain

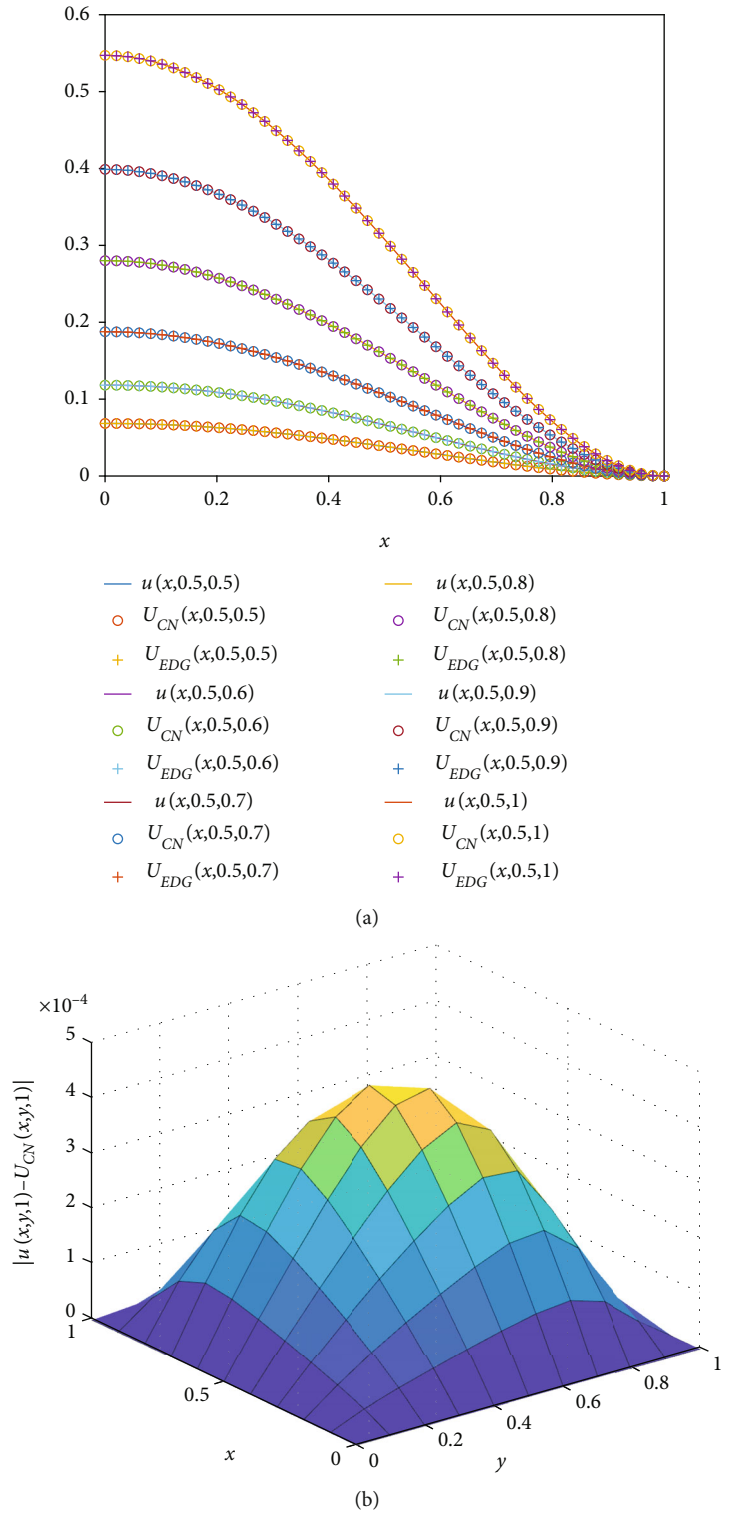

Figure 3: The exact, Crank–Nicolson, and EDG solutions in different values of t and $y = 0.5$ (a) and the absolute error of Crank–Nicolson method at $T = 1$ (b) of Example 13 for $\Delta t = 0.01$, Re $= 100$, $N = 49$, and $\alpha = 0.5$.

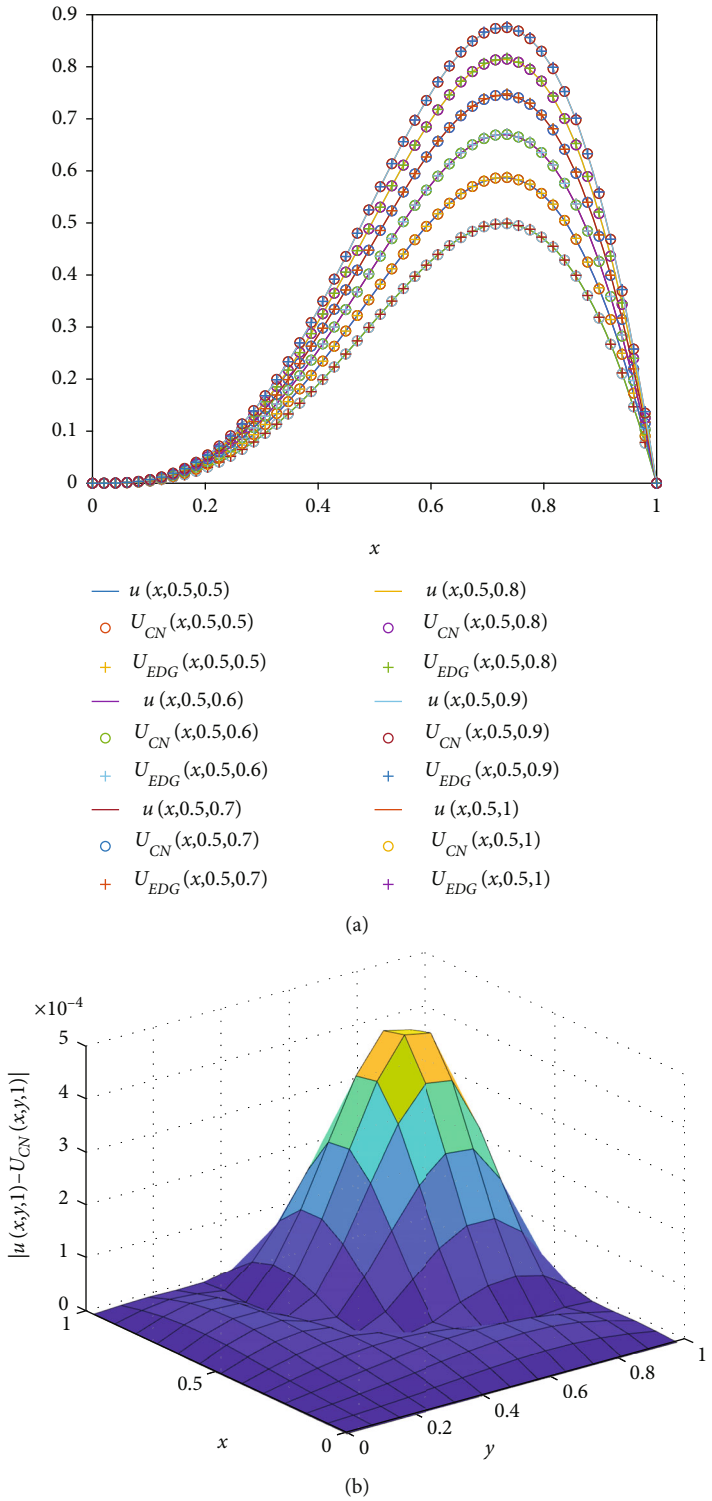

FIGURE 4: The exact, Crank–Nicolson and EDG solutions in different values of t and $y = 0.5$ (a) and the absolute error of Crank–Nicolson method at $T = 1$ (b) of Example 14 for $\Delta t = 0.01$, Re = 50, $N = 49$, and $\alpha = 0.5$.

Table 3: Absolute errors of Example 14 at $T = 1$ for Re = 100, $\Delta t = 0.01$, $\alpha = 0.1$, and $\alpha = 0.3$.

N	$\alpha = 0.1$				$\alpha = 0.3$			
	CN	Time	EDG	Time	CN	Time	EDG	Time
9	$4.1318e-03$	0.40	$1.0556e-02$	0.26	$3.7717e-03$	0.53	$9.8104e-03$	0.28
19	$8.8813e-04$	1.04	$2.6531e-03$	0.73	$8.1156e-04$	1.17	$2.5458e-03$	0.73
49	$1.3364e-04$	12.14	$4.1507e-04$	4.81	$1.2247e-04$	15.24	$4.0109e-04$	4.86
99	$3.4588e-05$	122.31	$1.0389e-04$	40.55	$3.1779e-05$	130.36	$1.0045e-04$	40.71

Table 4: Absolute errors of Example 14 at $T = 1$ for Re = 100, $\Delta t = 0.01$, $\alpha = 0.7$, and $\alpha = 0.9$.

N	$\alpha = 0.7$				$\alpha = 0.9$			
	CN	Time	EDG	Time	CN	Time	EDG	Time
9	$2.9459e-03$	0.57	$8.2550e-03$	0.34	$2.4730e-03$	0.96	$7.5148e-03$	0.26
19	$6.3611e-04$	1.39	$2.3322e-03$	0.84	$5.4346e-04$	1.56	$2.2536e-03$	0.84
49	$9.7981e-05$	15.19	$3.7198e-04$	5.69	$8.6200e-05$	17.26	$3.5924e-04$	5.32
99	$2.5774e-05$	126.65	$9.3273e-05$	44.77	$2.4146e-05$	136.80	$9.1092e-05$	43.01

Table 5: Absolute errors of Example 15 at $T = 1$ for Re = 5, $\Delta t = 0.01$, $\alpha = 0.1$, and $\alpha = 0.3$.

N	$\alpha = 0.1$				$\alpha = 0.3$			
	CN	Time	EDG	Time	CN	Time	EDG	Time
9	$2.1509-03$	0.51	$7.1351e-03$	0.24	$2.0937e-03$	0.19	$6.9914e-03$	0.12
19	$4.8726e-04$	1.09	$1.7356e-03$	0.59	$4.7437e-04$	0.91	$1.7078e-03$	0.56
49	$7.3239e-05$	11.88	$2.6457e-04$	4.86	$7.1213e-05$	11.80	$2.6032e-04$	5.04
99	$1.7989e-05$	121.06	$6.4817e-05$	40.01	$1.7399e-05$	120.95	$6.3688e-05$	40.27

Table 6: Absolute errors of Example 15 at $T = 1$ for Re = 5, $\Delta t = 0.01$, $\alpha = 0.7$, and $\alpha = 0.9$.

N	$\alpha = 0.7$				$\alpha = 0.9$			
	CN	Time	EDG	Time	CN	Time	EDG	Time
9	$1.9317e-03$	0.21	$6.5894e-03$	0.12	$1.8282e-03$	0.23	$6.3412e-03$	0.13
19	$4.3742e-04$	0.97	$1.6292e-03$	0.60	$4.1260e-04$	1.01	$1.5796e-03$	0.61
49	$6.4857e-05$	12.21	$2.4776e-04$	5.29	$5.9238e-05$	12.58	$2.3834e-04$	5.35
99	$1.5095e-05$	123.57	$5.9878e-05$	41.38	$1.2086e-05$	124.23	$5.5847e-05$	41.61

$$\left|\left\langle \sigma_4, e^{n+1}+e^n\right\rangle\right| \le c_0(1+\varepsilon_1+\varepsilon_2+\varepsilon_3+\varepsilon_4+\varepsilon_5)\left\|e^{n+1}\right\|^2 + c_0\left(1+\frac{1}{4\varepsilon_1}+\frac{1}{4\varepsilon_2}+\frac{1}{4\varepsilon_3}+\frac{1}{4\varepsilon_4}+\frac{1}{4\varepsilon_5}\right)\|e^n\|^2. \tag{77}$$

Similarly, we get

$$\left|\left\langle \sigma_5, e^{n+1}+e^n\right\rangle\right| \le c_0(1+\varepsilon_6+\varepsilon_7+\varepsilon_8+\varepsilon_9+\varepsilon_{10})\left\|e^{n+1}\right\|^2 + c_0\left(1+\frac{1}{4\varepsilon_6}+\frac{1}{4\varepsilon_7}+\frac{1}{4\varepsilon_8}+\frac{1}{4\varepsilon_9}+\frac{1}{4\varepsilon_{10}}\right)\|e^n\|^2. \tag{78}$$

Also for the fifth term, we have

$$\left|R^{n+\frac{1}{2}}, e^{n+1}+e^n\right| \le \left(\varepsilon_{11}+\frac{1}{4\varepsilon_{12}}\right)\left\|R^{n+\frac{1}{2}}\right\|^2 + \varepsilon_{12}\left\|e^{n+1}\right\|^2 + \frac{1}{4\varepsilon_{11}}\|e^n\|^2. \tag{79}$$

For the second term on the right-hand side of Equation (74), we get

$$w_1\left|\left|e^{n+1}, e^n\right|\right| \le w_1\left(\varepsilon_{13}\left\|e^{n+1}\right\|^2 + \frac{1}{4\varepsilon_{13}}\|e^n\|^2\right). \tag{80}$$

Combining Equations (76)–(80) in Equation (74) and using Lemma 1, we obtain

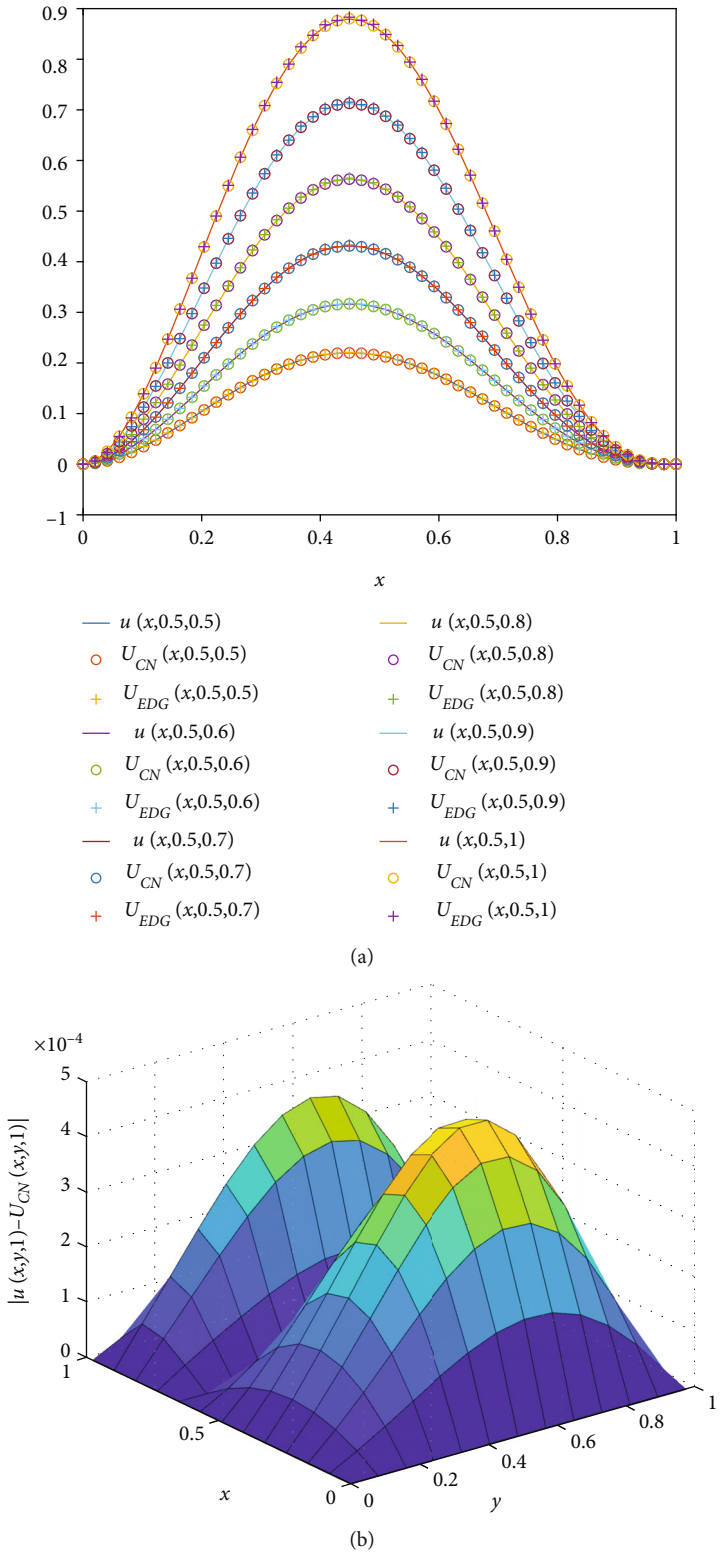

Figure 5: The exact, Crank–Nicolson and EDG solutions in different values of t and $y = 0.5$ (a) and the absolute error of Crank–Nicolson method at $T = 1$ (b) of Example 15 for $\Delta t = 0.01$, Re = 20, $N = 49$, and $\alpha = 0.5$.

Table 7: Absolute errors of Example 16 at $T = 1$ for Re = 2, $\Delta t = 0.01$, $\alpha = 0.2$, and $\alpha = 0.4$.

N	$\alpha = 0.2$				$\alpha = 0.4$			
	CN	Time	EDG	Time	CN	Time	EDG	Time
9	$2.5900e-03$	0.21	$2.1227e-02$	0.19	$2.5752e-03$	0.20	$2.1177e-02$	0.18
19	$5.9920e-04$	0.83	$5.3687e-03$	0.44	$5.9600e-04$	0.84	$5.3597e-03$	0.59
49	$9.3436e-05$	9.41	$8.2492e-04$	5.19	$9.2993e-05$	9.70	$8.2383e-04$	5.12
99	$2.5225e-05$	117.52	$2.0397e-04$	39.94	$2.5145e-05$	119.21	$2.0376e-04$	39.86

Table 8: Absolute errors of Example 16 at $T = 1$ for Re = 2, $\Delta t = 0.01$, $\alpha = 0.6$, and $\alpha = 0.8$.

N	$\alpha = 0.6$				$\alpha = 0.8$			
	CN	Time	EDG	Time	CN	Time	EDG	Time
9	$2.5546e-03$	0.22	$2.1112e-02$	0.20	$2.5253e-03$	0.24	$2.1039e-02$	0.22
19	$5.9150e-04$	0.84	$5.3476e-03$	0.60	$5.8469e-04$	0.88	$5.3318e-03$	0.62
49	$9.2340e-05$	9.88	$8.2234e-04$	5.05	$9.0870e-05$	10.19	$8.2010e-04$	5.51
99	$2.5001e-05$	119.14	$2.0348e-04$	41.28	$2.4238e-05$	123.96	$2.0280e-04$	41.67

$$D_0\|e^{n+1}\|^2 \le C\Delta t^2 \sum_{k=1}^{n-1} \left\|e^k\right\|^2 + \Delta t\left(\lambda_1 \left\|e^{n+1}\right\|^2 + \lambda_2 \|e^n\|^2\right) + \alpha\Delta t\left(\varepsilon_{11} + \frac{1}{4\varepsilon_{12}}\right)\left\|R^{n+1/2}\right\|^2, 1 \le n \le N, \tag{81}$$

where

$$\lambda_1 = \frac{\alpha c_0}{2}(2 + \varepsilon_1 + \varepsilon_2 + \varepsilon_3 + \varepsilon_4 + \varepsilon_5 + \varepsilon_6 + \varepsilon_7 + \varepsilon_8 + \varepsilon_9 + \varepsilon_{10}) + \alpha\varepsilon_{12} + C\varepsilon_{13} + C,$$

$$\lambda_2 = \frac{\alpha c_0}{2}\left(2 + \frac{1}{4\varepsilon_1} + \frac{1}{4\varepsilon_2} + \frac{1}{4\varepsilon_3} + \frac{1}{4\varepsilon_4} + \frac{1}{4\varepsilon_5} + \frac{1}{4\varepsilon_6} + \frac{1}{4\varepsilon_7} + \frac{1}{4\varepsilon_8} + \frac{1}{4\varepsilon_9} + \frac{1}{4\varepsilon_{10}}\right) + \frac{C}{4\varepsilon_{13}} + \frac{\alpha}{4\varepsilon_{11}} + 2C. \tag{82}$$

Therefore, we get

$$(C - \lambda_1)\left\|e^{n+1}\right\|^2 \le C\Delta t \sum_{k=1}^{n-1} \left\|e^k\right\|^2 + \lambda_2\|e^n\|^2 + \alpha\left(\varepsilon_{11} + \frac{1}{4\varepsilon_{12}}\right)\left\|R^{n+1/2}\right\|^2, 1 \le n \le N. \tag{83}$$

In the definition of λ_1, we choose epsilons which $C - \lambda_1$ be positive, so we have

$$\left\|e^{n+1}\right\|^2 \le C\Delta t \sum_{k=1}^{n-1} \left\|e^k\right\|^2 + C\|e^n\|^2 + \alpha C\left\|R^{n+1/2}\right\|^2, 1 \le n \le N. \tag{84}$$

Using Lemma 10 and $n\Delta t = T$, we get

$$\left\|e^{n+1}\right\|^2 \le C\left\|R^{n+1/2}\right\|^2 \le O\left(\Delta t + \Delta x^2 + \Delta y^2\right), 1 \le n \le N, \tag{85}$$

and this completes the proof.

Theorem 12. *The EDG method Equation (22) is convergent and the order of convergence is* $O(\Delta t + \Delta x^2 + \Delta y^2)$.

Proof. The proof is similar to Theorem 11.

6. Numerical Results

In this section, some numerical examples are considered to demonstrate the efficiency and accuracy of the proposed methods.

In numerical examples, we suppose that $u(x, t)$, $U_{\mathrm{CN}}(x, t)$, and $U_{\mathrm{EDG}}(x, t)$ denote the exact, Crank–Nicolson, and the EDG solution, respectively. Also in all Tables, the CN is an abbreviation for Crank–Nicolson Method.

The results obtained in this study show that the suggested methods have excellent stability, and they have verified the validity and effectiveness of the presented methods. Notably, we perform all of the computations by MATLAB R2019a software on a 64-bit PC with 2.30 GHz processor and 8 GB memory.

Example 13. Consider Equation (1) with the exact solution

$$u(x, y, t) = t^3\left(1 - x^2\right)^2\left(1 - y^2\right)^2, 0 \le x, y, t \le 1. \tag{86}$$

In Tables 1 and 2, the maximum of absolute errors and CPU Times for Crank–Nicolson and EDG methods for $\alpha = 0.1$, 0.3, and $\alpha = 0.7$, 0.9 with $T = 1$, $\Delta t = 0.01$, Re = 10, and different values of N are tabulated, respectively. These results confirm the convergent results. In Figure 3(a), the exact, Crank–Nicolson, and EDG solutions for $y = 0.5$, Re = 100,

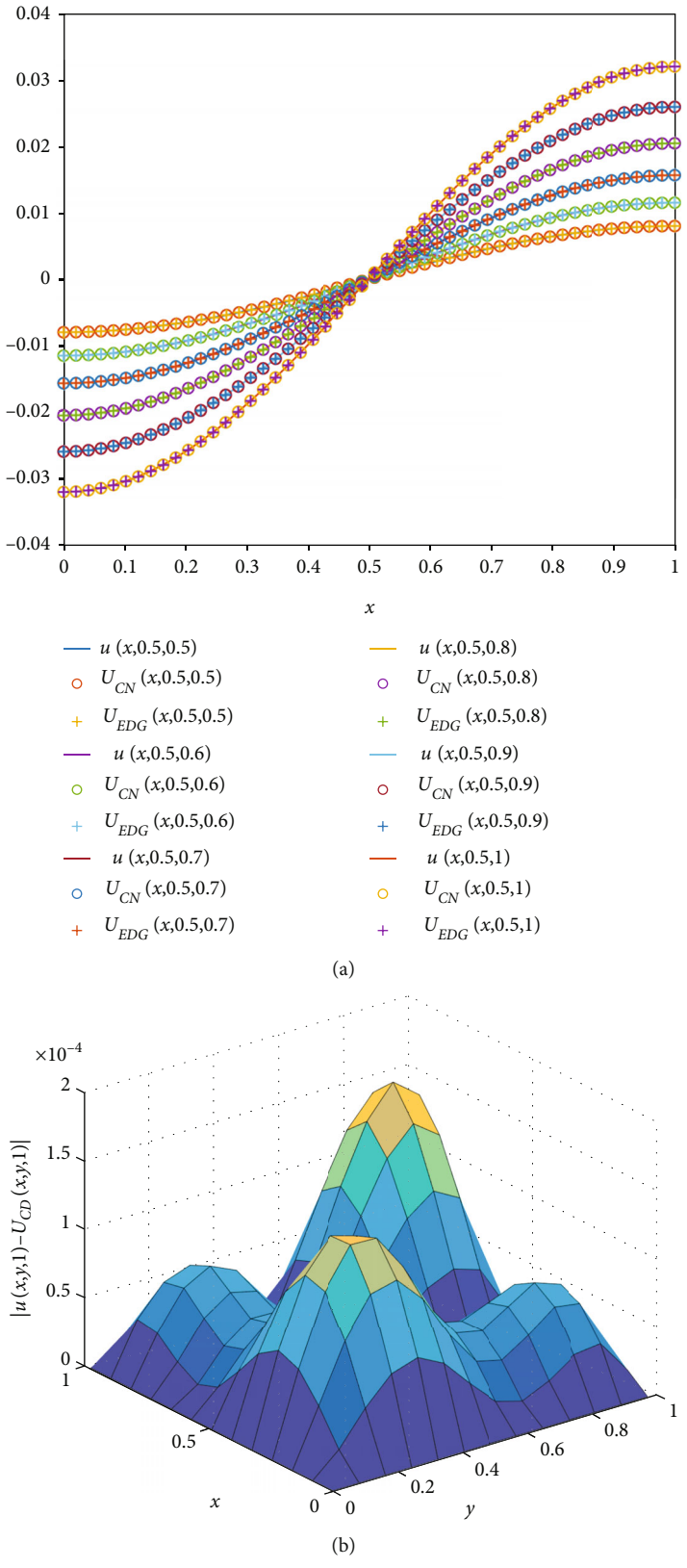

Figure 6: The exact, Crank–Nicolson, and EDG solutions in different values of t (a) and the absolute error of Crank–Nicolson method at $T = 1$ (b) of Example 16 for $\Delta t = 0.01$, Re = 10, $N = 49$, and $\alpha = 0.5$.

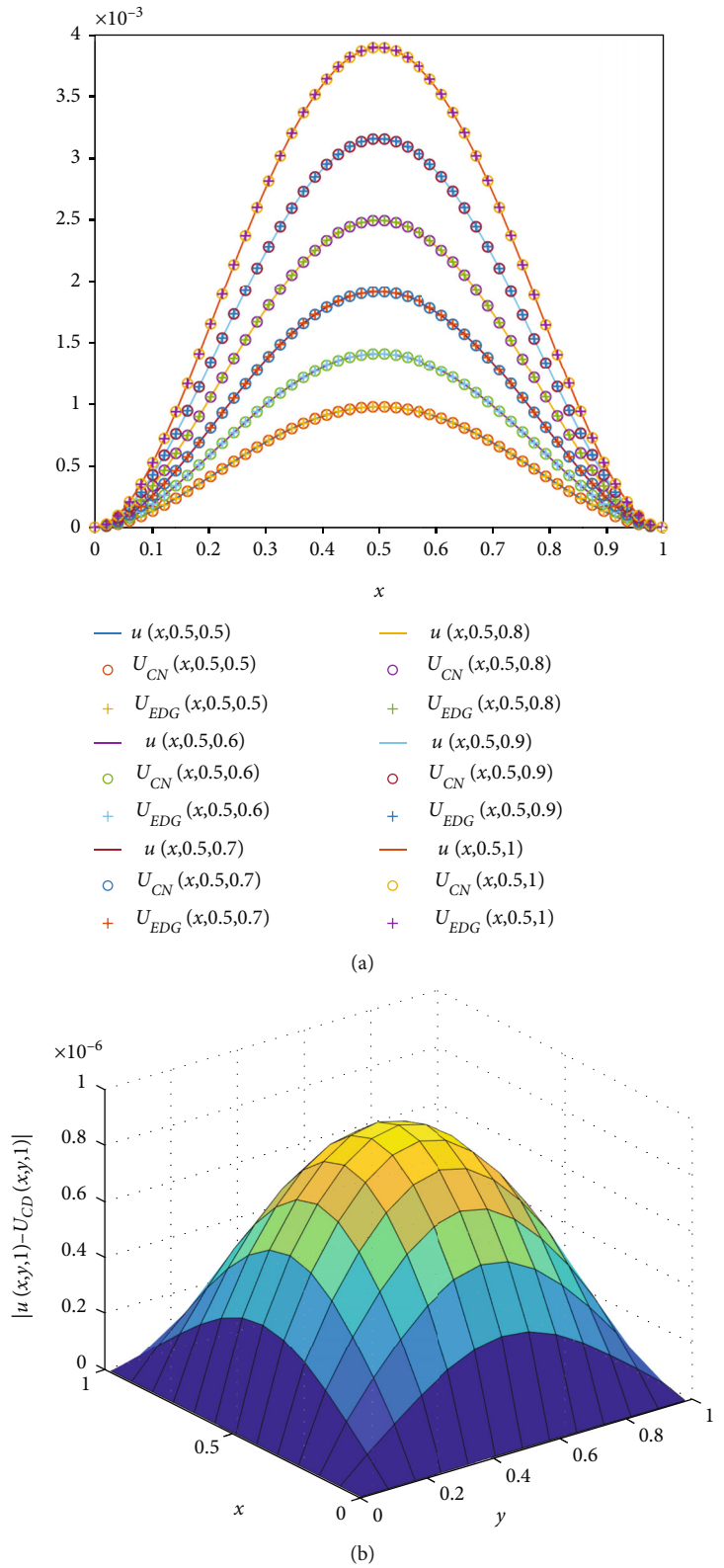

FIGURE 7: The exact, Crank–Nicolson and EDG solutions in different values of t (a) and the absolute error of Crank–Nicolson method at $T = 1$ (b) of Example 16 for $\Delta t = 0.01$, Re = 60, $N = 49$, and $\alpha = 0.5$.

Table 9: Absolute errors of Example 17 at $T = 1$ for Re = 100, $\Delta t = 0.01$, $\alpha = 0.2$, and $\alpha = 0.4$.

N	$\alpha = 0.2$				$\alpha = 0.4$			
	CN	Time	EDG	Time	CN	Time	EDG	Time
9	$2.3544e-05$	0.37	$1.2078e-04$	0.15	$2.0308e-05$	0.32	$1.1028e-04$	0.14
19	$5.3089e-06$	0.89	$3.7501e-05$	0.55	$4.5547e-06$	0.90	$3.5462e-05$	0.73
49	$7.8572e-07$	9.70	$6.1862e-06$	4.84	$6.5077e-07$	9.72	$5.9056e-06$	5.23
99	$1.9520e-07$	117.73	$1.5238e-06$	39.65	$1.9513e-07$	118.38	$1.4377e-06$	40.22

Table 10: Absolute errors of Example 17 at $T = 1$ for Re = 100, $\Delta t = 0.01$, $\alpha = 0.6$, and $\alpha = 0.8$.

N	$\alpha = 0.6$				$\alpha = 0.8$			
	CN	Time	EDG	Time	CN	Time	EDG	Time
9	$1.6919e-05$	0.32	$9.8582e-05$	0.26	$1.3331e-05$	0.37	$8.5506e-05$	0.27
19	$3.7515e-06$	0.89	$3.3183e-05$	0.82	$2.8606e-06$	0.94	$3.0637e-05$	0.79
49	$4.9131e-07$	9.91	$5.5845e-06$	5.41	$2.7513e-07$	10.06	$5.1849e-06$	5.50
99	$1.9501e-07$	118.22	$1.3268e-06$	41.16	$1.9462e-07$	119	$1.1529e-06$	41.91

$N = 49$, and $\Delta t = 0.01$ in different values of t are illustrated. Furthermore in Figure 3(b), the absolute error at $T = 1$ for Re = 100, $N = 49$, $\Delta t = 0.01$, and $\alpha = 0.5$ is portrayed. According to the Figures, we can see that our numerical solutions correspond to the exact solutions.

Example 14. In this example, we assume that the exact solution of Equation (1) is

$$u(x, y, t) = x^2 y^2 \sin(\pi x) \sin(\pi y) \sin(t), 0 \le x, y, t \le 1. \tag{87}$$

The values of initial and boundary conditions and f can be achieved using the exact solution. The exact, Crank–Nicolson, and EDG solutions for $y = 0.5$, Re = 50, $N = 49$, and $\Delta t = 0.01$ in different values of t are shown in Figure 4(a) and in Figure 4(b), the absolute error of Crank–Nicolson method at $T = 1$ for Re = 50, $N = 49$, $\Delta t = 0.01$, and $\alpha = 0.5$ is depicted. Based on the Figures, we can see that the numerical solutions are a good approximation of the exact solutions. In Tables 3 and 4, the maximum of absolute errors and CPU Times for Crank–Nicolson and EDG methods for $\alpha = 0.1$, 0.3, and $\alpha = 0.7$, 0.9 with $T = 1$, $\Delta t = 0.01$, Re = 100, and different values of N are tabulated, respectively. The EDG method generates the numerical solution with almost the same accuracy as the Crank–Nicolson method, but uses less time-consuming in comparison to the Crank–Nicolson method.

Example 15. Assume that the exact solution of Equation (1) is as follows:

$$u(x, y, t) = t^2 x^2 (1 - x)^3 \sin(\pi y) \exp(x + y), 0 \le x, y, t \le 1. \tag{88}$$

The maximum of absolute errors and CPU Times for Crank–Nicolson and EDG methods for $\alpha = 0.1$, 0.3, 0.7, 0.9 with $T = 1$, $\Delta t = 0.01$, Re = 5, and different values of N are shown in Tables 5 and 6, respectively. In Figure 5(a), the exact, Crank–Nicolson, and EDG solutions for $y = 0.5$, Re = 20, $N = 49$, and $\Delta t = 0.01$ in different values of t are illustrated. Also, the absolute error of Crank–Nicolson method at $T = 1$ for Re = 20, $N = 49$, $\Delta t = 0.01$, and $\alpha = 0.5$ is portrayed in Figure 5(b). The numerical experiments verified our theoretical results once again.

Example 16. Consider Equation (1) with the exact solution

$$u(x, y, t) = t^2 \cos(\pi x) \cos(\pi y), 0 \le x, y, t \le 1. \tag{89}$$

This example does not apply to the initial and boundary conditions of the article, but the results of this example are as good as other examples.

In Tables 7 and 8, the maximum of absolute errors and the CPU time consumed by our proposed methods for $\alpha =$ 0.2, 0.4, and 0.6, 0.8 at $T = 1$, $\Delta t = 0.01$, Re = 2 with different mesh sizes are presented, respectively. Similar to other examples, the EDG method is faster than the Crank–Nicolson method. The exact, Crank–Nicolson, and EDG solutions for $y = 0.5$, Re = 10, $N = 49$, $\alpha = 0.5$, and $\Delta t = 0.01$ in different values of t are displayed in Figure 6(a). In addition, the absolute error of the Crank–Nicolson method at $T = 1$, $\alpha = 0.5$, Re = 10, $N = 49$, and $\Delta t = 0.01$ is displayed in Figure 6(b).

Example 17. In this example, we assume that the exact solution of Equation (1) is

$$u(x, y, t) = t^2 \left(x - x^2\right)^2 \left(y - y^2\right)^2, 0 \le x, y, t \le 1. \tag{90}$$

In Figure 7(a), the exact, Crank–Nicolson, and EDG solutions for $y = 0.5$, Re = 60, $N = 49$, and $\Delta t = 0.01$ in different values of t are shown. Besides, the absolute error of Crank–Nicolson is demonstrated in Figure 7(b). Obviously, our schemes are very accurate and quickly converge to the exact solution. The maximum of absolute errors and CPU Times for Crank–Nicolson and EDG methods for $\alpha = 0.2$, 0.4, and

0.6, 0.8 at $T = 1$, $\Delta t = 0.01$, and Re = 100 with various mesh sizes are expressed in Tables 9 and 10, respectively.

7. Conclusion

In this paper, we introduced the Crank–Nicolson method and the EDG method which derived from 45° rotation of the Crank–Nicolson approximation point and Taylor expansion to solve the 2D time-fractional Burgers' equation with Caputo-Fabrizio derivative. The error analysis and local truncation error of these methods gave in detail. The stability of the proposed numerical methods is analyzed by the Von-Neumann method. The convergence analysis of the CN and EDG methods proved. Some test problems chose to investigate the applicability and practical efficiency. From Tables 1–10, the results showed a good agreement with the exact solution, and the EDG method was faster than the CN method. Numerical experiments showed the efficiency of the proposed methods in terms of CPU time and accuracy.

Data Availability

All results have been obtained by conducting the numerical procedure and the ideas can be shared for the researchers.

Conflicts of Interest

The authors declare that there are no conflicts of interest regarding the publication of this paper.

Acknowledgments

We are very grateful to anonymous referees for their careful reading and valuable comments which led to the improvement of this paper.

References

[1] F. Abdullaev and V. V. Konotop, *Nonlinear Waves: Classical and Quantum Aspects, Vol. 153*, Springer Science & Business Media, 2006.

[2] W. Gao, P. Veeresha, D. Prakasha, and H. M. Baskonus, "Novel dynamic structures of 2019-ncov with nonlocal operator via powerful computational technique," *Biology*, vol. 9, pp. 107–122, 2020.

[3] W. Gao, P. Veeresha, D. G. Prakasha, and H. M. Baskonus, "New numerical simulation for fractional benney–lin equation arising in falling film problems using two novel techniques," *Numerical Methods for Partial Differential Equations*, vol. 37, pp. 210–243, 2020.

[4] K. K. Ali, M. S. Osman, H. M. Baskonus, N. S. Elazabb, and E. İlhan, "Analytical and numerical study of the hiv-1 infection of $CD4^+$ T-cells conformable fractional mathematical model that causes acquired immunodeficiency syndrome with the effect of antiviral drug therapy," *Mathematical Methods in the Applied Sciences*, 2020.

[5] C. I. Muresan, P. Ostalczyk, and M. D. Ortigueira, "Fractional calculus applications in modeling and design of control systems," *Journal of Applied Nonlinear Dynamics*, vol. 6, pp. 131–134, 2017.

[6] C. Ionescu, A. Lopes, D. Copot, J. T. Machado, and J. Bates, "The role of fractional calculus in modeling biological phenomena: a review," *Communications in Nonlinear Science and Numerical Simulation*, vol. 51, pp. 141–159, 2017.

[7] H. Tang, D. Wang, R. Huang, X. Pei, and W. Chen, "A new rock creep model based on variable-order fractional derivatives and continuum damage mechanics," *Bulletin of Engineering Geology and the Environment*, vol. 77, pp. 375–383, 2018.

[8] Y. Zhuzhong, Z. Jiliu, and L. Fangnian, "Noise detection and image de-noising based on fractional calculus," *Journal of Image and Graphics*, vol. 19, pp. 1418–1429, 2014.

[9] X.-L. Gong, X.-H. Liu, and X. Xiong, "Chaotic analysis and adaptive synchronization for a class of fractional order financial system," *Physica A: Statistical Mechanics and its Applications*, vol. 522, pp. 33–42, 2019.

[10] M. Caputo and M. Fabrizio, "A new definition of fractional derivative without singular kernel," *Progress in Fractional Differentiation and Applications*, vol. 1, pp. 1–13, 2015.

[11] J. Shi and M. Chen, "A second-order accurate scheme for two-dimensional space fractional diffusion equations with time caputo-fabrizio fractional derivative," *Applied Numerical Mathematics*, vol. 151, pp. 246–262, 2020.

[12] H. Qiao, Z. Liu, and A. Cheng, "A fast compact finite difference method for fractional Cattaneo equation based on Caputo–Fabrizio derivative," *Mathematical Problems in Engineering*, vol. 2020, Article ID 3842946, 17 pages, 2020.

[13] Z. Korpinar, "On numerical solutions for the Caputo-Fabrizio fractional heat-like equation," *Thermal Science*, vol. 22, pp. 87–95, 2018.

[14] M. Zhang, Y. Liu, and H. Li, "High-order local discontinuous Galerkin method for a fractal mobile/immobile transport equation with the Caputo–Fabrizio fractional derivative," *Numerical Methods for Partial Differential Equations*, vol. 35, pp. 1588–1612, 2019.

[15] J. Singh, D. Kumar, Z. Hammouch, and A. Atangana, "A fractional epidemiological model for computer viruses pertaining to a new fractional derivative," *Applied Mathematics and Computation*, vol. 316, pp. 504–515, 2018.

[16] Z. Liu and X. Li, "A Crank–Nicolson difference scheme for the time variable fractional mobile–immobile advection–dispersion equation," *Journal of Applied Mathematics and Computing*, vol. 56, pp. 391–410, 2018.

[17] R. H. Shariffudin and A. R. Abdullah, "Hamiltonian circuited simulations of elliptic partial differential equations using a spark," *Applied Mathematics Letters*, vol. 14, pp. 413–418, 2001.

[18] N. Abdi, H. Aminikhah, A. H. Refahi Sheikhani, and J. Alavi, "A high-order compact alternating direction implicit method for solving the 3D time-fractional diffusion equation with the Caputo–Fabrizio operator," *Mathematical Sciences*, vol. 14, pp. 359–373, 2020.

[19] J. Jia and H. Wang, "A fast finite volume method on locally refined meshes for fractional diffusion equations," *East Asian Journal on Applied Mathematics*, vol. 9, pp. 755–779, 2019.

[20] H. Chen, S. Lü, and W. Chen, "Spectral methods for the time fractional diffusion–wave equation in a semi-infinite channel," *Computers & Mathematics with Applications*, vol. 71, pp. 1818–1830, 2016.

[21] Z. Chen, G. Huan, and Y. Ma, *Computational Methods for Multiphase Flows in Porous Media*, SIAM, 2006.

[22] A. R. Abdullah, "The four point explicit decoupled group (EDG) method: a fast poisson solver," *International Journal of Computer Mathematics*, vol. 38, pp. 61–70, 1991.

[23] M. K. M. Akhir, M. Othman, Z. A. Majid, M. Suleiman, and J. Sulaiman, "Four point explicit decoupled group iterative method applied to two-dimensional Helmholtz equation," *International Journal of Mathematical Analysis*, vol. 6, pp. 963–974, 2012.

[24] A. M. Saeed, "Solving 2d time-fractional diffusion equations by preconditioned fractional edg method," *Progressive Research in Mathematics*, vol. 14, pp. 1–7, 2018.

[25] A. T. Balasim and N. H. M. Ali, "Group iterative methods for the solution of two-dimensional time-fractional diffusion equation," in *AIP Conference Proceedings 1750, 030003*, 2016.

[26] J. Eng, A. Saudi, and J. Sulaiman, "Performance analysis of the explicit decoupled group iteration via five-point rotated Laplacian operator in solving poisson image blending problem," *Indian Journal of Science and Technology*, vol. 11, no. 12, pp. 1–6, 2018.

[27] D. Kong, Y. Xu, and Z. Zheng, "A hybrid numerical method for the KdV equation by finite difference and sinc collocation method," *Applied Mathematics and Computation*, vol. 355, pp. 61–72, 2019.

[28] Z. Liu, A. Cheng, and X. Li, "A second order Crank–Nicolson scheme for fractional Cattaneo equation based on new fractional derivative," *Applied Mathematics and Computation*, vol. 311, pp. 361–374, 2017.

[29] J. M. Holte, *Discrete Gronwall Lemma and Applications*, vol. 24, MAA-NCS meeting at the University of North Dakota, 2009.

Hindawi
Advances in Mathematical Physics
Volume 2021, Article ID 6652108, 15 pages
https://doi.org/10.1155/2021/6652108

Research Article

Numerical Study of the Inverse Problem of Generalized Burgers–Fisher and Generalized Burgers–Huxley Equations

Javad Alavi[1] **and Hossein Aminikhah**[1,2]

[1]*Department of Applied Mathematics and Computer Science, Faculty of Mathematical Sciences, University of Guilan, P.O. Box 1914, Rasht 41938, Iran*
[2]*Center of Excellence for Mathematical Modelling, Optimization and Combinational Computing (MMOCC), University of Guilan, P.O. Box 1914, Rasht 41938, Iran*

Correspondence should be addressed to Hossein Aminikhah; aminikhah@guilan.ac.ir

Received 31 December 2020; Revised 9 February 2021; Accepted 21 February 2021; Published 15 March 2021

Academic Editor: Sachin Kumar

In this paper, the boundary value inverse problem related to the generalized Burgers–Fisher and generalized Burgers–Huxley equations is solved numerically based on a spline approximation tool. B-splines with quasilinearization and Tikhonov regularization methods are used to obtain new numerical solutions to this problem. First, a quasilinearization method is used to linearize the equation in a specific time step. Then, a linear combination of B-splines is used to approximate the largest order of derivatives in the equation. By integrating from this linear combination, some approximations have been obtained for each of the functions and derivatives with respect to time and space. The boundary and additional conditions of the problem are also applied in these approximations. The Tikhonov regularization method is used to solve the system of linear equations using noisy data. Several numerical examples are provided to illustrate the accuracy and efficiency of the method.

1. Introduction

Most of the physical problems arising in various fields of physical science and engineering are modeled by nonlinear partial differential equations (NLPDEs) [1]. Two of the most famous NLPDEs are the generalized Burgers–Huxley and generalized Burgers–Fisher equations [2]. These equations describe the interaction between diffusion, convection, and reaction [3].

The generalized Burgers–Huxley and generalized Burgers–Fisher equations are of the form

$$u_t = \varepsilon u_{xx} - \alpha u^{\delta} u_x + \beta u\left(1 - u^{\delta}\right)\left(\eta u^{\delta} - \gamma\right), \quad a < x < b, t > 0, \tag{1}$$

with the initial condition

$$u(x, 0) = f(x), \quad a \le x \le b, \tag{2}$$

and Dirichlet boundary conditions

$$u(a, t) = q(t), \quad t \ge 0, \tag{3}$$

$$u(b, t) = g(t), \quad t \ge 0. \tag{4}$$

Also, in order to determine q, we consider an additional condition given at the interior point, $x = l$ of the region

$$u(l, t) = p(t), \quad a < l < b, t \ge 0, \tag{5}$$

where ε, α, β, γ, δ, and η are constants such that $0 < \varepsilon \le 1$, $\beta \ge 0$, $\delta > 0$, $\gamma \in (0, 1)$, and $\eta = 0, 1$, and g and f are considered known functions, while q and u are unknown functions.

If $\eta = 1$, (1) describes the generalized Burgers–Huxley equation, and in the case that $\eta = \gamma = 0$, (1) describes the generalized Burgers–Fisher equation.

In some cases, the exact solitary wave solutions of equation (1) are obtained using the relevant nonlinear transformations [4]. In the case that $\eta = 1$ and $\varepsilon = 1$, the exact

solution of the generalized Burgers–Huxley equation (1) is taken from [2], given by

$$u(x,t) = \left(\frac{\gamma}{2} + \frac{\gamma}{2}\tanh\left(w_1(x - w_2 t)\right)\right)^{1/\delta}, \quad (6)$$

where

$$w_1 = \frac{\nu\gamma\delta}{4(1+\delta)},$$

$$w_2 = \frac{\alpha\gamma}{1+\delta} - \frac{\nu(1+\delta-\gamma)}{2(1+\delta)}, \quad (7)$$

and $\nu = -\alpha + \sqrt{\alpha^2 + 4\beta(1+\delta)}$.

Note that, in here, to get the exact solution, we first assume that $u = w^{1/\delta}$. Then, by assuming $w(x,t) = w(x-ct) = w(\zeta)$, the equation transforms into an ordinary differential equation as the form $d^2w/d\zeta^2 = a^2(2w-\gamma)w(w-\gamma)$, which can be easily solvable.

If $\eta = 0$, $\varepsilon = 1$, and $\gamma = -1$, the exact solution of the generalized Burgers–Fisher equation (1) is taken from [2], given by

$$u(x,t) = \left(\frac{1}{2} + \frac{1}{2}\tanh\left(\theta_1(x - \theta_2 t)\right)\right)^{1/\delta}, \quad (8)$$

where

$$\theta_1 = \frac{-\alpha\delta}{2(1+\delta)},$$

$$\theta_2 = \frac{\alpha}{1+\delta} + \frac{\beta(1+\delta)}{\alpha}. \quad (9)$$

The boundary conditions are taken from the exact solution.

Burgers' equation was first introduced by Bateman [5] when he mentioned it as worthy of study and gave its steady solutions. Later on, Burgers [6] treated it as a mathematical model for turbulence and after whom such an equation is widely referred to as Burgers' equation. The study of Burgers' equation is important since it arises in the approximate theory of flow through a shock wave propagating in a viscous fluid and in the modeling of turbulence [7]. The generalized Burgers–Huxley equation describes a wide class of physical nonlinear phenomena, for instance, a prototype model for describing the interaction between reaction mechanisms, convection effects, and diffusion transports [8]. It has found its applications in many fields such as biology, metallurgy, chemistry, combustion, mathematics, and engineering [8, 9]. The generalized Burgers–Fisher equation has been found in many applications in fields such as gas dynamics, number theory, heat conduction, and elasticity [10]. The following are some works on these equations. Yadav and Jiwari [11] developed a finite element analysis and approximation of the Burgers–Fisher equation. Jiwrai and Mittal [12] presented a high-order numerical scheme for the singularly perturbed Burgers–Huxley equation. Also, they have a numerical study of the Burgers–Huxley equation by the differential quadrature method [13]. The Lie symmetry analysis and explicit solutions for the time fractional generalized Burgers–Huxley equation were studied by Inc et al. [14]. Korpinar et al. [15] studied the exact special solutions for the stochastic regularized long wave–Burgers equation. Dhawan et al. have a contemporary review of techniques for the solution of the nonlinear Burgers equation [16] (also, see [17, 18]).

In this article, for the first time, a boundary value inverse problem for the generalized Burgers–Huxley and generalized Burgers–Fisher equations will be studied. For this purpose, first, a quasilinearization method is used to linearize the equation in a specific time step. Then, a linear combination of B-splines is used to approximate the largest order of derivatives in the equation. By integrating from this linear combination, some new approximations have been obtained for each of the functions and derivatives with respect to time and space. In this new method, the boundary and additional conditions of the problem are also applied in these approximations. Then, the Tikhonov regularization method is used to solve the system of linear equations using noisy data. In the end, several numerical examples are provided and 2D and 3D graphical illustrations are reported to show the accuracy and efficiency of the method.

The rest of the article is organized as follows. In the first subsection of Section 2, the B-spline functions and their first- and second-order integrals are introduced. In the continuation of this section, the quasilinearization method is presented. The solution method is presented to solve the inverse problem (1), (2), (4), and (5) in Section 3. Some numerical experiments are given with graphical and tabular illustrations in Section 4. The conclusion of the presented method is given at the end of the paper in Section 5.

2. Preliminaries

In this section, first, the spline approximation, used in this article, is introduced and then the quasilinearization approximation will be obtained.

2.1. Cubic B-Spline. In this approach, the space derivatives are approximated using the cubic B-spline method. A mesh Ω, which is equally divided by knots x_i into M subintervals $[x_i, x_{i+1}]$, $i = 0, 1, \cdots, M-1$, such that $\Omega : a = x_0 < x_1 < \cdots < x_M = b$, is used. Also, let $S_4(\Omega)$ be the space of cubic splines on Ω. The corresponding set of cubic B-splines $\{B_{-1}, B_0, \cdots, B_{M+1}\}$, which is a basis for $S_4(\Omega)$, is defined using the recursive relation [19]:

$$b_{j,p}(x) = \frac{x - x_j}{x_{j+p} - x_j} b_{j,p-1}(x) + \frac{x_{j+p+1} - x}{x_{j+p+1} - x_{j+1}} b_{j+1,p-1}(x), \quad (10)$$

starting from

$$b_{j,0}(x) = \begin{cases} 1, & x_j \le x < x_{j+1}, \\ 0, & \text{otherwise}, \end{cases} \quad (11)$$

where $j = -3, -2, \cdots, M-1$, $x_{-3} = x_{-2} = x_{-1} = a$, $x_{M+1} = x_{M+2} = x_{M+3} = b$, $p = 1, 2, \cdots$, and $B_k(x) = b_{k-2,3}(x)$, $k = -1, 0, \cdots, M+1$, under the convention that fractions with zero denominators have the value zero. With the above definition, all the B-splines take the value zero at the endpoint b. Therefore, in

order to avoid asymmetry over the interval $[a, b]$, it is common to assume the B-splines to be left continuous at b. We will follow suit.

Using induction on recurrence relation (10), we deduce immediately the following basic properties of a B-spline [20]:

(i) A B-spline is right continuous; i.e., the value at a point x is obtained by taking the limit from the right

(ii) A B-spline is locally supported on the interval given by the extreme knots used in its definition. More precisely,

$$B_j(x) = 0, \quad x \notin \left[x_j, x_{j+4}\right). \tag{12}$$

(iii) A B-spline is nonnegative everywhere and positive inside its support, i.e.,

$$\begin{aligned} B_j(x) &\geq 0, \quad x \in \mathbb{R}, \\ B_j(x) &> 0, \quad x \in \left(x_j, x_{j+4}\right). \end{aligned} \tag{13}$$

(iv) From recurrence relation (10), one can find that the following formula for cubic B-splines:

$$B_j(x) = \begin{cases} \dfrac{(x-x_j)^3}{(x_{j+1}-x_j)(x_{j+2}-x_j)(x_{j+3}-x_j)}, & x \in [x_j, x_{j+1}), \\ \dfrac{(x-x_j)^2(x_{j+2}-x)}{(x_{j+2}-x_j)(x_{j+2}-x_{j+1})(x_{j+3}-x_j)} \\ \quad + \dfrac{(x-x_j)(x_{j+3}-x)(x-x_{j+1})}{(x_{j+3}-x_j)(x_{j+3}-x_{j+1})(x_{j+2}-x_{j+1})} \\ \quad + \dfrac{(x_{j+4}-x)(x-x_{j+1})^2}{(x_{j+2}-x_{j+1})(x_{j+3}-x_{j+1})(x_{j+4}-x_{j+1})}, & x \in [x_{j+1}, x_{j+2}), \\ \dfrac{(x-x_j)(x_{j+3}-x)^2}{(x_{j+3}-x_j)(x_{j+3}-x_{j+1})(x_{j+3}-x_{j+2})} \\ \quad + \dfrac{(x-x_{j+1})(x_{j+3}-x)(x_{j+4}-x)}{(x_{j+3}-x_{j+1})(x_{j+3}-x_{j+2})(x_{j+4}-x_{j+1})} \\ \quad + \dfrac{(x_{j+4}-x)^2(x-x_{j+2})}{(x_{j+4}-x_{j+1})(x_{j+4}-x_{j+2})(x_{j+3}-x_{j+2})}, & x \in [x_{j+2}, x_{j+3}), \\ \dfrac{(x_{j+4}-x)^3}{(x_{j+4}-x_{j+1})(x_{j+4}-x_{j+2})(x_{j+4}-x_{j+3})}, & x \in [x_{j+3}, x_{j+4}), \\ 0, \quad \text{o.w.}, \end{cases} \tag{14}$$

for $j = -3, -2, \cdots, M-1$.

Many other properties can be found in [19, 20] and references therein.

2.2. Spline Approximation. Now, let $f \in C[a, b]$; we consider a linear combination of B-splines $S_M(f)(x)$, as an approximation of $f(x)$, as follows:

$$S_M(f)(x) = \sum_{k=-1}^{M+1} c_k B_k(x) = C_M^T \Pi_M(x), \tag{15}$$

where $C_M = (c_{-1}, c_0, \cdots, c_{M+1})^T$ and $\Pi_M(x) = (B_{-1}(x), B_0(x), \cdots, B_{M+1}(x))^T$. Furthermore, in order to achieve a square system in numerical computations, the set of the nodes $\Omega^* = (\xi_i)_{i=-1}^{M+1}$ is used, where

$$\begin{cases} \xi_{-1} = x_0, \xi_0 = x_0 + \dfrac{h}{2}, \\ \xi_1 = x_1, \xi_2 = x_2, \cdots, \xi_{M-2} = x_{M-2}, \\ \xi_{M-1} = x_{M-1}, \xi_M = x_M - \dfrac{h}{2}, \xi_{M+1} = x_M, \end{cases} \tag{16}$$

where $h = (b-q)/M$.

Definition 1. Assume that B, I_1B, and I_2B are $(M+3)$-square matrices defined by

$$\begin{aligned} (B)_{i,j} &= B_i(\xi_j), \\ (I_1B)_{i,j} &= \int_a^{\xi_j} B_i(y)dy, \\ (I_2B)_{i,j} &= \int_a^{\xi_j}\int_a^{z} B_i(y)dydz, \end{aligned} \tag{17}$$

where $i, j = -1, 0, \cdots, M+1$. According to the definition of B_k, we have

$$B = \begin{pmatrix} 1 & \frac{1}{8} & & & & & & & & & \\ & \frac{19}{32} & \frac{1}{4} & & & & & & & & \\ & \frac{25}{96} & \frac{7}{12} & \frac{1}{6} & & & & & & & \\ & \frac{1}{48} & \frac{1}{6} & \frac{2}{3} & \frac{1}{6} & & & & & & \\ & & & \frac{1}{6} & \frac{2}{3} & \frac{1}{6} & & & & & \\ & & & & \ddots & \ddots & \ddots & & & & \\ & & & & & \frac{1}{6} & \frac{2}{3} & \frac{1}{6} & & & \\ & & & & & & \frac{1}{6} & \frac{2}{3} & \frac{1}{6} & \frac{1}{48} & \\ & & & & & & & \frac{1}{6} & \frac{7}{12} & \frac{25}{96} & \\ & & & & & & & & \frac{1}{4} & \frac{19}{32} & \\ & & & & & & & & & \frac{1}{8} & 1 \end{pmatrix}. \tag{18}$$

The matrices I_1B and I_2B are listed in the appendix.

Thus, we can write

$$\int_a^{\xi_j} S_M(f)(y)dy = C_n^T I_1^j, \tag{19}$$

$$\int_{ya}^{\xi_j}\int_a^z S_M(f)(y)dydz = C_n^T I_2^j, \tag{20}$$

where I_ν^j is the jth column of matrix $I_\nu B$, $\nu = 1, 2$.

2.3. The Quasilinearization Method. In equation (1), we have three nonlinear terms such as $u^\delta u_x$, $u^\delta u$, and $u^{2\delta}u$. In this section, a quasilinearization method is presented to linearize these terms. The quasilinearization technique is an application of the Newton–Raphson–Kantorovich approximation in function space [21–24].

Let $0 \le t \le T$ and $t_n = n\Delta t$, $n = 0, 1, \cdots, N$, are the equal parts of $[0, T]$, where $\Delta t = T/N$. Also, assume that $t \in [t_n, t_{n+1}]$, $u, v \in C[a, b] \times C[0, T]$, and $h(u, v) = u^\zeta v$. Using two-variable Taylor series for h in some open neighborhood around $(u, v) = (u^n, v^n)$, there is $c = (c_1, c_2)$, where $c_1, c_2 \in C[a, b] \times C[0, T]$, so that

$$h(x) = h(a) + (x - a) \cdot \nabla h(a) + (x - a) \cdot H(c) \cdot (x - a), \tag{21}$$

where $x = (u, v)$, $a = (u^n, v^n)$, $u^n = u(x, t_n)$, $v^n = v(x, t_n)$, and H is the Hessian matrix:

$$H(c) = \begin{pmatrix} h_{c_1c_1}(c) & h_{c_1c_2}(c) \\ h_{c_1c_2}(c) & h_{c_2c_2}(c) \end{pmatrix}. \tag{22}$$

Upon ignoring two-order terms, equation (21) becomes

$$h(x) \approx h(a) + (x - a) \cdot \nabla h(a). \tag{23}$$

Therefore,

$$\begin{aligned} h(u, v) &\approx \left(u^\zeta\right)^n v^n + (u - u^n, v - v^n) \cdot \left(\zeta\left(u^{\zeta-1}\right)^n v^n, \left(u^\zeta\right)^n\right) \\ &= \zeta\left(u^{\zeta-1}\right)^n v^n u - \zeta\left(u^\zeta\right)^n v^n + \left(u^\zeta\right)^n v. \end{aligned} \tag{24}$$

By placing $(\zeta, v) = (\delta, u_x)$, $(\zeta, v) = (\delta, u)$, and $(\zeta, v) = (2\delta, u)$ in (24), we obtain linear approximations for $u^\delta u_x$, $u^\delta u$, and $u^{2\delta}u$, respectively, as follows:

$$u^\delta u_x \approx \delta\left(u^{\delta-1}\right)^n (u_x)^n u - \delta\left(u^\delta\right)^n (u_x)^n + \left(u^\delta\right)^n u_x, \tag{25}$$

$$u^\delta u \approx \delta\left(u^\delta\right)^n u - \delta\left(u^{\delta+1}\right)^n + \left(u^\delta\right)^n u, \tag{26}$$

$$u^{2\delta}u \approx 2\delta\left(u^{2\delta}\right)^n u - 2\delta\left(u^{2\delta+1}\right)^n + \left(u^{2\delta}\right)^n u. \tag{27}$$

3. Solution Method for the Burgers–Huxley and Burgers–Fisher Equations

In this section, the inverse problem (1)–(5) is solved using S_M as an approximation tool. Assume that in (16), $l = \xi_\upsilon$, $\upsilon \in \{-1, 0, \cdots, M + 1\}$.

To discretize (1), the method of [25, 26] is used. We assume that $u_{txx}(x, t)$ can be expanded in terms of linear combination of cubic B-splines (15) as follows:

$$u_{txx}(x, t) = \sum_{k=-1}^{M+1} c_k^n B_k(x) = C_M^T \Pi_M(x), \tag{28}$$

where $t \in [t_n, t_{n+1}]$, and the row vector C_M^T is assumed constant in the subinterval $[t_n, t_{n+1}]$. By integrating (28) with respect to t from t_n to t, we obtain

$$u_{xx}(x, t) = u_{xx}(x, t_n) + (t - t_n) C_M^T \Pi_M(x). \tag{29}$$

Also, by integrating (28) with respect to x from l to x, we have

$$u_{tx}(x, t) = u_{tx}(l, t) + \sum_{k=-1}^{M+1} c_k^n \int_l^x B_k(y)dy. \tag{30}$$

Integrating (30) with respect to x from l to x gives

$$\begin{aligned} u_x(x, t) = {} & u_x(x, t_n) + u_x(l, t) - u_x(l, t_n) \\ & + (t - t_n) \sum_{k=-1}^{M+1} c_k^n \int_l^x B_k(y)dy. \end{aligned} \tag{31}$$

Again, by integrating (31) with respect to x from l to x, we gain

$$\begin{aligned} u(x, t) = {} & u(x, t_n) + p(t) - p(t_n) + (x - l)[u_x(l, t) - u_x(l, t_n)] \\ & + (t - t_n) \sum_{k=-1}^{M+1} c_k^n \int_l^x \int_l^z B_k(y)dydz. \end{aligned} \tag{32}$$

Putting $x = b$ in (32), we get

$$\begin{aligned} u_x(l, t) - u_x(l, t_n) = {} & \frac{1}{b - l}[g(t) - g(t_n) - p(t) + p(t_n) \\ & - (t - t_n) \sum_{k=-1}^{M+1} c_k^n \int_l^b \int_l^z B_k(y)dydz]. \end{aligned} \tag{33}$$

Substituting equation (33) into (31) and (32) and using (4) and (5) held

$$u_x(x,t) = u_x(x,t_n) + \frac{1}{b-l}[g(t) - g(t_n) - p(t) + p(t_n)] + (t-t_n)\sum_{k=-1}^{M+1} c_k^n \cdot \left(\int_l^x B_k(y)dy - \frac{1}{b-l}\int_l^b \int_l^z B_k(y)dydz\right), \tag{34}$$

$$u(x,t) = u(x,t_n) + p(t) - p(t_n) + \frac{x-l}{b-l} \cdot [g(t) - g(t_n) - p(t) + p(t_n)] + (t-t_n)\sum_{k=-1}^{M+1} c_k^n \cdot \left(\int_l^x \int_l^z B_k(y)dydz - \int_l^b \int_l^z B_k(y)dydz\right). \tag{35}$$

By integrating (28) twice with respect to x from l to x and using (5), we obtain

$$u_t(x,t) = \dot{p}(t) + (x-l)u_{tx}(l,t) + \sum_{k=-1}^{M+1} c_k^n \int_l^x \int_l^z B_k(y)dydz, \tag{36}$$

where $\dot{}$ denotes the differentiation with respect to t. By substituting $x = b$ in equation (36) and using (4), we get

$$u_{tx}(l,t) = \frac{1}{b-l}\left[\dot{g}(t) - \dot{p}(t) - \sum_{k=-1}^{M+1} c_k^n \int_l^b \int_l^z B_k(y)dydz\right]. \tag{37}$$

Substituting equation (37) into (36) held

$$u_t(x,t) = \dot{p}(t) + \frac{x-l}{b-l}[\dot{g}(t) - \dot{p}(t)] + \sum_{k=-1}^{M+1} c_k^n \cdot \left(\int_l^x \int_l^z B_k(y)dydz - \frac{x-l}{b-l}\int_l^b \int_l^z B_k(y)dydz\right). \tag{38}$$

Since

$$\int_l^x \int_l^z B_k(y)dydz = \int_a^x \int_a^z B_k(y)dydz - (x-l)\int_a^l B_k(y)dy - \int_a^l \int_a^z B_k(y)dydz, \tag{39}$$

from (34), (35), and (38), we obtain

$$u_x(x,t) = u_x(x,t_n) + \frac{1}{b-l} \cdot [g(t) - g(t_n) - p(t) + p(t_n)] + (t-t_n)\sum_{k=-1}^{M+1} c_k^n \mathcal{I}, \tag{40}$$

$$u(x,t) = u(x,t_n) + p(t) - p(t_n) + \frac{x-l}{b-l} \cdot [g(t) - g(t_n) - p(t) + p(t_n)] + (t-t_n)\sum_{k=-1}^{M+1} c_k^n \mathcal{J}, \tag{41}$$

$$u_t(x,t) = \dot{p}(t) + \frac{x-l}{b-l}[\dot{g}(t) - \dot{p}(t)] + \sum_{k=-1}^{M+1} c_k^n \mathcal{J}, \tag{42}$$

where

$$\mathcal{I} = \int_a^x B_k(y)dy - \frac{1}{b-l}\left(\int_a^b \int_a^z B_k(y)dydz - \int_a^l \int_a^z B_k(y)dydz\right),$$

$$\mathcal{J} = \int_a^x \int_a^z B_k(y)dydz + \frac{x-b}{b-l}\int_a^l \int_a^z B_k(y)dydz - \frac{x-l}{b-l}\int_a^b \int_a^z B_k(y)dydz. \tag{43}$$

Further, by discretizing (29), (40), (41), and (42), assuming $x \to \xi_j$ and $t \to t_{n+1}$, and using (19) and (20), we get

$$(u_{xx})_i^{n+1} = (u_{xx})_i^n + \Delta t C_M^T \Pi_M(\xi_i), \tag{44}$$

$$(u_x)_i^{n+1} = (u_x)_i^n + \frac{1}{b-l}\varphi_n + \Delta t C_M^T L^i, \tag{45}$$

$$(u_t)_i^{n+1} = \dot{p}(t_{n+1}) + d_i[\dot{g}(t_{n+1}) - \dot{p}(t_{n+1})] + C_M^T S^i, \tag{46}$$

$$u_i^{n+1} = u_i^n + p(t_{n+1}) - p(t_n) + d_i\varphi_n + \Delta t C_M^T S^i, \tag{47}$$

where

$$S^i = I_2^i + \nu_i I_2^v - d_i I_2^{M+1},$$

$$L^i = I_1^i - \frac{1}{b-l}\left(I_2^{M+1} - I_2^v\right),$$

$$\nu_i = \frac{\xi_i - b}{b-l},$$

$$d_i = \frac{\xi_i - l}{b-l},$$

$$\varphi_n = g(t_{n+1}) - g(t_n) - p(t_{n+1}) + p(t_n),$$

$$(u_{xx})_i^{n+1} = u_{xx}(x_i, t_{n+1}),$$

$$(u_x)_i^{n+1} = u_x(x_i, t_{n+1}),$$

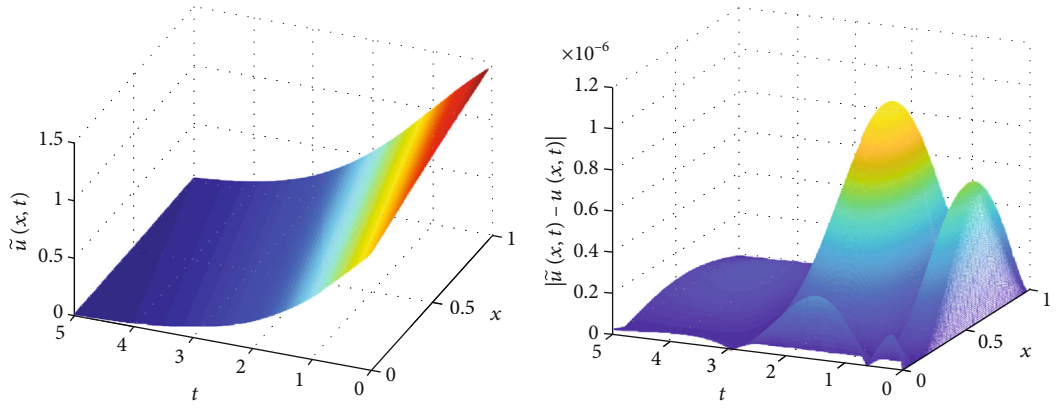

FIGURE 1: The exact solution (left) and the absolute error (right) of Example 1 with $\Delta t = 0.001$ and $h = 0.01$, without noise.

$$(u_t)_i^{n+1} = u_t(x_i, t_{n+1}),$$

$$(u)_i^{n+1} = u(x_i, t_{n+1}). \tag{48}$$

By substituting quasilinearization formulas (25)–(27) in (1), we get

$$\begin{aligned} u_t = {} & \varepsilon u_{xx} - \alpha\left(\delta(u^n)^{\delta-1}(u_x)^n u + (u^n)^\delta u_x\right) \\ & + \beta\left[(\eta+\gamma)(\delta+1)(u^n)^\delta - \eta(2\delta+1)(u^n)^{2\delta} - \gamma\right]u \\ & + \alpha\delta(u^n)^\delta(u_x)^n + \beta\left[2\eta\delta(u^n)^{2\delta+1} - (\eta+\gamma)\delta(u^n)^{\delta+1}\right]. \end{aligned} \tag{49}$$

Finally, substituting the approximation formulas (44)–(47) into (49) yields

$$C_M^T Z_i^n = \sigma_i^n, \tag{50}$$

where

$$\begin{aligned} Z_i^n = {} & \Delta t\left(\alpha(u_i^n)^\delta L^i - \varepsilon\Pi_M(\xi_i)\right) \\ & + (1 - \Delta t w_i^n)S^i, \end{aligned}$$

$$\begin{aligned} \sigma_i^n = {} & r_i^n + \varepsilon(u_{xx})_i^n - \dot{p}(t_{n+1}) \\ & - d_i(\dot{g}(t_{n+1}) - \dot{p}(t_{n+1})) \\ & - \alpha(u_i^n)^\delta\left((u_x)_i^n + \frac{1}{b-l}\varphi_n\right) \\ & + w_i^n(u_i^n + p(t_{n+1}) \\ & - p(t_n) + d_i\varphi_n), \end{aligned}$$

$$\begin{aligned} r_i^n = {} & \alpha\delta(u_i^n)^\delta(u_x)_i^n + \beta \\ & \cdot\left[2\eta\delta(u_i^n)^{2\delta+1} - (\eta+\gamma)\delta(u_i^n)^{\delta+1}\right], \end{aligned}$$

$$\begin{aligned} w_i^n = {} & \beta\Big[(\eta+\gamma)(\delta+1)(u_i^n)^\delta \\ & - \eta(2\delta+1)(u_i^n)^{2\delta} - \gamma\Big] \\ & - \alpha\delta(u_i^n)^{\delta-1}(u_x)_i^n. \end{aligned} \tag{51}$$

By organizing (50) with respect to $i = -1, 0, \cdots, M+1$, we obtain

$$Z^n C_M = R^n, \tag{52}$$

where

$$\begin{aligned} Z^n &= (Z_{-1}^n, Z_0^n, \cdots, Z_{M+1}^n)^T, \\ R^n &= (\sigma_{-1}^n, \sigma_0^n, \cdots, \sigma_{M+1}^n)^T. \end{aligned} \tag{53}$$

Note that for $n = 0$, we use equation (2) as $u_{xx}(x_i, t_0) = f''(x_i)$, $u_x(x_i, t_0) = f'(x_i)$, and $u(x_i, t_0) = f(x_i)$; otherwise, $u_{xx}(x_i, t_n)$, $u_x(x_i, t_n)$, and $u(x_i, t_n)$, are updated using (44), (45), and (47), respectively.

4. Numerical Examples

All examples in this section are solved once with the exact values of the right-hand metallurgy side vector R^0 and again by adding noise to it. We add the noise to the vector R^n in the form $R_\varepsilon^n = R^n + \vartheta \times \text{randn}(M+3)$, where ϑ is an absolute noise level and $\text{randn}(M+3)$ is a normal distribution vector with zero mean and unit standard deviation, and it is realized using the MATLAB function randn. In this article, we consider four noise levels $\vartheta = 0.0001, 0.001, 0.01$, and 0.1.

In the case that noise is added to the system (52), we will use the Tikhonov regularization method [27] to solve the system. By this technique, we have a minimization problem as follows:

$$\min_{x\in\mathbb{R}^{M+3}} \|Z^n C_M - R_\vartheta^n\|_2^2 + \lambda\|C_M\|_2^2, \tag{54}$$

where $\lambda > 0$ is the regularization parameter, which controls the trade-off between fidelity to the data and smoothness of

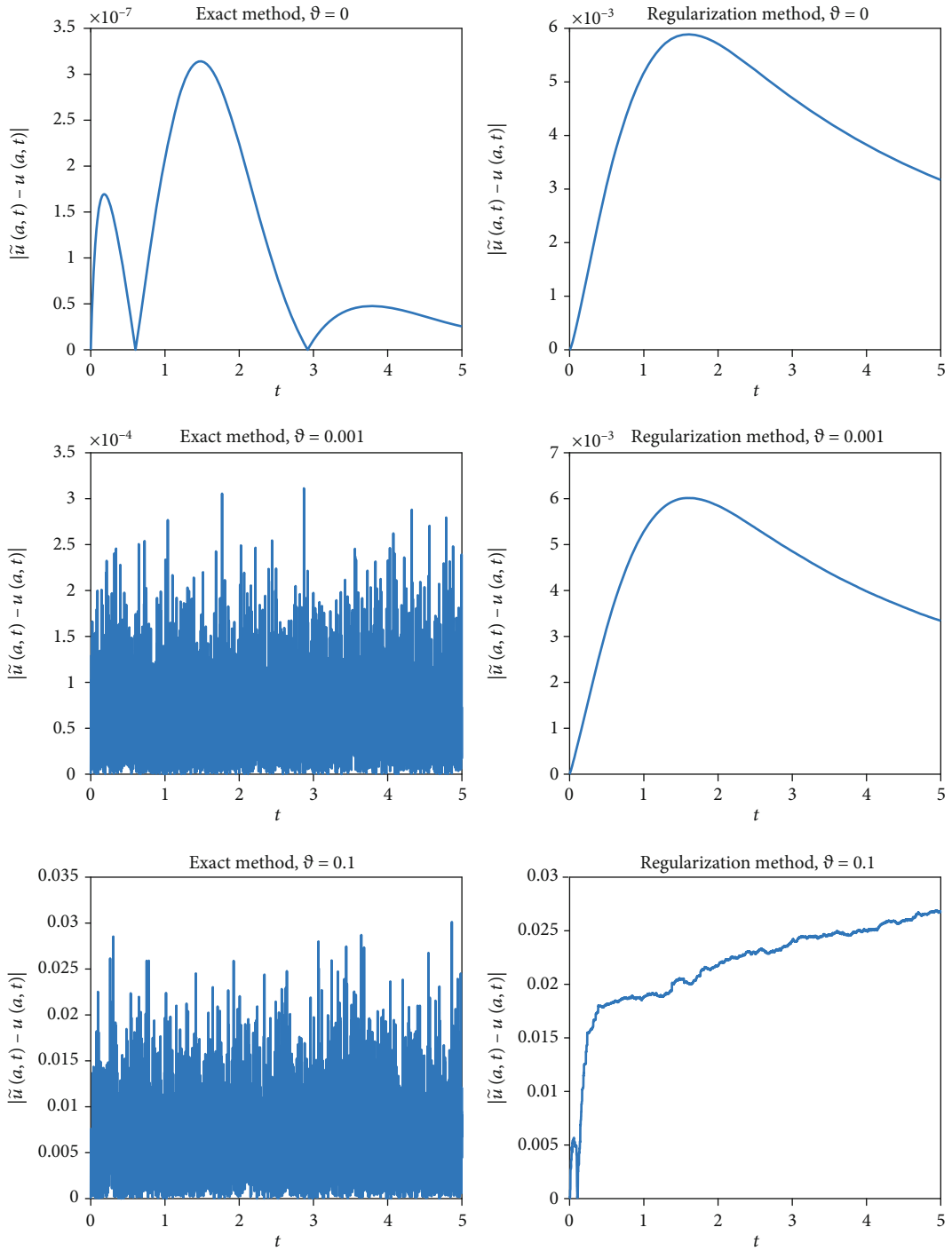

FIGURE 2: The absolute errors $|\tilde{u}(a,t) - u(a,t)|$, with the exact and regularization methods and different values of noises for Example 1 using $\Delta t = 0.001$ and $h = 0.05$.

Table 1: L_∞ errors of Example 1 for different values of Δt and ϑ with $h = 0.05$.

ϑ	Method	$\Delta t = \frac{1}{10}$	$\Delta t = \frac{1}{100}$	$\Delta t = \frac{1}{500}$	$\Delta t = \frac{1}{1000}$
0	Exact	$2.814715e-05$	$2.583762e-06$	$6.155098e-07$	$3.141230e-07$
0.0001	Exact	$3.621854e-05$	$1.145132e-05$	$1.462985e-05$	$3.314704e-05$
0.0001	Regularization	$4.802055e-05$	$1.106724e-05$	$4.894096e-03$	$5.889474e-03$
0.001	Exact	$1.049879e-04$	$1.147022e-04$	$1.588327e-04$	$3.328792e-04$
0.001	Regularization	$1.198265e-04$	$1.262147e-04$	$4.903954e-03$	$6.321994e-03$
0.01	Exact	$7.991674e-04$	$1.013317e-03$	$1.543202e-03$	$3.522300e-03$
0.01	Regularization	$6.676744e-04$	$1.020415e-03$	$5.201666e-03$	$6.770758e-03$
0.1	Exact	$1.134644e-02$	$1.124839e-02$	$1.672706e-02$	$3.645521e-02$
0.1	Regularization	$8.608509e-03$	$8.209530e-03$	$1.927866e-02$	$2.575360e-02$

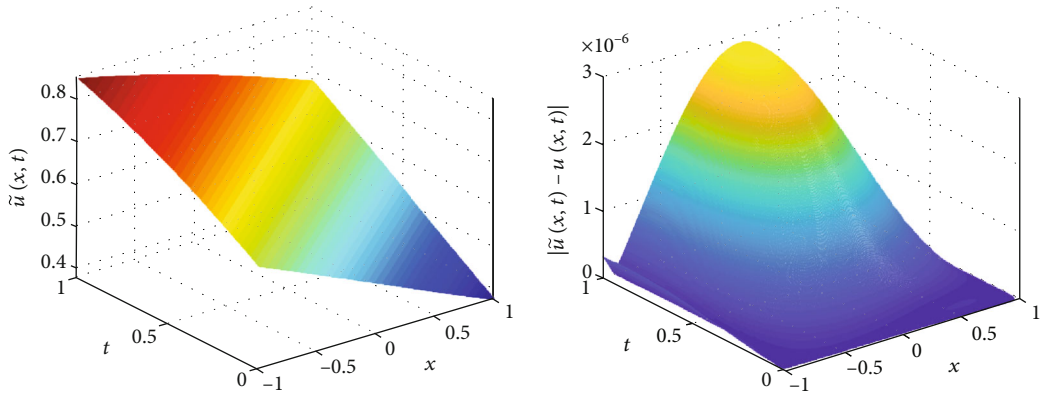

Figure 3: The exact solution (left) and the absolute error (right) of Example 2 with $\Delta t = 0.001$ and $h = 0.01$, without noise.

Table 2: L_∞ errors of Example 2 for different values of Δt and ϑ with $h = 0.05$.

ϑ	Method	$\Delta t = \frac{1}{10}$	$\Delta t = \frac{1}{100}$	$\Delta t = \frac{1}{500}$	$\Delta t = \frac{1}{1000}$
0	Exact	$3.612476e-05$	$2.959095e-06$	$6.619158e-07$	$3.353989e-07$
0.0001	Exact	$4.699528e-05$	$1.248949e-05$	$2.062944e-05$	$3.238930e-05$
0.0001	Regularization	$2.624024e-05$	$1.202468e-05$	$2.387568e-04$	$2.749732e-04$
0.001	Exact	$1.183073e-04$	$1.362642e-04$	$1.925736e-04$	$4.107127e-04$
0.001	Regularization	$1.363059e-04$	$8.611165e-05$	$2.450763e-04$	$3.206762e-04$
0.01	Exact	$1.525685e-03$	$1.297835e-03$	$1.956289e-03$	$3.485143e-03$
0.01	Regularization	$7.281806e-04$	$6.885447e-04$	$7.839071e-04$	$2.761185e-03$
0.1	Exact	$7.399248e-03$	$1.083570e-02$	$2.062804e-02$	$3.805156e-02$
0.1	Regularization	$9.402128e-03$	$9.843907e-03$	$1.193822e-02$	$2.510321e-02$

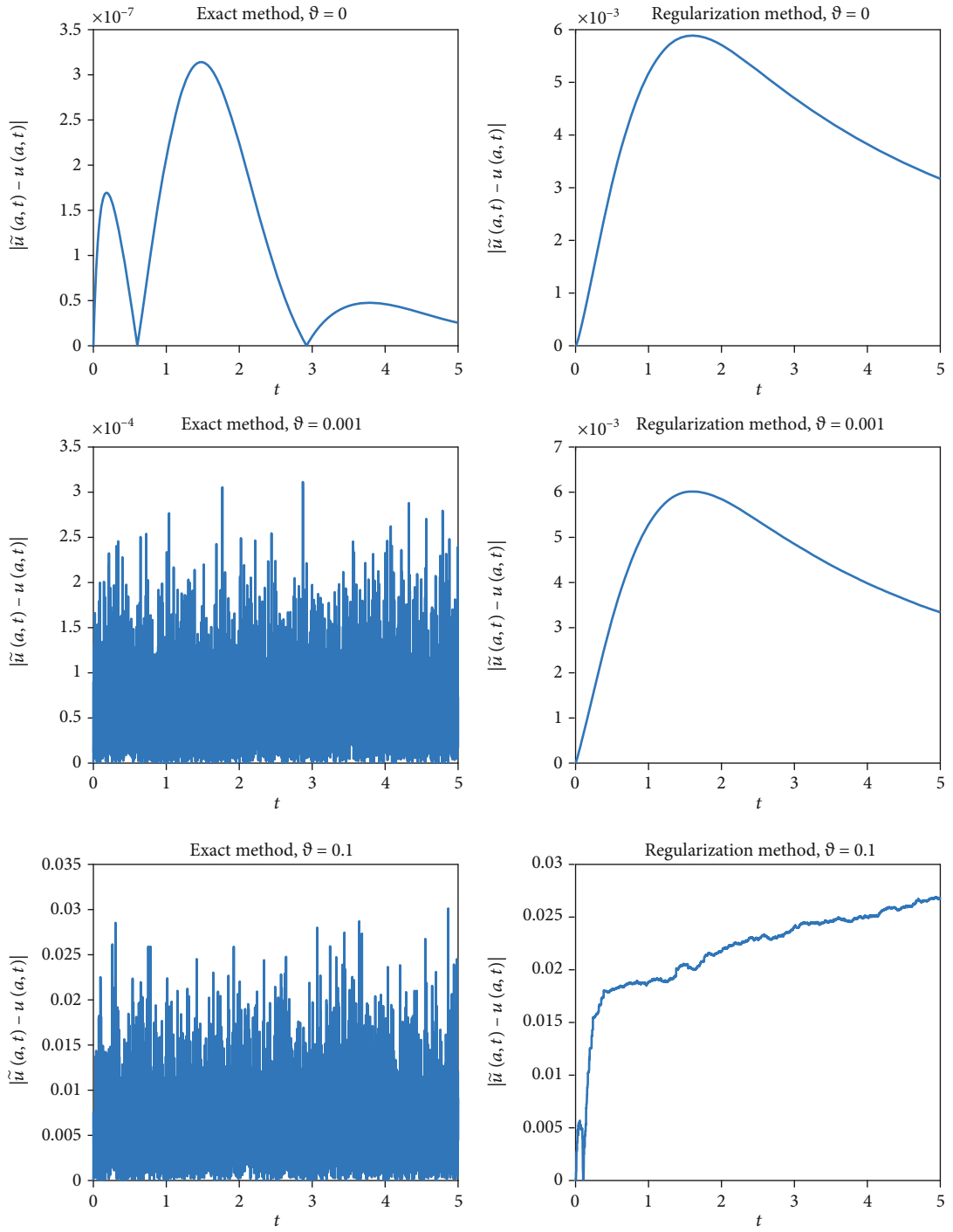

FIGURE 4: The absolute errors $|\tilde{u}(a,t) - u(a,t)|$, with the exact and regularization methods and different values of noises for Example 2 using $\Delta t = 0.001$ and $h = 0.05$.

Table 3: L_∞ errors of Example 3 for different values of Δt and ϑ with $h = 0.05$.

ϑ	Method	$\Delta t = \frac{1}{10}$	$\Delta t = \frac{1}{100}$	$\Delta t = \frac{1}{500}$	$\Delta t = \frac{1}{1000}$
0	Exact	$4.816528e-06$	$4.792704e-07$	$9.580090e-08$	$4.789637e-08$
0.0001	Exact	$2.351403e-05$	$2.514832e-05$	$4.071947e-05$	$7.494035e-05$
0.0001	Regularization	$2.801648e-05$	$5.715366e-05$	$1.121469e-04$	$1.220928e-04$
0.001	Exact	$1.306283e-04$	$2.291344e-04$	$3.901340e-04$	$7.325559e-04$
0.001	Regularization	$7.512398e-05$	$1.175376e-04$	$1.169995e-04$	$2.451920e-04$
0.01	Exact	$2.557327e-03$	$2.312663e-03$	$3.491372e-03$	$6.974782e-03$
0.01	Regularization	$1.193753e-03$	$4.763686e-04$	$4.462170e-04$	$2.318261e-03$
0.1	Exact	$1.812669e-02$	$2.584793e-02$	$3.202167e-02$	$7.193698e-02$
0.1	Regularization	$7.477861e-03$	$1.372036e-02$	$4.073468e-03$	$2.030713e-02$

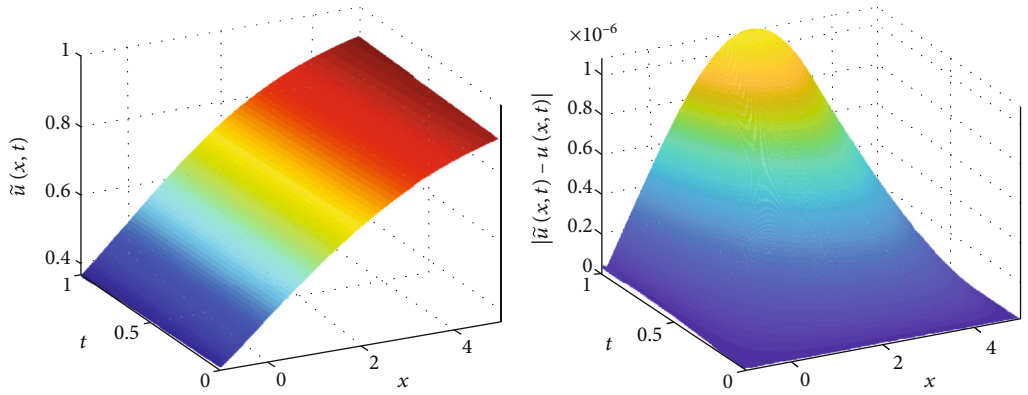

Figure 5: The exact solution (left) and the absolute error (right) of Example 3 with $\Delta t = 0.001$ and $h = 0.01$, without noise.

the solution. In this word, the generalized cross-validation (GCV) method [28] is used to determine the regularization parameter λ. In our computations, we will use the MATLAB codes developed by Hansen [29] for solving the ill-conditioned systems.

In numerical examples, we suppose that $\tilde{u}(x,t)$ denotes the exact solution and $u(x,t)$ denotes the estimated solution.

The versatility and accuracy of the methods are measured using the maximum absolute error norm L_∞, defined by [30]:

$$L_\infty = \max_{0 \le n \le N} |\tilde{u}(a,t_n) - u(a,t_n)|. \quad (55)$$

In all examples and for all different values of n and h, the conditional numbers of the coefficient matrices Z^n are less than 1000 but their smallest singular values are about 10^{-5} and relatively small. For this reason, we expect the ill-posedness of the systems to increase with increasing ϑ.

In all examples, solving the system by the decomposition method (Cholesky et al.) is called the "exact method" and solving the system using the Tikhonov regularization method is called the "regularization method."

It is notable that we perform all of the computations by MATLAB® R2019a software (V9.6.0.1072779, 64-bit (win64), License Number: 968398, MathWorks Inc., Natick, MA) running on a Sony VAIO Laptop (Intel® Core™ i5-2410M Processor 2.30 GHz with Turbo Boost up to 2.90 GHz, 8 GB of RAM, 64-bit) PC.

Example 1. We consider the problem (1)–(5) in the domain $[0,1]$ with $\varepsilon = 1$, $l = 0.1$, $T = 5$, $\eta = 1$, $\alpha = 1$, $\beta = 1$, $\gamma = 2$, and $\delta = 1$. The exact solution will be obtained using equation (6).

The exact solution and the absolute error using $\Delta t = 0.001$ and $h = 0.01$ are depicted in Figure 1. Also, the absolute errors $|\tilde{u}(a,t) - u(a,t)|$, by applying the exact and regularization methods and different values of ϑ with $\Delta t = 0.001$ and $h = 0.05$, are shown in Figure 2. In Table 1, the maximum absolute errors L_∞ are tabulated using $h = 0.05$ and different values of ϑ and Δt.

Example 2. In this example, we consider the problem (1)–(5) with $\varepsilon = 1$, $l = -0.9$, $T = 1$, $\eta = 0$, $\alpha = 1$, $\beta = 1$, $\gamma = -1$, and $\delta = 1$ in the domain $[-1,1]$. The exact solution will be obtained using equation (8).

In Figure 3, the exact solution and the absolute error using $\Delta t = 0.001$ and $h = 0.01$ are presented. In addition, the absolute errors $|\tilde{u}(a,t) - u(a,t)|$, using the exact and regularization methods and different values of ϑ with $\Delta t = 0.001$ and $h = 0.05$, are displayed in Figure 4. The L_∞ are shown using different values of ϑ and Δt and $h = 0.05$ in Table 2.

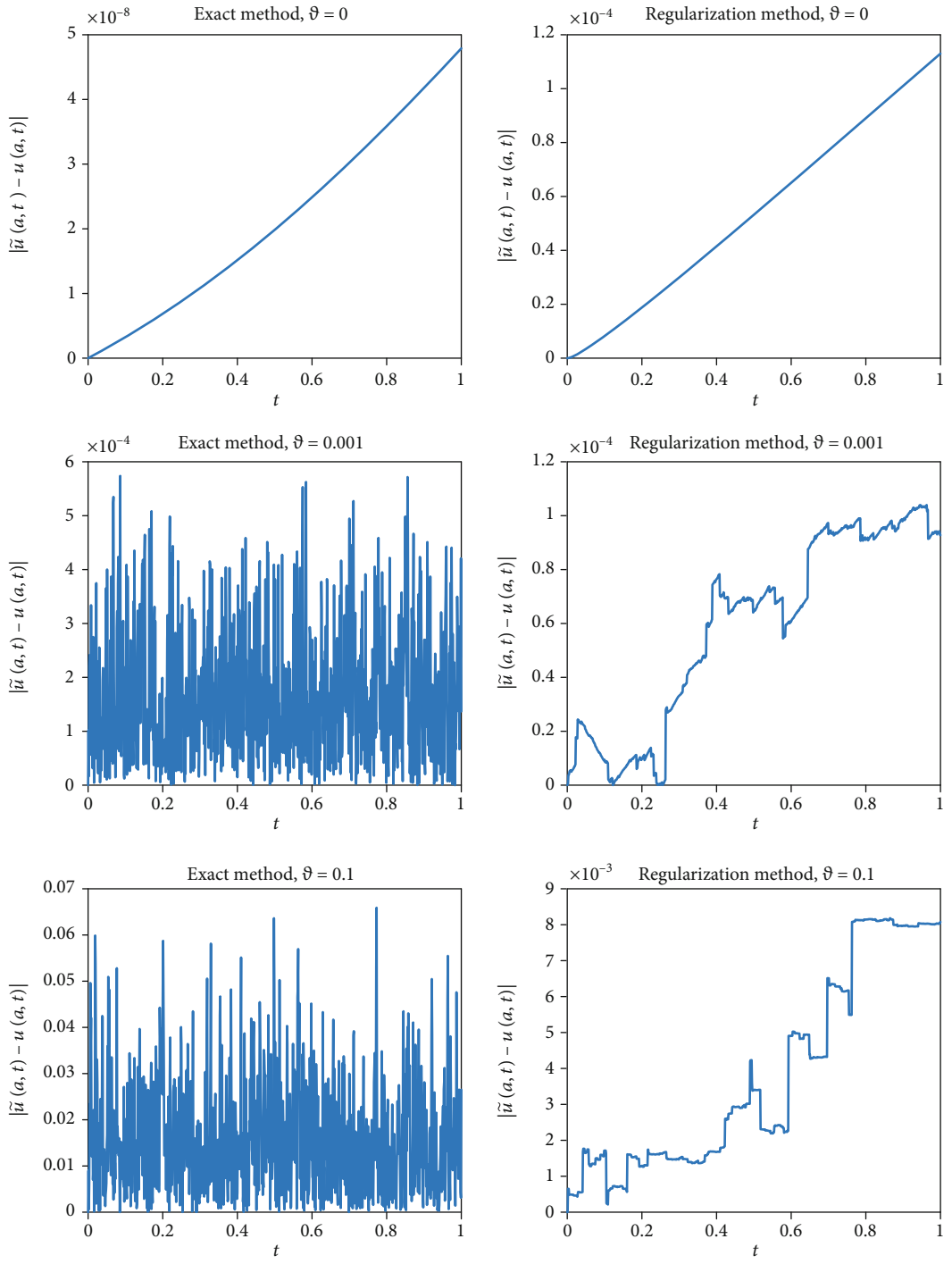

FIGURE 6: The absolute errors $|\tilde{u}(a,t) - u(a,t)|$, with the exact and regularization methods and different values of noises for Example 3 using $\Delta t = 0.001$ and $h = 0.05$.

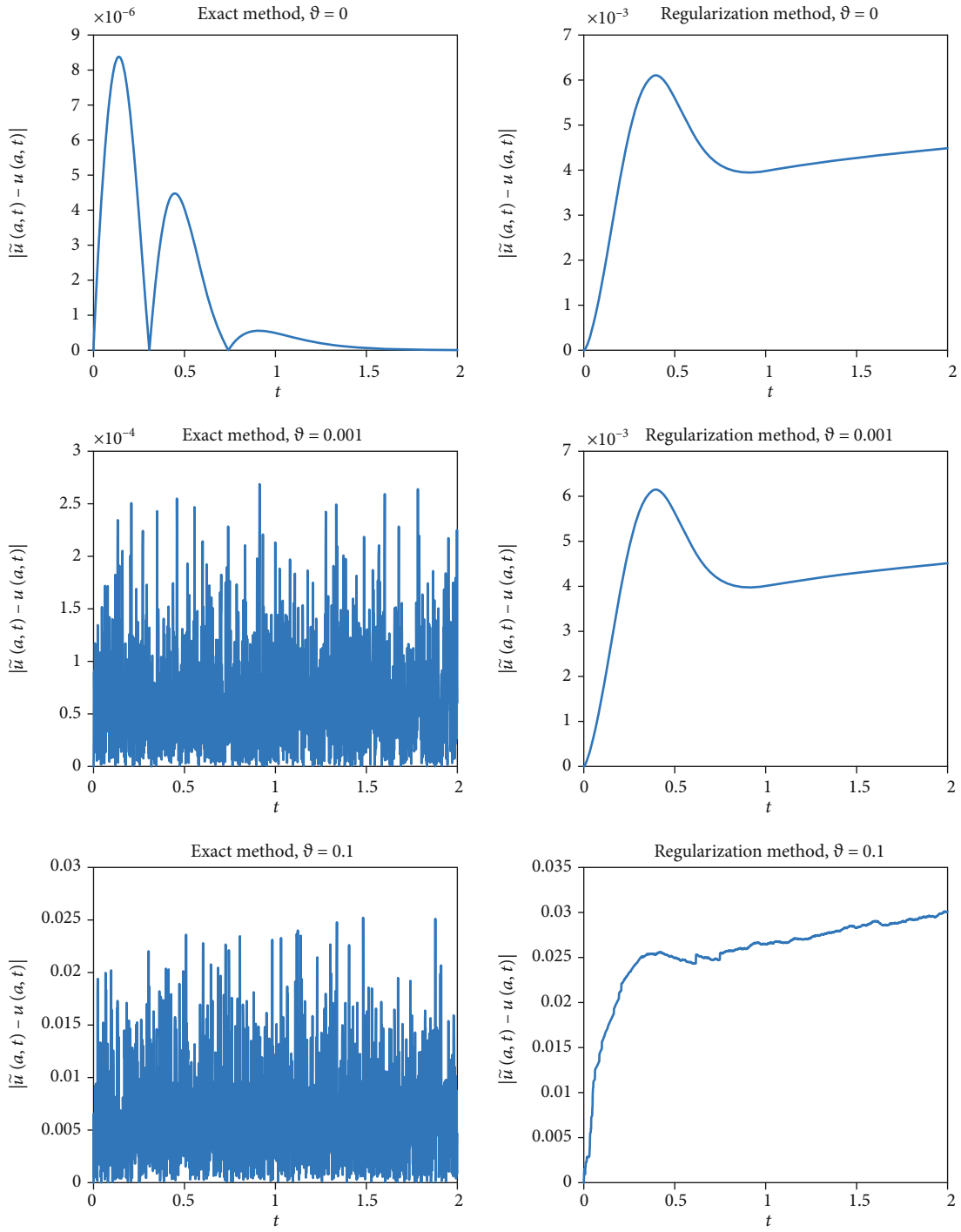

FIGURE 7: The absolute errors $|\tilde{u}(a,t) - u(a,t)|$, with the exact and regularization methods and different values of noises for Example 4 using $\Delta t = 0.001$ and $h = 0.05$.

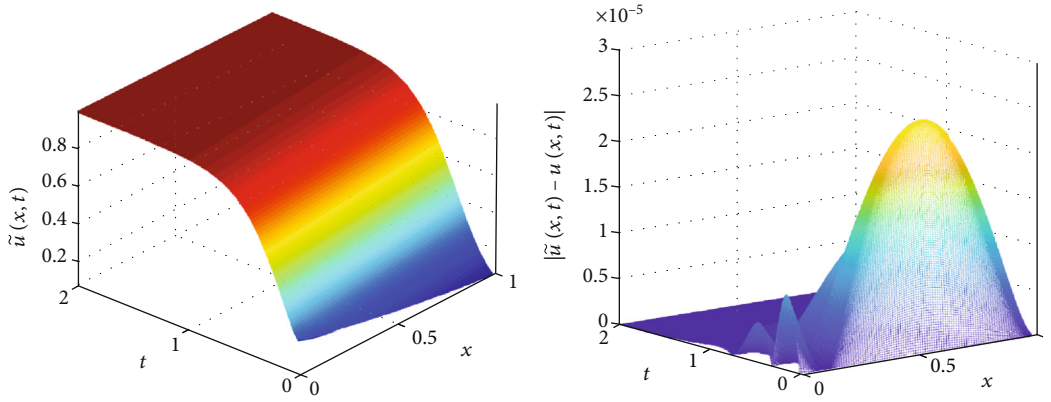

FIGURE 8: The exact solution (left) and the absolute error (right) of Example 4 with $\Delta t = 0.001$ and $h = 0.01$, without noise.

TABLE 4: L_∞ errors of Example 4 for different values of Δt and ϑ with $h = 0.05$.

ϑ	Method	$\Delta t = \frac{1}{10}$	$\Delta t = \frac{1}{100}$	$\Delta t = \frac{1}{500}$	$\Delta t = \frac{1}{1000}$
0	Exact	5.686819$e-03$	1.263590$e-04$	1.769301$e-05$	8.381687$e-06$
0.0001	Exact	5.685089$e-03$	1.327687$e-04$	3.060667$e-05$	3.335971$e-05$
0.0001	Regularization	5.332308$e-03$	1.069778$e-04$	5.492670$e-03$	6.108492$e-03$
0.001	Exact	5.701673$e-03$	1.770599$e-04$	1.672482$e-04$	2.856058$e-04$
0.001	Regularization	5.308533$e-03$	1.018102$e-04$	5.505681$e-03$	6.212021$e-03$
0.01	Exact	6.142029$e-03$	9.728911$e-04$	1.744781$e-03$	2.566482$e-03$
0.01	Regularization	5.132815$e-03$	1.078324$e-03$	4.795718$e-03$	6.132190$e-03$
0.1	Exact	1.584424$e-02$	1.078511$e-02$	1.603969$e-02$	3.379878$e-02$
0.1	Regularization	7.376052$e-03$	7.101563$e-03$	1.218363$e-02$	3.157183$e-02$

Example 3. Let $a = -1$, $b = 5$, $\varepsilon = 1$, $l = -0.9$, $T = 1$, $\eta = 1$, $\alpha = 0$, $\beta = 1$, and $\delta = 1$, in the problem (1)–(5). The exact solution of this example is given as [31]

$$u(x,t) = \frac{\gamma b_1 e^{(1/2)\left(\sqrt{2}\gamma x + \gamma^2 t\right)} + b_2 e^{(1/2)(\sqrt{2}x + t)}}{b_1 e^{(1/2)(\sqrt{2}\gamma x + \gamma^2 t)} + b_2 e^{(1/2)(\sqrt{2}x + t)} + b_3 e^{\gamma t}}, \tag{56}$$

where b_1, b_2, and b_3 are arbitrary constants. For the computation, we take $\gamma = 1/2$, $b_1 = 1$, $b_2 = 1$, and $b_3 = 1$.

The error norms L_∞ are tabulated using different values of ϑ and Δt and $h = 0.05$ in Table 3. The exact solution and the absolute error using $\Delta t = 0.001$ and $h = 0.01$ are presented in Figure 5. Moreover, the absolute errors $|\tilde{u}(a,t) - u(a,t)|$, using the exact and regularization methods and different values of ϑ with $\Delta t = 0.001$ and $h = 0.05$, are shown in Figure 6.

Example 4. We consider the problem (1)–(5) with $\varepsilon = 1$, $l = 0.1$, $T = 3$, $\eta = 0$, $\alpha = 0$, $\gamma = -1$, $\delta = 1$, $a = 0$, and $b = 1$. The exact solution is given by [32] as follows:

$$u(x,t) = \left(1 + e^{\sqrt{\beta/6}x - (5\beta/6)t}\right)^{-2}, \tag{57}$$

and we assume that $\beta = 6$.

In Figure 7, the absolute errors $|\tilde{u}(a,t) - u(a,t)|$, using the exact and regularization methods and different values of ϑ with $\Delta t = 0.001$ and $h = 0.05$, are depicted. In Figure 8, the exact solution and the absolute error using $\Delta t = 0.001$ and $h = 0.01$ are presented. The maximum absolute errors L_∞ are tabulated using $h = 0.05$ and different values of ϑ and Δt in Table 4.

5. Conclusions

The boundary value inverse problem related to the generalized Burgers–Fisher and generalized Burgers–Huxley equations was solved numerically. We considered the equation in a small time interval and then applied quasilinearization in time. We approximated the largest order of derivatives in the equation using a linear combination of B-splines. By integrating several times with respect to the time and space variables, we obtain approximations for the function and its partial derivatives. By substituting quasilinearization and the obtained approximations in the equation, a desired numerical scheme was obtained. In numerical examples, we saw that the obtained linear system from the numerical scheme has a relatively small condition number. The numerical results show that the solutions are very accurate. By adding large noise levels to the system, it was observed that the solutions were still appropriate.

Appendix

The matrices I_1B and I_2B are listed below.

$$I_1B = h\begin{pmatrix}
0 & \frac{15}{64} & \frac{1}{4} & \frac{1}{4} & \frac{1}{4} & \frac{1}{4} & \frac{1}{4} & \cdots & \frac{1}{4} & \frac{1}{4} & \frac{1}{4} \\
0 & \frac{55}{256} & \frac{7}{16} & \frac{1}{2} & \frac{1}{2} & \frac{1}{2} & \frac{1}{2} & \cdots & \frac{1}{2} & \frac{1}{2} & \frac{1}{2} \\
0 & \frac{37}{768} & \frac{13}{48} & \frac{17}{24} & \frac{3}{4} & \frac{3}{4} & \frac{3}{4} & \cdots & \frac{3}{4} & \frac{3}{4} & \frac{3}{4} \\
0 & \frac{1}{384} & \frac{1}{24} & \frac{1}{2} & \frac{23}{24} & 1 & 1 & \cdots & 1 & 1 & 1 \\
 & & & \frac{1}{24} & \frac{1}{2} & \frac{23}{24} & 1 & \cdots & 1 & 1 & 1 \\
 & & & & \ddots & \ddots & \ddots & \ddots & & & 1 \\
 & & & & & \frac{1}{24} & \frac{1}{2} & \frac{23}{24} & 1 & 1 & 1 \\
 & & & & & & \frac{1}{24} & \frac{1}{2} & \frac{23}{24} & \frac{383}{384} & 1 \\
 & & & & & & & \frac{1}{24} & \frac{23}{48} & \frac{539}{768} & \frac{3}{4} \\
 & & & & & & & & \frac{1}{16} & \frac{73}{256} & \frac{1}{2} \\
 & & & & & & & & & \frac{1}{64} & \frac{1}{4}
\end{pmatrix},$$

$$I_2B = h^2\begin{pmatrix}
0 & \frac{49}{640} & \frac{4}{20} & \frac{9}{20} & \frac{14}{20} & \frac{19}{20} & \frac{24}{20} & \cdots & \frac{4+5(2n-2)}{20} & \frac{20n-7}{40} & \frac{4+5(2n-1)}{20} \\
0 & \frac{107}{2560} & \frac{17}{80} & \frac{7}{10} & \frac{12}{10} & \frac{17}{10} & \frac{22}{10} & \cdots & \frac{7+5(2n-3)}{10} & \frac{20n-11}{20} & \frac{7+5(2n-2)}{10} \\
0 & \frac{49}{7680} & \frac{19}{240} & \frac{73}{120} & \frac{27}{20} & \frac{42}{20} & \frac{57}{20} & \cdots & \frac{27+15(2n-4)}{20} & \frac{60n-51}{40} & \frac{27+15(2n-3)}{20} \\
0 & \frac{1}{3840} & \frac{1}{120} & \frac{7}{30} & \frac{121}{120} & 2 & 3 & \cdots & 2n-3 & \frac{4n-5}{2} & 2n-2 \\
 & & & \frac{1}{120} & \frac{7}{30} & \frac{121}{120} & 2 & & 2n-4 & \frac{4n-7}{2} & 2n-3 \\
 & & & & \ddots & \ddots & \ddots & \ddots & & & \\
 & & & & & \frac{1}{120} & \frac{7}{30} & \frac{121}{120} & 2 & \frac{5}{2} & 3 \\
 & & & & & & \frac{1}{120} & \frac{7}{30} & \frac{121}{120} & \frac{5761}{3840} & 2 \\
 & & & & & & & \frac{1}{120} & \frac{11}{48} & \frac{4081}{7680} & \frac{9}{10} \\
 & & & & & & & & \frac{1}{80} & \frac{47}{512} & \frac{3}{10} \\
 & & & & & & & & & \frac{1}{640} & \frac{1}{20}
\end{pmatrix}. \tag{A.1}$$

Data Availability

All results have been obtained by conducting the numerical procedure, and the ideas can be shared with the researchers.

Conflicts of Interest

The authors declare that there are no conflicts of interest regarding the publication of this paper.

References

[1] E. Babolian and J. Saeidian, "Analytic approximate solutions to Burgers, Fisher, Huxley equations and two combined forms of these equations," *Communications in Nonlinear Science and Numerical Simulation*, vol. 14, no. 5, pp. 1984–1992, 2009.

[2] A. J. Khattak, "A computational meshless method for the generalized Burgers–Huxley equation," *Applied Mathematical Modelling*, vol. 33, no. 9, pp. 3718–3729, 2009.

[3] D. A. Hammada and M. S. El-Azab, "2N order compact finite difference scheme with collocation method for solving the generalized Burger's–Huxley and Burger's–Fisher equations," *Applied Mathematics and Computation*, vol. 258, pp. 296–311, 2015.

[4] X. Y. Wang, Z. S. Zhu, and Y. K. Lu, "Solitary wave solutions of the generalised Burgers-Huxley equation," *Journal of Physics A: Mathematical and General*, vol. 23, no. 3, pp. 271–274, 1990.

[5] H. Bateman, "Some recent researches on the motion of fluids," *Monthly Weather Review*, vol. 43, no. 4, pp. 163–170, 1915.

[6] J. M. Burgers, "A Mathematical Model Illustrating the Theory of Turbulence," in *Advances in Applied Mechanics*, pp. 171–199, Academic Press, New York, 1948.

[7] T. S. El-Danaf and A. R. Hadhoud, "Parametric spline functions for the solution of the one time fractional Burgers' equation," *Applied Mathematical Modelling*, vol. 36, no. 10, pp. 4557–4564, 2012.

[8] J. Satsuma, M. Ablowitz, B. Fuchssteiner, and M. Kruskal, *Topics in Soliton Theory and Exactly Solvable Nonlinear Equations*, World Scientific, Singapore, 1987.

[9] B. K. Singh and G. Arora, "A numerical scheme for the generalized Burgers–Huxley equation," *Journal of the Egyptian Mathematical Society*, vol. 24, no. 4, pp. 629–637, 2016.

[10] C. G. Zhu, "Numerical solution of Burgers–Fisher equation by cubic B-spline quasi-interpolation," *Applied Mathematics and Computation*, vol. 216, no. 9, pp. 2679–2686, 2010.

[11] O. P. Yadav and R. Jiwari, "Finite element analysis and approximation of Burgers–Fisher equation," *Numerical Methods for Partial Differential Equations*, vol. 33, no. 5, pp. 1652–1677, 2017.

[12] R. Jiwrai and R. C. Mittal, "A higher order numerical scheme for singularly perturbed Burger–Huxley equation," *Journal of applied mathematics & informatics*, vol. 29, pp. 813–829, 2011.

[13] R. C. Mittal and R. Jiwari, "Numerical study of Burger–Huxley equation by differential quadrature method," *Journal of Applied Mathematics and Mechanics*, vol. 5, no. 8, pp. 1–9, 2009.

[14] M. Inc, A. Yusuf, A. Isa Aliyu, and D. Baleanu, "Lie symmetry analysis and explicit solutions for the time fractional generalized Burgers–Huxley equation," *Optical and Quantum Electronics*, vol. 50, article 94, 2018.

[15] Z. Korpinar, M. Inc, A. S. Alshomrani, and D. Baleanu, "On exact special solutions for the stochastic regularized long wave–Burgers equation," *Advances in Difference Equations*, vol. 2020, no. 1, Article ID 433, 2020.

[16] S. Dhawan, S. Kapoor, S. Kumar, and S. Rawat, "Contemporary review of techniques for the solution of nonlinear Burgers equation," *Journal of Computational Science*, vol. 3, no. 5, pp. 405–419, 2012.

[17] T. Ak, S. Dhawan, and B. Inan, "Numerical solutions of the generalized Rosenau–Kawahara–RLW equation arising in fluid mechanics via B-spline collocation method," *International Journal of Modern Physics C*, vol. 29, no. 11, article 1850116, 2018.

[18] S. Dhawan, T. Ak, and G. Apaydin, "Algorithms for numerical solution of the equal width wave equation using multi-quadric quasi-interpolation method," *International Journal of Modern Physics C*, vol. 30, no. 11, article 1950087, 2019.

[19] C. De Boor, *A Practical Guide to Splines, Revised Edition*, Springer-Verlag New York, Inc, 2001.

[20] A. Kunoth, T. Lyche, G. Sangalli, and S. S. Capizzano, *Splines and PDEs: From Approximation Theory to Numerical Linear Algebra, Lecture Notes in Mathematics 2219*, Springer, Cetraro, Italy, 2017.

[21] R. Bellman and R. Kalaba, *Quasilinearization and Nonlinear Boundary–Value Problems*, Elsevier, 1965.

[22] M. El-Gebeily, "A generalized quasilinearization method for second-order nonlinear differential equations with nonlinear boundary conditions," *Journal of Computational and Applied Mathematics*, vol. 192, no. 2, pp. 270–281, 2006.

[23] B. Ahmad, J. Nieto, and N. Shahzad, "Generalized quasilinearization method for mixed boundary value problems," *Applied Mathematics and Computation*, vol. 133, no. 2-3, pp. 423–429, 2002.

[24] V. Lakshmikantham and A. Vatsala, *Generalized Quasilinearization for Nonlinear Problems*, MIA, Kluwer, Dordrecht, Boston, London, 1998.

[25] G. Hariharan and K. Kannan, "Review of wavelet methods for the solution of reaction-diffusion problems in science and engineering," *Applied Mathematical Modelling*, vol. 38, no. 3, pp. 799–813, 2014.

[26] R. Jiwari, "A Haar wavelet quasilinearization approach for numerical simulation of Burgers' equation," *Computer Physics Communications*, vol. 183, no. 11, pp. 2413–2423, 2012.

[27] A. N. Tikhonov and V. Y. Arsenin, *Solutions of Ill-Posed Problems*, Winston and Sons, Washington D.C, 1977.

[28] G. Wahba, *A Survey of Some Smoothing Problems and the Method of the Generalized Cross-Validation for Solving Them*, University of Wisconsin, Department of Statistics, 1976.

[29] P. C. Hansen, "Regularization tools: a MATLAB package for analysis and solution of discrete ill-posed problems," *Numerical Algorithms*, vol. 6, no. 1, pp. 1–35, 1994.

[30] Z. Balali, J. Rashidinia, and N. Taheri, "Numerical solution of singular boundary value problems using Green's function and Sinc-collocation method," *Journal of King Saud University*, vol. 32, no. 7, pp. 2962–2968, 2020.

[31] R. C. Mittal and A. Tripathi, "Numerical solutions of generalized Burgers–Fisher and generalized Burgers–Huxley equations using collocation of cubic B-splines," *International Journal of Computer Mathematics*, vol. 92, no. 5, pp. 1053–1077, 2014.

[32] A. M. Wazwaz and A. Gorguis, "An analytic study of Fisher's equation by using Adomian decomposition method," *Applied Mathematics and Computation*, vol. 154, no. 3, pp. 609–620, 2004.

Hindawi
Advances in Mathematical Physics
Volume 2021, Article ID 5544740, 10 pages
https://doi.org/10.1155/2021/5544740

Research Article

On Existence of Multiplicity of Weak Solutions for a New Class of Nonlinear Fractional Boundary Value Systems via Variational Approach

Fares Kamache,[1] Salah Mahmoud Boulaaras,[2,3] Rafik Guefaifia,[1] Nguyen Thanh Chung,[4] Bahri Belkacem Cherif,[2,5] and Mohamed Abdalla[6,7]

[1]*Laboratory of Mathematics, Informatics and Systems, Larbi Tebessi University, 12000 Tebessa, Algeria*
[2]*Department of Mathematics, College of Sciences and Arts, ArRass, Qassim University, Saudi Arabia*
[3]*Laboratory of Fundamental and Applied Mathematics of Oran (LMFAO), University of Oran 1, Oran, 31000 Oran, Algeria*
[4]*Department of Mathematics, Quang Binh University, 312 Ly Thuong Kiet, Dong Hoi, Quang Binh, Vietnam*
[5]*Preparatory Institute for Engineering Studies, Sfax, Tunisia*
[6]*Mathematics Department, College of Science, King Khalid University, Abha 61413, Saudi Arabia*
[7]*Mathematics Department, Faculty of Science, South Valley University, Qena 83523, Egypt*

Correspondence should be addressed to Bahri Belkacem Cherif; bahi1968@yahoo.com

Received 10 February 2021; Revised 1 March 2021; Accepted 5 March 2021; Published 13 March 2021

Academic Editor: Kamyar Hosseini

This paper deals with the existence of solutions for a new class of nonlinear fractional boundary value systems involving the left and right Riemann-Liouville fractional derivatives. More precisely, we establish the existence of at least three weak solutions for the problem using variational methods combined with the critical point theorem due to Bonano and Marano. In addition, some examples in $\mathbb{R}^3$ and $\mathbb{R}^4$ are given to illustrate the theoritical results.

1. Introduction

Fractional differential equations (FDEs) are a generalization of ordinary differential equations (ODEs), as they contain fractional derivatives whose degree is not necessarily an integer. This is what makes it receive great attention from researchers due to its ability to model some difficult and complex phenomena in many fields, including engineering, science, biology, economics, and physics (for more information, see [1–22]). One of the most investigated issues is the existence of solutions for the fractional initial and boundary value problems by using some fixed point theorems, coincidence degree theory, and monotone interactive method. Among the most important of these are the works mentioned in Oldham and Spanier and Podlubny's books (see [13, 23]) and the work of Metzler and Klafter (see [24]). Furthermore, the first to use the critical point theorem was Jiao and Zhou in [6] to study the following problem:

$$\begin{cases} {}_tD_T^{\alpha}({}_0D_t^{\alpha}u(t)) = \nabla F(t, u(t)), & \text{a.e } t \in [0, T], \\ u(0) = u(t) = 0, \end{cases} \tag{1}$$

where ${}_0D_T^{\alpha}$ and ${}_tD_T^{\alpha}$ are the left and right Riemann-Liouville fractional derivatives with $0 < \alpha \leq 1$, respectively, and $F : [0, T] \times \mathbb{R} \longrightarrow \mathbb{R}^n$ is a suitable function satisfying some hypothesis and $F(t, x)$ is the gradient of F with respect to x.

In [22], the authors have used variational methods to investigate the existence of weak solutions for the following system:

$$\begin{cases} {}_tD_T^{\alpha}(a(t){}_0D_t^{\alpha}u(t)) = \lambda F_u(t, u(t), v(t)), & \text{a.e } t \in [0, T], \\ {}_tD_T^{\beta}\left(b(t){}_0D_t^{\beta}v(t)\right) = \lambda F_v(t, u(t), v(t)), & \text{a.e } t \in [0, T], \\ u(0) = u(T) = 0, v(0) = v(T) = 0, \end{cases} \tag{2}$$

for ${}_0D_T^{\alpha}$ and ${}_tD_T^{\alpha}$ are the left and right Riemann-Liouville fractional derivatives with $0 < \alpha \leq 1$ and F_s denotes the partial derivative of F with respect to s. In [?], Zhao et al. obtained the existence of infinitely many solutions for system (2) with perturbed functions h_i, $i = 1, 2$.

Yet, there are a few findings for fractional boundary value problems which were established exploiting this approach due to its difficulty in establishing a suitable space and variational functional for fractional problems.

In this work, we shall study the existence of three weak solutions for the following system:

$$\begin{cases} {}_tD_T^{\alpha_i}\left(a_i(t){}_0D_t^{\alpha_i}u_i(t)\right) = \lambda F_{u_i}(t, u_1(t), u_2(t), \cdots, u_n(t)) + h_i(u_i(t)), & \text{a.e } t \in [0, T], \\ u_i(0) = u_i(T) = 0, \end{cases} \tag{3}$$

for $1 \leq i \leq n$, where $\alpha_i \in (0\,;1]$, ${}_0D_T^{\alpha_i}$ and ${}_tD_T^{\alpha_i}$ are the left and right Riemann–Liouville fractional derivatives of order α_i, respectively, $a_i \in L^{\infty}([0, T])$ with

$$a_{i0} = \operatorname{ess\,inf}_{[0,T]} a_i > 0, \quad \text{for } 1 \leq i \leq n, \tag{4}$$

$\lambda > 0$, $F : [0, T] \times \mathbb{R}^n \longrightarrow \mathbb{R}$ is a measurable function for all $(x_1, \cdots, x_n) \in \mathbb{R}^n$ and is C^1 with respect to $(x_1, \cdots, x_n) \in \mathbb{R}^n$ for a.e. $t \in [0, T]$, F_{u_i} denotes the partial derivative of F with respect to u_i, respectively, and $h_i : \mathbb{R} \longrightarrow \mathbb{R}$ are Lipschitz continuous functions with the Lipschitz constants $L_i > 0$, for $1 \leq i \leq n$, i.e.,

$$|h_i(x_1) - h_i(x_2)| \leq L_i|x_1 - x_2|, \tag{5}$$

for all $x_1, x_2 \in \mathbb{R}$ and $h_i(0) = 0$, for $1 \leq i \leq n$. In order to state the main results, we introduce the following conditions:

($F0$) For all $C > 0$ and any $1 \leq i \leq n$

$$\sup_{|(x_1,\cdots,x_n)|\leq C} \left|F_{u_i}(t, x_1, \cdots, x_n)\right| \in L^1([0, T]). \tag{6}$$

($F1$) $F(t\,; 0, \cdots, 0) = 0$, for a.e. $t \in [0\,; T]$.

In the present study, motivated by the results introduced in [12, 13, 25], using the three critical point theorems due to Ricceri ([26], see Theorem 2.6 in the next section), we ensure the existence of at least three solutions for system (3). For other applications of Ricceri's result for perturbed boundary value problems, the interested readers are referred to the papers [11–13, 23–25, 27].

We divided the paper as follows: in the second section, we put some preliminary facts, while in the third section we presented the main result and its proof. Finally, we proposed two practical examples of our theorem.

2. Preliminaries

In this section, introducing some necessary definitions and preliminary facts.

Definition 1 [28]. Let u be a function defined on $[0, T]$ and $\alpha_i > 0$ for $1 \leq i \leq n$. The left and right Riemann–Liouville fractional integrals of order α_i for the function u are defined by

$$\begin{aligned} {}_0D_t^{-\alpha_i}u(t) &= \frac{1}{\Gamma(\alpha_i)}\int_0^t (t-s)^{\alpha_i-1}u(s)ds, \quad t \in [0, T], \\ {}_0D_t^{-\alpha_i}u(t) &= \frac{1}{\Gamma(\alpha_i)}\int_t^T (s-t)^{\alpha_i-1}u(s)ds, \quad t \in [0, T], \end{aligned} \tag{7}$$

for $1 \leq i \leq n$, provided the RHS are pointwise given on $[0, T]$, where $\Gamma(\alpha_i)$ is the standard gamma function defined by

$$\Gamma(z) = \int_0^{+\infty} z^{\alpha_i-1}e^{-z}dz. \tag{8}$$

Definition 2 [25]. Let $0 < \alpha_i \leq 1$ for $1 \leq i \leq n$. The fractional derivative space $H_0^{\alpha_i}$ is given by the closure $C_0^{\infty}([0, T], \mathbb{R})$, that is

$$H_0^{\alpha_i} = C_0^{\infty}(\bar{[0, T]}, \mathbb{R}), \tag{9}$$

with the norm

$$\|u_i\|_{\alpha_i} = \left(\int_0^T a_i(t)\left|{}_0D_t^{\alpha_i}u_i(t)\right|^2 dt + \int_0^T |u_i(t)|^2 dt\right)^{1/2}, \tag{10}$$

for every $u_i \in H_0^{\alpha_i}$ and for $1 \leq i \leq n$.

We point out that $H_0^{\alpha_i}$ $(0 < \alpha_i \leq 1)$ is a reflexive and separable Banach space (see [22], Proposition 3.1) for details.

For every $u_i \in H_0^{\alpha_i}$, set

$$\begin{aligned} \|u_i\|_{L^s} &:= \left(\int_0^T |u_i(t)|^s dt\right)^{1/s}, \quad s \geq 1 \\ \|u_i\|_{\infty} &= \max_{t\in[0,T]} |u_i(t)|. \end{aligned} \tag{11}$$

Definition 3 [27]. We mean by a weak solution of system (3), any $u = (u_1, u_2, \cdots, u_n) \in X$ such that for all $v = (v_1, v_2, \cdots, v_n) \in X$,

$$\int_0^T \sum_{i=1}^n a_i(t)\,{}_0D_t^{\alpha_i}u_i(t)\,{}_0D_t^{\alpha_i}v_i(t)dt - \lambda\int_0^T \sum_{i=1}^n F_{u_i}(t,u_1(t),u_2(t),\cdots,u_n(t))v_i(t)dt - \int_0^T \sum_{i=1}^n h_i(u_i)v_i(t)dt = 0. \tag{12}$$

Lemma 4 [27]. *Let $0<\alpha_i\le 1$, for $1\le i\le n$. $\forall u_i\in H_0^{\alpha_i}$, we have*

$$\|u_i\|_{(L^2)} \le \frac{T^{\alpha_i}}{\Gamma(\alpha_i+1)}\left\|{}_0D_t^{\alpha_i}u_i\right\|_{L^2}. \tag{13}$$

Moreover,

$$\|u_i\|_\infty \le \frac{T^{\alpha_i}}{\Gamma(\alpha_i)\sqrt{(2\alpha_i-1)}}\left\|{}_0D_t^{\alpha_i}u_i\right\|_{L^2}. \tag{14}$$

From Lemma 4, we easily observe that

$$\|u_i\|_{L^2} \le \frac{T^{\alpha_i}}{\Gamma(\alpha_i+1)\sqrt{\alpha_{i0}}}\left(\int_0^T a_i(t)\left|{}_0D_t^{\alpha_i}u_i(t)\right|^2dt\right)^{1/2}. \tag{15}$$

for $0<\alpha_i\le 1$, and

$$\|u_i\|_\infty \le \frac{T^{\alpha_i-(1/2)}}{\Gamma(\alpha_i)\sqrt{a_{i0}(2\alpha_i-1)}}\left(\int_0^T a_i(t)\left|{}_0D_t^{\alpha_i}u_i(t)\right|^2dt\right)^{1/2}. \tag{16}$$

By using (15), the norm of (10) is equivalent to

$$\|u_i\|_{\alpha_i}\left(\int_0^T a_i(t)\left|{}_0D_t^{\alpha_i}u_i(t)\right|^2dt\right)^{1/2}, \quad \forall u_i\in H_0^{\alpha_i}. \tag{17}$$

Throughout this paper, let X be the Cartesian product of the n spaces $H_0^{\alpha_i}$ for $1\le i\le n$, i.e., $X=H_0^{\alpha_1}\times H_0^{\alpha_2}\times\cdots\times H_0^{\alpha_n}$; we equip X with the norm defined by

$$\|u\| = \sum_{i=1}^n \|u_i\|_{H_0^{\alpha_i}}, \quad u=(u_1,u_2,\cdots,u_n), \tag{18}$$

where $\|u_i\|_{H_0^{\alpha_i}}$ is given in (17). We have X compactly embedded in $C([0,T],\mathbb{R})^n$.

Theorem 5 [25]. *Let X be a reflexive real Banach space and $\Phi: X\longrightarrow\mathbb{R}$ be a coercive, continuously Gâteaux differentiable sequentially weakly lower semicontinuous functional whose Gâteaux derivative admits a continuous inverse on X^*, bounded on bounded subsets of X,$\Psi: X\longrightarrow\mathbb{R}$ a continuously Gâteaux differentiable functional whose Gâteaux derivative is compact such that*

$$\Phi(0)=\Psi(0)=0. \tag{19}$$

Suppose that $\exists r>0$ and $\bar{x}\in X$, with $r<\Phi(\bar{x})$, satisfying

(a_1) $\sup_{\Phi(u)\le r}(\Psi(u)/r) < (\Phi(\bar{x})/\Psi(\bar{x}))$.

(a_2) For each $\lambda\in\Lambda_\lambda; = (\Phi(\bar{x})/\Psi(\bar{x}), r/\sup_{\Phi(u)\le r}\Psi(u))$, the functional $\Phi-\lambda\Psi$ is coercive.

Hence, $\forall\lambda\in\Lambda_\lambda$, the functional $\Phi-\lambda\Psi$ has at least three critical points in the space X.

3. Main Results

In this section, by applying Theorem 5, we examine the existence of multiple solutions for system (3). For any $\sigma>0$, let us define

$$\pi(\sigma) = \left\{(x_1,\cdots,x_n)\in\mathbb{R}^n : \frac{1}{2}\sum_{i=1}^n |x_i|^2 \le \sigma\right\}. \tag{20}$$

This set will be used in some of our hypotheses with appropriate choices of σ. For $u=(u_1,u_2,\cdots,u_n)\in X$, we define

$$Y(u) := \sum_{i=1}^n Y_i(u_i) \tag{21}$$

where $Y_i(x)=\int_0^T H_i(x(s))ds$ and $H_i(x)=\int_0^x h_i(z)dz$ $1\le i\le n$, $\forall t\in[0;T]$ and $x\in\mathbb{R}$.

Furthermore, let

$$k := \max_{1\le i\le n}\left\{\frac{T^{2\alpha_i-1}}{(\Gamma(\alpha_i))^2 a_{i0}(2\alpha_i-1)}\right\},$$

$$M := \min_{1\le i\le n}\left\{1-\frac{L_iT^{2\alpha_i}}{(\Gamma(\alpha_i+1))^2 a_{i0}}\right\},$$

$$\tilde{k} := \max_{1\le i\le n}\left\{1+\frac{L_iT^{2\alpha_i}}{(\Gamma(\alpha_i+1))^2 a_{i0}}\right\}. \tag{22}$$

Theorem 6. *Let $1/2<\alpha_i\le 1$, for $1\le i\le n$, and suppose that $M>0$ and the conditions (F0) and (F1) are satisfied. Furthermore, assume that $\exists r>0$ and a function $\omega=(\omega_1,\omega_2,\cdots,\omega_n)\in X$ satisfying*

$$(i)\ \sum_{i=1}^n \frac{\|\omega_i\|_{\alpha_i}^2}{2} > \frac{r}{M},$$

$$(ii)\ 2r\frac{\int_0^T F(t,\omega_1,\omega_2,\cdots,\omega_n)dt}{\sum_{i=1}^n \|\omega_i\|_{\alpha_i}^2 - 2Y(\omega_1,\omega_2,\cdots,\omega_n)} - \int_0^T \max_{(x_1,\cdots,x_n)\in\pi\left(\frac{kr}{M}\right)}, \quad F(t,x_1,\cdots,x_n)dt > 0,$$

$$(iii)\ \lim_{(|x_1|,\cdots,|x_n|)\longrightarrow(+\infty,\cdots,+\infty)} \sup \frac{\sup_{t\in[0,T]} F(t,x_1,\cdots,x_n)}{\sum_{i=1}^n |x_i|^2/2} \le 0. \tag{23}$$

Then, setting

$$\Lambda = \left(\frac{\sum_{i=1}^{n}\left(\|\omega_i\|_{\alpha_i}^2/2\right) - Y(\omega_1,\omega_2,\cdots,\omega_n)}{\int_0^T F(t,\omega_1(t),\omega_2(t),\cdots,\omega_n(t))dt}, \frac{r}{\int_0^T \max_{(x_1,\cdots,x_n)\in\pi(M/kr)} F(t,x_1,\cdots,x_n)dt}\right). \tag{24}$$

$\forall\lambda\in\Lambda$ system (3) admits at least 3 weak solutions in X.

Proof. For each $u=(u_1,u_2,\cdots,u_n)\in X$, we introduce the functionals $\Phi,\Psi: X\longrightarrow\mathbb{R}$ as

$$\Phi(u)=\sum_{i=1}^{n}\frac{\|u_i\|_{\alpha_i}^2}{2} - Y(u), \tag{25}$$

$$\Psi(u)=\int_0^T F(t,u_1(t),u_2(t),\cdots,u_n(t))dt. \tag{26}$$

It is clear that Φ and Ψ are continuously Gâteaux differentiable functionals whose Gâteaux derivatives at the point $u\in X$ are defined by

$$\Phi'(u)(v)=\int_0^T\sum_{i=1}^{n} a_i(t)\,{}_0D_t^{\alpha_i}u_i(t)\,{}_0D_t^{\alpha_i}v_i(t)dt - \int_0^T\sum_{i=1}^{n}h_i(u_i(t))v_i(t)dt$$

$$\Psi'(u)(v)=\int_0^T\sum_{i=1}^{n}F_{u_i}(t,u_1(t),u_2(t),\cdots,u_n(t))v_i(t)dt, \tag{27}$$

for every $v=(v_1,v_2,\cdots,v_n)\in X$.

We have $\Phi'(u),\Psi'(u)\in X^*$, where X^* is the dual space of X. And the functional Φ is sequentially weakly lower semicontinuous and its Gâteaux derivative admits a continuous inverse on X^*; also $\lim_{\|u\|_X\longrightarrow+\infty}\Phi(u)=+\infty$ it is coercive. Now, we show that the functional Ψ is sequentially weakly upper semicontinuous and its derivative $\Psi': X\longrightarrow X^*$ is a compact operator. Let $u_m\rightharpoonup u$ in X, where $u_m(t)=(u_{m,1}(t),u_{m,2}(t),\cdots,u_{m,n}(t))$; then certainly u_m converges uniformly to u on the interval $[0,T]$. Then,

$$\begin{aligned}\limsup_{m\longrightarrow+\infty}\Psi(u_m) &\le \int_0^T \limsup_{m\longrightarrow+\infty} F(t,u_{m,1}(t),u_{m,2}(t),\cdots,u_{m,n}(t))dt\\ &= \int_0^T F(t,u_1(t),u_2(t),\cdots,u_n(t))dt=\Psi(u),\end{aligned} \tag{28}$$

which gets that Ψ is sequentially weakly upper semicontinuous.

Moreover, we have

$$\begin{aligned}&\lim_{m\longrightarrow+\infty}F(t,u_{m,1}(t),u_{m,2}(t),\cdots,u_{m,n}(t))\\ &\quad=F(t,u_1(t),u_2(t),\cdots,u_n(t)),\quad \text{for all } t\in[0,T].\end{aligned} \tag{29}$$

Note that $F(t,\cdot,\cdots,\cdot)\in C^1(\mathbb{R}^n)$. The Lebesgue control convergence theorem implies that $\Psi_m'(u)\longrightarrow\Psi'(u)$ strongly, hence yielding that Ψ' is strongly continuous on X. Then, $\Psi': X\longrightarrow X^*$ is a compact operator.

We show that required hypothesis $\Phi(\bar{x})>r$ follows from (i) and the definition of Φ by taking $\bar{x}=\omega$. Indeed, as (5) holds for all $x_1;x_2\in\mathbb{R}$ and $h_1(0)=\cdots=h_n(0)=0$; one has $|h_i(x)|\le L_i|x|$, $1\le i\le n$, for any $x\in\mathbb{R}$. It follows from (15) that

$$\begin{aligned}\Phi(\omega)&\ge\frac{\sum_{i=1}^n\|\omega_i\|_{\alpha_i}^2}{2}-\left|\int_0^T\sum_{i=1}^{n}H_i(\omega_i(t))dt\right|\\ &\ge\frac{\sum_{i=1}^n\|\omega_i\|_{\alpha_i}^2}{2}-\sum_{i=1}^{n}\frac{L_i}{2}\int_0^T|\omega_i(t)|^2dt\\ &\ge\sum_{i=1}^{n}\left(\frac{1}{2}-\frac{L_iT^{2\alpha_i}}{(\Gamma(\alpha_i+1))^2a_{i0}}\right)\|\omega_i\|_{\alpha_i}^2\\ &\ge\frac{M}{2}\sum_{i=1}^{n}\|\omega_i\|_{\alpha_i}^2.\end{aligned} \tag{30}$$

From (16), for every $u_i \in H_0^{\alpha_i}$, we have

$$\max_{t\in[0,T]} |u_i(t)|^2 \le k\|u_i\|_{\alpha_i}, \tag{31}$$

for $1 \le i \le n$. Hence,

$$\max_{t\in[0,T]} \sum_{i=1}^{n} |u_i(t)|^2 \le k \sum_{i=1}^{n} \|u_i\|_{\alpha_i}. \tag{32}$$

Assume that $u_0(t) = (0, \cdots, 0)$ and the supposition (i) deduces that $0 < r < \Phi(\omega)$ and they hold $\Phi(u_0(t)) = \Psi(u_0(t)) = 0$ from definitions (25) and (26), which are required assumptions in Theorem 5. Applying relations (16), (17), and (22) gives the following relation:

$$\begin{aligned}
\Phi^{-1}((-\infty;r]) &= \{u = (u_1, u_2, \cdots, u_n) \in X : \Phi(u) \le r\} \\
&= \left\{ u = (u_1, u_2, \cdots, u_n) \in X : \sum_{i=1}^{n} \frac{\|u_i\|_{\alpha_i}^2}{2} \le \frac{r}{M} \right\} \\
&\subseteq \left\{ u = (u_1, u_2, \cdots, u_n) \in X : \sum_{i=1}^{n} \right. \\
&\quad \left. \cdot \frac{(\Gamma(\alpha_i))^2 a_{10}(2\alpha_i - 1)}{2T^{2\alpha_i - 1}} \|u_i\|_{\infty}^2 \le \frac{r}{M} \right\} \\
&\subseteq \left\{ u = (u_1, u_2, \cdots, u_n) \in X : \frac{1}{2} \sum_{i=1}^{n} |u_i(t)|^2 \le \frac{kr}{M} \right\},
\end{aligned} \tag{33}$$

which implies that

$$\begin{aligned}
\sup_{u\in\Phi^{-1}((-\infty;r])} \Psi(u) &= \sup_{u\in\Phi^{-1}((-\infty;r])} \int_0^T F(t, u_1(t), u_2(t), \cdots, u_n(t))dt \\
&\le \int_0^T \max_{(x_1,\cdots,x_n)\in\pi\left(\frac{kr}{M}\right)} F(t, x_1, \cdots, x_n)dt.
\end{aligned} \tag{34}$$

Hence, under the condition (ii), we get the following inequality

$$\begin{aligned}
\frac{\sup_{u\in\Phi^{-1}((-\infty;r])} \Psi(u)}{r} &\le \int_0^T \max_{(x_1,\cdots,x_n)\in\pi\left(\frac{kr}{M}\right)} F(t, x_1, \cdots, x_n)dt \\
&< 2r \frac{\int_0^T F(t, \omega_1, \omega_2, \cdots, \omega_n)dt}{\sum_{i=1}^{n} \|\omega_i\|_{\alpha_i}^2 - 2Y(\omega_1, \omega_2, \cdots, \omega_n)} \\
&= r \frac{\int_0^T F(t, \omega_1, \omega_2, \cdots, \omega_n)dt}{\sum_{i=1}^{n} \left(\|\omega_i\|_{\alpha_i}^2/2 \right) - Y(\omega_1, \omega_2, \cdots, \omega_n)} \\
&= \frac{\Psi(\omega)}{\Phi(\omega)}.
\end{aligned} \tag{35}$$

Thus, the hypothesis (a_1) of Theorem 5 holds.

On the other hand, fix $0 < \varepsilon < (1/2Tk\lambda)$. From (iii) into account, there exist constants $\tau_\varepsilon \in \mathbb{R}$ such that

$$F(t, x_1, \cdots, x_n) \le \varepsilon \sum_{i=1}^{n} |x_i|^2 + \tau_\varepsilon, \tag{36}$$

for any $t \in [0, T]$ and $(x_1, \cdots, x_n) \in \mathbb{R}^n$, by using (36) and (15) yields, it follows that, for each $u \in X$,

$$\begin{aligned}
\Phi(u) - \lambda\Psi(u) &= \frac{1}{2} \sum_{i=1}^{n} \|u_i\|_{\alpha_i}^2 - \lambda \int_0^T F(t, u_1(t), u_2(t), \cdots, u_n(t))dt \\
&\ge \frac{1}{2} \sum_{i=1}^{n} \|u_i\|_{\alpha_i}^2 - T\lambda k\varepsilon \sum_{i=1}^{n} \|u_i\|_{\alpha_i}^2 - \lambda\tau_\varepsilon \\
&\ge \left(\frac{1}{2} - T\lambda k\varepsilon \right) \sum_{i=1}^{n} \|u_i\|_{\alpha_i}^2 - \lambda\tau_\varepsilon.
\end{aligned} \tag{37}$$

And from him,

$$\lim_{\|u\|_X \longrightarrow +\infty} \Phi(u) - \lambda\Psi(u) = +\infty. \tag{38}$$

Moreover, analogous to the case of $\tau_\varepsilon > 0$, we imply that $\Phi(u) - \lambda\Psi(u) \longrightarrow +\infty$ as $\|u\|_X \longrightarrow +\infty$ with $\tau_\varepsilon \le 0$. Then, the hypotheses of Theorem 5 hold, which means that system (3) admits at least 3 weak solutions in X, which completes the proof.

Now, we present some notations, before the corollary of Theorem 6.

Put

$$\begin{aligned}
A_i(\alpha_i) = \frac{16}{T^2} \Bigg\{ &\int_0^T a_i(t) t^{2(1-\alpha_i)} dt + \int_{T/4}^T a_i(t) \left(t - \frac{T}{4} \right)^{2(1-\alpha_i)} dt \\
&+ \int_{3T/4}^T a_i(t) \left(t - \frac{3T}{4} \right)^{2(1-\alpha_i)} dt - 2 \int_{T/4}^T a_i(t) \\
&\cdot \left(t^2 - \frac{T}{4} t \right)^{1-\alpha_i} dt - 2 \int_{3T/4}^T a_i(t) \left(t^2 - \frac{3T}{4} t \right)^{1-\alpha_i} dt \\
&+ 2 \int_{3T/4}^T a_i(t) \left(t^2 - Tt + \frac{3T^2}{16} t \right)^{1-\alpha_i} dt \Bigg\},
\end{aligned}$$

$$\begin{aligned}
\Delta_1 &= \min_{1\le i\le n} \{A_i(\alpha_i) \text{: for} 1 \le i \le n\}, \\
\Delta_2 &= \max_{1\le i\le n} \{A_i(\alpha_i) \text{: for} 1 \le i \le n\}.
\end{aligned} \tag{39}$$

Corollary 7. *Let $1/2 < \alpha_i \le 1$, $1 \le i \le n$ and supposition (iii) in Theorem 6 holds. Suppose that $\exists \tau > 0$ and d such that $(\tau/\Delta_1 kMn) < d^2$, and also*

$$\begin{aligned}
\left(i' \right) F(t, x_1, \cdots, x_n) \ge 0, \quad &for\ (t, x_1, \cdots, x_n) \\
&\in \left(\left[0, \frac{T}{4} \right] \cup \left[\frac{3T}{4}, T \right] \right. \\
&\left. \times [0, +\infty) \times \cdots \times [0, +\infty) \right),
\end{aligned}$$

$$(ii')\ \frac{\int_0^T \max_{(x_1,\cdots,x_n)\in\pi(\tau)} F(t,x_1,\cdots,x_n)dt}{\tau M} < \frac{\int_{T/4}^{3T/4} F(t,\Gamma(2-\alpha_1)d,\Gamma(2-\alpha_2)d,\cdots,\Gamma(2-\alpha_n)d)dt}{nk\tilde{k}\Delta_2 d^2},$$

$$(iii')\ \lim_{(|x_1|,\cdots,|x_n|)\longrightarrow(+\infty,\cdots,+\infty)} \sup \frac{\sup_{t\in[0,T]} F(t,x_1,\cdots,x_n)}{\sum_{i=1}^n |x_i|^2/2} \le 0. \tag{40}$$

Then, setting

$$\lambda \in \Lambda' = \left(\frac{n\tilde{k}\Delta_2 d^2}{\int_{T/4}^{3T/4} F(t,\Gamma(2-\alpha_1)d,\Gamma(2-\alpha_2)d,\cdots,\Gamma(2-\alpha_n)d)dt}, \frac{\tau}{k\int_0^T \max_{(x_1,\cdots,x_n)\in\pi(\tau)} F(t,x_1,\cdots,x_n)dt} \right) \tag{41}$$

Thus, system (3) admits at least three weak solutions in X.

Proof. Choose

$$\omega_i(t) = \begin{cases} \dfrac{4\Gamma(2-\alpha_i)d}{T}t, & t\in\left[0,\dfrac{T}{4}\right[, \\ \Gamma(2-\alpha_i)d, & t\in\left[\dfrac{T}{4},\dfrac{3T}{4}\right], \\ \dfrac{4\Gamma(2-\alpha_i)d}{hT}(T-t), & t\in\left]\dfrac{3T}{4},T\right]. \end{cases} \tag{42}$$

We derive

$${}_0D_t^{\alpha_i}\omega_i(t) = \begin{cases} \dfrac{4d}{T}t^{1-\alpha_i}, & t\in\left[0,\dfrac{T}{4}\right[, \\ \dfrac{4d}{T}\left(t^{1-\alpha_i}-\left(t-\dfrac{T}{4}\right)^{1-\alpha_i}\right), & t\in\left[\dfrac{T}{4},\dfrac{3T}{4}\right], \\ \dfrac{4d}{T}\left(t^{1-\alpha_i}-\left(t-\dfrac{T}{4}\right)^{1-\alpha_i}-\left(t-\dfrac{3T}{4}\right)^{1-\alpha_i}\right), & t\in\left]\dfrac{3T}{4},T\right]. \end{cases} \tag{43}$$

Moreover,

$$\begin{aligned} &\int_0^T a_i(t)\left|{}_0D_t^{\alpha_i}\omega_i(t)\right|^2 dt \\ &= \int_0^{T/4} + \int_{T/4}^{3T/4} + \int_{3T/4}^{T} a_i(t)\left|{}_0D_t^{\alpha_i}\omega_i(t)\right|^p dt \\ &= 2A_i(\alpha_i)d^2. \end{aligned} \tag{44}$$

Then, $\omega_i(0)=\omega_i(T)=0, \omega_i(t), {}_0D_t^{\alpha_i}\omega_i(t)\in L^2[0,T]$, $i=1,2,\cdots,n$; hence, $\omega=(\omega_1,\omega_2,\cdots,\omega_n)\in X$, and we have

$$\|\omega_i\|_{\alpha_i}^2 = \int_0^T a_i(t)\left|{}_0D_t^{\alpha_i}\omega_i(t)\right|^2 dt = 2A_i(\alpha_i)d^2. \tag{45}$$

By (25), for $1\le i\le n$, imply that

$$\begin{aligned} \Phi(\omega) &= \Phi(\omega_1,\omega_2,\cdots,\omega_n) \\ &= \sum_{i=1}^n \frac{\|\omega_i\|_{\alpha_i}^2}{2} - Y(\omega) \\ &\ge \frac{M}{2}\sum_{i=1}^n \|\omega_i\|_{\alpha_i}^2 \\ &= Md^2\sum_{i=1}^n A(\alpha_i) \\ &\ge nM\Delta_1 d^2. \end{aligned} \tag{46}$$

Similar to (30) and (46), we have $\Phi(\omega)\le n\tilde{k}\Delta_2 d^2$. Let $r=\tau M/k$. From $(\tau/\Delta_1 kMn)<d^2$, we have

$$\sum_{i=1}^n \frac{\|\omega_i\|_{\alpha_i}^2}{2} \ge \Phi(\omega) \ge nM\Delta_1 d^2 > nM\Delta_1 \times \frac{\tau}{\Delta_1 kMn} = \frac{r}{M}. \tag{47}$$

Thus, the assumption (ii) of Theorem 6 holds. (i') implies that

$$\begin{aligned} \Psi(\omega) &= \int_0^T F(t,\omega_1,\omega_2,\cdots,\omega_n)dt \\ &= \int_0^{T/4} F(t,\omega_1,\omega_2,\cdots,\omega_n)dt \\ &\quad + \int_{T/4}^{3T/4} F(t,\omega_1,\omega_2,\cdots,\omega_n)dt \\ &\quad + \int_{3T/4}^{T} F(t,\omega_1,\omega_2,\cdots,\omega_n)dt \\ &\ge \int_{T/4}^{3T/4} F(t,\omega_1,\omega_2,\cdots,\omega_n)dt. \end{aligned} \tag{48}$$

Moreover, by condition (ii'), we have

$$\begin{aligned}
&\frac{\int_0^T \max_{(x_1,\cdots,x_n)\in\pi(kr/M)} F(t,x_1,\cdots,x_n)dt}{r} \\
&= \frac{k\int_0^T \max_{(x_1,\cdots,x_n)\in\pi(kr/M)} F(t,x_1,\cdots,x_n)dt}{\tau M} \\
&< \frac{\int_{T/4}^{3T/4} F(t,\Gamma(2-\alpha_1)d,\Gamma(2-\alpha_2)d,\cdots,\Gamma(2-\alpha_n)d)dt}{n\tilde{k}\Delta_2 d^2} \\
&\le \frac{\int_{T/4}^{3T/4} F(t,\Gamma(2-\alpha_1)d,\Gamma(2-\alpha_2)d,\cdots,\Gamma(2-\alpha_n)d)dt}{\Phi(\omega)} \\
&\le \frac{2\int_0^T F(t,\omega_1,\omega_2,\cdots,\omega_n)dt}{\sum_{i=1}^n \|\omega_i\|_{\alpha_i}^2 - 2Y(\omega_1,\omega,\cdots,\omega_n)}.
\end{aligned} \tag{49}$$

Hence, the supposition (ii) of Theorem 6 is verified.

Moreover, the supposition (iii) of Theorem 6 holds under (iii') from $\Lambda' \subseteq \Lambda$. Theorem 6 is successfully employed to ensure the existence of at least 3 weak solutions for system (3). This completes of the proof.

4. Examples

In this section, we propose two practical examples of Theorem 6.

Example 1. Let $\alpha_1 = 0.7, \alpha_2 = 0.65, \alpha_3 = 0.6$, $a_1(t) = 1 + t^2, a_2(t) = 0.5 + t, a_3(t) = 1 + t, T = 1$. Then, system (3) gets the following form:

$$\begin{cases}
{}_tD_1^{0.7}\left(\left(1+t^2\right){}_0D_t^{0.7}u_1(t)\right) = \lambda F_{u_1}(t,u_1(t),u_2(t),u_3(t)) + h_1(u_1), & t\in[0,1], \\
{}_tD_1^{0.65}\left(\left(0.5+t\right){}_0D_t^{0.65}u_2(t)\right) = \lambda F_{u_2}(t,u_1(t),u_2(t),u_3(t)) + h_2(u_2), & t\in[0,1], \\
{}_tD_1^{0.6}\left(\left(1+t\right){}_0D_t^{0.6}u_3(t)\right) = \lambda F_{u_3}(t,u_1(t),u_2(t),u_3(t)) + h_3(u_3), & t\in[0,1], \\
u_1(0) = u_1(1) = 0, u_2(0) = u_2(1) = 0, u_3(0) = u_3(1) = 0,
\end{cases} \tag{50}$$

where $h_1(u_1) = 1/4 \sin u_1, h_2(u_2) = u_2/2$, and $h_3(u_3) = 1/20 \arctan u_3$.

Furthermore, $\forall(t; x_1, x_2, x_3) \in [0; 1] \times R^3$; put

$$F(t,x_1(t),x_2(t),x_3(t)) = \left(1+t^2\right)G(x_1,x_2,x_3), \tag{51}$$

where

$$\begin{aligned}
&G(x_1,x_2,x_3) \\
&= \begin{cases}
\left(x_1^2+x_2^2+x_3^2\right)^2, x_1^2+x_2^2+x_3^2 \le 1, \\
10\left(x_1^2+x_2^2+x_3^2\right)^{\frac{1}{2}} - 9\left(x_1^2+x_2^2+x_3^2\right)^{1/3}, x_1^2+x_2^2+x_3^2 > 1.
\end{cases}
\end{aligned} \tag{52}$$

Obviously $h_1, h_1, h_3 \longrightarrow \mathbb{R}$ are three Lipschitz continuous functions with Lipschitz constants $L_1 = 1/4, L_2 = 1/2, L_3 = 1/20$ and $h_1(0) = h_2(0) = h_3(0) = 0$. Clearly, $F(t,0,0,0) = 0, \forall t \in [0,1]$, by the direct calculation, we have $a_{10} = 1$, $a_{20} = 1$, and $a_{30} = 0.5$

$$\begin{aligned}
k &= \max\left\{\frac{1}{(\Gamma(0.7))^2(2\times0.7-1)}, \frac{1}{(\Gamma(0.65))^2(2\times0.65-1)}, \frac{1}{(\Gamma(0.6))^2\times0.5(2\times0.6-1)}\right\} \approx 4.509191, \\
M &= \min\left\{1-\frac{L_1}{(\Gamma(0.7)+1)^2}, 1-\frac{L_2}{(\Gamma(0.65)+1)^2}, 1-\frac{L_3}{(\Gamma(0.6)+1)^2\times0.5}\right\} \approx 0.912084
\end{aligned} \tag{53}$$

Taking

$$\begin{aligned}
\omega_1(t) &= \Gamma(1.3)t(1-t), \omega_2(t) \\
&= \Gamma(1.35)t(1-t), \omega_3(t) \\
&= \Gamma(1.4)t(1-t)
\end{aligned}$$

$$\begin{aligned}
{}_0D_t^{0.7}\omega_1(t) &= t^{0.3} - \frac{2\Gamma(1.3)}{\Gamma(2.3)}t^{1.3}, \\
{}_0D_t^{0.65}\omega_2(t) &= t^{0.35} - \frac{2\Gamma(1.35)}{\Gamma(2.35)}t^{1.35}, \\
{}_0D_t^{0.6}\omega_3(t) &= t^{0.4} - \frac{2\Gamma(1.4)}{\Gamma(2.4)}t^{1.4}.
\end{aligned} \tag{54}$$

By a simple calculation, we obtain

$$\begin{aligned}
\|\omega_1(t)\|_{0.7}^2 &\approx 0.130566, \|\omega_2(t)\|_{0.65}^2 \\
&\approx 0.078559, \|\omega_3(t)\|_{0.6}^2 \\
&\approx 0.102638.
\end{aligned} \tag{55}$$

Select $r = 1\times10^{-3}$, we find

$$\begin{aligned}
&\|\omega_1(t)\|_{0.7}^2 + \|\omega_2(t)\|_{0.65}^2 + \|\omega_3(t)\|_{0.6}^2 \\
&\approx 0.311763 > \frac{2r}{M} \approx 0.002192.
\end{aligned} \tag{56}$$

We deduce that the supposition (i) holds, and

$$\frac{\int_0^1 \max_{(x_1,x_2,x_3)\in\pi(kr/M)} F(t,x_1,x_2,x_3)dt}{r} = \frac{16k^2r}{3M^2} \approx 0.130355 < \frac{2\int_0^1 F(t,\omega_1,\omega_2,\omega_3)dt}{\left(\|\omega_1(t)\|_{0.7}^2 + \|\omega_2(t)\|_{0.65}^2 + \|\omega_3(t)\|_{0.6}^2\right) - Y(\omega_1,\omega_2,\omega_3)} \approx 0.365517,$$

$$\lim_{(|x_1|,|x_2|,|x_3|)\longrightarrow(+\infty,+\infty,+\infty)} \sup \frac{\sup_{t\in[0,T]} F(t,x_1,x_2,x_3)}{\left(|x_1|^2/2\right) + \left(|x_2|^2/2\right) + \left(|x_3|^2/2\right)} = 0. \tag{57}$$

Then, suppositions (ii) and (iii) are verified. Hence, in view of Theorem 6 for every $\lambda \in]2.7359,7.6714[$, system (50) has at least 3 weak solutions in the space $X = H_0^{0.7} \times H_0^{0.65} \times H_0^{0.6}$.

Example 2. Let $\alpha_1 = 0.65, \alpha_2 = 0.75, \alpha_3 = 0.85, \alpha_4 = 0.95$, $a_1(t) = 1 + t^3$, $a_2(t) = 1 + t^2$, $a_3(t) = 0.5 + t$, $a_4(t) = 1 + t$, $T = 1$.

Hence, system (3) gives

$$\begin{cases} {}_tD_1^{0.65}\left(\left(1+t^3\right){}_0D_t^{0.65}u_1(t)\right) = \lambda F_{u_1}(t,u_1(t),u_2(t),u_3(t),u_4(t)) + h_1(u_1), & t\in[0,1],\\ {}_tD_1^{0.75}\left(\left(1+t^2\right){}_0D_t^{0.75}u_2(t)\right) = \lambda F_{u_2}(t,u_1(t),u_2(t),u_3(t),u_4(t)) + h_2(u_2), & t\in[0,1],\\ {}_tD_1^{0.85}\left((0.5+t){}_0D_t^{0.85}u_3(t)\right) = \lambda F_{u_3}(t,u_1(t),u_2(t),u_3(t),u_4(t)) + h_3(u_3), & t\in[0,1],\\ {}_tD_1^{0.95}\left((1+t){}_0D_t^{0.95}u_4(t)\right) = \lambda F_{u_4}(t,u_1(t),u_2(t),u_3(t),u_4(t)) + h_4(u_4), & t\in[0,1],\\ u_1(0) = u_1(1) = 0, u_2(0) = u_2(1) = 0, u_3(0) = u_3(1) = 0, u_4(0) = u_4(1) = 0. \end{cases} \tag{58}$$

Taking

$$\begin{aligned} \omega_1(t) &= \Gamma(1.35)t(1-t), \omega_2(t)\\ &= \Gamma(1.25)t(1-t), \omega_3(t)\\ &= \Gamma(1.15)t(1-t), \omega_4(t)\\ &= \Gamma(1.05)t(1-t). \end{aligned} \tag{59}$$

Moreover, for all $(t; x_1, x_2, x_3, x_4) \in [0;1]\times R^4$, put

$$F(t,x_1(t),x_2(t),x_3(t),x_4(t)) = \left(1+t^2\right)G(x_1,x_2,x_3,x_4), \tag{60}$$

where

$$G(x_1,x_2,x_3,x_4) = \begin{cases} \left(x_1^2+x_2^2+x_3^2+x_4^2\right)^2, x_1^2+x_2^2+x_3^2+x_4^2 \le 1,\\ 10\left(x_1^2+x_2^2+x_3^2+x_4^2\right)^{\frac{1}{2}} - 9\left(x_1^2+x_2^2+x_3^2+x_4^2\right)^{\frac{1}{3}}, x_1^2+x_2^2+x_3^2+x_4^2 > 1. \end{cases} \tag{61}$$

Obviously $h_1, h_1, h_3, h_4 \longrightarrow \mathbb{R}$ are three Lipschitz continuous functions, $h_1(u_1) = 1/4 \sin u_1$, $h_2(u_2) = u_2/20$ and $h_3(u_3) = 1/100 \arctan u_3$, $h_4(u_4) = 1/10 \ln(u_4+1)$ for all $u_1, u_2, u_3, u_4 \in \mathbb{R}$ with Lipschitz constants $L_1 = 1/4, L_2 = 1/20, L_3 = 1/100, L_4 = 1/10$ and $h_1(0) = h_2(0) = h_3(0) = h_4(0) = 0$. Clearly, $F(t,0,0,0,0) = 0$ for any $t \in [0,1]$, $a_{10} = 1$, $a_{20} = 0.5$, $a_{30} = 1$, and $a_{40} = 1$

The direct calculation, gives

$$k = \max\left\{\frac{1}{(\Gamma(0.65))^2(2\times0.65-1)}, \frac{1}{(\Gamma(0.75))^2\times0.5(2\times0.75-1)}, \frac{1}{(\Gamma(0.85))^2(2\times0.85-1)}, \frac{1}{(\Gamma(0.95))^2(2\times0.95-1)}\right\} \approx 2.663742,$$

$$M = \min\left\{1 - \frac{L_1}{(\Gamma(0.65)+1)^2}, 1 - \frac{L_2}{(\Gamma(0.75)+1)^2\times0.5}, 1 - \frac{L_3}{(\Gamma(0.85)+1)^2}, 1 - \frac{L_4}{(\Gamma(0.95)+1)^2}\right\} \approx 0.956042,$$

$${}_0D_t^{0.65}\omega_1(t) = t^{0.35} - \frac{2\Gamma(1.35)}{\Gamma(2.35)}t^{1.35},$$

$${}_0D_t^{0.75}\omega_2(t) = t^{0.25} - \frac{2\Gamma(1.25)}{\Gamma(2.25)}t^{1.25},$$

$${}_0D_t^{0.85}\omega_3(t) = t^{0.15} - \frac{2\Gamma(1.15)}{\Gamma(2.15)}t^{1.15},$$

$$ {}_0D_t^{0.95}\omega_3(t) = t^{0.05} - \frac{2\Gamma(1.05)}{\Gamma(2.05)}t^{1.05}. \tag{62} $$

So that

$$ \begin{aligned} \|\omega_1(t)\|_{0.65}^2 &\approx 0.104555, \|\omega_2(t)\|_{0.75}^2 \\ &\approx 0.158153, \|\omega_3(t)\|_{0.85}^2 \\ &\approx 0.170894, \|\omega_4(t)\|_{0.95}^2 \\ &\approx 0.397611. \end{aligned} \tag{63} $$

Select $r = 1 \times 10^{-3}$; we find

$$ \begin{aligned} &\|\omega_1(t)\|_{0.65}^2 + \|\omega_2(t)\|_{0.75}^2 \\ &\quad + \|\omega_3(t)\|_{0.85}^2 + \|\omega_4(t)\|_{0.95}^2 \\ &\approx 0.831213 > \frac{2r}{M} \approx 0.002092. \end{aligned} \tag{64} $$

We deduce that the supposition (i) holds, and

$$ \begin{aligned} &\frac{\int_0^1 \max_{(x_1,x_2,x_3,x_4)\in\pi(kr/M)} F(t,x_1,x_2,x_3,x_4)dt}{r} = \frac{16k^2r}{3M^2} \approx 0.041403 \\ &< \frac{2\int_0^1 F(t,\omega_1,\omega_2,\omega_3,\omega_4)dt}{\left(\|\omega_1(t)\|_{0.65}^2 + \|\omega_2(t)\|_{0.75}^2 + \|\omega_3(t)\|_{0.85}^2 + \|\omega_4(t)\|_{0.95}^2\right) - Y(\omega_1,\omega_2,\omega_3,\omega_4)} \approx 0.135277, \\ &\lim_{(|x_1|,|x_2|,|x_3|,|x_4|)\longrightarrow(+\infty,+\infty,+\infty,+\infty)} \sup \frac{\sup_{t\in[0,T]} F(t,x_1,x_2,x_3,x_4)}{\left(|x_1|^2/2\right) + \left(|x_2|^2/2\right) + \left(|x_3|^2/2\right) + \left(|x_4|^2/2\right)} = 0. \end{aligned} \tag{65} $$

Then, suppositions (ii) and (iii) are verified. Hence, in view of Theorem 6 for every $\lambda \in]7.3922,24.1528[$, system (58) has at least 3 weak solutions in the space $X = H_0^{0.65} \times H_0^{0.75} \times H_0^{0.85} \times H_0^{0.95}$.

5. Conclusion

In this work, at least 3 weak solutions were obtained for a new class of nonlinear fractional BVPs using a critical three-point theorem due to Bonano and Marano. Some appropriate function spaces and variational frameworks were successfully created for system (3). Finally, we suggested two practical examples of Theorem 6 with a special case discussion $\mathbb{R}^3$. As for case $\mathbb{R}^4$, it was discussed. This makes our results prominent and distinct than previous ones. In the next work, we extend our recent work to the coupled system for this important problem. Also some numerical examples will be given in order to ensure the theory study by using some famous algorithms which are presented in ([28, 29]).

Data Availability

No data were used to support the study.

Conflicts of Interest

This work does not have any conflicts of interest.

Acknowledgments

The sixth author extend their appreciation to the Deanship of Scientific Research at King Khalid University for funding this work through Research Group Project under Grant No. R.G.P-2/1/42.

References

[1] H. M. Baskonus, "Complex surfaces to the fractional (2 + 1)-dimensional Boussinesq dynamical model with the local M-derivative," *The European Physical Journal Plus*, vol. 134, no. 7, p. 322, 2019.

[2] G. Bonanno and S. Marano, "On the structure of the critical set of non-differentiable functions with a weak compactness condition," *Applicable Analysis*, vol. 89, no. 1, pp. 1–10, 2010.

[3] G. W. C. Y. Ma, B. Shiri, and D. Baleanu, "New fractional signal smoothing equations with short memory and variable order," *Nonlinear Analysis*, vol. 218, p. 164507, 2020.

[4] H. E. Dadkhah, B. Shiri, and D. Baleanu, "Visco-elastic dampers in structural buildings and numerical solution with spline collocation methods," *Journal of Applied Mathematics and Computing*, vol. 63, no. 1-2, pp. 29–57, 2020.

[5] B. S. E. D. Khiabani, H. Ghaffarzadeh, and J. Katebi, "Spline collocation methods for seismic analysis of multiple degree of freedom systems with visco-elastic dampers using fractional models," *Journal of Vibration and Control*, vol. 26, no. 17-18, pp. 1445–1462, 2020.

[6] F. Jiao and Y. Zhou, "Existence results for fractional boundary value problem via critical point theory," *International Journal of Bifurcation and Chaos*, vol. 22, no. 4, article 1250086, 2012.

[7] W. Gao, P. Veeresha, D. G. Prakasha, H. M. Baskonus, and G. Ye, "A powerful approach for fractional Drinfeld-Sokolov-Wilson equation with Mittag-Leffler law," *Alexandria Engineering Journal*, vol. 58, no. 4, pp. 1301–1311, 2019.

[8] W. Gao, H. F. Ismael, S. A. Mohammed, H. M. Baskonus, and H. Bulut, "Complex and real optical Soliton properties of the paraxial non-linear Schrödinger equation in Kerr media with M-fractional," *Frontiers of Physics*, vol. 7, pp. 1–8, 2019.

[9] W. Gao, G. Yel, H. M. Baskonus, and C. Cattani, "Complex solitons in the conformable (2+1)-dimensional Ablowitz-Kaup-Newell-Segur equation," *AIMS Mathematics*, vol. 5, no. 1, pp. 507–521, 2020.

[10] G. Wei, P. Veeresha, D. G. Prakasha, H. M. Baskonus, and G. Yel, "New approach for the model describing the deathly disease in pregnant women using Mittag-Leffler function," *Solitons and Fractals*, vol. 134, p. 109696, 2020.

[11] M. J. H. J. Ul Rahman, D. Lu, and M. Ramzan, "He-Elzaki method for spatial diffusion of biological population," *Fractals*, vol. 27, no. 5, article 1950069, 2019.

[12] M. Suleman, D. Lu, J. H. He, U. Farooq, Y. S. Hui, and J. U. Rahman, "Numerical investigation of fractional HIV model using Elzaki projected differential transform method," *Fractals*, vol. 26, no. 5, article 1850062, 2018.

[13] I. Podlubny, *Fractional Differential Equations*, Academic Press, San Diego, 1999.

[14] B. Ricceri, "A three critical points theorem revisited," *Nonlinear Analysis*, vol. 70, no. 9, pp. 3084–3089, 2009.

[15] G. W. B. Shiri and D. Baleanu, "Collocation methods for terminal value problems of temperedfractional differential equations," *Applied Numerical Mathematics*, vol. 156, pp. 385–395, 2020.

[16] S. Rashid, F. Jarad, M. A. Noor, H. Kalsoom, and Y. M. Chu, "Inequalities by means of generalized proportional fractional integral operators with respect to another function," *Mathematics*, vol. 7, no. 12, pp. 1–18, 2019.

[17] S. Rashid, F. Jarad, H. Kalsoom, and Y. M. Chu, "On Pólya–Szegö and Čebyšev type inequalities via generalized k-fractional integrals," *Advances in Difference Equations*, vol. 2020, no. 1, 2020.

[18] S. Rashid, F. Jarad, and Y. M. Chu, "A note on reverse Minkowski inequality via generalized proportional fractional integral operator with respect to another function," *Mathematical Problems in Engineering*, vol. 2020, Article ID 7630260, 12 pages, 2020.

[19] E. Shivanian, "Existence of at least three distinct weak solutions for a class of nonlinear system of fractional differential equations," *Numerical Functional Analysis and Optimization*, vol. 41, no. 10, pp. 1228–1245, 2020.

[20] H. Y. Zhao and Q. Zhang, "Infinitely many solutions for fractional differential system via variational method," *Journal of Applied Mathematics and Computing*, vol. 50, no. 1-2, pp. 589–609, 2016.

[21] A. M. V. Kokilashvili and M. Ragusa, "Weighted extrapolation in grand Morrey spaces and applications to partial differential equations," *Rendiconti Lincei-Matematica e Applicazioni*, vol. 30, no. 1, pp. 67–92, 2019.

[22] H. Y. Zhao and B. Y. Qin, "Multiple solutions for a coupled system of nonlinear fractional differen-tial equations via variational methods," *Applied Mathematics and Computation*, vol. 257, pp. 417–427, 2015.

[23] K. Oldham and J. Spanier, *The Fractional Calculus Theory and Applications of Differentiationand Integration to Arbitrary Order*, Academic Press, New York, NY, 1974.

[24] R. Metzler and J. Klafter, "The restaurant at the end of the random walk: recent developments in the description of anomalous transport by fractional dynamics," *Journal of Physics A: Mathematical and General*, vol. 37, no. 31, pp. R161–R208, 2004.

[25] M. Ragusa, "Commutators of fractional integral operators on vanishing-Morrey spaces," *Journalof Global Optimization*, vol. 40, no. 1-3, pp. 361–368, 2008.

[26] B. Shiri and D. Baleanu, "Numerical solution of some fractional dynamical systems in medicineinvolving non-singular kernel with vector order," *Results in Nonlinear Analysis*, vol. 2, no. 4, pp. 160–168, 2019.

[27] B. Karaman, "Analytical investigation for modified Riemann-Louville fractional equal-with equation types based on (G '/G) expansion technique," *Miskolc Mathematical Notes*, vol. 21, no. 1, pp. 219–227, 2020.

[28] S. Boulaaras and M. Haiour, "The finite element approximation of evolutionary Hamilton-Jacobi-Bellman equations with nonlinear source terms," *Indagationes Mathematicae*, vol. 24, no. 1, pp. 161–173, 2013.

[29] S. Boulaaras and M. Haiour, "_L_ $^{\infty}$-asymptotic behavior for a finite element approximation in parabolic quasi-variational inequalities related to impulse control problem," *Applied Mathematics and Computation*, vol. 217, no. 14, pp. 6443–6450, 2011.

Hindawi
Advances in Mathematical Physics
Volume 2021, Article ID 6668355, 10 pages
https://doi.org/10.1155/2021/6668355

Research Article

Initial and Boundary Value Problems for a Class of Nonlinear Metaparabolic Equations

Huafei Di[1] **and Zefang Song**[2]

[1]*School of Mathematics and Information Science, Guangzhou University, Guangzhou, Guangdong 510006, China*
[2]*School of Economics and Statistics, Guangzhou University, Guangzhou 510006, China*

Correspondence should be addressed to Zefang Song; song_zefang@163.com

Received 18 December 2020; Revised 23 February 2021; Accepted 1 March 2021; Published 10 March 2021

Academic Editor: F. Rabiei

This paper is devoted to the initial and boundary value problems for a class of nonlinear metaparabolic equations $u_t - \beta u_{xx} - k u_{xxt} + \gamma u_{xxxx} = f(u_x)_x$. At low initial energy level ($J(u_0) < d$), we not only prove the existence of global weak solutions for these problems by the combination of the Galerkin approximation and potential well methods but also obtain the finite time blow-up result by adopting the potential well and improved concavity skills. Finally, we also discussed the finite time blow-up phenomenon for certain solutions of these problems with high initial energy.

1. Introduction

In this paper, we study the initial and boundary value problems for the following nonlinear metaparabolic equations

$$u_t - \beta u_{xx} - k u_{xxt} + \gamma u_{xxxx} = f(u_x)_x, \quad x \in \Omega,\ t > 0, \tag{1}$$

$$u(x, 0) = u_0(x), \quad x \in \Omega, \tag{2}$$

$$u(0, t) = u(1, t) = 0,\ u_{xx}(0, t) = u_{xx}(1, t) = 0, \quad t \geq 0, \tag{3}$$

in a bounded domain $\Omega = (0, 1)$, where $u_0(x)$ is the initial value function defined on Ω, $k > 0$ is the viscosity coefficient, $\gamma > 0$ is the interfacial energy parameter, and the nonlinear smooth function $f(s)$ satisfies the following assumptions:

$$\begin{cases} (i)\,|f(s)| \leq \alpha |s|^q, \quad \alpha > 0,\ 1 < q < +\infty,\ \forall s \in R, \\ (ii)\,(p+1)F(s) \geq s f(s) \text{ for some } p > 1, \quad \forall s \in R,\ F(s) = \int_0^s f(\tau) d\tau. \end{cases} \tag{4}$$

Equation (1) is a typical higher-order metaparabolic equation [1, 2], which has extensive physical background and rich theoretical connotation. This type of equation can be regarded as the regularization of Sobolev-Galpern equation by adding a fourth-order term u_{xxxx}. The Sobolev-Galpern equation appear in the study of various problems of fluid mechanics, solid mechanics, and heat conduction theory [3–5]. There have been many outstanding results about the qualitative theory for Sobolev-Galpern which include the existence, nonexistence, asymptotic behavior, regularities, and other some special properties of solutions. We also refer the reader to see [6, 7] and the papers cited therein. In (1), u is the concentration of one of the two phases, the fourth-order term γu_{xxxx} denotes the capillarity-driven surface diffusion, and the nonlinear term $f(u_x)_x$ is an intrinsic chemical potential. For example, differentiating (1) with respect to x and taking $v = u_x$, $\beta = 0$, then Equation (1) reduces to the well-known viscous Cahn-Hilliard equation

$$v_t - v_{xxt} + v_{xxxx} = \varphi(v)_{xx}, \quad x \in \Omega,\ t > 0. \tag{5}$$

Equation (5) appears in the dynamics of viscous first-order phase transitions in cooling binary solutions such as glasses, alloys, and polymer mixtures [8–10]. On the other hand, Equation (5) appears in the study of the regularization of nonclassical diffusion equations by adding a

fourth-order term v_{xxxx}. There have been many outstanding results about the qualitative theory for this type of equations [11–15]. For example, Liu and Yin [13] studied Equation (5) for $\varphi(v) = -v + \gamma_1 v^2 + \gamma_2 v^3$ in R^3; they proved the existence and nonexistence of global classical solutions and pointed out that the sign of γ_2 is crucial to the global existence of solutions. In [14], Grinfeld and Novick-Cohen studied a Morse decomposition of the stationary solutions of the one-dimensional viscous Cahn-Hilliard equation by explicit energy calculations. They also proved a partial picture of the variation in the structure of the attractor ($n = 1$) for the viscous Cahn-Hilliard equation as the mass constraint and homotopy parameter are varied. Zhao and Liu [15] considered the initial boundary problem for the viscous Cahn-Hilliard Equation (5). In their paper, the optimal control under boundary condition was given, and the existence of optimal solution was proved.

Let us mention that there is an abounding literature about the initial and boundary value problems or Cauchy problem to nonlinear parabolic and hyperbolic equations. We refer the reader to the monographs [16, 17] which devoted to the second-order parabolic and pseudoparabolic problems. For the fourth-order nonlinear parabolic and hyperbolic equations, there are also some results about the initial boundary value and Cauchy problems, especially on global existence/nonexistence, uniqueness/nonuniqueness, and asymptotic behavior [18–25]. Bakiyevich and Shadrin [21] studied the Cauchy problem of the metaparabolic equation

$$\begin{cases} u_t - \alpha u_{xx} - \gamma u_{xxt} + \beta u_{xxxx} = f(t,x), \quad x \in \mathbb{R},\ t > 0, \\ u(x,0) = \varphi(x), \quad x \in \mathbb{R}, \end{cases} \tag{6}$$

where $\alpha > 0$, $\beta \geq 0$, and $\gamma > 0$ are constants. They proved that the solutions are expressed through the sum of convolutions of functions $\varphi(x)$ and $f(t,x)$ with corresponding fundamental solutions.

In [22], Liu considered the metaparabolic equation

$$u_t - k u_{xxt} + A(u)_{xxxx} = f(x,t), \quad 0 \leq x \leq 1,\ 0 \leq t \leq T < +\infty, \tag{7}$$

where $A(u) = \int_0^u a(s)ds$, $a_0 + a_1|s|^b \leq a(s)$, and $|a''(s)| \leq a_2|s|^b$ (a_0, a_1, a_2, and b are positive constants). He proved the existence of weak solutions by using the method of continuity.

Khudaverdiyev and Farhadova [23] discussed the following fourth-order semilinear pseudoparabolic equation

$$u_t - \alpha u_{xxt} + u_{xxxx} = f(t,x,u,u_x,u_{xx},u_{xxx}), \quad 0 \leq x \leq 1,\ 0 \leq t \leq T < +\infty, \tag{8}$$

where $\alpha > 0$ is a fixed number. They proved the existence in large theorem (i.e., true for sufficiently large values of T) for generalized solution by means of Schauder stronger fixed-point principle.

In [24], Zhao and Xuan studied the generalized BBM-Burgers equation

$$u_t - \alpha u_{xx} - \gamma u_{xxt} + \beta u_{xxxx} + f(u)_x = 0, \quad x \in \mathbb{R},\ t > 0. \tag{9}$$

They obtained the existence and convergence behavior of the global smooth solutions for Equation (9).

Philippin [25] studied the following fourth-order parabolic equation

$$u_t - k_1(t)\Delta u + k_2(t)\Delta^2 u = k_3(t)u|u|^{p-1}, \quad x \in \Omega,\ t > 0, \tag{10}$$

where k_i, $i = 1, 2, 3$ are positive constants or in general positive derivable functions of time t. Under appropriate assumptions on the data, he proved that the solutions u cannot exist for all time, and an upper bound is derived.

Equation (1) is also closely connected with many equations [26–29]. For example, Yang [26] considered the initial and boundary value problems of the following equation

$$u_{tt} + \lambda u_t + \alpha u_{xxxx} = f(u_x)_x, \quad x \in (0,1),\ t > 0. \tag{11}$$

He studied the asymptotic property of the solution and gave some sufficient conditions of the blow-up. When the weak damping term u_t of Equation (11) is replaced by the strong damping term $-u_{xxt}$, we have the following fourth-order wave equation

$$u_{tt} - 2b u_{xxt} + \alpha u_{xxxx} = f(u_x)_x, \quad x \in (0,1),\ t > 0. \tag{12}$$

Chen and Lu [27] studied the initial and boundary value problems of Equation (12). They proved the existence and uniqueness of the global generalized solution and global classical solution by the Galerkin method. Furthermore, Xu et al. [28] considered the initial and boundary value problems and proved the global existence and nonexistence of solutions by adopting and modifying the so called concavity method under some conditions with low initial energy. Ali Khelghati and Khadijeh Baghaei [29] proved that the blow up for Equation (12) occurs in finite time for arbitrary positive initial energy.

Motivated by the above researches, in the present work, we mainly study the initial and boundary value problems (1)–(3) of metaparabolic equations. Hereafter, for simplicity, we set $\alpha = \beta = \gamma = 1$. Especially, the appearance of the dispersion term u_{xxt} and nonlinearity $f(u_x)_x$ for these problems cause some difficulties such that we cannot apply the normal Galerkin approximation, concavity, and potential methods directly; we have to invent some new skills and methods to overcome these difficulties.

Our paper is organized as follows. In Section 2, we introduce some functionals and potential wells and discuss the invariance of some sets which are needed for our work. In Sections 3 and 4, the existence and nonexistence of global weak solutions for problems (1)–(3) are proved by the Galerkin approximation and potential well and improved concavity methods at low initial energy ($J(u_0) < d$). Especially, the threshold result between global existence and nonexistence

is obtained under certain conditions. In the last section, we investigate the finite time blow-up for certain solutions of problems (1)–(3) with high initial energy.

2. Preliminaries

In this section, we introduce some functionals, potential wells, and important lemmas that will be needed in this paper. Throughout this paper, the following abbreviations are used for precise statement:

$$\begin{aligned} L^q(\Omega) &= L^q,\ W^{m,q}(\Omega) = W^{m,q}, \\ H^m(\Omega) &= W^{m,2}(\Omega) = H^m,\ H_0^m(\Omega) = H_0^m, \\ D &= \left\{u \in H^2(\Omega) | u(0,t) = u(1,t) \right. \\ &\quad \left. = 0,\ u_{xx}(0,t) = u_{xx}(1,t) = 0\right\}, \\ \|u\|_{L^q(\Omega)} &= \|u\|_q,\ \|u\|_{W^{m,q}(\Omega)} \\ &= \|u\|_{W^{m,q}},\ \|u\|_{H_0^m(\Omega)} = \|u\|_{H_0^m}. \end{aligned} \tag{13}$$

And the notation $(\cdot, \cdot)$ for the L^2-inner product will also be used for the notation of duality paring between dual spaces.

First of all, let us consider the functionals as follows. The "total energy" and "potential energy" associated with the problems (1)–(3) are defined by

$$\begin{aligned} E(t) &:= E(u(t)) = \int_0^t \|u_t(\tau)\|_{H^1}^2 d\tau + \frac{1}{2}\|u_x\|_{H^1}^2 + \int_\Omega F(u_x)dx, \\ J(u) &= \frac{1}{2}\|u_x\|_{H^1}^2 + \int_\Omega F(u_x)dx, \\ I(u) &= \|u_x\|_{H^1}^2 + \int_\Omega f(u_x)u_x dx. \end{aligned} \tag{14}$$

Then, by simple calculation, it follows that

$$J'(u) = \frac{d}{dt}J(u) = -\|u_t(t)\|_{H^1}^2 \le 0, \tag{15}$$

$$E(t) = J(u) + \int_0^t \|u_t(\tau)\|_{H^1}^2 d\tau = J(u_0) = E(0). \tag{16}$$

The corresponding "Nehari manifold" and "potential well depth" are given by

$$\begin{aligned} N &= \left\{u \in D \cap W^{1,q+1}(\Omega) | I(u) = 0,\ u \ne 0\right\}, \\ d &= \inf_{u \in N}(J(u)). \end{aligned} \tag{17}$$

In addition, we define

$$\begin{aligned} N^+ &= \left\{u \in D \cap W^{1,q+1}(\Omega) | I(u) > 0\right\} \cup \{0\}, \\ N^- &= \left\{u \in D \cap W^{1,q+1}(\Omega) | I(u) < 0\right\}. \end{aligned} \tag{18}$$

To obtain the results of this paper, we also introduce so called stable and unstable sets:

$$\begin{aligned} W &= \left\{u \in D \cap W^{1,q+1}(\Omega) | I(u) > 0, J(u) < d\right\} \cup \{0\}, \\ V &= \left\{u \in D \cap W^{1,q+1}(\Omega) | I(u) < 0, J(u) < d\right\}. \end{aligned} \tag{19}$$

Next, we shall give the following some essential lemmas which are important to obtain the main results of this paper.

Lemma 1. *Let $f(s)$ satisfy (4), $u \in D \cap W^{1,q+1}(\Omega)$, then the following hold:*

(1) If $0 < \|u_x\|_{H^1} < \gamma_0$, then $u \in N^+ (u \ne 0)$;

(2) If $u \in N^-$, then $\|u_x\|_{H^1} > \gamma_0$

(3) If $u \in N$, then $\|u_x\|_{H^1} \ge \gamma_0$, where

$$\begin{aligned} \gamma_0 &= \left(\frac{1}{\alpha C_*^{q+1}}\right)^{1/(q-1)}, \\ C_* &= \sup \frac{\|u_x\|_{q+1}}{\|u_x\|_{H^1}}, \\ &\left(u \in D \cap W^{1,q+1}(\Omega), u \ne 0\right). \end{aligned} \tag{20}$$

Proof.

(1) If $0 < \|u_x\|_{H^1} < \gamma_0$, then

$$\begin{aligned} -\int_\Omega f(u_x)u_x dx &\le \int_\Omega |f(u_x)u_x| dx \le \alpha \int_\Omega |u_x|^{q+1} dx \\ &\le \alpha C_*^{q+1}\|u_x\|_{H^1}^{q+1} = \alpha C_*^{q+1}\|u_x\|_{H^1}^{q-1}\|u_x\|_{H^1}^2 \\ &< \|u_x\|_{H^1}^2, \end{aligned} \tag{21}$$

which gives $I(u) > 0$ or $u \in N^+ (u \ne 0)$.

(2) If $u \in N^-$, then $u \ne 0$ and

$$\|u_x\|_{H^1}^2 < -\int_\Omega f(u_x)u_x dx \le \alpha C_*^{q+1}\|u_x\|_{H^1}^{q-1}\|u_x\|_{H^1}^2, \tag{22}$$

which gives $\|u_x\|_{H^1} > \gamma_0$.

(3) If $u \in N$, then from

$$\|u_x\|_{H^1}^2 = -\int_\Omega f(u_x)u_x dx \le \alpha C_*^{q+1}\|u_x\|_{H^1}^{q-1}\|u_x\|_{H^1}^2, \tag{23}$$

we have $\|u_x\|_{H^1} \ge \gamma_0$.

Lemma 2. *Let $f(s)$ satisfy (4) and $u \in N$, then*

$$d \ge d_0 = \frac{p-1}{2(p+1)}\gamma_0^2 = \frac{p-1}{2(p+1)}\left(\frac{1}{\alpha C_*^{q+1}}\right)^{2/(q-1)}. \tag{24}$$

Proof. For any $u \in N$, we have by Lemma 1 (3) that $\|u_x\|_{H^1} \geq \gamma_0$. Hence, from

$$\begin{aligned} J(u) &= \frac{1}{2}\|u_x\|_{H^1}^2 + \int_\Omega F(u_x)dx \\ &\geq \frac{1}{2}\|u_x\|_{H^1}^2 + \frac{1}{p+1}\int_\Omega f(u_x)u_x dx \\ &= \frac{p-1}{2(p+1)}\|u_x\|_{H^1}^2 + \frac{1}{p+1}I(u) \\ &= \frac{p-1}{2(p+1)}\|u_x\|_{H^1}^2 \geq \frac{p-1}{2(p+1)}\gamma_0^2, \end{aligned} \tag{25}$$

and the definition of potential depth d, we get $d \geq d_0$.

For simplicity, we define the weak solution of (1)–(3) over the interval $\Omega \times [0, T)$, but it is to be understood that T is either infinity or the limit of the existence interval.

Definition 3. We say that $u(x,t)$ is called a weak solution of the problems (1)–(3) on the interval $\Omega \times [0, T)$. If $u \in L^\infty([0,T]; D \cap W^{1,q+1}(\Omega))$, with $u_t \in L^2([0,T]; H_0^1(\Omega))$ satisfy the following conditions

(i) For any $v \in D \cap W^{1,q+1}(\Omega)$, such that

$$(u_t, v) + (u_{xt}, v_x) + (u_x, v_x) + (u_{xx}, v_{xx}) = -(f(u_x), v_x). \tag{26}$$

(ii) $u(x,0) = u_0$ in $D \cap W^{1,q+1}(\Omega)$.

(iii) The following energy inequality holds

$$J(u) \leq J(u_0), \tag{27}$$

for any $0 \leq t < T$.

Lemma 4. *Let $f(s)$ satisfy (4) and $u(x,t)$ be a solution of (1)–(3) over the interval $[0, T)$. If there exists a time $t_0 \in [0, T)$ such that $u(t_0) \in W$, then $u(t) \in W$ for any $t \in [t_0, T)$, where T is either infinity or the limit of the existence interval.*

Proof. Arguing by contradiction and considering the time continuity of $I(u)$ and $J(u)$, we suppose that there exists a time $t_1 \in [t_0, T)$ such that $u(x,t) \in W$ for any $t \in [t_0, t_1)$, but $u(t_1) \in \partial W$, which means that (1) $J(u(t_1)) = d$ or (2) $I(u(t_1)) = 0$, $\|u(t_1)\|_{H^2} \neq 0$. By (15) and $u(t_0) \in W$, we have $J(u(t_1)) \leq J(u(t_0)) < d$. It follows that case (1) is impossible. If $I(u(t_1)) = 0$, $\|u(t_1)\|_{H^2} \neq 0$, then by the definition of d, we have $J(u(t_1)) > d$ which contradicts $J(u(t_1)) \leq J(u(t_0)) < d$. The case (2) is also impossible.

Lemma 5. *Let $f(s)$ satisfy (4) and $u(x,t)$ be a solution of (1)–(3) over the interval $[0, T)$. If there exists a time $t_0 \in [0, T)$ such that $u(t_0) \in V$, then $u(t) \in V$ for any $t \in [t_0, T)$, where T is either infinity or the limit of the existence interval.*

Proof. The proof of Lemma 5 is similar to Lemma 4.

Lemma 6 (see [29, 30]). *Assume that the function $\phi(t) \in C^2$, $\phi(t) \geq 0$ satisfies*

$$\phi(t)\phi''(t) - (1+\delta)\phi'^2(t) \geq 0, \tag{28}$$

for certain real number $\delta > 0$, $\phi(0) > 0$, and $\phi'(0) > 0$. Then, there exists a real number $\tilde{T}$ with $0 < \tilde{T} \leq (\phi(0))/(\alpha\phi'(0))$ such that

$$\phi(t) \longrightarrow \infty, \quad ast \longrightarrow \tilde{T}^-. \tag{29}$$

We construct an approximate weak solution of the problems (1)-(3) by the Galerkin¡¯s method. Let $\{w_j\}_{j=1}^\infty$ be the eigenfunction system of problem

$$-w_{jxx} = \lambda w_j, \text{ in } \Omega, w_j(0) = w_j(1) = 0, j = 1, 2, \cdots. \tag{30}$$

Obviously, there exist some basis such that $\{w_j\}_{j=1}^\infty \subseteq D \cap W^{1,q+1}(\Omega)$, and it is dense in $D \cap W^{1,q+1}(\Omega)$. Now, suppose that the approximate weak solution of the problems (1)–(3) can be written

$$u_m(x,t) = \sum_{j=1}^m d_m^j(t) w_j(x). \tag{31}$$

According to Galerkin's method, these coefficients $d_m^j(t)$ need to satisfy the following initial value problem of the nonlinear differential equations

$$\begin{cases} (u_{mt}, w_j) + (u_{mxt}, w_{jx}) + (u_{mx}, w_{jx}) + (u_{mxx}, w_{jxx}) = -(f(u_{mx}), w_{jx}), \\ u_m|_{t=0} = u_{0m}(x), \end{cases} \tag{32}$$

where $u_{0m}(x) = \sum_{j=1}^m d_m^j(0) w_j(x)$, $u_{0m}(x) \longrightarrow u_0(x)$, in $D \cap W^{1,q+1}(\Omega)$.

The initial value problem (32) possesses a local solution in $[0, t_m)$, $0 < t_m < T$ for an arbitrary $T > 0$. Under some appropriate assumptions on the nonlinear terms and the initial data, we prove that the system (32) has global weak solutions in the interval $[0, T]$. Furthermore, we show that the solutions of the problems (1)–(3) can be approximated by the functions $u_m(x,t)$.

3. Existence of Global Weak Solutions

In this section, we shall prove the existence of global weak solution by the combination of the Galerkin approximation and potential well methods.

Theorem 7. *Assume that f satisfy (4), and $u_0 \in W$, then the problems (1)–(3) admits a global weak solution $u \in L^\infty([0, \infty); D \cap W^{1,q+1}(\Omega))$, with $u_t \in L^2([0,\infty); H_0^1(\Omega))$ and $u \in W$ for all $0 \leq t < \infty$.*

Proof. Multiplying (32) by $d_m^j(t)'$ and summing for $j = 1, \cdots, m$, then we have

$$(u_{mt}, u_{mt}) + (u_{mx}, u_{mxt}) + (u_{mxt}, u_{mxt}) + (u_{mxx}, u_{mxxt}) = -(f(u_{mx}), u_{mxt}). \tag{33}$$

By a direct calculation, it follows that

$$\int_0^t \|u_m(\tau)\|_{H^1}^2 d\tau + J(u_m) = J(u_{0m}), \tag{34}$$

where

$$J(u_m) = \frac{1}{2}\|u_{mx}\|_{H^1}^2 + \int_\Omega F(u_{mx})dx. \tag{35}$$

Utilizing the strong convergence of u_{0m} in $D \cap W^{1,q+1}(\Omega)$, we note that $J(u_{0m}) \longrightarrow J(u_0) < d$. Hence, we get $J(u_{0m}) < d$ for sufficiently large m. On the other hand, from $u_0 \in W$ and $u_{0m}(x) \longrightarrow u_0(x)$ in $D \cap W^{1,q+1}(\Omega)$, it follows that $u_{0m} \in W$ for sufficiently large m. Similar to the proof of Lemma 4, we have that the solution u_m constructed by (31) remains in W for $0 \le t < \infty$ and sufficiently large m.

Thus, from (4) and

$$\begin{aligned} d > J(u_m) &= \frac{1}{2}\|u_{mx}\|_{H^1}^2 + \int_\Omega F(u_{mx})dx \\ &\ge \frac{1}{2}\|u_{mx}\|_{H^1}^2 + \frac{1}{p+1}\int_\Omega f(u_{mx})u_{mx}dx \\ &\ge \frac{p-1}{2(p+1)}\|u_{mx}\|_{H^1}^2 + \frac{1}{p+1}I(u_m) \ge 0, \end{aligned} \tag{36}$$

we obtain

$$\begin{aligned} &\int_0^t \|u_m(\tau)\|_{H^1}^2 d\tau < d, \quad 0 \le t < \infty, \\ &\|u_{mx}\|_{H^1}^2 < \frac{2(p+1)}{p-1}d, \quad 0 \le t < \infty, \\ &\|u_{mx}\|_{q+1}^2 \le C_*^2\|u_{mx}\|_{H^1}^2 < C_*^2\frac{2(p+1)}{p-1}d, \quad 0 \le t < \infty, \\ &\|f(u_{mx})\|_r^r \le \alpha^r\|u_{mx}\|_{r+1}^{r+1} \\ &\qquad < \alpha^r C_*^{r+1}\left(\frac{2(p+1)}{p-1}d\right)^{(r+1)/2}, \quad 0 \le t < \infty, \end{aligned} \tag{37}$$

where $r = (q+1)/q$, $1/(q+1) + (1/r) = 1$. Therefore, there exist a subsequence of $\{u_m\}$ which from now on will be also denoted by $\{u_m\}$ such that as $m \longrightarrow \infty$

$$u_m \longrightarrow u \text{ in } L^\infty([0,\infty); D \cap W^{1,q+1}(\Omega)) \text{ weakly star}, \tag{38}$$

$$u_m \longrightarrow u \; a.e. Q = \Omega \times [0,\infty), \tag{39}$$

$$u_{mt} \longrightarrow u_t \text{ in } L^2([0,\infty); H_0^1(\Omega)) \text{ weakly}, \tag{40}$$

$$u_{mx} \longrightarrow u_x \text{ in } L^\infty([0,\infty); L^{q+1}(\Omega)) \text{ weakly star}, \tag{41}$$

$$f(u_{mx}) \longrightarrow \chi = f(u_x) \text{ in } L^\infty([0,\infty); L^r(\Omega)) \text{ weakly star}. \tag{42}$$

Convergences (38)–(42) permit us to pass to the limit in (32). Taking $m \longrightarrow \infty$, we obtain

$$(u_t, w_j) + (u_{xt}, w_{jx}) + (u_x, w_{jx}) + (u_{xx}, w_{jxx}) = -(f(u_x), w_{jx}), \tag{43}$$

for $j = 1, 2 \cdots$. Considering that the basis $\{w_j\}_{j=1}^\infty$ are dense in $D \cap W^{1,q+1}(\Omega)$, we choose a function $v \in L^\infty([0,\infty); D \cap W^{1,q+1}(\Omega))$ having the form $v(t) = \sum_{j=1}^\infty d^j(t)w_j$, where $\{d^j(t)\}_{j=1}^\infty$ are given functions. Multiplying (43) by $d^j(t)$ and summing $j = 1, 2, \cdots$, then we have

$$(u_t, v) + (u_{xt}, v_x) + (u_x, v_x) + (u_{xx}, v_{xx}) = -(f(u_x), v_x). \tag{44}$$

Moreover, (32) gives $u(x,0) = u_0(x)$ in $D \cap W^{1,q+1}(\Omega)$. Next, we will prove that u satisfies (27). Taking into account the nonlinear term of the functional $J(u)$, we deduce

$$\begin{aligned} &\left|\int_\Omega F(u_{mx})dx - \int_\Omega F(u_x)dx\right| \\ &\quad = \left|\int_\Omega f(u_x + \theta_m u_{mx})(u_{mx} - u_x)dx\right| \\ &\quad \le \|f(u_x + \theta_m u_{mx})\|_{q+1/q}\|u_{mx} - u\|_{q+1} \\ &\quad \le C\|u_{mx} - u_x\|_{q+1} \longrightarrow 0, \end{aligned} \tag{45}$$

as $m \longrightarrow \infty$, where $0 < \theta_m < 1$. Hence, we have

$$\lim_{m\longrightarrow\infty}\int_\Omega F(u_{mx})dx = \int_\Omega F(u_x)dx. \tag{46}$$

Then, making use of Fatou's Lemma and (34), (46), we deduce

$$\begin{aligned} \frac{1}{2}\|u_x\|_{H^1}^2 &\le \liminf_{m\longrightarrow\infty}\frac{1}{2}\|u_{mx}\|_{H^1}^2 = \liminf_{m\longrightarrow\infty}\left[J(u_m) - \int_\Omega F(u_{mx})dx\right] \\ &\le \lim_{m\longrightarrow\infty}\left[J(u_{0m}) - \int_\Omega F(u_{mx})dx\right] \\ &= J(u_0) - \int_\Omega F(u_x)dx, \end{aligned} \tag{47}$$

which yields (27). Thus, we obtain that u is a global weak solution of problems (1)–(3). Finally, making use of Lemma 4 again, we get $u(t) \in W$ for $0 \le t < \infty$.

4. Finite Time Blow-up of Solutions with $J(u_0) < d_0$

In this section, we consider the finite time blow up of solutions with $E(0) = J(u_0) < d_0$ for the problems (1)–(3).

Theorem 8. *Let f satisfy (4), and $u_0 \in D \cap W^{1,q+1}(\Omega)$. Assume that $I(u_0) < 0$ and $E(0) = J(u_0) < d_0$, where d_0 is defined in Lemma 2, then the weak solution $u(t)$ of problems (1)–(3) blow-up in finite time.*

Proof. Let $u(t)$ be any weak solution of the problems (1)–(3) with $I(u_0) < 0$ and $E(0) = J(u_0) < d_0$, $\tilde{T}$ be the maximal existence time of $u(t)$. Next, we will prove $\tilde{T} < +\infty$. Arguing by contradiction, we suppose $\tilde{T} = +\infty$. We define the function $\Psi : [0, T_1] \longrightarrow R^+$ by

$$\Psi(t) = \int_0^t \|u(\tau)\|_{H^1}^2 d\tau + (T_1 - t)\|u_0\|_{H^1}^2 + b(t + T_0)^2, \quad (48)$$

where b, T_0, and T_1 are positive constants to be chosen later. By simple calculation, we have

$$\begin{aligned}\Psi'(t) &= \|u(t)\|_{H^1}^2 - \|u_0\|_{H^1}^2 + 2b(t + T_0)\\ &= 2\int_0^t\int_\Omega u(\tau)u_t(\tau)dxd\tau\\ &\quad + 2\int_0^t\int_\Omega u_x(\tau)u_{xt}(\tau)dxd\tau + 2b(t + T_0),\\ \Psi''(t) &= 2\int_\Omega u(t)u_t(t)dx + 2\int_\Omega u_x(t)u_{xt}(t)dx + 2b.\end{aligned} \quad (49)$$

By (1), we obtain

$$\begin{aligned}\Psi''(t) &= 2\int_\Omega u\left[u_{xx} - u_{xxxx} + f(u_x)_x\right]dx + 2b\\ &= -2\|u_x\|_{H^1}^2 - 2\int_\Omega u_x f(u_x)dx + 2b.\end{aligned} \quad (50)$$

Therefore, we can get

$$\begin{aligned}&\Psi(t)\Psi''(t) - \frac{p+3}{4}\Psi'(t)^2\\ &= \Psi(t)\left[-2\|u_x\|_{H^1}^2 - 2\int_\Omega u_x f(u_x)dx + 2b\right]\\ &\quad - (p+3)\left[\int_0^t\int_\Omega u(\tau)u_t(\tau)dxd\tau\right.\\ &\quad \left. + \int_0^t\int_\Omega u_x(\tau)u_{xt}(\tau)dxd\tau + b(t + T_0)\right]^2\\ &= \Psi(t)\left[-2\|u_x\|_{H^1}^2 - 2\int_\Omega u_x f(u_x)dx + 2b\right]\\ &\quad + (p+3)\left\{\eta(t) - \left[\Psi(t) - (T_1 - t)\|u_0\|_{H^1}^2\right]\right.\\ &\quad \left.\cdot\left[\int_0^t \|u_t(\tau)\|_{H^1}^2 d\tau + b\right]\right\},\end{aligned} \quad (51)$$

where

$$\begin{aligned}\eta(t) &= \left[\int_0^t \|u(\tau)\|_{H^1}^2 d\tau + b(t + T_0)^2\right]\left[\int_0^t \|u_t(\tau)\|_{H^1}^2 d\tau + b\right]\\ &\quad - \left[\int_0^t\int_\Omega u(\tau)u_t(\tau)dxd\tau + \int_0^t\int_\Omega u_x(\tau)u_{xt}(\tau)dxd\tau\right.\\ &\quad \left. + b(t + T_0)\right]^2.\end{aligned} \quad (52)$$

Using the Schwarz and Young inequalities, we have

$$\left(\int_0^t (u(\tau), u_t(\tau))d\tau\right)^2 \le \int_0^t \|u(\tau)\|_2^2 d\tau \int_0^t \|u_t(\tau)\|_2^2 d\tau, \quad (53)$$

$$\left(\int_0^t (u_x(\tau), u_{xt}(\tau))d\tau\right)^2 \le \int_0^t \|u_x(\tau)\|_2^2 d\tau \int_0^t \|u_{xt}(\tau)\|_2^2 d\tau, \quad (54)$$

$$\begin{aligned}&\int_0^t (u(\tau), u_t(\tau))d\tau \int_0^t (u_x(\tau), u_{xt}(\tau))d\tau\\ &\le \frac{1}{2}\int_0^t \|u(\tau)\|_2^2 d\tau \int_0^t \|u_{xt}(\tau)\|_2^2 d\tau + \frac{1}{2}\int_0^t \|u_t\|_2^2 d\tau \int_0^t \|\nabla u\|_2^2 d\tau.\end{aligned} \quad (55)$$

Inserting (53)–(55) into (52), we have

$$\eta(t) \ge 0, \quad t \in [0, T_1]. \quad (56)$$

Thus,

$$\Psi''(t)\Psi(t) - \frac{p+3}{4}\Psi'(t)^2 \ge \Psi(t)\xi(t), \quad (57)$$

where

$$\begin{aligned}\xi(t) &= -2\|u_x\|_{H^1}^2 - 2\int_\Omega u_x f(u_x)dx + 2b\\ &\quad - (p+3)\left[\int_0^t \|u_t(\tau)\|_{H^1}^2 d\tau + b\right]\\ &\ge -(p+3)\int_0^t \|u_t(\tau)\|_{H^1}^2 d\tau - (p+1)b\\ &\quad - 2(p+1)\int_\Omega F(u_x)dx - 2\|u_x\|_{H^1}^2\\ &= -2(p+1)\left[E(t) - \frac{1}{2}\|u_x\|_{H^1}^2 - \int_0^t \|u_t(\tau)\|_{H^1} d\tau\right]\\ &\quad - (p+3)\int_0^t \|u_t(\tau)\|_{H^1}^2 d\tau - (p+1)b - 2\|u_x\|_{H^1}^2\\ &\ge -2(p+1)E(0) + (p-1)\|u_x\|_{H^1}^2\\ &\quad + (p-1)\int_0^t \|u_t(\tau)\|_{H^1}^2 d\tau - (p+1)b.\end{aligned} \quad (58)$$

From $I(u_0) < 0$, $E(0) = J(u_0) < d_0$ and Lemma 5, we have $I(u) < 0$ for all $t \in [0,\infty)$. Hence, by Lemma 1, it follows that

$\|u_x\|_{H^1}^2 > \gamma_0^2 = ((2(p+1))/(p-1))d_0 = (1/(\alpha C_*^{p+1}))^{2/(p-1)}$. Thus, we have from (58) that

$$\xi(t) > 2(p+1)(d_0 - J(u_0)) - (p+1)b. \tag{59}$$

We choose b small enough such that $b \le 2(d_0 - J(u_0))$, then we have

$$\Psi''(t)\Psi(t) - \frac{p+3}{4}\Psi'(t)^2 \ge \Psi(t)\xi(t) > 0, \tag{60}$$

for all $t \in [0, T_1]$. From $I(u) < 0$ for all $t \in [0, T_1)$ and (50), we get $\Psi''(t) > 0$. Hence, we have $\Psi'(t) > \Psi'(0) = 2bT_0 > 0$ for all $t \in (0, T_1)$.

From what has been discussed above, using Lemma 6 and letting $\delta = (p-1)/4$, we can obtain that there exists a finite time $\tilde{T} > 0$ such that

$$\lim_{t \longrightarrow \tilde{T}^-} \Psi(t) = +\infty, \tag{61}$$

or

$$\lim_{t \longrightarrow \tilde{T}^-} \left(\int_0^t \|u(\tau)\|_{H^1}^2 d\tau + (T_1 - t)\|u_0\|_{H^1}^2 + b(t + T_0)^2 \right) = +\infty, \tag{62}$$

where

$$\tilde{T} \le \frac{\Psi(0)}{\gamma\Psi'(0)} = \frac{2\left[T_1\|u_0\|_{H^1}^2 + bT_0^2\right]}{(p-1)bT_0}. \tag{63}$$

which contradicts $\tilde{T} = +\infty$. Hence, the desired assertion immediately follows.

From the discussed above in Sections 3 and 4, a threshold result of global existence and nonexistence of solutions for problems (1)–(3) has been obtained as follows.

Corollary 9. *Let f satisfy (4), and $u_0 \in D \cap W^{1,q+1}(\Omega)$. Assume that $E(0) = J(u_0) < d_0$. Then, problems (1)–(3) admits a global weak solution provided $I(u_0) \ge 0$ (includes $u_0 = 0$); Problems (1)–(3) dose not admit any global solution provided $I(u_0) < 0$.*

5. Finite Time Blow-up of Solutions with High Initial Energy

In this section, we shall state and prove the finite time blow-up result with high initial energy for the problems (1)–(3).

Theorem 10. *Let f satisfy (4), and $u_0 \in D \cap W^{1,q+1}(\Omega)$. Assume that*

$$0 \le J(u_0) \le \frac{(p-1)\lambda_1}{2(p+1)(1+\lambda_1)}\|u_0\|_{H^1}^2, \tag{64}$$

where λ_1 is the optimal constant satisfying the Poincáre inequality $\|u_x\|_2^2 \ge \lambda_1\|u\|_2^2$, then the weak solution $u(t)$ of problems (1)–(3) blow-up in finite time.

Proof. Arguing by contradiction, we suppose that $u(t)$ is a global weak solution of the problems (1)–(3). Considering that

$$\int_0^t u_t(\tau)d\tau = u(t) - u_0, \quad \forall t \in [0,\infty), \tag{65}$$

so we have

$$\begin{aligned}\int_0^t \|u_t(\tau)\|_{H^1} d\tau &\ge \left\|\int_0^t u_t(\tau)d\tau\right\|_{H^1} = \|u(t) - u_0\|_{H^1} \\ &\ge \|u(t)\|_{H^1} - \|u_0\|_{H^1}.\end{aligned} \tag{66}$$

From (16), (66) and Hölder's inequality, we obtain

$$\begin{aligned}\|u(t)\|_{H^1} &\le \|u_0\|_{H^1} + \int_0^t \|u_t(\tau)\|_{H^1} d\tau \\ &\le \|u_0\|_{H^1} + t^{1/2}\left(\int_0^t \|u_t(\tau)\|_{H^1}^2 d\tau\right)^{1/2} \\ &\le \|u_0\|_{H^1} + t^{1/2}(J(u_0) - J(u(t)))^{1/2}.\end{aligned} \tag{67}$$

Since assume that $u(t)$ is a global weak solution of the problems (1)–(3), we get $J(u(t)) \ge 0$ for all $t \in [0, \infty)$. Otherwise, there exists a time $t_0 \in [0,\infty)$ such that $J(u(t_0)) < 0$. Hence, from

$$\begin{aligned}0 > J(u(t_0)) &= \frac{1}{2}\|u_x(t_0)\|_{H^1}^2 + \int_\Omega F(u_x(t_0))dx \\ &\ge \frac{1}{2}\|u_x(t_0)\|_{H^1}^2 + \frac{1}{p+1}\int_\Omega f(u_x(t_0))u_x(t_0)dx \\ &\ge \frac{p-1}{2(p+1)}\|u_x(t_0)\|_{H^1}^2 + \frac{1}{p+1}I(u(t_0)),\end{aligned} \tag{68}$$

we have $I(u(t_0)) < 0$ and $J(u(t_0)) < 0$ which implies that $u(t_0) \in V$. Therefore, by the results of Theorem 8, we obtain that $u(x, t\,; u(t_0)) = u(x, t - t_0\,; u_0)$ blows up in finite time, which is a contradiction. Thus, we have

$$J(u_0) \ge J(u(t)) \ge 0, \quad \text{for all } t \in [0, \infty). \tag{69}$$

Next, combining (67) and (69), we get

$$\begin{aligned}\|u(t)\|_{H^1} &\le \|u_0\|_{H^1} + t^{1/2}(J(u_0) - J(u(t)))^{1/2} \\ &\le \|u_0\|_{H^1} + t^{1/2}(J(u_0))^{1/2},\end{aligned} \tag{70}$$

for all $t \in [0, \infty)$.

On the other hand, multiplying u on two sides of Equation (1) and integrating by parts, we have

$$(u_t, u) + (u_{xt}, u_x) + (u_x, u_x) + (u_{xx}, u_{xx}) = -(f(u_x), u_x). \tag{71}$$

The Poinca're inequality gives $\|u_x\|_2^2 \geq \lambda_1 \|u\|_2^2$, where λ_1 is the first eigenvalue of the problem

$$\begin{cases} w_{xx} + \lambda w = 0, \text{ in } \Omega, \\ w = 0, \text{ on } \partial\Omega. \end{cases} \tag{72}$$

Thus, we have

$$\|u\|_{H^1}^2 = \|u\|_2^2 + \|u_x\|_2^2 \leq \frac{1+\lambda_1}{\lambda_1}\|u_x\|_2^2 \leq \frac{1+\lambda_1}{\lambda_1}\|u_x\|_{H^1}^2. \tag{73}$$

By the combination of (4), (73), and Sobolev's inequality, we can get that

$$\begin{aligned} \frac{d}{dt}\left(\frac{1}{2}\|u\|_{H^1}^2\right) &= -\|u_x\|_{H^1}^2 - (f(u_x), u_x) \\ &\geq -\|u_x\|_{H^1}^2 - (p+1)\int_\Omega F(u_x)dx \\ &= \frac{p-1}{2}\|u_x\|_{H^1}^2 - (p+1)J(u(t)) \\ &\geq \frac{(p-1)\lambda_1}{2(1+\lambda_1)}\|u\|_{H^1}^2 - (p+1)J(u(t)). \end{aligned} \tag{74}$$

Since $(d/dt)J(u(t)) \leq 0$, for $\forall k > 0$, we have

$$\begin{aligned} &\frac{d}{dt}\left(\frac{1}{2}\|u\|_{H^1}^2 - kJ(u(t))\right) \\ &\geq \frac{d}{dt}\left(\frac{1}{2}\|u\|_{H^1}^2\right) \geq \frac{(p-1)\lambda_1}{2(1+\lambda_1)}\|u\|_{H^1}^2 - (p+1)J(u(t)), \\ &= \frac{(p-1)\lambda_1}{1+\lambda_1}\left[\frac{1}{2}\|u\|_{H^1}^2 - \frac{(p+1)(1+\lambda_1)}{(p-1)\lambda_1}J(u(t))\right]. \end{aligned} \tag{75}$$

Taking $k = ((p+1)(1+\lambda_1))/((p-1)\lambda_1)$ in (75) and $G(t) = 1/2\|u\|_{H^1}^2 - (((p+1)(1+\lambda_1))/((p-1)\lambda_1))J(u(t))$, then we have

$$\frac{d}{dt}G(t) \geq \frac{(p-1)\lambda_1}{1+\lambda_1}G(t). \tag{76}$$

Integrating the inequality (76) from 0 to t, we see

$$G(t) \geq e^{(((p-1)\lambda_1)/(1+\lambda_1))t}G(0), \quad t \in [0,\infty), \tag{77}$$

which means that

$$\begin{aligned} \|u\|_{H^1}^2 \geq{}& \frac{2(p+1)\lambda_1}{(p-1)(1+\lambda_1)}J(u(t)) \\ &+ 2e^{(((p-1)\lambda_1)/(1+\lambda_1))t}G(0), \quad t \in [0,\infty). \end{aligned} \tag{78}$$

From the assumption condition (64), we have $G(0) > 0$. Hence, we get from (69) and (78) that $\|u\|_{H^1}^2 \geq 2e^{(((p-1)\lambda_1)/(1+\lambda_1))t}G(0)$, i.e.,

$$\|u\|_{H^1} \geq [2G(0)]^{1/2}e^{(((p-1)\lambda_1)/(2(1+\lambda_1)))t}, \quad t \in [0,\infty). \tag{79}$$

From the combination of (70) and (79), we have

$$[2G(0)]^{1/2}e^{(((p-1)\lambda_1)/(2(1+\lambda_1)))t} \leq \|u_0\|_{H^1} + t^{1/2}(J(u_0))^{1/2}. \tag{80}$$

Clearly, the above inequality cannot hold for t large enough, this means that the solution u of problems (1)–(3) cannot exist all time.

Furthermore, by (80) and $e^{(((p-1)\lambda_1)/(2(1+\lambda_1)))t} \geq (((p-1)\lambda_1)/(2(1+\lambda_1)))t$, we can obtain the inequality

$$\frac{\sqrt{2G(0)}(p-1)\lambda_1}{2(1+\lambda_1)}t - (J(u_0))^{1/2}t^{1/2} - \|u_0\|_{H^1} \leq 0, \tag{81}$$

which implies that there exists a finite time $\tilde{T} > 0$ such that

$$\lim_{t \longrightarrow \tilde{T}^-}\|u\|_{H^1}^2 = +\infty, \tag{82}$$

and $\tilde{T}^{1/2}$ is the largest root of the following equation

$$\frac{\sqrt{2G(0)}(p-1)\lambda_1}{2(1+\lambda_1)}t^2 - (J(u_0))^{1/2}t - \|u_0\|_{H^1} = 0. \tag{83}$$

This completes the proof.

6. Conclusion and Future Work

In our work, we mainly study the qualitative properties of the solutions for the initial and boundary value problems (1)–(3). It is well known that Equation (1) is a typical higher-order metaparabolic equation, which has extensive practical background and rich theoretical connotation. For example, the solutions u of (1) can be used to denote the concentration of one of the two phases, the fourth-order term γu_{xxxx} presents the capillarity-driven surface diffusion, and the nonlinear term $f(u_x)_x$ is an intrinsic chemical potential. Especially, the interaction between the dispersion term u_{xxt} and nonlinearity $f(u_x)_x$ of these problems cause some difficulties such that we cannot apply the normal Galerkin approximation, concavity, and potential methods directly. Considering the above situation, at low initial energy level, we first prove the existence of global weak solutions for these problems by the Galerkin approximation and potential well methods and obtain the finite time blow-up result by the potential well and improved concavity skills. In addition, we establish the

finite time blow-up result for certain solutions with high initial energy. However, as far as we know, there is little information on the long-time behavior of global solutions for above problems. Whether the global solutions will exhibit a long-time dynamic behavior at low initial energy? Do both problems (1)–(3) have the global solutions and asymptotic property at high initial energy level? These questions are all opening, and we are now working on these problems. On the other hand, we note that the fractional partial differential equations have been applied in various areas of science, and their related theoretical results and applications have been investigated by some authors (see [31–33] and the references therein). The study of their qualitative properties is one of the hot topics. Do the conclusions of present paper also hold for the initial and boundary value problems of the fractional nonlinear metaparabolic equations? This question is very interesting and opening.

Data Availability

The data used to support the findings of this study are included within the article.

Conflicts of Interest

The authors declare that they have no competing interests.

Acknowledgments

This work is supported by the NSF of China (11801108 and 11701116), the Scientific Program of Guangdong Province (2016A030310262), and the College Scientific Research Project of Guangzhou University (YG2020005). Dr. Huafei Di also specially appreciates Prof. Yue Liu for his invitation of visiting to the University of Texas at Arlington.

References

[1] P. M. Brown, *Constructive Function-Theoretic Methods for Fourth Order Pseudo-Parabolic and Metaparabolic Equations*, Thesis, Indiana University, Bloomington, Indiana, 1973.

[2] R. P. Gilbert and G. C. Hsiao, "Constructive function theoretic methods for higher order pseudoparabolic equations," *Function Theoretic Methods for Partial Differential Equations, Lecture Notes in Mathematics, Springer, Berlin*, vol. 561, pp. 51–67, 1976.

[3] E. C. Aifantis, "On the problem of diffusion in solids," *Acta Mech.*, vol. 37, no. 3-4, pp. 265–296, 1980.

[4] K. Kuttler and E. Aifantis, "Quasilinear evolution equations in nonclassical diffusion," *SIAM Journal on Mathematical Analysis*, vol. 19, no. 1, pp. 110–120, 1988.

[5] T. W. Ting, "A cooling process according to two temperature theory of heat conduction," *Journal of Mathematical Analysis and Applications*, vol. 46, pp. 23–31, 1974.

[6] Y. D. Shang, "Blow-up of solutions for the nonlinear Sobolev-Galpern equations," *Mathem Atica Applicata*, vol. 13, no. 3, pp. 35–39, 2000.

[7] R. E. Showalter, "Sobolev equations for nonlinear dispersive systems," *Applicable Analysis*, vol. 7, pp. 297–308, 2007.

[8] Y. Y. Ke and J. X. Yin, "A note on the viscous Cahn-Hilliard equation," *Northeastern Mathematical Journal*, vol. 20, pp. 101–108, 2004.

[9] C. M. Elliott and I. N. Kostin, "Lower semicontinuity of a nonhyperbolic attractor for the viscous Cahn - Hilliard equation," *Nonlinearity*, vol. 9, no. 3, pp. 687–702, 1996.

[10] F. Bai, C. M. Elliott, A. Gardiner, A. Spence, and A. M. Stuart, "The viscous Cahn-Hilliard equation. I. computations," *Nonlinearity*, vol. 8, no. 2, pp. 131–160, 1995.

[11] C. M. Elliott and H. Garcke, "On the Cahn-Hilliard equation with degenerate mobility," *SIAM Journal on Mathematical Analysis*, vol. 27, no. 2, pp. 404–423, 1996.

[12] L. G. Reyna and M. J. Ward, "Metastable internal layer dynamics for the viscous Cahn-Hilliard equation," *Methods and Applications of Analysis*, vol. 2, no. 3, pp. 285–306, 1995.

[13] C. C. Liu and J. X. Yin, "Some properties of solutions for viscous Cahn-Hilliard equation," *Northeastern Mathematical Journal*, vol. 14, no. 4, pp. 455–466, 1998.

[14] M. Grinfeld and A. Novick-Cohen, "The viscous Cahn-Hilliard equation: Morse decomposition and structure of the global attractor," *Transactions of the American Mathematical Society*, vol. 351, no. 6, pp. 2375–2406, 1999.

[15] X. P. Zhao and C. C. Liu, "Optimal control problem for viscous Cahn-Hilliard equation," *Nonlinear Analysis: Theory, Methods & Applications*, vol. 74, pp. 6348–6357, 2011.

[16] A. B. Al'shin, M. O. Korpusov, and A. G. Siveshnikov, *Blow Up in Nonlinear Sobolev Type Equations*, Walter Gruyter, Berlin, 1 edition, 2011.

[17] B. Hu, *Blow-up Theories for Semilinear Parabolic Equations, Lecture Notes in Mathematics*, Springer, Heidelberg, 2011.

[18] H. F. Di, Y. D. Shang, and X. X. Zheng, "Global well-posedness for a fourth order pseudo-parabolic equation with memory and source terms," *Discrete & Continuous Dynamical Systems-B*, vol. 21, no. 3, pp. 781–801, 2016.

[19] H. F. Di and Y. D. Shang, "Blow-up phenomena for a class of generalized double dispersion equations," *Acta Mathematica Scientia*, vol. 39, no. 2, pp. 231–243, 2019.

[20] H. F. Di, Y. D. Shang, and J. L. Yu, "Existence and uniform decay estimates for the fourth order wave equation with nonlinear boundary damping and interior source," *Electronic Research Archive*, vol. 28, no. 1, pp. 221–261, 2020.

[21] N. I. Bakiyevich and G. A. Shadrin, "Cauchy problem for an equation in filtration theory," *Sb. Trudov Mosgospedinstituta*, vol. 7, pp. 47–63, 1978.

[22] C. C. Liu, "Weak solutions for a class of metaparabolic equations," *Applicable Analysis*, vol. 87, no. 8, pp. 887–900, 2008.

[23] K. I. Khudaverdiyev and G. M. Farhadova, "On global existence for generalized solution of one-dimensional non-self-adjoint mixed problem for a class of fourth order semilinear pseudo-parabolic equations," in *Proceedings of the Institute of Mathematics and Mechanics (PIMM), National Academy of Sciences of Azerbaijan, Volume 31*, pp. 119–134, 2009.

[24] H. J. Zhao and B. J. Xuan, "Existence and convergence of solutions for the generalized BBM-Burgers equations with dissipative term," *Nonlinear Analysis: Theory Methods & Applications*, vol. 28, no. 11, pp. 1835–1849, 1997.

[25] G. A. Philippin and S. Vernier Piro, "Behaviour in time of solutions to a class of fourth order evolution equations," *Journal of Mathematical Analysis and Applications*, vol. 436, no. 2, pp. 718–728, 2016.

[26] Z. J. Yang, "Global existence asymptotic behavior and blowup of solutions for a class of nonlinear wave equations with dissipative term," *Journal of Differential Equations*, vol. 187, pp. 520–540, 2003.

[27] G. W. Chen and B. Lu, "The initial-boundary value problems for a class of nonlinear wave equations with damping term," *Journal of Mathematical Analysis and Applications*, vol. 351, no. 1, pp. 1–15, 2009.

[28] R. Z. Xu, S. Wang, Y. B. Yang, and Y. H. Ding, "Initial boundary value problem for a class of fourth-order wave equation with viscous damping term," *Applicable Analysis*, vol. 92, no. 7, pp. 1403–1416, 2013.

[29] A. Khelghati and K. Baghaei, "Blow-up phenomena for a class of fourth-order nonlinear wave equations with a viscous damping term," *Mathematical Methods in the Applied Sciences*, vol. 41, no. 2, pp. 490–494, 2018.

[30] H. A. Levine and B. D. Sleeman, "A note on the non-existence of global solutions of initial boundary value problems for the Boussinesq equation $\sum_{i=1}^{n} i^3(n(n+i)/2)^2$," *Journal of mathematical analysis and applications*, vol. 107, pp. 206–210, 1985.

[31] K. Shah, H. Khalil, and R. A. Khan, "Analytical solutions of fractional order diffusion equations by natural transform method," *Iranian Journal of Science and Technology, Transactions A: Science*, vol. 42, no. 3, pp. 1479–1490, 2018.

[32] K. Shah, H. Khalil, and R. A. Khan, "A generalized scheme based on shifted Jacobi polynomials for numerical simulation of coupled systems of multi-term fractional-order partial differential equations," *LMS Journal of Computation and Mathematics*, vol. 20, no. 1, pp. 11–29, 2017.

[33] I. Ahmad, G. Ali, K. Shah, and T. Abdeljawad, "Iterative analysis of nonlinear bbm equations under nonsingular fractional order derivative," *Advances in Mathematical Physics*, vol. 2020, Article ID 3131856, 12 pages, 2020.

Hindawi
Advances in Mathematical Physics
Volume 2021, Article ID 5578391, 8 pages
https://doi.org/10.1155/2021/5578391

Research Article

Three-Dimensional Simulations of Offshore Oil Platform in Square and Diamond Arrangements

Saliha Nouri,[1] Zouhair Hafsia,[1] Salah Mahmoud Boulaaras,[2,3] Ali Allahem,[4] Salem Alkhalaf,[5] and Aldo Munoz Vazquez[6]

[1]*Department of Physics, College of Science and Arts at ArRass, Qassim University, Saudi Arabia*
[2]*Department of Mathematics, College of Science and Arts at ArRass, Qassim University, Saudi Arabia*
[3]*Laboratory of Fundamental and Applied Mathematics of Oran (LMFAO), University of Oran 1, Ahmed Benbella, Algeria*
[4]*Department of Mathematics, College of Science, Qassim University, Saudi Arabia*
[5]*Department of Computer Science, College of Science and Arts at ArRass, Qassim University, Saudi Arabia*
[6]*College of Engineering, Texas A&M University, 6200 Tres Lagos Blvd, Higher Education Center at McAllen, Texas 78504, USA*

Correspondence should be addressed to Ali Allahem; aallahem@qu.edu.sa

Received 19 January 2021; Revised 15 February 2021; Accepted 19 February 2021; Published 2 March 2021

Academic Editor: F. Rabiei

The interaction of the solitary wave with an oil platform composed of four vertical circular cylinders is investigated for two attack angle of the solitary wave $\beta = 0^\circ$ (square arrangement) and $\beta = 45^\circ$ (diamond arrangement). The solitary wave is generated using an internal source line as proposed by Hafsia et al. (2009). This generation method is extended to three-dimensional wave flow and is integrated into the PHOENICS code. The volume of fluid approach is used to capture the free surface evolution. The present model is validated in the case of a solitary wave propagating on a flat bottom for $H/h = 0.25$ where H is the wave height and h is the water depth. Compared to the analytical solution, the pseudowavelength and the wave crest are well reproduced. For a solitary wave interacting with square and diamond cylinders, the simulated results show that the maximum run-ups are well reproduced. For the diamond arrangements, the diffraction process seems to not affect the maximum run-ups, which approached the isolated cylinder. For the square arrangement, the shielding effect leads to a maximum wave force more pronounced for the upstream cylinder array.

1. Introduction

In the last decades, many researchers have focused on searching different wave structures of nonlinear partial differential equations. The interested readers can see [1–4]. The offshore oil platforms and the coastal bridges are composed of multiple cylinders disposed in different arrangements. When the wave run-up and the following wave forces exceed the expected values, the safety of these structures is compromised. The available analytical solutions in the literature are only valuable under some limiting assumptions. For this reason, experimental and numerical methods are adopted to solve this wave-platform interaction problem.

The interaction of a solitary wave (representing a real tsunami wave) with a single circular cylinder was studied experimentally by Yates and Wang (1994) in [5]. The effect of a single row of circular cylinders on the transmission and reflected coefficients is studied experimentally by Huang (2010) in [6]. The consequent results are that the wave force acting on a coastal structure protected by these cylinders can be reduced to about 60% for $S = 1.2\,D$, where S is the distance between the centers of adjacent cylinders, and D is the cylinder diameter. An experimental study was conducted by Huang (2007) in [7] to measure the reflection and transmission coefficients in the case of single and twin rows of rectangular cylinders, and simplified analytical expressions of these

coefficients are proposed. Wang et al. (2021) in [8] investigate experimentally, the back and front run-up and wave forces induced by solitary wave for different truncated vertical cylinders. Secondary peak for both the front run-up and wave forces are observed due to the return flow.

An alternative method to the experimental measurements of the free surface evolution is the use of a two-dimensional (2-D) or three-dimensional (3-D) numerical method. The first one is based on the depth averaged Boussinesq equations and can be used for a long-term simulation. Lin and Man (2007) in [9] validate the Boussinesq model for one-dimensional and two-dimensional wave transformations. Mohapatra et al. (2020) in [10] studied the regular wave diffraction by a floating fixed vertical cylinder by two methods: using a CFD code and analytically based on a Boussinesq model. Among the various Boussinesq models existing in the literature, the nonlinear effects cannot well be reproduced (Zhao et al., 2007 in [11], Wang and Ren, 1999 in [12], and Liu et al., 2012 in [13]). Hence, a full three-dimensional (3-D) Navier-Stokes model is required. In order to study the regular wave run-ups for a single and a group of vertical cylinders, numerical virtual wave probes were used by Cao and Wan (2017) in [14]. Frantzis et al. (2020) in [15] adopted a (3-D) numerical wave tank (NWT) to study the wave breaking induced by a single row of vertical cylinders for different ranges of cylinder diameter to depth ratios. The large eddy simulation (LES) model was used to reproduce the small scales of turbulence. Numerical results show that the effect of the cylinder diameter is more significant for larger values of solitary wave heights. Wang et al. (2018) in [16] conducted a series of laboratory experiments on the internal solitary wave (ISW) loads upon semisubmersible platforms in a density stratified fluid tank, and investigated the load components induced by different factors. The wave loads on a platform composed of 2×2 circular cylinders in side-by-side and tandem arrangements are numerically studied using the Reynolds-Averaged Navier-Stokes equations by Yang et al. (2015) in [17]. The desired monochromatic wave was generated by the prescribed velocity components at the inlet of the computational domain. Using a CFD code, Kamath et al. (2015) in [18] investigate the diffraction of sinusoidal wave by 3×3 square array cylinders placed in proximity and show that the wave force is highest when the distance between the cylinder center is less than half of the incident sinusoidal wave. The numerical results show that if $S > 4\,D$, there is no interaction between the platform cylinders. Xie et al. in [19] used a cut-cell method in a fully (3-D) code to simulate solitary wave interaction with a vertical circular cylinder and a thin horizontal plate. Several computational fluid dynamics (CFD) implemented a cut-cell algorithm permitting to identify the contribution of a portion of a rectangular grid to the convective and diffusive fluxes.

The main task of the present study is to investigate the interaction of the solitary wave with one or four circular cylinders in a square or diamond arrangement using a (3-D) numerical wave tank (NWT). The proposed wave generation method is based on an internal mass source. The cut-cell implemented in the PHOENICS code is used to reproduce the circular cylinder shape.

2. Mathematical Formulation

2.1. Computational Domain. The position of the still water level h and the location of the mass source line for solitary wave generation are shown in Figure 1(a). The direction of propagation of the solitary wave is the positive x-direction. In all simulated cases, the depth to cylinder radius ratio is taken: $h/a = 1$, and the distance from the center of cylinders is $S = 3\,a$. For the square platform, there is one cylinder in each corner of the square as indicated in Figure 1(b). The two upstream cylinders are denoted 3 and 4, and the two downstream cylinders are 1 and 2. The square arrangement corresponding to the attack angle of solitary wave $\beta = 0$. This angle is measured between the propagating direction and the symmetric line of the platform (the line parallel to the line joining 1 and 3). The diamond configuration of the platform is shown in Figure 1(c) and corresponds to $\beta = 45^{\circ}$. The effective computational domain has a length of $L = 55\,a$. Two dissipative zones are added in each open boundary to avoid wave reflection having a length of $(25\,a)$. The considered width is $(10\,a)$, $(13\,a)$, and $(12.25\,a)$, respectively, for a single cylinder, square platform, and diamond platform.

The overall grid and the grid around the oil platform are shown in Figure 2 for the diamond arrangement. Fine grids are adopted around the four cylinders, and coarse grids are imposed in the two dissipation regions. The cut-cell method is used to mesh the circular cylinders in the Cartesian coordinates system. Figure 2(b) shows the details of the cut-cell grids around the four cylinders. The number of grid in x, y, and z directions is, respectively $\mathrm{NX} \times \mathrm{NY} \times \mathrm{NZ} = 220 \times 110 \times 102$ for the diamond arrangement and $220 \times 100 \times 102$ for the square arrangement. For these two arrangements, the time step is $\Delta t = 0.01$ s.

2.2. Governing Transport Equations. The proposed (NWT) was based on the full three-dimensional (3-D) Navier-Stokes transport equations coupled to the volume of liquid (VOF) convective transport equation to reproduce the water wave interface. For unsteady flow and incompressible fluid, the mass and momentum conservation equations are written as:

(i) The mass conservation equation:

$$\frac{\partial \rho}{\partial t} + \frac{\partial u_i}{\partial x_i} = 0. \tag{1}$$

(ii) The momentum transport equation:

$$\frac{\partial u_i}{\partial t} + u_j \frac{\partial u_i}{\partial x_j} = -\frac{1}{\rho}\frac{\partial p}{\partial x_i} + \frac{\partial}{\partial x_j}\left[\nu\left(\frac{\partial u_i}{\partial x_j} + \frac{\partial u_j}{\partial x_i}\right)\right] + g_i + s_{d,i}, \tag{2}$$

where x_i is the Cartesian coordinates, u_i is the velocity components, ρ is the density of the mixture, p is the pressure, ν is the kinematic viscosity of the mixture, g is the

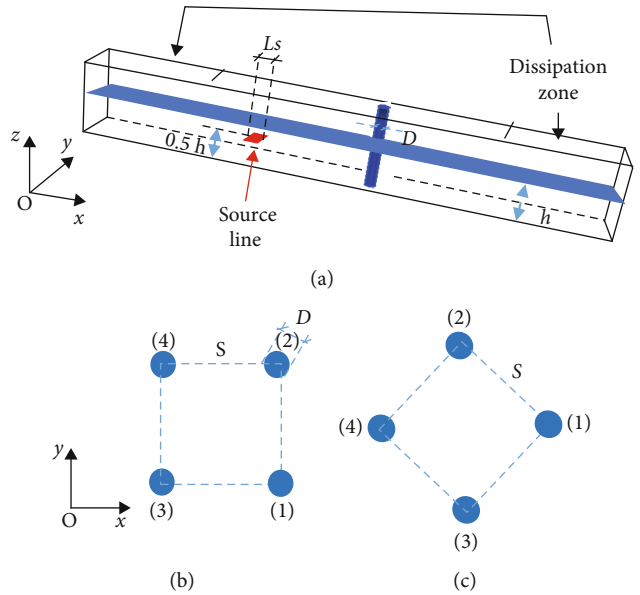

FIGURE 1: The computational domain and wave source line location; (a) side view; (b) top view.

acceleration due to gravity, and $s_{d,z}$ is a momentum source term added to the momentum equation along z-direction to avoid wave reflection at the open boundaries given by:

$$s_{d,z} = \gamma(x)\, w, \tag{3}$$

where $\gamma(x)$ is a linear damping function and w is the velocity component along the z-vertical direction.

2.3. Free Surface Capture. The air-water interface is modeled using the mixture model flow. If α_q denoted the volume fraction of the q^{th} fluid in a cell, then,

(i) The density of the mixture is given by:

$$\rho = \sum_{q=1}^{2} \rho_q\, \alpha_q, \tag{4}$$

where ρ_q is the density of the water when $(q = 1)$ and air when $(q = 2)$.

(ii) And dynamic viscosity of the mixture is

$$\mu = \sum_{q=1}^{2} \mu_q\, \alpha_q, \tag{5}$$

where μ_q is the dynamic viscosity of the water if $(q = 1)$ and air when $(q = 2)$.

The volume fraction of fluid is determined by the following mass conservation equation for each phase:

$$\frac{\partial \alpha_q}{\partial t} + \frac{\partial(\alpha_q u_i)}{\partial x_i} = 0. \tag{6}$$

When $\alpha_q = 0$, the cell is occupied by air, $\alpha_q = 1$, the cell is occupied by water, and $0 < \alpha_q < 1$, the cell contains the interface (Hirt and Nichols, 1981 in [20]).

2.4. Wave Generation. The desired solitary wave was generated by an internal source inlet across a source line as proposed by Hafsia et al. (2009) in [21]. The inlet vertical velocity is prescribed as a time-dependent inlet boundary condition:

$$w^I = \frac{2\, c\, \eta(x_s, t)}{L_s}, \tag{7}$$

where L_s is the length of the internal source line.

The wave celerity is given by (Dominguez et al., 2019 in [22]):

$$c = \sqrt{g\,(H + h)}. \tag{8}$$

The solitary wave surface elevation $\eta(x_s, t)$ is given by the following equation:

$$\eta = H\ \operatorname{sech}^2[k\,(x_s - c\,t)], \tag{9}$$

where H is the incident wave height and t is the time. The distance x_s permitting to have a negligible source at $t = 0\,s$ is determined by the following equation:

$$x_s = \frac{4\,h}{\sqrt{H/h}}. \tag{10}$$

The equivalent wave number k is

$$k = \sqrt{\frac{3\,H}{4\,h^2\,(H + h)}}. \tag{11}$$

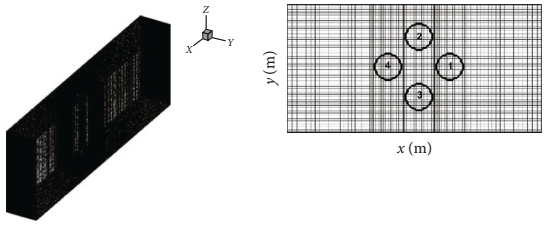

(a) (b)

Figure 2: The grid of computational domain for the diamond arrangement of the four circular cylinders; (a) side view; (b) top view of the grid details around the cylinders by cut-cell method.

Following this equivalent wave number, the pseudowavelength can be determined by:

$$L = \frac{2\pi}{k}. \tag{12}$$

The length L_s and the position of the source line are determined by the calibration procedure as indicated by Hafsia et al. (2009) in [21].

2.5. Wave Force. The wave force $\vec{F}$ acting on the cylinder is computed by integrating the water pressure p and the normal component of the viscous stress tensor τ on the wetted surface of the cylinder S:

$$\vec{F} = \int_S \left(-\vec{n}\, p + \vec{n}.\tau\right) dS, \tag{13}$$

where $\vec{n}$ is the normal unit vector pointing into the water.

From the component of this wave force along the x -direction, the force coefficient can be calculated as:

$$C_{f,x} = \frac{F_x}{\rho g h^2 a}. \tag{14}$$

2.6. Initial and Boundary Conditions. The following initial and boundary conditions are adopted for the governing transport equations. The imposed initial condition is still water with a depth h. For the top boundary, the pressure P is set equal to the atmospheric pressure. Two dissipation zones are adopted at the open boundaries (Figure 1). At all the other boundaries of the computational domain, symmetric boundary conditions are imposed.

2.7. Numerical Schemes. To solve this proposed model, we adopt the PHOENICS code (Parabolic Hyperbolic or Elliptic Numerical Integration Code Series). In this code, the SIMPLEST iterative algorithm is used to solve the pressure and velocity coupling in the Navier-Stokes equations (Artemov et al., 2009 in [23]). The upwind scheme is used for nonlinear convection terms and an implicit formulation for the transient term. The (VOF) method is used to predict the interface between the water wave and air. For all the presented simulation results, the cut-cell within the PARSOL (PARtial SOLid) treatment detects the solid-fluid interface, which is not aligned with the Cartesian grid. The proposed three-dimensional wave generation method is implemented in the PHOENICS code.

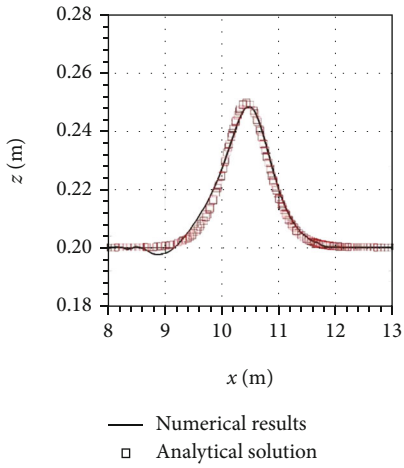

Figure 3: Comparison between the numerical and analytical free surface profiles at the centerline of the computational domain for $H/h = 0.25$.

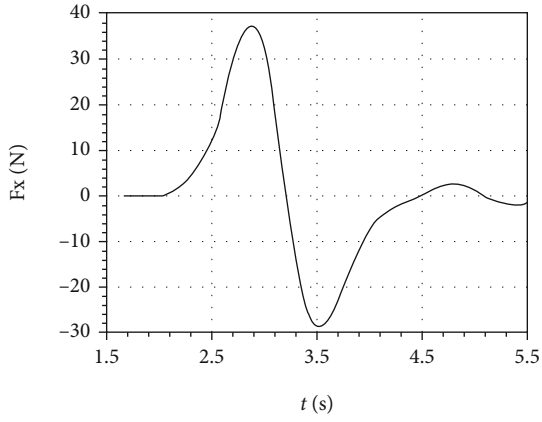

Figure 4: Time evolution of the in-line force on a single cylinder.

3. Numerical Results

3.1. Solitary Wave on a Single Cylinder. The proposed wave generation method based on an internal source line is validated for the nondimensional height $H/h = 0.25$. The

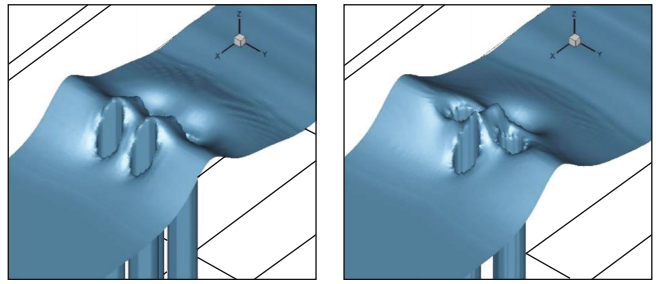

(a) (b)

Figure 5: A three-dimensional free-surface elevation at the maximum run-up of the cylinder 1 for $H/h = 0.25$: (a) square arrangement; (b) diamond arrangement.

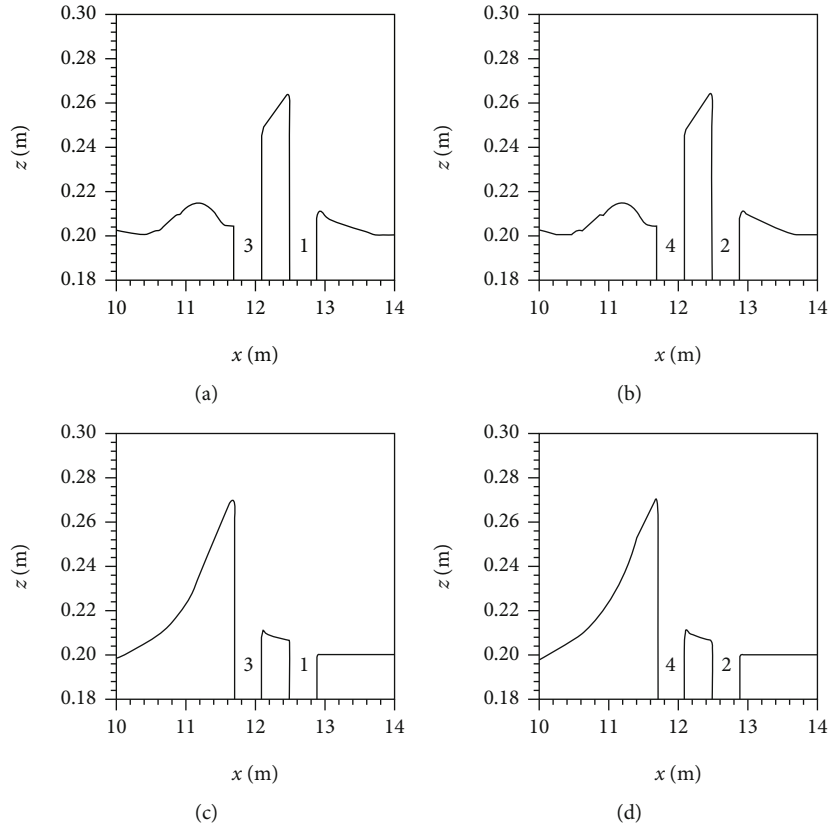

Figure 6: The maximum solitary wave run-ups at each cylinder for the square arrangement; (a) cylinder 1; (b) cylinder 2; (c) cylinder 3; (d) cylinder 4.

simulated results show that before reaching the vertical cylinder, the wave profile is invariant in the transverse direction and can be represented by two-dimensional profiles. Figure 3 represents the simulated wave profiles at the center of the computational domain before impacting the cylinder. The wave is not affected by the cylinder, and the free surface profiles agree very well with the analytical one. The wave crest and the pseudowavelength are in accordance with the analytical one.

When a solitary wave passes around the cylinder, run-up occurs at the front of the cylinder and the maximum run-up depended on the incident wave energy. Then, the water level drops at the front producing the rise of the water level at the rear of the cylinder by wave diffraction. In order to validate the cut-cell method, the maximum run-up is compared to the available literature. The maximum wave run-up is

Table 1: Comparison of the simulated maximum run-up to the wave height ratio with Zhao et al. (2007) in [11] for a diamond arrangement.

	Cylinder 1	Cylinder 2	Cylinder 3	Cylinder 4
Present study	1.36	1.38	1.38	1.36
Zhao et al. (2007) in [11]	1.33	1.37	1.38	1.37

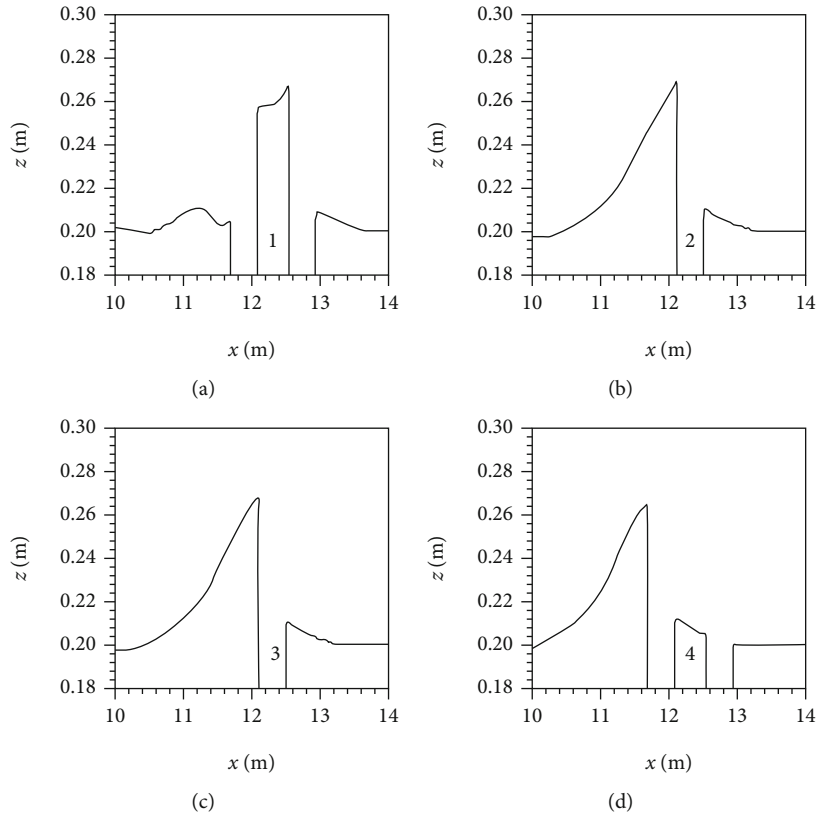

Figure 7: The maximum solitary wave run-ups at each cylinder for the diamond arrangement; (a) cylinder 1; (b) cylinder 2; (c) cylinder 3; (d) cylinder 4.

determined from the evolution of the solitary wave profiles along the centerline and is equal to $R_{max} = 0.068\,m$ corresponding to the ratio $R_{max}/H = 1.36$. Following the numerical study of Zhao et al. (2007) in [11] for the same $H/h = 0.25$ and $h/a = 1$, this ratio is found equal to 1.37. There is no significant difference between this nondimensional run-up. The maximum wave force occurs at the same time as the maximum run-up that is equal to $t = 2.9$ s. Figure 4 shows the time histories of the computed wave force on the x-direction acting on an isolated cylinder. The maximum wave force at this instant is equal to $F_{max} = 37.5$ N corresponding to the following force coefficient $C_{f,x} = 0.479$. The isolated cylinder is taken as a reference case for the computed force coefficient acting on each cylinder of the platform in the two studied configurations.

3.2. Solitary Wave Diffraction by an Oil Platform. The flow field due to the solitary wave diffraction by square and diamond platform is analyzed at the instant of the maximum run-up in terms of the free surface elevation, the maximum run-up R_{max} at each cylinder, and the maximum wave force F_{max}.

The perspective view of the free surface elevation is shown in Figure 5 at the instant of the maximum run-up at cylinder 1. The solitary wave crest has been altered by the diffraction process. Impacting the cylinder obstacle, the wave run-up is observed due to the transformation of the incident wave to potential energy. The R_{max} depends on the incoming

Table 2: Comparison of the simulated maximum run-up to the wave height ratio with Zhao et al. (2007) for a square arrangement.

	Cylinder 1	Cylinder 2	Cylinder 3	Cylinder 4
Present study	1.29	1.28	1.42	1.42
Zhao et al. (2007) in [11]	1.37	1.37	1.40	1.40

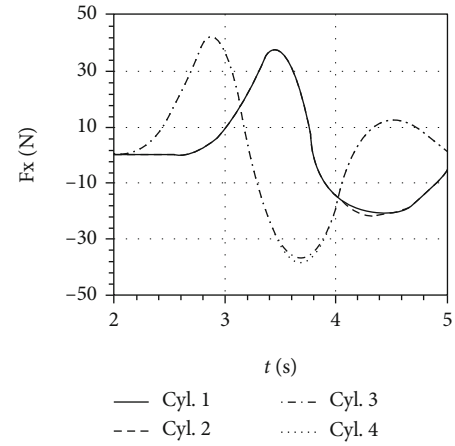

Figure 8: Time evolution of the in-line force on the square arrangement for $H/h = 0.25$.

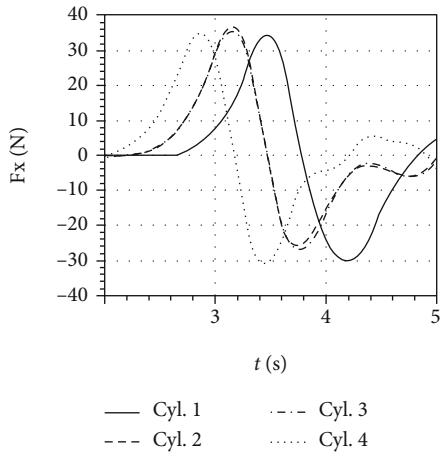

Figure 9: Time evolution of the in-line force on the diamond arrangement for $H/h = 0.25$.

wave and the nature of the obstacle. This interaction leads to a complicated flow field as shown in Figure 5.

For square arrangement, the R_{max} for the first array (cylinders 3 and 4) occurs at the instant $t = 2.90$s and the for second array (cylinders 1 and 2) at $t = 3.45$s. For diamond arrangement, the first R_{max} is observed for the most upstream cylinder (cylinder 4) at $t = 2.88$s. The maximum run-ups for cylinders 2 and 3 occur at the same instant ($t = 3.16$s) and due to nonlinear effect, the R_{max} for cylinder 1 is observed at $t = 3.48$s.

Figure 6 represents the free surface elevation at the instant of the maximum run-up R_{max} for each cylinder in the square arrangement (zero solitary wave incidence). The R_{max} on the downstream cylinders (1 and 2) is smaller than those on the upstream cylinders (3 and 4). The R_{max} on cylinders 1 and 2 is smaller than on the corresponding isolated cylinder. This can be explained by the fact that some of the incident wave energy has been reflected back by other cylinders before the solitary wave impacting the downstream cylinders array. The numerical results of Zhao et al. (2007) in [11] confirm these conclusions, and the calculated R_{max}/H is closely the same as shown by Table 1.

The free surface elevation at the instant of the maximum run-up R_{max} for each cylinder in the diamond arrangement is shown in Figure 7. The R_{max}/H for cylinders 4 and 1 is located at the centerline approach to that on the isolated cylinder. The R_{max}/H for cylinders 2 and 3 is slightly greater than on the isolated cylinder. Table 2 shows good agreement between the present simulations and Zhao et al. in [11] results for the diamond arrangement.

The time evolution of the wave force in the positive x–direction for each cylinder is presented in Figure 8 for the square arrangement. The maximum wave force F_{max} on the most downstream array of the cylinders (1 and 2) is slightly greater than on the isolated cylinder. The increase of the F_{max} relative to the isolated cylinder is more pronounced for the first cylinder array (cylinders 3 and 4). The platform and wave interactions lead to F_{max} for the first cylinders (3 and 4) array greater than on the second array (cylinders 1 and 2). This can be attributed to the shielding effect of the upstream cylinder array. These conclusions are in concordance with the computed run-ups previously discussed.

For the diamond arrangement, Figure 9 presents the time evolution of the wave force for each cylinder. The aligned cylinders 4 and 1 have the same F_{max}. Compared to the isolated cylinder, this F_{max} is significantly smaller. The two symmetric cylinders about the centerline of the computational domain are having the same F_{max} as the isolated cylinder. The approaching solitary wave for these cylinders seems to be not disturbed by the diffraction process.

4. Conclusions

A full three-dimensional numerical wave tank (NWT) was integrated on the PHOENICS code in order to study the solitary wave diffraction with diamond or square cylinders arrangements. The solitary wave was generated by an internal line source, and the cylinder structures are discretized using the cut-cell method. For the diamond platform arrangement, the maximum wave run-ups approach to that on the isolated cylinder indicating that the diffraction process does not affect the four cylinders. However, for a square arrangement, the shielding effect of the upstream cylinders leads to a maximum wave force for the first cylinders array greater than the most downstream array.

The cut-cell method can be generalized for more complex geometric coastal structures in the Cartesian coordinates system. The proposed model based on an internal line source for wave generation can be used to study the combined effects of wave and current on the forces acting on multiple cylinders. Different incident waves can be tested (monochromatic, Stokes, and cnoidal waves). The present model can be used to test the effect of the turbulence model, the effect of the wave height, and the distance between the cylinders on the wave forces and wave run-ups. Further wave-structure interaction cases can be studied such as the wave diffraction with floating structures.

Data Availability

No data were used to support the study.

Conflicts of Interest

This work does not have any conflicts of interest.

Acknowledgments

The third author would like to thank all the professors of the Mathematics Department at the University of Annaba in Algeria, especially his professors/scientists Pr. Mohamed Haiour, Pr. Ahmed-Salah Chibi, and Pr. Azzedine Benchettah for the important content of masters and PhD courses in pure and applied mathematics that he received during his studies. Moreover, he thanks them for the additional help they provided to him during office hours in their office about the few concepts/difficulties he had encountered, and he appreciates their talent and dedication for their postgraduate

students currently and previously. The authors gratefully acknowledge Qassim University, represented by the Deanship of Scientific Research, on the financial support for this research under the number (10261-cos-2020-1-3-I) during the academic year 1442 AH/2020 AD.

References

[1] K. Hosseini, M. Samavat, M. Mirzazadeh, W. X. Ma, and Z. Hammouch, "A new (3+1)-dimensional Hirota bilinear equation: its Bäcklund transformation and rational-type solutions," *Regular and Chaotic Dynamics*, vol. 25, no. 4, pp. 383–391, 2020.

[2] K. Hosseini, A. Seadawy, M. Mirzazadeh, M. Eslami, S. Radmehr, and D. Baleanu, "Multiwave, multicomplexiton, and positive multicomplexiton solutions to a (3 + 1)-dimensional generalized breaking soliton equation," *Alexandria Engineering Journal*, vol. 59, no. 5, pp. 3473–3479, 2020.

[3] K. Hosseini, W. A. Ma, R. Ansari, M. Mirzazadeh, M. Pouyanmehr, and F. Samadani, "Evolutionary behavior of rational wave solutions to the (4 + 1)-dimensional Boiti–Leon–Manna–Pempinelli equation," *Physica Scripta*, vol. 95, article 065208, 2020.

[4] H. Hafsia, S. Nouri, S. Boulaaras, A. Allahem, A. Alkhalaf, and A. M. Vazquez, "Solitary wave diffraction with a single and two vertical circular cylinders," *Mathematical Problems in Engineering*, vol. 2021, Article ID 6634762, 9 pages, 2021.

[5] G. T. Yates and K. H. Wang, "Solitary wave scattering by a vertical cylinder: experimental study," in *The Fourth International Offshore and Polar Engineering Conference*, Osaka, Japan, 1994.

[6] Z. Huang, "Wave interaction with one or two rows of closely spaced rectangular cylinders," *Ocean Engineering*, vol. 34, no. 11–12, pp. 1584–1591, 2007.

[7] Z. Huang and Z. Yuan, "Transmission of solitary waves through slotted barriers: a laboratory study with analysis by a long wave approximation," *Journal of Hydro-environment Research*, vol. 3, pp. 179–185, 2010.

[8] Q. Wang, Y. Fang, and H. Liu, "An experimental study of run-up and loads on a vertical truncated cylinder in a solitary wave," *Ocean Engineering*, vol. 219, pp. 1–10, 2021.

[9] P. Lin and C. Man, "A staggered-grid numerical algorithm for the extended Boussinesq equations," *Applied Mathematical Modelling*, vol. 31, no. 2, pp. 349–368, 2007.

[10] S. C. Mohapatra, H. Islam, and C. Guedes Soares, "Boussinesq model and CFD simulations of non-linear wave diffraction by a floating vertical cylinder," *Journal of Marine Science and Engineering*, vol. 8, no. 8, pp. 1–27, 2020.

[11] M. Zhao, L. Cheng, and B. Teng, "Numerical simulation of solitary wave scattering by a circular cylinder array," *Ocean Engineering*, vol. 34, no. 3-4, pp. 489–499, 2007.

[12] K.-H. Wang and X. Ren, "Interactions of cnoidal waves with cylinder arrays," *Ocean Engineering*, vol. 26, pp. 1–20, 1999.

[13] S. Liu, Z. Sun, and J. Li, "An unstructured FEM model based on Boussinesq equations and its application to the calculation of multidirectional wave run-up in a cylinder group," *Applied Mathematical Modelling*, vol. 36, no. 9, pp. 4146–4164, 2012.

[14] H. Cao and D. Wan, "Benchmark computations of wave run-up on single cylinder and four cylinders by naoe-FOAM-SJTU solver," *Applied Ocean Research*, vol. 65, pp. 327–337, 2017.

[15] C. Frantzis, D. G. E. Grigoriadis, and A. A. Dimas, "Numerical study of solitary waves past slotted breakwaters with a single row of vertical piles: wave processes and flow behavior," *Ocean Engineering*, vol. 211, no. 1, pp. 1–21, 2020.

[16] X. Wang, J. F. Zhou, Z. Wang, and Y. X. You, "A numerical and experimental study of internal solitary wave loads on semi-submersible platforms," *Ocean Engineering*, vol. 150, pp. 298–308, 2018.

[17] C. Yang, Y. Liu, and C. Liu, "Predicting wave loads on adjacent cylinder arrays with a 3D model," *Journal of Hydraulic Research*, vol. 53, no. 6, pp. 797–807, 2015.

[18] A. Kamath, M. Alagan Chella, H. Bihs, and Ø. A. Arntsen, "Evaluating wave forces on groups of three and nine cylinders using a 3D numerical wave tank," *Engineering Applications of Computational Fluid Mechanics*, vol. 9, no. 1, 2015.

[19] Z. Xie, T. Stoesser, S. Yan, Q. Ma, and P. Lin, "A Cartesian cut-cell based multiphase flow model for large-eddy simulation of three-dimensional wave-structure interaction," *Computers & Fluids*, vol. 213, no. 15, pp. 1–17, 2020.

[20] C. W. Hirt and B. D. Nichols, "Volume of fluid (VOF) method for the dynamics of free boundaries," *Journal of Computational Physics*, vol. 39, no. 1, pp. 201–225, 1981.

[21] Z. Hafsia, M. B. Hadj, H. Lamloumi, and K. Maalel, "Internal inlet for wave generation and absorption treatment," *Coastal Engineering*, vol. 56, no. 9, pp. 951–959, 2009.

[22] J. M. Domínguez, C. Altomare, J. Gonzalez-Caoa, and P. Lomonaco, "Towards a more complete tool for coastal engineering: solitary wave generation, propagation and breaking in an SPH-based model," *Coastal Engineering Journal*, vol. 61, pp. 1–15, 2019.

[23] V. Artemov, S. B. Beale, G. de Vahl Davis et al., "A tribute to DB Spalding and his contributions in science and engineering," *International Journal of Heat and Mass Transfer*, vol. 52, no. 17-18, pp. 3884–3905, 2009.

Hindawi
Advances in Mathematical Physics
Volume 2021, Article ID 5569043, 7 pages
https://doi.org/10.1155/2021/5569043

Research Article

Extinction Phenomenon and Decay Estimate for a Quasilinear Parabolic Equation with a Nonlinear Source

Dengming Liu and Luo Yang

School of Mathematics and Computational Science, Hunan University of Science and Technology, Xiangtan, Hunan 411201, China

Correspondence should be addressed to Dengming Liu; liudengming@hnust.edu.cn

Received 16 January 2021; Revised 2 February 2021; Accepted 4 February 2021; Published 20 February 2021

Academic Editor: Kamyar Hosseini

By energy estimate approach and the method of upper and lower solutions, we give the conditions on the occurrence of the extinction and nonextinction behaviors of the solutions for a quasilinear parabolic equation with nonlinear source. Moreover, the decay estimates of the solutions are studied.

1. Introduction

The main goal of this article is to investigate the extinction behavior and decay estimate of the following parabolic initial boundary value problem

$$\begin{cases} u_t = \operatorname{div}\left(u^{\alpha}|\nabla u|^{m-1}\nabla u\right) + \lambda u^{p}\displaystyle\int_{\Omega} u^{q}dx, & (x,t)\in\Omega\times(0,+\infty),\\ u(x,t)=0, & (x,t)\in\partial\Omega\times(0,+\infty),\\ u(x,0)=u_0(x), & x\in\bar{\Omega}. \end{cases} \tag{1}$$

Here, $\Omega\subset R^N$, $N\geq m+1$, is an open bounded domain with smooth boundary $\partial\Omega$, m, p, q, and λ that are positive parameters, $0<m+\alpha<1$, and $u_0^{m+\alpha/m}\in L^{\infty}(\Omega)\cap W_0^{1,m+1}(\Omega)$ is a nonzero nonnegative function.

It is well known that this type of equation describes lots of phenomena in nature, such as heat transfer, chemical reactions, and population dynamics (one can see [1–4] for more detailed physical background). In particular, problem (1) can be used to describe the nonstationary flows in a porous medium of fluids with a power dependence of the tangential stress on the velocity of displacement under polytropic conditions. In this physical context, $u(x,t)$ is the density of the fluid, $u^{\alpha}|\nabla u|^{m-1}\nabla u$ denotes the momentum velocity, and $\lambda u^{p}\int_{\Omega}u^{q}dx$ stands for the nonlinear nonlocal source. The parameter m acts as a characteristic of the medium, to be exact, the medium with $m=1$ is called Newtonian fluid, the medium with $m>1$ is called dilatant fluid, and that with $0<m<1$ is called pseudoplastic.

Extinction phenomenon, as one of the most remarkable properties that distinguish nonlinear parabolic problems from the linear ones, attracted extensive attentions of mathematicians in the past few decades (see [5–16] and the references therein). Especially, many authors devoted to concern with the extinction behavior of the following parabolic problem

$$\begin{cases} u_t - \operatorname{div}\left(a(x,t,u,\nabla\varphi(u))\right) = f(x,t,u), & (x,t)\in\Omega\times(0,+\infty),\\ u(x,t)=0, & (x,t)\in\partial\Omega\times(0,+\infty),\\ u(x,0)=u_0(x), & x\in\bar{\Omega}. \end{cases} \tag{2}$$

Gu [17] discussed (2) with $a(x,t,u,\nabla\varphi(u))=\nabla u$ and $f(x,t,u)=-u^{p}$, and concluded that the extinction phenomenon occurs if and only if $p\in(0,1)$. Tian and Mu [18] dealt with problem (2) with $a(x,t,u,\nabla\varphi(u))=|\nabla u|^{p-2}\nabla u$ and $f(x,t,u)=\lambda u^{p}$, and derived that $q=p-1$ is the critical extinction exponent of problem (2). The authors of [19, 20] generalized the results in [18] to $a(x,t,u,\nabla\varphi(u))=|\nabla u^{m}|^{p-2}\nabla u^{m}$.

The authors of [5, 21] concerned with the extinction behavior of problem (2) with $a(x,t,u,\nabla\varphi(u)) = |\nabla u^m|^{p-2}\nabla u^m$ and $f(x,t,u) = \lambda\int_\Omega u^q dx$, and they pointed out that the effect of the nonlocal source term $\lambda\int_\Omega u^q dx$ on the extinction behavior is very different from that of the local source λu^q. Recently, Zhou and Yang [22] dealt with the extinction singularity of problem (2) in the case $a(x,t,u,\nabla\varphi(u)) = \nabla u^m$ and $f(x,t,u) = \lambda u^p\int_\Omega u^q dx$. For some relevant works on other types of nonlinear evolution equations, the readers can refer to the references [23–28].

However, to our best knowledge, there is no literature on the study of the extinction and decay estimate of the solutions for problem (1). Motivated by those works above, we consider the extinction property of problem (1). More precisely, our purpose is to understand how the nonlinear nonlocal source affects the extinction behavior of problem (1). In other words, the aim of this article is to evaluate the competition between the diffusion term which may produce extinction phenomenon and the nonlinear nonlocal source which may prevent the occurrence of the extinction phenomenon. We want to find a critical extinction exponent and give a complete classification on the extinction and nonextinction cases of the solutions to problem (1). Meanwhile, we will deal with the decay estimates of the extinction solutions.

Since equation (1) is degenerate (or singular) at the points where $u = 0$ or $\nabla u = 0$, there is no classical solution in general, and hence we consider the nonnegative solution of (1) in some weak sense.

Definition 1. Let $\Sigma_T = \Omega\times(0,T)$, and

$$\mathfrak{S} = \Big\{u\in L^{2p}(\Sigma_T)\cap L^{2q}(\Sigma_T)\cap L^2(\Sigma_T);\, u\in C\cdot\big([0,T];L^1(\Omega)\big);\nabla u^{\frac{m+\alpha}{m}}\in L^{m+1}(\Sigma_T)\Big\}. \tag{3}$$

We say that a function $u(x,t)\in\mathfrak{S}$ is a weak lower solution of problem (1) if

$$\int_\Omega u(x,T)\zeta(x,T)dx + \iint_{\Sigma_T}\left[u^\alpha|\nabla u|^{m-1}\nabla u\cdot\nabla\zeta - u\zeta_t\right]dxdt \le \int_\Omega u(x,0)\zeta(x,0)dx + \iint_{\Sigma_T}\left(\lambda u^p\int_\Omega u^q dx\right)\zeta dxdt \tag{4}$$

holds for any $T>0$ and any nonnegative test function

$$\zeta\in\Big\{u\in L^2(\Sigma_T);\, u\in C\big([0,T];L^2(\Omega)\big);\, u_t\in L^2(\Sigma_T);\nabla u\in L^{m+1}(\Sigma_T);\, u\big|_{\partial\Omega}=0\Big\}. \tag{5}$$

Moreover,

$$u(x,0)\le u_0(x)\ \text{for}\ x\in\bar\Omega,\ \text{and}\ u(x,t)\le 0\ \text{for}\ (x,t)\in\partial\Omega\times(0,T). \tag{6}$$

Replacing "$\le$" by "$\ge$" in the inequalities (4) and (6) leads to the definition of the weak upper solution of problem (1). We say that u is a weak solution of problem (1) in Σ_T if it is both a weak lower solution and a weak upper solution of problem (1) in Σ_T.

Proposition 2. *Assume that $u_0(x)$ is a nonzero nonnegative function satisfying $u_0^{m+\alpha/m}\in L^\infty(\Omega)\cap W_0^{1,m+1}(\Omega)$. Then, problem (1) has at least one local weak solution $u(x,t)\in\mathfrak{S}$.*

Remark 3. The proof of Proposition 2 is based on an approximation procedure and the Leray-Schauder fixed-point theorem, and it is standard and lengthy; so, we omit it here, while one can refer to the proof of Proposition 2.1 in [5] (or Proposition 2.3 in [19]) for more details. On the other hand, it is necessary to point out that the weak solution of problem (1) is unique for $p\ge 1$ and $q\ge 1$. In the non-Lipschitz case $0<p<1$ or $0<q<1$, the uniqueness of the weak solution seems to be unknown (See Remark 44.1 of §44.1 in [29]).

The main results of this article are stated as follows.

Theorem 4. *Assume that $0<m+\alpha<p+q$. Then, the nonnegative weak solution of problem (1) vanishes in finite time provided that the nonnegative initial datum $u_0(x)$ is sufficiently small. Moreover,*

$$\begin{cases} \|u\|_{\frac{2m+\alpha}{m}} \le \|u_0\|_{\frac{2m+\alpha}{m}}(1-d_4t)^{\frac{1}{1-m-\alpha}}, & t\in[0,T_1),\\ \|u\|_{\frac{2m+\alpha}{m}} \equiv 0, & t\in[T_1,+\infty), \end{cases} \tag{7}$$

for $m(N-m-1/Nm+m+1-1)\le\alpha<1$, and $\{\|u\|_{N(1-m-\alpha)/m+1}\le\|u_0\|_{N(1-m-\alpha)/m+1}(1-d_8t)^{1/1-(m+\alpha)}, t\in[0,T_2)$, $\|u\|_{N(1-m-\alpha)/m+1}\equiv 0, t\in[T_2,+\infty)$,

for $-m<\alpha<m(N-m-1/Nm+m+1-1)$, where $T_1 = d_4^{-1}$, $T_2 = d_8^{-1}$, d_4, and d_8 are positive constants, given in Section 2.

Theorem 5. *Assume that $0<p+q<m+\alpha<1$ and λ are sufficiently large. Then, for any nonnegative initial datum $u_0(x)$, problem (1) admits at least one nonextinction weak solution.*

Theorem 6. *Assume that $0<m+\alpha=p+q<1$.*

(1) The nonnegative weak solution of problem (1) vanishes in finite time provided that λ is sufficiently small. Moreover,

$$\begin{cases} \|u\|_{\frac{2m+\alpha}{m}} \le \|u_0\|_{\frac{2m+\alpha}{m}}(1-d_{14}t)^{\frac{1}{1-m-\alpha}}, & t\in[0,T_3),\\ \|u\|_{\frac{2m+\alpha}{m}} \equiv 0, & t\in[T_3,+\infty), \end{cases} \tag{8}$$

for $m(N-m-1/Nm+m+1-1)\le\alpha<1$, and $\{\|u\|_{N(1-m-\alpha)/m+1}\le\|u_0\|_{N(1-m-\alpha)/m+1}(1-d_{15}t)^{1/1-m-\alpha}, t\in[0,T_4)$, $\|u\|_{N(1-m-\alpha)/m+1}\equiv 0, t\in[T_4,+\infty)$,

for $-m < \alpha < m(N - m - 1/Nm + m + 1 - 1)$, where $T_3 = d_{14}^{-1}$, $T_4 = d_{15}^{-1}$, d_{14}, and d_{15} are positive constants, given in Section 2.

(2) Problem (1) admits at least one non-extinction weak solution for any nonnegative initial datum $u_0(x)$ provided that λ is sufficiently large

2. Proofs of the Main Results

In this section, based on energy estimates approach and the method of upper and lower solutions, we will give the proofs of our main results.

Proof of Theorem 4. Multiplying equation (1) by u^s and integrating over Ω, one has

$$\frac{1}{s+1}\frac{d}{dt}\int_\Omega u^{s+1}dx + s\left(\frac{m+1}{m+\alpha+s}\right)^{m+1}\int_\Omega \left|\nabla u^{\frac{m+\alpha+s}{m+1}}\right|^{m+1}dx = \lambda\int_\Omega u^{p+s}dx\int_\Omega u^q dx, \tag{9}$$

where

$$s = \begin{cases} \dfrac{m+\alpha}{m}, & \text{if } m\left(\dfrac{N-m-1}{Nm+m+1}-1\right) \le \alpha < 1, \\ \dfrac{N(1-m-\alpha)-m-1}{m+1}, & \text{if } -m < \alpha < m\left(\dfrac{N-m-1}{Nm+m+1}-1\right). \end{cases} \tag{10}$$

We now divide the proof into two cases according to the different values of $p + q$.

Case 1. $m + \alpha < p + q \le 1$. For $m(N - m - 1/Nm + m + 1 - 1) \le \alpha < 1$. It follows from Hölder inequality and (9) that

$$\frac{m}{2m+\alpha}\frac{d}{dt}\int_\Omega u^{\frac{2m+\alpha}{m}}dx + \left(\frac{m}{m+\alpha}\right)^m\int_\Omega \left|\nabla u^{\frac{m+\alpha}{m}}\right|^{m+1}dx \le \lambda|\Omega|^{2-\frac{m(p+q)+m+\alpha}{2m+\alpha}}\left(\int_\Omega u^{\frac{2m+\alpha}{m}}dx\right)^{\frac{m(p+q)+m+\alpha}{2m+\alpha}}. \tag{11}$$

Using Hölder inequality and Sobolev embedding theorem, one has

$$\int_\Omega u^{\frac{2m+\alpha}{m}}dx \le |\Omega|^{1-\frac{(2m+\alpha)(N-m-1)}{N(m+1)(m+\alpha)}}\left(\int_\Omega u^{\frac{m+\alpha}{m}\frac{N(m+1)}{N-m-1}}dx\right)^{\frac{2m+\alpha}{m+\alpha}\frac{N-m-1}{N(m+1)}} \le \kappa_1|\Omega|^{1-\frac{(2m+\alpha)(N-m-1)}{N(m+1)(m+\alpha)}}\left(\int_\Omega \left|\nabla u^{\frac{m+\alpha}{m}}\right|^{m+1}dx\right)^{\frac{2m+\alpha}{(m+1)(m+\alpha)}}, \tag{12}$$

which is equivalent to

$$\kappa_1^{-\frac{(m+1)(m+\alpha)}{2m+\alpha}}|\Omega|^{1-\frac{m+1}{N}-\frac{(m+1)(m+\alpha)}{2m+\alpha}}\left(\int_\Omega u^{\frac{2m+\alpha}{m}}dx\right)^{\frac{(m+1)(m+\alpha)}{2m+\alpha}} \le \int_\Omega \left|\nabla u^{\frac{m+\alpha}{m}}\right|^{m+1}dx, \tag{13}$$

where $\kappa_1 = \kappa_1(\alpha, m, N)$ is the embedding constant. Inserting (13) into (11) yields

$$\frac{d}{dt}\int_\Omega u^{\frac{2m+\alpha}{m}}dx + d_1\left(\int_\Omega u^{\frac{2m+\alpha}{m}}dx\right)^{\frac{(m+1)(m+\alpha)}{2m+\alpha}} \le d_2\left(\int_\Omega u^{\frac{2m+\alpha}{m}}dx\right)^{\frac{m(p+q)+m+\alpha}{2m+\alpha}}, \tag{14}$$

where

$$d_1 = (2m+\alpha)m^{m-1}(m+\alpha)^{-m}\kappa_1^{-\frac{(m+1)(m+\alpha)}{2m+\alpha}}|\Omega|^{1-\frac{m+1}{N}-\frac{(m+1)(m+\alpha)}{2m+\alpha}}, \quad d_2 = \lambda(2m+\alpha)m^{-1}|\Omega|^{2-\frac{m(p+q)+m+\alpha}{2m+\alpha}}. \tag{15}$$

Now, if $u_0(x)$ is sufficiently small satisfying

$$d_3 = d_1 - d_2\left(\int_\Omega u_0^{\frac{2m+\alpha}{m}}dx\right)^{\frac{m(p+q-m-\alpha)}{2m+\alpha}} > 0, \tag{16}$$

then (14) leads to

$$\frac{d}{dt}\int_\Omega u^{\frac{2m+\alpha}{m}}dx + d_3\left(\int_\Omega u^{\frac{2m+\alpha}{m}}dx\right)^{\frac{(m+1)(m+\alpha)}{2m+\alpha}} \le 0. \tag{17}$$

By integration, one can deduce that

$$\|u\|_{\frac{2m+\alpha}{m}} \le \|u_0\|_{\frac{2m+\alpha}{m}}(1 - d_4 t)_+^{\frac{1}{1-m-\alpha}}, \tag{18}$$

which tells us that $u(x, t)$ vanishes in finite time $T_1 = d_4^{-1}$, where

$$d_4 = md_3(1-m-\alpha)(2m+\alpha)^{-1}\|u_0\|_{\frac{2m+\alpha}{m}}^{m+\alpha-1}. \tag{19}$$

For $-m < \alpha < m(N - m - 1/Nm + m + 1 - 1)$. By Sobolev embedding theorem, one obtains

$$\left(\int_\Omega u^{s+1}dx\right)^{\frac{m+\alpha+s}{(m+1)(s+1)}} = \left(\int_\Omega u^{\frac{N(\alpha+m+s)}{N-m-1}}dx\right)^{\frac{N-m-1}{N(m+1)}} \le \kappa_2\left(\int_\Omega \left|\nabla u^{\frac{\alpha+m+s}{m+1}}\right|^{m+1}dx\right)^{\frac{1}{m+1}}. \tag{20}$$

Here, $\kappa_2 = \kappa_2(\alpha, m, N)$ is the embedding constant. Combining (9) and (20), and in view of Hölder inequality, one arrives at

$$\frac{d}{dt}\int_\Omega u^{s+1}dx + d_5\left(\int_\Omega u^{s+1}dx\right)^{\frac{m+\alpha+s}{s+1}} \le d_6\left(\int_\Omega u^{s+1}dx\right)^{\frac{p+q+s}{s+1}}, \tag{21}$$

where

$$d_5 = s(s+1)\left[(m+1)(\kappa_2(m+\alpha+s))^{-1}\right]^{m+1},$$
$$d_6 = \lambda(s+1)|\Omega|^{2-\frac{p+q+s}{s+1}}. \tag{22}$$

Next, choosing $u_0(x)$ sufficiently small such that

$$d_7 = d_5 - d_6\left(\int_\Omega u_0^{s+1}dx\right)^{\frac{p+q-m-\alpha}{s+1}} > 0, \tag{23}$$

then from (21), one has

$$\frac{d}{dt}\int_\Omega u^{s+1}dx + d_7\left(\int_\Omega u^{s+1}dx\right)^{\frac{m+\alpha+s}{s+1}} \le 0. \tag{24}$$

Integrating (24) from 0 to t gives us that

$$\|u\|_{\frac{N(1-m-\alpha)}{m+1}} \le \|u_0\|_{\frac{N(1-m-\alpha)}{m+1}}(1-d_8t)_+^{\frac{1}{1-m-\alpha}}, \tag{25}$$

which means that $u(x,t)$ vanishes in finite time $T_2 = d_8^{-1}$, where

$$d_8 = d_7(m+1)(1-m-\alpha)[N(1-m-\alpha)]^{-1}\|u_0\|_{\frac{N(1-m-\alpha)}{m+1}}^{m+\alpha-1}. \tag{26}$$

Case 2. $m+\alpha < 1 < p+q$. If $p<1$ or $q<s+1$, then the proof is the same as that in Case 1. We only need to focus our attention on the subcase $p \ge 1$ and $q \ge s+1$. Let $\tilde{\Omega}$ be a bounded domain in R^N satisfying $\Omega \subset\subset \tilde{\Omega}$. Denote $\tilde{\lambda}_1$ be the first eigenvalue and $\tilde{\Psi}(x)$ be the corresponding eigenfunction of problem (One can see Lemma 2.3 of [18] for more details on the properties of the first eigenvalue and the corresponding eigenfunction of (27).)

$$\begin{cases} -\text{div}\left(\mathcal{U}^\alpha|\nabla\mathcal{U}|^{m-1}\nabla\mathcal{U}\right) = \lambda\mathcal{U}^{\alpha+1}|\mathcal{U}|^{m-1}, & x\in\tilde{\Omega}, \\ \mathcal{U}(x) = 0, & x\in\partial\tilde{\Omega}. \end{cases} \tag{27}$$

We assume that $\max_{x\in\tilde{\Omega}}\tilde{\Psi}(x) = 1$. Put

$$\mathrm{U}_1(x,t) = \mu\tilde{\Psi}(x) \text{ with } \mu \in \left(\max_{x\in\bar{\Omega}}\frac{u_0(x)}{\tilde{\Psi}(x)}, \left(\min_{x\in\bar{\Omega}}\frac{\tilde{\lambda}_1\tilde{\Psi}^{m+\alpha}(x)}{\lambda|\Omega|}\right)^{\frac{1}{p+q-m-\alpha}}\right). \tag{28}$$

Then, it is not difficult to show that $\mathrm{U}_1(x,t)$ is an upper solution of problem (1). Therefore, one has $u(x,t) \le \mu\tilde{\Psi}(x) \le \mu$ and

$$\lambda\int_\Omega u^{p+s}dx\int_\Omega u^q dx \le \lambda|\Omega|\mu^{p+q-1}\int_\Omega u^{s+1}dx. \tag{29}$$

It follows from (9) and (29) that

$$\frac{1}{s+1}\frac{d}{dt}\int_\Omega u^{s+1}dx + s\left(\frac{m+1}{m+\alpha+s}\right)^{m+1}\int_\Omega\left|\nabla u^{\frac{m+\alpha+s}{m+1}}\right|^{m+1}dx \le \lambda|\Omega|\mu^{p+q-1}\int_\Omega u^{s+1}dx. \tag{30}$$

For $m(N-m-1/Nm+m+1-1) \le \alpha < 1$. It follows from (13) and (30) that

$$\frac{d}{dt}\int_\Omega u^{\frac{2m+\alpha}{m}}dx + d_1\left(\int_\Omega u^{\frac{2m+\alpha}{m}}dx\right)^{\frac{(m+1)(m+\alpha)}{2m+\alpha}} \le d_9\int_\Omega u^{\frac{2m+\alpha}{m}}dx, \tag{31}$$

where

$$d_9 = \lambda|\Omega|(2m+\alpha)m^{-1}\mu^{p+q-1}. \tag{32}$$

Now, selecting $u_0(x)$ sufficiently small satisfying

$$d_{10} = d_1 - d_9\left(\int_\Omega u_0^{\frac{2m+\alpha}{m}}dx\right)^{\frac{m(1-m-\alpha)}{2m+\alpha}} > 0, \tag{33}$$

then (31) tells us that

$$\frac{d}{dt}\int_\Omega u^{\frac{2m+\alpha}{m}}dx + d_{10}\left(\int_\Omega u^{\frac{2m+\alpha}{m}}dx\right)^{\frac{(m+1)(m+\alpha)}{2m+\alpha}} \le 0. \tag{34}$$

A simple integration of (34) over $(0,t)$ gives

$$\|u\|_{\frac{2m+\alpha}{m}} \le \|u_0\|_{\frac{2m+\alpha}{m}}(1-d_4t)_+^{\frac{1}{1-m-\alpha}}, \tag{35}$$

which means that $u(x,t)$ vanishes in finite time, where

$$d_4 = md_{10}(1-m-\alpha)(2m+\alpha)^{-1}\|u_0\|_{\frac{2m+\alpha}{m}}^{m+\alpha-1}. \tag{36}$$

For $-m < \alpha < m(N-m-1/Nm+m+1-1)$. Recalling (20) and (30), one obtains

$$\frac{d}{dt}\int_\Omega u^{s+1}dx + d_5\left(\int_\Omega u^{s+1}dx\right)^{\frac{m+\alpha+s}{s+1}} \le d_{11}\int_\Omega u^{s+1}dx, \tag{37}$$

where

$$d_{11} = \lambda(s+1)|\Omega|\mu^{p+q-1}. \tag{38}$$

Next, if $u_0(x)$ is sufficiently small such that

$$d_{12} = d_5 - d_{11}\left(\int_\Omega u_0^{s+1}dx\right)^{\frac{1-m-\alpha}{s+1}} > 0, \tag{39}$$

then from (37), one arrives at

$$\frac{d}{dt}\int_\Omega u^{s+1}dx + d_{12}\left(\int_\Omega u^{s+1}\mathrm{d}x\right)^{\frac{m+\alpha+s}{s+1}} \le 0. \tag{40}$$

Integrating (40), one can claim that

$$\|u\|_{\frac{N(1-m-\alpha)}{m+1}} \le \|u_0\|_{\frac{N(1-m-\alpha)}{m+1}}(1-d_8t)_+^{\frac{1}{1-m-\alpha}}, \tag{41}$$

which tells us that $u(x,t)$ vanishes in finite time, where

$$d_8 = d_{12}(m+1)N^{-1}\|u_0\|_{\frac{N(1-m-\alpha)}{m+1}}^{m+\alpha-1}. \tag{42}$$

The proof of Theorem 4 is complete.

Proof of Theorem 5. Let λ_1 be the first eigenvalue and $\Psi(x)$ be the corresponding eigenfunction of the following problem

$$\begin{cases} -\mathrm{div}\left(\mathcal{U}^\alpha|\nabla\mathcal{U}|^{m-1}\nabla\mathcal{U}\right) = \lambda\mathcal{U}^{\alpha+1}|\mathcal{U}|^{m-1}, & x\in\Omega,\\ \mathcal{U}(x) = 0, & x\in\partial\Omega. \end{cases} \tag{43}$$

In what follows, we assume that $\Psi(x) > 0$ and $\max_{x\in\Omega}\Psi(x) = 1$. Define $f(t) = (1-e^{-ct})^{1/1-p-q}$, where $c\in(0,(1-p-q)(\lambda\|\Psi\|_q^q - \lambda_1))$. Then, it is easy to check that

$$f(0) = 0, \text{ and } f(t)\in(0,1) \text{ for } t>0. \tag{44}$$

In addition, one has

$$f'(t) + \lambda_1 f^{m+\alpha}(t) - \lambda\|\Psi\|_q^q f^{p+q}(t) \le 0. \tag{45}$$

Define $\mathrm{U}_2(x,t) = f(t)\Psi(x)$. Then, one can verify that

$$\begin{aligned} &\mathrm{U}_{2t} - \mathrm{d}iv\left(\mathrm{U}_2^\alpha|\nabla\mathrm{U}_2|^{m-1}\nabla\mathrm{U}_2\right) - \lambda\mathrm{U}_2^p\int_\Omega \mathrm{U}_2^q dx\\ &\quad= f'(t)\Psi(x) + \lambda_1 f^{m+\alpha}(t)\Psi^{m+\alpha}(x) - \lambda\|\Psi\|_q^q f^{p+q}(t)\Psi^p(x)\\ &\quad< \left(f'(t) + \lambda_1 f^{m+\alpha}(t) - \lambda\|\Psi\|_q^q f^{p+q}(t)\right)\Psi^p(x) \le 0, \end{aligned} \tag{46}$$

which implies that $\mathrm{U}_2(x,t)$ is a strict weak lower solution of problem (1) if $\lambda > \lambda_1\|\Psi\|_q^{-q}$.

Now, consider the following problem

$$\begin{cases} u_t = \mathrm{div}\left(u^\alpha|\nabla u|^{m-1}\nabla u\right) + \lambda(u_+ + 1)^p\int_\Omega (u_+ + 1)^q dx, & (x,t)\in\Omega\times(0,\infty),\\ u(x,t) = 0, & (x,t)\in\partial\Omega\times(0,\infty),\\ u(x,0) = u_0(x) \ge 0, & x\in\bar{\Omega}. \end{cases} \tag{47}$$

Using Leray-Schauder fixed-point theorem, we can prove that problem (47) admits at least one weak solution $\mathrm{U}_3(x,t)$, and we know that $\mathrm{U}_3(x,t)\ge 0$ by the weak maximum principle. In addition, the weak solution $\mathrm{U}_3(x,t)$ is also a weak upper solution of problem (1).

Up to now, we have constructed a pair of weak upper and lower solutions $\mathrm{U}_3(x,t)$, $\mathrm{U}_2(x,t)$. If $\mathrm{U}_2(x,t)\le \mathrm{U}_3(x,t)$, then problem (1) admits a weak solution $\tilde{u}$ satisfying $\mathrm{U}_2\le\tilde{u}\le\mathrm{U}_3$. By the definitions of U_2 and U_3, one has

$$\begin{aligned} &\int_\Omega (\mathrm{U}_2(x,t) - \mathrm{U}_3(x,t))\zeta(x,t)dx - \int_\Omega\\ &\quad\cdot(\mathrm{U}_2(x,0) - \mathrm{U}_3(x,0))\zeta(x,0)dx\\ &\quad+ \iint_{\Sigma_t}\left(\mathrm{U}_2^\alpha|\nabla\mathrm{U}_2|^{m-1}\nabla\mathrm{U}_2 - \mathrm{U}_3^\alpha|\nabla\mathrm{U}_3|^{m-1}\nabla\mathrm{U}_3\right)\cdot\nabla\zeta dxd\tau\\ &\quad- \iint_{\Sigma_t}(\mathrm{U}_2 - \mathrm{U}_3)\zeta_\tau dxd\tau\\ &\le \lambda\iint_{\Sigma_t}\left(\mathrm{U}_2^p\int_\Omega \mathrm{U}_2^q dx - (\mathrm{U}_{3+}+1)^p\int_\Omega(\mathrm{U}_{3+}+1)^q dx\right)\zeta dxd\tau\\ &= \lambda\iint_{\Sigma_t}\left[\mathrm{U}_2^p\int_\Omega\left(\mathrm{U}_2^q - (\mathrm{U}_{3+}+1)^q\right)dx + \left(\mathrm{U}_2^p - (\mathrm{U}_{3+}+1)^p\right)\right.\\ &\quad\left.\cdot\int_\Omega(\mathrm{U}_{3+}+1)^q dx\right]\zeta dxd\tau. \end{aligned} \tag{48}$$

Take $\zeta(x,t) = H_\varepsilon(\mathrm{U}_2^{m+\alpha/m} - \mathrm{U}_3^{m+\alpha/m})$, where $H_\varepsilon(r)$ is a monotone increasing smooth approximation of the following function

$$H(r) = \begin{cases} 1, & r>0,\\ 0, & \text{otherwise.} \end{cases} \tag{49}$$

It is easy to check that $H_\varepsilon'(r)\to\delta(r)$ as $\varepsilon\to 0$. Letting $\varepsilon\to 0$, it follows from (48) that

$$\begin{aligned} \int_\Omega(\mathrm{U}_2 - \mathrm{U}_3)_+dx &\le \lambda\iint_{\Sigma_t}\left[\mathrm{U}_2^p\int_\Omega\left(\mathrm{U}_2^q - (\mathrm{U}_{3+}+1)^q\right)dx\right]H\\ &\quad\cdot\left(\mathrm{U}_2^{\frac{m+\alpha}{m}} - \mathrm{U}_3^{\frac{m+\alpha}{m}}\right)dxd\tau + \lambda\iint_{\Sigma_t}\\ &\quad\cdot\left[\left(\mathrm{U}_2^p - (\mathrm{U}_{3+}+1)^p\right)\int_\Omega(\mathrm{U}_{3+}+1)^q dx\right]H\\ &\quad\cdot\left(\mathrm{U}_2^{\frac{m+\alpha}{m}} - \mathrm{U}_3^{\frac{m+\alpha}{m}}\right)dxd\tau\\ &\le d_{13}\iint_{\Sigma_t}(\mathrm{U}_2 - \mathrm{U}_3)_+dxd\tau, \end{aligned} \tag{50}$$

where d_{13} is a positive constant. Using Gronwall's inequality, one can conclude that $\mathrm{U}_2(x,t)\le\mathrm{U}_3(x,t)$, a.e., in $\Omega\times(0,\infty)$. Furthermore, since U_2 does not vanish, neither does $\tilde{u}$. The proof of Theorem 5 is complete.

Proof of Theorem 6.

(1) For $m(N-m-1/Nm+m+1-1)\le\alpha<1$. It follows from (14) that

$$\frac{d}{dt}\int_{\Omega} u^{\frac{2m+\alpha}{m}}dx \le (d_2 - d_1)\left(\int_{\Omega} u^{\frac{2m+\alpha}{m}}dx\right)^{\frac{(m+1)(m+\alpha)}{2m+\alpha}}. \tag{51}$$

If λ is sufficiently small such that $d_1 - d_2 \ge 0$, then above inequality tells us that

$$\|u\|_{\frac{2m+\alpha}{m}} \le \|u_0\|_{\frac{2m+\alpha}{m}}(1 - d_{14}t)_+^{\frac{1}{1-m-\alpha}}, \tag{52}$$

which means that $u(x,t)$ vanishes in finite time $T_3 = d_{14}^{-1}$, where

$$d_{14} = m(d_1 - d_2)(1 - m - \alpha)(2m + \alpha)^{-1}\|u_0\|_{\frac{2m+\alpha}{m}}^{m+\alpha-1}. \tag{53}$$

For $-m < \alpha < m(N - m - 1/Nm + m + 1 - 1)$. It follows from (21) that

$$\frac{d}{dt}\int_{\Omega} u^{\frac{N(1-m-\alpha)}{m+1}}dx \le (d_6 - d_5)\left(\int_{\Omega} u^{\frac{N(1-m-\alpha)}{m+1}}dx\right)^{\frac{N-m-1}{N}}. \tag{54}$$

If λ is sufficiently small such that $d_5 - d_6 \ge 0$, then (54) leads to

$$\|u\|_{\frac{N(1-m-\alpha)}{m+1}} \le \|u_0\|_{\frac{N(1-m-\alpha)}{m+1}}(1 - d_{15}t)_+^{\frac{1}{1-m-\alpha}}, \tag{55}$$

which implies that $u(x,t)$ vanishes in finite time $T_4 = d_{15}^{-1}$, where

$$d_{15} = (m+1)(d_5 - d_6)N^{-1}\|u_0\|_{\frac{2m+\alpha}{m}}^{m+\alpha-1}. \tag{56}$$

(2) Let

$$\mathrm{U}_4(x,t) = \left[(1 - p - q)\left(\lambda\|\Psi\|_q^q - \lambda_1\right)t\right]^{\frac{1}{1-p-q}}\Psi(x). \tag{57}$$

One can easily prove that $\mathrm{U}_4(x,t)$ is a weak nonextinction lower solution of problem (1) if $\lambda > \lambda_1\|\Psi\|_q^{-q}$. On the other hand, let $\mathrm{U}_5(x,t)$ be a weak solution of problem (47) with $p + q = m + \alpha$; then, $\mathrm{U}_5(x,t)$ is a weak upper solution of problem (1). Similar to the process of proof of Theorem 5, one can claim that problem (1) has at least one nonextinction weak solution $\tilde{u}$. The proof of Theorem 6 is complete.

3. Conclusion

In the present article, we mainly focus on the extinction phenomenon and the decay estimates of the solution to a quasilinear parabolic equation with a coupled nonlinear source. By analyzing the competition between the coupled nonlinear source term and the fast diffusion term, along with energy estimates approach and the method of upper and lower solutions, we show that $p + q = m + \alpha$ is the critical extinction exponent of the solutions. That is, if $m + \alpha < p + q$, then for sufficiently small initial datum, the solution possesses extinction property, while if $p + q < m + \alpha$, then for any nonnegative initial datum, problem (1) admits at least one nonextinction solution provided that λ is sufficiently large. In the critical case $p + q = m + \alpha$, whether the solution vanishes or not depends on the size of the parameter λ.

Our next work is to study the numerical extinction phenomenon of the parabolic problems like (1). We hope to give some numerical examples for our theoretical researches in the near future.

Data Availability

The data used to support the findings of this study are included within the article.

Conflicts of Interest

Conflict of interest statement is included without existing competing interests.

Acknowledgments

The first author is sincerely grateful to professor Chunlai Mu of Chongqing University for his encouragements and suggestions. The authors would like to thank the editor and anonymous referee for their careful reading and important comments and suggestions. This research is supported by the Natural Science Foundation of Hunan Province (Grant No. 2019JJ50160).

References

[1] A. S. Kalashnikov, "Some problems of the qualitative theory of second-order nonlinear degenerate parabolic equations," *Uspekhi Matematicheskikh Nauk*, vol. 42, no. 2, pp. 135–176, 1987.

[2] J. L. Vazquez, *The Porous Medium Equations: Mathematical Theory*, Oxford University Press, London, 2007.

[3] Z. Wu, J. Yin, H. Li, and J. Zhao, *Nonlinear Diffusion Equations*, World Scientific Publishing Co., Inc., River Edge, NJ, USA, 2001.

[4] D. M. Liu and C. L. Mu, "Cauchy problem for a doubly degenerate parabolic equation with inhomogeneous source and measure data," *Differential and Intergral Equations*, vol. 27, no. 11/12, pp. 1001–1012, 2014.

[5] Y. Z. Han and W. J. Gao, "Extinction and non-extinction for a polytropic filtration equation with a nonlocal source," *Applicable Analysis*, vol. 92, no. 3, pp. 636–650, 2013.

[6] R. M. P. Almeida, S. N. Antotesv, and J. C. M. Duque, "On a nonlocal degenerate parabolic problem," *Nonlinear Analysis: Real World Applications*, vol. 27, pp. 146–157, 2016.

[7] Y. J. Chen, J. Wang, and H. X. Zhang, "Extinction for a couple of fast diffusion systems with nonlinear sources," *Nonlinear Analysis: Real World Applications*, vol. 14, no. 4, pp. 1931–1937, 2013.

[8] Z. B. Fang and X. H. Xu, "Extinction behavior of solutions for the p-Laplacian equations with nonlocal sources," *Nonlinear Analysis: Real World Applications*, vol. 13, no. 4, pp. 1780–1789, 2012.

[9] D. M. Liu and C. L. Mu, "Critical extinction exponent for a doubly degenerate non-divergent parabolic equation with a

gradient source," *Applicable Analysis*, vol. 97, no. 12, pp. 2132–2141, 2018.

[10] D. M. Liu and C. L. Mu, "Extinction for a quasilinear parabolic equation with a nonlinear gradient source," *Taiwanese Journal of Mathematics*, vol. 18, no. 5, pp. 1329–1343, 2014.

[11] D. Liu and C. Mu, "Extinction for a quasilinear parabolic equation with a nonlinear gradient source and absorption," *Journal of Applied Analysis & Computation*, vol. 5, no. 1, pp. 114–137, 2015.

[12] W. Liu, "Extinction properties of solutions for a class of fast diffusive p-Laplacian equations," *Nonlinear Analysis: Theory, Methods & Applications*, vol. 74, no. 13, pp. 4520–4532, 2011.

[13] W. J. Liu and B. Wu, "A note on extinction for fast diffusivep-Laplacian with sources," *Mathematicsl Methods in the Applied Sciences*, vol. 31, no. 12, pp. 1383–1386, 2008.

[14] Y. F. Wang and J. X. Yin, "Critical extinction exponents for a polytropic filtration equation with absorption and source," *Mathematicsl Methods in the Applied Sciences*, vol. 36, no. 12, pp. 1591–1597, 2013.

[15] J. X. Yin and C. H. Jin, "Critical extinction and blow-up exponents for fast diffusivep-Laplacian with sources," *Mathematicsl Methods in the Applied Sciences*, vol. 30, no. 10, pp. 1147–1167, 2007.

[16] Y. Hongjun, L. Songzhe, G. Wenjie, X. Xiaojing, and C. Chunling, "Extinction and positivity for the evolution p-Laplacian equation in R^n," *Nonlinear Analysis: Theory, Methods & Applications*, vol. 60, no. 6, pp. 1085–1091, 2005.

[17] Y. G. Gu, "Necessary and sufficient conditions of extinction of solution on parabolic equations," *Acta Mathematica Sinica*, vol. 37, no. 1, pp. 73–79, 1994, (In Chinese).

[18] Y. Tian and C. L. Mu, "Extinction and non-extinction for a p-Laplacian equation with nonlinear source," *Nonlinear Analysis*, vol. 69, no. 8, pp. 2422–2431, 2008.

[19] C. H. Jin, J. X. Yin, and Y. Y. Ke, "Critical extinction and blow-up exponents for fast diffusive polytropic filtration equation with sources," *Proceedings of the Edinburgh Mathematical Society*, vol. 52, no. 2, pp. 419–444, 2009.

[20] J. Zhou and C. L. Mu, "Critical blow-up and extinction exponents for non-Newton polytropic filtration equation with source," *Bulletin of the Korean Mathematical Society*, vol. 46, no. 6, pp. 1159–1173, 2009.

[21] Y. Z. Han and W. J. Gao, "Extinction for a fast diffusion equation with a nonlinear nonlocal source," *Archiv der Mathematik*, vol. 97, no. 4, pp. 353–363, 2011.

[22] S. Zhou and Z. D. Yang, "Extinction and non-extinction behavior of solutions for a class of reaction-diffusion equations with a nonlinear source," *Acta Mathematica Scientia*, vol. 36A, no. 3, pp. 531–542, 2016, (In Chinese).

[23] S. Boulaaras, "Some new properties of asynchronous algorithms of theta scheme combined with finite elements methods for an evolutionary implicit 2-sided obstacle problem," *Mathematical Methods in the Applied Sciences*, vol. 40, no. 18, pp. 7231–7239, 2017.

[24] A. Choucha, S. Boulaaras, D. Ouchenane, and S. Beloul, "General decay of nonlinear viscoelastic Kirchhoff equation with Balakrishnan-Taylor damping, logarithmic nonlinearity and distributed delay terms," *Mathematical Methods in the Applied Sciences*, 2020.

[25] A. Choucha, S. Boulaaras, and D. Ouchenane, "Exponential decay of solutions for a viscoelastic coupled lame system with logarithmic source and distributed delay terms," *Mathematical Methods in the Applied Sciences*, 2020.

[26] S. Boulaaras and N. Doudi, "Global existence and exponential stability of coupled Lamé system with distributed delay and source term without memory term," *Boundary Value Problems*, vol. 2020, no. 1, 2020.

[27] N. Doudi and S. Boulaaras, "Global existence combined with general decay of solutions for coupled Kirchhoff system with a distributed delay term," *Revista de la Real Academia de Ciencias Exactas, Físicas y Naturales. Serie A. Matemáticas*, vol. 114, no. 4, 2020.

[28] D. M. Liu, C. L. Mu, and I. Ahmed, "Blow-up for a semilinear parabolic equation with nonlinear memory and nonlocal nonlinear boundary," *Taiwanese Journal of Mathematics*, vol. 17, no. 4, pp. 1353–1370, 2013.

[29] P. Quittner and P. Souplet, *Superlinear Parabolic Problems: Blow-Up, Global Existence and Steady States*, Birkhäuser Verlag AG, Basel, 2007.

Hindawi
Advances in Mathematical Physics
Volume 2021, Article ID 5555930, 7 pages
https://doi.org/10.1155/2021/5555930

Research Article

A New Result for a Blow-up of Solutions to a Logarithmic Flexible Structure with Second Sound

Ahlem Merah,[1] Fatiha Mesloub,[1] Salah Mahmoud Boulaaras,[2,3] and Bahri-Belkacem Cherif[4]

[1]*Laboratory of Mathematics, Informatics and Systems (LAMIS), Department of Mathematics and Computer Science, Larbi Tebessi University, 12002 Tebessa, Algeria*
[2]*Department of Mathematics, College of Sciences and Arts, ArRas, Qassim University, Buraydah, Saudi Arabia*
[3]*Laboratory of Fundamental and Applied Mathematics of Oran (LMFAO), University of Oran 1, Ahmed Benbella, Oran, Algeria*
[4]*Preparatory Institute for Engineering Studies in Sfax (I.P.E.I.S.Sfax), BP 1172 Sfax, Tunisia*

Correspondence should be addressed to Bahri-Belkacem Cherif; bahi1968@yahoo.com

Received 21 January 2021; Revised 2 February 2021; Accepted 4 February 2021; Published 11 February 2021

Academic Editor: Kamyar Hosseini

This paper is concerned with a problem of a logarithmic nonuniform flexible structure with time delay, where the heat flux is given by Cattaneo's law. We show that the energy of any weak solution blows up infinite time if the initial energy is negative.

1. Introduction

In this work, we consider the vibrations of an inhomogeneous flexible structure system with a constant internal delay and logarithmic nonlinear source term:

$$\begin{cases} m(x)u_{tt} - (p(x)u_x + 2\delta(x)u_{tx})_x + \eta\theta_x + \mu u_t(x, t-\tau_0) = u|u|^{p-2}\ln|u|^{\gamma}, & x \in (0, L), t > 0, \\ \theta_t + kq_x + \eta u_{tx} = 0 & x \in (0, L), t > 0, \\ \tau q_t + \beta q + k\theta_x = 0 & x \in (0, L), t > 0, \end{cases} \tag{1}$$

with boundary conditions

$$u(0, t) = u(L, t) = 0\,; \theta(0, t) = \theta(L, t) = 0, t \geq 0, \tag{2}$$

and initial conditions

$$u(x, 0) = u_0(x), u_t(x, 0) = u_1(x)\,; \theta(x, 0) = \theta_0(x)\,; q(x, 0) = q_0(x), x \in [0, L], \tag{3}$$

where $u(x, t)$ is the displacement of a particle at position $x \in [0, L]$, and the time $t > 0$. $\eta > 0$ is the coupling constant depending on the heating effect,$p \geq 2$,γ, β, and k are positive constants, and μ is a real number. $\tau > 0$ is the relaxation time describing the time lag in the response for the temperature, and $\tau_0 > 0$ represents the time delay in particular if $\tau = 0$(1.1) reduces to the viscothermoelastic system with delay, in which the heat flux is given by Fourier's law instead of Cattaneo's law, where $q = q(x, t)$ is the heat flux, and $m(x), \delta(x)$, and $p(x)$ are responsible for the inhomogeneous structure of the beam and, respectively, denote mass per unit length of structure, coefficient of internal material damping (viscoelastic property), and a positive function related to the stress acting on the body at a point x. The model of heat condition, originally due to Cattaneo, is of hyperbolic type. We recall the assumptions of $m(x), \delta(x)$, and $p(x)$ in [1, 2] such that

$$m, \delta, p \in W^{1,\infty}(0, L), m(x), \delta(x) \text{ and } p(x) > 0, \forall x \in [0, L]. \tag{4}$$

In these kinds of problems, Gorain [3] in 2013 has established uniform exponential stability of the problem

$$m(x)u_{tt} - (p(x)u_x + 2\delta(x)u_{tx})_x = f(x), on\ (0, L) \times \mathbb{R}^+, \tag{5}$$

which describes the vibrations of an inhomogeneous flexible

structure with an exterior disturbing force. More recently, Misra et al. [4] showed the exponential stability of the vibrations of a inhomogeneous flexible structure with thermal effect governed by the Fourier law.

$$\begin{aligned} m(x)u_{tt} - (p(x)u_x + 2\delta(x)u_{tx})_x - k\theta_x = f(x), \\ \theta_t - \theta_{xx} - ku_{xt} = 0. \end{aligned} \tag{6}$$

In addition, we can cite other works in the same form like the system in [5]; Racke studied the exponential stability in linear and nonlinear 1d of thermoelasticity system with second sound given by

$$\begin{cases} m(x)u_{tt} - (p(x)u_x + 2\delta(x)u_{tx})_x - k\theta_x = 0, on(0, L) \times \mathbb{R}^+ \\ \theta_t + kq_x + \eta u_{tx} = 0, on(0, L) \times \mathbb{R}^+ \\ \tau q_t + \beta q + k\theta_x = 0, on(0, L) \times \mathbb{R}^+, \end{cases} \tag{7}$$

Now for the multidimensional system, Messaoudi in [6] established a local existence and a blow-up result for a multidimensional nonlinear system of thermoelasticity with second sound (see in this regard Refs. [7–10]); for the same problem above, Alves et al. proved that system (7) is polynomial decay (see [1]), with boundary and initial conditions:

$$\begin{aligned} u(0, t) = u(L, t) = 0\,; \theta(0, t) = \theta(L, t) = 0, t \geq 0, \\ u(x, 0) = u_0(x), u_t(x, 0) = u_1(x)\,; \\ \theta(x, 0) = \theta_0(x)\,; q(x, 0) = q_0(x), x \in [0, L]. \end{aligned} \tag{8}$$

We know that the dynamic systems with delay terms have become a significant examination subject in differential condition since the 1970s of the only remaining century. The delay effect that is similar to memory processes is important in the research of applied mathematics such as physics, noninstant transmission phenomena, and biological motivation; model (7) is related to the following problem with delay terms:

$$\begin{cases} m(x)u_{tt} - (p(x)u_x + 2\delta(x)u_{tx})_x + \eta\theta_x + \mu u_t(x, t - \tau_0) = 0 & x \in (0, L), t > 0, \\ \theta_t + kq_x + \eta u_{tx} = 0 & x \in (0, L), t > 0, \\ \tau q_t + \beta q + k\theta_x = 0 & x \in (0, L), t > 0, \\ u(0, t) = u(L, t) = 0\,; \theta(0, t) = \theta(L, t) = 0, t \geq 0, \\ u(x, 0) = u_0(x), u_t(x, 0) = u_1(x)\,; \\ \theta(x, 0) = \theta_0(x)\,; q(x, 0) = q_0(x), x \in [0, L]. \end{cases} \tag{9}$$

The authors prove that the system (9) is well posed and exponential decay under a small condition on time delay (see [2]). Now in the presence of source term, the system (9) becomes the system studied in this work with a logarithmic source term; this type of problems is encountered in many branches of physics such as nuclear physics, optics, and geophysics. It is well known, from the quantum field theory, that such kind of logarithmic nonlinearity appears naturally in inflation cosmology and in supersymmetric field theories (see [11–13]).

This work is organized as follows: In "Statement of Problem," we talk briefly about the local existence of the systems (1), (2), and (3), and we define some space and theorem used. In "Blow-up of Solution," the blow-up result is proved.

2. Statement of Problem

Let us introduce the function

$$z(x, \rho, t) = u_t(x, t - \rho\tau_0), x \in (0, L), \rho \in (0, 1), t > 0. \tag{10}$$

Thus, we have

$$\tau_0 z_t(x, \rho, t) + z_\rho(x, \rho, t) = 0, x \in (0, L), \rho \in (0, 1), t > 0. \tag{11}$$

Then, problems (1)–(3) are equivalent to

$$\begin{cases} m(x)u_{tt} - (p(x)u_x + 2\delta(x)u_{tx})_x + \eta\theta_x & \\ +\mu z(x, 1, t) = u|u|^{p-2} \ln |u|^\gamma, & x \in (0, L), t > 0, \\ \tau_0 z_t(x, \rho, t) + z_\rho(x, \rho, t) = 0 & x \in (0, L), \rho \in (0, 1), t > 0, \\ \theta_t + kq_x + \eta u_{tx} = 0 & x \in (0, L), t > 0, \\ \tau q_t + \beta q + k\theta_x = 0 & x \in (0, L), t > 0, \end{cases} \tag{12}$$

$$\begin{cases} u(0, t) = u(L, t) = 0\,; \theta(0, t) = \theta(L, t) = 0, t \geq 0, \\ u(x, 0) = u_0(x), u_t(x, 0) = u_1(x)\,; \theta(x, 0) = \theta_0(x), x \in [0, L] \\ q(x, 0) = q_0(x), x \in [0, L] \\ z(x, 0, t) = u_t(x, t), x \in (0, L), t > 0, \\ z(x, \rho, 0) = f_0(x, -\rho\tau_0), x \in (0, L), \rho \in (0, 1). \end{cases} \tag{13}$$

We first state a local existence theorem that can be established by combining the arguments of related works [10,6].

Let $v = u_t$ and denote by

$$\Phi = (u, v, \theta, q, z)^T, \Phi(0) = \Phi_0 = (u_0, u_1, \theta_0, q_0, f_0)^T. \tag{14}$$

The state space of Φ is the Hilbert space

$$= H_0^1(0, L) \times L^2(0, L) \times L_*^2(0, L) \times L^2((0, 1) \times (0, L)). \tag{15}$$

Theorem 1. *Assume that*

$$2 < p \leq \frac{2n}{n-2}, \text{ if } n \geq 3. \tag{16}$$

Then, for every $\Phi_0 \in$, there exists a unique local solution in the class $\Phi \in C([0, T],)$.

3. Blow-up of Solution

In this section, we prove that the solutions for the problems (12)–(13) blow up in a finite time when the initial energy is negative. We use the improved method of Salim and Messaoudi [6]. We define the energy associated with problems (12)–(13) by

$$\begin{aligned} E(t) = {} & \frac{1}{2}\left(\|m(x)\|_\infty \|u_t(t)\|_2^2\right) + \frac{1}{2}\left(\|p(x)\|_\infty \|u_x\|_2^2\right) \\ & + \frac{\tau}{2}\|q\|_2^2 + \frac{1}{2}\|\theta\|_2^2 + \frac{\tau_0|\mu|}{2}\int_0^1 \|z(x,\rho,t)\|^2 d\rho \\ & + \frac{\gamma}{p^2}\|u\|_p^p - \frac{1}{p}\int_0^L |u|^p \ln |u|^\gamma dx. \end{aligned} \tag{17}$$

Lemma 2. *Suppose that*

$$2 < p \le \frac{2n}{n-2}, n \ge 3. \tag{18}$$

Then, there exists a positive constant $C > 0$ depending on $[0.L]$ only, such that

$$\left[\int_0^L |u|^p \ln |u|^\gamma dx\right]^{\frac{s}{p}} \le C\left[\int_0^L |u|^p \ln |u|^\gamma dx + \|u_x\|_2^2\right], \tag{19}$$

for any $u \in H_0^1(0,L)$ and $2 \le s \le p$, provided that $\int_0^L |u|^p \ln |u|^\gamma dx \ge 0$.

Proof. If $\int_0^L |u|^p \ln |u|^\gamma dx > 1$, then

$$\left[\int_0^L |u|^p \ln |u|^\gamma dx\right]^{\frac{s}{p}} \le \int_0^L |u|^p \ln |u|^\gamma dx. \tag{20}$$

If $\int_0^L |u|^p \ln |u|^\gamma dx \le 1$, then we set

$$\Gamma_1 = \{x \in [0,L] \,|\, |u| > 1\}, \tag{21}$$

and, for any $\beta \le 2$, we have

$$\begin{aligned} \left[\int_0^L |u|^p \ln |u|^\gamma dx\right]^{\frac{s}{p}} & \le \left[\int_0^L |u|^p \ln |u|^\gamma dx\right]^{\frac{\beta}{p}} \le \left[\int_{\Gamma_1} |u|^p \ln |u|^\gamma dx\right]^{\frac{\beta}{p}} \\ & \le \left[\int_{\Gamma_1} |u|^{p+1} dx\right]^{\frac{\beta}{p}} \le \left[\int_0^L |u|^{p+1} dx\right]^{\frac{\beta}{p}} = \|u\|_{p+1}^{\frac{\beta(p+1)}{p}}. \end{aligned} \tag{22}$$

We choose $\beta = 2p/(p+1) < 2$ to get

$$\left[\int_0^L |u|^p \ln |u|^\gamma dx\right]^{\frac{s}{p}} \le \|u\|_{p+1}^2 \le C\|u_x\|_2^2. \tag{23}$$

Combining (20) and (23), the result was obtained.

Lemma 3. *There exists a positive constant $C > 0$ depending on $[0,L]$ only, such that*

$$\|u\|_p^p \le C\left[\int_0^L |u|^p \ln |u|^\gamma dx + \|u_x\|_2^2\right], \tag{24}$$

for any $u \in H_0^1(0,L)$, provided that $\int_0^L |u|^p \ln |u|^\gamma dx \ge 0$.

Proof. We set

$$\Gamma_+ = \{x \in [0,L] \,|\, |u| > e\} \text{ and } \Gamma_- = \{x \in [0,L] \,|\, |u| \le e\}, \tag{25}$$

thus

$$\begin{aligned} \|u\|_p^p &= \int_{\Gamma_+} |u|^p dx + \int_{\Gamma_-} |u|^p dx \le \int_{\Gamma_+} |u|^p \ln |u|^\gamma dx + \int_{\Gamma_-} e^p \left|\frac{u}{e}\right|^p dx \\ &\le \int_{\Gamma_+} |u|^p \ln |u|^\gamma dx + e^p \int_{\Gamma_-} \left|\frac{u}{e}\right|^2 dx \\ &\le \int_0^L |u|^p \ln |u|^\gamma dx + e^{p-2} \int_0^L |u|^2 dx \\ &\le C\left\{\int_0^L |u|^p \ln |u|^\gamma dx + \|u_x\|_2^2\right\}. \end{aligned} \tag{26}$$

By using the inequalities $\|u\|_2^2 \le C\|u\|_p^2 \le C(\|u\|_p^p)^{2/p}$, we have the following corollary.

Corollary 4. *There exists a positive constant $C > 0$ depending on $[0,L]$ only, such that*

$$\|u\|_2^2 \le C\left[\left(\int_0^L |u|^p \ln |u|^\gamma dx\right)^{\frac{2}{p}} + \|u_x\|_2^{\frac{4}{p}}\right]. \tag{27}$$

provided that $\int_0^L |u|^p \ln |u|^\gamma dx \ge 0$.

Lemma 5. *There exists a positive constant $C > 0$ depending on $[0,L]$ only, such that*

$$\|u\|_p^s \le C\left[\|u\|_p^p + \|u_x\|_2^2\right], \tag{28}$$

for any $u \in H_0^1(0,L)$ and $2 \le s \le p$.

Proof. If $\|u\|_p \ge 1$, then

$$\|u\|_p^s \le \|u\|_p^p. \tag{29}$$

If $\|u\|_p \le 1$, then $\|u\|_p^s \le \|u\|_p^2$. Using the Sobolev embedding theorems, we have

$$\|u\|_p^s \le \|u\|_p^2 \le C\|u_x\|_2^2. \tag{30}$$

Now we are ready to state and prove our main result. For

this purpose, we define

$$H(t) = -E(t) = -\frac{1}{2}\left(\|m(x)\|_\infty \|u_t(t)\|_2^2\right) - \frac{1}{2}\left(\|p(x)\|_\infty \|u_x\|_2^2\right) - \frac{\tau}{2}\|q\|_2^2 - \frac{1}{2}\|\theta\|_2^2 - \frac{\tau_0|\mu|}{2}\int_0^1 \|z(x,\rho,t)\|^2 d\rho - \frac{\gamma}{p^2}\|u\|_p^p + \frac{1}{p}\int_0^L |u|^p \ln |u|^\gamma dx. \tag{31}$$

Corollary 6. *Assume that (18) holds. Then*

$$\|u\|_p^s \le C\left\{\left(1 - \frac{\gamma}{p\|p(x)\|_\infty}\right)\|u\|_p^p - \left(\frac{2}{\|p(x)\|_\infty}\right)H(t) - \left(\frac{\|m(x)\|_\infty}{\|p(x)\|_\infty}\right)\|u_t(t)\|_2^2 - \left(\frac{\tau}{\|p(x)\|_\infty}\right)\|q\|_2^2 - \left(\frac{1}{\|p(x)\|_\infty}\right)\|\theta\|_2^2 - \frac{\tau_0|\mu|}{\|p(x)\|_\infty}\int_0^1 \|z(x,\rho,t)\|^2 d\rho + \frac{2}{p\|p(x)\|_\infty}\int_0^L |u|^p \ln |u|^\gamma dx\right\}, \tag{32}$$

for any $u \in (H_0^1(0,L))^n$ *and* $2 \le s \le p$.

Theorem 7. *Assume that (18) holds. Assume further that*

$$E(0) = \frac{1}{2}\left(\|m(x)\|_\infty \|u_1(t)\|_2^2\right) + \frac{1}{2}\left(\|p(x)\|_\infty \|\nabla u_0\|_2^2\right) + \frac{\tau}{2}\|q_0\|_2^2 + \frac{1}{2}\|\theta_0\|_2^2 + \frac{\tau_0|\mu|}{2}\int_0^L\int_0^1 |f_0(x,-\rho\tau_0)|^2 d\rho dx + \frac{\gamma}{p^2}\|u_0\|_p^p - \frac{1}{p}\int_0^L |u_0|^p \ln |u_0|^\gamma dx < 0. \tag{33}$$

Then, the solution of (12) blows up in finite time.

Proof. we have

$$E(t) \le E(0) < 0, \tag{34}$$

and

$$H'(t) = -E'(t) = 2\left(\|\delta(x)\|_\infty \|u_{xt}(t)\|_2^2\right) + \beta\|q\|_2^2 + |\mu|\int_0^L |z(x,1,t)|^2 dx. \tag{35}$$

Hence

$$H'(t) \ge C_0\left\{\left(\|\delta(x)\|_\infty \|u_{xt}(t)\|_2^2\right) + |\mu|\int_0^L z^2(x,1,t)dx\right\} \ge 0; \forall t \in [0,T). \tag{36}$$

Consequently, we get

$$0 < H(0) \le H(t) \le \int_0^L |u|^p \ln |u|^\gamma dx; \forall t \in [0,T), \tag{37}$$

by virtue of (17) and (31). We then introduce

$$L(t) = H^{1-\alpha}(t) + \varepsilon\int_0^L \left[m(x)u_t(t)u(t) + 4\delta(x)|u_x|^2\right]dx + \varepsilon\int_0^L \frac{n\tau}{k} uq dx, \tag{38}$$

where $\varepsilon > 0$ to be specified later and

$$\frac{2(p-2)}{p^2} < \alpha < \frac{p-2}{2p} < 1. \tag{39}$$

A direct differentiation of $L(t)$ gives

$$L'(t) = (1-\alpha)H^{-\alpha}(t)H'(t) + \varepsilon\int_0^L m(x)|u_t|^2 dx + \varepsilon\frac{\eta\tau}{k}\int_0^L qu_t(t)dx - \varepsilon\int_0^L p(x)|u_x|^2 dx + 2\varepsilon\eta\int_0^L \theta u_x dx - \varepsilon\int_0^L \mu z(x,1,t)u dx + \varepsilon\int_0^L |u|^p \ln |u|^\gamma - \varepsilon\frac{\eta\beta}{k}\int_0^L q u dx, \tag{40}$$

using the inequality of young

$$2\varepsilon\eta\int_0^L \theta u_x dx \ge -\varepsilon\eta\|\theta\|_2^2 - \varepsilon\eta\|u_x\|_2^2, \tag{41}$$

$$-\varepsilon\int_0^L p(x)|u_x|^2 dx \ge -\varepsilon\|p(x)\|_\infty \|u_x\|_2^2, \tag{42}$$

$$\varepsilon\int_0^L m(x)|u_t|^2 dx \ge \varepsilon\|m(x)\|_\infty \|u_t\|_2^2, \tag{43}$$

$$\varepsilon\frac{\eta\tau}{k}\int_0^L qu_t(t)dx \ge -\varepsilon\frac{\eta\tau}{2k}\|u_t\|_2^2 - \varepsilon\frac{\eta\tau}{2k}\|q\|_2^2, \tag{44}$$

and

$$-\varepsilon\int_0^L \mu z(x,1,t)u dx \ge -\varepsilon|\mu|\left\{\frac{\xi_1}{2}\int_0^L |z(x,1,t)|^2 dx + \frac{1}{2\xi_1}\|u\|_2^2\right\}, \forall \xi_1 > 0, \tag{45}$$

$$-\varepsilon\frac{\eta\beta}{k}\int_0^L q u dx \ge \varepsilon\frac{\eta\beta}{k}\left\{\frac{\xi_2}{2}\|q\|_2^2 + \frac{1}{2\xi_2}\|u\|_2^2\right\}, \forall \xi_2 > 0. \tag{46}$$

Substituting (41), (42), (43), (44), (45), and (46) in (40),

we get

$$L'(t) \geq (1-\alpha)H^{-\alpha}(t)H'(t) + \varepsilon\left\{\|m(x)\|_\infty - \frac{\eta\tau}{2k}\right\}\|u_t\|_2^2 - \varepsilon\left\{\|p(x)\|_\infty + \eta\right\}\|u_x\|_2^2 - \varepsilon\eta\|\theta\|_2^2 - \varepsilon\left\{\frac{\tau\eta + \beta\eta\xi_2}{2k}\right\}\|q\|_2^2 + \varepsilon\int_0^L |u|^p \ln|u|^\gamma dx - \varepsilon|\mu|\frac{\xi_1}{2}\int_0^L |z(x,1,t)|^2 dx - \varepsilon\|u\|_2^2\left\{\frac{|\mu|}{2\xi_1} + \frac{\eta\beta}{2\xi_2 k}\right\}. \tag{47}$$

We obtain from (35) and (47) the following:

$$L'(t) \geq \left\{(1-\alpha)H^{-\alpha}(t) - \varepsilon\left(\frac{k\xi_1 + \eta\xi_2}{2k}\right)\right\}H'(t) + \varepsilon\left\{\|m(x)\|_\infty - \frac{\eta\tau}{2k}\right\}\|u_t\|_2^2 - \varepsilon\left\{\|p(x)\|_\infty + \eta\right\}\|u_x\|_2^2 - \varepsilon\eta\|\theta\|_2^2 - \varepsilon\frac{\tau\eta}{2k}\|q\|_2^2 + \varepsilon\int_0^L |u|^p \ln|u|^\gamma dx - \varepsilon\left\{\frac{|\mu|k}{2\xi_1 k} + \frac{\eta\beta}{2\xi_2 k}\right\}\|u\|_2^2. \tag{48}$$

We also set $\xi_1 = \xi_2 = H^{-\alpha}(t)$; hence, (48) gives

$$L'(t) \geq \{(1-\alpha) - \varepsilon C\}H^{-\alpha}(t)H'(t) + \varepsilon\left\{\|m(x)\|_\infty - \frac{\eta\tau}{2k}\right\}\|u_t\|_2^2 - \varepsilon\left\{\|p(x)\|_\infty + \eta\right\}\|u_x\|_2^2 - \varepsilon\eta\|\theta\|_2^2 - \varepsilon\frac{\tau\eta}{2k}\|q\|_2^2 + \varepsilon\int_0^L |u|^p \ln|u|^\gamma dx - \varepsilon\frac{M}{2k}H^\alpha(t)\|u\|_2^2, \tag{49}$$

where C and M are strictly positive constants depending only on $k, \eta, \beta, |\mu|$.

For $0 < a < 1$, we have

$$L'(t) \geq \{(1-\alpha) - \varepsilon C\}H^{-\alpha}(t)H'(t) + \varepsilon\left\{\|m(x)\|_\infty\left(1 + \frac{p}{2}(1-a)\right) - \frac{\eta\tau}{2k}\right\}\|u_t\|_2^2 + \varepsilon\left\{\|p(x)\|_\infty\left(\frac{p}{2}(1-a) - 1\right) + \eta\right\}\|u_x\|_2^2 + \varepsilon\left\{-\eta + \frac{p\varepsilon(1-a)}{2}\right\}\|\theta\|_2^2 + \varepsilon a\int_0^L |u|^p \ln|u|^\gamma dx + \varepsilon\left\{-\frac{\tau\eta}{2k} + \frac{p\tau(1-a)}{2}\right\}\|q\|_2^2 + \frac{\gamma\varepsilon(1-a)}{2}\|u\|_p^p + \varepsilon\frac{\tau_0 p(1-a)}{2}|\mu|\int_0^L\int_0^1 |z(x,\rho,t)|^2 d\rho dx - \varepsilon\frac{M}{2k}H^\alpha(t)\|u\|_2^2 + p\varepsilon(1-a)H(t). \tag{50}$$

Using (27), (37) and Young's inequality, we find

$$H^\alpha(t)\|u\|_2^2 \leq \left(\int_0^L |u|^p \ln|u|^\gamma dx\right)^\alpha \|u\|_2^2 \leq C\left[\left(\int_0^L |u|^p \ln|u|^\gamma dx\right)^{\alpha+\frac{2}{p}} + \left(\int_0^L |u|^p \ln|u|^\gamma dx\right)^\alpha \|u_x\|_2^{\frac{4}{p}}\right] \leq C\left[\left(\int_0^L |u|^p \ln|u|^\gamma dx\right)^{\frac{(\alpha p+2)}{p}} + \|u_x\|_2^2 + \left(\int_0^L |u|^p \ln|u|^\gamma dx\right)^{\frac{\alpha p}{p-2}}\right]. \tag{51}$$

Exploiting (39), we have

$$2 < \alpha p + 2 \leq p \text{ and } 2 < \frac{\alpha p^2}{p-2} \leq p. \tag{52}$$

Thus, lemma 1 yields

$$H^\alpha(t)\|u\|_2^2 \leq C\left\{\int_0^L |u|^p \ln|u|^\gamma dx + \|u_x\|_2^2\right\}. \tag{53}$$

Combining (50) and (53), we obtain

$$L'(t) \geq \{(1-\alpha) - \varepsilon C\}H^{-\alpha}(t)H'(t) + \varepsilon\left\{\|m(x)\|_\infty\left(1 + \frac{p}{2}(1-a)\right) - \frac{\eta\tau}{2k}\right\}\|u_t\|_2^2 + \varepsilon\left\{\|p(x)\|_\infty\left(\frac{p}{2}(1-a) - 1\right) + \eta - C\frac{M}{2k}\right\}\|u_x\|_2^2 + \varepsilon\left\{-\eta + \frac{p\varepsilon(1-a)}{2}\right\}\|\theta\|_2^2 + \varepsilon\left\{a - C\frac{M}{2k}\right\}\int_0^L |u|^p \ln|u|^\gamma dx + \varepsilon\left\{-\frac{\tau\eta}{2k} + \frac{p\tau(1-a)}{2}\right\}\|q\|_2^2 + \frac{\gamma\varepsilon(1-a)}{2}\|u\|_p^p + \varepsilon\frac{\tau_0 p(1-a)}{2}|\mu|\int_0^L\int_0^1 |z(x,\rho,t)|^2 d\rho dx + p\varepsilon(1-a)H(t). \tag{54}$$

At this point, we choose $a > 0$ so small that

$$-\eta + \frac{p\varepsilon(1-a)}{2} > 0, \quad \left(\frac{p}{2}(1-a) - 1\right) > 0, \quad \frac{\tau_0 p(1-a)}{2} > 0, \tag{55}$$

and k so large that

$$\begin{aligned}
\|p(x)\|_\infty\left(\frac{p}{2}(1-a)-1\right)+\eta-C\frac{M}{2k}>0,\\
a-C\frac{M}{2k}>0,\\
\|m(x)\|_\infty\left(1+\frac{p}{2}(1-a)\right)-\frac{\eta\tau}{2k}>0,\\
-\frac{\tau\eta}{2k}+\frac{p\tau(1-a)}{2}>0.
\end{aligned} \tag{56}$$

Once C and a are fixed, we pick ε so small so that

$$(1-\alpha)-\varepsilon C>0. \tag{57}$$

Hence, (54) becomes

$$\begin{aligned}
L'(t)\geq\{(1-\alpha)-\varepsilon C\}H^{-\alpha}(t)H'(t)+\varepsilon A_1\|u_t\|_2^2+\varepsilon A_2\|u_x\|_2^2\\
+\varepsilon A_3\|\theta\|_2^2+\varepsilon A_4\|q\|_2^2+\varepsilon\left\{a-C\frac{M}{2k}\right\}\int_0^L|u|^p\ln|u|^\gamma dx\\
+\varepsilon\frac{\tau_0 p(1-a)}{2}|\mu|\int_0^L\int_0^1|z(x,\rho,t)|^2d\rho dx\\
+\frac{\gamma\varepsilon(1-a)}{2}\|u\|_p^p+p\varepsilon(1-a)H(t),
\end{aligned} \tag{58}$$

where A_1-A_4 are strictly positive constants depending only on p,τ,η,k,a.

Thus, for some $A_0>0$, estimate (58) becomes

$$\begin{aligned}
L'(t)\geq A_0\Big\{H(t)+\|u_t\|_2^2+\|u_x\|_2^2+\|u\|_p^p\|q\|_2^2+\|\theta\|_2^2\\
+\int_0^L|u|^p\ln|u|^\gamma dx+\int_0^L\int_0^1|z(x,\rho,t)|^2d\rho dx\Big\},
\end{aligned} \tag{59}$$

and

$$L(t)\geq L(0)>0,\forall t\geq 0. \tag{60}$$

Next, using Hôlder's inequality and the embedding $\|u\|_2\leq C\|u\|_p$, we have

$$\left|\int_0^L m(x)uu_t dx\right|\leq\|m(x)\|_\infty\|u\|_2\|u_t\|_2\leq C\|u\|_2\|u_t\|_2, \tag{61}$$

and exploiting Young's inequality, we obtain

$$\left|\int_0^L m(x)uu_t dx\right|^{\frac{1}{1-\alpha}}\leq C\left\{\|u\|_p^{\frac{r}{1-\alpha}}+\|u_t\|_2^{\frac{r'}{1-\alpha}}\right\},\ \text{For}\ \frac{1}{r}+\frac{1}{r'}=1. \tag{62}$$

To be able to use Lemma 5, we take $r'=2(1-\alpha)$ which gives $r/1-\alpha=2/1-2\alpha\leq p$.

Therefore, for $s=2/1-2\alpha$, estimate (62) yields

$$\left|\int_0^L m(x)uu_t dx\right|^{\frac{1}{1-\alpha}}\leq C\left(\|u\|_p^s+\|u_t\|_2^2\right). \tag{63}$$

Hence, Lemma 5 gives

$$\left|\int_0^L m(x)uu_t dx\right|^{\frac{1}{1-\alpha}}\leq C_1\left(\|u\|_p^p+\|u_t\|_2^2+\|u_x\|_2^2\right),\forall C_1>0, \tag{64}$$

and with the same way, we get

$$\left|\varepsilon\int_0^L\frac{n\tau}{k}uqdx\right|^{\frac{1}{1-\alpha}}\leq C_2\left(\|u\|_p^p+\|q\|_2^2\right),\forall C_2>0, \tag{65}$$

$$\left|\varepsilon\int_0^L 4\delta(x)|u_x|^2dx\right|^{\frac{1}{1-\alpha}}\leq C_3\|u_x\|_2^2,\forall C_3>0. \tag{66}$$

From (64), (65), and (66) we obtain

$$L^{\frac{1}{1-\alpha}}(t)\leq C\left\{H(t)+\|u\|_p^p+\|q\|_2^2+\|u_x\|_2^2+\|u_t\|_2^2\right\};\forall t\geq 0,\forall C>0. \tag{67}$$

Combining (67) and (59), we arrive at

$$L'(t)\geq a_0L^{\frac{1}{1-\alpha}}(t),\forall t\geq 0, \tag{68}$$

where a_0 is a positive constant depending only on A_0 and C.

A simple integration of (68) over $(0,t)$ yields

$$L^{\frac{\alpha}{1-\alpha}}(t)\geq\frac{1}{L^{-\alpha/1-\alpha}(0)-\alpha a_0 t/(1-\alpha)}. \tag{69}$$

Therefore, $L(t)$ blows up in time

$$T^*\leq\frac{1-\alpha}{\alpha a_0 L^{\alpha/1-\alpha}(0)}. \tag{70}$$

The proof is completed.

4. Conclusion

In this work, we are interested with a problem of a logarithmic nonuniform flexible structure with time delay, where the heat flux is given by Cattaneo's law. We show that the energy of any weak solution blows up infinite time if the initial energy is negative. The delay effect that is similar to memory processes is important in the research of applied mathematics such as physics, noninstant transmission phenomena, and biological motivation. In the future work, we will try to study the local existence for this problem with respect to some proposal conditions.

Data Availability

No data were used to support the study.

Conflicts of Interest

This work does not have any conflicts of interest.

Acknowledgments

The authors are grateful to the anonymous referees for the careful reading and their important observations/suggestions for the sake of improving this paper.

References

[1] M. S. Alves, P. Gamboa, G. C. Gorain, A. Rambaud, and O. Vera, "Asymptotic behavior of aflexible structure with Cattaneo type ofthermal effect," *Indagationes Mathematicae*, vol. 27, no. 3, pp. 821–834, 2016.

[2] G. Li, Y. Luan, J. Yu, and F. Jiang, "Well-posedness and exponential stability of a flexible structure with second sound and time delay," *Applicable Analysis*, vol. 98, no. 16, pp. 2903–2915, 2019.

[3] G. C. Gorain, "Exponential stabilization of longitudinal vibrations of an inhomogeneous beam," *Non-Linear Oscillation*, vol. 16, pp. 157–164, 2013.

[4] S. Misra, M. Alves, G. Gorain, and O. Vera, "Stability of the vibrations of an inhomogeneous flexible structure with thermal effect," *International Journal of Dynamics and Control*, vol. 3, no. 4, pp. 354–362, 2015.

[5] R. Racke, "Thermoelasticity with second sound-exponential stability in linear and nonlinear 1d," *Mathematical Methods in the applied Sciences*, vol. 25, no. 5, pp. 409–441, 2001.

[6] S. A. Messaoudi, "Local existence and blow up in nonlinear thermoelasticity with second sound," *Communications in Partial Differential Equations*, vol. 27, no. 7-8, pp. 1681–1693, 2002.

[7] M. Aassila, "Nonlinear boundary stabilization of an inhomogeneous and anisotropic thermoelasticity system," *Applied Mathematics Letters*, vol. 13, no. 1, pp. 71–76, 2000.

[8] T. A. Apalara and S. A. Messaoudi, "An exponential stability result of a Timoshenko system with thermoelasticity with second sound and in the presence of delay," *Applied Mathematics and Optimization*, vol. 71, no. 3, pp. 449–472, 2015.

[9] C. M. Dafermos and L. Hsiao, "Development of singularities in solutions of the equations of nonlinear thermoelasticity," *Quarterly of Applied Mathematics*, vol. 44, no. 3, pp. 463–474, 1986.

[10] W. J. Hrusa and S. A. Messaoudi, "On formation of singularities on one-dimensional nonlinear thermoelasticity," *Archive for Rational Mechanics and Analysis*, vol. 3, pp. 135–151, 1990.

[11] I. Bialynicki-Birula and J. Mycielski, "Wave equations with logarithmic nonlinearities," *Bulletin de l'Academie Polonaise des Sciences: Serie des Sciences, Mathematiques, Astronomiques et Physiques*, vol. 23, pp. 461–466, 1975.

[12] P. Górka, "Logarithmic quantum mechanics: existence of the ground state," *Foundations of Physics Letters*, vol. 19, no. 6, pp. 591–601, 2006.

[13] M. Kafini and S. Messaoudi, "Local existence and blow up of solutions to a logarithmic nonlinear wave equation with delay," *Applicable Analysis*, vol. 99, no. 3, pp. 530–547, 2020.

Hindawi
Advances in Mathematical Physics
Volume 2021, Article ID 6630317, 8 pages
https://doi.org/10.1155/2021/6630317

Research Article

Uncertain Random Data Envelopment Analysis: Efficiency Estimation of Returns to Scale

Bao Jiang,[1] Shuang Feng,[1] Jinwu Gao,[1] and Jian Li[1,2]

[1]*Department of International Trade and Economy, Ocean University of China, Qingdao 266100, China*
[2]*Marine Development Studies Institute, Ocean University of China, Qingdao 266100, China*

Correspondence should be addressed to Jian Li; lijian@ouc.edu.cn

Received 30 November 2020; Revised 21 December 2020; Accepted 27 January 2021; Published 8 February 2021

Academic Editor: Mohammad Mirzazadeh

Evaluating efficiency according to the different states of returns to scale (RTS) is crucial to resource allocation and scientific decision for decision-making units (DMUs), but this kind of evaluation will become very difficult when the DMUs are in an uncertain random environment. In this paper, we attempt to explore the uncertain random data envelopment analysis approach so as to solve the problem that the inputs and outputs of DMUs are uncertain random variables. Chance theory is applied to handling the uncertain random variables, and hence, two evaluating models, one for increasing returns to scale (IRS) and the other for decreasing returns to scale (DRS), are proposed, respectively. Along with converting the two uncertain random models into corresponding equivalent forms, we also provide a numerical example to illustrate the evaluation results of these models.

1. Introduction

Data envelopment analysis (DEA) initiated by Charnes et al. [1], known as the CCR (Charnes, Cooper, and Rhodes) model, is one of the effective tools to evaluate efficiencies of DMUs with multiple inputs and multiple outputs. However, Banker [2] demonstrated that the CCR model only regarded that DMUs with constant returns to scale (CRS) were efficient. CRS is one of the states of returns to scale (RTS). Based on the RTS theory, RTS can be divided into three states as CRS, IRS (increasing returns to scale), and DRS (decreasing returns to scale) in accordance with the difference of output increment caused by input increment [3]. Subsequently, Banker et al. [4] proposed the BCC (Banker, Charnes, and Cooper) model to identify the efficient DMUs in the three states of RTS. The results revealed that the different states of RTS would affect the results of efficiency evaluation indeed. Afterwards, Fare and Grosskopf [5] refined the approach on measuring efficiencies of DMUs which exhibits DRS, and Seiford and Thrall [6] further estimated DMU's efficiency under IRS.

Along with the states of RTS affecting the results of efficiency evaluation, the inputs and outputs of DMUs that are not always observed accurately may affect the efficiency results as well. For example, early studies in DEA considered that such inputs and outputs as capital and labor are regarded as precise data. With more factors like carbon emission and social benefit taken into account in inputs and outputs nowadays, the traditional models are not suitable for dealing with these imprecise data. Then, some scholars regard these variables as random variables and treat them with probability theory. Therefore, many stochastic DEA models have been put forward including Li [7], Khodabakhshi et al. [8], and Cooper et al. [9].

However, some other scholars claim that these variables should be considered as uncertain variables because the uncertainty theory demonstrated that if the distribution function of a variable is not close enough to its real frequency, then it is better to treat it as an uncertain variable rather than a random variable [10]. Therefore, some uncertain DEA models are proposed via the application of uncertainty theory (Wen et al. [11], Lio and Liu [12], Jiang et al. [13], and Alireza and Lio [14]).

When the external environment becomes more complex, the imprecise inputs and outputs of DMUs may be not only a single random variable or uncertain variable but also both of

them. In this case, some scholars attempt to take the uncertain random variables into account and propose uncertain random DEA models to estimate DMU's overall efficiency (Jiang et al. [15]) and technical efficiency (Jiang et al. [16]). However, a specific uncertain random model of examining the influence of RTS on efficiency evaluation does not exist currently. Motivated by this, this paper proposes two uncertain random models by applying chance theory [17] to dealing with uncertain random variables. One model is for estimating the DMUs' efficiency under IRS, and the other one is for DRS.

The remainder of this article is organized as follows. The second section will present a number of basic knowledge of uncertainty theory and chance theory. The third section will introduce the new uncertain random DEA model for IRS, and the equivalent form will be verified. The fourth section will introduce the new uncertain random DEA model for DRS, and the equivalent form will be verified as well. A numerical example to test two new uncertain random DEA models will be provided in the fifth section. The final section will make concluding remarks.

2. Preliminaries

In this part, we will briefly introduce the primary concepts and theorems of uncertainty theory and chance theory for the preparation to structure the new uncertain random DEA models in the next two sections.

2.1. Uncertainty Theory. As a powerful mathematical tool for dealing with uncertain variables and analyzing the belief degree, uncertainty theory was founded by Liu [10] in 2007. The uncertain measure M was defined as a set function on a σ-algebra $\mathscr{L}$ over a nonempty set Γ by the following axioms:

Axiom 1 (normality axiom). $M\{\Gamma\} = 1$ for the universal set Γ.

Axiom 2 (duality axiom). $M\{\Lambda\} + M\{\Lambda^c\} = 1$ for any event Λ.

Axiom 3 (subadditivity axiom). For every countable sequence of events $\Lambda_1, \Lambda_2, \cdots$, we have

$$M\left\{\bigcup_{i=1}^{\infty} \Lambda_i\right\} \leq \sum_{i=1}^{\infty} M\{\Lambda_i\}. \tag{1}$$

Then, Liu [18] proposed a product axiom in 2009.

Axiom 4 (product axiom). Let $(\Gamma_k, \mathscr{L}_k, M_k)$ be uncertainty spaces for $k = 1, 2, \cdots$. The product uncertain measure M is an uncertain measure satisfying

$$M\left\{\prod_{k=1}^{\infty} \Lambda_k\right\} = \bigwedge_{k=1}^{\infty} M_k\{\Lambda_k\}, \tag{2}$$

where Λ_k are arbitrarily chosen events from $\mathscr{L}_k$ for $k = 1, 2, \cdots$, respectively.

Definition 5 (Liu [10]). *An uncertain variable is a function ξ from an uncertainty space $(\Gamma, \mathscr{L}, M)$ to the set of real numbers such that $\{\xi \in B\}$ is an event for any Borel set B of real numbers.*

Definition 6 (Liu [19]). *An uncertain variable ξ is called linear if it has a linear uncertainty distribution*

$$\Phi(x) = \begin{cases} 0, & \text{if } x \leq a, \\ \dfrac{x-a}{b-a}, & \text{if } a < x \leq b, \\ 1, & \text{if } x > b, \end{cases} \tag{3}$$

denoted by $\mathscr{L}(a, b)$ where a and b are real numbers with $a < b$.

Definition 7 (Liu [19]). *Let ξ be an uncertain variable with regular uncertainty distribution $\Phi(x)$. Then, the inverse function $\Phi^{-1}(\alpha)$ is called the inverse uncertainty distribution of ξ.*

Theorem 8 (Liu [19]). *Let $\xi_1, \xi_2, \cdots, \xi_n$ be independent uncertain variables with regular uncertainty distributions $\Phi_1, \Phi_2, \cdots, \Phi_n$, respectively. If $f(x_1, x_2, \cdots, x_n)$ is continuous, strictly increasing with respect to $x_1, x_2, \cdots, x_m$ and strictly decreasing with respect to $x_{m+1}, x_{m+2}, \cdots, x_n$, then*

$$\xi = f(\xi_1, \xi_2, \cdots, \xi_n) \tag{4}$$

has an inverse uncertainty distribution

$$\Psi^{-1}(\alpha) = f\left(\Phi_1^{-1}(\alpha), \cdots, \Phi_m^{-1}(\alpha), \Phi_{m+1}^{-1}(1-\alpha), \cdots, \Phi_n^{-1}(1-\alpha)\right). \tag{5}$$

Theorem 9 (Liu and Ha [20]). *Assume $\xi_1, \xi_2, \cdots, \xi_n$ are independent uncertain variables with regular uncertainty distributions $\Phi_1, \Phi_2, \cdots, \Phi_n$, respectively. If $f(\xi_1, \xi_2, \cdots, \xi_n)$ is strictly increasing with respect to $\xi_1, \xi_2, \cdots, \xi_m$ and strictly decreasing with respect to $\xi_{m+1}, \xi_{m+2}, \cdots, \xi_n$, then*

$$\xi = f(\xi_1, \xi_2, \cdots, \xi_n) \tag{6}$$

has an expected value

$$E[\xi] = \int_0^1 f\left(\Phi_1^{-1}(\alpha), \cdots, \Phi_m^{-1}(\alpha), \Phi_{m+1}^{-1}(1-\alpha), \cdots, \Phi_n^{-1}(1-\alpha)\right) d\alpha. \tag{7}$$

Uncertainty theory was subsequently studied by many researchers over the past decades, and many scholars have used uncertainty theory to model dynamic systems with uncertainty.

2.2. Chance Theory. Chance theory was put forward by Liu [17] in 2013 for modeling a complex system with the coexistence of uncertainty and randomness. Some elementary features and properties on uncertain random variables are defined as follows.

Definition 10 (Liu [21]). *An uncertain random variable is a function ξ from a chance space $(\Gamma, \mathscr{L}, M) \times (\Omega, \mathscr{A}, \Pr)$ to the set of real numbers such that $\{\xi \in B\}$ is an event in $\mathscr{L} \times \mathscr{A}$ for any Borel set B of real numbers.*

Definition 11 (Liu [21]). *Let ξ be an uncertain random variable. Then, its chance distribution is defined by*

$$\Phi(x) = \mathrm{Ch}\{\xi \leq x\} \tag{8}$$

for any $x \in \mathfrak{R}$.

Theorem 12 (Liu [17]). *Let $\eta_1, \eta_2, \cdots, \eta_m$ be independent random variables with probability distributions $\Psi_1, \Psi_2, \cdots, \Psi_m$, and let $\tau_1, \tau_2, \cdots, \tau_n$ be independent uncertain variables with regular uncertainty distributions $Y_1, Y_2, \cdots, Y_n$, respectively. Assume $f(\eta_1, \eta_2, \cdots, \eta_m, \tau_1, \tau_2, \cdots, \tau_n)$ is continuous, strictly increasing with respect to $\tau_1, \tau_2, \cdots, \tau_k$ and strictly decreasing with respect to $\tau_{k+1}, \tau_{k+2}, \cdots, \tau_n$. Then, the uncertain random variable*

$$\xi = f(\eta_1, \eta_2, \cdots, \eta_m, \tau_1, \tau_2, \cdots, \tau_n) \tag{9}$$

has a chance distribution

$$\Phi(x) = \int_{\mathfrak{R}^m} F(x; y_1, y_2, \cdots, y_m) d\Psi_1(y_1) d\Psi_2(y_2) \cdots d\Psi_m(y_m), \tag{10}$$

where $F(x; y_1, y_2, \cdots, y_m)$ is the root α of the equation

$$f\left(y_1, y_2, \cdots, y_m, Y_1^{-1}(\alpha), \cdots, Y_k^{-1}(\alpha), Y_{k+1}^{-1}(1-\alpha), \cdots, Y_n^{-1}(1-\alpha)\right) = x. \tag{11}$$

Theorem 13 (Liu [17]). *Let $\eta_1, \eta_2, \cdots, \eta_m$ be independent random variables with probability distributions $\Psi_1, \Psi_2, \cdots, \Psi_m$, and let $\tau_1, \tau_2, \cdots, \tau_n$ be independent uncertain variables with regular uncertainty distributions $Y_1, Y_2, \cdots, Y_n$, respectively. If f is a measurable function, then*

$$\xi = f(\eta_1, \eta_2, \cdots, \eta_m, \tau_1, \tau_2, \cdots, \tau_n) \tag{12}$$

has an expected value

$$E[\xi] = \int_{\mathfrak{R}^m} G(y_1, y_2, \cdots, y_m) d\Psi_1(y_1) d\Psi_2(y_2) \cdots d\Psi_m(y_m), \tag{13}$$

where

$$G(y_1, y_2, \cdots, y_m) = E[f(y_1, y_2, \cdots, y_m, \tau_1, \tau_2, \cdots, \tau_n)] \tag{14}$$

is the expected value of the uncertain variable $f(y_1, y_2, \cdots, y_m, \tau_1, \tau_2, \cdots, \tau_n)$ for any real numbers $y_1, y_2, \cdots, y_m$ and is determined by $Y_1, Y_2, \cdots, Y_n$.

Theorem 14 (Liu [17]). *Let $\eta_1, \eta_2, \cdots, \eta_m$ be independent random variables with probability distributions $\Psi_1, \Psi_2, \cdots, \Psi_m$, and let $\tau_1, \tau_2, \cdots, \tau_n$ be independent uncertain variables with regular uncertainty distributions $Y_1, Y_2, \cdots, Y_n$, respectively. If $f(\eta_1, \cdots, \eta_m, \tau_1, \cdots, \tau_n)$ is a continuous and strictly increasing function (or strictly decreasing function) with respect to $\tau_1, \cdots, \tau_n$, then the expected function*

$$E[f(\eta_1, \cdots, \eta_m, \tau_1, \cdots, \tau_n)] \tag{15}$$

is equal to

$$\int_{\mathfrak{R}^m} \int_0^1 f\left(y_1, \cdots, y_m, Y_1^{-1}(\alpha), \cdots, Y_n^{-1}(\alpha)\right) d\alpha d\Psi_1(y_1) \cdots d\Psi_m(y_m). \tag{16}$$

Based on the knowledge above, the two new uncertain random DEA models will be created in the following section.

3. Uncertain Random DEA Model for IRS

When the inputs and outputs of DMUs cannot be observed precisely, some of them were regarded as random variables and treated by probability theory, while some others were regarded as uncertain variables and treated by uncertainty theory. But in a more complex environment, the coexistence of random variables and uncertain variables in DMUs may occur. Therefore, a new approach to deal with uncertain random variables in estimating efficiency is necessary.

Suppose the number of DMUs is r. For each k with $1 \leq k \leq r$, the kth DMU consumes a random input vector x_k and an uncertain input vector $\tilde{x}_k$ to produce a random output vector y_k and an uncertain output vector $\tilde{y}_k$. For each DMU$_k$, we artificially set the expected ratio of weighted outputs to weighted inputs which is always less than or equal to unity, i.e.,

$$E\left[\frac{v^T \tilde{y}_k + v^T y_k}{\tilde{u}^T \tilde{x}_k + u^T x_k}\right] \leq 1, \quad k = 1, 2, \cdots, r, \tag{17}$$

where $\tilde{u}$, u, $\tilde{v}$, and v are nonnegative weight vectors. Subject to constraint (17), only a DMU which has CRS can find out a set of favorable weights $(\tilde{u}^*, u^*, \tilde{v}^*, v^*)$ such that the expected ratio of this DMU reaches up to 1, by which a DMU can be regarded as efficiency. The reason is that the increment of inputs of the DMU which exhibits CRS is equal to that of outputs.

According to the RTS theory, if the proportionate increases in outputs are larger than the proportionate increases in inputs, then the state of increasing returns to scale (IRS) arises [3]. In order to clarify the influence of IRS on efficiency values, we artificially set a factor, denoted as w, to adjust the proportion difference among input increment and output increment caused by IRS, and then, the constraint (17) is modified to

$$E\left[\frac{v^T\tilde{y}_k + v^T y_k - w}{\tilde{u}^T\tilde{x}_k + u^T x_k}\right] \le 1, \quad k = 1, 2, \cdots, r, \tag{18}$$

where w is less than or equal to 0, i.e., $w \le 0$. The new constraint (18) allows a DMU which exhibits IRS to also find out a set of favorable weights $(\tilde{u}^*, u^*, \tilde{v}^*, v^*)$ such that the expected ratio of this DMU reaches up to 1. In this way, the DMUs under IRS can be considered efficient as well. In order to verify if the target DMU, distinguished by subscript "o," is efficient under IRS, we may solve the following uncertain random DEA model:

$$\begin{cases} \max\limits_{\tilde{u},u,\tilde{v},v,w} \vartheta_{\text{IRS}} = E\left[\dfrac{v^T\tilde{y}_o + v^T y_o - w}{u^T\tilde{x}_o + u^T x_o}\right] \\ \text{subject to :} \\ E\left[\dfrac{v^T\tilde{y}_k + v^T y_k - w}{u^T\tilde{x}_k + u^T x_k}\right] \le 1, \quad k = 1, 2, \cdots, r, \\ u, u, v, v \ge 0, \\ w \le 0, \end{cases} \tag{19}$$

where $\tilde{x}_k$, $\tilde{y}_k$, x_k, and y_k are uncertain input vectors, uncertain output vectors, random input vectors, and random output vectors of DMU$_k$, $k = 1, 2, \cdots, r$, respectively; u, v, $\tilde{u}$, and $\tilde{v}$ are nonnegative weight vectors; and $w \le 0$.

Definition 15 (IRS efficiency). *DMU$_o$ is regarded IRS efficient if the optimal value ϑ^*_{IRS} of ((19)) reaches up to 1.*

Theorem 16. *Let uncertain variables $\tilde{x}_{k1}, \cdots, \tilde{x}_{kj}$, $\tilde{y}_{k1}, \cdots, \tilde{y}_{kn}$ be independent with uncertainty distributions $\tilde{Y}_{k1}, \cdots, \tilde{Y}_{kj}$, $\tilde{\Pi}_{k1}, \cdots, \tilde{\Pi}_{kn}$, and let random variables $x_{k1}, \cdots, x_{ki}$, $y_{k1}, \cdots, y_{km}$ be independent with probability distributions $\Phi_{k1}, \cdots, \Phi_{ki}$, $\Psi_{k1}, \cdots, \Psi_{km}$, $k = 1, 2, \cdots, r$, respectively. Then, the new uncertain random DEA model for IRS ((19)) can be indicated as follows:*

$$\begin{cases} \max\limits_{\tilde{u},u,\tilde{v},v,w} \vartheta_{IRS} = \displaystyle\int_{\Re^+_{m+i}} \int_0^1 \frac{\sum_{p=1}^m v_p z_{op} + \sum_{t=1}^n \tilde{v}_t \tilde{\Pi}^{-1}_{ot}(\alpha) - w}{\sum_{q=1}^i u_q h_{oq} + \sum_{s=1}^j \tilde{u}_s \tilde{Y}^{-1}_{os}(1-\alpha)} d\alpha d\mathbf{\Phi}_{\mathbf{o}}(\mathbf{h_o}) d\mathbf{\Psi}_{\mathbf{o}}(\mathbf{z_o}) \\ \textit{subject to :} \\ \displaystyle\int_{\Re^+_{m+i}} \int_0^1 \frac{\sum_{p=1}^m v_p z_{kp} + \sum_{t=1}^n \tilde{v}_t \tilde{\Pi}^{-1}_{kt}(\alpha) - w}{\sum_{q=1}^i u_q h_{kq} + \sum_{s=1}^j \tilde{u}_s \tilde{Y}^{-1}_{ks}(1-\alpha)} d\alpha d\mathbf{\Phi}_{\mathbf{k}}(\mathbf{h_k}) d\mathbf{\Psi}_{\mathbf{k}}(\mathbf{z_k}) \le 1, \\ k = 1, 2, \cdots, r, \\ \tilde{u} = (\tilde{u}_1, \tilde{u}_2, \cdots, \tilde{u}_j) \ge 0, \\ u = (u_1, u_2, \cdots, u_i) \ge 0, \\ \tilde{v} = (\tilde{v}_1, \tilde{v}_2, \cdots, \tilde{v}_n) \ge 0, \\ v = (v_1, v_2, \cdots, v_m) \ge 0, \\ w \le 0, \end{cases} \tag{20}$$

where

$$\begin{aligned} d\mathbf{\Phi}_{\mathbf{o}}(\mathbf{h_o}) &= d\Phi_{o1}(h_{o1}), d\Phi_{o2}(h_{o2}) \cdots d\Phi_{oi}(h_{oi}), \\ d\mathbf{\Psi}_{\mathbf{o}}(\mathbf{z_o}) &= d\Psi_{o1}(z_{o1}), d\Psi_{o2}(z_{o2}) \cdots d\Psi_{om}(z_{om}), \\ d\mathbf{\Phi}_{\mathbf{k}}(\mathbf{h_k}) &= d\Phi_{k1}(h_{k1}), d\Phi_{k2}(h_{k2}) \cdots d\Phi_{ki}(h_{ki}), \\ d\mathbf{\Psi}_{\mathbf{k}}(\mathbf{z_k}) &= d\Psi_{k1}(z_{k1}), d\Psi_{k2}(z_{k2}) \cdots d\Psi_{km}(h_{km}). \end{aligned} \tag{21}$$

The uncertainty distributions of $\tilde{x}_{o1}, \cdots, \tilde{x}_{oj}$, $\tilde{y}_{o1}, \cdots, \tilde{y}_{on}$ are $\tilde{Y}_{o1}, \cdots, \tilde{Y}_{oj}$ and $\tilde{\Pi}_{o1}, \cdots, \tilde{\Pi}_{on}$, and the probability distributions of $x_{o1}, \cdots, x_{oi}$, $y_{o1}, \cdots, y_{om}$ are $\Phi_{o1}, \cdots, \Phi_{oi}$, $\Psi_{o1}, \cdots, \Psi_{om}$, respectively.

Proof. Since the function $(v^T y_k + \tilde{v}^T\tilde{y}_k - w)/(u^T x_k + \tilde{u}^T\tilde{x}_k)$ is a measurable function for each k with $1 \le k \le r$, it follows from Theorem 13 and we can obtain

$$\xi = \frac{v^T y_k + \tilde{v}^T\tilde{y}_k - w}{u^T x_k + \tilde{u}^T\tilde{x}_k} \tag{22}$$

has an expected value

$$E[\xi] = \int_{\Re^+_{m+i}} G(h_{k1}, \cdots, h_{ki}, z_{k1}, \cdots, z_{km}) d\mathbf{\Phi}_{\mathbf{k}}(\mathbf{h_k}) \mathrm{d}\mathbf{\Psi}_{\mathbf{k}}(\mathbf{z_k}) \tag{23}$$

for $k = 1, 2, \cdots, r$, where

$$\begin{aligned} G(h_{k1}, \cdots, h_{ki}, z_{k1}, \cdots, z_{km}) &= E\left[\frac{v^T z_k + \tilde{v}^T\tilde{y}_k - w}{u^T h_k + \tilde{u}^T\tilde{x}_k}\right], \\ d\mathbf{\Phi}_{\mathbf{k}}(\mathbf{h_k}) &= d\Phi_{k1}(h_{k1}) d\Phi_{k2}(h_{k2}) \cdots d\Phi_{ki}(h_{ki}), \\ d\mathbf{\Psi}_{\mathbf{k}}(\mathbf{z_k}) &= d\Psi_{k1}(z_{k1}) d\Psi_{k2}(z_{k2}) \cdots d\Psi_{km}(z_{km}), \end{aligned} \tag{24}$$

$k = 1, 2, \cdots, r$.

For each k with $1 \le k \le r$, since the function $(v^T z_k + \tilde{v}^T\tilde{y}_k - w)/(u^T h_k + \tilde{u}^T\tilde{x}_k)$ is strictly increasing with respect to $\tilde{y}_k$ and strictly decreasing with respect to $\tilde{x}_k$, by using Theorem 8, we can get the inverse uncertainty distribution is

$$R^{-1}_k(\alpha) = \frac{\sum_{p=1}^m v_p z_{kp} + \sum_{t=1}^n \tilde{v}_t \tilde{\Pi}^{-1}_{kt}(\alpha) - w}{\sum_{q=1}^i u_q h_{kq} + \sum_{s=1}^j \tilde{u}_s \tilde{Y}^{-1}_{ks}(1-\alpha)}. \tag{25}$$

Moreover, from Theorem 14, we can obtain

$$E\left[\frac{v^T z_k + \tilde{v}^T\tilde{y}_k - w}{u^T h_k + \tilde{u}^T\tilde{x}_k}\right] = \int_0^1 \frac{\sum_{p=1}^m v_p z_{kp} + \sum_{t=1}^n \tilde{v}_t \tilde{\Pi}^{-1}_{kt}(\alpha) - w}{\sum_{q=1}^i u_q h_{kq} + \sum_{s=1}^j \tilde{u}_s \tilde{Y}^{-1}_{ks}(1-\alpha)} d\alpha, \tag{26}$$

$k = 1, 2, \cdots, r$. Then, the equivalent form of equation (23) is

$$E[\xi] = \int_{\Re^+_{m+i}} \int_0^1 \frac{\sum_{p=1}^m v_p z_{kp} + \sum_{t=1}^n \tilde{v}_t \tilde{\Pi}_{kt}^{-1}(\alpha) - w}{\sum_{q=1}^i u_q h_{kq} + \sum_{s=1}^j \tilde{u}_s \tilde{Y}_{ks}^{-1}(1-\alpha)} d\alpha d\Phi_{\mathbf{k}}(\mathbf{h_k}) d\Psi_{\mathbf{k}}(\mathbf{z_k}), \tag{27}$$

where

$$\begin{aligned} d\Phi_{\mathbf{k}}(\mathbf{h_k}) &= d\Phi_{k1}(h_{k1}) d\Phi_{k2}(h_{k2}) \cdots d\Phi_{ki}(h_{ki}), \\ d\Psi_{\mathbf{k}}(\mathbf{z_k}) &= d\Psi_{k1}(z_{k1}) d\Psi_{k2}(z_{k2}) \cdots d\Psi_{km}(z_{km}), \end{aligned} \tag{28}$$

$k = 1, 2, \cdots, r$. The proof is completed.

4. Uncertain Random DEA Model for DRS

In this part, we propose the uncertain random DEA model for DRS. According to RTS theory, if the proportionate increases in outputs are smaller than the proportionate increases in inputs, then the state of decreasing returns to scale (DRS) prevails [3]. Then, the constraint (17) is modified to

$$E\left[\frac{v^T \tilde{y}_k + v^T y_k - w}{\tilde{u}^T \tilde{x}_k + u^T x_k}\right] \le 1, \quad k = 1, 2, \cdots, r, \tag{29}$$

where w is greater than or equal to 0, i.e., $w \ge 0$. The new constraint (29) allows a DMU which exhibits DRS to also find out a set of favorable weights $(\tilde{u}^*, u^*, \tilde{v}^*, v^*)$ such that the expected ratio of this DMU reaches up to 1. In this way, the DMUs under DRS can be considered efficient as well. We still distinguish target DMU by subscript "o," then verify if it is efficient under DRS, and may solve the following uncertain random DEA model:

$$\begin{cases} \max\limits_{\tilde{u},u,\tilde{v},v,w} \vartheta_{\mathrm{DRS}} = E\left[\dfrac{v^T \tilde{y}_o + v^T y_o - w}{u^T \tilde{x}_o + u^T \mathrm{x}_o}\right] \\ \text{subject to}: \\ E\left[\dfrac{v^T \tilde{y}_k + v^T y_k - w}{u^T \tilde{x}_k + u^T x_k}\right] \le 1, \quad k = 1, 2, \cdots, r, \\ u, u, v, v \ge 0, \\ w \ge 0, \end{cases} \tag{30}$$

where $\tilde{x}_k$, $\tilde{y}_k$, x_k, and y_k are uncertain input vectors, uncertain output vectors, random input vectors, and random output vectors of DMU_k, $k = 1, 2, \cdots, r$, respectively; u, v, $\tilde{u}$, and $\tilde{v}$ are nonnegative weight vectors; and $w \ge 0$.

Definition 17 (DRS efficiency). *DMU_o is regarded DRS efficient if the optimal value $\vartheta^*_{\mathrm{DRS}}$ of ((30)) reaches up to 1.*

Theorem 18. *Let uncertain variables $\tilde{x}_{k1}, \cdots, \tilde{x}_{kj}, \tilde{y}_{k1}, \cdots, \tilde{y}_{kn}$ be independent with uncertainty distributions $\tilde{Y}_{k1}, \cdots, \tilde{Y}_{kj}, \tilde{\Pi}_{k1}, \cdots, \tilde{\Pi}_{kn}$, and let random variables $x_{k1}, \cdots, x_{ki}, y_{k1}, \cdots, y_{km}$ be independent with probability distributions $\Phi_{k1}, \cdots, \Phi_{ki}, \Psi_{k1}, \cdots, \Psi_{km}$, $k = 1, 2, \cdots, r$, respectively. Then, the new uncertain random DEA model for DRS ((30)) can be indicated as follows:*

$$\begin{cases} \max\limits_{\tilde{u},u,\tilde{v},v,w} \vartheta_{DRS} = \displaystyle\int_{\Re^+_{m+i}} \int_0^1 \frac{\sum_{p=1}^m v_p z_{op} + \sum_{t=1}^n \tilde{v}_t \tilde{\Pi}_{ot}^{-1}(\alpha) - w}{\sum_{q=1}^i u_q h_{oq} + \sum_{s=1}^j \tilde{u}_s \tilde{Y}_{os}^{-1}(1-\alpha)} d\alpha d\Phi_{\mathbf{o}}(\mathbf{h_o}) d\Psi_{\mathbf{o}}(\mathbf{z_o}) \\ \text{subject to}: \\ \displaystyle\int_{\Re^+_{m+i}} \int_0^1 \frac{\sum_{p=1}^m v_p z_{kp} + \sum_{t=1}^n \tilde{v}_t \tilde{\Pi}_{kt}^{-1}(\alpha) - w}{\sum_{q=1}^i u_q h_{kq} + \sum_{s=1}^j \tilde{u}_s \tilde{Y}_{ks}^{-1}(1-\alpha)} d\alpha d\Phi_{\mathbf{k}}(\mathbf{h_k}) d\Psi_{\mathbf{k}}(\mathbf{z_k}) \le 1, \\ k = 1, 2, \cdots, r, \\ \tilde{u} = (\tilde{u}_1, \tilde{u}_2, \cdots, \tilde{u}_j) \ge 0, \\ u = (u_1, u_2, \cdots, u_i) \ge 0, \\ \tilde{v} = (\tilde{v}_1, \tilde{v}_2, \cdots, \tilde{v}_n) \ge 0, \\ v = (v_1, v_2, \cdots, v_m) \ge 0, \\ w \ge 0, \end{cases} \tag{31}$$

where

$$\begin{aligned} d\Phi_{\mathbf{o}}(\mathbf{h_o}) &= d\Phi_{o1}(h_{o1}), d\Phi_{o2}(h_{o2}) \cdots d\Phi_{oi}(h_{oi}), \\ d\Psi_{\mathbf{o}}(\mathbf{z_o}) &= d\Psi_{o1}(z_{o1}), d\Psi_{o2}(z_{o2}) \cdots d\Psi_{om}(z_{om}), \\ d\Phi_{\mathbf{k}}(\mathbf{h_k}) &= d\Phi_{k1}(h_{k1}), d\Phi_{k2}(h_{k2}) \cdots d\Phi_{ki}(h_{ki}), \\ d\Psi_{\mathbf{k}}(\mathbf{z_k}) &= d\Psi_{k1}(z_{k1}), d\Psi_{k2}(z_{k2}) \cdots d\Psi_{km}(h_{km}). \end{aligned} \tag{32}$$

The uncertainty distributions of $\tilde{x}_{o1}, \cdots, \tilde{x}_{oj}, \tilde{y}_{o1}, \cdots, \tilde{y}_{on}$ are $\tilde{Y}_{o1}, \cdots, \tilde{Y}_{oj}$ and $\tilde{\Pi}_{o1}, \cdots, \tilde{\Pi}_{on}$, and the probability distributions of $x_{o1}, \cdots, x_{oi}$, $y_{o1}, \cdots, y_{om}$ are $\Phi_{o1}, \cdots, \Phi_{oi}$, $\Psi_{o1}, \cdots, \Psi_{om}$, respectively.

Proof. Since the function $(v^T y_k + \tilde{v}^T \tilde{y}_k - w)/(u^T x_k + \tilde{u}^T \tilde{x}_k)$ is a measurable function for each k with $1 \le k \le r$, it follows from Theorem 13 and we can obtain

$$\varsigma = \frac{v^T y_k + \tilde{v}^T \tilde{y}_k - w}{u^T x_k + \tilde{u}^T \tilde{x}_k} \tag{33}$$

has an expected value

$$E[\varsigma] = \int_{\Re^+_{m+i}} G(h_{k1}, \cdots, h_{ki}, z_{k1}, \cdots, z_{km}) d\Phi_{\mathbf{k}}(\mathbf{h_k}) d\Psi_{\mathbf{k}}(\mathbf{z_k}) \tag{34}$$

for $k = 1, 2, \cdots, r$, where

$$\begin{aligned} G(h_{k1}, \cdots, h_{ki}, z_{k1}, \cdots, z_{km}) &= E\left[\frac{v^T z_k + \tilde{v}^T \tilde{y}_k - w}{u^T h_k + \tilde{u}^T \tilde{x}_k}\right], \\ d\Phi_{\mathbf{k}}(\mathbf{h_k}) &= d\Phi_{k1}(h_{k1}) d\Phi_{k2}(h_{k2}) \cdots d\Phi_{ki}(h_{ki}), \\ d\Psi_{\mathbf{k}}(\mathbf{z_k}) &= d\Psi_{k1}(z_{k1}) d\Psi_{k2}(z_{k2}) \cdots d\Psi_{km}(z_{km}), \end{aligned} \tag{35}$$

$k = 1, 2, \cdots, r$.

Table 1: Fifteen DMUs with three inputs and three outputs.

DMU$_k$	Output variables			Input variables		
	$\tilde{y}_1$ (uncertain)	$\tilde{y}_2$ (uncertain)	y_3 (random)	$\tilde{x}_1$ (uncertain)	$\tilde{x}_2$ (uncertain)	x_3 (random)
1	$\mathscr{L}(51, 65)$	$\mathscr{L}(45, 55)$	$U(60, 78)$	$\mathscr{L}(8, 13)$	$\mathscr{L}(10, 15)$	$U(9, 14)$
2	$\mathscr{L}(64, 71)$	$\mathscr{L}(60, 69)$	$U(76, 88)$	$\mathscr{L}(17, 20)$	$\mathscr{L}(12, 19)$	$U(10, 16)$
3	$\mathscr{L}(55, 60)$	$\mathscr{L}(80, 96)$	$U(77, 89)$	$\mathscr{L}(10, 19)$	$\mathscr{L}(11, 20)$	$U(10, 21)$
4	$\mathscr{L}(47, 55)$	$\mathscr{L}(79, 95)$	$U(62, 80)$	$\mathscr{L}(15, 24)$	$\mathscr{L}(12, 21)$	$U(12, 23)$
5	$\mathscr{L}(49, 62)$	$\mathscr{L}(54, 67)$	$U(60, 75)$	$\mathscr{L}(10, 16)$	$\mathscr{L}(13, 19)$	$U(14, 17)$
6	$\mathscr{L}(46, 52)$	$\mathscr{L}(55, 68)$	$U(65, 76)$	$\mathscr{L}(11, 19)$	$\mathscr{L}(16, 22)$	$U(13, 19)$
7	$\mathscr{L}(52, 60)$	$\mathscr{L}(67, 80)$	$U(70, 83)$	$\mathscr{L}(13, 21)$	$\mathscr{L}(10, 17)$	$U(12, 18)$
8	$\mathscr{L}(54, 67)$	$\mathscr{L}(65, 75)$	$U(55, 69)$	$\mathscr{L}(11, 16)$	$\mathscr{L}(14, 20)$	$U(8, 16)$
9	$\mathscr{L}(45, 55)$	$\mathscr{L}(62, 76)$	$U(63, 78)$	$\mathscr{L}(10, 15)$	$\mathscr{L}(8, 12)$	$U(14, 21)$
10	$\mathscr{L}(48, 57)$	$\mathscr{L}(54, 63)$	$U(60, 73)$	$\mathscr{L}(11, 17)$	$\mathscr{L}(9, 18)$	$U(8, 17)$
11	$\mathscr{L}(56, 69)$	$\mathscr{L}(64, 76)$	$U(66, 83)$	$\mathscr{L}(8, 12)$	$\mathscr{L}(10, 20)$	$U(11, 18)$
12	$\mathscr{L}(60, 78)$	$\mathscr{L}(63, 70)$	$U(74, 83)$	$\mathscr{L}(6, 13)$	$\mathscr{L}(7, 15)$	$U(15, 20)$
13	$\mathscr{L}(58, 66)$	$\mathscr{L}(80, 97)$	$U(78, 90)$	$\mathscr{L}(5, 11)$	$\mathscr{L}(12, 25)$	$U(10, 17)$
14	$\mathscr{L}(47, 58)$	$\mathscr{L}(68, 78)$	$U(70, 88)$	$\mathscr{L}(12, 19)$	$\mathscr{L}(14, 22)$	$U(14, 25)$
15	$\mathscr{L}(44, 53)$	$\mathscr{L}(53, 69)$	$U(63, 72)$	$\mathscr{L}(14, 20)$	$\mathscr{L}(9, 15)$	$U(13, 21)$

For each k with $1 \le k \le r$, since the function $(v^T z_k + \tilde{v}^T \tilde{y}_k - w)/(u^T h_k + \tilde{u}^T \tilde{x}_k)$ is strictly increasing with respect to $\tilde{y}_k$ and strictly decreasing with respect to $\tilde{x}_k$, by using Theorem 8, we can get the inverse uncertainty distribution is

$$R_k^{-1}(\alpha) = \frac{\sum_{p=1}^{m} v_p z_{kp} + \sum_{t=1}^{n} \tilde{v}_t \tilde{\Pi}_{kt}^{-1}(\alpha) - w}{\sum_{q=1}^{i} u_q h_{kq} + \sum_{s=1}^{j} \tilde{u}_s \tilde{Y}_{ks}^{-1}(1-\alpha)}. \tag{36}$$

Moreover, from Theorem 14, we can obtain

$$E\left[\frac{v^T z_k + \tilde{v}^T \tilde{y}_k - w}{u^T h_k + \tilde{u}^T \tilde{x}_k}\right] = \int_0^1 \frac{\sum_{p=1}^{m} v_p z_{kp} + \sum_{t=1}^{n} \tilde{v}_t \tilde{\Pi}_{kt}^{-1}(\alpha) - w}{\sum_{q=1}^{i} u_q h_{kq} + \sum_{s=1}^{j} \tilde{u}_s \tilde{Y}_{ks}^{-1}(1-\alpha)} d\alpha, \tag{37}$$

$k = 1, 2, \cdots, r$. Then, the equivalent form of equation (34) is

$$E[\varsigma] = \int_{\Re_{m+i}^{+}} \int_0^1 \frac{\sum_{p=1}^{m} v_p z_{kp} + \sum_{t=1}^{n} \tilde{v}_t \tilde{\Pi}_{kt}^{-1}(\alpha) - w}{\sum_{q=1}^{i} u_q h_{kq} + \sum_{s=1}^{j} \tilde{u}_s \tilde{Y}_{ks}^{-1}(1-\alpha)} d\alpha \Phi_{\mathbf{k}}(\mathbf{h_k}) d\Psi_{\mathbf{k}}(\mathbf{z_k}), \tag{38}$$

where

$$\begin{aligned} d\Phi_{\mathbf{k}}(\mathbf{h_k}) &= d\Phi_{k1}(h_{k1}) d\Phi_{k2}(h_{k2}) \cdots d\Phi_{ki}(h_{ki}), \\ d\Psi_{\mathbf{k}}(\mathbf{z_k}) &= d\Psi_{k1}(z_{k1}) d\Psi_{k2}(z_{k2}) \cdots d\Psi_{km}(z_{km}), \end{aligned} \tag{39}$$

$k = 1, 2, \cdots, r$. The proof is completed.

5. A Numerical Example

In order to examine the two new uncertain random DEA models, this section presents fifteen DMUs with three inputs and three outputs to demonstrate an illustrative example. Among these inputs and outputs, two inputs and two outputs are uncertain variables subject to linear uncertainty distributions represented as $\mathscr{L}(a, b)$, and one input and one output are random variables subject to uniform distributions represented as $U(a, b)$. The original data of these DMUs are provided in Table 1.

According to the data in Table 1, we can obtain each DMU's IRS efficiency by calculating the optimal value ϑ_{IRS}^* of model (19) and DRS efficiency by calculating the optimal value ϑ_{DRS}^* of model (30). In addition, to further clarify the influence of RTS on efficiency values, we have also examined two other cases, one for overall efficiency and the other for technical efficiency. If $w = 0$, overall efficiencies of DMUs can be calculated, represented as η^*, and technical efficiencies of DMUs, represented as φ^*, can be gained under the condition that w is unconstrained in sign. The results of the four kinds of efficiencies of each DMU are shown in Table 2.

As shown in Table 2, the second column represents DMUs' IRS efficiencies. It is obvious that the five DMUs are IRS efficient because the optimal values ϑ_{IRS}^* of them reach up to 1, and the other ten are IRS inefficient. Similarly, four DMUs are DRS efficient shown in the third column. Among these efficient DMUs, some like DMU$_3$, DMU$_8$, and DMU$_9$ are IRS efficient but DRS inefficient, while some like DMU$_1$ and DMU$_2$ are DRS efficient but IRS inefficient. However, there are also two DMUs (DMU$_{12}$ and DMU$_{13}$) that are both IRS efficient and DRS efficient. Does it mean that these two DMUs are overall efficient as well?

Table 2: The efficiency evaluation results of different uncertain random DEA models.

DMU_k	Optimal values			
	ϑ^*_{IRS}	ϑ^*_{DRS}	η^*	φ^*
1	0.9702	1.0000	0.4366	1.0000
2	0.9745	1.0000	0.5699	1.0000
3	1.0000	0.8829	0.5678	1.0000
4	0.8784	0.8803	0.2686	0.9185
5	0.6766	0.4042	0.3251	0.8219
6	0.6584	0.3746	0.3433	0.6062
7	0.9542	0.4382	0.3451	0.9583
8	1.0000	0.5223	0.3661	1.0000
9	1.0000	0.8316	0.3600	1.0000
10	0.7588	0.4123	0.3535	0.9047
11	0.9569	0.7897	0.4859	0.9405
12	1.0000	1.0000	1.0000	1.0000
13	1.0000	1.0000	1.0000	1.0000
14	0.7667	0.7667	0.3275	0.7362
15	0.7525	0.3414	0.4764	0.6200

Overall efficiencies of DMUs are exhibited in the fourth column of Table 2, represented as η^*. It is clear that only two DMUs, DMU_{12} and DMU_{13}, can be regarded as overall efficient among fifteen DMUs. Therefore, it can be inferred that if a DMU prevails IRS efficiency and DRS efficiency simultaneously, it prevails overall efficiency as well. The result is in accordance with the assumption that the efficiency value is affected by the RTS state.

The last column shows DMUs' technical efficiencies, represented as φ^*. There are a total of seven DMUs that can be considered technical efficient. The number is just the aggregation of DMUs which are both IRS efficient and DRS efficient. This phenomenon demonstrates that the technical efficiency compounds three kinds of different efficiencies caused by RTS, although it cannot differ IRS efficiency and DRS efficiency.

6. Conclusions

In this paper, we introduced two new models, uncertain random DEA model for IRS and uncertain random DEA model for DRS, so as to focus on efficiency evaluation of DMUs under the uncertain random environment. Meanwhile, we presented the equivalent forms of the two new models and provided detailed proof processes. Finally, a numerical example was given to demonstrate the evaluation results of these two models. Considering the situation that uncertain variables and random variables coexist in the inputs and outputs of DMUs simultaneously, our work broadens the application of chance theory in efficiency evaluation in practice. In addition, this paper is also expected to be applied in the field of logistics in the future.

Data Availability

No data were used to support this study.

Conflicts of Interest

The authors declare that they have no conflicts of interest.

Acknowledgments

This work was supported by the National Natural Science Foundation of China Grant No. 61873329 and Research Program of Natural Science Foundation of Shandong Province Grant No. ZR2020MG044.

References

[1] A. Charnes, W. W. Cooper, and E. Rhodes, "Measuring the efficiency of decision making units," *European Journal of Operational Research*, vol. 2, no. 6, pp. 429–444, 1978.

[2] R. D. Banker, "Estimating most productive scale size using data envelopment analysis," *European Journal of Operational Research*, vol. 17, no. 1, pp. 35–44, 1984.

[3] M. T. Douglas, F. Christopher, and P. Michael, *Economics*, Addison-Wesley Longman, Australia, 3rd edition, 1999.

[4] R. D. Banker, A. Charnes, and W. W. Cooper, "Some models for estimating technical and scale efficiencies in data envelopment analysis," *Management Science*, vol. 30, no. 9, pp. 1078–1092, 1984.

[5] R. Fare and S. Grosskopf, "Nonparametric cost approach to scale efficiency," *Scandinavian Journal of Economics*, vol. 87, no. 4, pp. 594–604, 1985.

[6] L. M. Seiford and R. M. Thrall, "Recent developments in DEA: the mathematical programming approach to frontier analysis," *Journal of Econometrics*, vol. 46, no. 1-2, pp. 7–38, 1990.

[7] S. X. Li, "Stochastic models and variable returns to scales in data envelopment analysis," *European Journal of Operations Research*, vol. 104, no. 3, pp. 532–548, 1998.

[8] M. Khodabakhshi, Y. Gholami, and H. Kheirollahi, "An additive model approach for estimating returns to scale in imprecise data envelopment analysis," *Applied Mathematical Modeling*, vol. 34, no. 5, pp. 1247–1257, 2010.

[9] W. W. Cooper, H. Deng, Z. M. Huang, and S. X. Li, "Chance constrained programming approaches to congestion in stochastic data envelopment analysis," *European Journal of Operational Research*, vol. 155, no. 2, pp. 487–501, 2004.

[10] B. Liu, *Uncertainty Theory*, Springer-Verlag, Berlin, 2nd edition, 2007.

[11] M. Wen, L. Guo, R. Kang, and Y. Yang, "Data envelopment analysis with uncertain inputs and outputs," *Journal of Applied Mathematics*, vol. 2014, Article ID 307108, 6 pages, 2014.

[12] W. Lio and B. Liu, "Uncertain data envelopment analysis with imprecisely observed inputs and outputs," *Fuzzy Optimization and Decision Making*, vol. 17, no. 3, pp. 357–373, 2018.

[13] B. Jiang, Z. Zou, W. Lio, and J. Li, "The uncertain DEA models for specific scale efficiency identification," *Journal of Intelligent and Fuzzy Systems*, vol. 38, no. 3, pp. 3403–3417, 2020.

[14] G. Alireza and W. Lio, "Network data envelopment analysis in uncertain environment," *Computers and Industrial Engineering*, vol. 148, article 106657, 2020.

[15] B. Jiang, W. Feng, and J. Li, *Uncertain random data envelopment analysis for technical efficiency*, 2020, Technical report.

[16] B. Jiang, Y. Zhou, W. Lio, and J. Li, *Evaluation of technical efficiency in uncertain random data envelopment analysis*, 2020, Technical report.

[17] Y. H. Liu, "Uncertain random programming with applications," *Fuzzy Optimization and Decision Making*, vol. 12, no. 2, pp. 153–169, 2013.

[18] B. Liu, "Some research problems in uncertainty theory," *Journal of Uncertain Systems*, vol. 3, no. 1, pp. 3–10, 2009.

[19] B. Liu, *Uncertainty Theory: A Branch of Mathematics for Modeling Human Uncertainty*, Springer-Verlag, Berlin, 2010.

[20] Y. H. Liu and M. H. Ha, "Expected value of function of uncertain variables," *Journal of Uncertain Systems*, vol. 4, no. 3, pp. 181–186, 2010.

[21] Y. H. Liu, "Uncertain random variables: a mixture of uncertainty and randomness," *Soft Computing*, vol. 17, no. 4, pp. 625–634, 2013.

Hindawi
Advances in Mathematical Physics
Volume 2021, Article ID 6676400, 6 pages
https://doi.org/10.1155/2021/6676400

Research Article

Improvement of the Nonparametric Estimation of Functional Stationary Time Series Using Yeo-Johnson Transformation with Application to Temperature Curves

Sameera Abdulsalam Othman [1] **and Haithem Taha Mohammed Ali** [2]

[1]*Department of Mathematics, College of Basic Education, University of Duhok, Kurdistan Region, Iraq*
[2]*Department of Economics, College of Administration and Economics, Nawroz University, Kurdistan Region, Iraq*

Correspondence should be addressed to Sameera Abdulsalam Othman; sameera.othman@uod.ac

Received 22 November 2020; Revised 26 December 2020; Accepted 13 January 2021; Published 30 January 2021

Academic Editor: F. Rabiei

In this article, Box-Cox and Yeo-Johnson transformation models are applied to two time series datasets of monthly temperature averages to improve the forecast ability. An application algorithm was proposed to transform the positive original responses using the first model and the stationary responses using the second model to improve the nonparametric estimation of the functional time series. The Box-Cox model contributed to improving the results of the nonparametric estimation of the original data, but the results become somewhat confusing after attempting to make the transformed response variable stationary in the mean, while the functional time series predictions were more accurate using the transformed stationary datasets using the Yeo-Johnson model.

1. Introduction

Forecasting the future is the main function of time series analysis. Proceeding from this idea, researchers have developed several techniques that are concerned with the improvement of accuracy of forecasts by treating the time series as a stochastic process. A functional data analytic approach or so-called a stochastic forecast [1] allows dealing with the observations as a function [2] freely outside of the conditions of parametric and fully nonparametric modeling. This handling of observations in time series data makes it sequential and can be separated into successive time periods [3]. Thus, the dimensions of the time series are reduced with a limited loss of information [4] and represent the data in a linear combination of a few functions (carefully selected) instead of treating the data in its original form as a single vector of values [2], that is, processing and transforming the structure of time series data in line with the structure of regression models. Shang in 2019 showed that with the time dependence of observations in some datasets, the principal component method may lead to erroneous estimates. Therefore, the two authors believe that this problem may be exacerbated in some time series data, especially those that are characterized by the presence of seasonal changes. However, it has become known in practical applications of time series that they are rarely stationary and that seasonal changes, trend, and dependence on external factors have become the rules, not the exception [5]. For this reason, it can be said that the data transformation has become a part of the traditional parametric and nonparametric analysis of complex time series.

In this article, the two authors have used the Yeo-Johnson transformations to improve the nonparametric estimation of the functional time series. The use of both approaches, transformation, and functional analysis without considering the modeling conditions is an attempt to focus the analyzing goal and the efficiency criterion in the context of forecast ability.

The rest of the article is organized as follows. The Box-Cox and Yeo-Johnson transformations are presented in the next section. The third section contains the formulation of

the problem and the proposed application methodology. The practical examples are included in the fourth section, while the fifth section contained some conclusions.

2. Box-Cox and Yeo-Johnson Transformations

Box and Cox [6] suggested the Box-Cox transformation (BCT) methodology in regression models to reduce anomalies in data, reduce nonlinearity, and achieve normality random errors. The methodology assumes, for any response variable $Z > 0$ and $\lambda \in R$, the transformed variable $\Psi(Z) = (Z^{\lambda} - 1)/\lambda$ when $\lambda \neq 0$ and $\Psi(Z) = \mathrm{Ln}Z$ when $\lambda = 0$. And when λ is equal to 1, the data is analyzed in its original scale, whereas the case $\lambda = 0$ corresponds to the natural logarithmic transformation of the data. BCT is based on the assumption of the transformed response normality and then defining the probability density function of the original response as a "backward transformed" of change of variables technique.

Yeo and Johnson [7] generalized the BCT to include negative and positive values in datasets [7]. They used a smoothness condition to combine the transformations for positive and negative observations, thus obtaining a one-parameter transformation family [8]. For $Z \in R$, the YJT is given by

$$\psi(Z) = \begin{cases} \dfrac{(Z+1)^{\lambda} - 1}{\lambda}, & \lambda \neq 0 \text{ and } Z \geq 0, \\ \mathrm{Ln}(Z+1), & \lambda = 0 \text{ and } Z \geq 0, \\ \dfrac{-\left((-Z+1)^{2-\lambda} - 1\right)}{2-\lambda}, & \lambda \neq 2 \text{ and } Z < 0, \\ \mathrm{Ln}(-Z+1), & \lambda = 2 \text{ and } Z < 0. \end{cases} \tag{1}$$

This transformation is appropriate for correcting both left and right skew when $\lambda > 1$ and $\lambda < 1$, respectively, while the linear relationship is achieved when $\lambda = 1$ [9]. Also, Yeo-Johnson transformations (YJT) can hold the properties of the log-mean standardization after the inverse transformation since $\Psi(Z)$ is invertible [10].

In 1970, Box and Jenkins recommended for the first time the use of power transformation in ARIMA models [11]. After that date, many authors took up this topic and made numerous proposals in many mathematical and applied aspects of the time series. Also, some of them indicated some failures in practical cases, for example, the success limitation of the normality assumption of the transformed data, and that it could lead to noticeable improvements in the simplicity of the data models and the accuracy of the estimate [12] especially in the models with skewness for variables [10]. Cook and Olive, [13] and Atkinson [8] also point out that the estimation of the transformation parameter can be particularly sensitive to outliers. And in some practical cases of time series, the BCT may not lead to an improvement in forecasting performance [11], or as Chen and Lee [14] say, it does not consistently produce superior forecasts.

Some problems in practical applications occur for two reasons: the first is the difficulty in obtaining an optimum value of the transformation parameter, so that at the same time, the conditions of the fitting of assumed distribution of the transformed data are met, and the model errors are minimal, while the second is that the transformations lead to a change in the nature of the relationships between the variables of the model, which may lead to a lack of balance between the efficiency of statistical inference and the ability to interpret the sizes of the variables' influence [15].

3. Formulation of the Problem

Let us consider a univariate time series $\{Z_t, t \in R\}$, by redividing the time series sample into $(p-1)$ statistical samples of size $(n = N - s - p + 1)$. This division allows the time series to be redefined as functional data $\{(\mathbf{X}_i, Y_i)\}_{i=1,..,n}$ in such the variation trends between times of the series are diagnosed through the functional analysis tools [1]. Thus, the relationship can be described as a standard regression model.

$$Y = m(\mathbf{X}) + \varepsilon, \tag{2}$$

where $m(\mathbf{X})$ is the smooth functional data, ε is a sequence of independent identically distributed function white noise sequence in such $E(\varepsilon/\mathbf{X}) = 0$. $\mathbf{X}_1, \mathbf{X}_2, \cdots, \mathbf{X}_n$ are identically distributed as the functional random variable $\mathbf{X}_i = (Z_{i-p+1}, \cdots, Z_i)$ and $Y_i = Z_{i+s}, i = p, \cdots, N - s$ as a scalar response. In order to characterize the relationship, the response Y, given the functional variable $\mathbf{X}$, assumes that $N = n\tau$ for some $n \epsilon N$ and some $\tau > 0$. And then, we get a statistical sample of curves $\mathbf{X}_i = \{Z(t), (i-1)\tau < t \leq i\tau\}$ of size $(n-1)$ and the response $Y_i = Z(i\tau + s), i = 1, \cdots, n-1$ [16, 17]. The usual nonparametric estimation of the functional relation has several advantages and can be very well adapted to local features of time series data [18] and robustness to functional form misspecification [19]. The kernel regression estimator is evaluated at a given function $m(\mathbf{X})$ by

$$\widehat{m}(\mathbf{X}) = \frac{\sum_{i=1}^{n} Y_i K\left(h^{-1}\, d\,(X, \mathbf{X}_i)\right)}{\sum_{i=1}^{n} K\left(h^{-1}\, d\,(X, \mathbf{X}_i)\right)}, \tag{3}$$

where K is a kernel function, h (depending on n) is a positive real bandwidth, and $d\,(X, \mathbf{X}_i)$ denotes any semimetric (index of proximity) between the observed curves. The authors suggest several ways to find equation (3) including kernel regression estimator, functional conditional quantiles, and conditional mode.

A number of useful explanatory methods can be used to measure the closeness (proximities) between the curves of the functional variables in a reduced dimensional space. Ferraty and Vieu [16] refer to at least three families of semimetrics to measure $d\,(X, \mathbf{X}_i)$, for example, the functional principal component analysis (FPCA) in which the proximity is measured by the square root of the quantity $\int (\mathbf{X}_i(t) - \mathbf{X}_j(t))^2 dt$. Also, there is another measure which is based on the second derivative, where the proximity is measured by the square root of the quantity $\int (\mathbf{X}_i^{(2)}(t) - \mathbf{X}_j^{(2)}(t))^2 dt$ (Dauxois et al. (1982), Castre et al.

(1986), Ferraty and Vieu [16], and Febrero-Bande and Oviedo de la Fuente (2012)).

Regarding the kernel estimator (3), Wand et al. [20] indicated that it is not working well when the data are asymmetric, as for the standard PCA which may not be the suitable technique to apply when the data distribution is skewed or there are outliers [21]. Therefore, power transformation is considered one of the important alternatives to improve the efficiency of nonparametric estimation of functional data (for more details, see [12, 22, 23]).

Most transformation approaches have a common analytical path, which is the choice of the power transformation model, and propose an algorithm for estimating the power parameters in parallel with the mechanisms of estimating the traditional parameters of the model. Also, there are two common directions of the power parameter's estimation; the first is the parametric direction in which the power parameters are estimated under the statistical modeling assumptions. The most important methodology of this direction is the Box-Cox transformation (BCT) to improve the efficiency of the multiple linear regression model under the normality assumption of transformed response [6]. Also, Wand et al. [20] used the same methodology of Box-Cox to improve the efficiency of density estimation under the assumption of some distributions of the transformed variable [20] (see also [24, 25, 26]).

The second direction is the nonparametric estimation of power parameters without any assumptions about the response and error distributions or what might be called the model-independent approach [27] (see also [28, 29]). In this direction, the power parameters can estimate according to some decision rules such as minimizing or maximizing some indicators of model efficiency.

4. Application Methodology

It is known that the power transformations are important for making the time series stationary in the variance, while the differencing is useful for making the time series stationary in the mean. Generally, none of these approaches can be a substitute for the other. However, sometimes power transformations can make the time series stationary. And because the BCT is used to transform the positive responses, it becomes important to use it to transform the original data as a first stage and then calculate the differences to achieve the stationary of the time series. And as a result, the variance stabilizing obtained from the power transformation will be affected by the differencing process. In this regard, Dittmann and Granger [30] indicate that for every nonstationary process, the polynomial transformations are also nonstationary and have a stochastic trend in mean and invariance. To overcome these problems, the authors believe that the use of YJT will be appropriate to improve forecastability, because it can be used to stabilize the variance in stationary time series. Also, the estimation of the power parameter according to a certain decision rule that we have referred to would be appropriate as long as the issue is related to the nonparametric functional analysis.

The application methodology includes estimating the smooth functional data $m(\mathbf{X})$ in the regression equation (2) according to the kernel estimator equation (3) after transforming the time series dataset. The BCT was applied to the original time series dataset, while the YJT was applied to the stationary time series dataset. So, the statistical sample of curves was redefined by the expression

$$\Psi_\lambda(\mathbf{X}_i) = \{\Psi_\lambda(Z(t)), (i-1)\tau < t \le i\tau\}, \tag{4}$$

and the response by the expression

$$\Psi_\lambda(Y_i) = \Psi_\lambda(Z(i\tau + s)), \tag{5}$$

where $i = 1, \cdots, n-1$ and Ψ_λ represents a data transformation function by the power parameter λ.

For each transformation model, the decision rule adopted for selecting the optimal estimate of power parameter λ is that which corresponds to the lowest estimates of the mean squares of the forecasting errors of the last curve of functional variable according to the equation $\mathrm{MSE}(\mathbf{X}_n) = (1/s)\sum_{j=1}^{s} (Z_j^{\wedge} - Z_j)^2$, where $Z_j^{\wedge}$ and Z_j are the j-th estimated and real values in the last curve. As for $Z_j^{\wedge}$ values, they are computed from the inversions of BCT and YJT, or what we might call the retransformation from the transformed data metric to the original metric.

So, the application algorithm of BCT and YJT models and nonparametric estimation of the transformed functional time series were as follows:

(1) Fix τ to define expressions (4) and (5)

(2) Remove the seasonality patterns by taking the differences to make the time series stationary

(3) Fix $\lambda \epsilon \Lambda$, where $\Lambda = \{-3, 3\}$

(4) For each $\lambda \epsilon \Lambda$, BCT is used to transform the original time series $Z(t)$ and YJT is used to transform the stationary time series of k differences $\Delta^k Z(t)$ to get the two explanatory functional matrices $\Psi_\lambda(\mathbf{X}) = [\Psi_\lambda(Z)]_{nx\tau}$ and $\Psi_\lambda(\mathbf{X}) = [\Psi_\lambda(\Delta^k Z)]_{nx\tau}$, (for more details about the matrices fille organizing in R program, see [16, 31]).

(5) Evaluate the explanatory function estimation of the relationship $\Psi_\lambda(Y_i) = m(\Psi_\lambda(\mathbf{X})) + \varepsilon$ according to the following kernel estimator:

$$\widehat{m}(\Psi_\lambda(\mathbf{X})) = \frac{\sum_{i=1}^{n} \Psi_\lambda(Y_i) K\left(h^{-1}\, d\left(\Psi_\lambda(X), \Psi_\lambda(\mathbf{X}_i)\right)\right)}{\sum_{i=1}^{n} K\left(h^{-1}\, d\left(\Psi_\lambda(X), \Psi_\lambda(\mathbf{X}_i)\right)\right)}. \tag{6}$$

The optimal value λ^* of the power parameter λ is the one that minimizes the $\mathrm{MSE}(\mathbf{X}_n)$ of the last functional variable.

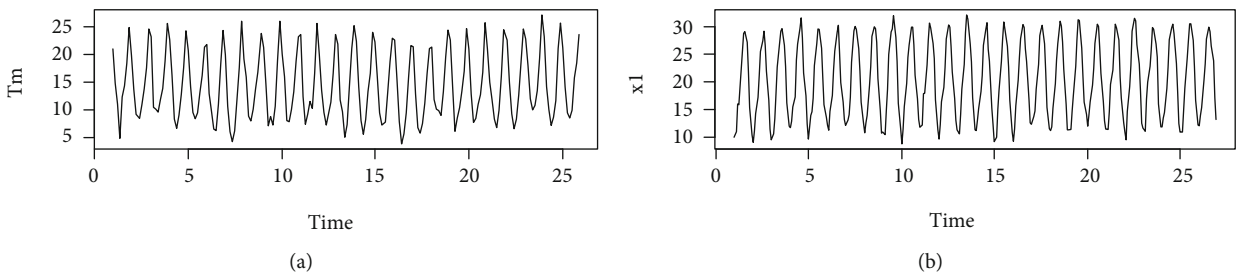

Figure 1: Plots of the monthly temperature averages series: (a) Nineveh City in Iraq for the period 1976 to 2000; (b) Tunisia (TSN) for the period 1991 to 2015.

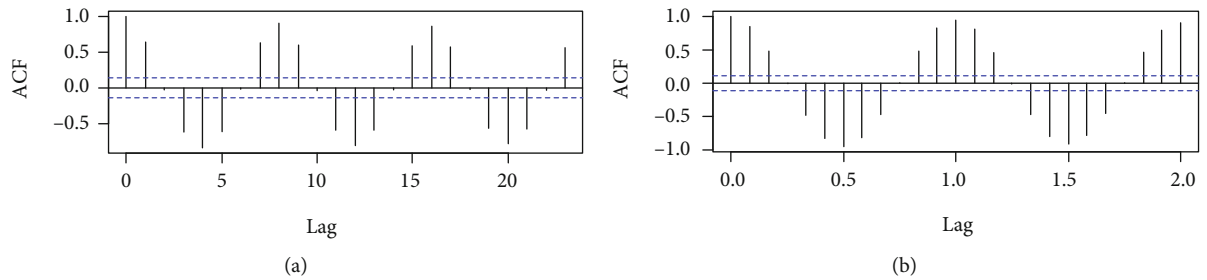

Figure 2: The ACF plots of the two time series: (a) TSN; (b) TST.

Table 1: Optimal parameters of the BCT model and MSE estimates of the last curve of functional variable for the two time series datasets.

Time series	TSN		TST	
Power parameters	$\lambda = 1$	$\lambda^* = 2.1$	$\lambda = 1$	$\lambda^* = 1.7$
MSE($\mathbf{X}_n$) of the original and transferred time series	2.0365	1.5620	0.5214	0.3402
MSE($\mathbf{X}_n$) after making the original and transferred time series stationary	1.7616	1.7494	0.4303	0.5118

Table 2: Optimal parameters of the two transformation models and MSE estimates of the last curve of functional variable $\mathbf{X}_n$ for the two time series datasets.

Time series	TSN				TST			
Transformation models	BCT		YJT		BCT		YJT	
Power parameters	λ	λ^*	λ	λ^*	λ	λ^*	λ	λ^*
	1	2.1	1	−1.9	1	1.7	1	0.3
MSE($\mathbf{X}_n$)	1.7616	1.7494	1.7616	0.8955	0.4303	0.5118	0.4303	0.1706

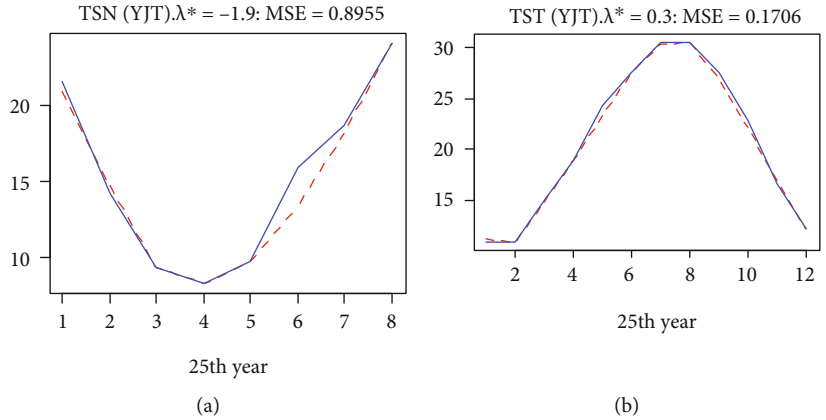

Figure 3: The plots of the original (blue) and predicted values (red) for the latest curve (25th year) of the inverse of the data transformed by the YJT model for the two time series: (a) TSN; (b) TST.

5. Applications

The two transformation models, BCT and YJT, were applied to two time series examples of monthly temperature averages, and an R program was used to analyze the data. The first time series has a size of 200 observations of Nineveh City in Iraq (TSN) for the eight rainy months in every year. We take the monthly average of the meteorological station of Nineveh for the period 1976 to 2000 (Figure 1(a)). The second has a size of 300 observations of Tunisia (TST) for all months of the period 1991 to 2015. The data can be found at https://climateknowledgeportal.worldbank.org (Figure 1(b)).

It was found that the two time series are not stationary, and this is clearly demonstrated by the values of the autocorrelation functions (ACF) outside the confidence levels in Figure 2.

By applying BCT model to the two time series according to the five-step algorithm suggested in Section 4, we obtained the results shown in Table 1.

As expected, it is evident from the results shown in Table 1 that the estimate of MSE has decreased when using BCT compared to its value resulting from the analysis of the original data when $\lambda = 1$. These confusing results were overcome when the YJT model was used according to the same five-step algorithm.

As for the attempt to make the original and transformed time series stationary by the first-order differences, the MSE estimation increased in the two transformed series and decreased in the original series. By applying the YJT model according to the same five-step algorithm, more accurate predictions of fewer errors were obtained compared to the error estimates obtained by using the BCT model (Table 2). Figure 3 shows the plots of the original and predicted values for the latest curve (25th year) after smoothing the data using the YJT model for the two time series.

6. Conclusions

It is important to note that the optimum power parameters λ^* for both transformation models are significantly different even though YJT represents the extended version of the BCT model. The authors believe that this difference and the amount of displacement in the original data generated by both models were due to the use of a nonparametric estimation method to choose the optimal power parameter as an alternative to the parametric method for the hypothesis of normality of transformed response, in addition to the differences in the level of homogeneity between stationary and nonstationary time series datasets.

The application methodology in this article demonstrates that YGT could be a successful alternative to BCT to improve the nonparametric estimation of the functional time series. Also, the nonparametric estimation of the power parameters not restricted by the conditions of the probability distribution provides the researcher with wide options to ensure the accuracy of the prediction.

Data Availability

The datasets supporting the conclusions of this article are included in the article.

Conflicts of Interest

The authors declare that they have no conflict of interest.

References

[1] H. L. Shang, P. W. F. Smith, J. Bijak, and A. Wisniowski, "A functional data analysis approach for forecasting population: a case study for the United Kingdom," in *Centre for Population Change*, Working paper, number 41, 2013.

[2] L. Kidzinski, "Functional time series," *arXiv: Methodology*, 2015, arXiv:1502.07113v1.

[3] A. Aue, D. D. Norinho, and S. Hörmann, "On the prediction of stationary functional time series," *Journal of the American Statistical Association*, vol. 110, no. 509, pp. 378–392, 2015.

[4] H. L. Shang, "Forecasting intraday S&P 500 index returns: a functional time series approach," *Journal of Forecasting*, vol. 36, no. 7, pp. 741–755, 2017.

[5] V. Chavez-Demoulin and A. C. Davison, "Modelling time series extremes," *Revstat – Statistical Journal*, vol. 10, no. 1, pp. 109–133, 2012.

[6] G. E. P. Box and D. R. Cox, "An analysis of transformations (with discussion)," *Journal of the Royal Statistical Society*, vol. 26, no. 2, pp. 211–252, 1964.

[7] I.-K. Yeo and R. A. Johnson, "A new family of power transformations to improve normality or symmetry," *Biometrika*, vol. 87, no. 4, pp. 954–959, 2000.

[8] A. C. Atkinson, "The Box-Cox transformation: review and extensions," *Statistical Science.*, pp. ISSN 0883–ISSN 4237, 2020, http://eprints.lse.ac.uk/103537/.

[9] B. Bean, X. Xu, and S. MacEachern, "Transformations and Bayesian density estimation," *Electronic Journal of Statistics*, vol. 10, no. 2, pp. 3355–3373, 2016.

[10] S. Soleymani, "Exact Box-Cox analysis," *A Thesis Submitted in Partial Fulfillment of the Requirements for the Degree in Doctor of Philosophy in Statistics and Actuarial Sciences*, The University of Western Ontario, 2018.

[11] T. Proietti and H. Lutkepohl, "Does the Box-Cox transformation help in forecasting macroeconomic time series?," *International Journal of Forecasting*, vol. 29, no. 1, pp. 88–99, 2013.

[12] H. L. Shang, "Selection of the optimal Box-Cox transformation parameter for modelling and forecasting age-specific fertility," *Journal of Population Research*, vol. 32, no. 1, pp. 69–79, 2015.

[13] R. D. Cook and D. J. Olive, "A note on visualizing response transformations in regression," 2001, https://opensiuc.lib.siu.edu/cgi/viewcontent.cgi?article=1006&context=math_articles.

[14] C. W. S. Chen and J. C. Lee, "On selecting a power transformation in time-series analysis," *Journal of Forecasting*, vol. 16, no. 5, pp. 343–354, 1997.

[15] J. Pek, O. Wong, and A. C. Wong, "Data transformations for inference with linear regression: clarifications and recommendations," *practical assessment, research, and evaluation*, vol. 22, 2017.

[16] F. Ferraty and P. Vieu, *Nonparametric Functional Data Analysis - Theory and Practice*, Springer Series in Statistics, 2006.

[17] G. Aneiros-perez, R. Cao, and J. M. Vilar-Fernandez, "Functional methods for time series prediction: a nonparametric approach," *Journal of Forecasting*, vol. 30, no. 4, pp. 377–392, 2011.

[18] J. M. Vilar-Fernandez and R. CAO, "Nonparametric forecasting in time series—a comparative study," *Communications in Statistics - Simulation and Computation*, vol. 36, no. 2, pp. 311–334, 2007.

[19] Z. Cai, Q. Li, and J. Y. Park, "Functional-coefficient models for nonstationary time series data," *Journal of Econometrics*, vol. 148, no. 2, pp. 101–113, 2009.

[20] M. P. Wand, J. S. Marron, and D. Ruppert, "Transformations in density estimation," *Journal of the American Statistical Association*, vol. 86, no. 414, pp. 343–353, 1991.

[21] M. Maadooliat, J. Z. Huang, and J. Hu, "Integrating data transformation in principal components analysis," *Journal of Computational and Graphical Statistics*, vol. 24, no. 1, pp. 84–103, 2015.

[22] H. L. Shang, P. W. F. Smith, J. Bijak, and A. Wiśniowski, "A multilevel functional data method for forecasting population, with an application to the United Kingdom," *International Journal of Forecasting*, vol. 32, no. 3, pp. 629–649, 2016.

[23] P. Legendre and D. Borcard, "Box–Cox-chord transformations for community composition data prior to beta diversity analysis," *Ecography*, vol. 41, no. 11, pp. 1820–1824, 2018.

[24] C. Bolance, M. Guillen, and J. P. Nilsen, "Kernel density estimation of actuarial loss functions," *Insurance: Mathematics and Economics*, vol. 32, no. 1, pp. 19–36, 2003.

[25] D. Pitt, M. Guillen, and C. Bolancé, "Estimation of parametric and nonparametric models for univariate claim severity distributions - an approach using R," *XREAP*, 2011, 2011. SSRN: https://ssrn.com/abstract=1856982.

[26] K. M. Sakthivel and C. S. Rajitha, "Kernel density estimation for claim size distributions using shifted power transformation," *International Journal of Science and Research (IJSR)*, vol. 5, no. 4, pp. 2025–2028, 2016.

[27] V. M. Guerrero and R. Perera, "Variance stabilizing power transformation for time series," *Journal of Modern Applied Statistical Methods*, vol. 3, no. 2, pp. 357–369, 2004.

[28] D. Nychka and D. Ruppert, "Nonparametric transformations for both sides of a regression model," *Journal of the Royal Statistical Society: Series B (Methodological)*, vol. 57, no. 3, pp. 519–532, 1995.

[29] H. T. Alyousif, Department of Economics, C. Administration et al., "Develop a nonlinear model for the conditional expectation of the Bayesian probability distribution (gamma – gamma)," *Journal of Al-Nahrain University Science*, vol. 17, no. 2, pp. 205–212, 2014.

[30] I. Dittmann and C. W. J. Granger, "Properties of nonlinear transformations of fractionally integrated processes," *Journal of Econometrics*, vol. 110, no. 2, pp. 113–133, 2002.

[31] S. A. Othman and H. T. Mohammed Ali, "Studying of nonparametric multivariate time series analysis with applications methodology," *Journal of Xi'an University of Architecture & Technology*, vol. 12, no. 6, pp. 1500–1514, 2020.

Hindawi
Advances in Mathematical Physics
Volume 2021, Article ID 6643512, 12 pages
https://doi.org/10.1155/2021/6643512

Research Article

Application of the Multiple Exp-Function, Cross-Kink, Periodic-Kink, Solitary Wave Methods, and Stability Analysis for the CDG Equation

Haifa Bin Jebreen [1] **and Yurilev Chalco-Cano** [2]

[1]*Mathematics Department, College of Science, King Saud University, Riyadh, Saudi Arabia*
[2]*Departamento de Mathematica, Universidad de Tarapaca, Casilla 7D, Arica, Chile*

Correspondence should be addressed to Haifa Bin Jebreen; hjebreen@ksu.edu.sa

Received 23 November 2020; Revised 16 December 2020; Accepted 31 December 2020; Published 16 January 2021

Academic Editor: Sachin Kumar

In this article, the exact wave structures are discussed to the Caudrey-Dodd-Gibbon equation with the assistance of Maple based on the Hirota bilinear form. It is investigated that the equation exhibits the trigonometric, hyperbolic, and exponential function solutions. We first construct a combination of the general exponential function, periodic function, and hyperbolic function in order to derive the general periodic-kink solution for this equation. Then, the more periodic wave solutions are presented with more arbitrary autocephalous parameters, in which the periodic-kink solution localized in all directions in space. Furthermore, the modulation instability is employed to discuss the stability of the available solutions, and the special theorem is also introduced. Moreover, the constraint conditions are also reported which validate the existence of solutions. Furthermore, 2-dimensional graphs are presented for the physical movement of the earned solutions under the appropriate selection of the parameters for stability analysis. The concluded results are helpful for the understanding of the investigation of nonlinear waves and are also vital for numerical and experimental verification in engineering sciences and nonlinear physics.

1. Introduction

It is known that these exact solutions of nonlinear evolution equations (NLEEs), especially the soliton solutions [1–3], can be given by using a variety of different methods [4, 5], such as Jacobi elliptic function expansion method [6], inverse scattering transformation (IST) [7, 8], Darboux transformation (DT) [9], extended generalized DT [10], Lax pair (LP) [11], Lie symmetry analysis [12], Hirota bilinear method [13], and others [14, 15]. The Hirota bilinear method is an efficient tool to construct exact solutions of NLEEs, and there exists plenty of completely integrable equations which are studied in this way. For instance, generalized bilinear equations [16], the lump-type solutions in a homogenous-dispersive medium [17], the $(2+1)$-dimensional KdV equation [18], the $(3+1)$-D potential-YTSF equation [19], the generalized BKP equation [20], the $(3+1)$-dimensional BKP-Boussinesq equation [21], the $(3+1)$ dimensional generalized KP-Boussinesq equation [22], the $(2+1)$-dimensional integrable Boussinesq model [23], and the $(2+1)$-dimensional Breaking Soliton equation [24, 25]. More recently, lump waves and rogue waves have attracted a growing amount of attention, and many theoretical and experimental studies of lump waves are mentioned [26–33]. A novel method for finding the special rogue waves with predictability of NLEEs is proposed by using the Hirota bilinear method by powerful researchers in Refs. [34, 35], in which some results are very helpful for us to study some physical phenomena in engineering.

The Caudrey-Dodd-Gibbon equation introduced by Aiyer et al. [36] who describes the inelastic interactions between the solitary waves under strong physical contexts

in certain integrable or nonintegrable systems and has been investigated the related dynamic behavior [37], which reads

$$\Phi_t + \Phi_{xxxxx} + 30\Phi\Phi_{xxx} + 30\Phi_x\Phi_{xx} + 180\Phi^2\Phi_x = 0. \quad (1)$$

In 2006, the tanh solutions of the equation [38] and, in 2008, the multiple-soliton solutions utilizing the Hirota bilinear method combined with the simplified Hereman method [39] for the above equation are derived by Wazwaz. Also, the physical comprehension of Equation (1) was demonstrated by plenty of scholars who investigated its solitary type solutions and given in Refs. [40] and [41]. The homotopy perturbation method has been utilized to find solutions for the aforementioned equation [42–44]. Based on the obtained transformation of integrating Equation (1), we get to the following nonlinear PDE [45]:

$$\Lambda_t + 60\Lambda_x^3 + 30\Lambda_x\Lambda_{xxx} + \Lambda_{xxxxx} = 0. \quad (2)$$

According to [46], the Hirota bilinear from of the CDG equation reads

$$\Lambda = 2(\ln \Gamma)_x, (\Phi = \Lambda_x) \quad (3)$$

and, also by applying the dependent variable transformation, turns into the Hirota bilinear form

$$\left(D_{xt} + D_x^6\right)\Gamma.\Gamma = 0, \quad (4)$$

where D is a bilinear operator. By deeming the D-operator defined with the aid of the functions Γ_1 and Γ_2, we get to the following relation:

$$D_x^{\pi_1}D_t^{\pi_2}(\Gamma_1.\Gamma_2) = \left(\frac{\partial}{\partial x} - \frac{\partial}{\partial x'}\right)^{\pi_1}\left(\frac{\partial}{\partial t} - \frac{\partial}{\partial t'}\right)^{\pi_2}\Gamma_1(x,t).\Gamma_2\left(x',t'\right)\Big|_{x}^{\prime=x,t\prime=t}. \quad (5)$$

With the help of the transformation Equation (3), the general periodic-kink solutions of Equation (1) can be given. We get to the bilinear form the of Γ as

$$\Gamma\Gamma_{xt} - \Gamma_x\Gamma_t + \Gamma\Gamma_{xxxxxx} - 6\Gamma_x\Gamma_{xxxxx} + 15\Gamma_{xx}\Gamma_{xxxx} - 10\Gamma_{xxx}^2 = 0. \quad (6)$$

Moreover, the stability analysis and the more general periodic-wave solutions and special rogue waves with predictability are investigated in our paper, which have never been studied. Various types of studies were investigated by capable authors in which some of them can be mentioned, for example, the Caudrey–Dodd–Gibbon equation [47], the pZK equation using Lie point symmetries [48], group-invariant solutions of the $(3+1)$-dimensional generalized KP equation [49], optimal system and dynamics of solitons for a higher-dimensional Fokas equation [50], dynamics of solitons for $(2+1)$-dimensional NNV equations [51], the combined MCBS-nMCBS equation [52], Lie symmetry reductions for $(2+1)$-dimensional Pavlov equation [53], Schrödinger-Hirota equation with variable coefficients [54], the $(2+1)$-dimension paraxial wave equation [55], the fractional Drinfeld-Sokolov-Wilson equation [56], the $(3+1)$-dimensional extended Jimbo-Miwa equations [57], and a high-order partial differential equation with fractional derivatives [58]. In the valuable work, the capable authors studied the periodic wave solutions and stability analysis for the KP-BBM equation [59] and breather and periodic wave solution for generalized Bogoyavlensky-Konopelchenko equation [60] with the aid of Hirota operator.

To make this paper more self-contained, a combination of general exponential function, periodic function, and hyperbolic function of the $(3+1)$-dimensional CDG equation is constructed with the help of a bilinear operator, which is crucial to obtain the periodic-wave solution of Equation (1). Based on the Hirota bilinear form Equation (6), the general periodic-wave solution is derived in Section 2 and the novel periodic solutions which can be arisen with twenty one classes. In Section 4, we shall investigate the stability analysis to obtain the modulation stability spectrum of this equation. The final section will be reserved for the conclusions and the discussions.

2. Multiple Exp-Function Method

In this section, according to [61–63] so that it can be further employed to the nonlinear partial differential equation (NLPDE) in order to furnish its exact solutions, it can be presented as:

Step 1. The following is the NLPDE:

$$\mathcal{P}\left(x, y, t, \Psi, \Psi_x, \Psi_y, \Psi_z, \Psi_t, \Psi_{xx}, \Psi_{tt}, \cdots\right) = 0. \quad (7)$$

We commence a sequence of new variables $\xi_i = \xi_i(x,t)$, $1 \le i \le n$, by solvable PDEs, for example, the linear ones,

$$\xi_{i,x} = \alpha_i\xi_i, \xi_{i,t} = \delta_i\xi_i, \quad 1 \le i \le n, \quad (8)$$

where α_i, $1 \le i \le n$, is the angular wave number and δ_i, $1 \le i \le n$, is the wave frequency. It should be pointed that this is frequently the initiating step for constructing the exact solutions to NLPDEs, and moreover, solving such linear equations redounds to the exponential function solutions:

$$\xi_i = \varpi_i e^{\theta_i}, \theta_i = \alpha_i x - \delta_i t, \quad 1 \le i \le n, \quad (9)$$

in which ϖ_i, $1 \le i \le n$, are undetermined constants.

Step 2. Determine the solution of Equation (7) as the following form in terms of the new variables ξ_i, $1 \le i \le n$:

$$\Psi(x,t) = \frac{\Delta(\xi_1, \xi_2, \cdots, \xi_n)}{\Omega(\xi_1, \xi_2, \cdots, \xi_n)}, \quad \Delta = \sum_{r,s=1}^{n}\sum_{i,j=0}^{M}\Delta_{rs,ij}\xi_r^i\xi_s^j, \Omega = \sum_{r,s=1}^{n}\sum_{i,j=0}^{N}\Omega_{rs,ij}\xi_r^i\xi_s^j, \quad (10)$$

in which $\Delta_{rs,ij}$ and $\Omega_{rs,ij}$ are the amounts to be settled. Appending Equation (10) into Equation (7) and ordering the numerator of the rational function to zero, we can achieve

a series of nonlinear algebraic equations about the variables $\alpha_i, \delta_i, \Delta_{rs,ij}$ and $\Omega_{rs,ij}$. Solving the solutions for these nonlinear algebraic equations and putting these solutions into Equation (10), the multiple soliton solutions to Equation (7) can be obtained in the below form as

$$\Psi(x,t) = \frac{\Delta\left(\varpi_1 e^{\alpha_1 x - \delta_1 t}, \cdots, \varpi_n e^{\alpha_n x - \delta_n t}\right)}{\Omega\left(\varpi_1 e^{\alpha_1 x - \delta_1 t}, \cdots, \varpi_n e^{\alpha_n x - \delta_n t}\right)}, \tag{11}$$

in which $\Omega \neq 0$, and also, we have

$$\Delta_t = \sum_{i=1}^{n} \Delta_{\xi_i} \xi_{i,t}, \Omega_t = \sum_{i=1}^{n} \Omega_{\xi_i} \xi_{i,t}, \Delta_x = \sum_{i=1}^{n} \Delta_{\xi_i} \xi_{i,x}, \Omega_x = \sum_{i=1}^{n} \Omega_{\xi_i} \xi_{i,x},$$
$$\Psi_t = \frac{\Omega \sum_{i=1}^{n} \Delta_{\xi_i} \xi_{i,t} - \Delta \sum_{i=1}^{n} \Omega_{\xi_i} \xi_{i,t}}{\Omega^2}, \Psi_x = \frac{\Omega \sum_{i=1}^{n} \Delta_{\xi_i} \xi_{i,x} - \Delta \sum_{i=1}^{n} \Omega_{\xi_i} \xi_{i,x}}{\Omega^2}. \tag{12}$$

3. Multiple Soliton Solutions for the CDG Equation

3.1. Set I: One-Wave Solution. We start up with one-wave function based on the explanation in Step 2 in the previous section, we deem that Equation (1) has the below form of one-wave solution as

$$\Psi(x,t) = \frac{\eta_1}{\eta_2}, \quad \eta_1 = \sigma_1 + \sigma_2 e^{\alpha_1 x - \delta_1 t}, \eta_2 = 1 + \rho_1 + \rho_2 e^{\alpha_1 x - \delta_1 t}, \tag{13}$$

in which ρ_1, ρ_2, σ_1, and σ_2 are the unfound constants. Plugging (13) into Equation (1), we get to the following cases:

Case 1.

$$\alpha_1 = \alpha_1, \beta_1 = \beta_1, \rho_1 = \frac{\rho_2 \sigma_1 - \sigma_2}{\sigma_2}, \rho_2 = \rho_2,$$
$$\sigma_1 = \sigma_1, \sigma_2 = \sigma_2, \delta_1 = \alpha_1^5. \tag{14}$$

Case 2.

$$\alpha_1 = \alpha_1, \beta_1 = \beta_1, \rho_1 = -1, \rho_2 = \rho_2,$$
$$\sigma_1 = \sigma_1, \sigma_2 = \sigma_2, \delta_1 = \alpha_1^5. \tag{15}$$

Case 3.

$$\alpha_1 = \alpha_1, \beta_1 = \beta_1, \rho_1 = \rho_1, \rho_2 = \frac{\sigma_2(1+\rho_1)}{\sigma_1},$$
$$\sigma_1 = \sigma_1, \sigma_2 = \sigma_2, \delta_1 = \delta_1. \tag{16}$$

For example, the resulting one-wave solution for Cases 1 to 3 will be read, respectively, as

$$\Psi_1(x,t) = \frac{\sigma_1 + \sigma_2 e^{-t\alpha_1{}^5 + x\alpha_1}}{1 + ((\rho_2\sigma_1 - \sigma_2)/\sigma_2) + \rho_2 e^{-t\alpha_1{}^5 + x\alpha_1}},$$
$$\Psi_2(x,t) = \frac{\sigma_1 + \sigma_2 e^{-t\alpha_1{}^5 + x\alpha_1}}{\rho_2 e^{-t\alpha_1{}^5 + x\alpha_1}}, \tag{17}$$
$$\Psi_1(x,t) = \frac{\sigma_1 + \sigma_2 e^{-t\delta_1 + x\alpha_1}}{1 + \rho_1 + \left(\left(\sigma_2(1+\rho_1)e^{-t\delta_1 + x\alpha_1}\right)/\sigma_1\right)}.$$

3.2. Set II: Two-Wave Solutions. We start up with two-wave functions based on the explanations in Step 2 in the previous section; we deem that Equation (1) has the bellow form of two-wave solutions as

$$\Psi(x,t) = \frac{\eta_1}{\eta_2}, \tag{18}$$

$$\eta_1 = \rho_0 + \rho_1 e^{\alpha_1 x - \delta_1 t} + \rho_2 e^{\alpha_2 x - \delta_2 t} + \rho_1 \rho_2 \rho_{12} e^{(\alpha_1 + \alpha_2)x - (\delta_1 + \delta_2)t}, \tag{19}$$

$$\eta_2 = 1 + \sigma_1 e^{\alpha_1 x - \delta_1 t} + \sigma_2 e^{\alpha_2 x - \delta_2 t} + \sigma_1 \sigma_2 \sigma_{12} e^{(\alpha_1 + \alpha_2)x - (\delta_1 + \delta_2)t}. \tag{20}$$

Plugging (18) along with (19) into Equation (1), we gain the following cases:

Case 1.

$$\alpha_1 = 0, \alpha_2 = \alpha_2, \delta_1 = \delta_1, \delta_1 = \delta_1, \rho_0 = \frac{\rho_2}{\sigma_2},$$
$$\rho_1 = 0, \rho_2 = \rho_2, \rho_{12} = \rho_{12}, \sigma_1 = \sigma_1, \sigma_2 = \sigma_2, \sigma_{12} = 1. \tag{21}$$

Case 2.

$$\alpha_1 = 0, \alpha_2 = \alpha_2, \delta_1 = \delta_1, \delta_2 = \delta_2, \rho_0 = \frac{1}{\rho_{12}},$$
$$\rho_1 = \rho_1, \rho_2 = \frac{\sigma_2}{\rho_{12}}, \rho_{12} = \rho_{12}, \sigma_1 = 0, \sigma_2 = \sigma_2, \sigma_{12} = \sigma_{12}. \tag{22}$$

Case 3.

$$\alpha_1 = 0, \alpha_2 = \alpha_2, \delta_1 = \delta_1, \delta_2 = \alpha_2^5, \rho_0 = \frac{1}{\rho_{12}},$$
$$\rho_1 = \rho_1, \rho_2 = \rho_2, \rho_{12} = \rho_{12}, \sigma_1 = \sigma_1, \sigma_2 = 0, \sigma_{12} = \sigma_{12}. \tag{23}$$

Case 4.

$$\alpha_1 = 0, \alpha_2 = \alpha_2, \delta_1 = \delta_1, \delta_2 = \delta_2, \rho_0 = \frac{\rho_2}{\sigma_2},$$
$$\rho_1 = \rho_1, \rho_2 = \rho_2, \rho_{12} = \frac{\sigma_2}{\rho_2}, \sigma_1 = \sigma_1, \sigma_2 = \sigma_2, \sigma_{12} = 1. \tag{24}$$

Case 5.

$$\alpha_1 = \alpha_1, \alpha_2 = \alpha_2, \delta_1 = \alpha_1^5, \delta_2 = \alpha_2^5,$$
$$\rho_0 = \frac{\alpha_1{}^4 - 3\,\alpha_1{}^3\alpha_2 + 4\,\alpha_1{}^2\alpha_2{}^2 - 3\,\alpha_1\alpha_2{}^3 + \alpha_2{}^4}{\rho_{12}(\alpha_1{}^2 + \alpha_1\alpha_2 + \alpha_2{}^2)(\alpha_1 + \alpha_2)^2},$$
$$\rho_1 = \rho_1, \rho_2 = \rho_2, \rho_{12} = \rho_{12}, \sigma_1 = 0, \sigma_2 = 0, \sigma_{12} = \sigma 12. \tag{25}$$

Case 6.

$$\alpha_1 = \alpha_1, \alpha_2 = \alpha_2, \delta_1 = \alpha_1^5, \delta_2 = \delta_2, \rho_0 = \frac{1}{\rho_{12}},$$
$$\rho_1 = \rho_1, \rho_2 = \frac{\sigma_2}{\rho_{12}}, \rho_{12} = \rho_{12}, \tag{26}$$
$$\sigma_1 = 0, \sigma_2 = \sigma_2, \sigma_{12} = \sigma 12.$$

Case 7.

$$\alpha_1 = \alpha_1, \alpha_2 = \alpha_2, \delta_1 = \delta_1, \delta_2 = \delta_2, \rho_0 = \frac{\rho_2}{\sigma_2},$$
$$\rho_1 = \frac{\rho_2\sigma_1}{\sigma_2}, \rho_2 = \rho_2, \rho_{12} = \frac{\sigma_2\sigma_{12}}{\rho_2}, \sigma_1 = 0, \sigma_2 = \sigma_2, \sigma_{12} = \sigma_{12}. \tag{27}$$

For example, the resulting two-wave solution for Cases 1–7 will be read, respectively, as

$$\Psi_1(x,t) = \frac{(\rho_2/\sigma_2) + \rho_2 e^{-t\delta_2 + x\alpha_2}}{1 + \sigma_1 e^{-t\delta_1} + \sigma_2 e^{-t\delta_2 + x\alpha_2} + \sigma_1\sigma_2 e^{-t\delta_1 - t\delta_2 + x\alpha_2}},$$
$$\Psi_2(x,t) = \frac{\rho_{12}{}^{-1} + \rho_1 e^{-t\delta_1} + \left((\sigma_2 e^{-t\delta_2 + x\alpha_2})/\rho_{12}\right) + \rho_1\sigma_2 e^{-t\delta_1 - t\delta_2 + x\alpha_2}}{1 + \sigma_2 e^{-t\delta_2 + x\alpha_2}},$$
$$\Psi_3(x,t) = \frac{\rho_{12}{}^{-1} + \rho_1 e^{-t\delta_1} + \rho_2 e^{-t\alpha_2{}^5 + x\alpha_2} + \rho_1\rho_2\rho_{12} e^{-t\alpha_2{}^5 - t\delta_1 + x\alpha_2}}{1 + \sigma_1 e^{-t\delta_1}},$$
$$\Psi_4(x,t) = \frac{(\rho_2/\sigma_2) + \rho_1 e^{-t\delta_1} + \rho_2 e^{-t\delta_2 + x\alpha_2} + \rho_1\sigma_2 e^{-t\delta_1 - t\delta_2 + x\alpha_2}}{1 + \sigma_1 e^{-t\delta_1} + \sigma_2 e^{-t\delta_2 + x\alpha_2} + \sigma_1\sigma_2 e^{-t\delta_1 - t\delta_2 + x\alpha_2}},$$
$$\Psi_5(x,t) = \frac{\alpha_1{}^4 - 3\,\alpha_1{}^3\alpha_2 + 4\,\alpha_1{}^2\alpha_2{}^2 - 3\,\alpha_1\alpha_2{}^3 + \alpha_2{}^4}{\rho_{12}(\alpha_1{}^2 + \alpha_1\alpha_2 + \alpha_2{}^2)(\alpha_1 + \alpha_2)^2} + \rho_1 e^{-t\alpha_1{}^5 + x\alpha_1} + \rho_2 e^{-t\alpha_2{}^5 + x\alpha_2} + \rho_1\rho_2\rho_{12} e^{-t\alpha_1{}^5 - t\alpha_2{}^5 + x\alpha_1 + x\alpha_2},$$
$$\Psi_6(x,t) = \frac{\rho_{12}{}^{-1} + \rho_1 e^{-t\alpha_1{}^5 + x\alpha_1} + \left((\sigma_2 e^{-t\delta_2 + x\alpha_2})/\rho_{12}\right) + \rho_1\sigma_2 e^{-t\alpha_1{}^5 - t\delta_2 + x\alpha_1 + x\alpha_2}}{1 + \sigma_2 e^{-t\delta_2 + x\alpha_2}},$$
$$\Psi_7(x,t) = \frac{(\rho_2/\sigma_2) + \left((\rho_2\sigma_1 e^{-t\delta_1 + x\alpha_1})/\sigma_2\right) + \rho_2 e^{-t\delta_2 + x\alpha_2} + \rho_2\sigma_{12} e^{-t\delta_1 - t\delta_2 + x\alpha_1 + x\alpha_2}}{1 + \sigma_1 e^{-t\delta_1 + x\alpha_1} + \sigma_2 e^{-t\delta_2 + x\alpha_2} + \sigma_1\sigma_2\sigma_{12} e^{-t\delta_1 - t\delta_2 + x\alpha_1 + x\alpha_2}}. \tag{28}$$

3.3. Set III: Three-Wave Solutions. We start up with three-wave functions according to the given explanations in Step 2 in the previous section, we deem that Equation (1) has the below form of three-wave solutions as

$$\Psi(x,t) = \frac{df(\eta_1)/dx}{\eta_1}, \tag{29}$$

$$\begin{aligned}\eta_1 = {} & 1 + \rho_1 e^{\Lambda_1} + \rho_2 e^{\Lambda_2} + \rho_3 e^{\Lambda_3} \\ & + \rho_1\rho_2\rho_{12} e^{\Lambda_1 + \Lambda_2} \\ & + \rho_1\rho_3\rho_{13} e^{\Lambda_1 + \Lambda_3} + \rho_2\rho_3\rho_{23} e^{\Lambda_2 + \Lambda_3} \\ & + \rho_1\rho_2\rho_3\rho_{12}\rho_{13}\rho_{23} e^{\Lambda_1 + \Lambda_2 + \Lambda_3},\end{aligned} \tag{30}$$

in which $\Lambda_i = \alpha_i x - \delta_i t, i = 1, 2, 3$. Appending (29) along with (30) into Equation (1), we obtain the following case:

$$\begin{aligned}&\alpha_i = \alpha_i, \delta_i = \alpha_i^5, \quad i = 1, 2, 3, \\ &\rho_{ij} = \rho_{ij}, \quad i, j = 1, 2, 3, i \neq j.\end{aligned} \tag{31}$$

Therefore, three-wave solution will be as

$$\begin{aligned}\Psi_1(x,t) = {} & \rho_1\alpha_1 e^{-t\alpha_1{}^5 + x\alpha_1} + \rho_2\alpha_2 e^{-t\alpha_2{}^5 + x\alpha_2} + \rho_3\alpha_3 e^{-t\alpha_3{}^5 + x\alpha_3} \\ & + \rho_1\rho_2\rho_{12}(\alpha_1 + \alpha_2) e^{-t\alpha_1{}^5 - t\alpha_2{}^5 + x\alpha_1 + x\alpha_2} \\ & + \rho_1\rho_3\rho_{13}(\alpha_1 + \alpha_3) e^{-t\alpha_1{}^5 - t\alpha_3{}^5 + x\alpha_1 + x\alpha_3} \\ & + \rho_2\rho_3\rho_{23}(\alpha_2 + \alpha_3) e^{-t\alpha_2{}^5 - t\alpha_3{}^5 + x\alpha_2 + x\alpha_3} \\ & + \rho_1\rho_2\rho_3\rho_{12}\rho_{13}\rho_{23}(\alpha_1 + \alpha_2 + \alpha_3) e^{-t\alpha_1{}^5 - t\alpha_2{}^5 - t\alpha_3{}^5 + x\alpha_1 + x\alpha_2 + x\alpha_3} / \\ & \cdot \Big(1 + \rho_1 e^{-t\alpha_1{}^5 + x\alpha_1} + \rho_2 e^{-t\alpha_2{}^5 + x\alpha_2} + \rho_3 e^{-t\alpha_3{}^5 + x\alpha_3} \\ & + \rho_1\rho_2\rho_{12} e^{-t\alpha_1{}^5 - t\alpha_2{}^5 + x\alpha_1 + x\alpha_2} + \rho_1\rho_3\rho_{13} e^{-t\alpha_1{}^5 - t\alpha_3{}^5 + x\alpha_1 + x\alpha_3} \\ & + \rho_2\rho_3\rho_{23} e^{-t\alpha_2{}^5 - t\alpha_3{}^5 + x\alpha_2 + x\alpha_3} \\ & + \rho_1\rho_2\rho_3\rho_{12}\rho_{13}\rho_{23} e^{-t\alpha_1{}^5 - t\alpha_2{}^5 - t\alpha_3{}^5 + x\alpha_1 + x\alpha_2 + x\alpha_3}\Big).\end{aligned} \tag{32}$$

3.4. Cross-Kink Solutions. Here, we will consider the cross-kink wave solution with selecting the below function which for Equation (1) has been taken as

$$\begin{aligned}f = {} & \exp(\tau_1) + \theta_{10}\exp(-\tau_1) + \sinh(\tau_2) \\ & + \sin(\tau_3) + \theta_{11}, \tau_1 = \theta_1 x + \theta_2 t \\ & + \theta_3, \tau_2 = \theta_4 x + \theta_5 t \\ & + \theta_6, \tau_3 = \theta_7 x + \theta_8 t + \theta_9,\end{aligned} \tag{33}$$

$$\Psi(x,t) = \ln(f)_{xx}, \tag{34}$$

where $\theta_i, i = 1, \cdots, 11$, are undetermined amounts which should be detected. Appending (34) into Equation (1) and afterwards collecting the coefficients, we obtain the following consequences:

Case 1.

$$\begin{aligned}&\theta_1 = \theta_4 = i\theta_7, \theta_2 = \theta_5 = -16i\theta_7^5, \\ &\theta_8 = -16\theta_7^5, \theta_{11} = 0, i^2 = -1.\end{aligned} \tag{35}$$

Substituting (35) into (33) and (34), we achieve a cross-kink wave solution of Equation (1) as follows:

$$f = e^{-16\,i\theta_7{}^5 t + i\theta_7 x + \theta_3} + \theta_{10} e^{16\,i\theta_7{}^5 t - i\theta_7 x - \theta_3} - \sinh\left(16\,i\theta_7{}^5 t - i\theta_7 x - \theta_6\right) - \sin\left(16\,\theta_7{}^5 t - \theta_7 x - \theta_9\right),$$

$$\Psi_1 = \frac{-\theta_7{}^2 e^{-16\,i\theta_7{}^5 t + i\theta_7 x + \theta_3} - \theta_{10}\theta_7{}^2 e^{16\,i\theta_7{}^5 t - i\theta_7 x - \theta_3} + \sinh\left(16\,i\theta_7{}^5 t - i\theta_7 x - \theta_6\right)\theta_7{}^2 + \sin\left(16\,\theta_7{}^5 t - \theta_7 x - \theta_9\right)\theta_7{}^2}{e^{-16\,i\theta_7{}^5 t + i\theta_7 x + \theta_3} + \theta_{10} e^{16\,i\theta_7{}^5 t - i\theta_7 x - \theta_3} - \sinh\left(16\,i\theta_7{}^5 t - i\theta_7 x - \theta_6\right) - \sin\left(16\,\theta_7{}^5 t - \theta_7 x - \theta_9\right)}$$

$$- \frac{\left(i\theta_7 e^{-16\,i\theta_7{}^5 t + i\theta_7 x + \theta_3} - i\theta_{10}\theta_7 e^{16\,i\theta_7{}^5 t - i\theta_7 x - \theta_3} + i\cosh\left(16\,i\theta_7{}^5 t - i\theta_7 x - \theta_6\right)\theta_7 + \cos\left(16\,\theta_7{}^5 t - \theta_7 x - \theta_9\right)\theta_7\right)^2}{\left(e^{-16\,i\theta_7{}^5 t + i\theta_7 x + \theta_3} + \theta_{10} e^{16\,i\theta_7{}^5 t - i\theta_7 x - \theta_3} - \sinh\left(16\,i\theta_7{}^5 t - i\theta_7 x - \theta_6\right) - \sin\left(16\,\theta_7{}^5 t - \theta_7 x - \theta_9\right)\right)^2}. \tag{36}$$

Case 2.

$$\theta_1 = \sqrt{3}\theta_7 = i\sqrt{3}\theta_4, \theta_2 = -\sqrt{3}\theta_8 = 16\sqrt{3}i\theta_4^5,$$
$$\theta_5 = -16\theta_4^5, \theta_{10} = 0, \theta_{11} = 0, i^2 = -1. \tag{37}$$

Substituting (37) into (33) and (34), we achieve a cross-kink wave solution of Equation (1) which can be written as follows:

$$f = e^{16\sqrt{3}\theta_4{}^5 it + \sqrt{3}i\theta_4 x + \theta_3} - \sinh\left(16\,t\theta_4{}^5 - x\theta_4 - \theta_6\right) - \sin\left(16\,\theta_4{}^5 it - i\theta_4 x - \theta_9\right),$$

$$\Psi_1 = \frac{3\,i^2\theta_4{}^2 e^{16\sqrt{3}\theta_4{}^5 it + \sqrt{3}i\theta_4 x + \theta_3} - \sinh\left(16\,t\theta_4{}^5 - x\theta_4 - \theta_6\right)\theta_4{}^2 + \sin\left(16\,\theta_4{}^5 it - i\theta_4 x - \theta_9\right)i^2\theta_4{}^2}{e^{16\sqrt{3}\theta_4{}^5 it + \sqrt{3}i\theta_4 x + \theta_3} - \sinh\left(16\,t\theta_4{}^5 - x\theta_4 - \theta_6\right) - \sin\left(16\,\theta_4{}^5 it - i\theta_4 x - \theta_9\right)}$$

$$- \frac{\left(\sqrt{3}i\theta_4 e^{16\sqrt{3}\theta_4{}^5 it + \sqrt{3}i\theta_4 x + \theta_3} + \cosh\left(16\,t\theta_4{}^5 - x\theta_4 - \theta_6\right)\theta_4 + \cos\left(16\,\theta_4{}^5 it - i\theta_4 x - \theta_9\right)i\theta_4\right)^2}{\left(e^{16\sqrt{3}\theta_4{}^5 it + \sqrt{3}i\theta_4 x + \theta_3} - \sinh\left(16\,t\theta_4{}^5 - x\theta_4 - \theta_6\right) - \sin\left(16\,\theta_4{}^5 it - i\theta_4 x - \theta_9\right)\right)^2}. \tag{38}$$

3.5. Periodic-Kink Wave Solutions. Here, we will consider the periodic-kink wave solution with selecting the below function which for Equation (1) has been taken as

$$f = \exp(\tau_1) + \theta_{10}\exp(-\tau_1) + \cosh(\tau_2) + \cos(\tau_3) + \theta_{11}, \tau_1 = \theta_1 x + \theta_2 t + \theta_3, \tau_2 = \theta_4 x + \theta_5 t + \theta_6, \tau_3 = \theta_7 x + \theta_8 t + \theta_9, \tag{39}$$

$$\Psi(x,t) = \ln(f)_{xx}, \tag{40}$$

where $\theta_i, i = 1, \cdots, 11$, are undetermined amounts which should be detected. Appending (40) into Equation (1) and afterwards collecting the coefficients, we obtain the following consequences:

Case 1.

$$\theta_1 = \theta_4 = i\theta_7, \theta_2 = \theta_5 = -16i\theta_7^5, \theta_8 = -16\theta_7^5, \theta_{11} = 0, i^2 = -1. \tag{41}$$

Substituting (41) into (39) and (40), we achieve a periodic-kink wave solution of Equation (1) which can be written as follows:

$$f = e^{-16\,i\theta_7{}^5 t + i\theta_7 x + \theta_3} + \theta_{10} e^{16\,i\theta_7{}^5 t - i\theta_7 x - \theta_3} + \cosh\left(-16\,i\theta_7{}^5 t + i\theta_7 x + \theta_6\right) + \cos\left(-16\,\theta_7{}^5 t + \theta_7 x + \theta_9\right),$$

$$\Psi_2 = \frac{i^2\theta_7{}^2 e^{-16\,i\theta_7{}^5 t + i\theta_7 x + \theta_3} + \theta_{10} i^2\theta_7{}^2 e^{16\,i\theta_7{}^5 t - i\theta_7 x - \theta_3} + \cosh\left(16\,i\theta_7{}^5 t - i\theta_7 x - \theta_6\right)i^2\theta_7{}^2 - \cos\left(16\,t\theta_7{}^5 - x\theta_7 - \theta_9\right)\theta_7{}^2}{e^{-16\,i\theta_7{}^5 t + i\theta_7 x + \theta_3} + \theta_{10} e^{16\,i\theta_7{}^5 t - i\theta_7 x - \theta_3} + \cosh\left(16\,i\theta_7{}^5 t - i\theta_7 x - \theta_6\right) + \cos\left(16\,t\theta_7{}^5 - x\theta_7 - \theta_9\right)}$$

$$- \frac{\left(i\theta_7 e^{-16\,i\theta_7{}^5 t + i\theta_7 x + \theta_3} - \theta_{10} i\theta_7 e^{16\,i\theta_7{}^5 t - i\theta_7 x - \theta_3} - \sinh\left(16\,i\theta_7{}^5 t - i\theta_7 x - \theta_6\right)i\theta_7 + \sin\left(16\,t\theta_7{}^5 - x\theta_7 - \theta_9\right)\theta_7\right)^2}{\left(e^{-16\,i\theta_7{}^5 t + i\theta_7 x + \theta_3} + \theta_{10} e^{16\,i\theta_7{}^5 t - i\theta_7 x - \theta_3} + \cosh\left(16\,i\theta_7{}^5 t - i\theta_7 x - \theta_6\right) + \cos\left(16\,t\theta_7{}^5 - x\theta_7 - \theta_9\right)\right)^2}. \tag{42}$$

Case 2.

$$\theta_1 = \sqrt{3}\theta_7 = i\sqrt{3}\theta_4, \theta_2 = -\sqrt{3}\theta_8 = 16\sqrt{3}i\theta_4^5, \quad \theta_5 = -16\theta_4^5, \theta_{10} = 0, \theta_{11} = 0, i^2 = -1. \tag{43}$$

Substituting (43) into (39) and (40), we achieve a periodic-kink wave solution of Equation (1) as follows:

$$\begin{aligned} f &= e^{16\sqrt{3}\theta_4{}^5 it + \sqrt{3}i\theta_4 x + \theta_3} + \sinh\left(-16\, t\theta_4{}^5 + x\theta_4 + \theta_6\right) + \sin\left(-16\,\theta_4{}^5 it + i\theta_4 x + \theta_9\right), \\ \Psi_2 &= \frac{3\, i^2\theta_4{}^2 e^{16\sqrt{3}\theta_4{}^5 it + \sqrt{3}i\theta_4 x + \theta_3} + \cosh\left(16\, t\theta_4{}^5 - x\theta_4 - \theta_6\right)\theta_4{}^2 - \cos\left(16\,\theta_4{}^5 it - i\theta_4 x - \theta_9\right) i^2\theta_4{}^2}{e^{16\sqrt{3}\theta_4{}^5 it + \sqrt{3}i\theta_4 x + \theta_3} + \cosh\left(16\, t\theta_4{}^5 - x\theta_4 - \theta_6\right) + \cos\left(16\,\theta_4{}^5 it - i\theta_4 x - \theta_9\right)} \\ &\quad - \frac{\left(\sqrt{3}i\theta_4 e^{16\sqrt{3}\theta_4{}^5 it + \sqrt{3}i\theta_4 x + \theta_3} - \sinh\left(16\, t\theta_4{}^5 - x\theta_4 - \theta_6\right)\theta_4 + \sin\left(16\,\theta_4{}^5 it - i\theta_4 x - \theta_9\right) i\theta_4\right)^2}{\left(e^{16\sqrt{3}\theta_4{}^5 it + \sqrt{3}i\theta_4 x + \theta_3} + \cosh\left(16\, t\theta_4{}^5 - x\theta_4 - \theta_6\right) + \cos\left(16\,\theta_4{}^5 it - i\theta_4 x - \theta_9\right)\right)^2}. \end{aligned} \tag{44}$$

3.6. Periodic Type Wave Solutions-I. Here, we will consider the periodic type wave solution with selecting the below function which for Equation (1) has been taken as

$$f = \theta_{10}\exp(\tau_1) + \theta_{11}\exp(-\tau_2) + \theta_{12}\cos(\tau_3), \tau_1 = \theta_1 x + \theta_2 t + \theta_3, \tau_2 = \theta_4 x + \theta_5 t + \theta_6, \tau_3 = \theta_7 x + \theta_8 t + \theta_9, \tag{45}$$

$$\Psi(x,t) = \ln(f)_{xx}, \tag{46}$$

where $\theta_i, i = 1, \cdots, 11$, are undetermined amounts which should be detected. Appending (46) into Equation (1) and afterwards collecting the coefficients, we obtain the following consequences:

Case 1.

$$\theta_1 = \sqrt{3}\theta_7, \theta_2 = 16\sqrt{3}\theta_7^5, \theta_8 = -16\theta_7^5, \theta_{11} = 0. \tag{47}$$

Substituting (47) into (45) and (46), a periodic type wave solution of Equation (1) can be obtained as follows:

$$\begin{aligned} f &= \theta_{10} e^{16\theta_7{}^5\sqrt{3}t + \sqrt{3}\theta_7 x + \theta_3} + \theta_{12}\cos\left(16\, t\theta_7{}^5 - x\theta_7 - \theta_9\right), \\ \Psi_1 &= \frac{3\,\theta_{10}\theta_7{}^2 e^{16\theta_7{}^5\sqrt{3}t + \sqrt{3}\theta_7 x + \theta_3} - \theta_{12}\cos\left(16\, t\theta_7{}^5 - x\theta_7 - \theta_9\right)\theta_7{}^2}{\theta_{10} e^{16\theta_7{}^5\sqrt{3}t + \sqrt{3}\theta_7 x + \theta_3} + \theta_{12}\cos\left(16\, t\theta_7{}^5 - x\theta_7 - \theta_9\right)} \\ &\quad - \frac{\left(\theta_{10}\sqrt{3}\theta_7 e^{16\theta_7{}^5\sqrt{3}t + \sqrt{3}\theta_7 x + \theta_3} + \theta_{12}\sin\left(16\, t\theta_7{}^5 - x\theta_7 - \theta_9\right)\theta_7\right)^2}{\left(\theta_{10} e^{16\theta_7{}^5\sqrt{3}t + \sqrt{3}\theta_7 x + \theta_3} + \theta_{12}\cos\left(16\, t\theta_7{}^5 - x\theta_7 - \theta_9\right)\right)^2}. \end{aligned} \tag{48}$$

Case 2.

$$\theta_1 = -\theta_4 = -\sqrt{3}\theta_7, \theta_2 = -\theta_5 = -16\sqrt{3}\theta_7^5, \theta_8 = -16\theta_7^5. \tag{49}$$

Substituting (49) into (45) and (46), a periodic type wave solution of Equation (1) can be obtained as follows:

$$\begin{aligned} f &= \theta_{10} e^{-16\theta_7{}^5\sqrt{3}t - \sqrt{3}\theta_7 x + \theta_3} + \theta_{11} e^{-16\theta_7{}^5\sqrt{3}t - \sqrt{3}\theta_7 x - \theta_6} + \theta_{12}\cos\left(16\, t\theta_7{}^5 - x\theta_7 - \theta_9\right), \\ \Psi_2 &= \frac{3\,\theta_{10}\theta_7{}^2 e^{-16\theta_7{}^5\sqrt{3}t - \sqrt{3}\theta_7 x + \theta_3} + 3\,\theta_{11}\theta_7{}^2 e^{-16\theta_7{}^5\sqrt{3}t - \sqrt{3}\theta_7 x - \theta_6} - \theta_{12}\cos\left(16\, t\theta_7{}^5 - x\theta_7 - \theta_9\right)\theta_7{}^2}{\theta_{10} e^{-16\theta_7{}^5\sqrt{3}t - \sqrt{3}\theta_7 x + \theta_3} + \theta_{11} e^{-16\theta_7{}^5\sqrt{3}t - \sqrt{3}\theta_7 x - \theta_6} + \theta_{12}\cos\left(16\, t\theta_7{}^5 - x\theta_7 - \theta_9\right)} \\ &\quad - \frac{\left(-\theta_{10}\sqrt{3}\theta_7 e^{-16\theta_7{}^5\sqrt{3}t - \sqrt{3}\theta_7 x + \theta_3} - \theta_{11}\sqrt{3}\theta_7 e^{-16\theta_7{}^5\sqrt{3}t - \sqrt{3}\theta_7 x - \theta_6} + \theta_{12}\sin\left(16\, t\theta_7{}^5 - x\theta_7 - \theta_9\right)\theta_7\right)^2}{\left(\theta_{10} e^{-16\theta_7{}^5\sqrt{3}t - \sqrt{3}\theta_7 x + \theta_3} + \theta_{11} e^{-16\theta_7{}^5\sqrt{3}t - \sqrt{3}\theta_7 x - \theta_6} + \theta_{12}\cos\left(16\, t\theta_7{}^5 - x\theta_7 - \theta_9\right)\right)^2}. \end{aligned} \tag{50}$$

3.7. Periodic Type Wave Solutions-II. Here, we will consider the periodic wave solution with selecting the below function which for Equation (1) has been taken as

$$f = \theta_{10}\exp(\tau_1) + \theta_{11}\exp(-\tau_2) + \theta_{12}\sin(\tau_3), \tau_1 = \theta_1 x + \theta_2 t + \theta_3, \tau_2 = \theta_4 x + \theta_5 t + \theta_6, \tau_3 = \theta_7 x + \theta_8 t + \theta_9, \tag{51}$$

$$\Psi(x,t) = \ln(f)_{xx}, \tag{52}$$

where $\theta_i, i = 1, \cdots, 11$, are undetermined amounts which should be detected. Appending (52) into Equation (1) and afterwards collecting the coefficients, we obtain the following consequences:

Case 1.

$$\theta_1 = \sqrt{3}\theta_7, \theta_2 = 16\sqrt{3}\theta_7^5, \theta_8 = -16\theta_7^5, \theta_{11} = 0. \tag{53}$$

Substituting (53) into (51) and (52), a periodic type wave solution of Equation (1) can be obtained as follows:

$$\begin{aligned} f &= \theta_{10}e^{16\theta_7{}^5\sqrt{3}t+\sqrt{3}\theta_7 x+\theta_3} + \theta_{12}\sin\left(-16\,t\theta_7{}^5 + x\theta_7 + \theta_9\right), \\ \Psi_1 &= \frac{3\,\theta_{11}\theta_7{}^2 e^{16\theta_7{}^5\sqrt{3}t+\sqrt{3}\theta_7 x+\theta_3} + \theta_{12}\sin\left(16\,t\theta_7{}^5 - x\theta_7 - \theta_9\right)\theta_7{}^2}{\theta_{11}e^{16\theta_7{}^5\sqrt{3}t+\sqrt{3}\theta_7 x+\theta_3} - \theta_{12}\sin\left(16\,t\theta_7{}^5 - x\theta_7 - \theta_9\right)} \\ &\quad - \frac{\left(\theta_{11}\sqrt{3}\theta_7 e^{16\theta_7{}^5\sqrt{3}t+\sqrt{3}\theta_7 x+\theta_3} + \theta_{12}\cos\left(16\,t\theta_7{}^5 - x\theta_7 - \theta_9\right)\theta_7\right)^2}{\left(\theta_{11}e^{16\theta_7{}^5\sqrt{3}t+\sqrt{3}\theta_7 x+\theta_3} - \theta_{12}\sin\left(16\,t\theta_7{}^5 - x\theta_7 - \theta_9\right)\right)^2}. \end{aligned} \tag{54}$$

Case 2.

$$\theta_1 = -\theta_4 = -\sqrt{3}\theta_7, \theta_2 = -\theta_5 = -16\sqrt{3}\theta_7^5, \theta_8 = -16\theta_7^5. \tag{55}$$

Substituting (55) into (51) and (52), a periodic type wave solution of Equation (1) can be obtained as follows:

$$\begin{aligned} f &= \theta_{10}e^{-16\theta_7{}^5\sqrt{3}t-\sqrt{3}\theta_7 x+\theta_3} + \theta_{11}e^{-16\theta_7{}^5\sqrt{3}t-\sqrt{3}\theta_7 x-\theta_6} - \theta_{12}\sin\left(16\,t\theta_7{}^5 - x\theta_7 - \theta_9\right), \\ \Psi_2 &= \frac{3\,\theta_{10}\theta_7{}^2 e^{-16\theta_7{}^5\sqrt{3}t-\sqrt{3}\theta_7 x+\theta_3} + 3\,\theta_{11}\theta_7{}^2 e^{-16\theta_7{}^5\sqrt{3}t-\sqrt{3}\theta_7 x-\theta_6} + \theta_{12}\sin\left(16\,t\theta_7{}^5 - x\theta_7 - \theta_9\right)\theta_7{}^2}{\theta_{10}e^{-16\theta_7{}^5\sqrt{3}t-\sqrt{3}\theta_7 x+\theta_3} + \theta_{11}e^{-16\theta_7{}^5\sqrt{3}t-\sqrt{3}\theta_7 x-\theta_6} - \theta_{12}\sin\left(16\,t\theta_7{}^5 - x\theta_7 - \theta_9\right)} \\ &\quad - \frac{\left(-\theta_{10}\sqrt{3}\theta_7 e^{-16\theta_7{}^5\sqrt{3}t-\sqrt{3}\theta_7 x+\theta_3} - \theta_{11}\sqrt{3}\theta_7 e^{-16\theta_7{}^5\sqrt{3}t-\sqrt{3}\theta_7 x-\theta_6} + \theta_{12}\cos\left(16\,t\theta_7{}^5 - x\theta_7 - \theta_9\right)\theta_7\right)^2}{\left(\theta_{10}e^{-16\theta_7{}^5\sqrt{3}t-\sqrt{3}\theta_7 x+\theta_3} + \theta_{11}e^{-16\theta_7{}^5\sqrt{3}t-\sqrt{3}\theta_7 x-\theta_6} - \theta_{12}\sin\left(16\,t\theta_7{}^5 - x\theta_7 - \theta_9\right)\right)^2}. \end{aligned} \tag{56}$$

3.8. Solitary Wave Solutions. Here, we will consider the solitary wave solution with selecting the below function which for Equation (1) has been taken as

$$\begin{aligned} f &= \theta_7 + \theta_8\exp(\tau_1) + \theta_9\exp(-\tau_2), \tau_1 = \theta_1 x \\ &\quad + \theta_2 t + \theta_3, \tau_2 = \theta_4 x + \theta_5 t + \theta_6, \end{aligned} \tag{57}$$

$$\Psi(x,t) = \ln(f)_{xx}, \tag{58}$$

where $\theta_i, i = 1, \cdots, 9$, are undetermined amounts which should be detected. Appending (58) into Equation (1) and afterwards collecting the coefficients, we obtain the below consequences:

Case 1.

$$\begin{aligned} \theta_2 &= -\theta_1{}^5 - 5\,\theta_1{}^4\theta_4 - 10\,\theta_1{}^3\theta_4{}^2 - 10\,\theta_1{}^2\theta_4{}^3 \\ &\quad - 5\,\theta_1\theta_4{}^4 - \theta_4{}^5 - \theta_5, \theta_7 = 0. \end{aligned} \tag{59}$$

Substituting (59) into (57) and (58), a solitary wave solution of Equation (1) can be written as follows:

$$\begin{aligned} f &= \theta_8 e^{\left(-\theta_1{}^5 - 5\,\theta_1{}^4\theta_4 - 10\,\theta_1{}^3\theta_4{}^2 - 10\,\theta_1{}^2\theta_4{}^3 - 5\,\theta_1\theta_4{}^4 - \theta_4{}^5 - \theta_5\right)t + \theta_1 x + \theta_3} \\ &\quad + \theta_9 e^{-t\theta_5 - x\theta_4 - \theta_6}, \end{aligned} \tag{60}$$

$$\Psi_1 = \frac{\theta_8\theta_1{}^2 e^{\left(-\theta_1{}^5 - 5\,\theta_1{}^4\theta_4 - 10\,\theta_1{}^3\theta_4{}^2 - 10\,\theta_1{}^2\theta_4{}^3 - 5\,\theta_1\theta_4{}^4 - \theta_4{}^5 - \theta_5\right)t + \theta_1 x + \theta_3} + \theta_9\theta_4{}^2 e^{-t\theta_5 - x\theta_4 - \theta_6}}{\theta_8 e^{\left(-\theta_1{}^5 - 5\,\theta_1{}^4\theta_4 - 10\,\theta_1{}^3\theta_4{}^2 - 10\,\theta_1{}^2\theta_4{}^3 - 5\,\theta_1\theta_4{}^4 - \theta_4{}^5 - \theta_5\right)t + \theta_1 x + \theta_3} + \theta_9 e^{-t\theta_5 - x\theta_4 - \theta_6}}$$
$$- \frac{\left(\theta_8\theta_1 e^{\left(-\theta_1{}^5 - 5\,\theta_1{}^4\theta_4 - 10\,\theta_1{}^3\theta_4{}^2 - 10\,\theta_1{}^2\theta_4{}^3 - 5\,\theta_1\theta_4{}^4 - \theta_4{}^5 - \theta_5\right)t + \theta_1 x + \theta_3} - \theta_9\theta_4 e^{-t\theta_5 - x\theta_4 - \theta_6}\right)^2}{\left(\theta_8 e^{\left(-\theta_1{}^5 - 5\,\theta_1{}^4\theta_4 - 10\,\theta_1{}^3\theta_4{}^2 - 10\,\theta_1{}^2\theta_4{}^3 - 5\,\theta_1\theta_4{}^4 - \theta_4{}^5 - \theta_5\right)t + \theta_1 x + \theta_3} + \theta_9 e^{-t\theta_5 - x\theta_4 - \theta_6}\right)^2}. \tag{61}$$

By using suitable values of parameters, the analytical treatment of periodic wave solution is presented in Figure 1 including 3D plot and 2D plot with three points of time including $t = 0$, $t = 0.02$, and $t = 0.04$.

Case 2.

$$\theta_1 = -\theta_4, \theta_2 = \theta_4^5, \theta_5 = -\theta_4^5. \tag{62}$$

Substituting (62) into (57) and (58), a solitary wave solution of Equation (1) can be obtained as follows:

$$\begin{aligned} f &= \theta_7 + \theta_8 e^{t\theta_4{}^5 - x\theta_4 + \theta_3} + \theta_9 e^{t\theta_4{}^5 - x\theta_4 - \theta_6}, \\ \Psi_2 &= \frac{\theta_4{}^2\left(\theta_8 e^{t\theta_4{}^5 - x\theta_4 + \theta_3} + \theta_9 e^{t\theta_4{}^5 - x\theta_4 - \theta_6}\right)\theta_7}{\left(\theta_7 + \theta_8 e^{t\theta_4{}^5 - x\theta_4 + \theta_3} + \theta_9 e^{t\theta_4{}^5 - x\theta_4 - \theta_6}\right)^2}. \end{aligned} \tag{63}$$

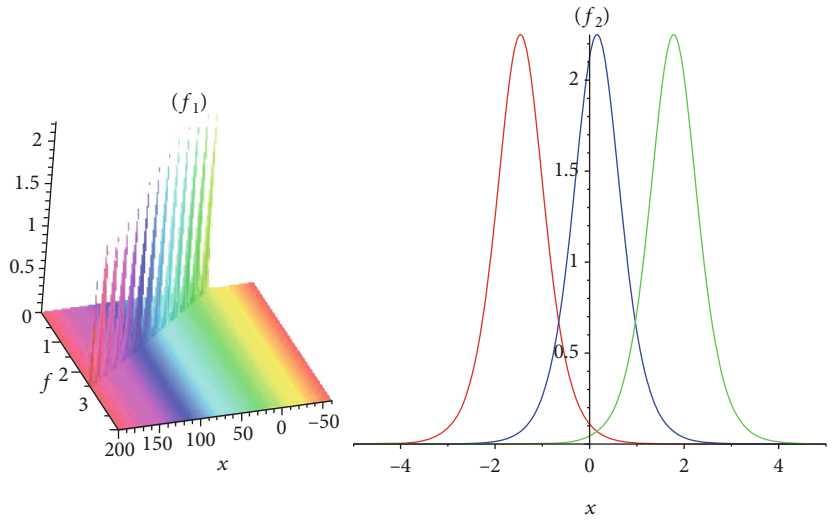

Figure 1: The solitary wave (61) at $\theta_1 = 1, \theta_4 = 2, \theta_3 = 2, \theta_5 = .5, \theta_6 = 3, \theta_8 = 1.3, \theta_9 = 2.4$.

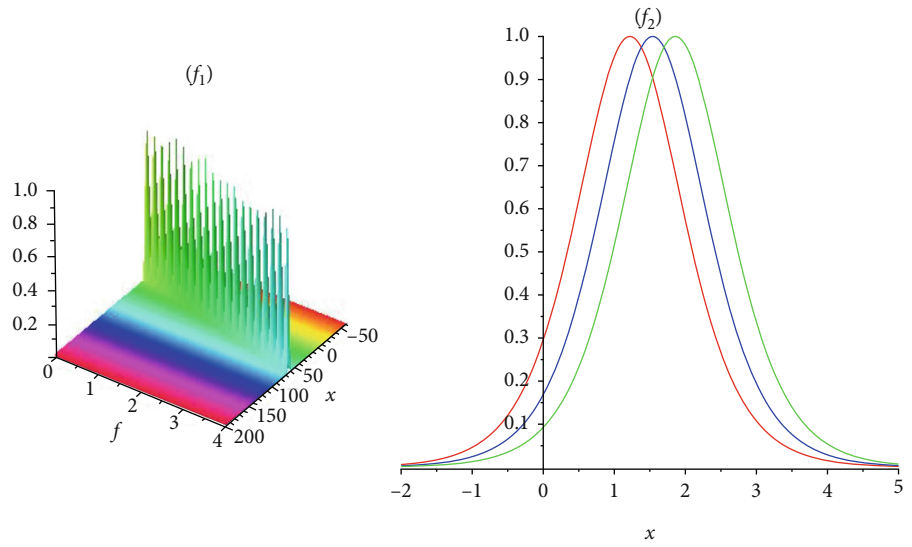

Figure 2: The solitary wave (63) at $\theta_4 = 2, \theta_3 = 2, \theta_6 = 3, \theta_7 = 1.3, \theta_8 = 2, \theta_9 = 2.4$.

By using suitable values of parameters, the analytical treatment of periodic wave solution is presented in Figure 2 including 3D plot and 2D plot with three points of time including $t = 0$, $t = 0.02$, and $t = 0.04$.

Case 3.

$$\theta_1 = -\frac{1}{2}\left(-1 \pm \sqrt{3}i\right)\theta_4, \theta_2 = \frac{1}{2}\left(1 \pm \sqrt{3}i\right)\theta_4^5, \theta_5 = -\theta_4^5. \quad (64)$$

Substituting (64) into (57) and (58), we achieve a solitary wave solution of Equation (1) as follows:

$$f = \theta_7 + \theta_8 e^{(1/2)t\theta_4^5\left(i\sqrt{3}+1\right)-(1/2)x\theta_4\left(i\sqrt{3}-1\right)+\theta_3} + \theta_9 e^{t\theta_4^5 - x\theta_4 - \theta_6},$$

$$\Psi_3 = \frac{(1/4)\theta_8\theta_4^2\left(i\sqrt{3}-1\right)^2 e^{(1/2)t\theta_4^5\left(i\sqrt{3}+1\right)-(1/2)x\theta_4\left(i\sqrt{3}-1\right)+\theta_3} + \theta_9\theta_4^2 e^{t\theta_4^5 - x\theta_4 - \theta_6}}{\theta_7 + \theta_8 e^{(1/2)t\theta_4^5\left(i\sqrt{3}+1\right)-(1/2)x\theta_4\left(i\sqrt{3}-1\right)+\theta_3} + \theta_9 e^{t\theta_4^5 - x\theta_4 - \theta_6}} - \frac{\left(-(1/2)\theta_8\theta_4\left(i\sqrt{3}-1\right)e^{(1/2)t\theta_4^5\left(i\sqrt{3}+1\right)-(1/2)x\theta_4\left(i\sqrt{3}-1\right)+\theta_3} - \theta_9\theta_4 e^{t\theta_4^5 - x\theta_4 - \theta_6}\right)^2}{\left(\theta_7 + \theta_8 e^{(1/2)t\theta_4^5\left(i\sqrt{3}+1\right)-(1/2)x\theta_4\left(i\sqrt{3}-1\right)+\theta_3} + \theta_9 e^{t\theta_4^5 - x\theta_4 - \theta_6}\right)^2}. \quad (65)$$

4. Stability Analysis of CDG Equation

According to [59], in order to analyze the propagation characteristics of the rogue wave in detail, we choose the linear stability analysis for the CDG equation via the following

function along with appropriate parameters:

$$\Phi(x,t) = \theta + \delta\Omega(x,t), \tag{66}$$

where the relation constant θ is a steady state solution of Equation (66). Appending (66) into Equation (1), one can obtain

$$\begin{aligned}
&\delta\frac{\partial}{\partial t}\Omega(x,t) + \delta\frac{\partial^5}{\partial x^5}\Omega(x,t) + 30\delta\left(\frac{\partial^3}{\partial x^3}\Omega(x,t)\right)\theta \\
&+ 30\delta^2\left(\frac{\partial^3}{\partial x^3}\Omega(x,t)\right)\Omega(x,t) + 30\delta^2\left(\frac{\partial}{\partial x}\Omega(x,t)\right) \\
&\cdot\frac{\partial^2}{\partial x^2}\Omega(x,t) + 180\delta\left(\frac{\partial}{\partial x}\Omega(x,t)\right)\theta^2 + 360\delta^2\left(\frac{\partial}{\partial x}\Omega(x,t)\right) \\
&\cdot\theta\Omega(x,t) + 180\delta^3\left(\frac{\partial}{\partial x}\Omega(x,t)\right)(\Omega(x,t))^2 = 0.
\end{aligned} \tag{67}$$

By linearization of Equation (67), we get

$$\begin{aligned}
&\delta\frac{\partial}{\partial t}\Omega(x,t) + \delta\frac{\partial^5}{\partial x^5}\Omega(x,t) + 30\delta\left(\frac{\partial^3}{\partial x^3}\Omega(x,t)\right)\theta \\
&+ 180\delta\left(\frac{\partial}{\partial x}\Omega(x,t)\right)\theta^2 = 0.
\end{aligned} \tag{68}$$

Theorem 1. *Presume that the solution of Equation (68) has the following form:*

$$\Omega(x,t) = \rho_1 e^{i(\alpha x+\beta t)}, \tag{69}$$

where α, β are the normalized wave numbers, by putting (69) into Equation (68), then by solving for β, we can achieve the following form

$$\beta(\alpha) = -\alpha^5 + 30\,\alpha^3\theta - 180\alpha\theta^2. \tag{70}$$

Proof. By appending the equality (69) in the linear PDE (68), we obtain

$$\begin{aligned}
&\delta\frac{\partial}{\partial t}\Omega(x,t) + \delta\frac{\partial^5}{\partial x^5}\Omega(x,t) + 30\delta\left(\frac{\partial^3}{\partial x^3}\Omega(x,t)\right)\theta \\
&+ 180\delta\left(\frac{\partial}{\partial x}\Omega(x,t)\right)\theta^2 = ie^{i(\alpha x+\beta t)} \\
&\cdot\delta\rho_1\left(\alpha^5 - 30\,\alpha^3\theta + 180\,\alpha\theta^2 + \beta\right) = 0.
\end{aligned} \tag{71}$$

By solving and simplifying, we can find the value of $\beta(\alpha)$ as follows:

$$\beta(\alpha) = -\alpha^5 + 30\alpha^3\theta - 180\alpha\theta^2. \tag{72}$$

After that, we get to the needed solution. Hence, the proof of the theorem is complete.

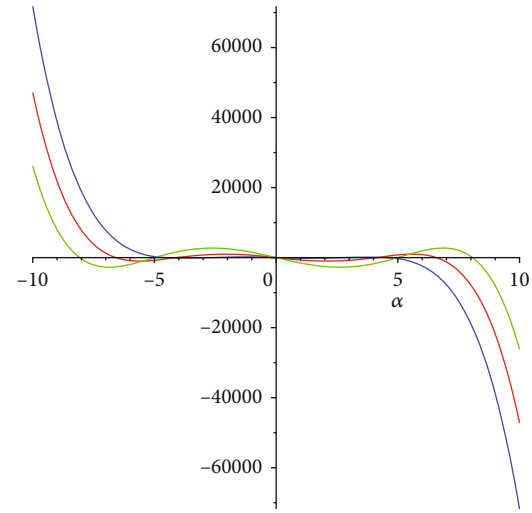

Figure 3: The behavior of stability analysis $\beta(\alpha)$ and wave number α with the disparate amounts $\theta = 1, \theta = 2, \theta = 3$.

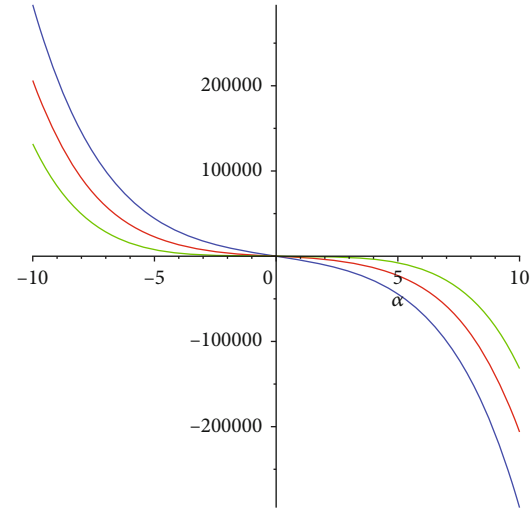

Figure 4: The behavior of stability analysis $\beta(\alpha)$ and wave number α with the disparate amounts $\theta = -5, \theta = -3, \theta = -1$.

In Figures 3–5, it can be seen that when the sign of $\beta(\alpha)$ is positive for all amounts of α, then any superposition of solutions of the form $e^{i(\alpha x+\beta t)}$ will come to ascent, while the sign of $\beta(\alpha)$ is negative for all amounts of α, then any superposition of solutions of the form $e^{i(\alpha x+\beta t)}$ will come to decay and the steady condition is stable. After that, in Figures 3 and 4, it can be observed that if the $\beta(\alpha)$ is positive or negative for some amounts of α, then with increasing time some components of a superposition will become descent, and the steady condition is stable. Finally, in Figure 5, it can be perceived that when the sign of $\beta(\alpha)$ is positive for all amounts of α, then any superposition of solutions of the form $e^{i(\alpha x+\beta t)}$ will come to ascent, while the sign of $\beta(\alpha)$ is negative for all amounts of α, then any superposition of solutions of the form $e^{i(\alpha x+\beta t)}$ will come to decay and the steady condition is stable.

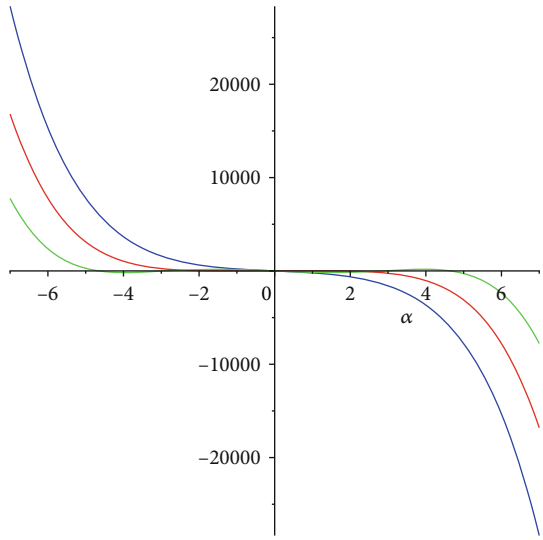

Figure 5: The behavior of stability analysis $\beta(\alpha)$ and wave number α with the disparate amounts $\theta = -1, \theta = 0, \theta = 1$.

5. Conclusion

In this work, the multiple exp-function, cross-kink, periodic-kink, and solitary wave methods with predictability of the $(1 + 1)$-dimensional CDG equation are investigated with more arbitrary autocephalous parameters. It is not hard to see that the general periodic-kink solution is an algebraically wave solution, and we noticed that some obtained solutions are singular periodic solitary wave solution which is periodic wave or periodic-kink, or solitary wave solutions in $x - t$ direction. Also, the other presented solution is a breather type of two-solitary wave solution which contains a periodic wave and two solitary waves, whose amplitude periodically oscillates with the evolution of time. Moreover, the kink and periodic solutions were analyzed and investigated. In addition, the periodic-kink waves appeared when the periodic solution cut by a stripe soliton before or after a special time. Meanwhile, the modulation instability was applied to discuss the stability of earned solutions. Finally, we show some graphs to explain these solutions.

Data Availability

The datasets supporting the conclusions of this article are included within the article and its additional file.

Conflicts of Interest

The authors declare that they have no conflicts of interest.

Acknowledgments

This project was supported by Researchers Supporting Project number (RSP-2020/210), King Saud University, Riyadh, Saudi Arabia.

References

[1] M. S. Osman, H. Rezazadeh, and M. Eslami, "Traveling wave solutions for (3+1) dimensional conformable fractional Zakharov-Kuznetsov equation with power law nonlinearity," *Nonlinear Engineering*, vol. 8, no. 1, pp. 559–567, 2019.

[2] D. Lu, K. U. Tariq, M. S. Osman, D. Baleanu, M. Younis, and M. M. A. Khater, "New analytical wave structures for the (3 + 1)-dimensional Kadomtsev- Petviashvili and the generalized Boussinesq models and their applications," *Results in Physics*, vol. 14, p. 102491, 2019.

[3] D. Kumar, C. Park, N. Tamanna, G. C. Paul, and M. S. Osman, "Dynamics of two-mode Sawada-Kotera equation: mathematical and graphical analysis of its dual-wave solutions," *Results in Physics*, vol. 19, article 103581, 2020.

[4] Y. Ding, M. S. Osman, and A. M. Wazwaz, "Abundant complex wave solutions for the nonautonomous Fokas-Lenells equation in presence of perturbation terms," *Optik*, vol. 181, pp. 503–513, 2019.

[5] M. S. Osman, M. Inc, J. G. Liu, K. Hosseini, and A. Yusuf, "Different wave structures and stability analysis for the generalized (2+1)-dimensional Camassa-Holm-Kadomtsev-Petviashvili equation," *Physica Scripta*, vol. 95, no. 3, article 035229, 2020.

[6] V. S. Kumar, H. Rezazadeh, M. Eslami, F. Izadi, and M. S. Osman, "Jacobi elliptic function expansion method for solving KdV equation with conformable derivative and dual-power law nonlinearity," *International Journal of Applied and Computational*, vol. 5, no. 5, p. 127, 2019.

[7] F. Yu and L. Li, "Inverse scattering transformation and soliton stability for a nonlinear Gross- Pitaevskii equation with external potentials," *Applied Mathematics Letters*, vol. 91, pp. 41–47, 2019.

[8] A. Ramani, "Inverse scattering, ordinary differential equations of painlevé-type, and Hirota's bilinear formalism," *Annals of the New York Academy of Sciences*, vol. 373, no. 1, pp. 54–67, 1981.

[9] Y. Li, R. Li, B. Xue, and X. Geng, "A generalized complex mKdV equation: Darboux transformations and explicit solutions," *Wave Motion*, vol. 98, article 102639, 2020.

[10] B. Q. Li and Y. L. Ma, "Extended generalized Darboux transformation to hybrid rogue wave and breather solutions for a nonlinear Schrodinger equation," *Applied Mathematics and Computation*, vol. 386, article 125469, 2020.

[11] X. W. Yan, "Lax pair, Darboux-dressing transformation and localized waves of the coupled mixed derivative nonlinear Schrodinger equation in a birefringent optical fiber," *Applied Mathematics Letters*, vol. 107, article 106414, 2020.

[12] M. S. Osman, D. Baleanu, A. R. Adem, K. Hosseini, M. Mirzazadeh, and M. Eslami, "Double-wave solutions and Lie symmetry analysis to the (2 + 1)-dimensional coupled Burgers equations," *Chinese Journal of Physics*, vol. 63, pp. 122–129, 2020.

[13] R. Hirota, *The Direct Method in Soliton Theory*, Cambridge University Press, 2009.

[14] M. S. Osman and H. I. Abdel-Gawad, "Multi-wave solutions of the (2+1)-dimensional Nizhnik-Novikov-Veselov equations with variable coefficients," *The European Physical Journal Plus*, vol. 130, no. 10, p. 215, 2015.

[15] J. G. Liu, W. H. Zhu, M. S. Osman, and W. X. Ma, "An explicit plethora of different classes of interactive lump solutions for an extension form of 3D-Jimbo–Miwa model," *The European Physical Journal Plus*, vol. 135, no. 5, p. 412, 2015.

[16] W. X. Ma, Y. Zhou, and R. Dougherty, "Lump-type solutions to nonlinear differential equations derived from generalized bilinear equations," *International Journal of Modern Physics B*, vol. 30, no. 28n29, article 1640018, 2016.

[17] J. G. Liu, M. S. Osman, W. H. Zhu, L. Zhou, and D. Baleanu, "The general bilinear techniques for studying the propagation of mixed-type periodic and lump-type solutions in a homogenous-dispersive medium," *AIP Advances*, vol. 10, no. 10, article 105325, 2020.

[18] C. J. Wang, "Spatiotemporal deformation of lump solution to (2+1)-dimensional KdV equation," *Nonlinear Dynamics*, vol. 84, no. 2, pp. 697–702, 2016.

[19] M. R. Foroutan, J. Manafian, and A. Ranjbaran, "Lump solution and its interaction to (3+1)-D potential-YTSF equation," *Nonlinear Dynamics*, vol. 92, no. 4, pp. 2077–2092, 2018.

[20] L. Kaur and A. M. Wazwaz, "Lump, breather and solitary wave solutions to new reduced form of the generalized BKP equation," *International Journal of Numerical Methods for Heat and Fluid Flow*, vol. 29, no. 2, pp. 569–579, 2019.

[21] L. Kaur and A. M. Wazwaz, "Bright-dark lump wave solutions for a new form of the (3+1)-dimensional BKP-Boussinesq equation," *Romanian Reports in Physics*, vol. 71, pp. 1–11, 2019.

[22] L. Kaur and A. M. Wazwaz, "Dynamical analysis of lump solutions for (3 + 1) dimensional generalized KP–Boussinesq equation and its dimensionally reduced equations," *Physica Scripta*, vol. 93, no. 7, article 075203, 2018.

[23] S. Singh, L. Kaur, K. Sakkaravarthi, R. Sakthivel, and K. Murugesan, "Dynamics of higher-order bright and dark rogue waves in a new (2+1)-dimensional integrable Boussinesq model," *Physica Scripta*, vol. 95, no. 11, article 115213, 2020.

[24] J. Manafian, B. Mohammadi Ivatlo, and M. Abapour, "Lump-type solutions and interaction phenomenon to the (2+1)-dimensional breaking soliton equation," *Applied Mathematics and Computation*, vol. 13, pp. 13–41, 2019.

[25] O. A. Ilhan and J. Manafian, "Periodic type and periodic cross-kink wave solutions to the (2+1)-dimensional breaking soliton equation arising in fluid dynamics," *Modern Physics Letters B*, vol. 33, no. 23, article 1950277, 2019.

[26] L. L. Huang and Y. Chen, "Lump solutions and interaction phenomenon for (2+1)-dimensional Sawada–Kotera equation," *Communications in Theoretical Physics*, vol. 67, no. 5, pp. 473–478, 2017.

[27] J. Q. Lu and S. D. Bilige, "Lump solutions of a (2+1)-dimensional bSK equation," *Nonlinear Dynamics*, vol. 90, no. 3, pp. 2119–2124, 2017.

[28] J. Manafian and M. Lakestani, "Lump-type solutions and interaction phenomenon to the bidirectional Sawada-Kotera equation," *Pramana*, vol. 92, no. 3, p. 41, 2019.

[29] J. Zhao, J. Manafian, N. E. Zaya, and S. A. Mohammed, "Multiple rogue wave, lump-periodic, lump-soliton, and interaction betweenk-lump andk-stripe soliton solutions for the generalized KP equation," *Mathematical Methods in the Applied Sciences*, 2020.

[30] J. Manafian, S. A. Mohammed, A. Alizadeh, H. M. Baskonus, and W. Gao, "Investigating lump and its interaction for the third-order evolution equation arising propagation of long waves over shallow water," *European Journal of Mechanics - B/Fluids*, vol. 84, pp. 289–301, 2020.

[31] B. He and Q. Meng, "Bilinear form and new interaction solutions for the sixth-order Ramani equation," *Applied Mathematics Letters*, vol. 98, pp. 411–418, 2019.

[32] J. Manafian and M. Lakestani, "N-lump and interaction solutions of localized waves to the (2+1)-dimensional variable-coefficient Caudrey-Dodd-Gibbon-Kotera-Sawada equation," *Journal of Geometry and Physics*, vol. 150, p. 103598, 2020.

[33] J. Wang, H. L. An, and B. Li, "Non-traveling lump solutions and mixed lump kink solutions to (2+1)-dimensional variable-coefficient Caudrey Dodd Gibbon Kotera Sawada equation," *Modern Physics Letters B*, vol. 33, no. 22, article 1950262, 2019.

[34] Z. D. Dai, J. Liu, X. P. Zeng, and Z. J. Liu, "Periodic kink-wave and kinky periodic-wave solutions for the Jimbo-Miwa equation," *Physics Letters A*, vol. 372, no. 38, pp. 5984–5986, 2008.

[35] W. X. Ma and Z. Zhu, "Solving the (3 + 1)-dimensional generalized KP and BKP equations by the multiple exp-function algorithm," *Applied Mathematics and Computation*, vol. 218, no. 24, pp. 11871–11879, 2012.

[36] R. N. Aiyer, B. Fuchssteiner, and W. Oevel, "Solitons and discrete eigenfunctions of the recursion operator of non-linear evolution equations. I. the Caudrey-Dodd-Gibbon-Sawada-Kotera equation," *Journal of Physics A: Mathematical and General*, vol. 19, no. 18, pp. 3755–3770, 1986.

[37] Y. G. Xu, X. W. Zhou, and L. Yao, "Solving the fifth order Caudrey-Dodd-Gibbon (CDG) equation using the exp- function method," *Applied Mathematics and Computation*, vol. 206, no. 1, pp. 70–73, 2008.

[38] A. M. Wazwaz, "Analytic study of the fifth order integrable nonlinear evolution equations by using the tanh method," *Applied Mathematics and Computation*, vol. 174, no. 1, pp. 289–299, 2006.

[39] A. M. Wazwaz, "Multiple-soliton solutions for the fifth order Caudrey-Dodd-Gibbon (CDG) equation," *Applied Mathematics and Computation*, vol. 197, no. 2, pp. 719–724, 2008.

[40] C. Cao, Y. Wu, and X. Geng, "On quasi-periodic solutions of the 2+1 dimensional Caudrey-Dodd-Gibbon-Kotera-Sawada equation," *Physics Letters A*, vol. 256, no. 1, pp. 59–65, 1999.

[41] S. Y. Lou, "Twelve sets of symmetries of the Caudrey-Dodd-Gibbon-Sawada-Kotera equation," *Physics Letters A*, vol. 175, no. 1, pp. 23–26, 1993.

[42] J. H. He, "New interpretation of homotopy perturbation method," *International Journal of Modern Physics B*, vol. 20, pp. 2561–2568, 2012.

[43] H. Tari, D. D. Ganji, and M. Rostamian, "Approximate solutions of K (2,2), KdV and modified KdV equations by variational iteration method, homotopy perturbation method and homotopy analysis method," *International Journal of Nonlinear Sciences and Numerical Simulation*, vol. 8, pp. 203–210, 2007.

[44] T. Ozis and A. Yildirim, "Traveling wave solution of Korteweg–de Vries equation using He's homotopy perturbation method," *International Journal of Nonlinear Sciences and Numerical Simulation*, vol. 8, pp. 239–242, 2007.

[45] A. H. Salas, O. G. Hurtado, and J. E. C. Hernández, "Computing multi-soliton solutions to Caudrey-Dodd- Gibbon equation by Hirota's method," *Eur. Int. J. Phys. Sc.*, vol. 6, no. 34, 2011.

[46] A. Yusuf, T. A. Sulaiman, M. Inc, and M. Bayram, "Breather wave, lump-periodic solutions and some other interaction

phenomena to the Caudrey-Dodd-Gibbon equation," *The European Physical Journal Plus*, vol. 135, no. 7, p. 563, 2020.

[47] D. Kumar and S. Kumar, "Some more solutions of Caudrey–Dodd–Gibbon equation using optimal system of lie symmetries," *International Journal of Applied and Computational Mathematics*, vol. 6, no. 4, p. 125, 2020.

[48] D. Kumar and S. Kumar, "Solitary wave solutions of pZK equation using Lie point symmetries," *The European Physical Journal Plus*, vol. 135, p. 162, 2020.

[49] S. Kumar, W. X. Ma, and A. Kumar, "Lie symmetries, optimal system and group-invariant solutions of the (3+1)-dimensional generalized KP equation," *Chinese Journal of Physics*, vol. 69, pp. 1–23, 2021.

[50] S. Kumar, D. Kumar, and A. Kumar, "Lie symmetry analysis for obtaining the abundant exact solutions, optimal system and dynamics of solitons for a higher-dimensional Fokas equation," *Chaos, Solitons & Fractals*, vol. 29, p. 110507, 2020.

[51] S. Kumar, M. Niwas, and A. M. Wazwaz, "Lie symmetry analysis, exact analytical solutions and dynamics of solitons for (2 +1)-dimensional NNV equations," *Physica Scripta*, vol. 95, no. 9, article 095204, 2020.

[52] S. Kumar and D. Kumar, "Lie symmetry analysis, complex and singular solutions of (2+1)-dimensional combined MCBS-nMCBS equation," *International Journal of Dynamics and Control*, vol. 7, no. 2, pp. 496–509, 2019.

[53] S. Kumar and S. Rani, "Lie symmetry reductions and dynamics of soliton solutions of (2+1)-dimensional Pavlov equation," *Pramana*, vol. 94, no. 1, p. 116, 2020.

[54] L. Kaur and A. M. Wazwaz, "Bright-dark optical solitons for Schrödinger-Hirota equation with variable coefficients," *Optik*, vol. 179, pp. 479–484, 2019.

[55] W. Gao, H. F. Ismael, H. Bulut, and H. M. Baskonus, "Instability modulation for the (2+1)-dimension paraxial wave equation and its new optical soliton solutions in Kerr media," *Physica Scripta*, vol. 95, no. 3, article 035207, 2020.

[56] W. Gao, P. Veeresha, D. G. Prakasha, H. M. Baskonus, and G. Yel, "A powerful approach for fractional Drinfeld-Sokolov-Wilson equation with Mittag-Leffler law," *Alexandria Engineering Journal*, vol. 58, no. 4, pp. 1301–1311, 2019.

[57] J. Manafian, "Novel solitary wave solutions for the (3+1)-dimensional extended Jimbo-Miwa equations," *Computers & Mathematcs with Applications*, vol. 76, no. 5, pp. 1246–1260, 2018.

[58] O. İlhan, S. G. Kasimov, S. Q. Otaev, and H. M. Baskonus, "On the solvability of a mixed problem for a high-order partial differential equation with fractional derivatives with respect to time, with Laplace operators with spatial variables and nonlocal boundary conditions in Sobolev classes," *Mathematics*, vol. 7, no. 3, p. 235, 2019.

[59] J. Manafian, O. A. Ilhan, and A. Alizadeh, "Periodic wave solutions and stability analysis for the KP-BBM equation with abundant novel interaction solutions," *Physica Scripta*, vol. 95, no. 6, article 065203, 2020.

[60] J. Manafian, B. Mohammadi Ivatlo, and M. Abapour, "Breather wave, periodic, and cross-kink solutions to the generalized Bogoyavlensky-Konopelchenko equation," *Mathematical Methods in the Applied Sciences*, vol. 43, no. 4, pp. 1753–1774, 2019.

[61] Y. Yakup and Y. Emrullah, "Multiple exp-function method for soliton solutions of nonlinear evolution equations," *Chinese Physics B*, vol. 26, no. 7, pp. 20–26, 2017.

[62] A. G. Alnowehy, "The multiple exp-function method and the linear superposition principle for solving the (2+1)-dimensional Calogero-Bogoyavlenskii-Schiff equation," *Zeitschrift für Naturforschung A*, vol. 70, no. 9, pp. 775–779, 2015.

[63] R. A. Abdullahi, "The generalized (1+1)-dimensional and (2 +1)-dimensional Ito equations: multiple exp-function algorithm and multiple wave solutions," *Computers & Mathematcs with Applications*, vol. 71, pp. 1248–1258, 2016.